Primitive ankaramitic melts in island arcs: evidence from melt inclusions

by

Fernando N. Della-Pasqua BSc. (Hons.)

Submitted in fulfilment of the requirements
for the degree of Doctor of Philosophy (Geology)

University of Tasmania Dept of Geology

Hobart 1997

Statement

This thesis contains the results of research done at the Department of Geology, University of Tasmania, Hobart between 1992 and 1997. Part of the material presented in this thesis has been published as:

Della-Pasqua F. N., Kamenetsky V. S., Gasparon M., Crawford A. J. & Varne R. (1995). Al-spinels in primitive arc volcanics.
Mineralogy and Petrology 53, 1-26

and

Della-Pasqua F. N.& Varne R. (1997).
Primitive ankaramitic magmas in volcanic arcs: a melt-inclusion approach.
The Canadian Mineralogist 35, 291-312.

This thesis contains no material which has been accepted for the award of any other higher degree or graduate diploma in any tertiary institution and to the best of the author's knowledge and belief, the thesis contains no material previously published or written by another person, except where due reference is made in the text of the thesis.

This thesis may be available for loan and limited copying in accordance with the Copyright Act 1968.

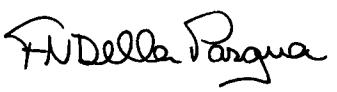

Fernando N. Della-Pasqua
Department of Geology
University of Tasmania
Hobart
(November, 1997)

Contents

page

Chapter 4: "Fe-loss" in melt inclusions hosted in olivine

Chapter 5: Dry, hydrous, and CO_2-bearing phase relations of an ankaramite composition based on melt inclusion compositions

page

Chapter 6: The formation of Al-spl in melt inclusions

page

List of tables

List of figures

page

Chapter 1

Chapter 2

Chapter 3

Chapter 4

Chapter 5

page

Chapter 6

Frequently used abbreviations

Al-spl	aluminous spinel
$Al\text{-}spl_d$	daughter Al-spl crystal in melt inclusion
$Al\text{-}spl_s$	solid inclusion of Al-spl
°C	degree Celsius (Centigrade)
cpx	clinopyroxene
cs	larnite
Cr#	100Cr/(Cr+Al)
Cr-spl	chromian spinel
di	diopside
Fe*	all iron as Fe^{2+}
g	gram
GPa	gigapascal=10 Kbar=10^9 N/m^2
grt	garnet
gross	grossular
hy	hypersthene
$K_D{}^{*\ Ol\text{-}Melt}_{Fe\text{-}Mg}$	Fe-Mg partitioning between olivine and melt, $=(Fe/Mg)_{ol}/(Fe^*/Mg)_{melt}$
$K_D{}^{Ol\text{-}Melt}_{Fe\text{-}Mg}$	Fe-Mg partitioning between olivine and melt, $=(Fe/Mg)_{ol}/(Fe^{2+}/Mg)_{melt}$
lu	leucite
µm	micron = 0.01 mm
mg	milligram
Mg#	100Mg/(Mg+Fe*)
mg#	$100Mg/(Mg+Fe^{2+})$
MH-buffer	magnetite-haematite buffer
ne	nepheline
ol	olivine
opx	orthopyroxene
P	pressure
plg	plagioclase
qtz	quartz
$R_{(mi/spl)}$	(melt inclusion/$Al\text{-}spl_d$) radius ratio
spess	spessartine
spl	spinel
T	temperature
T_c	dry liquidus T calculated using the olivine-melt thermometer of Ford *et al.* (1983)
T_h	temperature of homogenization
T_q	temperature of experimental quenching

Mineral names abbreviated in italics are used in the text to indicate molecular CIPW normative components.

Acknowledgments

Throughout the duration of this thesis I greatly benefited from the knowledge, help and friendship of many people. All of them have contributed towards the fulfilment of this thesis and without them it would have not been possible. To all of them I am indebted and I extend my thanks.

First I should acknowledge the advice and financial assistance of my supervisor Prof. R. Varne. I am indebted to Prof. R. Varne for making available opportunities which I would otherwise not have had.

I also like to acknowledge the associate supervision of Prof. A.J. Crawford. I thank Tony for his enthusiasm, interest and willingness to help at all times. I am also indebted to Tony for his willingness to review the final version of this thesis and help to improve it.

K.L. Harris is also acknowledged for his supervision, expert advise and guidance through the high pressure experimental work carried out in this thesis. I specially thank K.L. Harris for his patience and forgiveness during "lab-training", and for his instruction on numerous aspects of experimental petrology. The contribution of his knowledge and help during the experimental work is greatly acknowledged and has greatly improved the quality of the results presented in this thesis.

Prof. D.H. Green is acknowledged for bringing to my attention the possible role of CO_2 in the generation of ankaramitic melts and for his advise on the theoretical basis for the high pressure experimental work carried out in this thesis.

Dr. L.V Danyushevsky and Dr. V.L. Kamenetsky are thank for their instruction, supervision and helpful discussions during the course of melt inclusion work. I thank them both for bringing to my attention and helping me disentangle a wealth of information hidden within the world of melt inclusions. Dr. V.L. Kamenetsky is thank for his helpful reviews and constructive criticism of early versions of this thesis. Chapter 4 was greatly improved through the careful reviews and constructive criticism of Dr. L.V. Danyushevsky. I specially thank Dr. L.V. Danyushevsky for bringing to my attention the re-equilibration processes within melt inclusions and for the provision of a computer program for the recalculation of melt inclusions affected by "Fe-loss".

The advise and guidance of Dr. S. Eggins and Prof. D. H. Green during early stages of this thesis is greatly appreciated.

The final writing of this thesis was immensely helped by the grammar corrections and careful editing of the text made by Robina Sharpe. I am indebted to Robina for her invaluable help and her willingness to perform the tedious task of turning the text into "readable" english.

I like to thank W. Jablonski (Central Science Laboratory) for the long hours of instruction on the use of the SX-50 Cameca electron microprobe. His assistance specially after-hours and his dedication to keep the probe running at optimal conditions are greatly acknowledged.

S. Stephens and N. Deards are thanked for their instructions on the preparation of high quality electron microprobe mounts.

Graham Rowbottom (Central Science Laboratory) is thanked for carrying out CO_2 and H_2O determinations.

Dr. Khin Zaw is specially thanked for analysing fluid inclusions.

The work in this thesis was also greatly benefited from many helpful discussions with fellow students and staff, especially Dr. Ron Berry, Dr. Massimo Gasparon, Dr. Alicia Verbeeten, Dr. J. Adam, Dr. Jan Van Moort, Dr. Tom Troll, Dr. Joe Stolz, Dr. Wayne Taylor, Andrew McNeill, Dr. Marcell Kamperman and Dr. Trevor Falloon.

I also thank all my other fellow students and staff at the department of geology and CODES through out the years, Dr. Paul Kitto, Dr. Udi Hartono, Dr. Ai Yang, Russel Fulton, Dr. Sampan Singharajwarapan, Dr. Garry Davidson, Dr. Aung Pwa, Dr. Mohamad Adabi and many others. S. Hunns is specially thanked for his willingness to proof read part of the text.

I especially thank all the students with whom I shared room 338 (Geoff Nicholls, Ingvar Atli Sigurdsson, Greg Yaxley, Ruth Lanyon, Massimo Gasparon, Alicia Verbeeten, Robina Sharpe, Rohan Wolfe and Cathryn Gifkins) for creating an exceptionally unique environment within the room through the years. I like to thank them all for their friendship and for their tolerance.

I thank all the staff of the Geology department and CODES for their help specially Jaeanette Hankin, Christine Higgins, Marylin Feast, Peter Cornish, Julie Beattie and Cathy Stait. I like to thank Mike Harlow, Darren Turner and especially June Pongratz for their willingness to help and solve numerous unexpected computer problems.

I would like to thank the encouragement of many friends throughout the years specially the moral support of Chris Hockings, Dr. Neville Jones, Dr. Peter Sedwick, Ben Stockwin, James Hannon, Toby Chesworth, Tod Fisher and many others. I like to thank Kristy Boon for her close friendship and for tolerating me as a house mate for so many years. I also like to thank the Stockwin Family for welcoming me to their home and for the enjoyed hospitality.

My special thanks go to my parents Ada and Nestor, to my sister Laura and to Robina Sharpe. I am indebted to them for all the love and care that they always offer me.

Financial support for this project was provided by an Australian Post-Graduate Research Award at the University of Tasmania and generously supplemented by research grants to Prof. R. Varne for which I am grateful.

Abstract

Primitive ankaramite rocks differ from picrite by their richness in clinopyroxene (cpx>ol), their high CaO/Al_2O_3 values (>1, wt%) and their high normative *di/ol* values (>0.7, mol%). Ankaramite rocks are generally interpreted as a variety of basalt enriched in clinopyroxene crystals yet some studies suggest that ankaramite rocks crystallized from primitive ankaramitic melts. The origin of ankaramitic melts is of interest because their compositions differ from the picritic compositions of experimentally produced partial melts in equilibrium with mantle peridotite, yet many of their of their characteristics are similar to those of primitive mantle melts, i.e. high Mg# values, high Ni and Cr, and magnesian olivine phenocrysts.

The four primitive ankaramite suites studied in this thesis are from the Ulakan Formation in Bali, and the Rinjani volcano in Lombok (Sunda arc), and from Merelava and Epi (Vanuatu arc). Primary melt inclusions in magnesian olivine phenocrysts ($Fo_{>90}$) from each suite are studied to investigate the early stages of ankaramite magma evolution. The composition of these melt inclusions after homogenization are quite unlike picrite and have CaO/Al_2O_3 values which range up to ~1.7, and are therefore ankaramitic. Additionally, the CaO/Al_2O_3 values of melt inclusions within the same grain are similar, but vary between phenocrysts.

Critical assessment of the data suggests that the composition of melt inclusions trapped in olivine can be modified by Fe-Mg re-equilibration with the host, before the magma is erupted. This process might lower the original FeO* content of the trapped melt by several wt% ("Fe-loss"). The extent of "Fe-loss" depends on (1) the time spent by the host olivine phenocryst in the magma before eruption (residence time) and (2) the rate at which the re-equilibration occurred. Most of the compositions of homogenized melt inclusions in this study are affected by "Fe-loss" and are therefore not directly representative of the original trapped melt. A recalculation procedure is developed to reconstruct the original composition of the melt at the moment of trapping. Both, before and after recalculation, the compositions of melt inclusions display *di/ol* values >1, thus retaining their ankaramitic affinities. The CaO/Al_2O_3 values of melt inclusions are unaffected by this procedure. The recalculated melt inclusion compositions are also more silica-undersaturated (*ne*-, *lc*- and *cs*-normative) than the host ankaramite rocks, which range from *ne*- to *hy*-normative.

If the melt inclusions are aliquots of the parent melts, these results suggest that the ankaramite magma formed by the aggregation of strongly-silica-undersaturated primitive ankaramite melts with high CaO/Al_2O_3 and high *di/ol* values. A link may therefore exist between these trapped melts, the hypothetical primary melts and the formation of ankaramitic magmas. This link is explored experimentally at high pressures, using the composition of a representative melt inclusion in Fo_{91} from the Lombok ankaramite suite as a starting mix composition. Liquidus and near-liquidus phase relations of this melt, under dry, hydrous, CO_2-H_2O- and CO_2-bearing conditions, and between 1 to 3 GPa pressures, lack orthopyroxene near the liquidus. Therefore a direct origin is excluded for this composition by partial melting of mantle peridotite (i.e. not a primary melt). Instead, the trapped melt inclusions may have been derived from even more mafic primary melts that were generated at higher temperatures and pressures than those prevailing when the ankaramitic magma aggregated. Two mechanisms are considered for the formation of these

primary melts that have high CaO/Al_2O_3 values (>1): (a) partial melting of lherzolite at high pressures (>5 GPa) and (b) partial melting of lherzolite at lower pressures (<5 GPa) in the presence of CO_2-rich mantle fluids.

The natural phenocryst assemblage and composition of the host ankaramite rock are only duplicated experimentally under hydrous conditions. With increasing CO_2 content in the fluid, the compositions of synthesized clinopyroxene crystals become less calcic and are unlike the natural phenocrysts. Thus the crystallization and aggregation of the ankaramite magma may have taken place under hydrous conditions at depths where olivine and clinopyroxene are co-crystallizing as phenocryst phases. In the case of the Lombok ankaramite suite, these conditions correspond to pressures equivalent to depths of around ~35 km below the base of the arc crust. The aggregated ankaramite magma may mix and continue to crystallize isobarically and in-situ, thus producing the wide compositional range observed in olivine ($\sim Fo_{75\text{-}91}$) and clinopyroxene ($\sim Wo_{45\text{-}47}En_{50\text{-}41}Fs_{5\text{-}12}$) phenocrysts, as well as the variable zoning and resorption textures. Reaction and re-equilibration of this aggregated magma with the sub-arc mantle before eruption, may cause the silica-enrichment that distinguishes the wholerock ankaramite compositions from the melt inclusions in their olivine phenocrysts.

Tiny pleonastic daughter spinel crystals with up to 65 wt% Al_2O_3 and virtually no chromium, occur within melt inclusions in olivine phenocrysts. These aluminous spinels could form in melt inclusions provided the trapped melt becomes sufficiently Al-enriched and Cr-depleted, following the fractional crystallization of olivine on the walls. Daughter aluminous spinels were found in the melt inclusions of olivine phenocrysts from all four ankaramite suites studied and may therefore, also occur in melt inclusions of other basaltic rocks. The occurrence of aluminous spinels in melt inclusions is therefore not evidence for the trapping of contaminant aluminous melts.

This thesis attempts to 1) demonstrate that ankaramitic melts with CaO/Al_2O_3 values (>1) and normative *di/ol* values >0.7 exist and can be parental to ankaramite rocks; 2) describe the Fe-Mg re-equilibration ("Fe-loss") process that affects melt inclusions in olivine phenocrysts before magma eruption; and 3) re-interpret the formation of aluminous spinel crystals in melt inclusions that have previously been interpreted as evidence for contaminant aluminous melts in basaltic magma chambers.

Chapter 1: Characteristics of ankaramite rocks

1.1 Introduction

For decades an ankaramite rock was distinguished from a picrite by its abundance in clinopyroxene crystals irrespective of composition, chemical affinity or tectonic setting. The term ankaramite was originally introduced to classify a suite of basaltic rocks from Ankaramy, Madagascar, that had an unusually clinopyroxene-rich assemblage with minor olivine and rare plagioclase phenocrysts (Lacroix 1916). For example Nicholls (1955) wrote that: "*...large phenocrysts of green pyroxene and yellow olivine in a grey aphanitic groundmass characterize the ankaramites. Plagioclase is sparse and only very rarely forms phenocrysts. Thus these rocks conform to the original definition of ankaramite (Lacroix, 1916, p. 182)...*". Similar comparisons by other petrologists recognized the Madagascar suite as a "type locality" for the classification of ankaramite rocks (e.g., Tomkeieff 1983, LeMaitre 1989, Mitchell 1985). The term ankaramite has been used in this textural sense until recently[1] and consequently, it includes a diverse range of rock compositions (Table 1.1).

The absence of a strict definition for ankaramite rocks means that petrographically, ankaramite and picrite grade into one another. Ankaramite and picrite rocks may share similar "primitive" characteristics. These include magnesian olivines (>Fo_{90}) with chromian spinel inclusions ($Cr^{\#}$[2]>75) and magnesian diopsidic clinopyroxenes. Ankaramites are also rich in MgO (>13 wt%) with high $Mg^{\#}$ values (>70) and in many cases have Cr and Ni contents as high as those of picrites. An ankaramite rock therefore may appear picritic, when compared with a different suite of ankaramite rocks that are richer in clinopyroxene. Thus, the distinction between ankaramite and picrite rock suites has become vague.

This thesis aims to characterize the formation of ankaramite rocks through the recognition of distinctive chemical characteristics, as well as mineralogical and textural attributes, which typify ankaramite, and thus construct a model for their petrogenesis. It has been long recognized that the unique chemical composition of ankaramite rocks strongly reflect the high content of clinopyroxene crystals (Section 1.2 to 1.4). There has been also a popular view that ankaramites simply represent picritic basalts that are enriched in clinopyroxene (Section 1.4). However, some studies conclude that the distinct chemical composition of ankaramite rocks may reflect chemical characteristics of the melt from which they crystallize (Section 1.5). This has significant ramifications as it implies the existence of primitive ankaramitic melts which, are unlike picrite.

---

[1] Barsdell & Berry (1990), Sheraton *et al.* (1990), Frey *et al.* (1991), Harangi (1994), Govorov *et al.* (1994), Nono *et al.* (1994).

[2] $Cr^{\#}$=100Cr/(Cr+Al), also $Mg^{\#}$=100Mg/(Mg+Fe*) and $mg^{\#}$=100Mg/(Mg+Fe^{2+}).

TABLE 1.1

no.	Rock type	Mineral assemblage	Locality	Setting	Mg#	Comments and source reference
1	Basalt	cpx+ol	Madagascar	IP	79	(3) Lacroix (1916), in: Dawson *et al.* (1970)
2	Trachybasalt	cpx(30)+ol(7)	North Johore	IP	64	Grubb (1965)
3	Basalt	cpx(32)+ol(7)	Jan Mayen	IP	73	Maaløe *et al.* (1986)
4	Basalt	cpx(14)+ol(13)	Hawaii	IP	63	(1) Frey *et al.* (1991)
5	Basanite	cpx+ol	Hawaii	IP	61	Macdonald & Powers (1968)
6	Basalt	cpx+ol±(bi,phl,amph,plg)	East Antartica	IP	71	(1) Sheraton *et al.* (1990)
7	Basalt	cpx(30)+ol(14)+plg(8)	Comores archipelago	IP	64	(1) Thompson & Flower (1971b)
8	Basalt	cpx+ol	Crozet archipelago	IP	68	(1) Gunn *et al.* (1970)
9	Basalt	cpx+ol±bi	Marcus-Wake Rise	IP	72	(1) Govorov *et al.* (1994)
10	Picrobasalt	cpx+ol	Cook Is.	IP	70	Wood (1978)
11	Basalt	cpx+ol	Cook Is.	IP	n/a	Nakamura & Tatsumoto (1988)
12	Basalt	cpx+ol+plg	Jan Mayen	IP	n/a	Nicholls (1955)
13	Basaltic Andesite	cpx+ol+plg	Eastern Australia	IA	67	Sivell & Waterhouse (1988)
14	Basalt	cpx(3)+ol(12)	Gaua, Vanuatu	IA	67	(1) Mallick & Ash (1975, Table 3)
15	Basalt	cpx(36)+ol(8)	Merelava, Vanuatu	IA	75	(2) Barsdell (1988)
16	Basalt	cpx+ol (≈26:10)	Epi, Vanuatu	IA	73	(2) Barsdell & Berry (1990)
17	Basalt	cpx(20)+plg(15)+ol(5)+phl(2)	Lesser Antilles	IA	55	Arculus (1978)
18	Basalt	cpx+ol	Aoba, Vanuatu	IA	75	Warden (1970)
19	Basalt	cpx+ol+plg	New Zealand	IA	77	Sivell & Rankin (1983)
20	Trachybasalt	cpx(13)+ol(7)+(amph,phl)	Sangean Api, Indonesia	IA	62	Foden & Varne (1983)
21	Basalt	cpx(37)+ol(12)+pl(4)	Lombok, Indonesia	IA	73	(2) Foden (1979)
22	Basalt	cpx(38)+ol(14)	Bali, Indonesia	IA	75	(2) Wheller (1986)
23	Basalt	cpx+ol	South Hungary	R	63	Harangi (1994)
24	Basalt	cpx+ol	Tanzania	R	79	Dawson *et al.* (1970)
25	Basanite	cpx(24)+amph(33)+ol(2)	Cameroon	R	59	(1) Nono *et al.* (1994)
26	Basalt	cpx+ol	Ethiopia	R	67	De Fino *et al.* (1973)

Listing of some ankaramite rock occurrences. Rock types are as recommended by the IUGS Subcommission on the Systematics of Igneous Rocks (LeMaitre 1989). Mineral assemblages are listed in order of abundance. cpx=clinopyroxene, ol=olivine, plg=plagioclase, amph=amphibole, phl=phlogopite, bi=biotite, ne=nepheline. Numbers in brackets indicate modal abundances. Comments: (1) indicates localities where ankaramite occurs in association with picrite, (2) indicate ankaramite suites studied in this thesis, (3) indicates ankaramite type locality. IP= Intra Plate, IA= Island arc, R= Rift. Mg# calculated as 100Mg/(Mg+Fe*) unless analyses unavailable (n/a).

This controversy in the origin of ankaramite is the topic explored throughout this thesis.

It should be noted that the terms "melt" and "magma", as used in this thesis, are not synonyms and have different connotations. "Melt" is strictly used in reference to the liquid whereas "magma" represents an aggregate of melt plus crystals. The ankaramitic chemical affinities of a primitive clinopyroxene rich magma (i.e., melt+crystals) may be the result of clinopyroxene accumulation. The ankaramitic affinities of a melt however, cannot be produced by clinopyroxene accumulation and are therefore likely to be primary. This thesis therefore focuses on the origin of ankaramite rocks by studying the composition of primary melt inclusions trapped in magnesian olivine phenocrysts of primitive ankaramite rocks.

1.2 The composition of ankaramite

Geochemically, the high clinopyroxene content of ankaramite rocks is associated with high CaO/Al_2O_3, Sc/Ni, Cr/Ni and normative diopside/olivine (*di/ol*) values (Dawson *et al.* 1970, Thompson & Flower 1971, Arculus 1976, Foden & Varne 1983, Thirwall & Graham 1984, Barsdell 1988, Barsdell & Berry 1990, Frey *et al.* 1991 and Govorov *et al.* 1994).

Wholerock analyses of eight separate ankaramite-picrite pairs are listed in Table 1.2, where ankaramite is distinguished from picrite by various authors using the relative abundance of clinopyroxene crystals. For each pair, CaO/Al_2O_3 and normative *di/ol* values are plotted in Figure 1.1a-b and demonstrate that these ratios are typically higher in ankaramite compared to associated picrite rocks. However, there are inconsistencies between these pairs due to the ambiguities in the definition of ankaramite. Figures 1.1c-b incorporate analyses from a larger data compilation of ankaramite and picrite rock occurrences listed in Appendix 1.1. Figure 1.1c-d indicates that primitive ankaramite ($Mg^{\#}$>~65) is characterized by CaO/Al_2O_3 values typically >1.0 (Figure 1.1c) and by *di/ol* values typically >0.7 (Figure 1.1d). These values are adopted in this study to indicate primitive ($Mg^{\#}$>65) ankaramitic affinities and to quantitatively distinguish ankaramite from picrite. The classification of ankaramite rocks used in this thesis is summarized in Table 1.3.

TABLE 1.3

	Picrite	Ankaramite
a) cpx/ol[1]	<1	>1
b) CaO/Al_2O_3[2]	<1	>1
c) *di/ol*[3]	<0.7	>0.7

[1]Modal proportions of clinopyroxene and olivine phenocrysts. [2]Wholerock (wt%) value. [3]Molecular CIPW normative diopside and olivine components.

1.3 Diversity of ankaramite petrogenetic models: why?

Because many clinopyroxene-rich basaltic rocks have been classified as ankaramite irrespective of their chemical composition, the ankaramite term now includes rocks with a vast range of compositions. Thus evaluation of the mechanisms for the generation of ankaramitic rocks has been confused throughout the years by the reported diversity in composition. Petrogenetic models

TABLE 1.2

	A	P	A	P	A	P	A	P	A	P	A	P	A	P	A	P
Analysis	1	2	3	4	5	6	7	8	9	10	11	12	13	14	15	16
Major elements (wt%)																
SiO_2	**47.55**	48.65	**45.40**	45.92	**47.40**	44.30	**47.22**	47.12	**46.77**	44.98	**45.45**	45.13	**44.52**	46.37	**43.69**	40.69
TiO_2	**2.27**	1.78	**2.59**	1.88	**2.41**	1.50	**0.75**	0.75	**1.48**	1.57	**1.88**	2.54	**2.19**	2.30	**3.37**	3.81
Al_2O_3	**10.57**	11.65	**11.26**	8.98	**7.51**	7.23	**11.25**	11.51	**7.70**	7.73	**7.59**	9.31	**9.19**	12.16	**12.00**	13.78
FeO*	**11.90**	11.82	**11.50**	10.75	**9.91**	11.55	**11.37**	10.59	**11.21**	12.13	**12.52**	12.81	**12.89**	11.25	**12.23**	14.16
MgO	**12.03**	12.09	**13.51**	18.94	**14.26**	23.12	**13.08**	15.01	**20.55**	24.57	**17.16**	16.51	**16.77**	13.63	**12.04**	9.82
CaO	**12.36**	10.65	**12.04**	10.75	**16.50**	9.66	**13.66**	11.94	**10.79**	7.48	**12.91**	9.30	**11.36**	10.49	**12.85**	12.04
MnO	**0.18**	0.17	**0.16**	0.16	**0.17**	0.21	**0.19**	0.26	**0.16**	0.19	**0.19**	0.19	**0.19**	0.20	**0.21**	0.21
Na_2O	**2.00**	2.25	**2.22**	1.66	**0.91**	1.51	**1.65**	2.07	**0.96**	1.09	**1.55**	2.21	**2.20**	2.50	**2.42**	3.44
K_2O	**0.75**	0.59	**0.95**	0.70	**0.36**	0.50	**0.61**	0.61	**0.23**	0.08	**0.57**	1.56	**0.53**	0.93	**0.54**	1.17
P_2O_5	**0.39**	0.34	**0.37**	0.26	**0.56**	0.41	**0.22**	0.15	**0.15**	0.16	**0.19**	0.43	**0.15**	0.17	**0.65**	0.89
TOTAL	**100**	100	**100**	100	**100**	100	**100**	100	**100**	100	**100**	100	**100**	100	**100**	100
Mg#	**64.3**	64.6	**67.7**	75.9	**72.0**	78.1	**67.3**	71.7	**76.6**	78.3	**71.0**	69.7	**69.9**	68.4	**63.7**	55.3
CaO/Al_2O_3	**1.17**	0.91	**1.07**	1.20	**2.20**	1.34	**1.21**	1.04	**1.40**	0.97	**1.70**	1.00	**1.24**	0.86	**1.07**	0.87
CIPW norm (molecular proportions)																
Or	**3.43**	2.61	**4.10**	2.91	**1.64**	1.98	**2.73**	2.65	**0.92**	0.30	**2.37**	6.42	**2.17**	4.01	**2.34**	
Ab	**11.92**	15.11	**5.02**	6.02	**5.87**	3.02	**6.33**	7.30	**5.78**	6.25	**1.96**	4.65	**2.67**	9.02	**4.27**	
An	**13.57**	14.89	**13.08**	10.50	**11.73**	7.62	**16.37**	14.98	**10.71**	10.14	**8.48**	7.58	**9.45**	14.06	**14.76**	12.53
Ne	**1.89**		**9.47**	4.46	**0.38**	5.99	**4.92**	6.37			**7.85**	9.21	**10.97**	7.46	**11.58**	20.69
Lc																4.62
Di	**31.63**	22.95	**28.62**	25.72	**48.09**	22.42	**34.08**	27.91	**24.44**	12.78	**35.73**	22.63	**28.83**	23.23	**28.63**	17.86
Hy		9.47							**12.61**	11.93						
Ol	**31.09**	30.00	**32.80**	45.53	**25.31**	55.16	**33.36**	38.72	**41.97**	54.99	**38.82**	42.93	**40.51**	36.18	**29.24**	27.98
Cs																6.65
Ilm	**6.08**	4.64	**6.56**	4.61	**6.42**	3.47	**1.98**	1.92	**3.44**	3.48	**4.62**	6.18	**5.26**	5.87	**8.56**	8.88
Hap	**0.39**	0.33	**0.35**	0.24	**0.56**	0.36	**0.22**	0.15	**0.13**	0.13	**0.17**	0.40	**0.14**	0.17	**0.62**	0.78
TOTAL	**100**	100	**100**	100	**100**	100	**100**	100	**100**	100	**100**	100	**100**	100	**100**	100
Di/Ol	**1.02**	0.76	**0.87**	0.56	**1.90**	0.41	**1.02**	0.72	**0.58**	0.23	**0.92**	0.53	**0.71**	0.64	**0.98**	0.64

Wholerock analyses of some ankaramite (A, bold) and picrite (P) pairs. Analyses are recalculated to 100% after omission of volatiles and recalculation of all iron as FeO. Sample numbers and column heading as follows.

1-2: samples AJ35 and AJ32, Anjouan Is., Comores archipelago, Western Indian Ocean (Thompson & Flower 1971);
3-4: samples CE0021 and CE0411, East Island, Crozet archipelago, Western Indian Ocean (Gunn *et al.* 1970);
5-6: samples D209d and D51/5, Marcus-Wake Rise, Central Pacific Ocean (Govorov *et al.* 1994);
7-8: samples GM17 and G20, Gaua Is, Vanuatu island arc (Mallick & Ash 1975, and Barsdell 1980, respectively);
9-10: samples 11 and 3, Manua Kea volcano, Hawaii (Frey *et al.* 1991, Table 2c);
11-12: samples 5823 and 5954, Bunger Hill, East Antarctica (Sheraton *et al.* 1990);
13-14: samples 6 and 2, Cook Is. (Wood 1978);
15-16: samples 220 and 129W, Tchabal-Nganha volcano, Cameroon (Nono *et al.* 1994).

indicates total iron as FeO. Mg#=100Mg/(Mg+Fe)

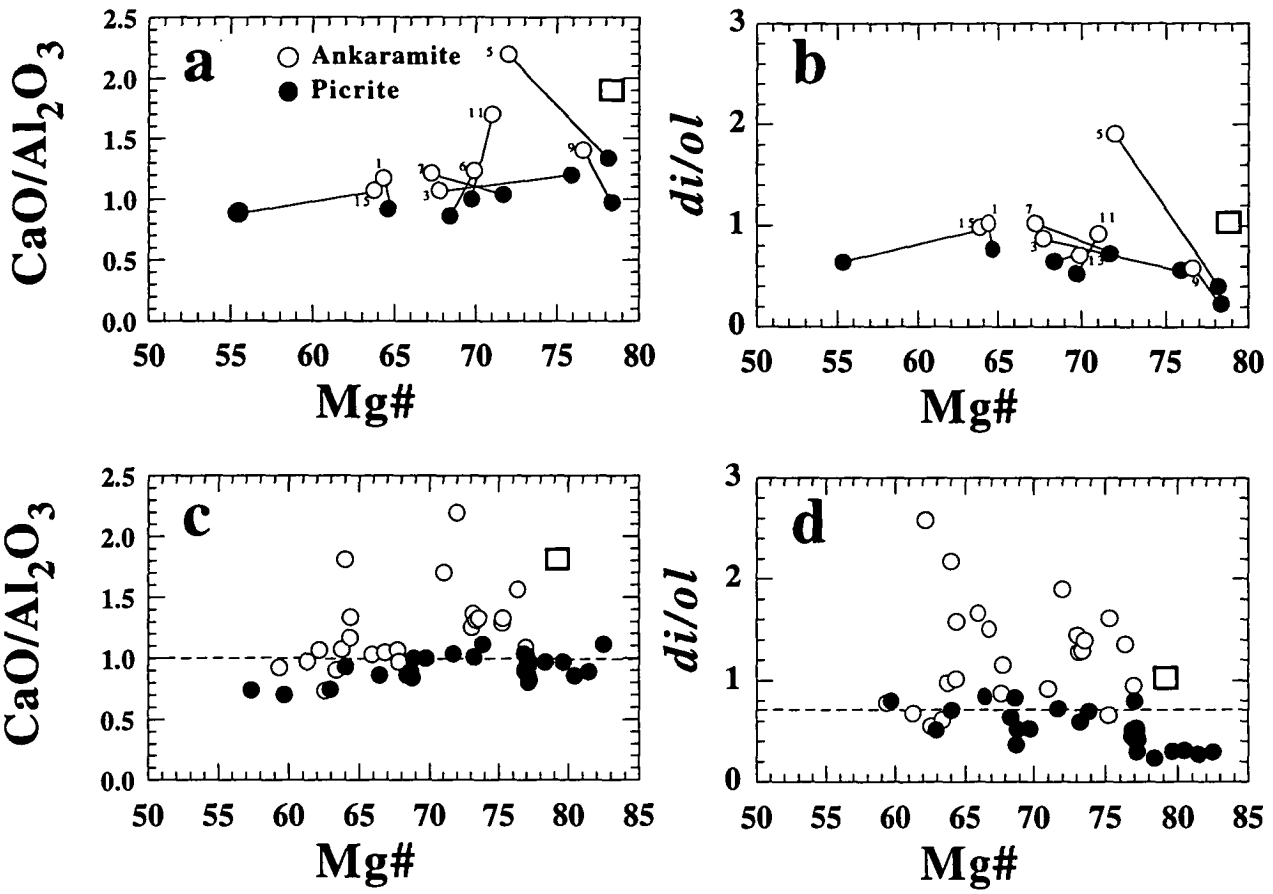

Figure 1.1 CaO/Al_2O_3 and *di/ol* values of ankaramite (open circles) and picrites (filled circles) *versus* Mg# =100Mg/(Mg+Fe*) of wholerock analyses. (a) and (b) are ankaramite-picrite pairs from Table 1.2. Numbers next to symbols refer to analysis numbers listed in Table 1.2. Tie-lines connect the composition of coexisting ankaramite and picrites from different localities. Plotted in (c) and (d) are the wholerock analyses of ankaramite and picrite rockss compiled in Appendix 1.1. Square symbol indicates the composition of ankaramite type specimen from Ankaramy, Madagascar (Lacroix 1916).

dealing with the generation of ankaramitic melts must explain the origin of ankaramitic chemical characteristics listed in Table 1.3 (b and c). Petrogenetic models dealing with the origin of supposedly ankaramite rocks, which lack the ankaramitic affinities outlined in Table 1.3, are not sufficiently constrained and therefore do not directly address the problem of ankaramite petrogenesis directly. Thus the various developments of the petrogenetic models for ankaramite rocks may reflect their diversity in chemical composition.

1.4 Aims of this thesis

Arguments that primary ankaramitic parent melts may exist are based on wholerock geochemistry and often compromised by the presence of abundant clinopyroxene crystals in the rock. This thesis investigates the composition of parent melts to ankaramite directly by studying the composition of primary melt inclusions trapped in primitive olivine phenocrysts of ankaramite. If ankaramite are the result of clinopyroxene accumulation then the CaO/Al_2O_3 values of its melt inclusions will not exceed 1. Alternatively, if ankaramites are derived from ankaramitic parent melts, then the CaO/Al_2O_3 values of their melt inclusions will be >1 and comparable to wholerock values. This concept is applied here to assess the case for clinopyroxene accumulation in producing the characteristic wholerock compositions of four well-studied primitive arc-ankaramite suites. In general, the results from this study are also applicable to other suites, but are particularly important for arc-suites because primitive arc magmas are rare and many, have ankaramitic affinities.

In summary, the compositions of primary melt inclusions in ankaramite are compared to that of its host ankaramite rock to establish if parent ankaramitic melts exist.

1.5 Thesis outline

Each chapter deals with different aspects of the research topic of this thesis.

• The reminder of chapter 1 discusses the petrogenetic significance of CaO/Al_2O_3 and *di/ol* values and presents a summary for the evidence for ankaramitic melts.

• Chapter 2 summarizes the geochemistry of four well-studied arc-ankaramite suites and describes the mineralogy of particularly Mg-rich, rocks including their primary melt and fluid inclusions. These suites were selected for this study because they have typical ankaramitic affinities (Table 1.3).

• Chapter 3 is the heart of this thesis. It includes the results of melt inclusion homogenization experiments on melt inclusions in primitive olivine (Fo>88) phenocrysts of the four ankaramite suites described in Chapter 2. A possible petrogenetic model for the formation of ankaramite rocks, constrained by the melt inclusion data, is presented.

• Chapter 4 deals with the phenomenon of "Fe-loss" in melt inclusions hosted in olivine phenocrysts. An attempt is made to explain the variation in FeO* content observed in most of the homogenized melt inclusions (Chapter 3) by Fe-Mg re-equilibration between the host olivine and the trapped melt before eruption.

• Chapter 5 presents the results of a high-pressure liquidus study aimed to test if the composition of a representative melt inclusion (ANK2376) can be the product of lherzolite partial melting at high pressures in the presence of CO_2-rich fluids.

• Chapter 6 discusses the origin of rare aluminous spinel crystals in primary melt inclusions. Such spinels have been considered as evidence for contaminant aluminous melts in basaltic magma chambers. It is argued in this thesis that the aluminous spinels form as a result of fractional crystallization within the inclusion.

• Chapter 7 summarizes the main conclusion presented in each of the previous chapters.

Some of the work from chapters 3 and 6 of this thesis has already been published in Della-Pasqua *et al.* (1995) and in Della-Pasqua and Varne (1997).

1.6 Comparison of ankaramite compositions with experimental partial melts

The petrogenetic significance of CaO/Al_2O_3 values has been emphasized by Frey *et al.* 1978, Herzberg & Ohtani 1988 and Frey *et al.* 1991. In a partial melting event, the CaO/Al_2O_3 values of primary melts are inherited from the source (mantle) and controlled by the composition of the major phases in the residue. If the residue consists predominantly of olivine and orthopyroxene (harzburgite), then after partial melting the CaO/Al_2O_3 values of the primary melt will be similar to the original bulk CaO/Al_2O_3 value of the source. Current estimates of bulk CaO/Al_2O_3 values of the mantle differ, but mostly fall within the range 0.8 to 0.9 (Frey *et al.* 1991, Herzberg *et al.* 1990 and Allègre *et al.* 1995), and therefore primary melts in equilibrium with a harzburgite residue should inherit this value.

If the residue retains clinopyroxene in addition to orthopyroxene and olivine (lherzolite source), then after partial melting the primary melts will inherit CaO/Al_2O_3 values that are lower. Even so, the CaO/Al_2O_3 value of the primary melt should be no higher than the mantle source. The observed CaO/Al_2O_3 values of picrite (<1, Figure 1.1c) which are likely to represent mantle-derived magmas, support this argument.

Experimental studies of the melting behaviour of lherzolite provide a guide to the likely compositions of primary mantle-derived magmas. Primary melts produced in partial melting experiments of mantle peridotite to ~3 GPa, have a range in CaO/Al_2O_3 values that are similar to those of picrite (<1), but which are unlike those of ankaramite and are typically higher than one. Experiments to 3 GPa with fertile (cpx-rich) and depleted (cpx-poor) lherzolite bulk compositions indicate that changes in the source composition do not lead to changes in the partial melt composition toward an ankaramitic bulk composition (Green *et al.* 1987, Falloon *et al.* 1988, Hirose & Kushiro 1993, Baker & Stolper 1994). The compositional range of these partial melts in equilibrium with mantle lherzolite is displayed in Figure 1.2b and d, projected from the Ol (olivine) and Jd+CaTs (Jadeite+Cacium Tschermak's molecule) apexes in the basalt tetrahedron Ol-Jd+CaTs-Di(diopside)-Qtz(quartz) (Falloon *et al.* 1988). Also plotted in this figure are the compositional fields of ankaramite and picrite constructed from Figure 1.2a and c.

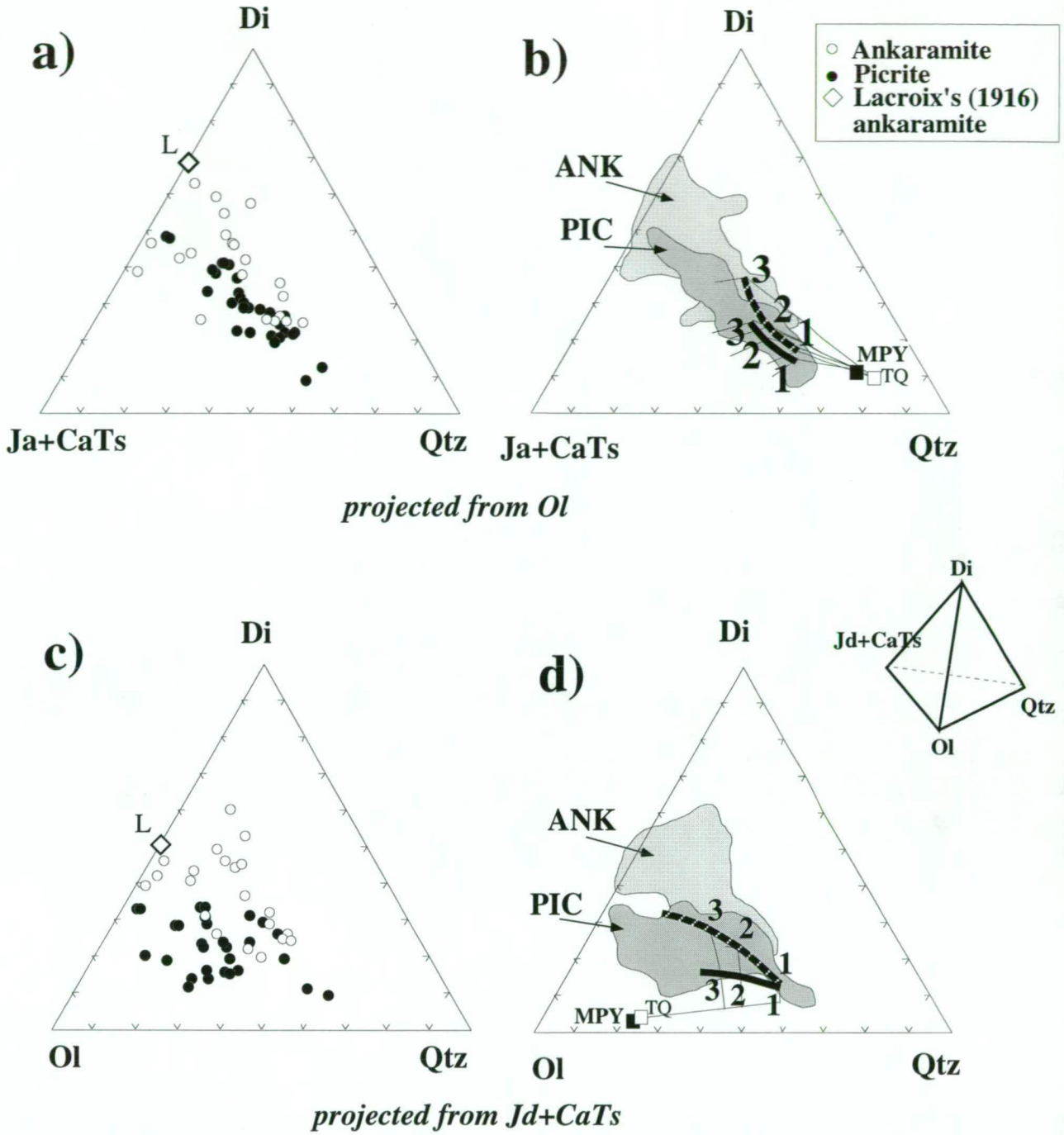

Figure 1.2 Wholerock analyses of ankaramite and picrite (Appendix 1.1) plotted in the CIPW molecular normative basalt tetrahedron Ol(olivine)-Qtz(quartz)-Jd+CaTs(Jadeite+Calcium Tschermak's molecule)-Di(diopside). Algorithm for the projections after Falloon & Green (1988).

a-b) projected from Ol onto the face Di=*di*, Jd+CaTs=*ab+an+ne*, Qtz=*ab+an+en+qtz-ne*,
c-d) projected from Jd+CaTs onto the face diopside Di=*di*, Ol=*ol+opx*, Qtz=*ab+an+opx+qtz-ne*.

b) and d) show fields of ankaramite and picrite from a) and c). Also shown in b) and d) are the compositions of primary liquids produced by partial melting of two sources at pressures up to 3 GPa: MORB Pyrolite (MPY filled square) and a more depleted Tenaquillo Lherzolite (TQ open square). Grid lines represent composition of primary liquids in equilibrium with ol+opx+cpx±grt±spl, ol+opx and ol, produced by increased partial melting. Thick full line and thick dashed line are locus of points where clinopyroxene is eliminated from the MPY and TQ residue respectively. Experimental results are from Jaques & Green (1980), Falloon & Green (1987, 1988) and Falloon *et al.* (1988).

These projections show that ankaramite are unlike picrite, as ankaramite are richer in clinopyroxene component than the experimental primary melts and therefore, unlikely to be derived by partial melting.

With increasing pressure in the range of 1 to 3 GPa, melts become increasingly nepheline(*ne*)-normative (poorer in Qtz component, Figure 1.2b) but do not attain the high normative *di* content of ankaramite (Figure 1.2b-d). These partial melts are still picritic rather than ankaramitic, and although CaO/Al_2O_3 values increase with the degree of melting until clinopyroxene is exhausted (Kinzler & Grove 1992b), these will not exceed the wholerock value of the source and are unlikely to reach ~1. With a greater extent of melting, melts become relatively poorer in clinopyroxene component, and eventually become picritic. Thus, as indicated by Barsdell (1988) "....high pressure (0.8-2 GPa) experiments do not provide an explanation for the high normative diopside component in these parent melts....".

Experimental results from melting experiments at even higher pressures (>4 GPa) by Herzberg & Ohtani (1988), Herzberg *et al.* (1990) and Herzberg (1992), indicate that garnet remains a residue phase during partial melting. The presence of garnet as a residual phase during melting would be expected to impart high CaO/Al_2O_3 values to the primary melts, as was demonstrated by Herzberg's experiments in which CaO/Al_2O_3 values of primary melts become greater than 1 above ~5 GPa. These results have successfully accounted for the high CaO/Al_2O_3 values (>1.7) of some low-alumina komatiite rocks (Herzberg 1992). The possible implications from Herzberg's work for the formation of ankaramitic rocks will be considered in Chapter 3.

1.7 Ankaramite as a product of "clinopyroxene addition"?

A porphyritic rock may not necessarily represent the melt composition from which it crystallized, as there are many magmatic processes capable of modifying the modal proportion of phenocrysts phases in the magma. A commonly-cited process is "crystal accumulation" in which the accumulated phenocrysts mix with relatively evolved melts to cause a change in bulk magma composition (Frey *et al.* 1991). "Compensated crystal settling" instead is a process in which crystals lost downwards by gravity settling are balanced by the addition of crystals settling from above (Krishnamurthy & Cox 1977). Thus, this process enables the magma to achieve high degrees of crystallization and fractionation. If crystals are not separated from the crystallizing magma, crystal fractionation does not occur and place "in-situ crystallization" occurs (Langmuir 1989). "In-situ crystallization" within a replenishing magma chamber could therefore significantly modify the bulk magma composition. Alternatively, crystal fractionation may be "delayed" if it occurs after some degree of crystallization (Maaløe *et al.* 1988). Both "in-situ crystallization" and "delayed fractionation" cause the main body of magma to evolve along a chemical path that differs from that produced by fractional crystallization. Bulk magma compositions may also be strongly affected after eruption by "phenocryst re-distribution" due to gravity settling, flotation and dynamic sorting (Staudigel & Bryan 1981).

All these processes could lead to significant phenocryst enrichment in the magma and the reported widespread occurrence of such processes in volcanic rocks, led to the consideration of

clinopyroxene "addition" as a process for the formation of ankaramitic magmas[3]. Examples in which addition of a clinopyroxene component has occurred are ankaramite rocks with abundant clinopyroxene xenocrysts (Foden & Varne 1983) and ankaramite rocks where clinopyroxene has been strongly resorbed (Trønnes 1990, Hasteen 1991). These examples are clear evidence that the magma has been modified by the assimilation of a "clinopyroxene component".

An alternative mechanism of generating magmas with abundant clinopyroxene crystals (i.e., ankaramitic) involves the addition of disrupted of cumulate pyroxenite material from the lower crust, during tectonic movements (Foden & Varne 1983). This mechanism was linked to tectonic extension by Ballard (1987) and the relationship between ankaramite occurrences and extension was later demonstrated by the presence of ankaramite in extension zones such as Jan Mayen Island, characterized by fissure activity adjacent to a transform fault (Maaløe *et al.* 1986; in Eastern Australia, during the opening of the Tasman sea (Sivell & Waterhouse 1988); in Central Europe during the extension in the Cretaceous (Harangi 1994) and in the Cameroon Line of Central West Africa (Nono *et al.* 1994). A similar association is also inferred for ankaramite rocks at the Wake-Rise, West Pacific, and thought to be derived from deep magma chambers generated during "tectonomagmatic activity" (Govorov *et al.* 1994).

In summary clinopyroxene addition models view the formation of ankaramite rocks from olivine basalts or picritic rocks that have undergone the addition of a clinopyroxene component by the process of crystal accumulation. These schemes can explain the origin of most ankaramite rocks yet some are unsuccessful and suggest that ankaramite rocks may be derived from ankaramitic melts. The chemical characteristics of ankaramite rocks (Table 1.3) are therefore not solely explained by clinopyroxene accumulation.

1.8 Evidence for primitive ankaramitic melts

Clinopyroxene-addition models (Section 1.7) do not convincingly explain all occurrences of ankaramite rocks. The possibility that ankaramite rocks may be derived from more primitive ankaramitic melts has been considered by Thompson & Flower (1971), Maaløe *et al.* (1986), Barsdell (1988) and Barsdell & Berry (1990). However, models proposed by these authors have conflicting arguments for ankaramite formation (see for example: Thompson & Flower 1971 and Frey *et al.* 1991), as they invoke more than one process of producing primitive melts with ankaramitic affinities rather than picritic. Evidence to support the occurrence of ankaramitic melts is outlined below.

1) CaO/Al_2O_3 values >1 do not only occur in basaltic rocks that are clinopyroxene-rich, but also occur in primitive basaltic rocks that are either clinopyroxene-poor or have no clinopyroxene phenocrysts at all (Table 1.4). The high CaO/Al_2O_3 values of these rocks are unusual because they are unlikely to be caused by clinopyroxene addition and may represent primary characteristics inherited from the parent melt. An important example is the olivine-phyric komatiite rocks that attain CaO/Al_2O_3 values of ~2 (Table 1.3, analysis 8). Also notable is the silica-undersaturated nature of these rocks which, with the exception of analyses 8 in Table 1.3, are all *ne*-normative.

---

[3] MacDonald & Powers (1968), Gunn *et al.* (1970), Warden (1970), Mallick & Ash (1975), Hughes (1982), Sivell & Rankin (1983), Nakamura & Tatsumoto (1988), Sivell & Waterhouse (1988) and Frey *et al.* (1991).

Table 1.5 lists analysis of mantle-derived rocks with high CaO/Al_2O_3 values (>1) whose compositions are interpreted to represent those of primary magmas. Most of these rocks are silica-undersaturated, as are those listed in Table 1.4. A negative correlation between CaO/Al_2O_3 values and SiO_2 content has been previously noted (Dawson *et al.* 1970, Bultitude & Green 1971, Adam 1988), which contrasts with the silica-enrichment trend that would be associated with clinopyroxene addition. The association between high CaO/Al_2O_3 values and silica-undersaturation is significant and discussed in the results of melt inclusion studies in Chapter 3.

2) Mass balance calculations indicate that up to ~30 to 40 vol% of clinopyroxene is required to "convert" a picritic composition with CaO/Al_2O_3 values ~0.8 and *di/ol* ~0.5, to an ankaramitic composition with CaO/Al_2O_3 values ~1.8 and *di/ol* ~2.2 (Figure 1.3). If the accumulated material contains olivine as well as clinopyroxene, then even larger amounts are required to attain ankaramitic affinities. Therefore, the "clinopyroxene addition" model may become unrealistic and is not supported by the petrographic and geochemical evidence of some ankaramite rocks (Barsdell & Berry 1990).

3) Statistical correlation of compatible trace elements (e.g., Cr/Ni) and phenocryst proportions with wholerock $Mg^{\#}$ values of ankaramite are unlikely to reflect random crystal accumulation. Random crystal accumulation would tend to produce random variation diagrams unless the accumulated (or fractionated) crystals maintained fairly fixed crystallizing proportions (Thompson & Flower 1971, Barsdell & Berry 1990).

4) The co-crystallisation of clinopyroxene ($Mg^{\#}94$) with olivine (Fo_{90-92}), as defined by olivine-clinopyroxene inclusion pairs, suggests that ankaramite fractionated from liquids that were saturated early in both these phases (Barsdell 1988, Barsdell & Berry 1990). Support is also drawn from liquidus studies on natural ankaramite compositions (Dawson *et al.* 1970, Thompson & Flower 1971, Arculus 1975, Arculus 1978, Graham 1981). Further evidence in favour of primary ankaramitic melts comes from the demonstrated co-existence of such ankaramitic melts with spinel-lherzolite mineralogy at 2 GPa (Maaløe *et al.* 1986). These experiments indicate that ankaramitic liquids can be generated directly by partial melting of peridotite. The generation of melts with chemical compositions similar to ankaramite by the partial melting program SILMIN (Ghiorso & Carmichael 1985) also supports the possibility that ankaramitic melts may exist (Barsdell & Berry 1990).

In summary available evidence favours the possibility that high CaO/Al_2O_3 >1.0 and *di/ol* values >0.7 in ankaramite rocks may be inherited from a primitive ankaramitic melt.

1.9 Models for the generation of primary ankaramitic melts

Limited petrological and geochemical evidence from several independent studies suggest that ankaramite rocks may be derived from primary melts with ankaramitic characteristics as listed in Table 1.3 (Section 1.8). The particular mechanisms that lead to the generation of these ankaramitic melts are contentious (Section 1.3)

TABLE 1.4

Analysis no.	1	2	3	4	5	6	7	8	9	10
Major elements (wt%)										
SiO_2	39.88	41.98	37.50	39.71	36.56	43.97	39.44	45.30	37.63	36.40
TiO_2	3.42	3.29	3.21	3.10	2.65	2.01	2.37	0.22	3.36	2.72
Al_2O_3	9.60	10.25	9.12	9.57	10.00	8.40	5.84	2.30	8.06	7.1
FeO*	15.46	10.51	13.84	12.81	14.24	11.99	12.88	10.92	11.04	10.83
MgO	14.11	11.88	13.72	13.98	11.71	16.07	17.67	30.64	18.76	21.51
CaO	11.37	14.26	13.85	12.71	14.84	10.99	12.24	5.74	10.81	11.85
MnO	0.20	0.16	0.15	0.19	0.27	0.21	0.17	0.17	0.18	0.19
Na_2O	3.03	3.29	2.69	2.96	4.91	1.94	1.97	0.07	3.70	3.2
K_2O	1.55	2.62	0.63	1.06	1.72	0.54	0.99	0.01	2.54	2.15
P_2O_5	1.10	1.14	0.90	0.89	1.51	0.16	0.81	0.02	1.30	1.4
TOTAL	99.72	99.38	95.61	96.98	98.41	96.28	94.38	95.39	97.38	97.35
Mg#	62.0	66.9	63.9	66.1	59.5	70.5	71.0	83.4	75.2	78.0
CaO/Al_2O_3	1.2	1.4	1.5	1.3	1.5	1.3	2.1	2.5	1.3	1.7
CIPW norm molecular proportions										
or						2.34		0.03		
ab						5.31		0.35		
an	5.29	3.68	7.50	6.63	0.10	9.25	2.88	3.28		
ne	17.97	19.92	16.54	18.17	27.33	7.45	12.22		17.90	15.59
lc	6.05	10.44	2.55	4.28	6.30		4.04		9.29	7.60
ns									1.30	0.80
di	19.44	25.70	17.37	22.96	5.49	29.94	25.65	12.40	5.90	0.05
hy								39.11		
ol	38.54	24.87	38.49	35.02	36.87	40.42	43.90	44.39	46.32	54.35
cs	3.89	6.65	9.09	4.77	16.97		4.88		11.01	14.83
ilm	7.87	7.73	7.66	7.38	5.72	5.13	5.70	0.42	7.24	5.67
ap	0.95	1.00	0.81	0.79	1.22	0.15	0.73	0.01	1.05	1.10
Total	100.00	100.00	100.00	100.00	100.00	100.00	100.00	100.00	100.00	100.00
di/ol	0.50	1.03	0.45	0.66	0.15	0.74	0.58	0.28	0.13	<0.01

Wholerock analyses of aphyric or olivine-phyric rocks with high CaO/Al_2O_3 values (>1). Source of analysis as follows:

1: Olivine-phyric nephelinite (Frey *et al.* 1978, Table 2, analysis 11);
2: Microphyric melilitite (Hawkins & Natland 1975, Table 1, sample 6624);
3: Aphyric melilitite (Cross 1915, p17, analysis 43);
4: Olivine-phyric limburgite (Black & Brothers 1965, Table 1, analysis B);
5: Olivine-phyric (3%) olivine-melilitite (Adam 1990, Table 1, sample 496);
6: Olivine-phyric basanite (Wood 1978, Table 1, analysis 1);
7: Olivine-phyric ankaramite (Dawson *et al.* 1970, Table 1, sample DB780);
8: Olivine-phyric komatiite (Smith & Erlank 1982, Table 2.3a, sample HSS-8);
9: Aphanitic alnoite (Nixon *et al.* 1980, Table 1, sample 3544);
10: Olivine-phyric alnoite (Nixon et al. 1980, Table 1, sample 3565).

Total iron as FeO. Mg#=100Mg/(Mg+Fe*). CIPW norm calculated with analyses summed to 100%.

TABLE 1.5

Analysis	1	2	3	4	5
Major elements (wt%)					
SiO_2	36.73	37.60	43.70	37.10	46.77
TiO_2	2.84	2.60	3.41	2.70	0.33
Al_2O_3	10.78	8.20	10.00	9.30	3.42
FeO*	13.77	13.18	10.60	12.78	11.07
MgO	12.74	18.60	11.20	15.90	31.51
CaO	13.70	15.50	13.80	12.80	5.67
MnO	0.12	0.20	0.21	0.20	
Na_2O	3.88	2.90	1.89	3.70	0.12
K_2O	0.91	1.50	2.90	1.40	0.08
P_2O_5	1.10	0.90	0.52	1.30	0.03
TOTAL	96.57	101.18	98.23	97.18	99.00
Mg#	62.29	71.59	65.36	68.96	83.56
CaO/Al_2O_3	1.27	1.89	1.38	1.38	1.66
CIPW normative molecular proportions					
or					0.25
ab					0.58
an	6.10	2.92	7.42	2.94	4.58
ne	22.84	15.43	12.30	21.06	
lc	3.53	5.25	12.42	5.24	
di	9.32	1.11	35.93	7.77	10.38
hy					38.69
ol	38.57	50.18	20.93	43.86	44.88
cs	12.22	19.04	1.91	12.08	
ilm	6.48	5.37	8.61	5.96	0.62
ap	0.94	0.70	0.49	1.08	0.02
Total	100.00	100.00	100.00	100.00	100.00
di/ol	0.24	0.02	1.72	0.18	0.23

Wholerock analyses of mantle derived rocks with CaO/Al_2O_3 values >1 interpreted to be representative of primary magma compositions. Source of analyses as follows:
1: Melilite-nephelinite (Kushiro & Kuno 1963, Table 2, analysis 8a);
2: Olivine-melilitite (Bultitude & Green 1971, Table 1, analysis 12);
3: Leucitite (Fergurson & Cundary 1975, Table 2, analysis 7);
4: Olivine-melilitite (Brey & Green 1975, Table 1, analysis 1;
5: Aphyric komatiite (Smith & Erlank 1982, Table 2.2, sample HSS-15).
Mg#=100Mg/(Mg+Fe*). *Total iron as FeO*. CIPW norm calculated with analyses summed to 100%.

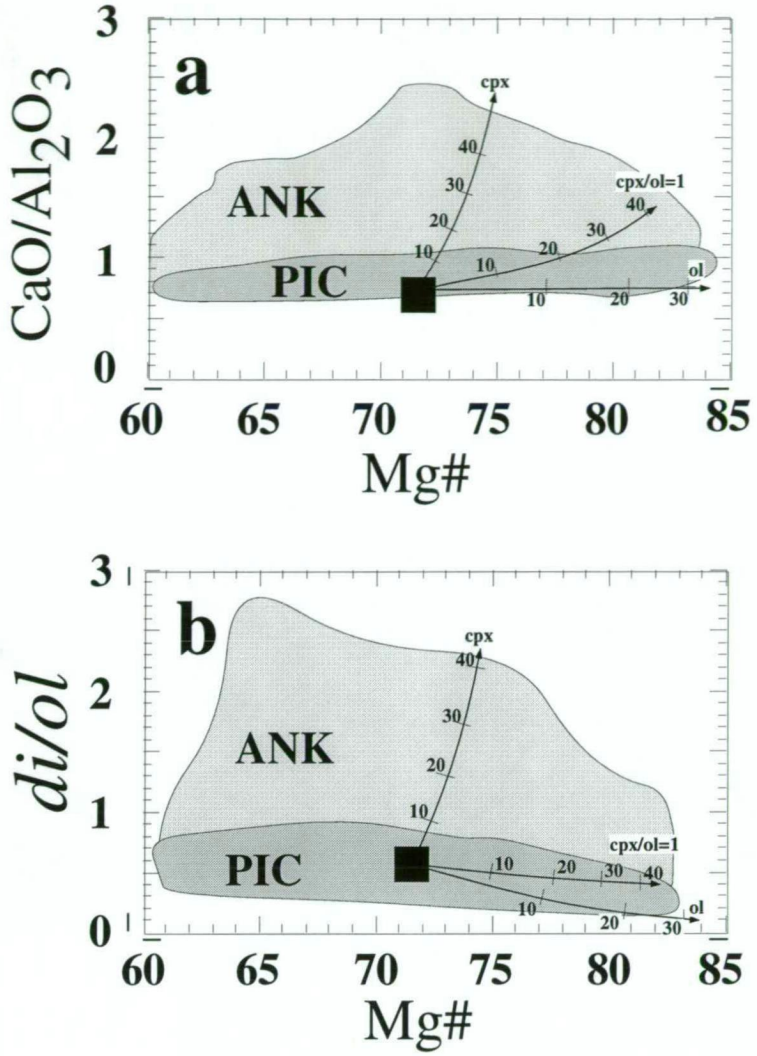

Figure 1.3 Possible shift in a) CaO/Al_2O_3 values and b) *di/ol* values of a hypothetical picritic rock (filled square) after the addition of up to 40 vol% clinopyroxene (cpx), olivine (ol) and equal proportions of clinopyroxene+olivine (cpx/ol=1). The starting picrite composition used here is from Manua Kea (average of samples MK1-3 and MK1-8, Frey *et al.* 1991, Table 1) which contain ~15% Ol and trace amounts of clinopyroxene phenocrysts. Numbers 10, 20, 30 and 40 indicate proportion (vol%) of phenocrysts added to picrite. Field of ankaramite (ANK) and picrite (PIC) are defined from Figure 1.1c and d. Addition of at least 30 to 40% is required to "convert" the composition of this picritic rock with CaO/Al_2O_3 values of ~0.8 and *di/ol* values of ~0.5 into a composition with values of ~2.2 and ~1.8, respectively, and thus to an ankaramitic composition.

Mechanisms ankaramite formation are exemplified by the models of Thompson & Flower (1971), Maaløe *et al.* (1986) and Barsdell & Berry (1990), and are summarized below.

Thompson & Flower (1971): On Anjouan Island in the Comores archipelago ankaramites form a *hy*-normative suite that is genetically associated with two other suites, one basanitic and the other alkalic. The most primitive ankaramite sample has affinities that are typical of ankaramite, with cpx>ol, $Mg^{\#}$=64, CaO/Al_2O_3=1.2 and *di/ol*=1 (sample AJ35, Table 1.2, analysis 1). The wholerock composition of this ankaramite, together with compositions of the most primitive samples from the two other suites, are considered to represent near-primary melts generated by high pressure melting of lherzolite. Differences in composition are attributed to different degrees of partial melting. These primary melts are considered to have crystallized at lower pressures in order to produce the observed low pressure fractionation series. Thompson & Flower (1971) conclude that the ankaramite textures are formed by "...prolonged in situ crystallization of an initially all-liquid magma...", instead of clinopyroxene accumulation, that has a composition similar to AJ35. The key ingredients in the model postulated by Thompson & Flower (1971) are high pressure melting and later crystallization at lower pressures, and are significant with respect to the model discussed in this thesis, in Chapters 3 and 5.

Maaløe et al. (1986): On Jan Mayen Island, Maaløe *et al.* (1986) differentiated between ankaramite with wholerock compositions representative of primary melts, from ankaramites whose wholerock composition had been affected by crystal accumulation. The inferred ankaramitic parental melt to this suite has $Mg^{\#}$=77.4, CaO/Al_2O_3=1.3, *di/ol*=1.3 and is *hy*-normative (Sample JM2, Appendix 1.1). Based on a liquidus study of this ankaramitic composition at high pressures, ankaramite can coexist with dry spinel lherzolite at around ~1400°C and ~2 GPa. Maaløe *et al.* (1986) used this result to support a primary origin by partial melting. However, orthopyroxene saturation at these conditions was not achieved (due to the reaction of opx with the melt) and the only phases that coexist in the ankaramitic melt at the liquidus are ol+cpx+spl . As for the Thompson & Flower model, these ankaramitic melts are considered to rise and crystallize at low pressures. Retention of phenocrysts phases (ol+cpx) as the magma crystallizes at low pressures lead to the highly porphyritic textures distinctive of the ankaramite and thus, is not the result of crystal accumulation.

Barsdell & Berry (1990): The authors conclude that the melt parental to the ankaramite suite of Epi Island in the Vanuatu arc has $Mg^{\#}$=73.0, CaO/Al_2O_3=1.34, *di/ol*=1.32 and is *hy*-normative (Sample UTas71046, Appendix 1.1). These ankaramitic attributes are successfully duplicated by the partial melting program SILMIN of Ghiorso & Carmichael (1985) at around 0.5-1 GPa and ~1450°C, under the assumption that orthopyroxene is not included in the source. Thus, the results of Barsdell & Berry (1990) differ from previous partial melting models as they exclude mantle lherzolite as a source for primary ankaramite melts. Instead, their model considers the partial melting of a "cumulate clinopyroxenite source" in the lower crust, where melting is triggered by ascending peridotite diapirs.

A number of authors have also inferred a mantle origin for the generation of ankaramite melts. For example Sheraton *et al.* (1990) conclude that isotopic and geochemical data from a suite of genetically related ankaramitic and picritic dykes of Bunger Hill of East Antarctica represent ankaramite formed from relatively larger and smaller degrees of partial melting. The most primitive

ankaramitic dike in this suite is *ne*-normative, and has Mg#=74, CaO/Al_2O_3=1.7, *di/ol*=1.5, with cpx>ol (Sample 5823, Table 1.2, analysis 11) and is a typical ankaramite (Table 1.3).

1.10 Conclusions

A compilation of primitive ankaramite and picrite wholerock analyses highlights ankaramite to be typically characterized by CaO/Al_2O_3 >1.0 and normative *di/ol* values >0.7 (Table 1.3). These characteristics have previously been attributed to the accumulation of clinopyroxene crystals, with some evidence to suggests the existence of parental ankaramitic melts. Interestingly, most (but not all) ankaramite rocks have *ne*-normative compositions (Table 1.2), as do olivine-phyric rocks with high CaO/Al_2O_3 values (Table 1.4). A negative correlation between CaO/Al_2O_3 values and silica content is previously noted, and will be referred to in Chapter 3, where the results from melt inclusions are used to constrain a model for the generation of ankaramitic melts. If the compositions of ankaramite rocks represent a melt, then the criteria in Table 1.3 should serve as useful constraints for any petrogenetic model dealing with the formation of ankaramitic melts. In addition, these criteria expand the original textural definition of ankaramite rocks, that clinopyroxene is more abundant than olivine.

Models dealing with the generation of primitive melts with ankaramitic affinities (Table 1.3) mainly involve partial melting mechanisms. Petrogenetic models that consider the formation of supposedly ankaramitic rocks, which do not satisfy the geochemical criteria of Table 1.3, have not surprisingly contributed to an increase in the diversity of models.

Chapter 2: Primitive arc-ankaramite samples from Indonesia and Vanuatu

2.1 Introduction

Primitive volcanic rocks may preserve some of the primary geochemical signature of the primary liquids from which they formed. These primitive rocks therefore provide an opportunity to study the generation of primitive magmas. In particular, primitive ankaramitic rocks have been investigated from many perspectives but conflicting interpretations persist concerning their origin (cf. Chapter 1). This chapter describes four primitive arc-ankaramite suites that were selected to compare wholerock and melt inclusion compositions. Two of the ankaramite suites are from Lombok and Bali islands in the Sunda arc of Indonesia, and the other two are from the islands of Merelava and Epi, in the Vanuatu arc (Figure 2.1). The petrology and geochemistry of these suites are well documented, with each suite having distinctive ankaramitic affinities (Section 2.2 below). Melt inclusion studies were carried out on olivine and some clinopyroxene phenocrysts of the most primitive samples in each suite. These primitive samples are described in this chapter together with the various types of melt and fluid inclusions found. Melt inclusion homogenization experiments are presented separately in Chapter 4.

2.2 Previous work and sample selection

The Sunda-Banda arc contains the widest compositional range in mafic magmatism of any active volcanic arc (Wheller *et al.* 1987). Although basalts are common, picrites are not known in this island arc and the most primitive rocks are ankaramites. These rocks occur in the Ulakan Formation of eastern Bali (Wheller 1986), and in the Rinjani volcano of Lombok Island (Foden & Varne 1981a,b) (Figure 2.1a). In addition, ankaramite lavas are also documented from Sangeang Api Island (Foden & Varne 1983) and in the Ringit-Besser volcano on Java (Figure 2.1a, R. Varne unpubl. data), but these are not be discussed here. Unlike the Sunda arc, the Vanuatu island arc is characterized by the widespread occurrence of picrite (Eggins 1989; Barsdell 1980, 1988; Barsdell & Berry 1990; Monzier *et al.* 1993). Primitive ankaramite rocks are also present in the Vanuatu arc but are less common and constitute the mafic end members of some fractionation series, such as the Merelava Island ankaramite suite (Barsdell 1988) and the Epi Island ankaramite suite (Barsdell & Berry 1990) (Figure 2.1b). The ankaramite suites from the Vanuatu arc are olivine(*ol*)- and hypersthene(*hy*)-normative. In contrast, the Sunda rocks are nepheline(*ne*)-normative (Table 2.2).

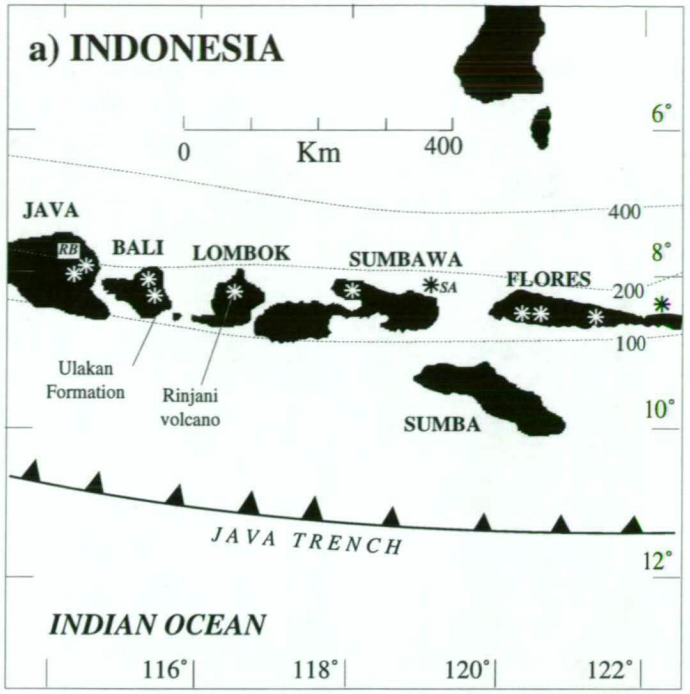

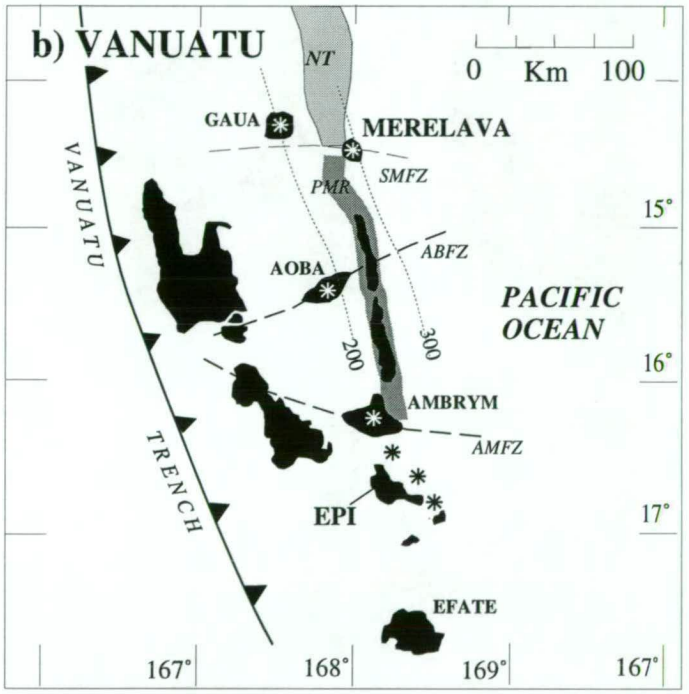

Figure 2.1a) Portion of the Sunda arc, Indonesia, showing the location of Rinjani volcano in Lombok and the Ulakan Formation in Bali. *SA*= Sangean Api volcano, *RB*= Ringgit Beser volcano. After Foden (1979).

b) Location of Merelava and Epi islands in the Vanuatu arc, Vanuatu. Dashed lines indicate fracture zones. *NT*= Northern Trough, *PMR*=Pentecost-Maewo Ridge, *SMFZ*=Santa Maria Fracture Zone, *ABFZ*= Aoba Fracture Zone, *AMFZ*=Ambrym Fracture Zone. After Barsdell (1980) and Greene *et al.* (1988).

Dotted lines indicate approximate depth (Km) and contour of Benioff zone. Stars (✳) indicate active volcanoes.

In all four ankaramite suites the most magnesian samples have high CaO/Al_2O_3 values (>1) compared to chondritic CaO/Al_2O_3 values (~0.8, Frey *et al.* 1978), picritic CaO/Al_2O_3 values (≤1, Section 1.2) and typical CaO/Al_2O_3 values of other primitive arc volcanic rocks (≤1, Perfit *et al.* 1980). The highest CaO/Al_2O_3 values (>1) occur in the most magnesian rocks, and within each suite CaO/Al_2O_3 values decrease with decreasing $Mg^{\#}$ (Figure 2.2). Ankaramite samples selected from each suite to study the melt inclusions are listed in Table 2.1. Samples labelled "UTas" form part of the University of Tasmania collection whereas the samples from Merelava were kindly donated by Dr. Mark Barsdell from the University of Auckland collection. These samples are typical ankaramites (Table 1.3) and are the most magnesian from each suite, which are briefly described below.

TABLE 2.1

Sample	Location	Sampler
UTas48001	Rinjani volcano, Lombok Is., Sunda arc	Foden (1979)
UTas67424	Ulakan Formation, Bali Is., Sunda arc	Wheller (1986)
UTas71046	Epi Is., Vanuatu arc	Barsdell & Berry (1990)
BC-13, 31551	Merelava Is., Vanuatu arc	Mallick & Ash (1977), Barsdell (1988)

Ankaramite samples used for melt inclusion study.

2.2.1 Ankaramite suite from Rinjani volcano

On Lombok, lavas of Early Quaternary age and younger are high-Al basalts, andesites and dacites (Figure 2.3a). The mafic lavas are represented by ankaramite ($Mg^{\#}$ 62 to 73) and the age of ankaramite lavas predates Pleistocene volcanic activity (Foden 1979, 1983, Foden & Varne 1981a, Varne & Foden 1986). The ankaramite rocks have a range in MgO contents from 8 to 14 wt%, with Al_2O_3 contents <16 wt% and high CaO, Cr and Ni contents. Compositional variation within the Rinjani ankaramite suite is characterized by simultaneous depletion of Cr, Ni, MgO and CaO, and enrichment in Al_2O_3, K_2O and TiO_2 with decreasing $Mg^{\#}$. SiO_2 and FeO* are relatively invariable throughout. These associations are consistent with the crystal fractionation of the clinopyroxene-dominated, plagioclase-free phenocryst assemblage of the Rinjani ankaramites (Foden 1983). The most mafic sample (UTas48001, Table 2.2) has abundant clinopyroxene phenocrysts (~37%), and minor olivine phenocrysts (12%) that contain rare inclusions of Cr-spinel. Plagioclase rarely occurs as phenocrysts (<4%) and the groundmass contains clinopyroxene, olivine, plagioclase, magnetite and possibly nepheline and/or sanidine (Foden 1979). This sample has a cpx/ol[1] value of ~3, a CaO/Al_2O_3 value of 1.37, a *di/ol* value of ~1.3 and $Mg^{\#}$ 73.0 (Table 2.2), thus it has chemical characteristics that are typical of ankaramite (Table 1.3).

Compositionally, the ankaramites form a separate, unrelated group to other Rinjani basaltic rocks (Foden 1983) and constitute a distinct *ne*-normative rock-type (Table 2.2). Foden & Varne (1981) conclude that at least two primitive mafic magmas must be present in the Rinjani volcano.

[1]cxp/ol= modal abundance of clinopyroxene/olivine. *di/ol*= molecular normative content of diopside/olivine

TABLE 2.2

	Sunda arc				Vanuatu arc		
	Rinjani volcano		Ulakan Formation		Merelava Island		Epi Island
Sample	UTas48001	UTas48002	UTas67424	UTas67422	BC-13	31551	UTas71046
SiO_2	48.32	47.95	46.44	46.86	50.20	51.33	48.20
TiO_2	0.69	0.83	0.56	0.79	0.46	0.59	0.39
Al_2O_3	10.53	13.78	9.12	11.84	10.30	13.10	11.50
FeO*	9.19	10.16	10.30	10.20	8.08	8.20	8.91
MgO	14.02	10.61	17.48	13.30	13.71	10.67	13.50
CaO	14.38	13.14	11.78	11.84	13.69	12.45	14.40
MnO	0.17	0.17	0.20	0.19	0.17	0.22	0.16
Na_2O	1.50	1.78	1.22	1.59	1.60	1.78	1.05
K_2O	0.90	1.20	0.61	0.94	0.38	0.35	0.31
P_2O_5	0.15	0.21	0.21	0.28	0.05	0.07	0.07
TOTAL	99.85	99.83	97.92	97.83	98.64	98.76	98.49
Mg#	73.1	65.1	75.2	70.0	75.2	69.9	73.0
mg#	77.6	70.3	78.1	73.3	77.5	72.5	75.0
Eq-Fo*	90.1	86.1	91.0	88.6	91.0	88.6	90.0
Eq-Fo	92.0	88.8	92.3	90.2	92.0	89.8	90.9
Ni (ppm)	151	125	392	246	137		172
Cr (ppm)	510	307	1055	618	695		820
CaO/Al_2O_3	1.37	0.95	1.29	1.00	1.33	0.95	1.25
CIPW norm (molecular %)							
or	4.04	5.61	2.69	4.36	1.68	1.45	1.40
ab	5.24	8.25	7.16	9.76	10.78	11.22	7.19
an	14.70	20.63	13.16	17.60	14.85	18.76	19.64
ne	4.99	4.40	1.02	1.46			
di	38.78	29.88	29.49	27.13	35.85	24.29	34.49
hy					13.25	36.66	10.04
ol	30.26	28.73	44.81	37.24	22.33	6.12	26.14
ilm	1.83	2.29	1.46	2.16	1.20	1.44	1.04
ap	0.15	0.22	0.21	0.29	0.05	0.06	0.07
di/ol	1.28	1.04	0.66	0.73	1.61	3.97	1.32
Phenocryst modes							
cpx	36.5		37.5		36.0	20.7	72.0†
ol	12.0		13.9		8.2	10.3	28.0†
plg	4.5					15.5	
cpx/ol	~3.0		~2.7		~4.4	~2.0	~2.6

Wholerock analysis of magnesian samples in the ankaramite suites from Rinjani volcano (Foden 1979), Ulakan Formation (Wheller 1986), Merelava Island (Barsdell 1988) and Epi Island (Barsdell & Berry 1990). * indicates all iron as Fe^{2+}. Mg#=100Mg/(Mg+Fe*), mg#=100Mg/(Mg+Fe^{2+}), Eq-Fo*=Fosterite content in equilibrium with wholerock composition calculated using all iron as FeO, Eq-Fo=Fosterite content in equilibrium with wholerock composition calculated using $(Fe_2O_3/FeO)_{melt}$ values from Section 2.5.3 and a $K_D^{Mg\text{-}Fe}$ value for olivine-melt of 0.30 (Roeder & Emslie 1970). Molecular CIPW norm calculated with analyses summed to 100% and with all iron as FeO. (†) Indicates modal proportion of olivine (ol) relative to clinopyroxene (cpx). Pl=plagioclase. Trace and rare earth element analyses of Indonesian samples listed in Table 2.3.

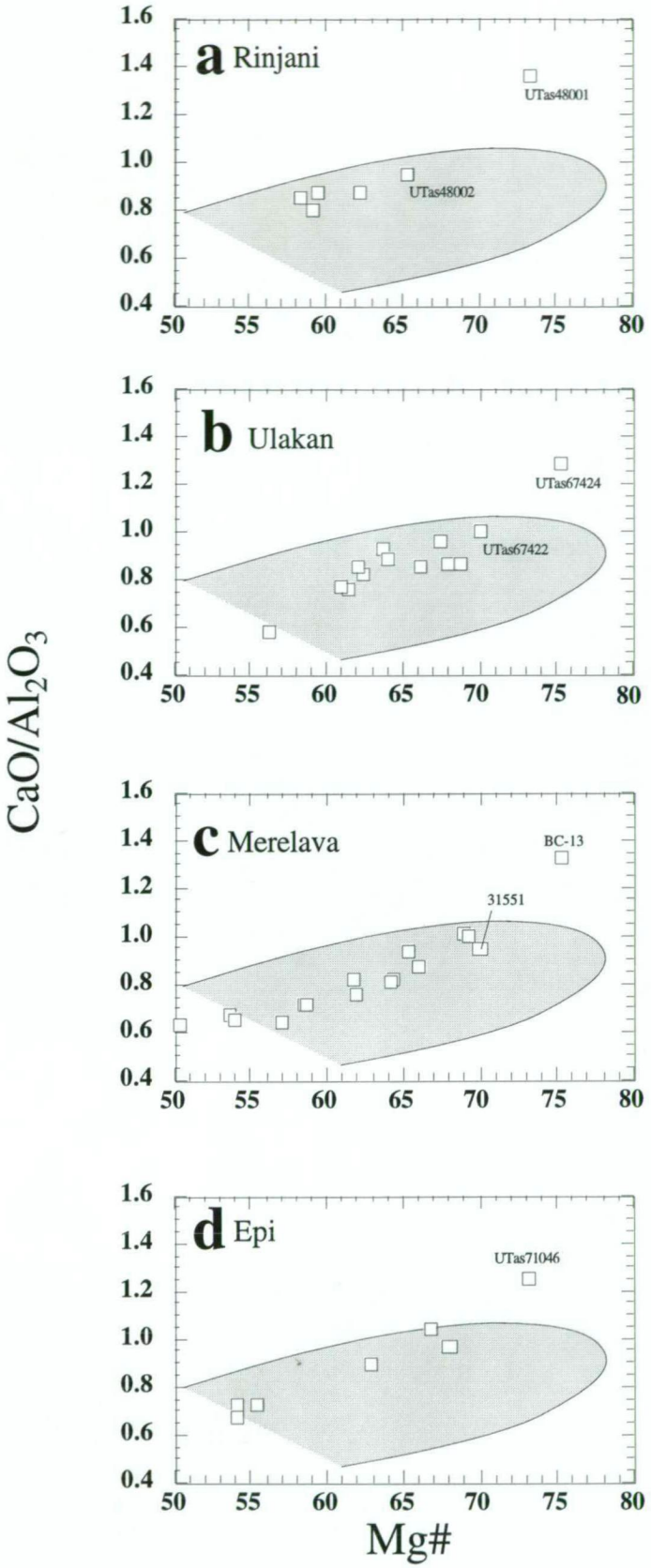

Figure 2.2 Wholerock CaO/Al_2O_3 values *versus* Mg# (=100Mg/(Mg+Fe*)) in samples of ankaramite suites from a) Rinjani volcano, b) Ulakan Formation, c) Merelava Island and d) Epi Island. Analyses of magnesian samples are listed in Table 2.1. Shaded area indicates the field of primitive arc lavas (Perfit *et al.* 1980). Data from Foden (1979), Wheller (1986), Barsdell & Berry (1990) and Barsdell (1988).

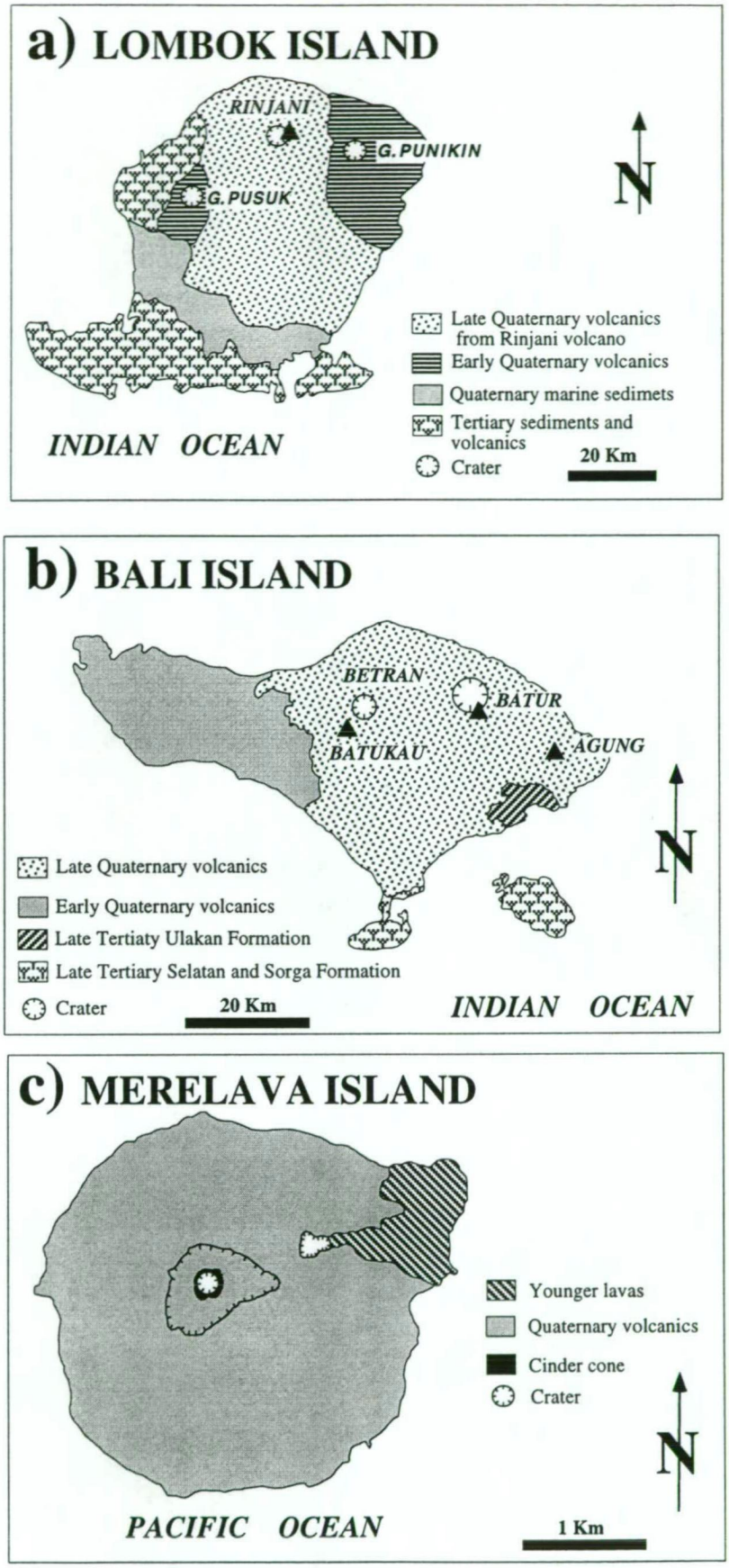

Figure 2.3 Geology of a) Lombok, after Foden (1979), b) Bali, after Wheller (1986) and c) Merelava Island, after Barsdell (1988).

One that fractionates to give the compositional range observed in ankaramites lavas and the other to yield the other basalts. Sr, Nd and Pb isotopic ratios of ankaramite sample UTas48001, the only Rinjani ankaramite so far isotopically analysed (Varne & Foden 1986), are unlike those of more evolved Rinjani basalts. However, isotopically they resemble those of shoshonitic olivine trachybasalts from Tambora volcano in Sumbawa to the east. REE analyses of the two most primitive samples in this suite, samples UTas48001 and UTas48002 (Table 2.3) show similar LREE enrichment with La/Yb values of ~7.9 (Figure 2.4a, Table 2.3). Sample UTas48001 has slight Eu and Ce anomalies that are not present in the less magnesian UTas48002 sample.

2.2.2 Ankaramite suite from the Ulakan Formation

Most of Bali is covered by Quaternary volcanics although older volcanic sequences are exposed as a result of uplift. The Ulakan Formation in eastern Bali (Figure 2.3b) is an exposed submarine sequence with ankaramitic pillow basalts of Late Miocene age. These rocks are the oldest and most mafic volcanic rocks exposed in Bali (Whitford 1975, Wheller 1986). In Bali, younger Quaternary volcanic sequences do not include ankaramite, but contain common basalts (Whitford 1975, Whitford *et al.* 1979, Wheller 1986). Ankaramites from the Ulakan Formation contain abundant, large, euhedral phenocryst of clinopyroxene (38%) and olivine (14%), as well as micro-phenocrysts of plagioclase and Ti-magnetite in some rocks (Wheller 1986). Cr-spinels occur as small euhedral inclusions in olivine. Rarely inclusions of aluminous green spinels also occur in olivine and clinopyroxene phenocrysts (Chapter 6).

The most magnesian ankaramite from the Ulakan Formation (sample UTas67424) has 37.5% clinopyroxene, 13.9% olivine and no plagioclase phenocrysts. Its wholerock composition contains 17.5 wt% MgO, 1055 ppm Cr, 392 ppm Ni and it has a $Mg^{\#}$ value of 75 (Table 2.2). Sample UTas67424 has a cpx/ol value of ~2.7 and a CaO/Al_2O_3 value of 1.29 that are typical of ankaramite, but a *di/ol* value of ~0.7 makes this sample transitional to a picrite (Table 1.3).

Although these Bali ankaramites have typical orogenic affinities with low TiO_2 and Nb contents, several other geochemical characteristics, such as high Ba/K_2O, La/Zr and Ba/La values make these ankaramites compositionally distinct from other Balinese volcanics (Wheller 1986). In the most magnesian sample UTas67424 shows weak LREE enrichment, with La/Yb~6.1, compared to more evolved ankaramite samples in the suite (sample UTas67422) and other volcanics from Bali (Figure 2.4b). The ankaramites from the Ulakan Formation are also K_2O-rich, with mildly *ne*-normative compositions and shoshonitic affinities (Wheller 1986). Distinctly different petrographic and chemical characteristics to other volcanics on Bali suggest that these ankaramites are derived from a distinctive magma source. These primitive rocks are therefore unlikely parental magmas to the younger differentiated series of volcanic rocks exposed on Bali, that range from basalt through andesite to dacite (Wheller 1986).

TABLE 2.3

Location	Rinjani volcano		Ulakan Formation	
Sample	UTas48001	UTas48002	UTas67424	UTas67422
Ba	516	351	208	347
La	8.98	12.8	8.52	13.5
Ce	10.9	30.5	20.1	28.6
Nd	12.7	16.8	11.9	14.5
Sm	3.16	4.07	2.77	3.84
Eu	0.82	1.32	0.77	1.19
Tb	0.58	0.71	0.52	0.59
Ho	0.64	0.83	0.68	0.68
Yb	1.14	1.62	1.4	1.4
Lu	0.16	0.2	0.17	0.2
Th	1.98	2.25	1.87	2.56
Hf	1.17	1.57	1.44	1.49
Ta	0.79	0.76	<DL	<DL
La/Yb	7.88	7.90	6.09	9.64

Trace and rare earth element analyses (ppm) obtained by neutron activation on the two most magnesian ankaramite samples from Rinjani and Ulakan. <DL indicates values below detection limit (Appendix 2.1).

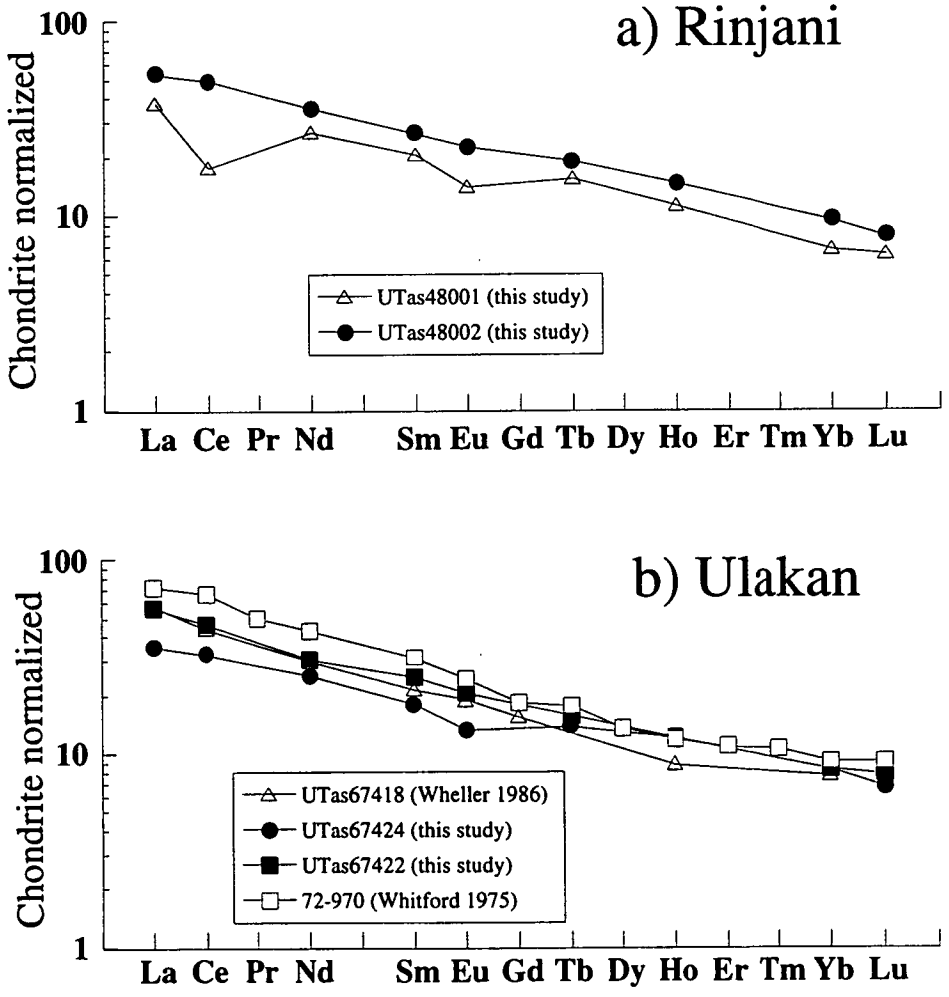

Figure 2.4 REE analyses (Table 2.2) of the two most magnesian samples from a) Rinjani volcano ankaramite suite (UTas48001 and UTas48002) and b) the Ulakan Formation ankaramite suite (UTas67424 and UTas67422). Normalization values taken from Sun & McDonough 1989.

2.2.3 Ankaramite suite from Merelava Island

Merelava island is a dormant volcano in the Vanuatu island arc that is situated on oceanic crust (~17 km thick) and approximately 300 Km above the Benioff zone (Barsdell 1988). Despite its proximity to back-arc basins, between the Pentecost-Maewo Ridge and the Northern Trough (Figure 2.1b), the volcanic rocks on Merelava preserve chemical characteristics that are typically orogenic (Barsdell & Berry 1990, Mallick & Ash 1975, Barsdell 1988, Gaetani *et al.* 1994). Merelava is mainly composed of Quaternary ankaramitic tholeiitic basalt flows that have abundant crystals of clinopyroxene, and lesser olivine phenocrysts that contain rare inclusions of Cr-spinel (Barsdell 1980). The most magnesian sample of the suite (sample BC-13, Table 2.2) contains 36% clinopyroxene, 8% olivine and lacks phenocrysts of plagioclase. Sample BC-13 has features typical of ankaramite rocks, with a cpx/ol value of ~4.4, a CaO/Al_2O_3 value of 1.33, a *di/ol* value of ~1.6 and Mg#75.2. Samples BC-13 and 31551 represents the most primitive end-members of a differentiated volcanic sequence that ranges from ankaramite through to dacite, with MgO contents varying from ~14 to ~4 wt% respectively (Barsdell 1980, 1988). Within this compositional range, wholerock chemical variations indicate crystal fractionation with cpx/ol values as observed in the suite (~3:1) and with negligible contribution from plagioclase. Groundmass phases consist of clinopyroxene, plagioclase, titanomagnetite and hypersthene. Cumulate ultramafic xenoliths are also present in these lavas and are mainly clinopyroxenites (Barsdell 1988, Barsdell & Smith 1989).

2.2.4 Ankaramite suite from Epi Island

Located along the volcanic front of the Vanuatu island arc, Epi island consists of uplifted Pleistocene submarine sequences to the west, and younger subaerial volcanic cones on the east (Gorton 1977, Barsdell & Berry 1990, Gaetani *et al.* 1994). Primitive lavas in western Epi are ankaramitic and are parental to differentiated basalt, andesite and dacite series (MgO ~1 to ~14 wt%). Trace elements and isotopic signatures are typical of island arc affinities (Barsdell & Berry 1990). As in Merelava, these ankaramites are characterized by abundant clinopyroxene and olivine phenocrysts. Additionally, orthopyroxene also occurs as a phenocryst phase in andesite and dacite but is absent from the groundmass. The groundmass phases for this suite are clinopyroxene, plagioclase and titanomagnetite, with olivine occurring in the more mafic samples.

The most primitive sample UTas71046 has a cpx/ol value of ~2.6, a CaO/Al_2O_3 value of 1.25, a *di/ol* value of 2.6 and Mg# 73.0 (Table 2.2). Barsdell & Berry (1990) rule out a mechanism involving clinopyroxene assimilation for the formation of ankaramites, instead showing instead that wholerock compositions of these primitive ankaramite rocks represent olivine-clinopyroxene cotectic liquids produced by melting of lower crustal clinopyroxenite cumulates (cf. Section 1.6).

2.3 Sample preparation

The samples were crushed, sieved, and phenocryst grains (olivine and clinopyroxene) carefully hand-picked from the crushed material using a binocular microscope. The grains were then set in epoxy mounts, sectioned and polished to exposed their magmatic inclusions. Each one of the

primary melt and mineral inclusions exposed by polishing, was studied optically and then analysed by electron microprobe. The host was analysed adjacent the inclusions within a distance of around 100 μm. Microprobe analytical conditions are described in Appendix 2.1 and representative mineral analyses are tabulated in Appendix 2.2 to 2.5. Over 200 grains from each suite were studied by this method to asses the variation in chemical composition of mineral phases, but principally to sample a larger number of melt inclusions in the most primitive phenocrysts. Using this technique, olivine compositions that are equally or more magnesian than previously reported for these suites were found. In addition, the rare occurrence of aluminous spinels in melt inclusions was also documented (Chapter 6). After probing, grains were selected for homogenization experiments based on their primitive composition (~$Mg^{\#}$>88) and the presence of suitable primary melt inclusions. These grains were extracted from their epoxy mounts and individually prepared for further study. Results on homogenization experiments are presented in Chapters 3 and 4.

2.4 Mineralogy of the primitive samples

Considered as a group, the primitive samples from each of the four suites are highly porphyritic and typically contain abundant phenocrysts of clinopyroxene, minor olivine and traces of plagioclase. Their compositions are described below as a group by combining previous and new mineral data generated from olivine and clinopyroxene grain mounts.

2.4.1 Olivine

Olivine phenocrysts in ankaramite from the Rinjani volcano are rounded and embayed. The most magnesian olivine attains $Fo_{90.8}$ and olivines range down to ~Fo_{74} (Figure 2.5a). CaO contents of olivine range between 0.22 to 0.46 wt% and increases with decreasing Fo content, with the maximum CaO values occurring at around $Fo_{89.5}$ (Figure 2.6a). This trend is confirmed by two olivine grains with $Fo_{91.0}$, re-analysed by electron microprobe for trace elements Ca, Mn, Ni, Cr (Appendix 2.5a) which also have low CaO contents (~0.28 wt% CaO, Figure 2.6a, filled symbols). Within this range of increasing CaO content, corresponding to a range from ~Fo_{91} down to ~Fo_{88}, the NiO content of olivine decreases rapidly from 0.25 wt% to 0.12 wt% (Figure 2.6e).

Olivine phenocrysts in the Ulakan ankaramite range in composition from $Fo_{92.6}$ down to ~Fo_{74} (Figure 2.5b). Within this range, the CaO content in olivine varies between 0.24 to 0.50 wt% (Figure 2.6b, open symbols). Grains re-analysed by microprobe using trace element analytical conditions reveal an increase in CaO content (~0.28 to 0.45 wt%) with decreasing Fo and maximum CaO values around Fo_{90} (Figure 2.6b, filled symbols). The NiO content in olivine also decreases rapidly from 0.34 wt% in $Fo_{92.6}$ down to ~0.20 wt% in Fo_{90} and more gradually in less magnesian olivines (Figure 2.6f).

Olivine phenocrysts in ankaramite from Merelava show reversely zoned inner rims with typical core to rim variation from $Fo_{90.5}$ to $Fo_{91.3}$ (Barsdell 1988) and a range in composition from $Fo_{91.5}$ (Barsdell 1988) to Fo_{77} (Figure 2.5c). The CaO content in olivine varies between 0.23 and 0.30 wt% (Figure 2.6c) and does not show the rise of CaO content observed in the most primitive

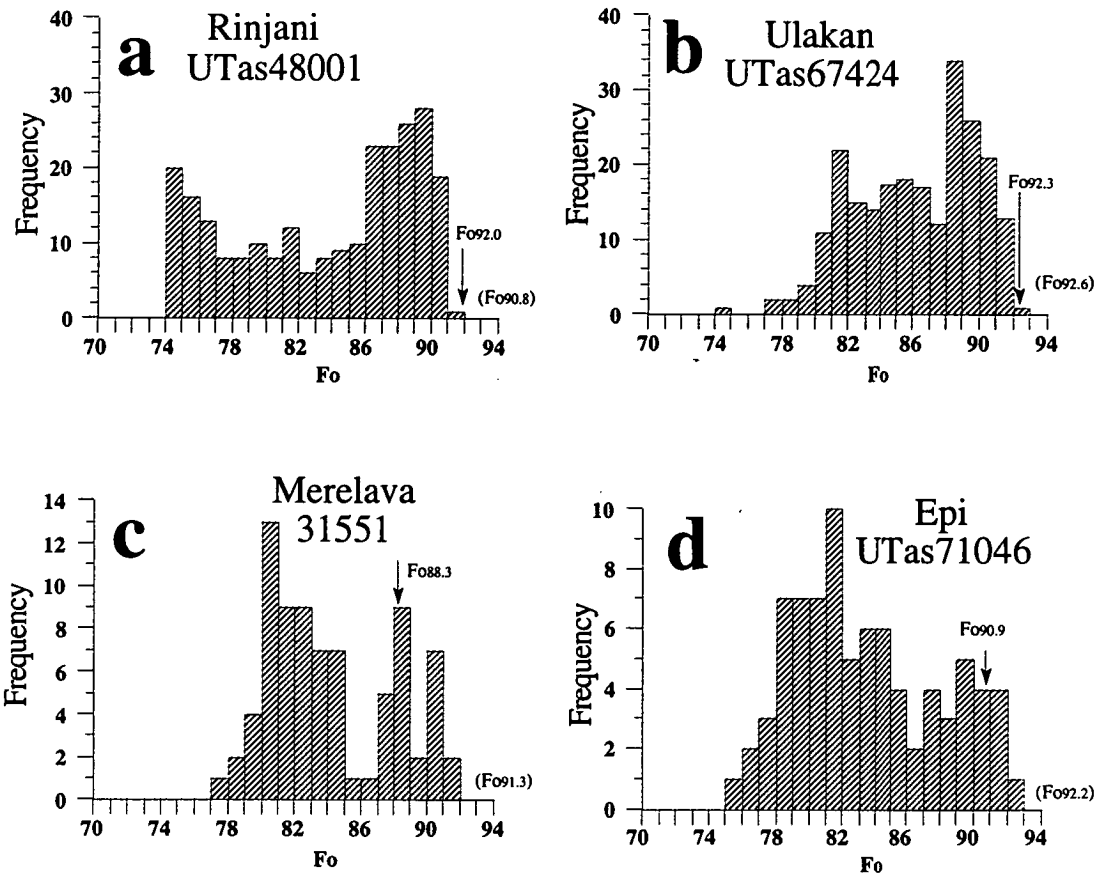

Figure 2.5 Histograms of the olivine Fo content in ankaramite from a) Rinjani volcano, b) Ulakan Formation, b) Merelava and c) Epi. Arrow indicates Fo value in equilibrium with wholerock composition of sample. The highest Fo content in each sample is indicated in brackets. Representative olivine analyses listed in Appendix 2.2

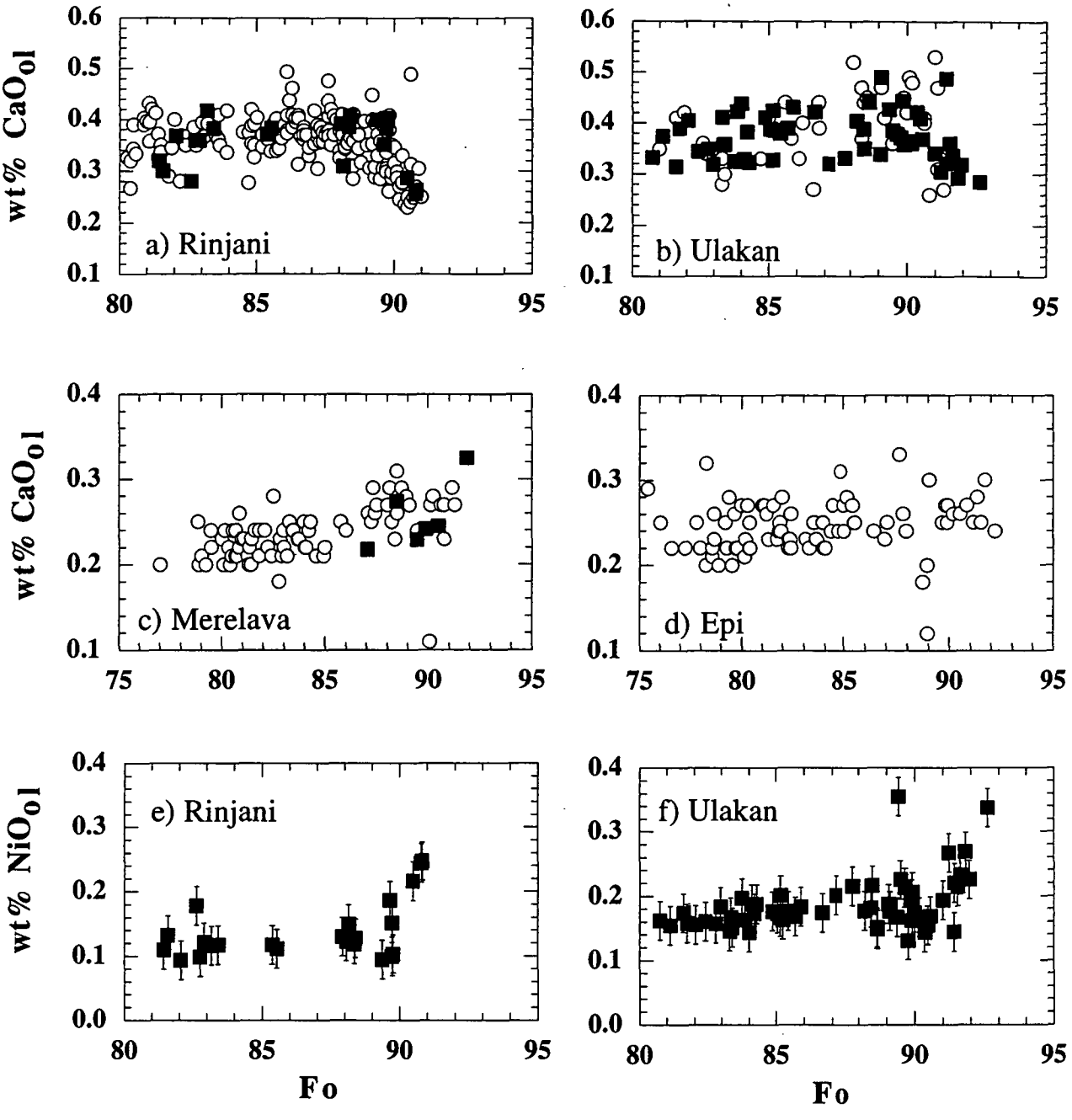

Figure 2.6a-d) Concentration of CaO (±0.05 wt%) *versus* Fo content in olivines in ankaramite suites from a) Rinjani volcano (UTas48001), b) Ulakan Formation (UTas67424), c) Merelava Island (31551) and d) Epi Island (UTas71046). Square filled symbols are electron microprobe analyses under trace element operating conditions (200 nA current, 20 μm beam size, 20 kV accelarating voltage and 120 seconds counting time, Appendix 2.1) which yield analytical uncertainties smaller than symbols (±0.01 wt%). Representative analyses are listed in Appendix 2.5. Note the decline in CaO content in olivines from Rinjani and Ulakan with decreasing Fo, which suggest the late crystallization of clinopyroxene after olivine in these two ankaramite suites (Section 2.6).

e-f) Concentration of NiO (wt%) in olivine versus Fo content in e) Rinjani and f) Ulakan. Error bars are ±0.03 wt% NiO and indicate maximun range of duplicate analyses under the trace element conditions described above.

olivines in ankaramite samples from Rinjani and Ulakan Formation (Figure 2.6a and b). NiO contents in the most magnesian olivine range up to 0.25 wt% (Barsdell 1988).

Olivine phenocrysts in ankaramite from Epi show an Fo range from 92.2 to ~75 (Figure 2.5d) and lack the reversely zoned rims observed in Merelava olivines (Barsdell & Berry 1990). Variation in CaO content is, however, similar to Merelava, with some low values around Fo_{89} (Figure 2.6d). NiO content in primitive olivine ranges up to 0.21 (Barsdell & Berry 1990).

Besides CaO, the SiO_2 content of the melt has the greatest influence on the CaO content of olivine phenocrysts (Stormer 1973, Jurewicz & Watson 1988). This agrees with observations of Sigurdsson (1994, his Figure 3.4b) where, among rocks with similar CaO and MgO contents, those with relatively lower SiO_2 contents have less calcic olivines. In Figure 2.6a and b, the range in CaO content of olivines from Lombok and Bali (0.25 to 0.45 wt%) are higher to those observed from Merelava and Epi (0.20 to 0.30 wt%, Figure 2.6c and d). Thus the observed differences in CaO content may reflect the *ne*-normative nature of the Indonesian ankaramites, compared to those from the Vanuatu arc that are *hy*-normative (Table 2.2).

2.4.2 Clinopyroxene

Clinopyroxene typically forms large euhedral crystals which, in the Merelava and Rinjani ankaramites are up to 2 cm long. In clinopyroxene from Rinjani and Ulakan, resorption textures are common, whereas clinopyroxenes from Merelava and Epi occasionally show minor resorption (Barsdell 1988, Barsdell & Berry 1990). Whether from Merelava, Epi, Rinjani or Ulakan, the magnesian clinopyroxenes have high CaO (>23 wt%, Appendix 2.3) and their compositions are mainly diopsidic (Figure 2.7). The composition of Merelava clinopyroxene does, however, vary to lower Ca contents and include augite, in accord with the tholeiitic affinities of this suite. The $Mg^{\#}_{cpx}$ values range up to 90 in Rinjani, 92 in Ulakan Formation, 93 in Merelava and 94.4 in Epi (Figure 2.8). Zoning in clinopyroxene crystals is also observed. In the ankaramite from Rinjani, clinopyroxene crystals have a sharp transition from Cr-diopside cores to augite rims (Foden & Varne 1981a) and this feature is also present in clinopyroxenes from the Ulakan Formation (Wheller 1986). Comparatively, clinopyroxenes from Epi have a narrow compositional variation. In Merelava the compositional differences between clinopyroxene cores and internal rims are relatively small, although some clinopyroxene phenocrysts may show a wider (diopside-augite) range in composition from $Wo_{47}En_{50}Fs_3$ to $Wo_{38}En_{45}Fs_{17}$ (Barsdell 1988). Many of the clinopyroxenes from Merelava have narrow (100 to 200 μm), "reversely zoned internal rims" that range from $Mg^{\#}$ 92.5 to 94 and may also have a lower-temperature normally zoned outer rim resultant upon localized oxidation (Barsdell 1988).

2.4.3 Plagioclase

Plagioclase is a rare phenocryst phase in all four ankaramite suites and appears late in the crystallisation sequence. In Rinjani, rare plagioclase phenocrysts are relatively unzoned and are as calcic as An_{90}, ranging down to An_{85} (Foden 1983). In the ankaramite from the Ulakan Formation,

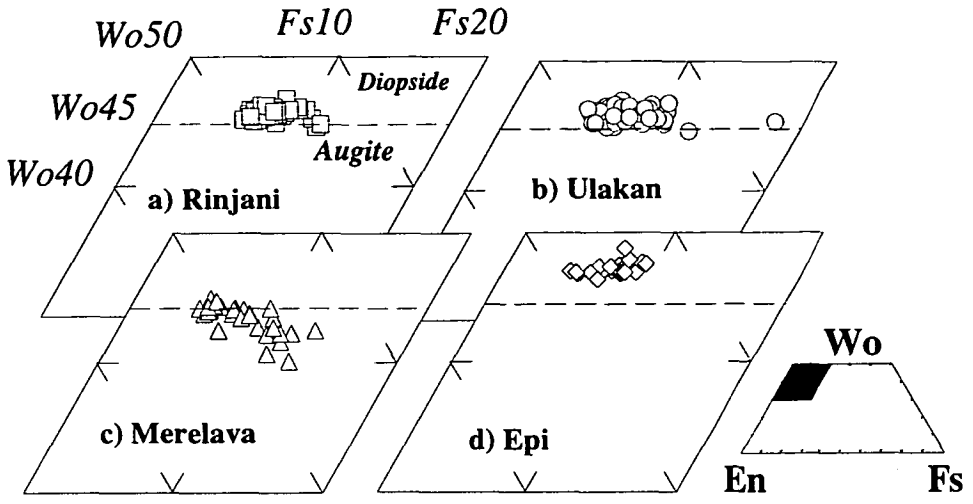

Figure 2.7 Clinopyroxene compositions in ankaramite from a) Rinjani volcano (UTas48001), b) Ulakan Formation (UTas67424), c) Merelava (31551) and d) Epi (UTas71046). Quadrilateral Wo-En-Fs after Moromito (1989).

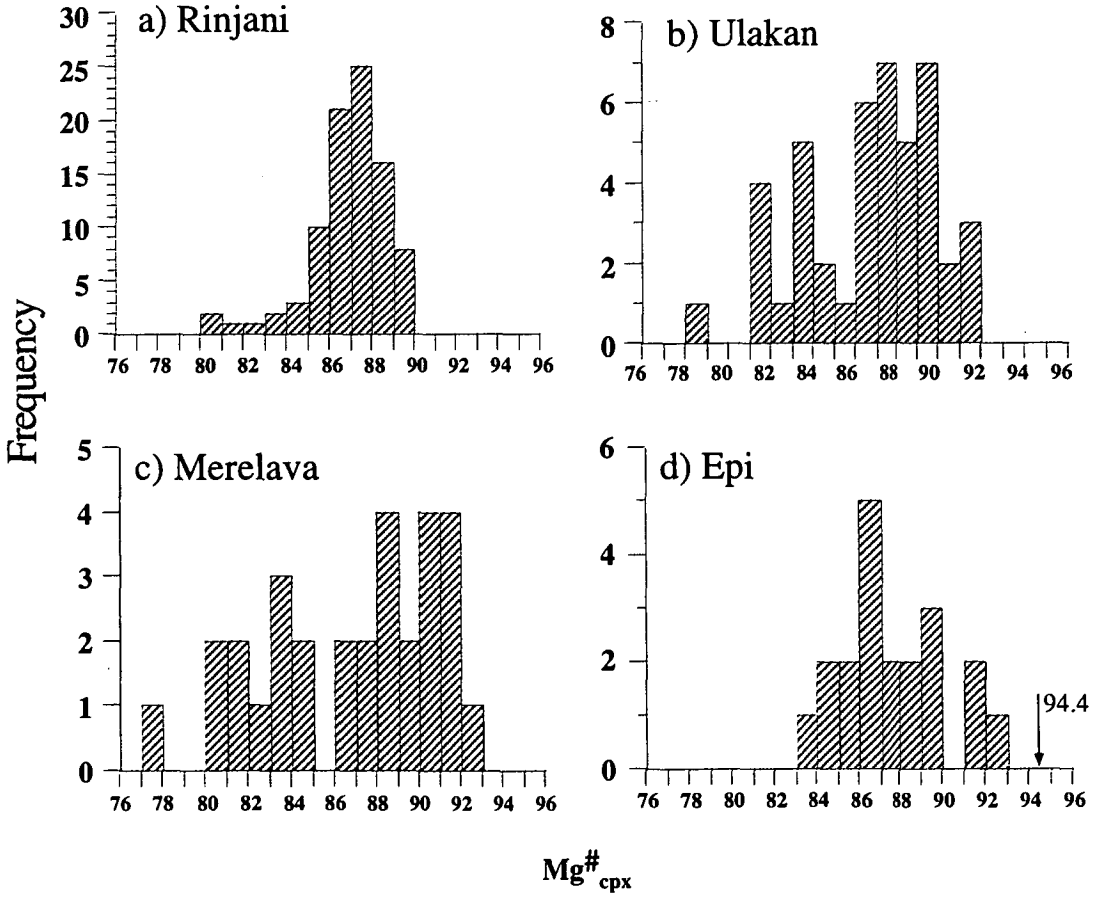

Figure 2.8 Mg# of clinopyroxene ($Mg\#_{cpx}$=100Mg/(Mg+Fe*)) from ankaramite suites of a) Rinjani volcano (UTas48001), b) Ulakan Formation (UTas67424), c) Merelava (31551) and d) Epi (UTas71046). The arrow indicating $Mg\#_{cpx}$=94.4 from Epi is the most magnesian clinopyroxene composition reported by Barsdell & Berry (1990).

rare microphenocrysts of plagioclase attain at least An_{80}, and rare plagioclase phenocrysts in ankaramite from Merelava vary from An_{93} to An_{44} (Barsdell 1988). In the most mafic sample from Merelava (BC-13, Table 2.2), plagioclase phenocrysts are absent and Mallick & Ash (1975) report a groundmass plagioclase composition of An_{90}. In Epi, plagioclase microphenocrysts range from $An_{94.6}$ to An_{39} and start to co-crystallize with olivine of around ~Fo_{82} (Barsdell & Berry 1990).

2.4.4 Groundmass

Groundmass assemblages are typically composed of clinopyroxene, plagioclase and titaniferous magnetite. In addition, Merelava ankaramites contain hypersthene and pigeonite (e.g., sample BC-13, Barsdell 1988) whereas in the ankaramite from Epi these phases only occur in the groundmass of the more evolved andesitic rocks. Compositions of groundmass olivine range down to Fo_{43} on Epi (Barsdell & Berry 1990) and Fo_{49} on Merelava (Barsdell 1988). Groundmass clinopyroxenes in Merelava are augite, Mg-pigeonite and hypersthene with ferrosilite (Fs) contents ranging from 11 to 36 (Barsdell 1988). Groundmass plagioclase ranges up to An_{70} in Ulakan, An_{90} in Rinjani (Foden & Varne 1981a), An_{90} in Merelava (sample BC-13, Barsdell 1988), and An_{94} in Epi (Barsdell & Berry 1990).

2.5 Magmatic inclusions

2.5.1 Classification used in this study

There are four types of magmatic inclusions in phenocrysts: melt inclusions (**L**), solid inclusions (**S**), fluid inclusions (**V**) and composite inclusions (Roedder 1984). Composite inclusions may be a combination of the first three types (ie. L±V±S). These four inclusion types can in turn be classified into primary, pseudo-secondary or secondary as illustrated in Figure 2.9a-b. Primary inclusions form when melt is trapped by a growing crystal as a result of growth irregularities. Pseudo-secondary inclusions form by the healing of fractures produced during crystal growth. Secondary inclusions instead, are trapped by the healing of fractures formed at a stage after crystal formation (Roedder 1979, 1984, Sobolev *et al.* 1991). Primary melt inclusions are hence the only inclusion type that can provide information on the composition of the parent melt from which the host mineral grew. Therefore primary inclusions are the only type investigated in this study.

After entrapment, crystallization of the host continues on the wall of the inclusion ("S_1", Figure 2.9c-d) and with a continued decrease in temperature, other daughter phases may also nucleate and grow from the residual melt within the inclusion ("S_2", Figure 2.9c) to produce a crystalline texture (Roedder 1979, Roedder 1984). These types of melt inclusions are known as "crystalline" melt inclusions (Roedder 1984, Sobolev *et al.* 1989). Alternatively, after crystallization of the host on the wall, the residual melt may be "naturally quenched" to a glass due to relatively rapid cooling. These types of melt inclusions are known as "vitreous" (Sobolev *et al.* 1989) or more commonly as "glassy" melt inclusions (Roedder 1984) (Figure 2.9d).

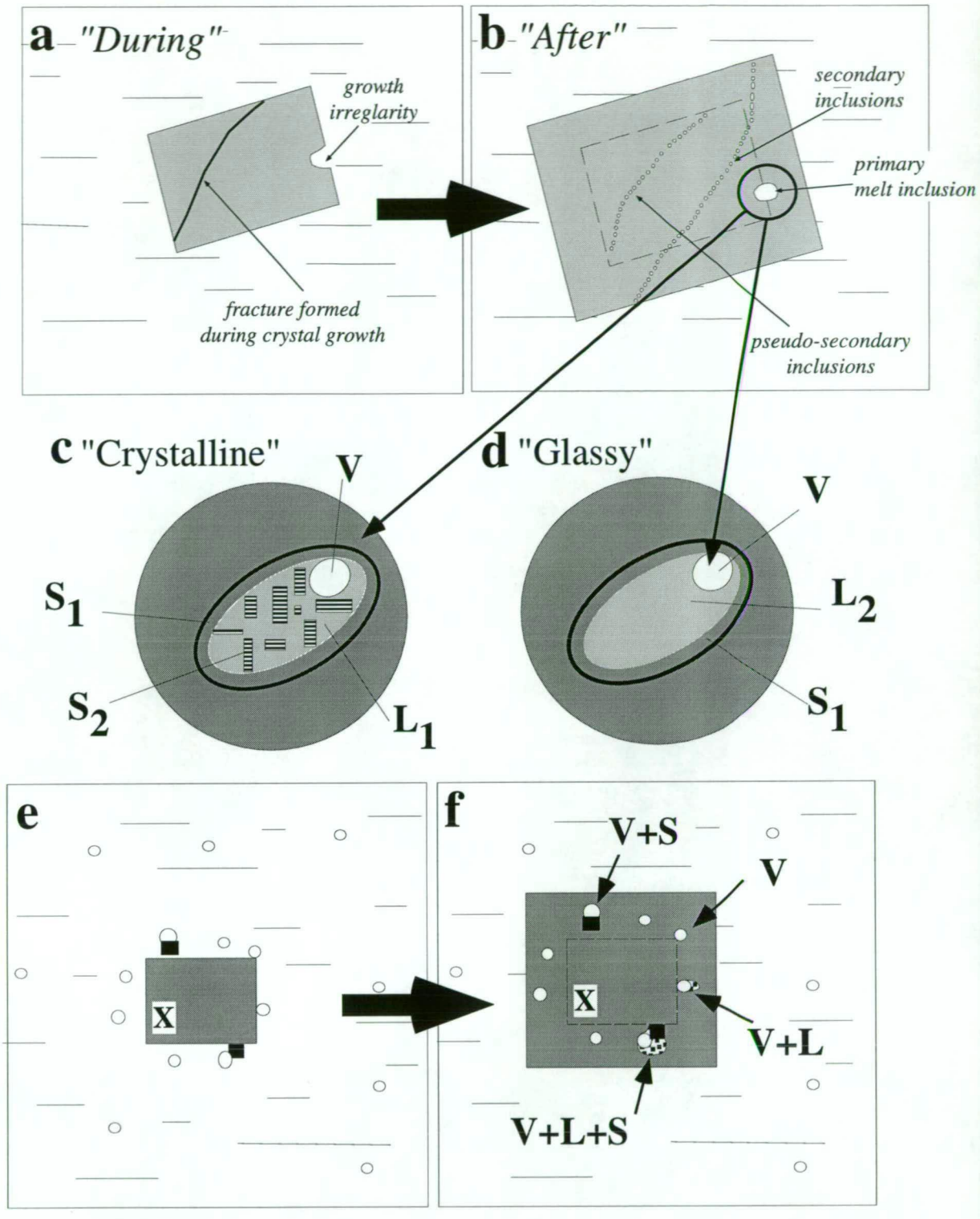

Figure 2.9a-f) Illustrating of the formation of:

a) "pseudo-secondary" inclusions trapped by the healing of fractures and "primary" melt inclusions trapped by growth irregularities synchronous with crystal growth. Both types are produced during crystal growth and become enclosed in the crystal as growth continues,

b) "secondary" inclusions trapped by the healing of fractures produced after crystal growth.

c) "crystalline" melt inclusion textures. After entrapment, crystallization of the host mineral continues on the wall ("S_1") and a shrinkage bubble forms ("V"). With continued decrease in temperature other phases may crystallize inside the inclusion to form daughter crystals ("S_2") and a residual glass (L_1).

d) "glassy" melt inclusion textures. Fast cooling rates after entrapment may naturally-quench the residual melt to a glass (L_2) without the growth of daugther phases.

e-f) Entrapment of a primary fluid inclusion (V), and "composite" primary inclusions (V+S, V+L, V+L+S) by a growing crystal.

Figures modified after Roedder (1979).

Cooling of a melt inclusion after trapping also leads to the formation of a shrinkage bubble ("V", Figure 2.9c-d). This bubble forms due to a change in density, and thus volume, inside the inclusion as a result of the growth of daughter phases, which also leads to an increased volatile pressure within the melt inclusion. As a shrinkage bubble forms, volatile species dissolved in the trapped melt may partition into the shrinkage bubble, which may or may not approach a vacuum, depending on the original concentration of volatiles in the melt (Roedder 1984). Information therefore can be obtained from L+V type primary inclusions on the volatile species that may have been dissolved in the parent melt (Bacon *et al.* 1992, Tait 1992). Alternatively, if the magma was volatile oversaturated, the immiscible fluid bubbles in the magma may be (1) accidentally trapped by a growing phenocryst to form V±L primary fluid inclusions or, (2) attached to a pre-existing crystal such as chromian spinel and later trapped by a growing phenocryst to form a combined V+S±L type primary inclusion, as illustrated in Figure 2.9e-f. In the latter type of inclusions, the glass-bubble volume ratio will be random as opposed to the L+V inclusion type described above, where glass/bubble volume ratios are constant (Sisson & Layne 1993).

2.5.2 Spinel inclusions in olivine

The compositional range of spinel inclusions in olivine is illustrated in an "oxidized" spinel prism in Figure 2.10 Analyses of rare green spinel inclusions with high Al_2O_3 (>60 wt%) and virtually no chromium from Ulakan and Epi are also shown for comparison (Figure 2.10b-d). The chemical characteristics and significance of these aluminous spinels are given in Della-Pasqua *et al.* (1995) and their possible origin is discussed separately in Chapter 6.

Reddish brown chromian spinels are most common in the olivines from the ankaramite suite of the Ulakan Formation ($Cr^{\#}$40-80), less common in the Rinjani volcano and Epi suites ($Cr^{\#}$56-74 and $Cr^{\#}$52-88 respectively) and rare in the Merelava suite ($Cr^{\#}$64-84) (Figure 2.11a-d). For a given Fo content, Cr# values of spinels from Merelava and Epi (Figure 2.11c-d) are higher than spinels from the Indonesian suites which have Cr# values <80 (Figure 2.11a-b), indicating a less refractory source (Dick & Bullen 1984, Duncan & Green 1987). Linear correlation between $Mg^{\#}_{spl}$ and Fo_{host} (Figure 2.11e-h) reflect Fe-Mg exchange between olivine and spinel as well as the evolution of spinels in a fractionating magma (e.g., Dick & Bullen 1984, Ballhaus *et al.* 1991). The TiO_2 contents of chromian spinels vary typically between 0.5 and 1.0 wt% in Rinjani and Ulakan Formation (Figure 2.11q-r) but are below ~0.5 wt% in Epi and Merelava (Figure 2.11s-t).

2.5.3 Fe_2O_3/FeO value in the melt

The calculated[2] $Fe^{3+}/(Fe^{2+}+Fe^{3+})$ values of spinel inclusions in magnesian olivines (~Fo>88) from all four ankaramite suites are plotted in Figure 2.11m-p. Also shown in Figure 2.11m-p is the range in $Fe^{3+}/(Fe^{2+}+Fe^{3+})$ values used for the calculation of Fe_2O_3/FeO_{melt} values summarized in Table 2.4. These values are calculated using the equation of Maurel & Maurel (1982):

$$\log_{10}(Fe^{2+}/Fe^{3+})_{spl}=0.764\ \log_{10}(Fe^{2+}/Fe^{3+})_{melt} - 0.343$$

[2] Fe^{2+} and Fe^{3+} species calculated assuming perfect stochiometry using the method of Robinson (1980).

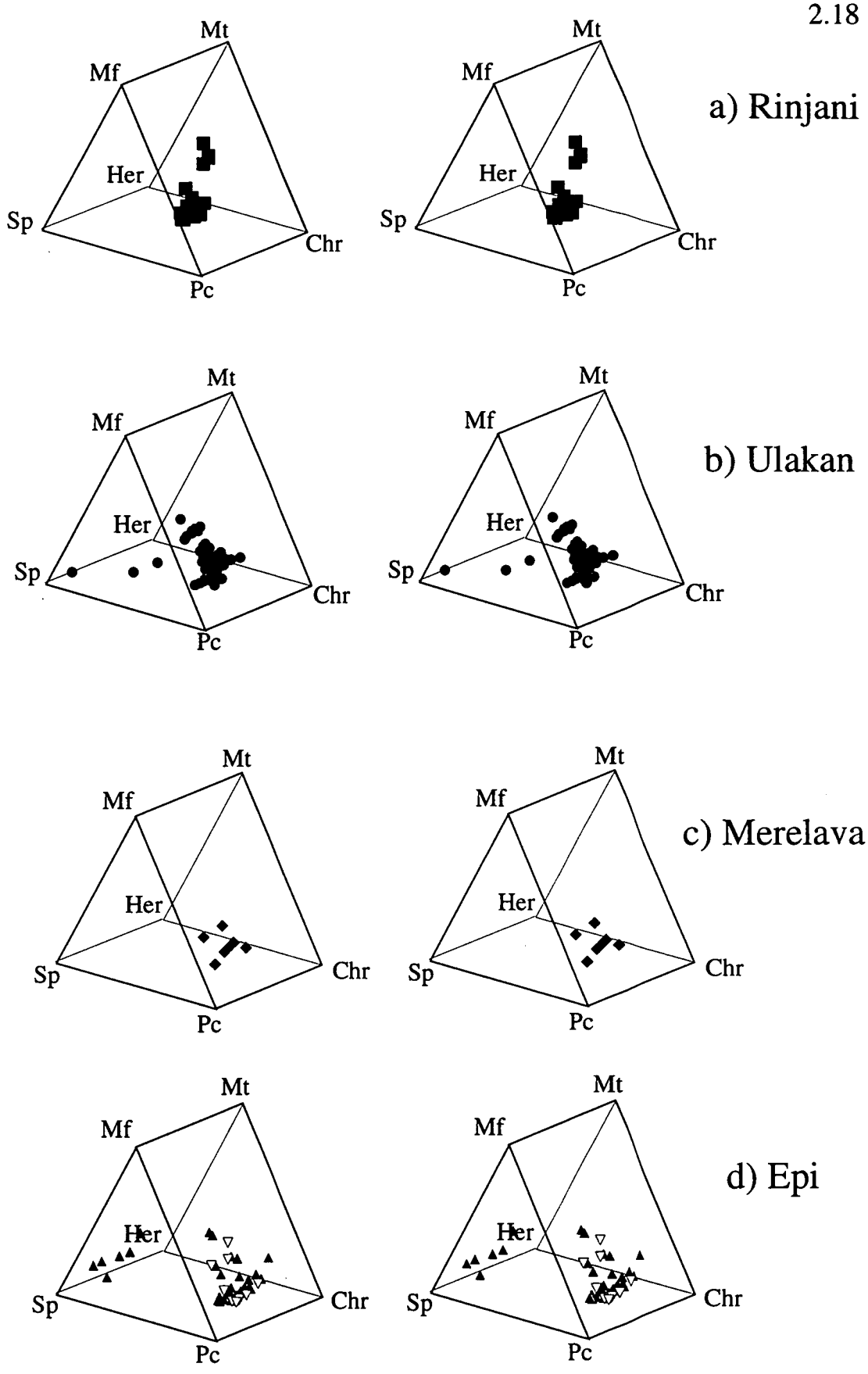

Figure 2.10 Stereopair projections of the composition of spinel inclusions in olivine phenocrysts from four ankaramite suites in the oxidized (magnetite) spinel prism (Williams *et al.* 1990). a) Rinjani, b) Ulakan formation, c) Merelava and d) Epi. Open symbols in the Epi are analyses from Barsdell & Berry (1990). Data from Appendix 2.4.

In this prism spinel analyses are subdivided into three series according to whether the trivalent ion is Al, Fe^{3+} or Cr.

Spinel series [Sp-Her]: Spinel($MgAl_2O_4$) - Hercynite($Fe^{2+}Al_2O_4$),
Magnetite series [Mf-Mt]: Magnesioferrite($MgFe^{3+}{}_2O_4$) - Magnetite($Fe^{2+}Fe^{3+}O_4$),
Chromite series [Pc-Chr]: Magnesiochromite($MgCr_2O_4$) - Chromite($Fe^{2+}Cr_2O_4$)

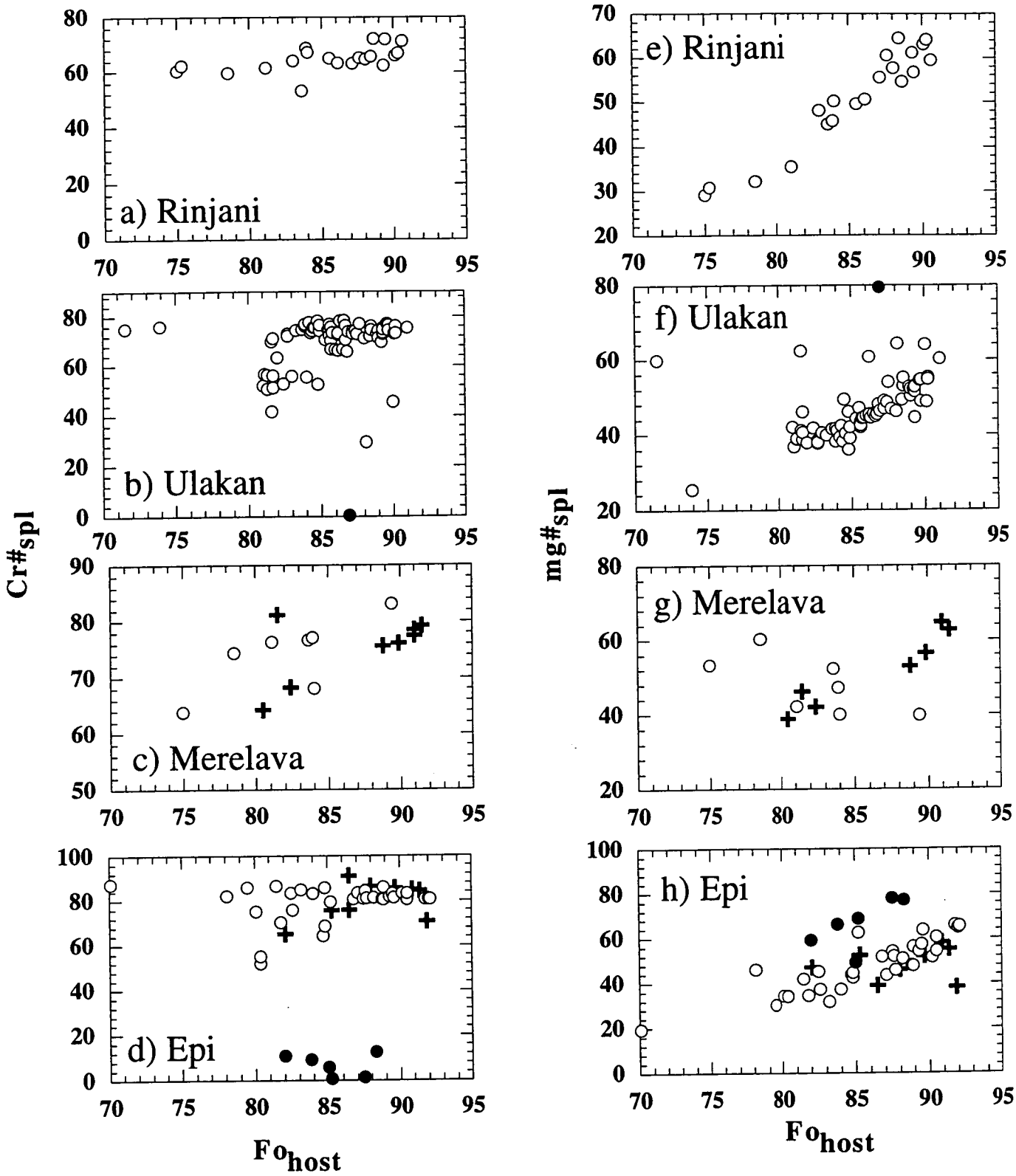

Figure 2.11 Compositional variation of olivine and spinel inclusion pairs from each of the ankaramite suite. a) to d) Cr# *versus* Fo_{host} olivine, e) to h) $mg\#_{spl}$ *versus* Fo_{host}. Fe^{3+} and Fe^{2+} species in spinel calculated assuming perfect stochiometry following the method of Robinson (1989, p419). Filled symbols in Ulakan and Epi are composition of spinel inclusion with more than 50 wt% Al_2O_3. Crosses in Merelava and Epi are analyses from Barsdell (1988) and Barsdell & Berry (1990).

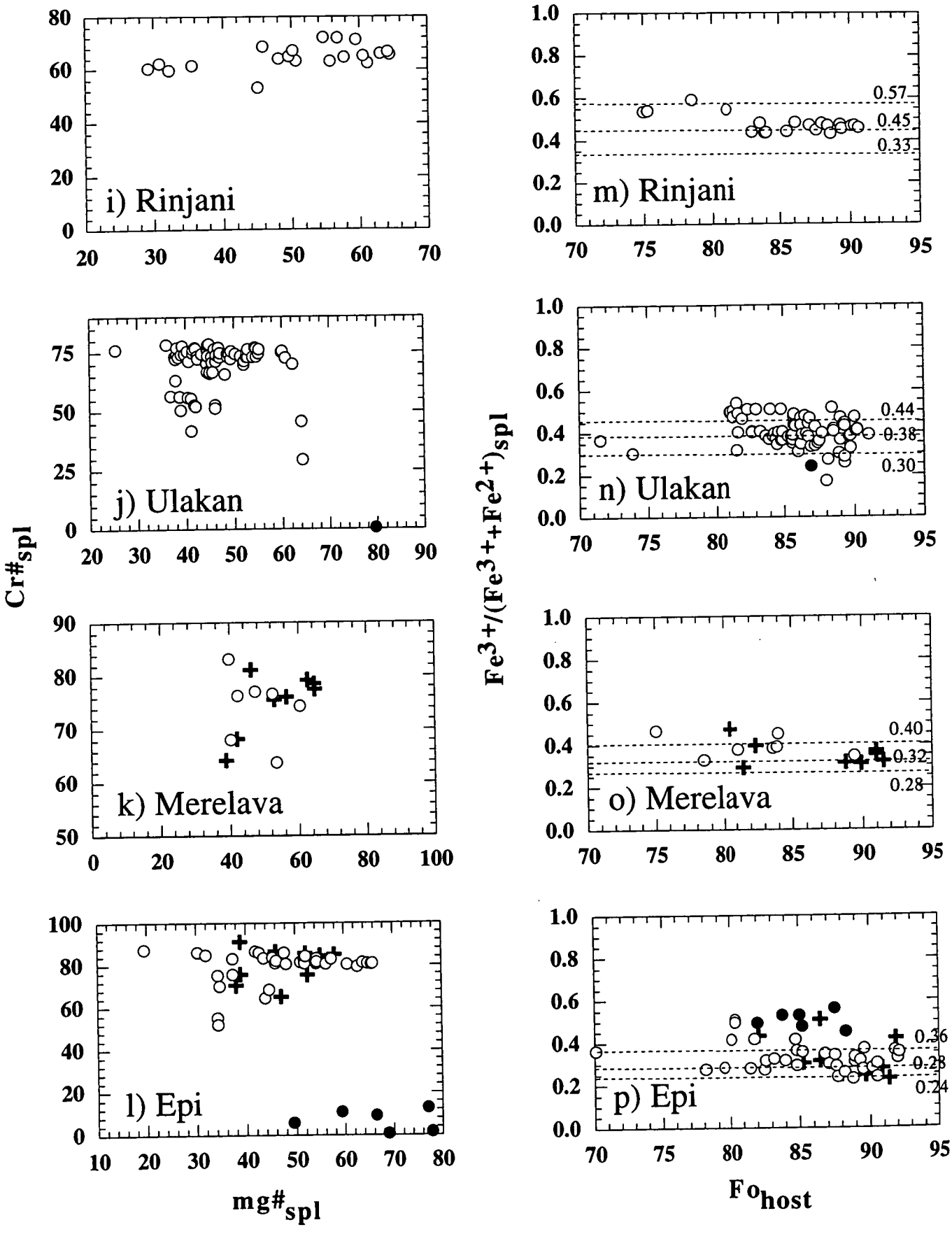

Figure 2.11 continued. i) to l) $Cr\#_{spl}$ *versus* $Mg\#_{spl}$, m) to p) $Fe^{3+}/(Fe^{3+}+Fe^{2+})_{spl}$ *versus* Fo_{host}. Dashed lines in m) to p) indicate the range of $Fe^{3+}/(Fe^{3+}+Fe^{2+})_{spl}$ value used for Fe_2O_3/FeO_{melt} determination from each location (Table 2.4).

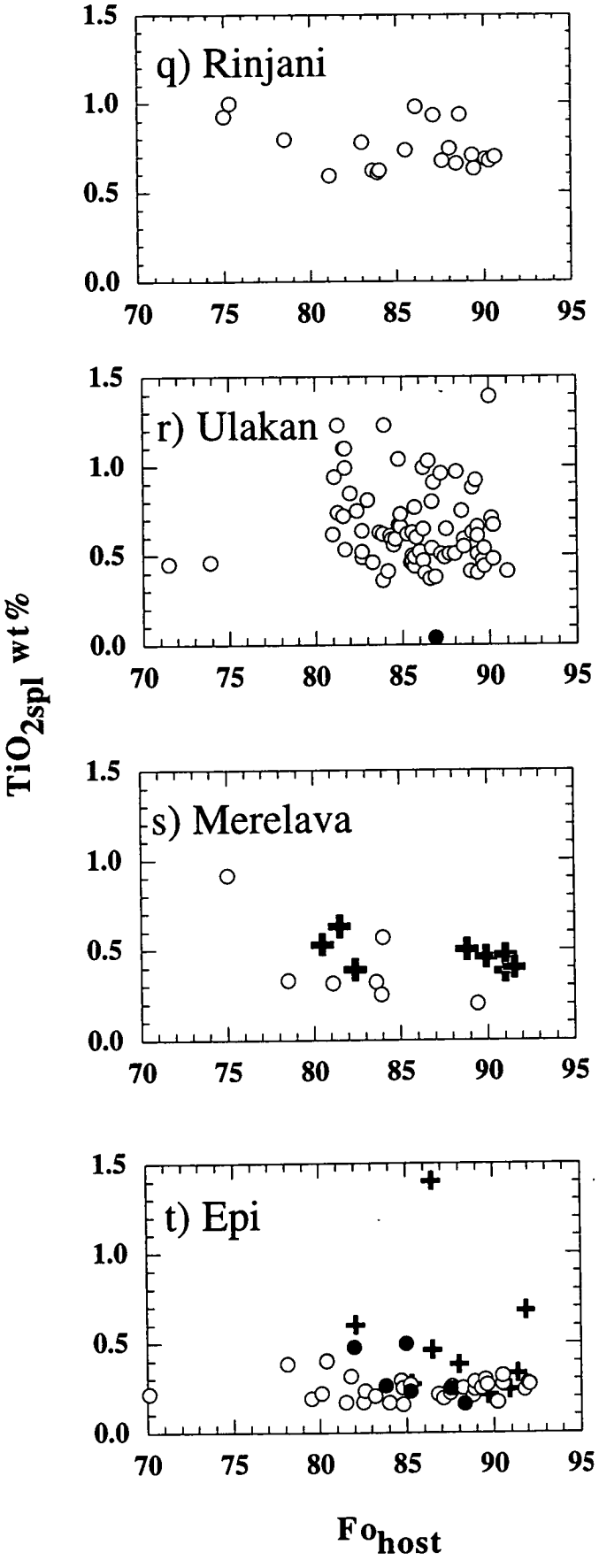

Figure 2.11 continued. q) to t) TiO_{2spl} *versus* Fo_{host}.

and are used in Chapter 4 for the recalculation of melt inclusion compositions. The estimated Fe_2O_3/FeO_{melt} values are, Rinjani ~0.30, Ulakan ~0.20, Merelava ~0.15 and Epi ~0.12.

TABLE 2.4

Suite	$Fe^{3+}/\Sigma Fe_{spl}$	Fe_2O_3/FeO_{spl}	Fe^{2+}/Fe^{3+}_{spl}	Fe^{2+}/Fe^{3+}_{melt}	Fe_2O_3/FeO_{melt}
	0.57	1.47	0.75	1.94	0.57
Rinjani	**0.45**	**0.91**	**1.22**	**3.66**	**0.30**
	0.33	0.55	2.03	7.10	0.16
	0.44	0.87	1.27	3.86	0.29
Ulakan	**0.38**	**0.68**	**1.63**	**5.34**	**0.21**
	0.3	0.48	2.33	8.52	0.13
	0.4	0.74	1.50	4.78	0.23
Merelava	**0.32**	**0.52**	**2.13**	**7.54**	**0.15**
	0.28	0.43	2.57	9.68	0.11
	0.36	0.63	1.78	5.97	0.19
Epi	**0.28**	**0.43**	**2.57**	**9.68**	**0.11**
	0.24	0.35	3.17	12.71	0.09

Calculated range in Fe_2O_3/FeO_{melt} values from olivine-spinel inclusion pairs (Maurel & Maurel 1982) used in Chapter 4 for the recalculation of melt inclusion compositions.

2.5.4 Primary melt inclusions

Olivine and clinopyroxene phenocrysts within ankaramite contain crystalline and glassy primary melt inclusions (Figures 2.12a-c). Primary inclusions vary from abundant to absent within a single grain from any sample. Generally inclusions hosted by olivine are most common in ankaramite from the Ulakan Formation, less common in ankaramite from Rinjani, and rare in ankaramites from Merelava and Epi. The sizes of inclusions range between 20 to 40 μm and very rarely exceed 100 μm. The larger inclusions contain a shrinkage bubble whereas smaller melt inclusions (<10 μm) tend to be glassy and lack a shrinkage bubble. Daughter phases in crystalline melt inclusions are always clinopyroxene and tend to form aggregates of tiny crystals (Figure 2.12a-b). Daughter olivine crystallizes on the walls of all inclusions hosted by olivine.

Crystalline melt inclusions are more common in magnesian olivine phenocrysts (~Fo≥88) whereas glassy melt inclusions tend to be more typical in less magnesian olivines. This association reflects the differences in cooling rates (Roedder 1984) that can be reconciled with the residence time of olivine phenocrysts in the magma chamber. Melt inclusions trapped during the formation of early magnesian olivine phenocrysts are likely to undergo crystallization in a slowly cooling magma chamber and therefore form crystalline textures. Melt inclusions in less magnesian olivines erupted shortly after trapping undergo rapid cooling and are therefore likely to have glassy textures.

Composite inclusions consist typically of an accidentally trapped chromian spinel crystal together with variable proportions of melt, and an associated shrinkage bubble (i.e., S+L+V, Figure 2.12d-e). In some cases, composite inclusions only consist of spinel and vapour (S+V). These types of inclusions are described below and suggest the presence of a separate fluid phase in the magma as a result of saturation.

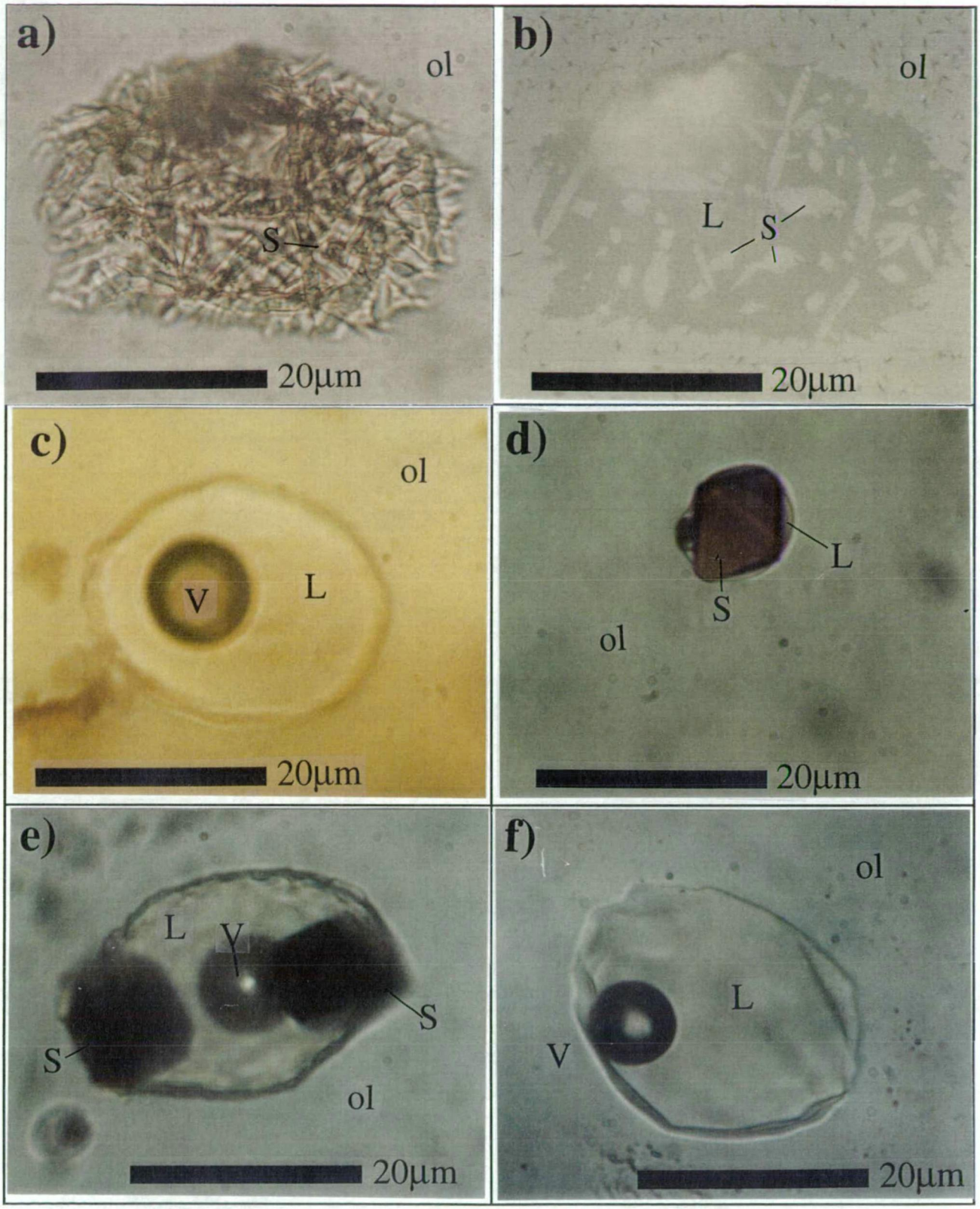

Figure 2.12 Photomicrographs of common primary inclusion types in olivine (ol) phenocrysts from ankaramite. Bar length represents approximately 20 µm.

a) "Crystalline" melt inclusion. S= daughter clinopyroxene. Daughter olivine has possibly crystallized on the wall of the inclusion. Sample 31551 from Merelava, plane polarized light (PPL), 100x.

b) Same inclusion in (a) showing visible daughter crystals under reflected light, 100x.

c) "Glassy" melt inclusion. L=melt, V=shrinkage bubble. Sample 31551 from Merelava, PPL, 100x.

d) "Composite" inclusion. S=chromian spinel octahedra, L=melt. Sample UTas67424 from Ulakan, PPL, 100x.

e) "Composite" inclusion. S=chromian spinel, L=melt, V=shrinkage bubble. Sample UTas67424 from Ulakan. PPL, 100x.

f) optically homogenized ("heated") melt inclusion hosted in olivine. Tq=1250°C. Sample UTas48001 from Rinjani, PPL, 100X.

2.5.5 Primary fluid inclusions

Primitive ankaramite samples were initially studied using grain mounts and doubly polished thin-sections ~250 μm thick. Primary fluid inclusions were found adjacent to chromian spinel inclusions in olivine phenocrysts from ankaramites of the Rinjani volcano, Ulakan Formation and Merelava (Figure 2.13). These V+S type inclusions suggest volatile saturation of the melt. A DILOR MICRODIL-28® Laser Raman microprobe at the Australian Geological Survey Organisation (AGSO), Canberra, was used to scan for CO_2 and CH_4 fluid species in the fluid bubble of V+S type inclusions (Figure 2.13a-f) and in the shrinkage bubbles of L+V type inclusions (Figure 2.12c) trapped in olivine phenocrysts (Fo_{88-90}) from the Rinjani ankaramite. CO_2 was present in V+S type inclusions but none was detected in shrinkage bubbles of L+V type (Figure 2.14). CH_4 was not detected in any of the inclusions.

These reconnaissance results suggest that the Rinjani ankaramite magma was saturated in CO_2-bearing fluids early in its evolution. This interpretation can be extended to the ankaramite suites from Ulakan and Merelava, where similar V+S primary inclusions are also found (Figure 2.13d-f). Although CO_2 was not detected in shrinkage bubbles, this may in part be due to low concentrations of CO_2 present, as well as the small volume of the analysed bubble (diameter <1 μm).

2.6 Crystallisation sequence of ankaramites

Barsdell (1988) and Barsdell & Berry (1990) found no evidence for early crystallization of clinopyroxene prior to olivine in ankaramites from Merelava or Epi. They conclude that olivine co-precipitated with clinopyroxene even in the most magnesian samples (BC-13 and UTas71046) where olivine Fo_{92} coexists with clinopyroxene of $Mg^{\#}$ 94. Co-precipitation of olivine and clinopyroxene in the Vanuatu mafic ankaramite samples is also suggested by the near constant CaO contents of olivine phenocryst with decreasing Fo (Figure 2.6c-d). If the most magnesian olivines had crystallized before clinopyroxene, CaO contents of these olivines would first increase as their Fo decreased, and then decrease when clinopyroxene joined olivine as a crystallizing phase. Thus the decline in the CaO content of olivine phenocrysts within the ankaramite from Rinjani at approximately ~$Fo_{89.5}$ and in the Ulakan Formation at approximately ~Fo_{90} (Figure 2.6a-b), suggests that these two suites crystallized olivine before clinopyroxene. Only four olivine-clinopyroxene inclusion pairs were found in these suites; one in Rinjani and three in the Ulakan Formation. In Rinjani, $Fo_{85.2}$ contains a clinopyroxene with $mg^{\#}$ 91.0, whereas the most magnesian pair from Ulakan has clinopyroxene with $mg^{\#}$ 93.8 in $Fo_{90.1}$. These inclusion pairs are insufficient to confirm the late appearance of clinopyroxene but, nevertheless their Fo_{host}-$mg^{\#}_{cpx}$ values are consistent with established relationships of co-magmatic inclusion (Figure 2.15). Chromian spinel occurs as co-magmatic inclusions throughout a range of olivine crystallization ranging from most magnesian (Fo_{91-93}) down to ~Fo_{75} in Rinjani, ~Fo_{81} in Ulakan, ~Fo_{75} in Merelava and ~Fo_{79} in Epi (Figure 2.11a-d). The decline in the Al_2O_3 content of clinopyroxene indicates that plagioclase commenced crystallization at around ~$Mg^{\#}_{cpx}82$ in Merelava and Epi (Barsdell & Berry 1990 and Figure 2.16c-d) and below ~$Mg^{\#}_{cpx}80$ in Rinjani and Ulakan (Figures 2.16a-b).

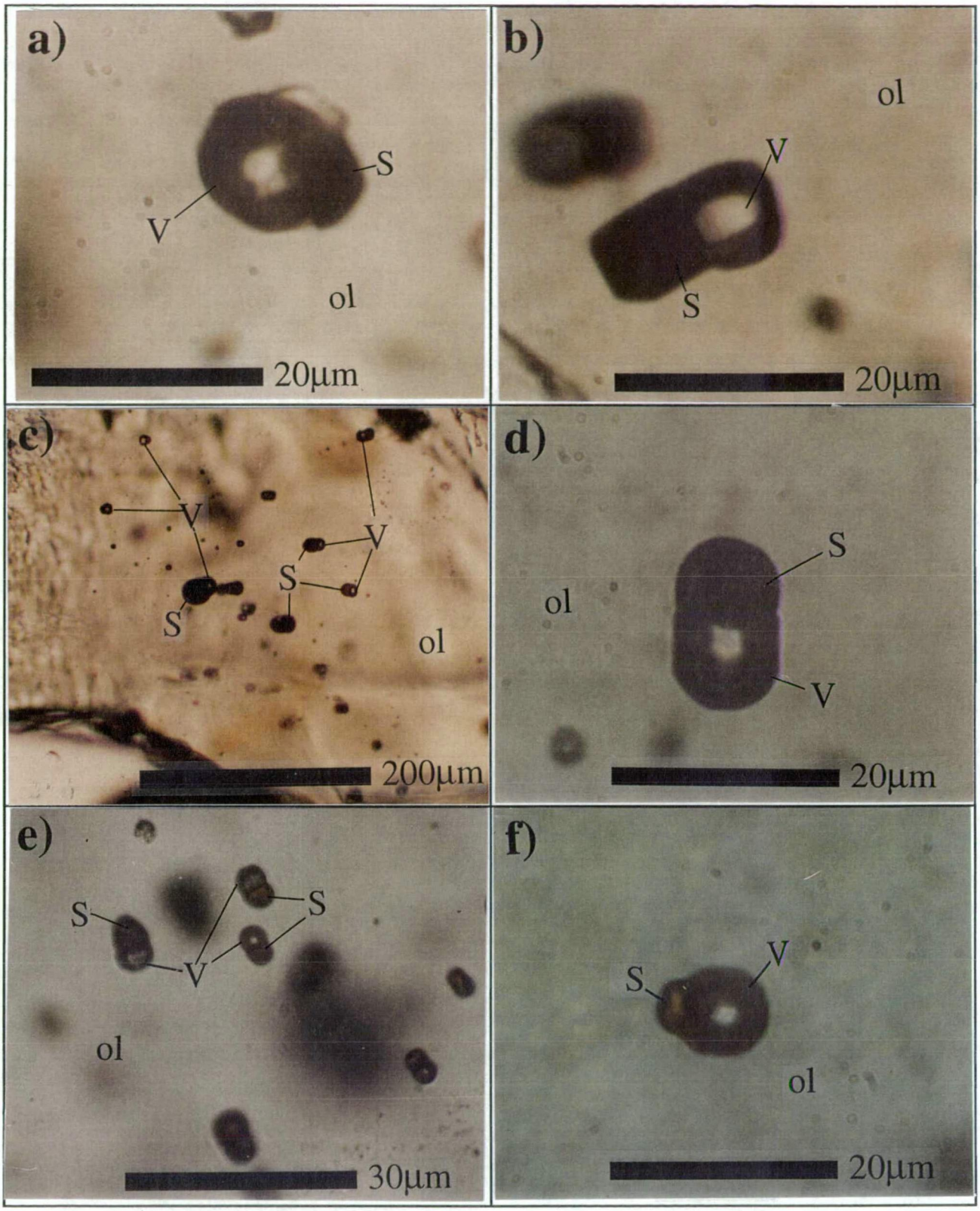

Figure 2.13 Photomicrographs of typical primary fluid inclusion types found in olivine (ol) phenocrysts of ankaramite.
a-b) "Composite" primary V+S type inclusions. Sample UTas48001, PPL, 100x.
c) Co-existing composite primary V+S type inclusions. Sample UTas48001 from Rinjani, 10x, PPL.
d) "Composite" primary V+S type inclusion. Sample UTas67424 from Ulakan, 100x, PPL.
e) Co-existing composite primary V+S type inclusions. Sample UTas67424 from Ulakan, 40x, PPL.
f) "Composite" primary V+S type inclusion. Sample 31551 from Merelava, 100x, PPL.
S= chromian spinel, V=fluid bubble.

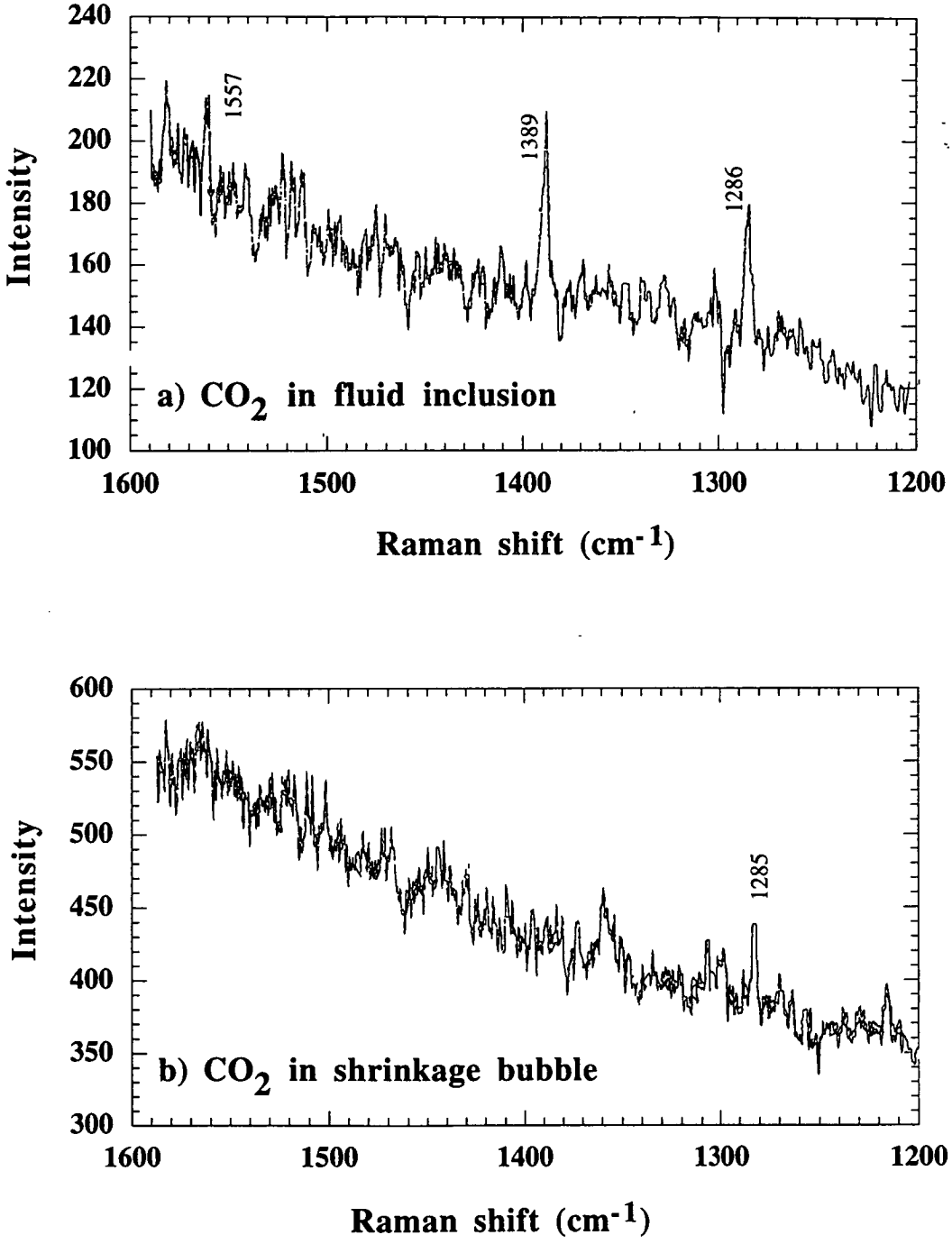

Figure 2.14 Laser Raman scan for CO_2 in a) the fluid bubble of a composite V+S+L type inclusion and b) the shrinkage bubble of a primary melt inclusion. Both inclusions are within olivine phenocrysts (~Fo_{89}) from the ankaramite suite of Rinjani volcano (sample UTas48001). CO_2 was not deteted in the shrinkage bubbles of the melt inclusions, but is present in primary fluid inclusions types. Laser power 400mW (on sample) with ~3 cm^{-1} band pass. Spectra are averaged from 10 accumulations at 10 second counting times.

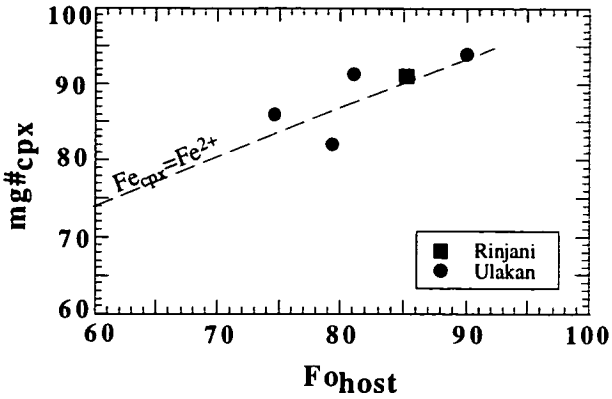

Figure 2.15 mg#=100Mg/(Mg+Fe^{2+}) *versus* Fo content of the host of clinopyroxene inclusions in olivine phenocrysts from the ankaramite suites of Rinjani volcano (square) and Ulakan Formation (circles). Fe^{3+} in clinopyroxene calculated assuming perfect stochiometry (Robinson 1989). Dashed line indicates established olivine-clinopyroxene relationship from Barsdell (1988).

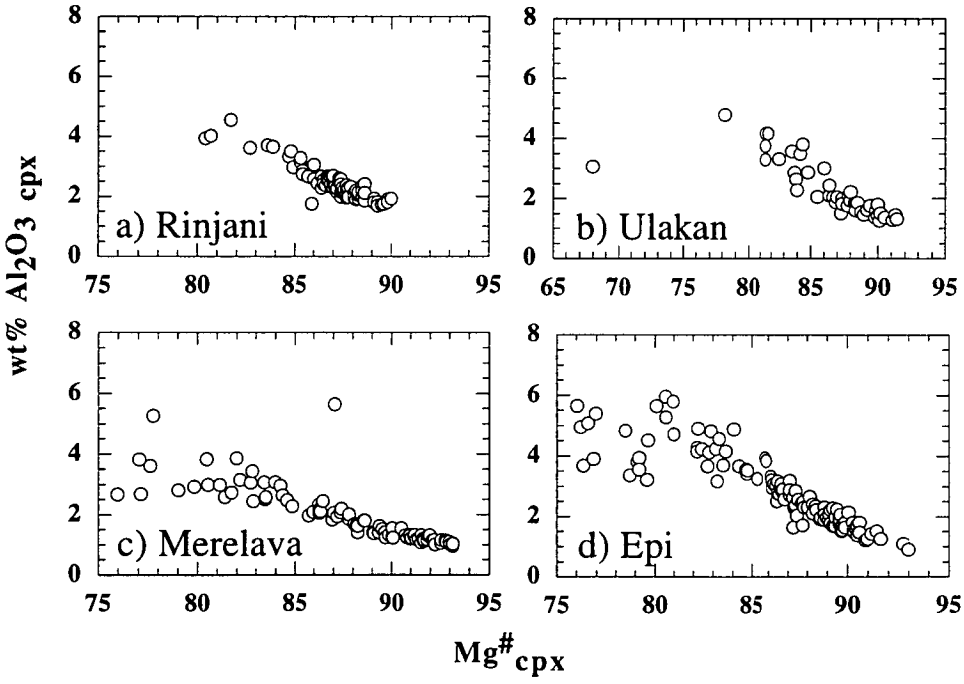

Figure 2.16 Variation in wt% Al_2O_3 *versus* $Mg^{\#}$ (=100Mg/(Mg+Fe*)) of clinopyroxene phenocrysts in the ankaramite suites from a) Rinjani volcano, b) Ulakan Formation, c) Merelava and d) Epi.

In summary, olivine is considered an early crystallizing phase with chromian spinel only in the ankaramite suites from Rinjani and Ulakan. In Rinjani suite, clinopyroxene appears in the crystallization sequence at around $Fo_{89.5}$ and in the Ulakan suite at around Fo_{90}. Plagioclase appears late in the crystallization sequence of all suites. In the ankaramites from Merelava and Epi, olivine and clinopyroxene are co-crystallizing phases.

2.7 Summary

Olivine and chromian spinel are early crystallizing phenocryst phases in the ankaramite suites of Rinjani and Ulakan. Clinopyroxene joins the crystallization sequence after olivine and and is followed by plagioclase. Comparatively, the ankaramite suites from Vanuatu indicate that olivine and clinopyroxene are both early co-crystallizing phases. If basaltic magmas fractionate by continuous crystal setting, then all phenocrysts present in the magma should show a small compositional range. This type of crystallization does not apply for the primitive ankaramite rocks described here. Instead, their range in composition (e.g., Fo_{74-92} and $Mg^{\#}_{cpx}$80-93) indicates that early formed phenocrysts remained in the magma as they crystallized. Thus, the range in phenocryst composition observed in these highly porphyritic rocks suggests that crystallization could have occurred in situ.

The most magnesian samples in each ankaramite suite will be compared in Chapter 3, on the basis of wholerock and melt inclusion compositions. This comparison is aimed at determining the extent to which the composition of the parental melt has been modified by crystal fractionation. Primary melt inclusions in the magnesian olivines are, however, crystalline rather than glassy and therefore direct microprobe analysis is not possible. This problem is overcome with a melt inclusion homogenization technique (Chapter 3), whereby daughter phases within the inclusion are remelted by heating and then quenched to a homogeneous glass for microprobe analysis. Primary fluid inclusions trapped in olivine phenocrysts suggest the presence of CO_2-bearing fluids early in the crystallization history of the ankaramite magma. The implications will be considered in Chapter 3.

Chapter 3: Primitive ankaramitic melts in volcanic arcs: evidence from melt inclusions

3.1 Introduction

A crucial task in petrogenetic studies of ankaramite rocks has been to determine whether geochemical characteristics such as high CaO/Al_2O_3 values (>1), represent those of the melts from which they formed, or instead is the result of clinopyroxene accumulation (Chapter 1). In this Chapter, this problem is tackled directly by investigating the compositions of melt inclusions in four primitive ankaramite suites.

The study of melt inclusions has been widely documented[1], and provides a tool to explore the early stages of magma evolution. After melt entrapment however, the continued crystallization of the host and other daughter phases within the melt inclusion modify the composition of the trapped melt. This problem is circumvented here using a melt inclusion heating stage at the University of Tasmania, based on the design of Sobolev *et al.* (1980). In this technique, daughter phases are redissolved and the homogeneous melt quenched to a glass that can be later prepared for electron microprobe analysis. This technique has been extensively described by other authors (Sigurdsson 1994, Sobolev & Danyushevsky 1994) and is only briefly described in section 3.3.

Ideally, the composition of homogenized melt inclusion glasses should resemble the original composition of the trapped melt. In practice however, the composition of these glasses may differ from the original due to diffusion and re-equilibration of the melt with the host, before eruption. (Sobolev & Danyushevsky 1994). The interpretation of these bulk glass analyses may therefore in some cases, be limited. Nonetheless, the ratios of incompatible major elements in these glasses are not changed by this technique, and may be used to recognize primitive chemical characteristics of the parent melt[2]. In particular, melt inclusions in magnesian olivine phenocrysts provide a direct tool to investigate the range of high CaO/Al_2O_3 values in the parent melts of ankaramite rocks. Inclusions hosted by clinopyroxene and spinel are not as suitable for this purpose because their CaO/Al_2O_3 values are be easily modified if crystallisation of the host occurs.

The rationale of this melt inclusion study is the following: if ankaramite rocks represent an ordinary basalt enriched in clinopyroxene, melt inclusions should have picritic CaO/Al_2O_3 values (i.e., ~1 or less). Conversely, if ankaramite rocks are derived from melts with ankaramitic

---

[1] e.g, Roedder (1971 1979, 1984), Anderson (1974), Watson (1976), Weiblen (1977), Clocchiatti & Massare (1985), Sobolev *et al.* (1991), Jambon *et al.* (1992), Sisson & Layne (1993)

[2] e.g. Anderson & Wright (1972), Donaldson & Brown (1977), Dungan & Rhodes (1978), Falloon & Green (1986), Sullivan (1991), Sigurdsson (1994), Sobolev & Danyushevsky (1994)

characteristics, the melt inclusion in primitive olivine phenocrysts (~Fo>90) should have CaO/Al_2O_3 values higher than picrite (i.e., >1) and similar to those of the rock sample.

In this chapter it is suggested that primitive ankaramite rocks are derived from primitive ankaramitic melts with CaO/Al_2O_3 values >1. A model is described in which primitive ankaramitic magmas form from an aggregate of silica-undersaturated primitive melts with variable CaO/Al_2O_3 values as opposed to clinopyroxene accumulation. Part of the material presented in this chapter has been published in Della-Pasqua & Varne (1997).

3.2 Samples selected for this study

Ankaramites with olivine and clinopyroxene phenocrysts containing vitreous and crystalline inclusions were sampled from Rinjani volcano in Lombok, and from the Ulakan Formation in Bali, both from the Sunda island arc, and from Merelava and Epi islands, both from the Vanuatu island arc. Each of these four ankaramitic suites and samples studied are fully described in Chapter 2 and their sample numbers listed in Table 2.1. Types of melt inclusions found in these rocks are described in Section 2.5.

3.3 Experimental methods

This study focuses on the compositions of silicate melt inclusions in magnesian olivine and some clinopyroxene phenocrysts from ankaramite samples. Grains with primary melt inclusions were selected for experimental work and extracted from their probe mounts for further study and homogenization. Sample preparation procedures were described in Section 2.3.

3.3.1 The homogenization technique

Experiments were carried out using a melt inclusion heating stage at the University of Tasmania, based on the design of Sobolev *et al.* (1980) which allows visual monitoring and manual control of temperature during heating. Each inclusion-bearing grain is progressively heated in an ultra-pure He atmosphere while the melting behaviour of the inclusion is observed and the temperature at which the various phases disappeared is recorded. This technique is most appropriate for fluid-saturated melts because it relies on fluid bubble disappearance to dictate the point of homogenization. After trapping, crystallization on to the walls of the inclusion leads to a decrease in pressure that causes this bubble to nucleate. During a homogenization experiment, pressure inside the inclusion increases as daughter phases dissolve, and the bubble will disappear when the pressure inside the inclusion is equal to the pressure at the moment of trapping. At this moment all daughter phases that formed during cooling are molten and the composition of the melt theoretically corresponds to the composition of the trapped melt. At this stage the melt inclusion is "homogenized" and it can be quenched to a glass for microprobe analysis.

In the ankaramitic melt inclusions studied here, complete homogenization was not achieved, and bubbles remained as a separate phase even after considerable overheating (~1400°C). This suggests volatile oversaturation as also suggested by the presence of fluid bubbles attached to chromian spinel inclusion in olivine (Figure 2.13). Kinetic effects however may also play a

significant role in preventing complete homogenisation of the melt inclusion (Danyushevsky *et al.* 1992, Gurenko *et al.* 1992). This problem compromised the use of standard homogenization techniques that depend on bubble disappearance as an indicator of homogenization, and led instead, to the use of an "optical homogenization" technique in this work.

3.3.2 Optical homogenization technique

In this technique melt inclusions are individually heated up to temperatures at which the last daughter crystals are observed to melt, therefore becoming optically homogeneous (Gurenko *et al.* 1988, 1992, Hansteen 1991, Sobolev *et al.* 1990). Once optical homogenization of the inclusions has been achieved in the experiment, the host grains are quickly cooled, and the molten inclusion quenched to homogeneous glass. The host grains are then mounted in epoxy and individually sectioned and polished to expose the homogenized melt inclusions within them for electron microprobe analysis.

The composition of optically homogenized glasses however may still be modified by the incomplete remelting of the host on the wall or the melting of the host. Thus, the temperatures at which these melt inclusions were quenched (Tq), shown in Figure 3.1, are not necessarily representative of the magmatic temperatures at which the inclusions were trapped. The implications if this is discussed in Section 3.4.

3.3.3 Electron microprobe

Homogenized melt inclusions and host grains were analyzed using a CAMECA SX-50 electron microprobe at University of Tasmania, under analytical conditions described in Appendix 2.1. The beam size used on the melt inclusion glasses was restricted by the size of the inclusions, occasionally 100 μm but average 30 to 50 μm in diameter. The risk that the excited volume of the electron beam might interact with the host grain, when small melt inclusions were being analyzed, was reduced by using a focussed beam in the centre of the inclusion. An allowance of 5 μm was adopted for edge effects based on the results of microprobe traverses across melt inclusions by Roedder (1979) and Sullivan (1991). Melt inclusions with diameters less than ~20 μm were not analyzed and the smallest beam size used on the quenched glass was 4 μm. After each analysis, the correct positioning of analytical points was checked and inspected for any likely interaction of the electron beam with the host grain. Provided the melt inclusions are sufficiently large (>10μm) the use of transmitted and reflected light images in conjunction with the back-scattered electron image makes the selection and correct positioning of analytical points in exposed melt inclusions a relatively simple procedure.

Volatilization under these beam conditions was assessed following methods described by Falloon & Green (1987), Sisson & Layne (1993) and Spray & Rae (1995) in which spot and broad area analyses of a glass standard are compared with its known bulk composition. Table 3.1 shows analyses of glass standard VG-A99 (USNM113498/1, Jarosewich *et al.* 1980) using 1, 4 and 10 μm beam sizes. Na_2O and K_2O values under focussed beam conditions and 10 μm beam size agree with standard values shown in Table 3.1. With a 4 μm beam size, Na_2O

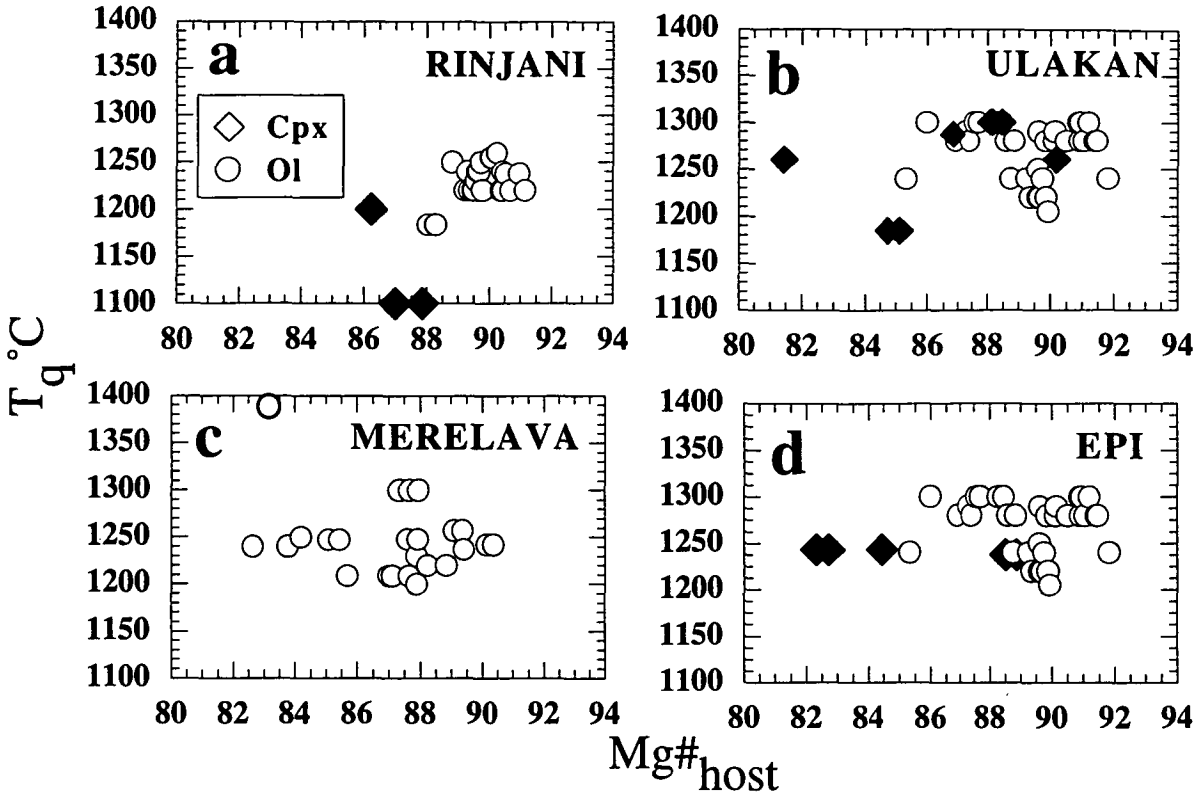

Figure 3.1 Temperature of quenching (Tq) of heated melt inclusions *versus* Mg# (=100Mg/Mg+Fe*) of the host olivine (circles) and clinopyroxene (filled diamonds) phenocrysts. Filled circle in c indicates overheated melt inclusion to 1390°C.

TABLE 3.1

	1 μm			4 μm			10 μm			VG-A99**
	av.	std.		av	std.		av.	std.		
SiO_2	51.13	0.25	*51.53*	50.58	0.26	*51.57*	50.59	0.21	*51.56*	50.94 *51.36*
TiO_2	3.99	0.08	*4.02*	4.00	0.12	*4.08*	4.04	0.09	*4.12*	4.06 *4.09*
Al_2O_3	12.35	0.26	*12.45*	12.14	0.05	*12.38*	12.08	0.41	*12.31*	12.49 *12.59*
FeO*	13.34	0.63	*13.45*	13.38	0.59	*13.64*	13.22	0.38	*13.47*	13.30 *13.41*
MgO	5.08	0.55	*5.12*	4.79	0.35	*4.89*	5.01	0.13	*5.10*	5.08 *5.12*
CaO	9.47	0.58	*9.54*	9.25	0.24	*9.43*	9.25	0.08	*9.42*	9.30 *9.38*
MnO	0.26	0.03	*0.26*	0.24	0.05	*0.24*	0.25	0.04	*0.26*	0.15 *0.15*
Na_2O	2.44	0.15	*2.46*	2.53	0.05	*2.58*	2.57	0.12	*2.62*	2.66 *2.68*
K_2O	0.73	0.08	*0.74*	0.76	0.04	*0.77*	0.78	0.04	*0.80*	0.82 *0.83*
P_2O_5	0.43	0.02	*0.44*	0.41	0.03	*0.42*	0.34	0.18	*0.35*	0.38 *0.38*
Sum	99.21			98.07			98.12			99.18

Microprobe analyses of basaltic glass standard VG-A99 at 1, 4 and 10 μm beam size. Operating conditions: 15 kV accelerating voltage, 10 nA beam current, 20 seconds counting times except Na_2O (10 seconds), focussed beam. av.= average of 10 analyses, std.= standard deviation. Numbers in italics are averages summed to 100%. (*) All iron as FeO. (**) Standard glass USNM113498/1, Joresewich *et al* . (1980).

and K_2O values are only slightly lower than standard, by ~0.1 wt%, (Table 3.1). With a beam size of 1 μm, Na_2O contents are ~0.2 wt% lower than the standard value.

Analytical conditions for glasses adopted in this study may therefore cause some loss of alkalis but this loss is insufficient to invalidate the conclusions reached here. These analytical conditions reduce the potential risk of edge effects introduced by a defocussed beam on small melt inclusion sizes. Compositional homogeneity of the glass was confirmed wherever possible by analysing the centre and rim of melt inclusions.

3.4 Assessment of experimental results

The main experimental uncertainty encountered in determinations of the composition of the melts that were originally trapped in the phenocrysts is related to the "optical homogenization" technique adopted in this study. This uncertainty results because the host continues to crystallize within the melt inclusions during post-entrapment cooling. Within melt inclusions hosted by olivine phenocrysts for example, olivine is deposited as a thin shell on the walls of the melt inclusion. This shell is difficult to distinguish optically, from the primary host olivine. With the "optical homogenization" technique employed here (Section 3.3.2), some of this olivine shell might not all be remelted during experimental heating. Alternatively, some of the host olivine phenocryst might instead be melted into the melt inclusion because of overheating. Similarly, if a melt inclusion in clinopyroxene was overheated, the melt derived from the host might be added to the inclusion. Conversely, underheating might result in incomplete remelting of clinopyroxene from the walls. Thus the composition of melt inclusions that were heated using this optical homogenization technique may still be affected by post-entrapment crystallization of the host on the walls and thus their compositions may not be directly representative of the trapped melt. Several tests performed on the analytical data (Appendix 3) confirm that this problem has occurred and are summarized below.

(1) If at the moment of melt-entrapment, the growing phenocrysts are at chemical equilibrium with the surrounding melt in the magma, then the composition of the successfully homogenized melt inclusions should also be at equilibrium with their hosts. This equilibrium can be checked using the mineral-melt thermometer of Ford *et al.* (1983) which calculates the dry-liquidus temperature (T_c°C) from the compositions of olivine-melt pairs. Thus, in a homogenized inclusion, T_c is equal to the temperature of quenching (T_q), provided that the melt was dry. If volatiles were present in the trapped melt, then homogenization should occur at lower temperatures and therefore T_q will be less than T_c. T_c is only lower than T_q when bad quenching occurs. During bad quenching, olivine grows on the walls of the inclusion and depletes the melt in olivine component, which therefore gives lower calculated liquidus temperatures. The melt inclusion data is now assessed considering these three possibilities.

Figure 3.2a is a T_c *versus* T_q diagram illustrating all three cases described above. The calculated temperatures (T_c) of optically homogenized melt inclusions from all four suites are plotted using a range of Fe_2O_3/FeOmelt values (Section 2.5.3) against Tq in Figure 3.2c-f. Most melt inclusions have T_c lower than T_q indicating bad quenching. An extreme example of bad quenching is illustrated by a melt inclusion from Merelava, which was quenched at a temperature of 1390°C but

has a T_c of ~1150°C. Some melt inclusions have T_q lower that T_c and suggest the presence of volatiles in the melt. Runs least affected by quenching have T_c varying from ~20°C below the dry-liquidus in Epi, up to ~150°C in Ulakan.

(2) The composition of optically homogenized melt inclusions hosted in olivine are, naturally, olivine-saturated and therefore their MgO contents are function of T_q. This relationship is illustrated in Figure 3.3 by a good correlation between MgO_{melt} and T_q in melt inclusion from all four suites. The composition of an overheated melt inclusion (T_q~1390°C) hosted in olivine ($Fo_{83.2}$) also lies well within this trend (Figure 3.3c). Superimposed on this trend however, is a variation in MgO_{melt} content at a constant T_q of up to 4 wt%. This variation in MgO is due to the growth of olivine during quenching and therefore indicates bad quenching.

(3) Inconsistency in the melt inclusion data is also indicated by uncorrelated MgO_{melt} *versus* $Mg^{\#}_{host}$ (Figure 3.1) and T_q *versus* $Mg^{\#}_{host}$ (Figure 3.4) values. The scatter in these plots is atypical of a melt with uniform composition, undergoing crystal fractionation. The range in T_q of up to 100°C at a constant Fo in Figure 3.1b is introduced by the optical homogenization technique adopted here and therefore leads to variable MgO_{melt} contents at a constant Fo (Figure 3.4b).

(4) Chemical Fe-Mg disequilibrium between the melt inclusion and host olivine is indicated by the large scatter at constant Fo of, calculated $K_D^{Ol\text{-}Melt}_{Fe\text{-}Mg}$ values (Figure 3.5c) and calculated equilibrium Fo values (Fo_c) (Figure 3.6). The calculated equilibrium olivine compositions of heated melt inclusions differ up to ±5 fosterite units from the host olivine phenocryst. Although this scatter may suggest that the melt inclusions were trapped by olivine xenocrysts, they more likely indicate that the compositions of these melts are removed from equilibrium with their host olivine.

As homogenization did not occur, the compositions of these melt inclusions cannot be used directly as representative of true melt compositions from which the ankaramite formed; and although optical homogenization was achieved, the tests 1 to 4 above demonstrate that these compositions are still modified by the crystallization of the host on the wall. Addition or substruction of olivine as a procedure to reconstruct the composition of heated melt inclusion by restoring their Fe-Mg equilibrium is possible (cf. Gurenko *et al.* 1988, 1992, Sobolev *et al.* 1990), but has one main drawback: the likelihood the melt inclusions were affected by "Fe-loss" before the magma was erupted.

Fe-loss is a phenomenon whereby Fe and Mg re-equilibration occurs between the fractionating residual melt within an inclusion and its host olivine at magmatic temperatures. The result of this re-equilibration is a loss of Fe from the melt before eruption. The re-equilibration process involves Fe, Mg diffusion, and is driven by the chemical disequilibrium between the host olivine and the residual melt as it undergoes fractional crystallization within the inclusion. A detailed description of this process given in Chapter 4. In Chapter 4 it will also be shown that most of the melt inclusions in this study are affected by Fe-loss and thus their composition cannot be simply recalculated by the addition or substruction of olivine. A program written by L.D. Danyushevsky is used to recalculate the composition of optically homogenized melt inclusions that are affected by Fe-loss. The recalculation

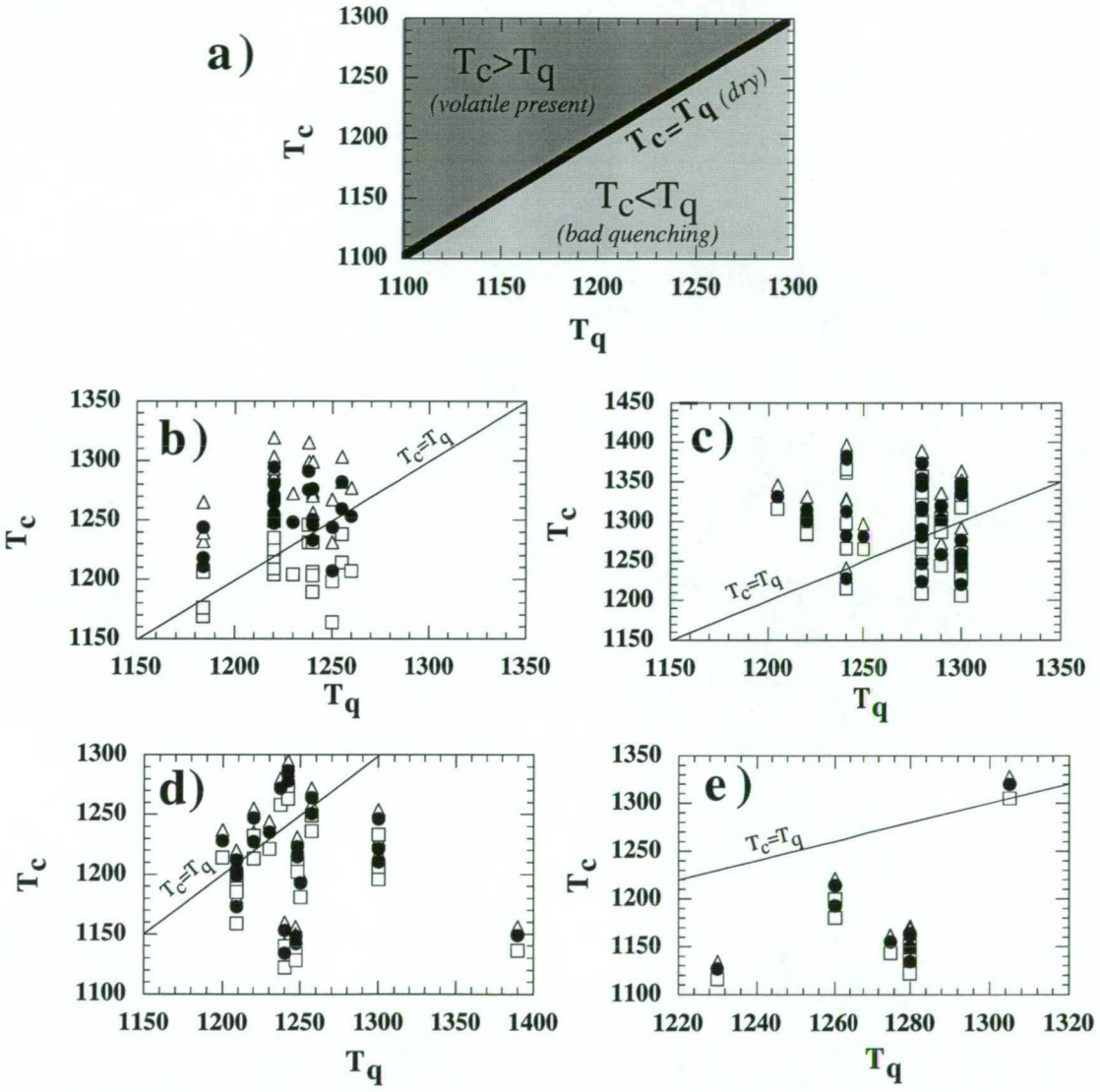

Figure 3.2 a) diagram illustrating the temperature fields of melt inclusions that are unhydrous (T_c=T_q, full line), contain dissolved volatiles (T_c>T_q, dark shaded area) or are affected by bad quenching (T_c<T_q, light shaded area). b-e) Variations of calculated melt temperatures (T_c) *versus* temperature of quenching (T_q) of opicaly homogenized melt inclusions hosted in olivine phenocrysts from ankaramites of b) Rinjani, c) Ulakan, d) Merelaba and e) Epi. T_c is calculated using the olivine-melt thermometer of Ford *et al.* (1983) for a range of Fe_2O_3/FeO_{melt} values (triangles=high, circles=average, square=low) as listed Table 2.4.

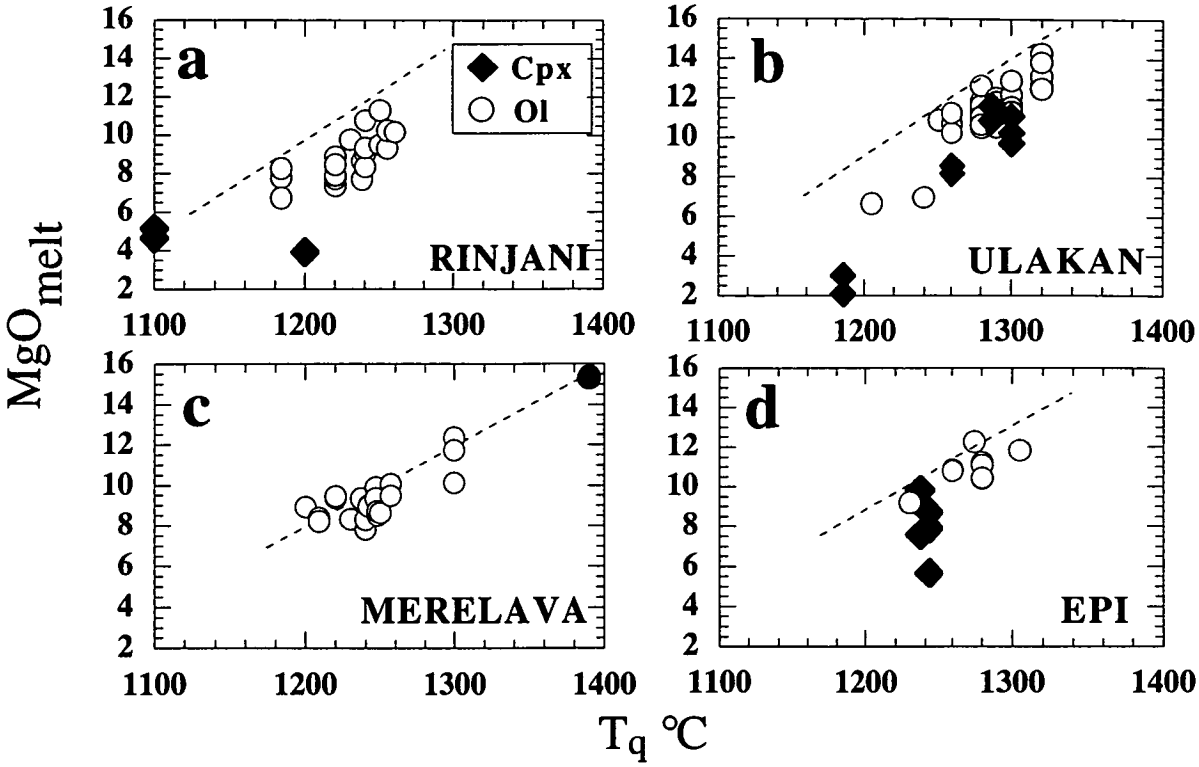

Figure 3.3 MgO content (wt%) *versus* temperature of quenching (Tq) of heated melt inclusions in olivine (circles) and clinopyroxene (diamonds) phenocrysts. Dashed lines show trend of increasing MgO with temperature for melt inclusions hosted in olivines. Note overheated melt inclusion to 1390°C in C (filled circle).

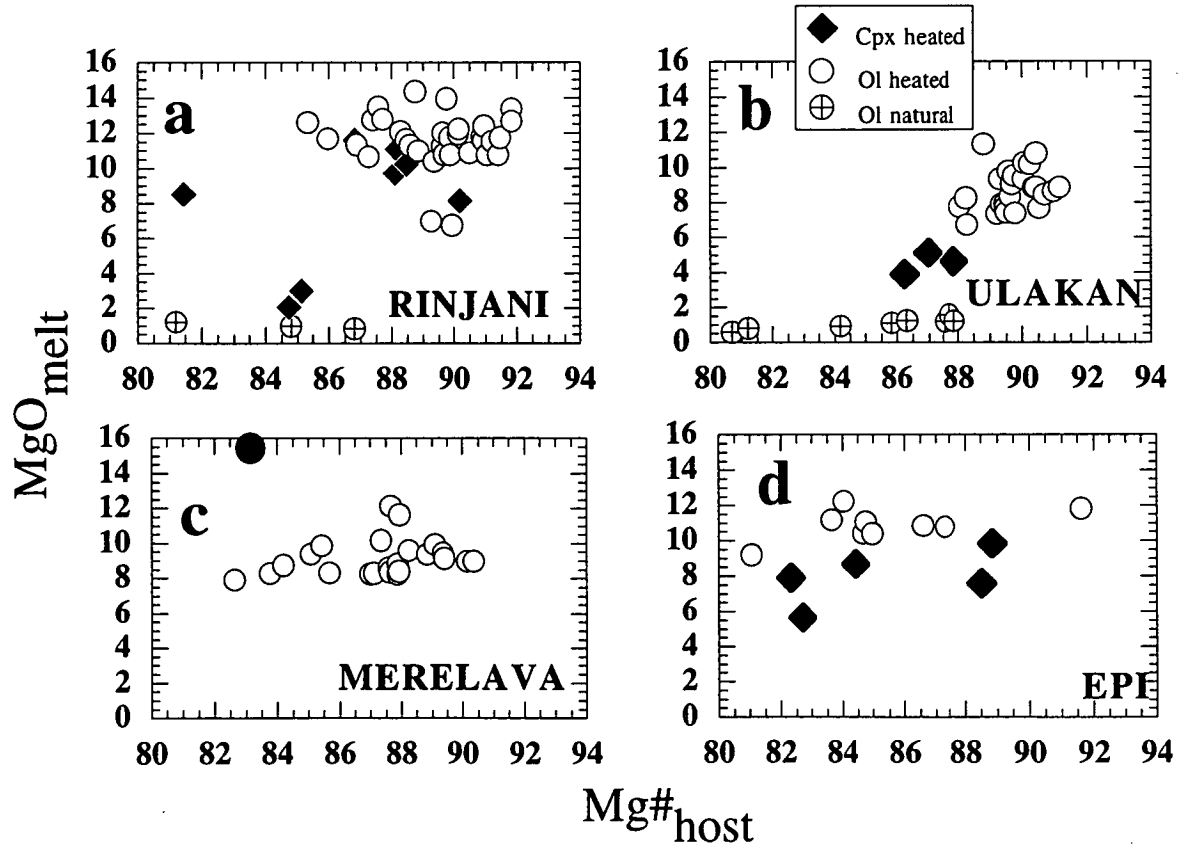

Figure 3.4 MgO content (wt%) of heated melt inclusions *versus* Mg# (=100Mg/Mg+Fe*) of their host olivine (circles) and clinopyroxene (diamonds) phenocrysts. Filled circle in c represents an overheated melt inclusion to 1390°C. Circles with crosses are naturally quenched melt inclusions in olivine.

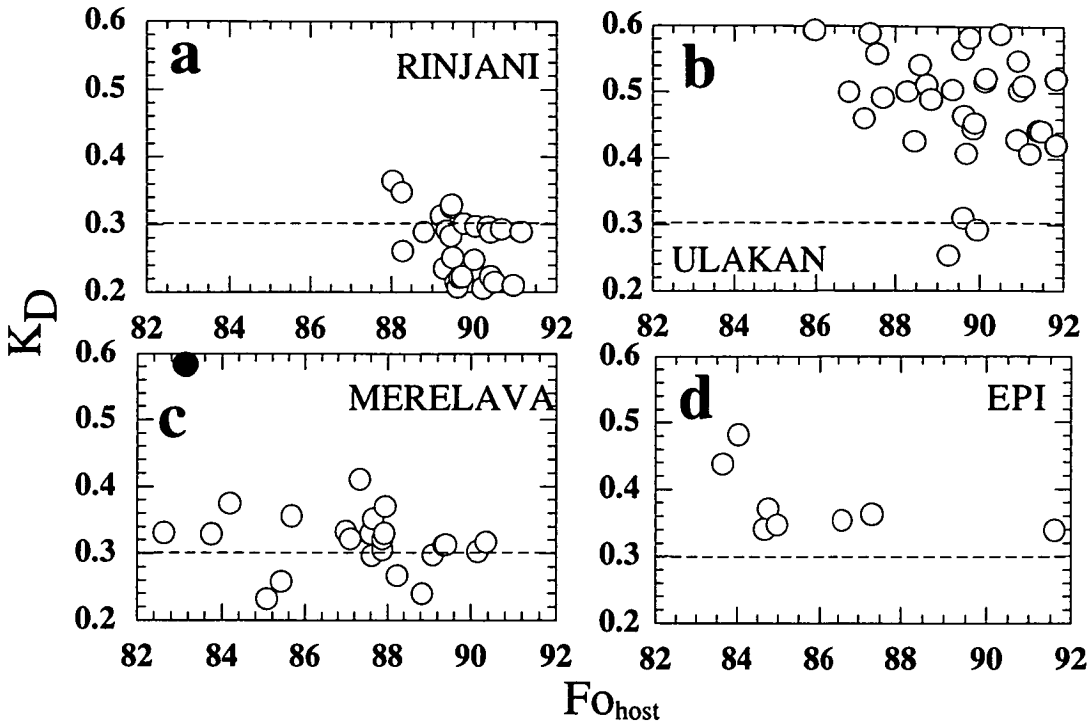

Figure 3.5 K_D values for Fe and Mg between heated inclusions and host olivine versus Fo. K_D calculated as $(Fe/Mg)_{ol}/(Fe^*/Mg)_{melt}$. Dashed line indicates K_D value of 0.3 (Roeder & Emslie 1970). Note overheated melt inclusion (1390°C) in C (filled circle).

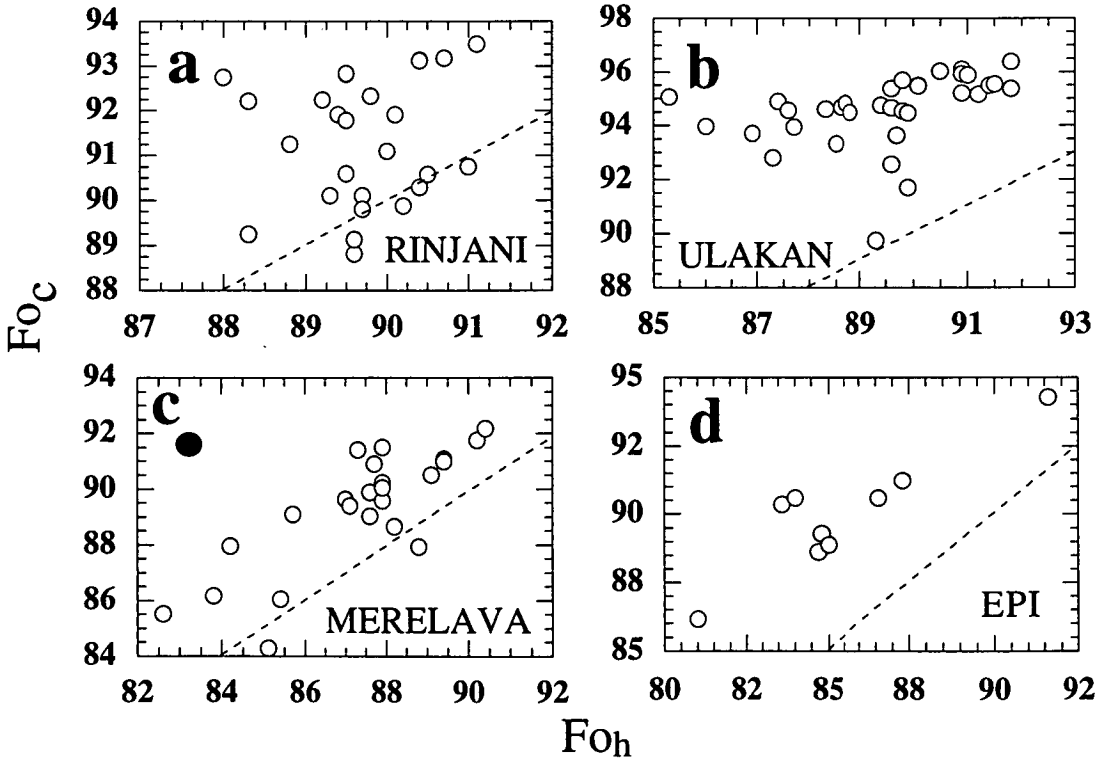

Figure 3.6 Calculated Fo content (Fo_c) in equilibrium with the composition of optically homogenized melt inclusion (Ford *et al.* 1983). Note overheated melt inclusion (1390°C) in c (filled circle).

procedure used in this program is also described in Chapter 4 and in Appendix 4. Results of this recalculation are listed in Appendix 3.1.

In short, the compositions of melt inclusions in these experiments are modified by two processes: (1) crystallization or melting of the host on the wall of the inclusion, and (2) loss of Fe-loss from the melt. The interpretation of bulk melt inclusion analyses in this work is therefore limited; however, the ratios of elements that are incompatible in olivine should not be affected. This study therefore focuses on the CaO/Al_2O_3 values of optically homogenized melt inclusions hosted in olivine. These values are unaffected by Fe-loss nor the addition and subtraction of olivine from the melt, and indicate ankaramitic affinities. The possible effects of underheating, overheating, and Fe loss on the melt inclusion data are described in the following sections.

3.5 Compositions of melt inclusions in olivine and clinopyroxene phenocrysts

The main aim of this chapter is to discover whether the melt inclusions trapped in the earliest-formed phenocrysts in the most primitive ankaramites have compositions with ankaramitic affinities, with characteristically high CaO/Al_2O_3 values (>1). Representative compositions of heated inclusions in olivine phenocrysts from primitive ankaramites are listed in Table 3.2 and the complete set of analytical data is given in Appendix 3.1. Composition of naturally quenched inclusions in olivine are listed in Table 3.3, and those of heated melt inclusions hosted in clinopyroxene in Table 3.4. These are described below as the compositions of glassy (naturally quenched) melt inclusions (Section 3.5.1), the compositions of heated (optically homogenized) melt inclusions (Section 3.5.2), and the compositions of heated melt inclusions following correction for the possible effects of iron loss (Section 3.5.3).

3.5.1 Glassy (naturally quenched) melt inclusions

Glassy melt inclusions in which the only daughter phases are olivine on the walls and quenched glass, were found in relatively low magnesian olivine phenocrysts from Rinjani and in olivine phenocrysts from Ulakan. In the ankaramite from Rinjani, glass inclusions were found only in olivine grains with composition of up to $Fo_{87.8}$ (analysis 1 to 8, Table 3.3). These inclusions attain maximum CaO/Al_2O_3 value of 1.09 (Figure 3.7a) and are not much higher than 1, as typical of ankaramite (Section 1.4). Primary melt inclusions in more Mg-rich olivines are crystalline, not glassy, and cannot be directly analysed by microprobe without further preparation. The positive correlation between CaO/Al_2O_3 values and Fo content (Figure 3.7a) suggests that higher values could be found in these more mg-rich olivines with Fo≥90. Moreover, this trend (Figure 3.7a) coincides with the wholerock trend defined by the Rinjani suite, demonstrating that CaO/Al_2O_3 values of the rock samples have not been significantly modified by crystal accumulation despite their highly porphyritic texture. Three glass inclusions from the Ulakan Formation were found in olivine with compositions with up to $Fo_{84.8}$ and attain a maximum CaO/Al_2O_3 value of 0.89 (analysis 10, Table 3.3) which is not typical of ankaramite. However these three inclusions are consistent with the whole-rock trend (Figure 3.7b) and it is possible that higher values may be found in the crystalline inclusions in more magnesian olivines. Two examples of glass inclusions hosted by clinopyroxene

TABLE 3.2

Location	Rinjani			*Ulakan*				
Sample #	UTas48001		UTas48001	UTas67424		UTas67424		UTas67424
Fo host	90.2		*whole*	90.9		90.3		*whole*
Run	84/1		*rock*	R109/1		R109/3		*rock*
T_q (°C)	1260			1300		1300		
Type	H	R		OH	R	OH	R	
Ol added		0.71			12.96		13.40	
SiO_2	45.08	45.06	*48.41*	47.78	45.71	47.04	45.16	*47.45*
TiO_2	0.96	0.96	*0.69*	1.29	1.10	1.18	1.00	*0.57*
Al_2O_3	12.75	12.66	*10.55*	10.87	9.27	11.88	10.12	*9.32*
FeO*	9.55	9.51	*9.18*	4.37	10.51	4.91	10.50	*10.50*
MgO	10.17	10.47	*14.04*	12.39	13.43	11.80	13.37	*17.86*
CaO	18.34	18.21	*14.40*	18.64	15.90	19.31	16.44	*12.03*
MnO	0.17	0.16	*0.17*	0.07	0.06	0.07	0.06	*0.20*
Na_2O	1.62	1.61	*1.50*	1.56	1.33	1.45	1.24	*1.24*
K_2O	1.01	1.01	*0.90*	2.41	2.06	1.82	1.55	*0.62*
P_2O_5	0.07	0.07	*0.15*	0.41	0.35	0.28	0.24	*0.21*
Total	99.72	99.72	*100.00*	99.79	99.72	99.74	99.68	*100.00*
CaO/Al_2O_3	1.44	1.44	*1.36*	1.71	1.72	1.63	1.62	*1.29*
Mg#	65.5	66.3	*73.2*	83.5	69.5	81.1	69.5	*75.2*
K_D*	0.21	0.21		0.51	0.23	0.46	0.24	
FeO	7.52	7.48	*7.23*	3.70	8.91	4.16	8.90	*8.89*
mg#	70.7	71.4	77.6	85.7	72.9	83.5	72.8	*78.2*
K_D	0.26	0.27		0.60	0.27	0.54	0.29	
T_q (°C)	1244	1253		1323	1342	1299	1335	
CIPW norm (mol%)								
or			4.04					2.69
ab			5.28					7.20
an	18.35	18.14	14.73	11.51	9.58	15.34	12.69	13.19
ne	10.88	10.77	4.95	10.37	8.64	9.73	8.09	0.96
lc	4.46	4.45		10.54	8.81	8.04	6.65	
di	35.85	35.50	38.78	45.49	37.85	42.74	35.31	29.51
hy								
ol	21.15	21.90	30.25	13.62	28.03	14.74	29.45	44.79
cs	6.75	6.68		4.75	3.99	6.07	5.05	
ilm	2.50	2.49	1.82	3.33	2.77	3.07	2.53	1.46
ap	0.07	0.07	0.15	0.40	0.33	0.27	0.23	0.20

Location	*Merelava*			Epi		
Sample #	31551		BC13	UTas71046		UTas71046
Fo host	90.4		*whole*	91.6		*whole*
Run	64/1		*rock*	R15/1		*rock*
T_q (°C)	1242			1305		
Type	OH	R		OH	R	
Ol added		13.01			7.61	
SiO_2	48.57	46.20	*50.89*	44.94	43.14	*44.01*
TiO_2	0.56	0.49	*0.47*	0.60	0.53	*0.55*
Al_2O_3	15.66	13.68	*10.44*	14.73	12.94	*13.44*
FeO*	5.4	9.00	*8.19*	5.70	9.00	*9.00*
MgO	8.99	12.47	*13.90*	11.81	14.89	*12.68*
CaO	17.75	15.53	*13.88*	19.46	17.12	*17.76*
MnO	0.07	0.09	*0.17*	0.05	0.05	*0.05*
Na_2O	1.77	1.55	*1.62*	2.00	1.76	*1.82*
K_2O	0.64	0.56	*0.39*	0.45	0.40	*0.41*
P_2O_5	0.47	0.41	*0.05*	0.16	0.14	*0.15*
Total	99.88	99.96	*100.00*	99.90	99.96	*99.87*
CaO/Al_2O_3	1.13	1.13	*1.33*	1.32	1.32	*1.32*
Mg#	74.8	71.2	*75.2*	78.7	74.7	*71.6*
K_D*	0.32	0.26		0.34	0.27	
FeO	4.76	7.93	*7.22*	5.14	8.12	*7.63*
mg#	77.1	73.7	77.5	80.4	76.6	*74.8*
K_D	0.36	0.30		0.38	0.30	
T_q (°C)	1199	1287		1296	1320	
CIPW norm (mol%)						
or	3.10	2.51	1.71			
ab	5.37	1.71	10.76			
an	27.00	21.99	14.85	21.90	18.33	19.72
ne	7.67	8.91		13.16	11.00	11.80
lc				1.95	1.63	1.75
di	42.76	34.89	35.87	30.33	20.90	27.28
hy			13.20			
ol	11.98	28.28	22.35	22.10	37.01	29.94
cs				8.88	9.72	7.97
ilm	1.60	1.30	1.21	1.53	1.28	1.38
ap	0.50	0.41	0.05	0.15	0.13	0.14

Composition of heated melt inclusions in olivine. $Mg^{\#}$=100Mg/(Mg+Fe*), mg#=100Mg/(Mg+Fe^{2+}), K_D*=$(Mg/Fe^*)_{glass}/(Mg/Fe)_{Ol}$, K_d=$(Mg/Fe^{2+})_{glass}/(Mg/Fe)_{olv}$. Fe_2O_3/FeO values as follows: Rinjani=0.30, Ulakan=0.20, Merelava=0.15, Epi=0.12. Run: grain number/melt inclusion number within that grain. Analysis in bold italics indicate re-calculated (R) compositions of heated (H) melt inclusions. R† indicates recalculation by olivine addition only because no iron loss occurred. T_q: temperature of quenching. Ol addeed: wt% of host olivine material added to the composition (H) of melt inclusions after correction for Fe-loss. See Section 3.5.3 for explanation of recalculation procedure. Wholerock analyses are the most primitive sample in each suite, UTas48001: Foden (1979), BC13: Barsdell (1988), UTas67424: Wheller (1986), UTas71046: Barsdell & Berry (1990).

TABLE 3.3

Location	Rinjani volcano								Ulakan Formation			
Analysis	1	2	3	4	5	6	7	8	9	10	11	12
SiO_2	50.98	43.16	50.70	50.48	49.73	46.21	46.27	49.17	49.50	49.98	54.64	54.30
TiO_2	2.14	2.65	2.12	1.56	1.25	1.43	1.26	1.13	1.00	1.08	1.45	1.10
Al_2O_3	22.52	22.37	20.48	20.59	20.25	19.43	19.49	20.17	22.07	21.07	20.23	21.14
FeO*	2.60	2.79	2.58	2.85	2.81	2.66	2.79	2.42	2.18	2.27	2.03	2.18
MgO	0.59	1.11	0.80	0.93	1.24	1.57	1.19	1.21	1.22	0.98	0.73	0.18
CaO	14.93	19.89	16.30	16.55	17.98	21.18	20.11	18.27	15.36	18.81	13.60	15.25
MnO	0.11	0.11	0.08	0.08	0.11	0.01	0.07	0.11	0.94	0.02	0.01	-
Na_2O	4.57	3.07	3.79	0.82	3.53	3.14	3.30	3.53	2.96	2.88	3.00	3.75
K_2O	2.38	2.72	1.91	2.39	2.13	1.35	1.82	1.01	2.44	2.12	3.23	2.28
P_2O_5	0.40	1.94	0.47	0.34	0.51	1.56	0.92	0.45	0.70	0.32	0.55	0.33
Total	101.21	99.81	99.23	96.59	99.55	98.53	97.23	97.47	98.37	99.53	99.47	100.51
Mg#	28.7	41.5	35.6	36.8	44.1	51.3	43.3	47.2	50.0	43.5	39.1	12.8
mg#	33.8	47.4	41.2	42.5	50.1	57.2	49.2	53.2	54.1	47.6	43.1	14.8
Fo_{max}	80.7	85.8	81.2	84.2	86.3	87.7	87.6	87.9	81.2	84.8	79.9	79.9
K_D	0.10	0.12	0.13	0.11	0.13	0.15	0.11	0.12	0.23	0.14	0.16	0.04
CaO/Al_2O	0.66	0.89	0.80	0.80	0.89	1.09	1.03	0.91	0.70	0.89	0.67	0.72

Electron microprobe analyses of glassy melt inclusions in olivine. Mg#= 100Mg/(Mg+Fe*), mg#= 100Mg/(Mg+Fe^{2+}), K_D= $(Fe/Mg)_{ol}/(Fe^*/Mg)_{melt}$. (*) all iron as FeO.

TABLE 3.4

Location	*Ulakan Formation*									*Epi*					*Rinjani*		
Sample	67422	67422	67422	67422	67422	67424	67424	67424	67424	71046	71046	71046	71046	71046	48002	48002	48002
Run	31/3	31/1	32/1	32/2	33/2	34/1	34/3	35/1	35/4	25/1	25/2	25/3	28/1	46/2	44/1	45/1	45/2
T_q (°C)	1300	1300	1260	1260	1300	1185	1185	1287	1287	1243	1243	1243	1237	1237	1200	1100	1100
Res Phase						Al-Spl	Al-Spl										
SiO_2	51.22	51.20	50.90	53.17	51.01	61.38	67.85	52.74	52.30	57.07	53.18	52.54	53.24	55.39	56.89	53.96	54.17
TiO_2	0.59	0.58	0.52	0.34	0.59	0.68	0.33	0.51	0.58	0.47	0.39	0.42	0.35	0.48	0.40	1.01	0.63
Al_2O_3	9.64	9.21	11.34	12.08	8.71	16.45	16.46	8.78	8.49	15.38	13.94	13.55	9.14	11.92	16.26	17.18	16.07
Cr_2O_3	0.05	0.05	0.12	0.10	0.02	0.01	0.08	0.21	0.28	0.09	0.07	0.05	0.04	0.09	0.04	0.02	0.00
FeO	7.60	7.77	6.49	4.78	8.44	2.39	1.68	6.25	6.01	4.69	6.83	7.00	7.74	6.23	5.81	5.87	5.46
MgO	9.71	10.25	8.53	8.14	11.08	3.00	2.07	10.86	11.60	5.65	7.89	8.68	9.82	7.57	3.89	5.11	4.61
CaO	16.26	15.72	14.27	13.02	18.27	6.39	4.71	17.80	17.71	10.94	13.79	14.27	14.33	12.37	9.00	7.70	8.32
MnO	0.00	0.06	0.12	0.06	0.08	0.00	0.22	0.11	0.04	0.05	0.16	0.00	0.00	0.17	0.07	0.13	0.24
Na_2O	1.50	1.48	1.94	2.32	1.34	3.87	4.10	1.42	1.23	3.78	1.75	1.80	1.20	1.33	3.74	3.04	3.21
K_2O	1.64	1.80	2.65	3.36	1.02	3.80	4.32	1.16	0.96	1.64	0.49	0.48	0.33	0.45	3.09	2.26	2.08
P_2O_5	0.49	0.66	0.84	0.97	0.38	0.21	0.22	0.46	0.39	0.14	0.09	0.11	0.06	0.10	0.67	0.34	0.53
Total	98.69	98.76	97.71	98.33	100.94	98.17	102.02	100.29	99.58	99.90	98.58	98.90	96.25	96.10	99.86	96.62	95.32
Mg#	69.5	70.2	70.1	75.3	70.1	69.2	68.8	75.6	77.5	68.3	67.4	68.9	69.4	68.5	54.5	60.9	60.1
CaO/Al_2O_3	1.69	1.71	1.26	1.08	2.10	0.39	0.29	2.03	2.09	0.71	0.99	1.05	1.57	1.04	0.55	0.45	0.52
Host clinopyroxene																	
Wo	46.5	45.8	46.6	46.2	46.0	46.0	44.6	46.4	45.7						46.1	46.2	45.8
En	48.2	48.8	45.3	49.4	48.3	46.2	48.5	45.6	47.5						47.6	48.1	48.5
Fs	5.4	5.5	8.1	4.5	5.7	7.9	7.0	8.0	6.9						6.3	5.6	5.7
Mg#	88.1	88.5	81.5	90.2	88.2	85.2	84.8	78.4	86.8	82.7	82.3	84.4	88.9	88.5	86.3	87.0	87.9

Electron microprobe analyses of heated melt inclusions in clinopyroxene. Run notation indicates: grain number/melt inclusion number. T_q (°C): temperature of quenching. Res Phase: Residual daughter phase in melt inclusion after heating. Mg#= 100Mg(Mg+Fe*). Wo=Ca, En=Mg, Fs=Fe^{2+}+Fe^{3+}.

phenocrysts and heated to low temperatures (1100°C) are listed in Table 3.4 to illustrate the effect of continued crystallization on the wall (Run 45/1 and 45/2 of Rinjani). In this case CaO/Al_2O_3 values in the glass are significantly lower (~0.5) compared to those of glasses in olivine (Figure 3.7a). Two coexisting glass inclusions in a spinel crystal ($Cr^{\#}$ 73) trapped by olivine ($Fo_{90.6}$) instead, show much higher CaO/Al_2O_3 values (~1.9 and ~2.6, Table 3.5, and Figure 3.7a).

The low MgO (<2 wt%) and FeO* (<3 wt%) contents of the glass inclusions hosted in olivine (Table 3.3), partly reflect the continued fractional crystallization of daughter olivine on the inclusion wall. In Figure 3.8, $K_D{}^{Ol\text{-}Melt}_{Fe\text{-}Mg}$ values between these glasses and their host range between 0.10 and 0.20 and are thus much lower than the accepted equilibrium value of ~0.3 (Roeder & Emslie 1970). Alternatively, $K_D{}^{Ol\text{-}Melt}_{Fe\text{-}Mg}$ values between of the glass inclusions trapped by the spinel described above and its host olivine, are ~0.40 (Table 3.5), much higher than those calculated for glassy inclusions in olivine (Figure 3.8). This indicates that the nature of Fe-Mg re-equilibration operating in melt inclusion hosted by spinel may differ significantly from those of inclusion hosted by olivine.

3.5.2 Heated melt inclusions

Melt inclusions in olivine phenocrysts, analyzed after heating and optical homogenization, have CaO/Al_2O_3 values that overlap with those of naturally quenched glasses (Figure 3.9a and b) and which range up to values characteristic of ankaramitic bulk compositions (~1.2 to 1.6, Figure 3.9). CaO/Al_2O_3 values are similar among melt inclusions within a single olivine grain (Figure 3.10, and Runs 83, 43, 64, 2, R109 in Table 3.2), but vary over a wide range among melt inclusions from various olivine phenocrysts (Figure 3.10a). CaO/Al_2O_3 values also vary more in inclusion compositions than in ankaramitic bulk-rock compositions (Figure 3.9 and 3.9). These variations within a narrow Fo range are inconsistent with crystal fractionation from a single melt.

Incomplete melting of clinopyroxene causes depletion in CaO/Al_2O_3, as is demonstrated by the composition of underheated inclusions in clinopyroxene from Rinjani volcano and the Ulakan Formation (Table 3.4, Figure 3.9 and 3.6). These values are lower than those in glass inclusions in which olivine is the only phase (Figure 3.7). CaO/Al_2O_3 values in heated melt inclusions in olivine are above these values (Figure 3.9) and indicate the complete melting of clinopyroxene daughter crystals during the experiment. Another possibility is that some clinopyroxene crystals were accidentally trapped and then remelted during the heating experiment to produce variable (and high) CaO/Al_2O_3 values. This is, however, highly unlikely considering the similarity of CaO/Al_2O_3 values within the same grain (Figure 3.10).

Inclusion compositions in olivines are also more silica-undersaturated than ankaramitic host compositions: inclusion CIPW norms contain nepheline, leucite, and larnite, (Table 3.2) whereas Rinjani and Ulakan ankaramites are *ne*-normative and those from Merelava and Epi are olivine- and hypersthene-normative. Although the compositions of these heated inclusions are not representative of the trapped melt (Section 3.4), it is difficult to explain why the inclusions would yield these silica-undersaturated compositions on analysis if they actually have compositions like the ankaramite host rocks. The analytical conditions for glasses adopted in this study might cause some loss of alkalis

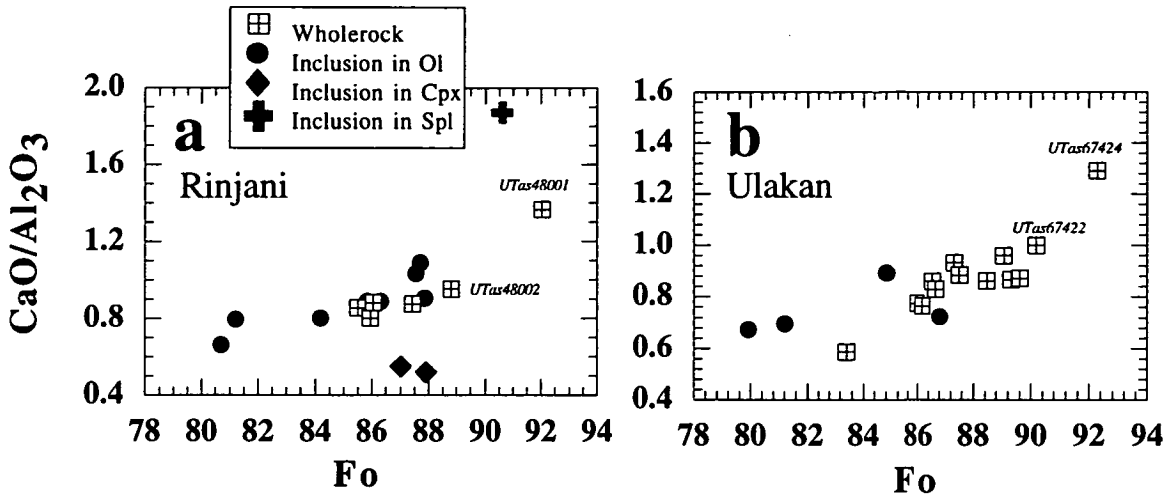

Figure 3.7 CaO/Al2O3 values of primary glass inclusions in olivine phenocrysts (filled circles) from ankaramite rocks of a: Rinjani volcano and b: Ulakan Formation. Equilibrium olivine composition of each ankaramite sample are calculated with a KD value of 0.3 (Roeder & Emslie 1970) and Fe2O3/FeO values of 0.3 for Rinjani and 0.2 for Ulakan (Chapter 2). The composition of two inclusions in a clinopyroxene heated to low temperature (1100°C, filled diamonds) and the composition of one inclusion in a spinel crystal (Cr#73) trapped by olivine (Fo90.6, cross) are to show the effect of the host on compatible elements. Analyses are from Tables 3.3, 3.4 and 3.5.

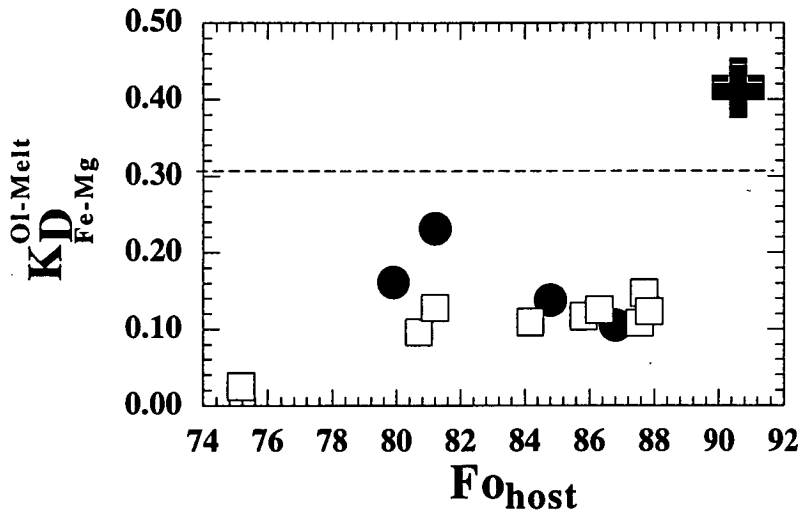

Figure 3.8 KD values, calculated as (Fe/Mg)ol/(Fe*/Mg)melt of glass inclusions in olivine phenocrysts from Rinjani (squares) and Ulakan (circle) *versus* Fo content of the host. Cross shows KD value of two glass inclusions trapped in a spinel crystal (Cr#73) in olivine (Fo90.6). Analyses are listed in Tables 3.3 and 3.5. Dashed line indicates KD value of 0.3 (Roeder & Emslie 1970)

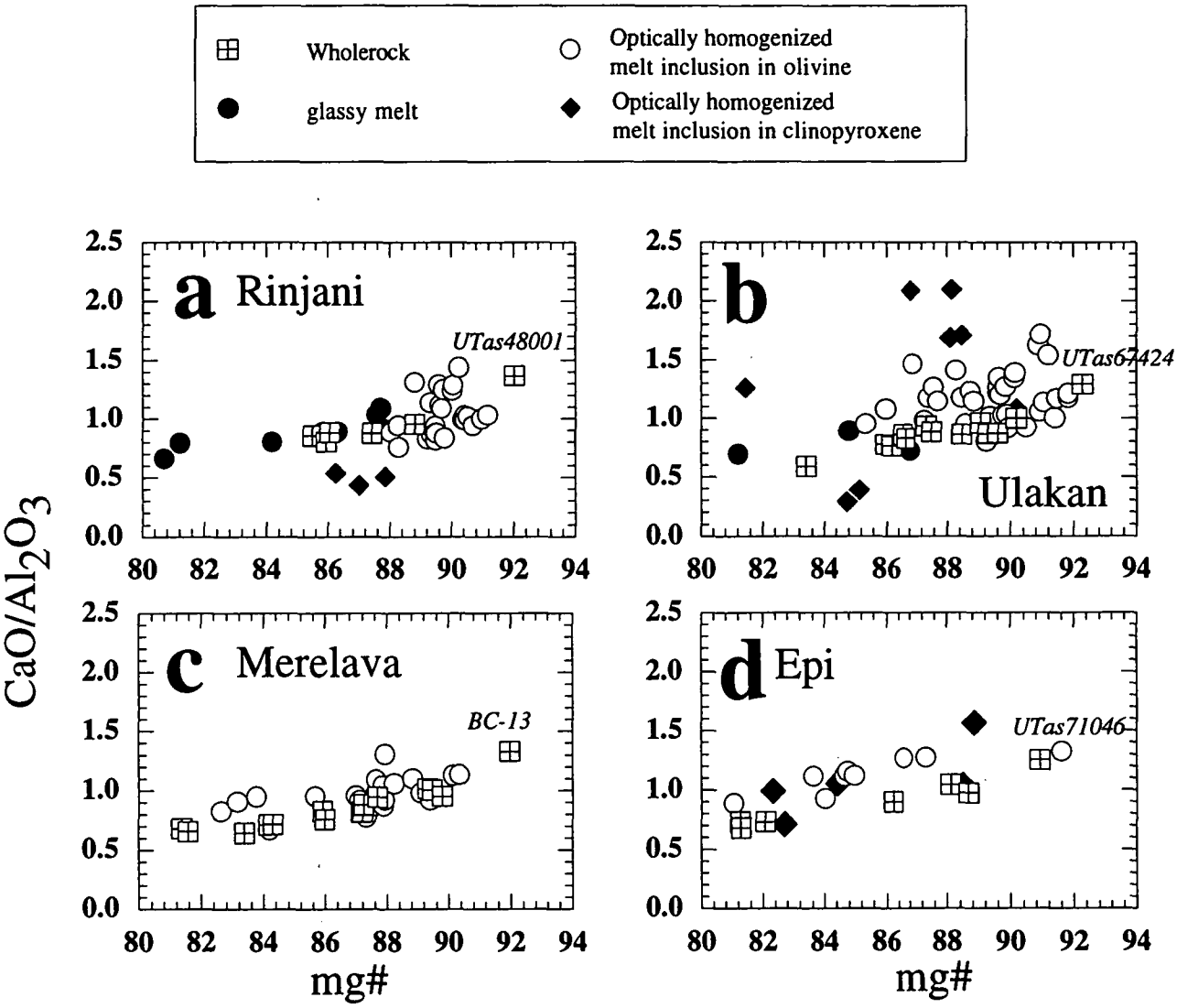

Figure 3.9 CaO/Al2O3 in melt inclusions *versus* mg# (=100Mg/(Mg+Fe^{2+})) of the host. Open circles: compositions of heated melt inclusions in olivine. Filled circles: glassy melt inclusions hosted in olivine. Filled diamonds: composition of heated melt inclusions in clinopyroxene. Wholerock CaO/Al2O3 values are also shown for comparison (square with crosses) with their equilibrium olivine composition calculated using melt Fe2O3/FeO values (Rinjani=0.30, Ulakan=0.20, Merelava=0.15, Epi=0.12) obtained from olivine-spinel inclusion pairs (Maurel & Maurel 1984). Sample numbers of the most primitive sample in each suite are in italics.

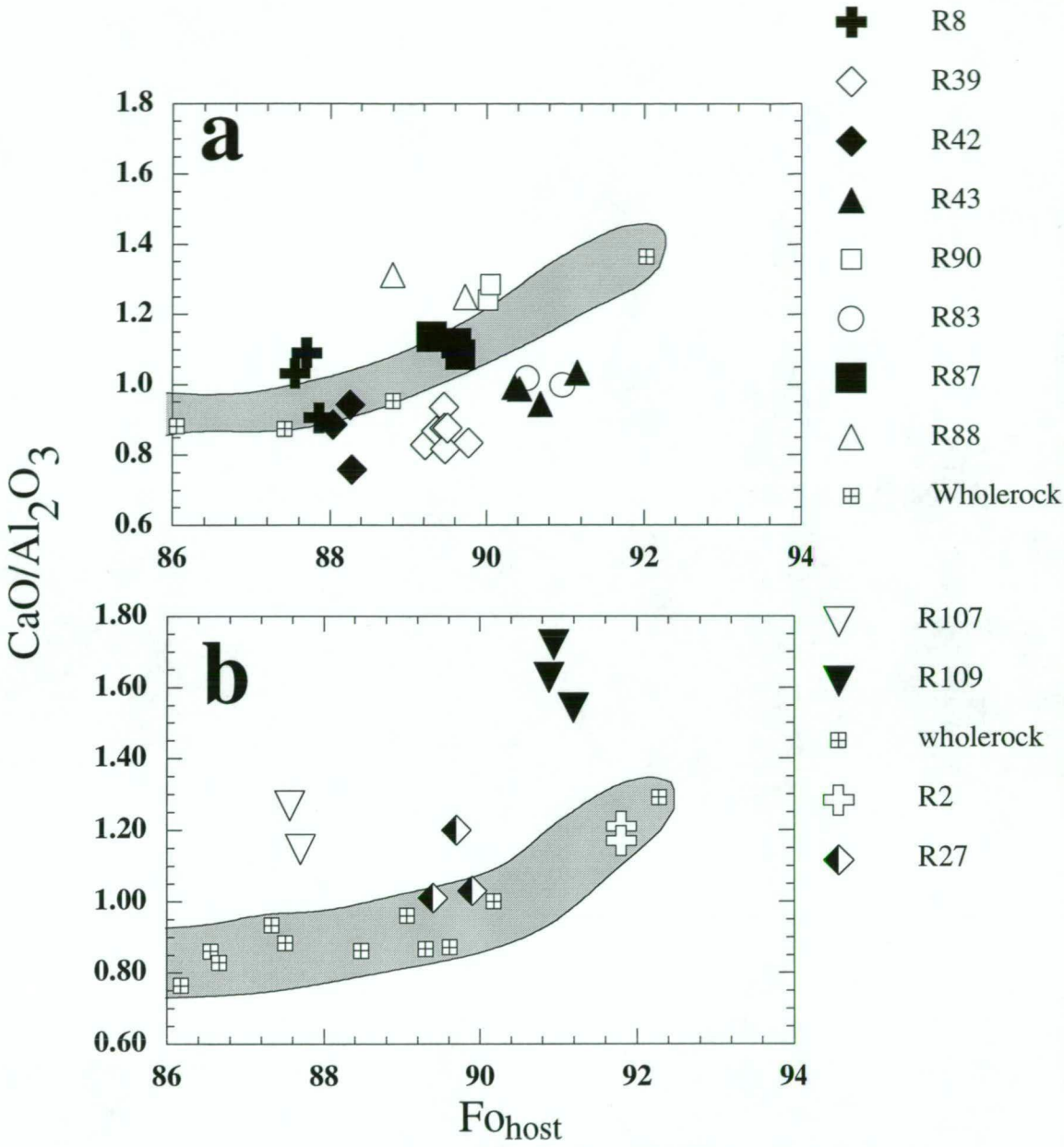

Figure 3.10 Diagram illustrating the larger difference in variation of CaO/Al2O3 between grains compared to within grains. CaO/Al2O3 values are from optically homogenized melt inclusions that coexist in the same olivine grain plotted *versus* Fo from a: Rinjani volcano and b: Ulakan Formation. Each type of symbol represents a separate grain as indicated in the legend (Appendix 3). R8 are compositions of glassy melt inclusions (Table 3.3). Field encloses compositions of wholerock analyses (squares with crosses) of ankaramite suites from Rinjani (Foden 1983) and Ulakan (Wheller 1986).

but this would make the compositions less silica-undersaturated, not more. In addition, if the trapped glasses originally had ankaramitic compositions but lost iron, the modified compositions would again have become less silica-undersaturated than the originals, not more. And if the inclusions were composed of melt plus trapped crystals of olivine and clinopyroxene, or were subjected to over- or under-heating during experimental homogenization, then the compositions would simply become more- or less-rich in normative olivine and diopside. It is therefore concluded that the silica-undersaturated nature of the inclusions are representative of the melts as trapped.

CaO/Al_2O_3 values of clinopyroxene-hosted melt inclusions are also plotted against $Mg^{\#}$ content of their host grains in Figure 3.9a, b and d. Their CaO/Al_2O_3 values vary much more widely than those of olivine-hosted melt inclusions. In some cases the homogenization procedure may have remelted some of the host clinopyroxene crystal in addition to the post-entrapment clinopyroxene precipitated on melt inclusion walls: this would produce higher CaO/Al_2O_3 values than those of the original trapped melt. The composition of an overheated (1300°C) melt inclusion from an Ulakan clinopyroxene (Table 3.4: Sample 67424, Run 33/2) may reflect this process. The CaO/Al_2O_3 of this composition is 2.1, compared with ~1.2 for the olivine-hosted inclusions that were quenched at temperatures of 1240°C. Its CaO and normative diopside (~60 %) contents are also substantially higher than those of the olivine-hosted inclusions.

If, however, an inclusion was reheated to a temperature lower than its original trapping temperature, some post-entrapment crystals of olivine and clinopyroxene may be left unmelted, which would result in CaO/Al_2O_3 values lower than those of the original trapped melt. Rinjani inclusions 44/1 and 45/1-2 are likely examples of underheating during homogenization (Table 3.4).

Therefore, recalling that the main aim is to discover whether the melt inclusions trapped in the earliest-formed phenocrysts in the most primitive ankaramites have compositions with ankaramitic affinities, most emphasis is placed on the composition of melt inclusions in early crystallized olivine phenocrysts.

3.5.3 Heated melt inclusions in olivine corrected for iron loss

Analyses of heated melt inclusions in olivine are recalculated following a method described in Chapter 4. This recalculation reverses the effect of iron loss caused by Mg# re-equilibration between the melt and the host olivine after trapping, and corrects for the effect of crystallization (or melting) of host olivine on the walls of the inclusion. Some examples of melt compositions obtained by this recalculation procedure are listed in Table 3.2, for comparison with their corresponding uncorrected analyses after heating. FeO* and MgO are changed by this correction procedure; SiO_2, CaO and Al_2O_3 are slightly diluted (~<2 wt%) due to the addition of olivine to the melt and TiO_2, MnO, Na_2O, K_2O and P_2O_5 are slightly changed (<0.5 wt%); but the ratios of incompatible elements such as CaO/Al_2O_3 are unaffected (Table 3.2) .

3.6 Deductions from each suite

3.6.1 Rinjani volcano

Recalculated melt inclusions in magnesian olivine phenocrysts (Fo_{89-91}) have CaO/Al_2O_3 values that range from ~0.8 to ~1.5, and overlap with the composition of the most primitive ankaramite sample UTas48001, which has a CaO/Al_2O_3 value of ~1.4, (Figure 3.9a). Some of the trapped melts, therefore, have ankaramitic characteristics (not picritic), but their large range of values at a constant Fo content is inconsistent with fractionation from a common parent melt, (Figure 3.10). CaO/Al_2O_3 of melt inclusions that coexist in a single grain, however, are much the same (Figure 3.10a), suggesting that the magma aggregated from parental melts that differed in CaO/Al_2O_3 values. It was shown in chapter 1 (Table 1.3) that *di/ol* value of ankaramite rocks are typically 0.7 whereas the values of picrite rocks are <0.7. In Rinjani, the *di/ol* values of recalculated melt inclusions are greater than 0.7 and range up to values of ~3.5 (Figure 3.11a). This range of *di/ol* indicates that the parent melts to the ankaramite rocks of Rinjani had ankaramitic affinities, not picritic. The compositions of recalculated melt inclusions are also *ne*-, *lc*-, and *cs*-normative and therefore more silica-undersaturated than the wholerock compositions, which are *ne*-normative, (Table 3.2).

3.6.2 Ulakan formation

The most primitive ankaramite in the Ulakan suite (UTas67424) with $mg^{\#}$= 75.2 has a CaO/Al_2O_3 of 1.4, (Table 3.2). Recalculated melt inclusions from olivine (Fo_{90-92}) in this sample have ankaramitic CaO/Al_2O_3 values that range from 0.9 to 1.7 and $mg^{\#}$ from 73 to 77 (Figure 3.9, and Table 3.2). These values resemble those of Ulakan wholerock analyses, but they tend to be richer in normative nepheline contents, and are also *lc*-, *cs*-normative, (Table 3.2). As found in the melt inclusions from Rinjani, variations of CaO/Al_2O_3 values in melt inclusion that coexist in the same grain are also much smaller than the variations amongst several grains of similar Fo content (Figure 3.10b). Thus, the Ulakan rocks also seem to have formed from parent melts that have variable CaO/Al_2O_3 values. The *di/ol* values of recalculated met inclusions vary between ~1 and ~3 and indicate ankaramitic affinities (Figure 3.11b). It is also notable that at similar run temperatures, the differences in composition between Rinjani and Ulakan melt inclusions reflect those between the ankaramite hosts, with the Ulakan compositions being richer in Mg, poorer in Ca, and with higher $Mg^{\#}$ values (Table 3.2).

3.6.3 Merelava

Two coexisting melt inclusions in ~Fo_{90} olivine have identical compositions with CaO/Al_2O_3 values ~1.1 and $Mg^{\#}$ ~74, (Table 3.2). These are *ne*-normative and resemble compositionally ankaramites from Ulakan and Rinjani more than they do the Merelava ankaramites, which are olivine- and hypersthene-normative. Melt inclusions suitable for homogenization experiments were not found in olivine with Fo>90, although olivine compositions in Merelava ankaramites range up to Fo_{92}. An

inclusion hosted in olivine with Fo88 has CaO/Al_2O_3 of 1.30, similar to that of the wholerock composition of sample BC-13, and therefore ankaramitic (Table 3.2). The *di/ol* values of recalculated melt inclusions vary from ~1 up to ~3 and indicate ankaramitic affinities (Figure 3.11c).

3.6.4 Epi

One melt inclusion in Fo92 olivine contains a CaO/Al_2O_3 value of ~1.3 and $Mg^{\#}$ 75, resembling the bulk composition of the most primitive ankaramite sample from Epi, with CaO/Al_2O_3 = 1.25. The inclusion composition is therefore ankaramitic but silica-undersaturated (*ne*-normative) whereas wholerock analyses are not (Table 3.2). The *di/ol* values of recalculated melt inclusions from Epi range from 1 to ~3.5 (Figure 3.11d) and indicate ankaramitic affinities.

3.7 Petrogenesis of primitive ankaramitic magmas

From the high CaO/Al_2O_3 values and *di/ol* values observed in melt inclusions, it seems unlikely that the wholerock compositions of primitive ankaramite samples in each suite are the result of clinopyroxene accumulation, as they are similar to those of their melt inclusions in olivine (Fo_{90-92}) phenocrysts. The recalculated composition of melt inclusions in magnesian olivines (Fo>89) are plotted in Figure 3.12 for comparison with the wholerock compositional trends of each ankaramite suite. It can be seen form Figure 3.12 that the compositions of recalculated melt inclusions are ankaramitic, not picritic, and plot within the compositional field defined by primitive ankaramite rocks. In Chapter 1, it was concluded that a primary ankaramite melt, with its characteristic CaO/Al_2O_3 values greater than 1 and richness in normative diopside could not be produced by partial melting of anhydrous mantle peridotite at pressures of up to 3 GPa. In this Chapter, two alternative mechanisms are considered: one involving partial melting of mantle lherzolite at pressures below 4 GPa, but in the presence of H_2O-CO_2-rich fluids, and a second mechanism involving partial melting of mantle lherzolite at pressures above 4 GPa.

3.7.1 Mechanism 1 - Melting of lherzolite in the presence of H_2O and CO_2 at pressures less than 4 GPa

It is notable that the two chemical characteristics common to all ankaramitic melt inclusion studied here namely, silica-undersaturation and high CaO/Al_2O_3, are also typical of highly silica-undersaturated primitive rocks such as nephelinites and melilitites (Section 1.6). The compositions of these rocks resemble those of the melt inclusions, but are unlike the ankaramite host. A link therefore could exist between "parental" primary silica-undersaturated melts with CaO/Al_2O_3 values >1, similar to those found in melt inclusions, and the formation of ankaramitic magmas. Extensive experimental work on the genesis of undersaturated primitive melts (cf. Mysen & Boettcher 1975a,b, Brey & Green 1975, 1977, Eggler 1978, Brey *et al.* 1977, Frey *et al.* 1978, Adam 1988, Green *et al.* 1987, Taylor & Green 1987) suggest that such compositions may form in the mantle by small degrees of partial melting of lherzolite at pressures <3 GPa, provided CO_2-rich fluids are present. Some examples of these melts are listed in Table 3.6, for comparison with the composition of heated melt inclusions (Table 3.2). Their high CaO/Al_2O_3 and silica undersaturation

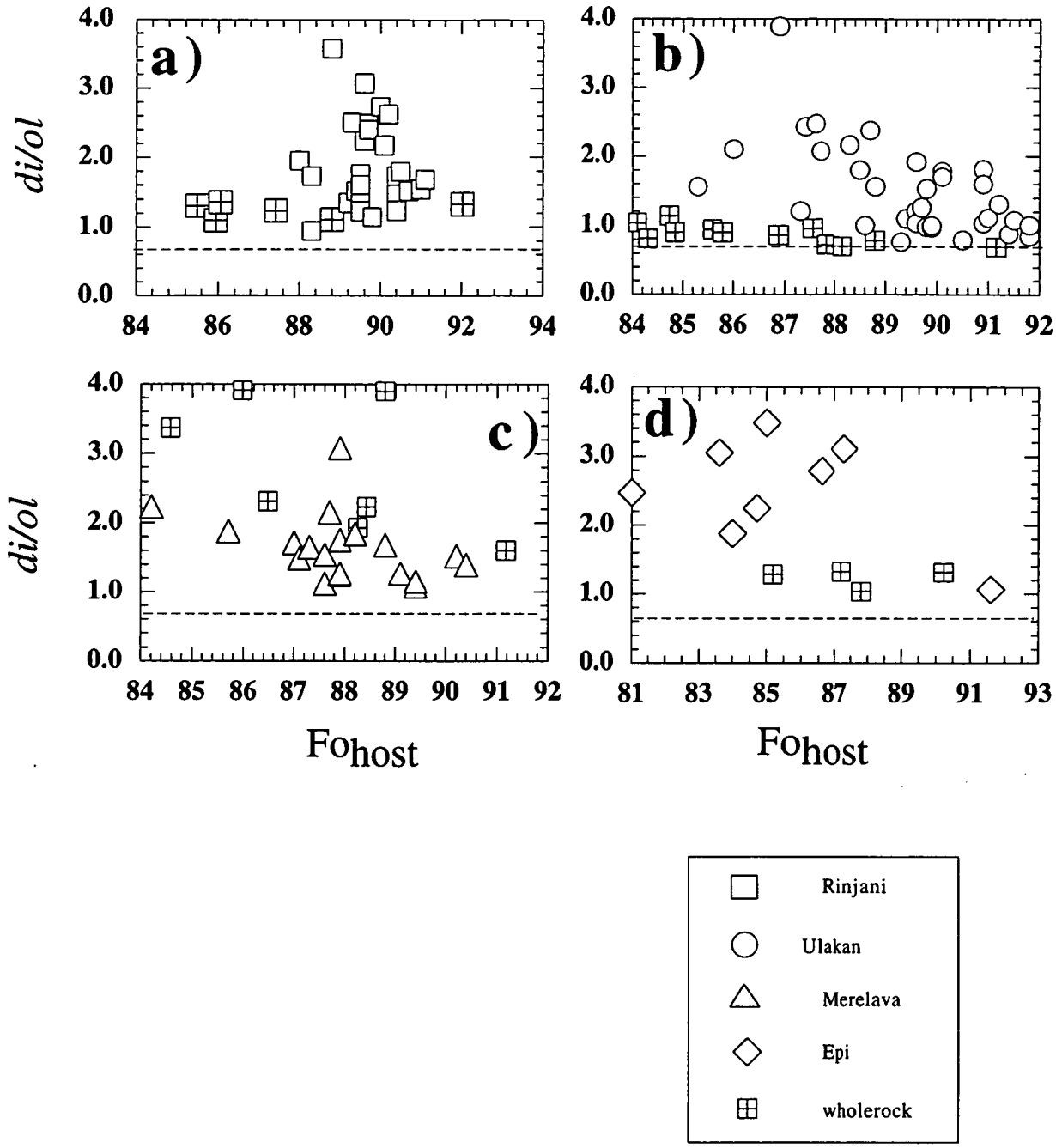

Figure 3.11 Normative *di/ol* values of recalculated melt inclusions *versus* Fo content of the host olivine phenocrysts from the ankaramite suites of a) Rinjani, b) Ulakan, c) Merelava and d) Epi. Normative *di/ol* values of the rock suite is also shown for comparison, using calculated equilibrium Fo contents. Dashed lines in a-d) indicate di/ol value of 0.7. *di/ol* values >0.7 indicate ankaramitic affinities (Table 1.3).

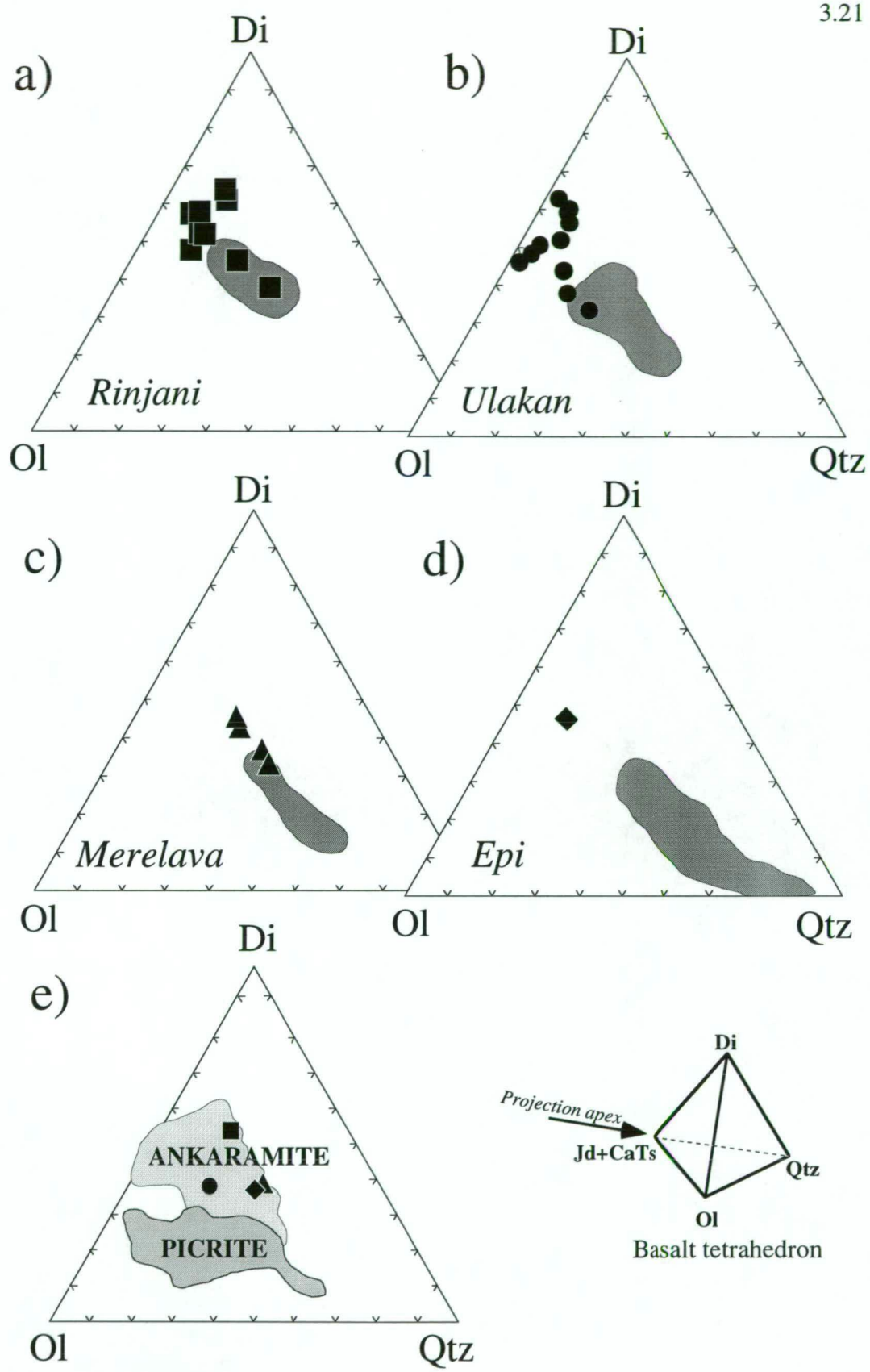

Figure 3.12 Compositions projected from the Jd+CaTs apex of the basalt tetrahedron onto the face Ol-Di-Qtz. Projection parameters are described in Chapter 1.

a-d) Composition of melt inclusions in olivine phenocrysts from ankaramite rocks of a) Rinjani, b) Ulakan, c) Merelava and c) Epi. Filled symbols indicate compositions of melt inclusions hosted by >Fo90 in a-b, by >Fo89 in c and by Fo91.5 in d. Fields in a-b enclose variation in wholerock composition within each suite.

e) Compositional variations of primitive ankaramite and picrite rocks from Chapter 1. Filled symbols indicate wholerock composition of the most mafic ankaramite sample from each suite: Rinjani (square), Ulakan (circle), Merelava (triangle) and Epi (diamond).

are considered to reflect the increased stability of garnet and orthopyroxene as a function of CO_2. Thus CO_2 may play a crucial role in the formation of ankaramitic magmas. Moreover, variable CO_2 concentrations in the source could produced the variations in CaO/Al_2O_3 values found in their melt inclusions. The possibility that the compositions of melt inclusions in ankaramite may represent a primary melt produced by partial melting in the presence of CO_2-rich fluids is investigated further in Chapter 5.

3.7.2 Mechanism 2 - Melting of anhydrous lherzolite at pressures above 4 GPa

The CaO/Al_2O_3 values of partial melts in equilibrium with peridotite are inherited from the source and controlled by the residual mineralogy (Herzberg 1992). The field of stability of garnet enlarges with increasing pressure, and the appearance of garnet as a residual phase plays a key role in imparting higher CaO/Al_2O_3 values to the partial melts (Takahashi 1986, Kato *et al.* 1988, Wei *et al.* 1990, Herzberg 1992, Moryama *et al.* 1992, Trønnes *et al.* 1992, Ohtani *et al.* 1995). Herzberg (1992) showed that the CaO/Al_2O_3 values of partial melts, in equilibrium with ol+opx+cpx+grt, increase with pressures and become >1 above 5 GPa (i.e., ankaramitic).

In peridotitic systems, the field of stability of olivine on the liquidus contracts with increasing pressure. Shift of the olivine-pyroxene liquidus boundary curve with increasing pressure is illustrated to 14 GPa in Figure 3.13 (thin lines). This interpretation is based on experimental results of Shibata (1976), Walker (1979), Green *et al.* (1986), Takahashi (1986), Falloon *et al.* (1988), Herzberg (1992), Kinzler & Grove (1992a), Hirose & Kushiro (1993), and Baker & Stolper (1994). If the pressure-related trends on the cotectic established to ~4 GPa persist to higher pressures, a possible ol+opx+cpx+grt cotectic can be extrapolated to ~14 GPa (Figure 3.13, dashed line). This extrapolation is based on olivine-pyroxene boundary curves to 14 GPa taken from experimental data of Takahashi (1986), Herzberg (1992) and Hirose & Kushiro (1993). The evolution of a representative picritic melt, generated at the ol+cpx+opx+grt cotectic at some pressure above 5 GPa (composition X, Figure 3.13), as it rises through the mantle can now be considered.

As pressure decreases and the liquidus field of olivine enlarges, the location of the ol+Px+grt cotectic migrates away from composition X, thereby leaving the melt within the liquidus field of olivine. Olivine will continue to precipitate from the melt as it rises and cools. Olivine crystallization will cause the melt's composition to move away from the olivine apex towards the olivine-pyroxene cotectic, but if the melt continues to rise, falling pressure will lead to enlargement of the liquidus field of olivine, and the location of the olivine-pyroxene cotectic will continue to migrate away from the liquid composition, so that it will continue to precipitate olivine, becoming richer in pyroxene components and retaining the high CaO/Al_2O_3 value acquired as a primary melt. A protracted period of olivine crystallization as the melt ascends would cause the residual melt to become more and more ankaramitic, until eventually clinopyroxene joins olivine.

TABLE 3.5

	glassy inclusion		*host Spl*	*host Ol*
	a	*b*		
SiO_2	50.93	47.10	0.01	39.82
TiO_2	0.32	0.48	0.44	
Al_2O_3	6.20	7.12	12.26	
Cr_2O_3	0.89	0.91	49.28	0.05
FeO*	7.16	7.34	23.13	9.13
MgO	16.36	16.46	12.77	49.36
CaO	16.20	13.34		0.33
MnO	0.27	0.20	0.19	0.10
Na_2O	1.04	0.86		
K_2O	0.14	0.23		
P_2O_5	0.38	0.33		
NiO				0.12
TOTAL	99.89	94.37	98.08	98.91
Mg#	80.3	80.0	61.6	90.6
K_D	0.42	0.41		
CaO/Al_2O_3	2.61	1.87		
Fe_2O_3			9.89	
FeO			14.23	
Cr#			73.0	

Analyses of two glassy inclusions (a and b) coexisting in a spinel crystal trapped by a olivine phenocryst from Rinjani ankaramite UTas 48001, Grain FM38-3-4. Mg#= 100Mg/(Mg+Fe*), KD= (Fe/Mg)Ol/(Fe*/Mg) Melt.

TABLE 3.6

Source	Gt-lherz.	Spl-lherz.	Pyrolite
P (GPa)	2.0	1.5	2.7
T (°C)	1460	1150	1160
Fluid	H_2O-CO_2	H_2O-CO_2	H_2O-CO_2
Analysis	1	2	3
SiO_2	45.10	43.50	39.40
TiO_2	1.10	0.50	2.90
Al_2O_3	11.00	10.50	9.80
FeO*	13.60	13.00	12.60
MgO	13.70	10.70	16.30
CaO	13.40	13.80	13.40
MnO	0.30	0.30	0.40
Na_2O	1.10	2.90	3.70
K_2O	0.50	0.40	1.40
P_2O_5			1.30
TOTAL	99.80	95.60	101.20
Mg#	64.3	59.5	69.8
CaO/Al_2O_3	1.22	1.31	1.37

Molecular CIPW norm			
Analysis	1	2	3
or	2.20		
ab	2.35		
an	17.61	10.83	3.65
ne	5.03	19.51	20.23
lc		1.77	5.04
di	32.00	39.67	8.56
ol	37.95	26.50	42.24
cs		0.40	14.14
ilm	2.86	1.30	6.15

Composition of experimentally produced melts by partial melting of mantle lherzolite. Analysis 1: Mysen & Kushiro (1977), Table 3, Run 4-84, Residue: ol+opx+cpx. Analysis 2: Mysen & Boettcher (1975b), Table 11, Run 521, Residue: ol+opx+cpx+spl. Analysis 3: represents composition inferred to be at equilibrium with ol+opx+cpx+grt, Brey & Green (1977). Mg#= 100Mg/(Mg+Fe*). (*) all iron as FeO.

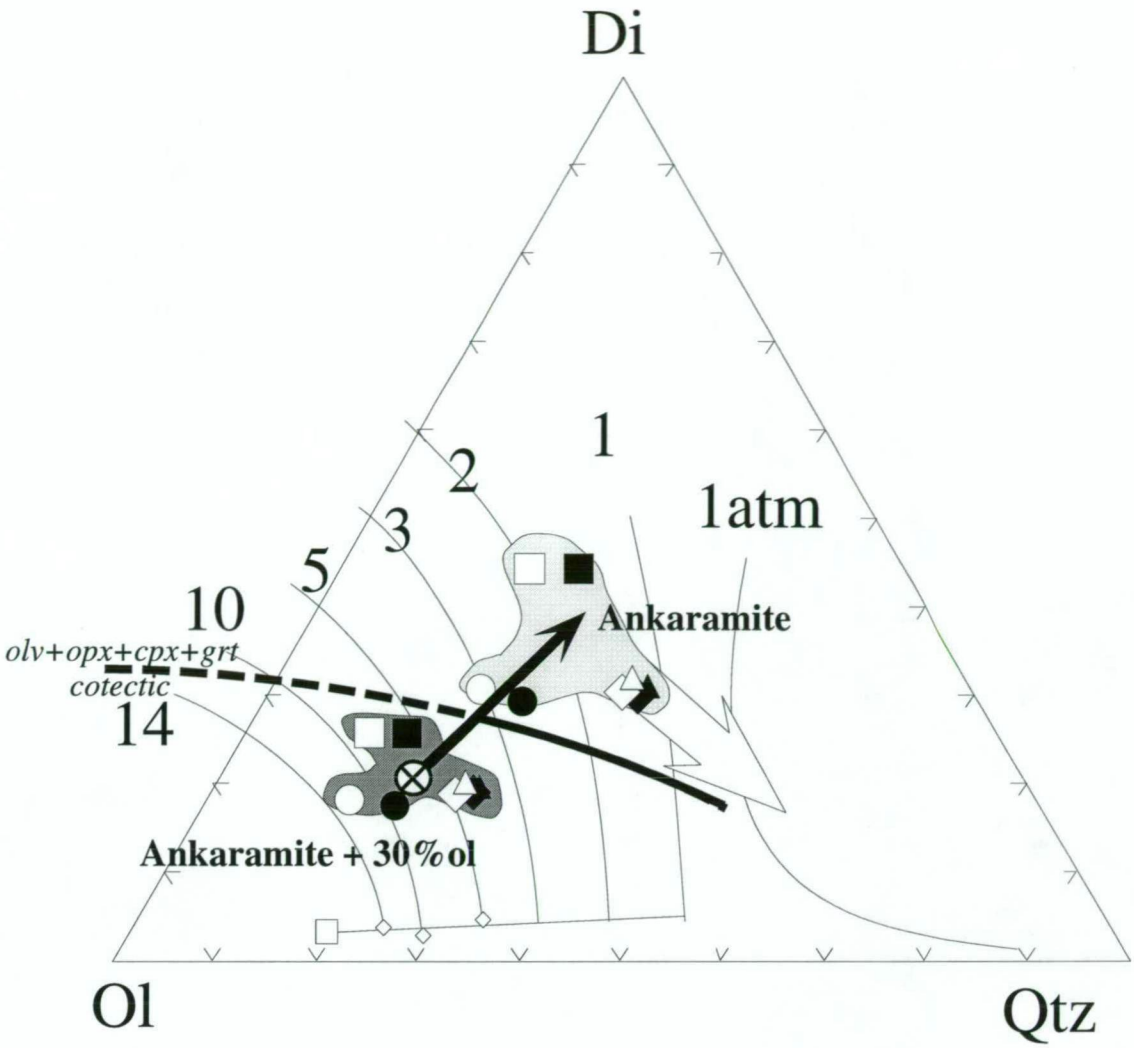

Figure 3.13 Compositions projected from Jadite+CaTs in the molecular normative basalt tetrahedron Ol-Di-(Jd+CaTs)-Qtz. A detailed explanation for the projection is given in Figure 1.2. Thin lines illustrate the likely shift of the olivine-pyroxene liquidus boundary curve with pressure, based on experimental work of Shibata (1976), Walker (1979), Green *et al.* (1986), Takahashi (1986), Falloon *et al.* (1988), Kinzler & Grove (1992a), Herzberg (1992), Hirose & Kushiro (1993), and Baker & Stolper (1994). Grid lines above 5 GPa are extrapolated using experimental data of Takahashi (1986), Herzberg (1992), and Hirose & Kushiro (1993) assuming that pressure-related trends on the cotectic established to 4 GPa (full line), persist to higher pressures (dashed line). Light-shaded area includes wholerock compositions of the most primitive ankaramite sample in each suite. Dark-shaded area includes recalculated bulk-rock compositions of the ankaramites with 30% equilibrium olivine added. Symbols are as follows, Square=Rinjani, circle=Ulakan, triangle=Merelava, diamond=Epi. Open symbols use Fe^{3+}/Fe^{2+} as determined from olivine-spinel inclusion pairs (Rinjani=0.27, Ulakan=0.18, Merelava=0.14, and Epi=0.11 after Maurel & Maurel, 1982). Filled symbols use all iron as FeO.

Melts generated above 5 GPa (e.g. X) have CaO/Al_2O_3 values greater than 1 (Herzberg, 1992). On the way to the surface and as pressure on the melt decreases, the olv-px-grt-melt cotectic will migrate away from composition X, leaving melt composition X in the olivine liquidus field. Olivine will now precipitate from the melt, thereby shifting the melt composition away from the olivine apex and causing the residual melt to become more and more ankaramitic, until eventually clinopyroxene precipitates. Numbers indicate pressure in GPa.

3.8 Discussion

Figure 3.14 helps to illustrate the model in discussion. Experimental studies suggest that partial melting of mantle lherzolite could yield primary melts with high CaO/Al_2O_3 values by partial melting either in the presence of CO_2-rich fluids at pressures <4 GPa or by anhydrous partial melting at pressures above 5 GPa (Figure 3.14, Stage: 1a and 1b, respectively), or by some combination of these factors at intermediate pressures. Partial melts produced experimentally by lherzolite melting in the presence of CO_2-rich fluids at pressures <4 GPa are markedly silica-undersaturated, and thus similar to the compositions of olivine-hosted melt inclusions, whereas the compositions of partial melts produced by anhydrous high-pressure melting of lherzolite are picritic.

The possibility that the ankaramitic melts represent non-primary but primitive liquid compositions derived by olivine fractionation from a high-pressure picritic melt with komatiitic affinities, is tested by adding equilibrium olivine to the most primitive ankaramitic bulk-rock compositions in each suite. Figure 3.13 shows that addition of 10-30% olivine is sufficient to bring the hypothetical parental picritic liquid close to the hypothetical 5-10 GPa ol+opx+cpx+grt cotectic (Figure 3.13, dashed line). The compositions of primitive ankaramites with 30% equilibrium olivine added are shown for each suite in Table 3.7. These calculated hypothetical parental liquids have ~24-28 wt% MgO, $Mg^{\#}$ ~83-87 and their calculated equilibrium olivine composition is ~Fo_{94-96} (Table 3.7). The composition of these liquids resemble those of naturally occurring, but rare, alnöitic rocks (Table 3.7) interpreted as possible primary melts generated by partial melting at pressures >4 GPa and in the presence of CO_2-rich fluids (Nixon *et al.* 1980). The composition of these rocks also have high CaO/Al_2O_3 values (>1) and a strong silica-undersaturation which resembles the composition of melt inclusions observed in magnesian olivines of ankaramite rocks. Thus, the calculated liquids could well represent the composition of near-primary melts parental to ankaramitic melts prior to olivine fractionation (Figure 3.14, Stage: 1).

Highest NiO contents in the magnesian olivine phenocrys (~Fo_{90-92}) of ankaramite rocks studied here range from 0.21 to 0.34 wt% (Barsdell 1988, Barsdell & Berry 1990, and Figure 3.2) and extrapolate to ~0.4 to 0.5 wt% in ~Fo94-95 (Figure 3.15). This range resembles NiO contents of olivines from Ringgit-Beser volcano, situated immediately west of Bali (R-B, Figure 2.10), with up to 0.63 wt% in Fo94 (R. Varne, unpublished data) and of other primitive olivines (Sato *et al.* 1991, Chen 1993). Adopting a NiO content in olivine of ~0.50 wt%, with a range in values for the partitioning coefficient of Ni between olivine and melt ($D_{Ni}^{Ol-Melt}$) from ~2.0 to ~2.5 (Beattie *et al.* 1991), the Ni content of the hypothetical picritic liquid ranges from ~2000 to ~1600 ppm Ni, much higher than those of primitive ankaramite bulk-rock compositions (~130 to 390 ppm Ni, Table 2.3), but matching those of ~1000 to 2000 ppm Ni postulated for highly magnesian (>20 wt% MgO) primary liquids (cf. Clarke 1970, Smith & Erlank 1982, Liang & Elthon 1990, Barnes *et al.* 1995, Lesher & Arndt 1995). This postulated course of evolution of the primary komatiitic melt supposes that the fractionating liquid does not react with the mantle through which it is passing, which is unlikely. Also, although these fractionated liquids will resemble ankaramite wholerock compositions, they are less silica-undersaturated than those preserved in melt inclusions.

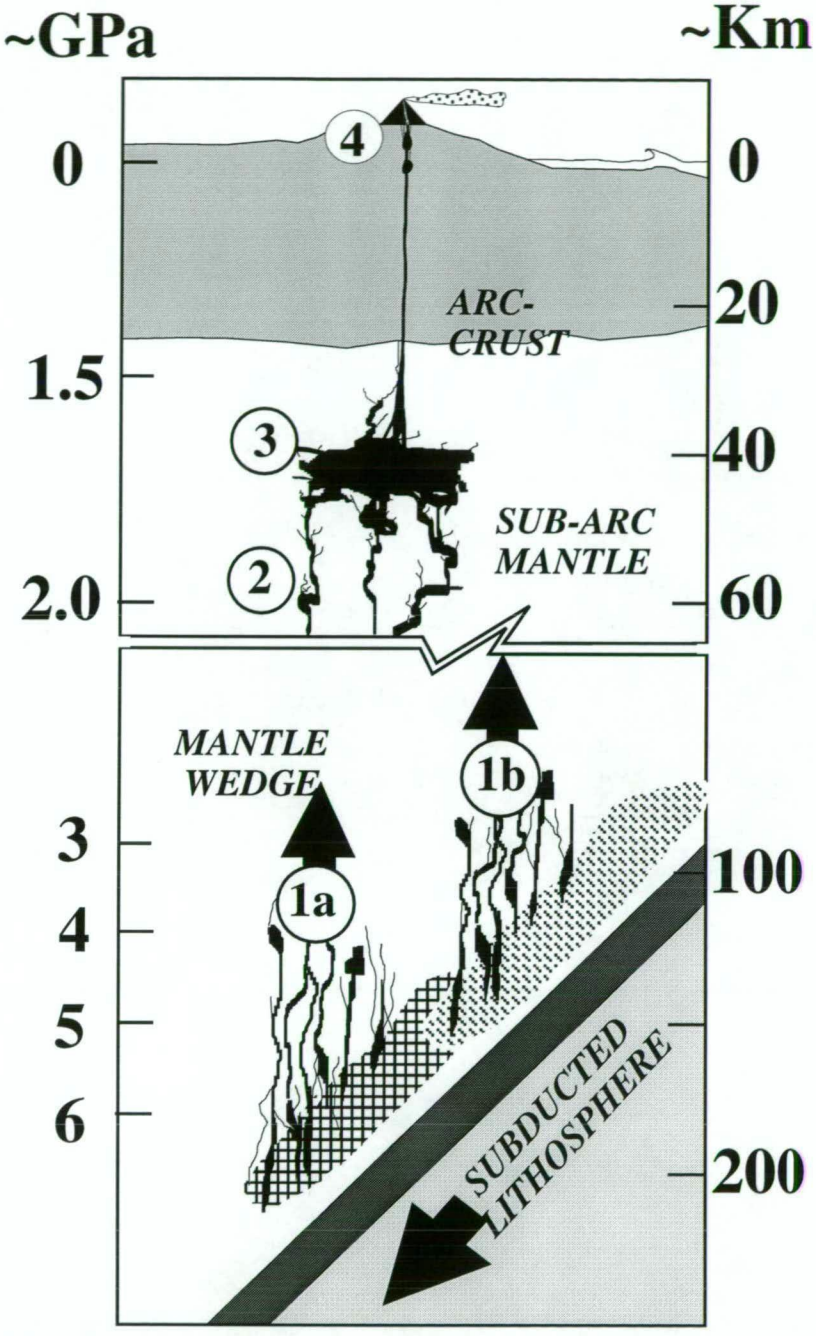

Figure 3.14 Schematic model illustrating possible stages in the formation of ankaramitic magmas in volcanic arcs. Stage 1: Generation of primary melts with variable CaO/Al_2O_3 values (*e.g.*, 0.8 to 1.6) by partial melting at pressures greater than 5 GPa (1a, cross-hatched area), or by partial melting at pressures less than 5 GPa in the presence of CO_2-rich fluids (1b, diagonal hatched area) or by some combination of these conditions. Stage 2: Trapping of ascending primary melts by early formed phenocrysts (*e.g.*, Fo>90). Stage 3: Aggregation at lower pressures of fractionating melts, possibly accompanied by re-equilibration with sub-arc mantle and magma-mantle reaction (Kelemen *et al.* 1992). Stage 4: Accumulation of melts, accompanied by differentiation in subvolcanic environment, followed by eruption. See Section 3.7 for further discussion.

TABLE 3.7

	Sunda Arc				Vanuatu Arc			
Sample	UTas48001		UTas67424		BC-13		UTas71046	
Location	Lombok		Bali		Merelava		Epi	
Fe^{3+}/Fe^{2+}		0.27		0.18		0.14		0.11
SiO_2	46.48	46.57	45.82	45.88	48.21	48.25	46.87	46.91
TiO_2	0.49	0.49	0.40	0.40	0.33	0.33	0.28	0.28
Al_2O_3	7.42	7.42	6.55	6.55	7.36	7.36	8.22	8.22
FeO*	8.64	8.21	9.48	9.18	7.76	7.54	8.53	8.33
MgO	24.92	25.27	27.67	27.91	24.99	25.17	24.68	24.84
CaO	10.13	10.13	8.47	8.47	9.79	9.79	10.29	10.29
MnO	0.12	0.12	0.14	0.14	0.12	0.12	0.11	0.11
Na_2O	1.06	1.06	0.88	0.88	1.14	1.14	0.75	0.75
K_2O	0.63	0.63	0.44	0.44	0.27	0.27	0.22	0.22
P_2O_5	0.11	0.11	0.15	0.15	0.04	0.04	0.05	0.05
Fe_2O_3		1.94		1.56		1.16		0.90
FeO		6.46		7.78		7.76		7.52
equil. Fo	94.49	95.88	94.56	95.52	95.04	95.76	94.51	95.16
Mg#	83.74	84.61	83.90	84.45	85.19	85.63	83.78	84.19
D_{Ni}	2.41	2.42	1.89	1.90	2.45	2.46	2.46	2.47
CaO/Al_2O_3	1.37	1.37	1.29	1.29	1.33	1.33	1.25	1.25
CIPW norm (mol%)								
or	2.50	2.50	1.71	1.70	1.05	1.05	0.86	0.86
ab	3.80	3.80	4.97	4.98	6.71	6.70	4.45	4.45
an	9.16	9.14	8.29	8.27	9.29	9.28	12.17	12.16
ne	2.60	2.58	0.21	0.20				
di	24.13	24.07	18.65	18.62	22.39	22.36	21.36	21.33
hy					9.52	9.50	8.21	8.23
ol	56.57	56.68	65.13	65.18	50.25	50.32	52.26	52.29
ilm	1.15	1.14	0.91	0.91	0.75	0.75	0.64	0.64
ap	0.10	0.10	0.13	0.13	0.03	0.03	0.04	0.04

Wholerock analyses of the most primitive sample in each of the four ankaramite suites with 30 wt% of equilibrium olivine added using a $K_{D\,Fe\text{-}Mg}$ values for olivine and melt of 0.30 (Roeder & Emslie 1970). Analyses in italics are composition calculated with Fe^{3+}/Fe^{2+} values determined from olivine-spinel inclusion pairs as listed. (*) all iron as FeO. Mg#=100Mg/(Mg+Fe*). D_{Ni} is the partitioning coefficients for Ni between olivine and liquid using equation of Beattie *et al.* (1991).

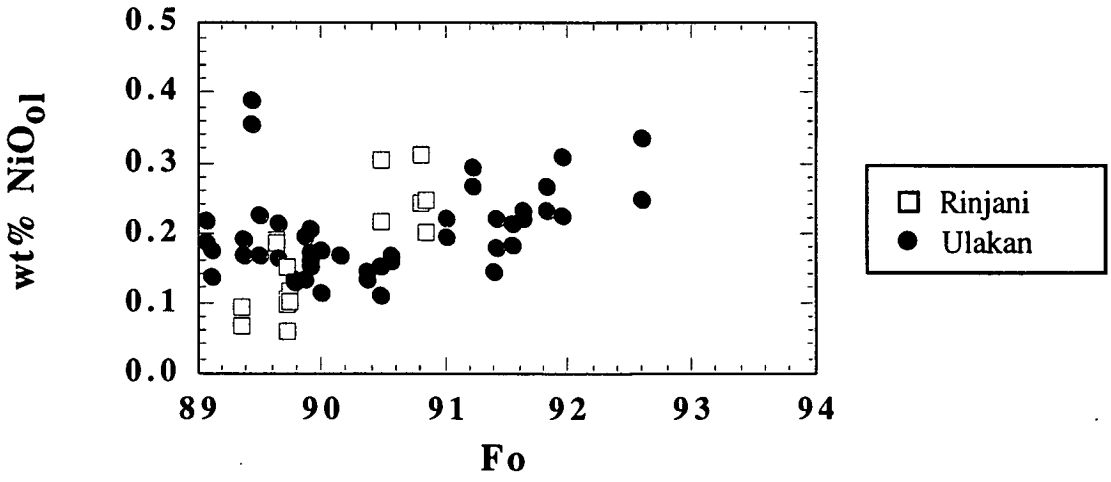

Figure 3.15 Concentration of Ni (wt%NiO) in olivine *versus* Fo in ankaramite samples from Rinjani volcano (Lombok), and Ulakan Formation (Bali). These are results of electron-microprobe analyses operating at conditions suitable for trace elements (Ca, Ni, Mn and Cr); current 200nA, beam size 2 μm, 20kV accelerating voltage and 120 seconds counting time.

If the melt inclusions in olivines and clinopyroxenes in the aggregated magma (= crystals plus melts) are samples of the melts in contact with the crystals when they grew, these melts would have been at or near their liquidus temperatures when trapped. The earliest phases to crystallize (of those which survive) in the ankaramites from Rinjani and Ulakan appear to have been the magnesian olivines and the chromian spinels (Section 2.5), later joined by clinopyroxene. The melts trapped in olivines may therefore include some melt fractions that were in existence at higher temperatures and pressures than those prevailing when the aggregated ankaramitic magmas (= crystals plus melts) adjusted to low pressure conditions before eruption, and may therefore represent primitive magmas parental to the ankaramites. Furthermore, the large variations in CaO/Al_2O_3 observed among grains (Figure 3.10) supports the aggregation of melts with variable CaO/Al_2O_3 values.

It is suggested that ascending near-primary melts with variable CaO/Al_2O_3 values and strong silica-undersaturation (Figure 3.14, Stage: 2) attain a diopside-rich normative character *via* decompression induced olivine fractionation. These melts collect, aggregate and mix at lower pressures to form the ankaramitic magma (Figure 3.14, Stage: 3). In the case of Rinjani, these pressures are constrained to less than ~2.0 GPa, by the high pressure phase relations of a melt inclusion composition in Fo_{91} (Chapter 5).

Although the composition of melt inclusions are markedly more silica-undersaturated than the host ankaramite rock, continued reaction and re-equilibration at low pressures of the aggregated magma with the surrounding sub-arc mantle could lead to silica enrichment by a process of melt-rock interaction (Kelemen *et al.* 1992). During melt-rock interaction primary liquids are modified by the dissolution of pyroxene from the wall-rock, leading to the silica-enrichment which distinguishes the ankaramite rock compositions from the compositions of primitive melt inclusions trapped in early crystallized olivine crystals (Table 3.2).

Olivine and clinopyroxene phenocrysts from the ankaramites vary in composition, are zoned, and display resorption textures. These textural features also suggest that ankaramite rocks may form as mixtures of crystals and melts at low pressures, as opposed to simple differentiation of a common parent melt. Continued crystallization and reaction in the sub-arc reservoir (Figure 3.14, Stage: 3) of these aggregated melts could account for their compositional characteristics and for the wide compositional ranges and textural features observed in the phenocrysts of erupted ankaramitic rocks (e.g., olivine ranging from ~Fo_{74} to ~Fo_{92}, and clinopyroxene ranging from $Mg^{\#}$~80 to ~93) as well as for their relative abundances (cpx:ol ~3:1, Table 2.3) and the reversely zoned rims observed in primitive olivine and clinopyroxene phenocrysts of ankaramites from Merelava (Barsdell 1988) and Epi (Barsdell & Berry 1990).

3.9 Conclusion

Melt inclusions in magnesian (Fo>90) olivine phenocrysts in primitive arc ankaramites have CaO/Al_2O_3 values about or greater than unity, and high $Mg^{\#}$ >70. If the host ankaramites crystallized from picritic or basaltic magmas enriched with clinopyroxene crystals, then the melt inclusions in olivine would have lower CaO/Al_2O_3 values. These inclusion compositions clearly

have ankaramitic affinities, suggesting that the primitive ankaramites of each suite may have been derived from ankaramitic parental melts.

The heated, homogenized olivine-hosted inclusion compositions are generally *ne*- and *lc*-normative, and some are also *cs*-normative. The primitive ankaramites from Rinjani and Ulakan have *ne*-normative wholerock compositions, and in general the inclusion compositions from their olivine phenocrysts resemble those of these ankaramite hosts but are clearly more silica-undersaturated. The more silica-undersaturated inclusion compositions also resemble leucite basanites and tephrites from the Sangenges, Soromundi and Batu Tara volcanic centres in the eastern Sunda arc to the east, so could well be representative of magmatic compositions involved in the genesis of Rinjani and Ulakan ankaramites. Compositions of olivine-hosted melt inclusions from Merelava and Epi are also *ne*-normative despite the olivine- hypersthene-normative character of their host ankaramite.

In short, it is proposed that the primitive melt inclusions with their variable CaO/Al_2O_3 values, trapped in olivines (Fo_{89-92}) in ankaramite rocks from Rinjani volcano (CaO/Al_2O_3 of 0.8 to 1.5, Figure 3.9a) and the Ulakan Formation (CaO/Al_2O_3 of 0.9 to 1.8, Figure 3.9b) represent aliquots of primary melts trapped by early formed phenocrysts (Figure 3.14, Stage: 2) before the magmas aggregated, mixed, and re-equilibrated at low pressures in the sub-arc mantle. Primitive ankaramitic magmas in volcanic arcs are viewed here as an aggregate of silica-undersaturated primitive melts with variable CaO/Al_2O_3 values, similar in composition to the melt inclusions. These melts are considered derive from more mafic precursors, generated by the high pressure partial melting of lherzolite in the presence of CO_2-H_2O rich fluids. These melts rise to sub-volcanic arc-mantle reservoirs where they aggregate and continue to crystallize, At these relatively lower pressures, reaction and re-equilibration by melt-rock interaction with the surrounding mantle impart the relative silica enrichment observed in wholerock analyses of ankaramite.

Chapter 4:
"Fe-loss" in melt inclusions hosted in olivine

4.1 Introduction

This chapter describes a phenomenon known as "Fe-loss" whereby re-equilibration between the melt inclusion and the host olivine at temperatures lower than trapping results in decreasing FeO* contents. This process has important implications for the interpretation of homogenized melt inclusion compositions and an attempt is made is this chapter to explain how it may occur.

After trapping, fractional crystallization of the host and other daughter phases, modify the original composition of the melt in the inclusion. This process can be reversed through homogenization heating experiments to remelt daughter phases and obtain the original composition of the trapped melt. However, while most major element contents of homogenized melt inclusions trapped in olivine overlap with the trends defined by the host rock suite, FeO* contents of melt inclusions trapped in olivine phenocrysts from island arc suites are often as much as ~5 wt% lower (Sobolev & Danyushevsky 1994). This is known as the phenomenon of "Fe-loss", whereby the trapped melt re-equilibrates with the host in such a way as to cause the melt to lose Fe (Gurenko *et al.* 1988, 1992, Danyushevsky *et al.* 1992 and Sobolev & Danyushevsky 1994). This re-equilibration involves diffusion of Fe from the melt into the host, and is driven by the $Mg^{\#}$ disequilibrium between the fractionated residual melt and the host olivine crystal while still in the magma.

It will be shown in this chapter that the FeO* content of heated melt inclusions trapped in olivine in all four ankaramite suites, have been re-equilibrated by "Fe-loss". As a result the compositions of these inclusions have significantly lower FeO* content compared to their original composition and cannot be used directly as representative of the melt from which the host crystal formed. This chapter describes how this re-equilibration process may operate with particular reference to those melt inclusion trapped in olivine studied in this thesis.

4.2 *Evidence for "Fe-loss"*

Sobolev and Danyushevsky (1994) note that homogenized melt inclusions that have re-equilibrated with their host by "Fe-loss" have (1) systematically lower FeO* contents at a given MgO compared to the natural glassy groundmass and wholerock compositions and (2) high $K_D{}^{Ol\text{-}Melt}_{Fe\text{-}Mg}$ values »0.30. In the melt inclusion heating experiments presented in this thesis,

complete homogenization was not achieved (Section 3.3). The compositions of heated melt inclusions are therefore depleted in MgO content as a result of the unmelting of daughter olivine from the wall (*i.e.*, underheating). This counteracts the effect of "Fe-loss", and makes $K_D^{Ol\text{-}Melt}_{Fe\text{-}Mg}$ values an inadequate indicator of "Fe-loss". In the heated inclusions, $K_D^{Ol\text{-}Melt}_{Fe\text{-}Mg}$ values vary over a wide range above and below the equilibrium $K_D^{Ol\text{-}Melt}_{Fe\text{-}Mg}$ values (Figure 3.4), and for this reason the assessment of "Fe-loss" will be based upon variations in FeO* content alone.

4.2.1 FeO content of heated melt inclusions*

FeO* contents of heated melt inclusions in the Rinjani and Ulakan suites vary between those of their glassy melt inclusions and those of the ankaramitic host rocks (Figure 4.1a-b). In Rinjani volcano heated melt inclusions in Fo_{90} have variable FeO* contents that range from as low as 5 wt% up to values similar to the host rock trend with ~10 wt% FeO* (Figure 4.1a). Heated melt inclusions trapped in magnesian olivines (Fo>90) of the Ulakan suite have lowest FeO* content (~3 wt%), compared to those melt inclusions trapped in less magnesian olivines tend to have higher FeO* content (Figure 4.1b). In Merelava, heated inclusions in Fo_{88} also have a wide range in FeO* content, and their lowest value in all olivines increases with decreasing Fo (Figure 4.1c). Inclusions in Fo<84 from Merelava have FeO* contents within the wholerock field. In Epi, heated melt inclusions in olivine also have decreasing FeO* contents with increasing Fo (Figure 4.1d). Inclusions in olivines with $<Fo_{85}$ have FeO* content similar to the wholerock values, whereas those in more magnesian olivines have much lower FeO*.

Two trends are therefore recognizable from Figure 4.1. Trend I, defined by the lowest FeO* content at any given Fo with increasing Fo (Figure 4.1b-d), and Trend II defined by the range in FeO* content of heated melt inclusion at a constant Fo content (Figure 4.1a-c). The ramifications of these two trends are discussed in Section 4.6 where it will be shown that the variations of these trends are governed by (1) $Mg^{\#}$ re-equilibration rates between the trapped melt and the host, and (2) by the residence time of the host phenocrysts in the magma. These two trends (I and II) together with the wholerock trend also define a "Fe-loss triangle" zone (Figure 4.2). The model presented here describes the origin of this triangle and explains why the composition of heated melt inclusions in olivine are to be found within it.

*4.2.2 Evidence from variations in FeO**

The compositions of most heated melt inclusions in these experiments are affected by incomplete remelting of olivine on the wall, whereas some instead, are affected by overheating and therefore acquired much higher MgO contents (Chapter 3). In both cases nonetheless, FeO* contents should remain much the same (~±1wt% FeO*), provided the FeO* content of the host olivine and the original rapped melt were approximately similar. This is illustrated by the

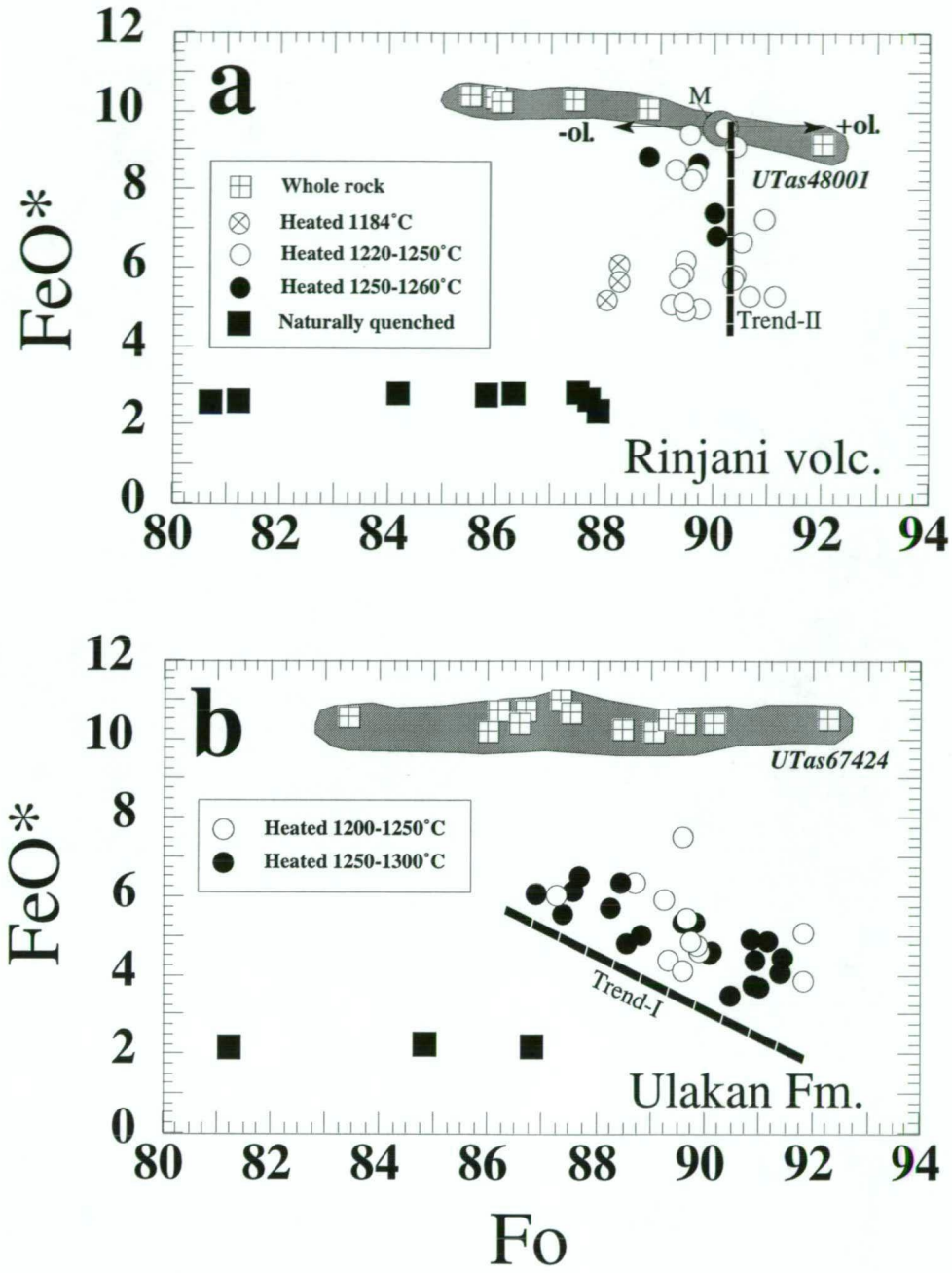

Figure 4.1 FeO* *versus* Fo content of heated (circles) and naturally quenched (filled squares) melt inclusions in olivine. FeO* content of whole rock analyses are shown for comparison (squares with crosses) with their equilibrium Fo calculated using KD=0.3 (Roeder & Emslie, 1970) and Fe2O3/FeO values for the melt (Rinjani=0.30, Ulakan=0.20, Merelava=0.15 and Epi=0.12) obtained from olivine-spinel inclusion pairs using relations of Maurel & Maurel (1982) (Chapter 2). In all four suites FeO* content of wholerock analyses show slight variation (mostly within 1 wt%) due to the combined effects of fractionation and accumulation of olivine and clinopyroxene. Horizontal arrows in (a) indicate evolution of the melt by substruction (+ol.) or addition (-ol.) of equilibrium olivine. Dashed line labeled Trend-I in Figure b, c, and d, indicate general trend of decreasing FeO* content of heated melt inclusions with increasing Fo content. Dashed line labeled Trend-II in Figure a, and c indicates wide range in FeO* content in melt inclusions hosted by olivine of similar Fo content. See text for explanation. Analyses for glassy inclusions from Table 3.3, for heated melt inclusions from Appendix 2 and for wholerock analyses from Table 2.1.

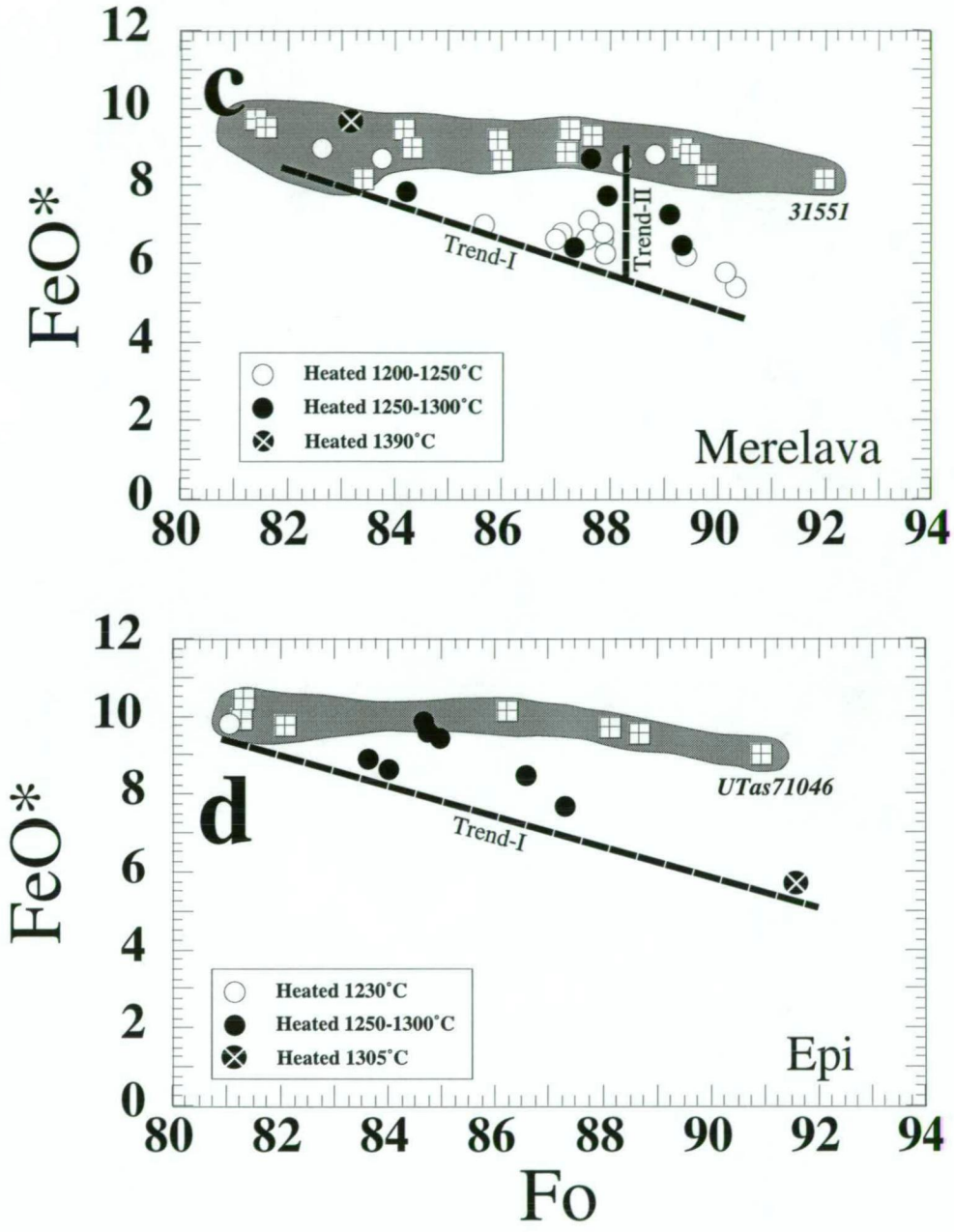

Figure 4.1 continued.

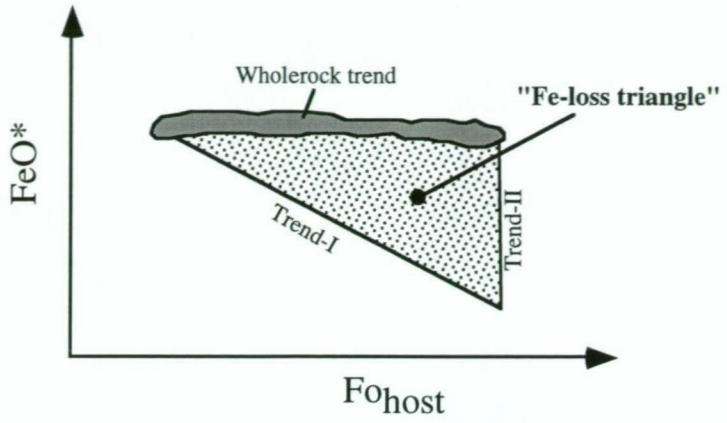

Figure 4.2 Variation in FeO* content of homogenized melt inclusions trapped in olivine. Trend-I is governed by the residence time of the olivine phenocrysts in the magma chamber whereas Trend-II is governed by the rate of re-equilibration. The wholerock trend is defined by the compositional variation of the rock suite. These three trends define a "Fe-loss triangle" within which the composition of melt inclusions after homogenization are to be found.

differentiation path that would be followed by the removal (-ol) or addition (+ol) of equilibrium olivine from a hypothetical primitive melt (M) in equilibrium with Fo$_{90}$ (horizontal arrows, Figure 4.1a). This path is sub-parallel to the olivine+clinopyroxene fractionation trend defined by wholerock analyses (shaded area) and oblique to Trend II. Thus the variation in FeO* contents of melt inclusions at constant Fo (e.g., 5 to 10 wt% FeO* in ~Fo$_{90}$, Figure 4.1a) can not be explained by olivine fractionation of a common melt alone. These variations in FeO* at constant Fo require an alternative explanation.

All four ankaramite suites show little variation in wholerock FeO* content with decreasing $Mg^{\#}$, which is typical of olivine+clinopyroxene dominated fractionation (Figure 4.1). Trend I however, is oblique to this trend and can not represent the composition of trapped primitive melts, evolving by olivine+clinopyroxene fractionation. The variation in FeO* content in heated inclusions with decreasing Fo defined by Trend I therefore, also requires an alternative explanation to crystal fractionation.

Models of mantle melting indicate that the calculated FeO* content of primary melt (1-4 GPa) increase with pressure (Langmuir *et al.* 1992). Melting experiments on a wide range of peridotite compositions also indicate similar trends (Jaques & Green 1980, Falloon & Green 1988, Falloon *et al.* 1988). The FeO* contents of primary melts are mostly governed by the partitioning of FeO between the residual olivine and melt ($K_D{}^{Ol\text{-}Melt}_{FeO}$). $K_D{}^{Ol\text{-}Melt}_{FeO}$ increases with increasing pressure but with increasing depth of melting along the mantle solidus the temperature effect dominates causing $K_D{}^{Ol\text{-}Melt}_{FeO}$ to decrease (Langmuir *et al.* 1992). The composition of primary

melts therefore become richer in FeO* with increasing pressure. If this temperature-depth relationship applies for the arc mantle wedge, then the variations in FeO* of homogenized melt inclusions (Trend-I and Trend-II, Figure 4.2) may be attributed to variable depth of melting (i.e., varying pressures). Early formed magnesian olivine phenocrysts could trap aliquots of these near-primary melt fractions at different depths before mixing, thus preserving their variable FeO contents prior to aggregation of the ankaramitic magma (Trend-III, Figure 4.2).

The CaO/Al_2O_3 values of primary mantle melts increase systematically with pressure (Herzberg 1992), yet the FeO* content of melt inclusions in magnesian olivines (>Fo_{90}) show no correlation with their CaO/Al_2O_3 values (Figure 4.3). Moreover, if the variations in FeO* content of melt inclusions are caused by partial melting at different pressures, then the low FeO* content of some melt inclusions from Ulakan (<4 wt%, Figure 4.1b) would indicate that partial melting occurred at pressures much less than ~1 GPa (Langmuir *et al.* 1992). Such low pressures are inconsistent with a high pressure origin for ankaramitic melts (Chapter 3). In addition, if the variable FeO* content observed in melt inclusions reflects different melting pressures, then the less magnesian olivine phenocrysts are likely to contain melt inclusions with lower FeO* contents, not higher, and thus inconsistent with Trend-I (Figure 4.2). Another feature contrary to the effect of pressure is the lack of "Fe-loss" in melt inclusions from settings other than arc setting, e.g. melt inclusions in MORB olivines (L. V. Danyushevsky, pers. comm.). Thus, the likelihood that the variations in FeO* of homogenized melt inclusions are pressure related is discarded.

In summary, if the composition of homogenized melt inclusions are only affected by olivine crystallization on the walls then FeO* contents should vary along an olivine fractionation trend. Trends I and II are inconsistent with olivine fractionation and must therefore reflect another process, and although the FeO* content of primary mantle melts are pressure dependent, such process is considered too constrained to account for the observed variations in FeO*. This

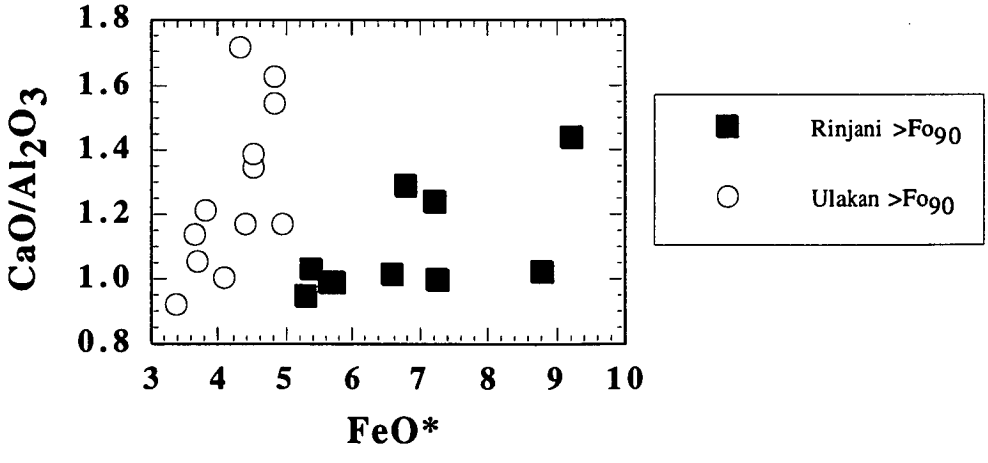

Figure 4.3 CaO/Al_2O_3 values *versus* FeO* content of optically homogenized melt inclusions hosted in magnesian olivine phenocrysts (Fo_{90-91}) from Rinjani and Ulakan ankaramite suites.

observations together with the abnormally low FeO* contents compared to wholerock values suggest that "Fe-loss" has occur. The highest FeO* contents of three melt inclusions from Rinjani overlap with the wholerock field and these are therefore considered to have undergone least "Fe-loss".

4.3 The re-equilibration of melt inclusions in olivine

In this section, a model after L.V. Danyushevsky (pers. comm) is described to explain how the re-equilibration between a melt inclusion with its host olivine may modify the original composition of the trapped melt. This model is then applied to the observed FeO* contents of heated melt inclusions in this study to explain the observed variations in FeO* and to assess the extent of "Fe-loss".

4.3.1 Basic model

The possible fractional crystallization and re-equilibration path of a hypothetical melt M (Mg# 74.5, Fe_2O_3/FeO= 0.2) trapped at high temperatures in equilibrium with olivine (Fo_{92}) are illustrated in Figure 4.4. In this model, it is assumed that at the moment of eruption the liquid in the host magma, and the residual melt in the inclusion, have approximately the same MgO content buffered by the temperature of olivine-saturated liquids. Continued fractional crystallization of olivine on the inclusion walls after trapping and before eruption, forms a zoned rim that rapidly depletes the residual melt in MgO, (path M to A, Figure 4.4). After fractional crystallization of approximately 30 wt% olivine, the olivine rim is zoned from Fo_{92} to Fo_{83}, and it surrounds a residual melt of Mg# 55.4 in equilibrium. This process occurs while the host olivine phenocrysts is in the magma.

While still in the magma, at high temperatures (>1000°C) and before eruption, the $Mg^{\#}$ of this zoned olivine rim (Fo_{83-92}) chemically re-equilibrates with the host to Fo_{92}, by Fe-Mg diffusion. Diffusion rates in the melt (which at this point still liquid) are faster than in the host olivine crystal, and therefore, the residual melt also re-equilibrates simultaneously as the composition of the zoned rim in contact with the melt changes. This re-equilibration continues until the $Mg^{\#}$ of the residual melt is at chemical equilibrium with the host olivine. This residual melt attains chemical equilibrium with the host (Fo_{92}) by: 1) the diffusion of Fe from the melt to the host ("Fe-loss") and 2) the diffusion of Mg from the host into the melt. The change in composition of the host olivine caused by the diffusion of Fe from the melt is however undetectable due to its relatively larger volume. The MgO content of the melt is however controlled by temperature and therefore the addition of Mg by diffusion leads to some extra

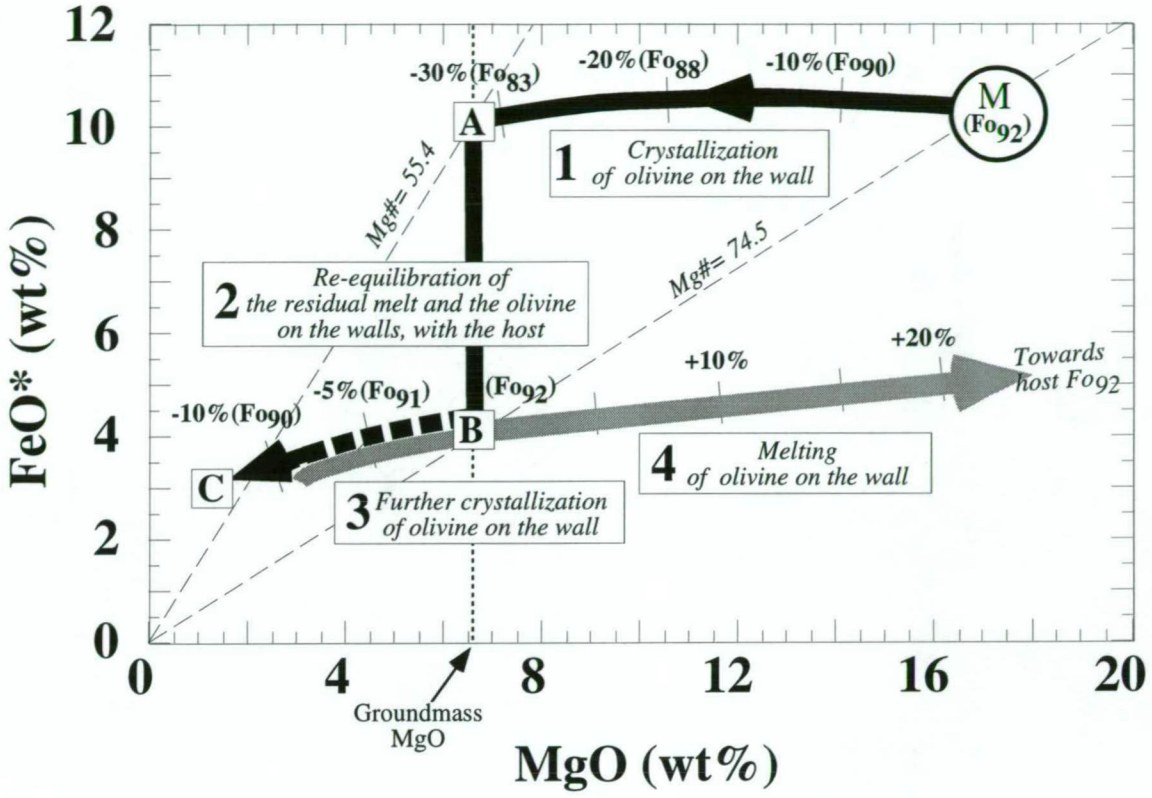

Figure 4.4 Possible crystallization-reequilibration-crystallization-melting path (thick dark arrows) of a hypothetical melt "M" (Mg#74.5, Fe_2O_3/FeO=0.2) trapped in equilibrium with olivine (Fo92). Three main stages of this path are,

Stage 1: Depletion in olivine component by the crystallization of an outer-rim of zoned olivine on the walls of the inclusion (path M to A).

Stage 2: mg# reequilibration of the outer-rim of zoned olivine and residual melt, with the host olivine (path A to B).

Stage 3: Further depletion in olivine components by the growth of an inner-rim of zoned olivine during rapid cooling during and after eruption (path B to C).

Stage 4: During a heating experiment path B to C is reversed, but with increasing temperature the composition of the melt is driven towards the composition of the host olivine (Fo92) not M. This occurs because the reequilibration path A-B is irreversible. Note that if reequilibration does not occur (i.e., A-B=0), then the original FeO* content of the melt M is recovered by heating along the path C-M.

Negative percentages indicate approximate wt% of olivine fractionated. Fractional crystallization paths are calculated by stepwise mass balance substruction of equilibrium olivine at increments of 1 wt% assuming a Fe_2O_3/FeO in the melt of 0.2. Dashed lines represent FeO*/MgO values in the melt in equilibrium with Fo83 and Fo92. Dotted line indicates a hypothetical MgO content for the liquid of the host magma (now groundmass) at the moment of eruption. Positive percentages indicate wt% of host added to the melt. Fo values in brackets indicate composition of equilibrium olivine on the rim.

precipitation of olivine on the walls. The net result of this re-equilibration is therefore a decrease in FeO* and an increase in the $mg^{\#}$ of the melt from 55.4 to 74.5. Its MgO content however, is largely controlled by temperature, and thus will remain approximately constant during re-equilibration and similar to the MgO content of the liquid in the host magma. Thus, re-equilibration between the residual melt and the host olivine produces, in this ideal case, a decrease in FeO* at constant MgO (path A to B, Figure 4.4). With increasing re-equilibration of the residual melt at high temperatures, its FeO* content is driven towards B. At B, the residual melt has Mg# 74.5 and is in equilibrium with the host (Fo_{92}). At this stage, re-equilibration between the residual melt and the host olivine is complete.

During eruption relatively faster cooling cause rapid crystallization of olivine on the walls, which further depletes the residual melt in MgO (path B to C, Figure 4.4), and quenched the residual melt to a glass at C. This produces an additional inner rim of zoned olivine on the walls. After crystallization of approximately 10 wt% olivine this inner rim is zoned from Fo_{92} to Fo_{90} and the residual melt contains ~2 wt% MgO and ~3 wt% FeO*. However the composition of this liquid as it fractionates can not be accurately ascertained because crystallization may not be controlled by equilibrium K_D values. At this relatively low subsolidus temperatures re-equilibration is inhibited and the residual glass and the zoned inner rim of olivine preserve their compositions

During a melt inclusion heating experiment, melting of the inner zoned rim reverses the composition of the residual melt along the path C to B. At B, the inner rim is completely dissolved by heating and melting of the outer re-equilibrated rim begins. Further heating however, will drive the residual melt towards Fo_{92} not M, and thus the crystallization path (M-A-B) will not be reversed. As a result, heated melt inclusions inherit relatively low FeO* contents. Thus the composition of quenched glasses from heated melt inclusions hosted in olivine, may have significantly lower FeO* contents compared to their host if re-equilibration between the residual melt and the host olivine occurred at high temperatures after trapping but before eruption (path A to B, Figure 4.4).

4.3.2 Model considering simultaneous re-equilibration

A more realistic model considers re-equilibration of the residual melt simultaneously with crystallization of olivine on the walls (*i.e.*, decreasing temperature in the magma chamber). In this case, paths M to A, and A to B (Figure 4.4) occur in small increments such that the resultant path is a curve joining M to B whose slope depends on the rate of re-equilibration. The possible paths for crystallization, and simultaneous re-equilibration at three different rates, of a hypothetical melt M are illustrated in Figure 4.5. Along path M-B1 (Figure 4.5a) no re-equilibration occurs, and the residual melt evolves by fractional crystallization (C) of olivine on the walls. At B1, after

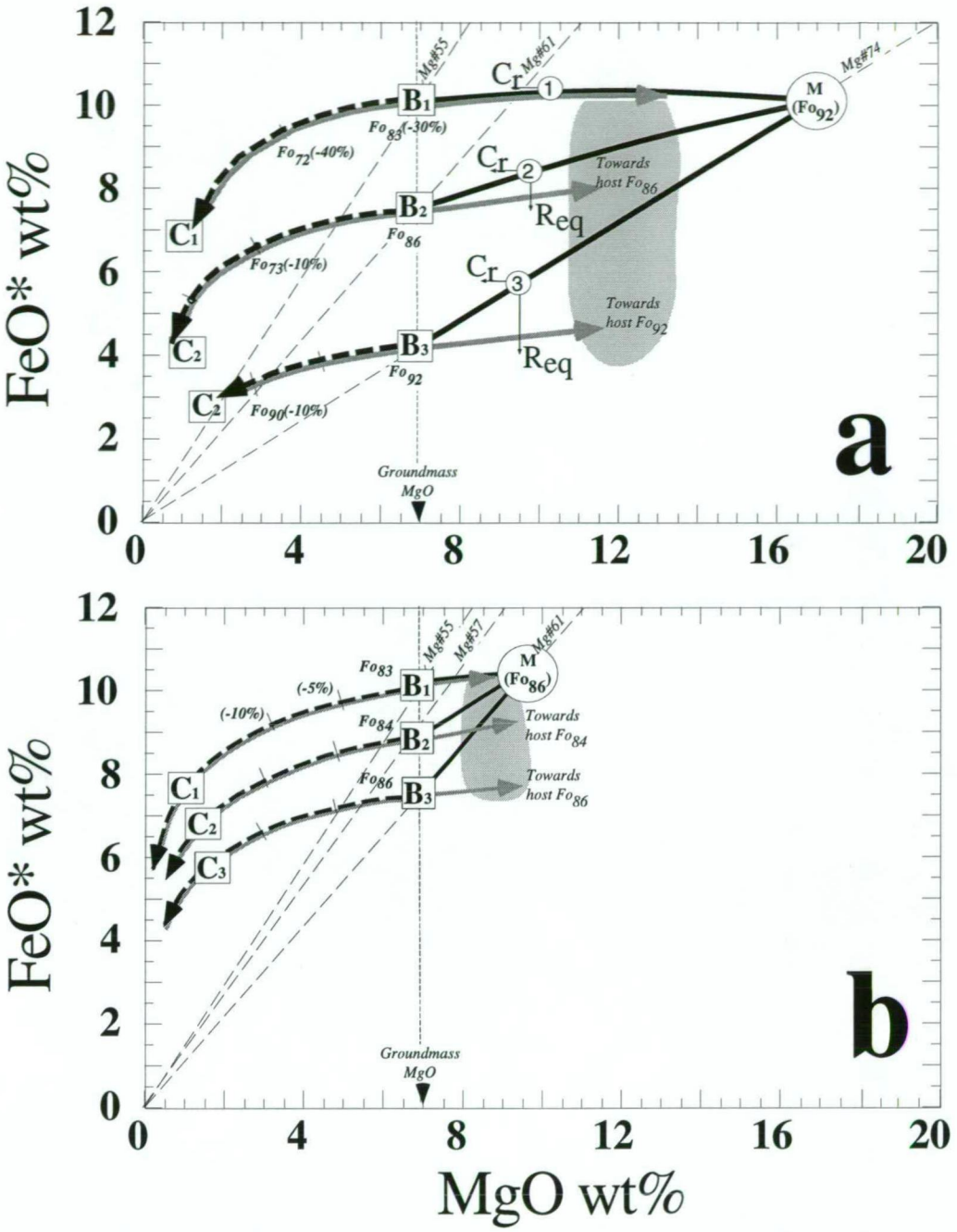

Figure 4.5 Possible model for the simultaneous reequilibration of the residual melt with the host olivine, at different rates.

(a) A melt M (Mg# 74) trapped in equilibrium with Fo92. Thick arrows represent crystallization and re-equilibration paths. Light thick arrow represent melting path during experiment. Eruption is considered to occur when the MgO in the melt is 7 wt%. Fe_2O_3/FeO=0.2. Path M-B1-C1 represents crystallization with no reequilibration. Path M-B2-C2 represents crystallization with partial reequilibration. Path M-B3-C3 represents crystallization with complete re-equilibration. Paths M-B1, MB-2 and M-B3 represent increasing rates of re-equilibration (R_{eq}) relative to crystallization (C_r). B represents the composition of the residual melt at the moment of eruption, and C after further crystallization during natural quenching. Negative percentages indicate wt% of olivine fractionated. Dashed line represent FeO*/MgO value of melt in equilibrium with host (Fo92) and with olivine on the rim. See text for explanation. From this diagram it can be seen that heated melt inclusions in similarly magnesian olivines can inherit a range of FeO* values provided that the residual melts in each inclusion re-equilibrate at different rates.

(b) A hypothetical melt M (Mg#61) trapped in equilibrium by a relatively less magnesian olivine (Fo86). Symbols as in (a) above. Paths M-B1-C1, M-B2-C2, and M-B3-C3 represent increasing rates of re-equilibration between the residual glass and the host (Fo86). The relatively smaller fractionation interval between trapping (M) and eruption (B) reduces the possible maximum extent of Fe-loss. From this diagram it can be seen that for a given constant re-equilibration rate, heated melt inclusions hosted in relatively less magnesian olivines experience lesser degree of Fe-loss relative to those inclusions hosted in more magnesian olivines. This is because they are trapped at a later stage and had a shorter interval of pre-eruption crystallization.

30% crystallization, olivine on the rim is zoned from Fo_{92} to Fo_{83} and the residual melt has Mg# 55. During eruption and before quenching, more olivine crystallizes on the walls of the inclusion that further depletes the melt in MgO (path A1 to C1, Figure 4.5a). During a melt inclusion heating experiment, olivine from the walls is remelted and the composition of the residual melts follows the reverse path (C1-A1-M, Figure 4.5a). Because re-equilibration did not occur, FeO* content of heated melt inclusions are only affected by the addition (overheating) or substruction (underheating) of olivine from the wall.

Path M-B2-C2 of Figure 4.5a is similar to M-B1-C1, but along the latter, partial re-equilibration (R) occurs simultaneously while olivine crystallizes on the wall (C). At B2, the olivine rim is zoned from Fo_{92} to Fo_{86} and the residual melt has Mg# 61. However, the olivine inner rim that forms after B2 and drives the residual melt towards C2, does not re-equilibrate, and during a heating experiment this path is reverted (C2 to B2, Figure 4.5a). Melting of the re-equilibrated rim (now of average composition Fo_{86}) formed along M-C2, drives the melt towards Fo_{86} and not M. Thus these heated melt inclusions have moderately lower FeO* content.

If the re-equilibration rate is fast compared to the growth rate of olivine on the walls (*i.e.*, cooling rate), the residual glass keeps re-equilibrating with the host (Fo_{92}) by "Fe-loss", maintaining Mg# 74 (Path: M-B3, Figure 4.5a). At B3, the olivine rim is Fo_{92} (unzoned) and the residual melt has initial $Mg^{\#}$ 74. After eruption the residual melt evolves towards C3. During heating, this path is reversed (C3 to B3, Figure 4.5a), but after B3 the melt is driven towards (Fo_{92}), not M as a result of re-equilibration. These heated inclusions show lowest FeO* content because of their complete re-equilibration with the host (Fo_{92}) at high temperatures.

From Figure 4.5a, therefore, it can be seen that melt inclusions in similarly magnesian olivines (e.g., Fo_{92}), can undergo a range of "Fe-loss" (light shaded area) provided that the residual melt re-equilibrates at various rates within each inclusion. Thus, heated melt inclusion in similarly magnesian olivines can inherit a range of FeO* (light shaded area) contents provided that each inclusion re-equilibrates at different rates.

According to the model described in Figure 4.5a, only melt inclusions that do not re-equilibrate with the host preserve the original FeO* content. However, inclusions trapped immediately before eruption may also show no "Fe-loss" because of their relatively smaller fractionation interval between trapping and eruption. This case is described below.

The possible fractional crystallization and re-equilibration path of a hypothetical melt M (Mg# 61) trapped in equilibrium with a less magnesian olivine (Fo_{86}) is illustrated in Figure 4.5b. Paths M-B1-C1, M-B2-C2, and M-B3-C3 (Figure 4.5b) represent increasing rates of re-equilibration between the residual melt and the host (Fo_{86}). The relatively smaller fractionation interval between trapping (M) and eruption (B) reduces the possible maximum extent of "Fe-loss"

(shaded area, Figure 4.5b). Therefore, given a constant re-equilibration rate, melt inclusions hosted by less magnesian olivines undergo relatively lesser degree of "Fe-loss" (Figure 4.5).

The re-equilibration process described above and illustrated in Figure 4.5 explains the relatively low FeO* content observed in heated melt inclusions in olivine from all four suites of ankaramites. Thus the decreasing FeO* content with increasing Fo of the host (Trend I, Figure 4.1) represents the increasing fractionation interval in melt inclusion before eruption trapped in more magnesian olivines (Figure 4.5a) compared to those in less magnesian olivines (Figure 4.5b). Also, the range in FeO* for a given Fo content (Trend II, Figure 4.1) represents varying rates of re-equilibration. In all cases, the largest extent of "Fe-loss" (lowest FeO* content) is defined by two parameters, (1) the $Mg^{\#}$ of the melt at the moment of trapping (dashed line, Figure 4.5), and (2) the MgO content of the residual melt at the moment of eruption (dotted line, Figure 4.5). Both parameters are independently defined by (1) the composition of host olivine and Fe_2O_3/FeO values of the melt, and (2) the MgO content of the groundmass, respectively. "Fe-loss" by re-equilibration is not likely to continue to the left of B in Figure 4.5 and therefore B3 defined the lowest FeO* content, i.e., the maximum extent of "Fe-loss" possible.

4.4 Assessment of "Fe-loss" in heated melt inclusions

The re-equilibration processes described in Figure 4.5 are now applied to the observed FeO-MgO composition of heated melt inclusions in olivines from the four ankaramite suites (Figure 4.6). Possible fractionation paths, considering re-equilibration after trapping, are constructed for a melt M in equilibrium with the host. In these models, Fe_2O_3/FeO values in the melt are values determined from olivine-spinel inclusion pairs (Maurel & Maurel 1982) (Chapter 2), K_D= 0.3 (Roeder & Emslie 1970), and FeO* content of the melt M is defined by the whole rock trend.

4.4.1 FeO content of heated melt inclusion from Rinjani*

In Figure 4.6a, a melt M ($Mg^{\#}$73) is trapped in equilibrium with Fo_{90}. Along path M to B1, no re-equilibration occurs and the residual melt evolves by fractional crystallization of olivine on the wall. Paths M to B2, M to B3, and M to B4 are three possible fractionation paths, each representing crystallization at faster re-equilibration rates. A broad range of paths are possible, however, between M-B1 and M-B4, and only two examples are shown here. At B2 and B3, the residual melt has partially re-equilibrated to $Mg^{\#}$55 and $Mg^{\#}$63, and the olivine rim to Fo_{80} and Fo_{85}, respectively. Along M-B4, the residual melt rapidly re-equilibrates with the host (Fo_{90}) and maintains $Mg^{\#}$73. With heating, the crystallization path M to B1 is reversed and the inclusion regains their original FeO* content. However, melt inclusions that re-equilibrated are driven with increasing temperature from B2, B3 and B4 towards Fo_{80}, Fo_{85}, and Fo_{90}, respectively.

The heated melt inclusion in Fo_{90} therefore, appear to have partially re-equilibrated at various rates whereas others have FeO* content similar to the trapped melt M and show no "Fe-loss" compared to the host rock (UTas48001). According to this model, the lowest possible FeO* by re-equilibration is defined by the path: B4 towards Fo_{90}, yet heated melt inclusions have higher FeO* values. This suggest only partial re-equilibration of the residual melt. Variation in MgO content of heated melt inclusion result primarily from variations in heating temperatures: 1220°C to 1240°C (filled triangles, Figure 4.6a), and 1250°C to 1260°C (filled triangles in circles).

4.4.3 FeO content of heated melt inclusion from Ulakan Fm.*

In Figure 4.6b, FeO* content of heated melt inclusion in Fo_{87} (filled diamonds, 1280°C to 1310°C) and Fo_{91} (filled triangles, 1280°C to 1300°C) are lower than the host rock (UTas67424) and differ from each other. Melts M1 and M2, with Mg# 67 and Mg# 75, represent melts trapped in equilibrium with Fo_{87} and Fo_{91}. With continued crystallization and rapid re-equilibration at high temperatures, the trapped melt is driven from M1 and M2, towards B1 and B2, respectively. B marks the moment of eruption. Beyond this point re-equilibration is negligible and the residual melt evolves by fractional crystallization (paths B1 to C1 and B2 to C2, respectively) before being naturally quench to a glass (C1 and C2). During heating, these paths are reversed but beyond B1 and B2, the heated melt inclusions are driven towards Fo_{87} and Fo_{91}, respectively. Heated melt inclusion in Fo_{87} (filled diamonds) and Fo_{91} (filled triangles) cluster close to these olivine control lines, in accord with re-equilibration by "Fe-loss".

4.4.3 FeO content of heated melt inclusions from Merelava*

Heated melt inclusions in Fo_{90} (filled triangles, 1242°C) and Fo_{84} (filled diamonds: 1240°C, filled diamond in circle: 1250°C, open diamond in filled circle: 1390°C) from Merelava (Figure 4.6c) have FeO* contents within the range predicted by re-equilibration of the residual melt with the host at high temperatures: M1 to B1 and M2 to B2, respectively. With increased heating the composition of melt inclusions progress from B1 and B2, towards Fo_{84} and Fo_{90}, respectively. These trends are highlighted by the composition of an overheated melt inclusion (1390°C) which lies along this Fo_{84} control line and has been affected by the melting of host olivine (open diamond in filled circle). The relatively lower FeO* content of two heated melt inclusions in Fo_{90} (~4 wt% lower) compared to the three melt inclusions in Fo_{84}, represents the larger extent of re-equilibration at high temperatures.

4.4.4 FeO content of heated melt inclusions from Epi*

Heated melt inclusions in Fo_{84} (filled diamond: 1280°C, filled diamond in circle: 1230°C to) and Fo_{90} (filled triangle, 1305°C) from Epi are shown in Figure 4.6d. Melts M1 and M2, are

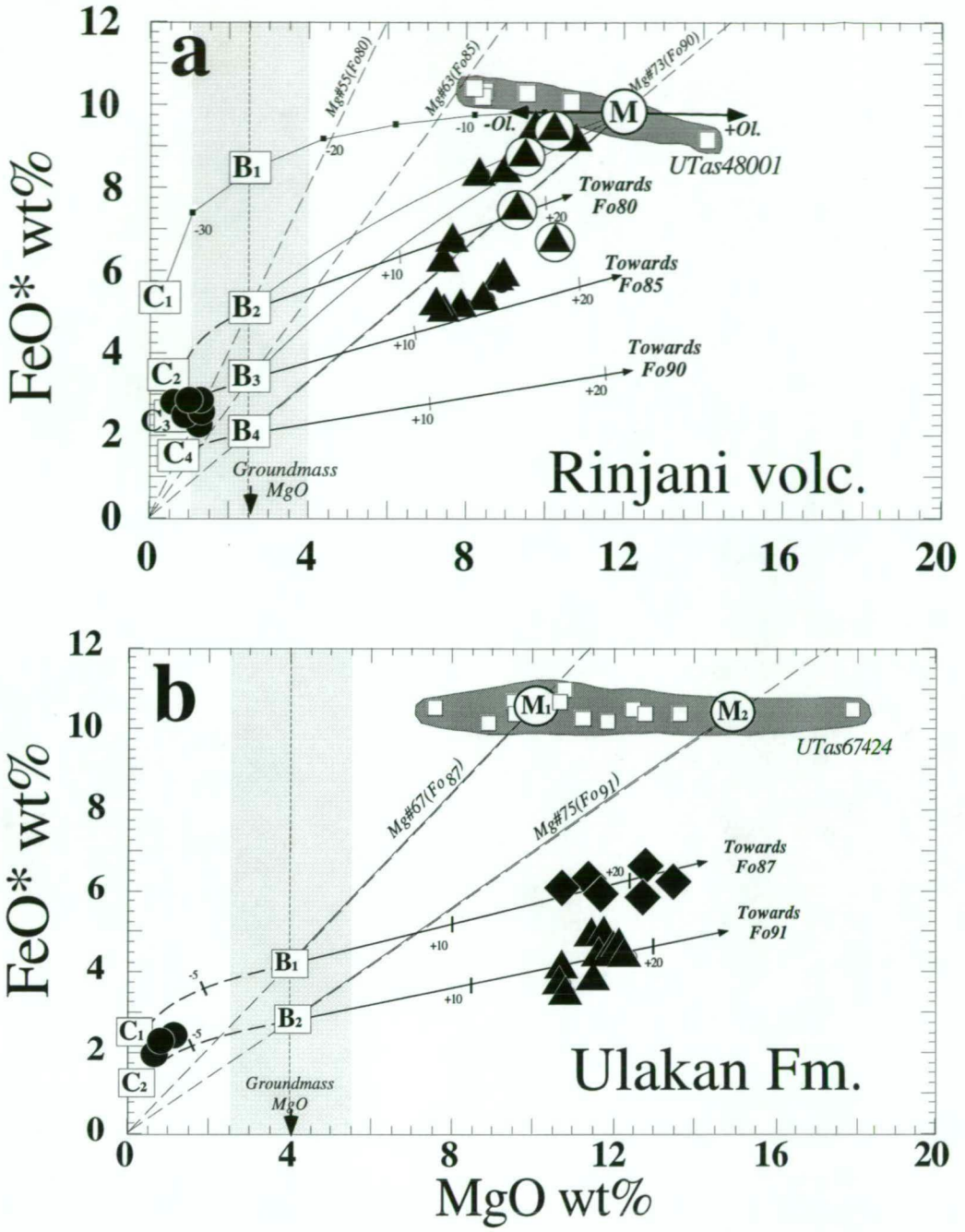

Figure 4.6 FeO*, MgO content of heated melt inclusions (filled triangles and filled diamonds), and naturally quenched inclusions (filled circles), compared to FeO*, MgO content of whole rock analyses (open squares) from four suites of ankaramite. Possible fractionation path considering crystallization and re-equilibration after trapping are shown for a hypothetical melt M in equilibrium with its host. This re-equilibration process illustrated in Figure 4.3, and described in the text. Fe_2O_3/FeO in the melt determined from olivine-spinel inclusion pairs (Chapter 2), K_D=0.3 (Roeder & Emslie 1970).

(a) Four possible fractionation paths at different re-equilibration rates for a melt M (Mg#73) trapped in equilibrium with Fo90 from Rinjani volc. Heating temperatures as follows, filled triangles: 1220 to 1240°C, filled triangles in circles: 1250°C to 1260°C. Vertical dotted line at MgO~2.5 wt% represents residual melt at the moment of eruption. B1: FeO* content at the moment of eruption after fractional crystallization of olivine on the wall. Numbers along path indicate amount (wt%) of olivine fractionated (-) during natural cooling or added (+) during the heating experiment to the melt. B2, B3, and B4: FeO* content of the residual melts at the moment of eruption after increasing rates of Fe-loss at high temperatures. Dashed lines: FeO*/MgO values that correspond to the Mg# value in equilibrium with the olivine rim (Fo85 and Fo80). C1, C2, C3 and C4: approximate FeO*, MgO content of the residual melt after further crystallization of ≈10 wt% olivine after eruption. Filled circles: naturally quenched inclusion in Fo81-88. Groundmass MgO content estimated by mass balance substruction of phenocryst phases (average analysis) from whole rock analysis on the basis of modal proportions: ol=10%, cpx=38%, plag=2% (959 points counted) and specific densities: ol=3.3, cpx=3.2, plag=2.8 (Deer *et al.* 1985) and melt= 2.7 (Andesite-dacite, Telford *et al.* 1976). Shaded area indicates uncertainty in the MgO value (±1.5 wt%) by this method.

(b) FeO*, MgO content of melt inclusion in Fo87 heated to 1280°C to 1310°C, (filled diamonds), and Fo91 heated to 1280°C to 1300°C, (filled triangles) from Ulakan Fm. (open squares) sample UTas67424. M1 (Mg#67) and M2 (Mg#75), are melts trapped in equilibrium with Fo87 and Fo91, respectively. M1 to B1 and M2 to B2, are crystallization paths with fast re-equilibration. Groundmass MgO content of sample UTas67424 estimated by mass balance substruction of phenocryst phases (average analysis) from whole rock analysis on the basis of modal proportions: ol=14%, cpx=38%, Wheller 1986) and densities (gm/mm^3): ol=3.3, cpx=3.2 (Deer *et al.* 1985) and melt= 2.54 (Andesite-dacite, Telford *et al.* 1976). Shaded area indicates uncertainty in the MgO value (±1.5 wt%) by this method. Residual melt C1 and C2, after further crystallization of ~10 wt% olivine are compared to naturally quenched melt inclusion hosted in Fo80 to Fo85 (filled circles). Numbers next to paths indicate amount (wt%) of olivine fractionated (-) during natural cooling or added (+) during experimental heating to the melt.

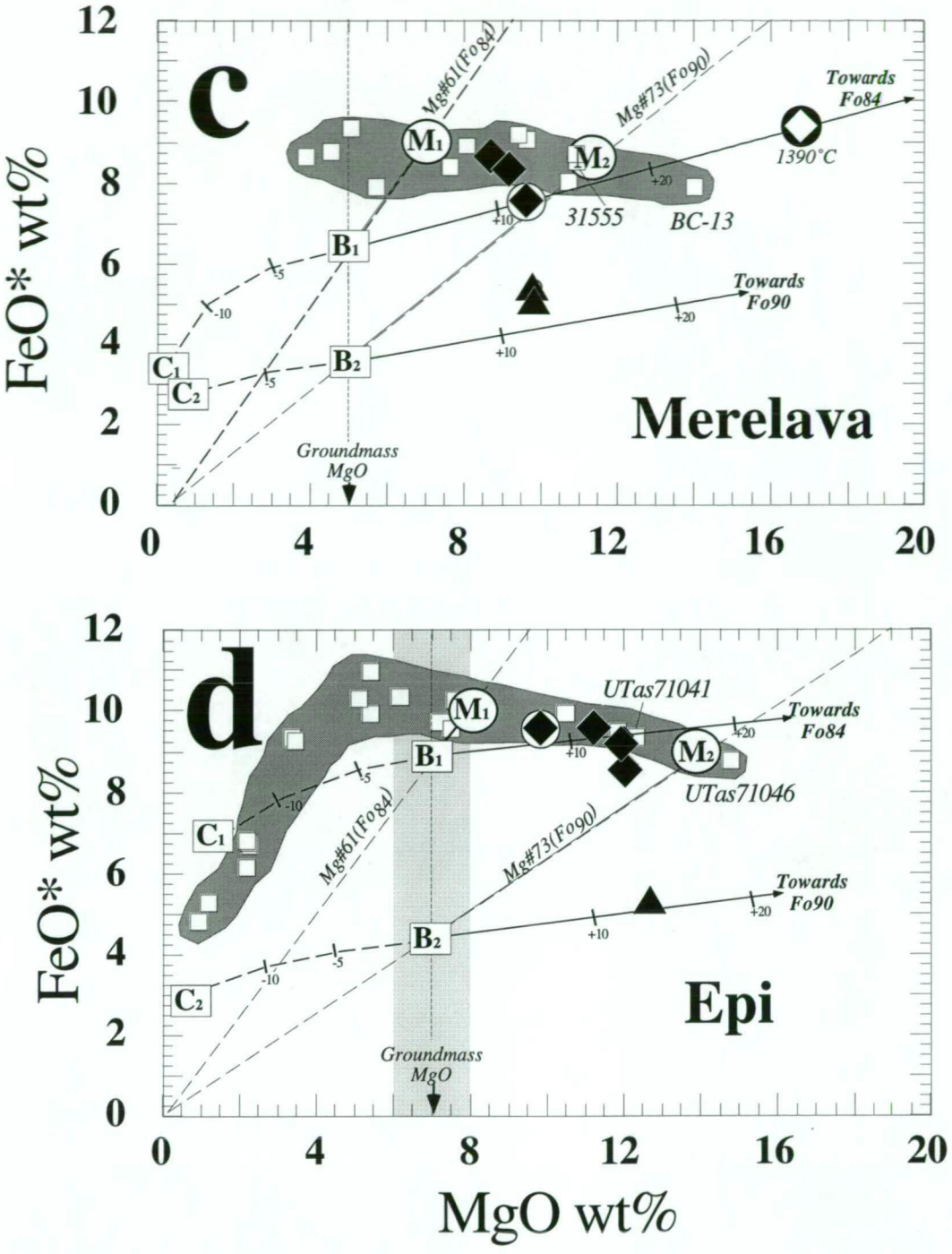

Figure 4.6 continued,

(c) Heated melt inclusions in Fo90 (filled triangle, 1242°C) and Fo84 (filled diamonds: 1240°C, filled diamond in circle: 1250°C, open diamond in filled circle: 1390°C) from Merelava. M1 to B1 and M2 to B2 are re-equilibration trends at high temperature. Groundmass MgO~5 wt% is from sample 31555 (Barsdell 1988). B1 and B2, towards Fo84 and Fo90, are olivine addition control line as a result of heating. Note overheated composition (1390°C) of a melt inclusion along Fo84 control line. The relatively lower FeO* content of a heated melt inclusion in Fo90 (~4wt% lower) with respect to inclusion in Fo84, represents larger extent of reequilibration at high temperatures.

(d) FeO*, MgO content of heated melt inclusions in Fo84 (filled diamonds: 1280°C, filled diamond in open circle: 1230°C), and in Fo90 (filled triangle, 1305°C) from Epi. Melts M1 and M2, trapped in equilibrium with Fo84 and Fo90 have Mg#61 and Mg#73, respectively. M1 to B1, and M2 to B2, are fractionation paths with rapid re-equilibration. Groundmass MgO of ~7wt% can be constrained by groundmass analyses of samples UTas71046 and UTas71041 which contain ~8wt% and ~6wt% MgO, respectively (light shaded area, Barsdell & Berry 1990). B1 to C1, and B2 to C2 represent crystallization after eruption, and are reversible by heating. B1 and B2, towards Fo84 and Fo90, respectively represent heating tends. The similar and relatively lower FeO* content of heated melt inclusions in Fo84 and Fo90 to the host rock trend (~4wt% lower), represent minor and larger extents of re-equilibration at high temperatures, respectively, after trapping.

in equilibrium with Fo_{84} and Fo_{90}, and have $Mg^{\#}61$ and $Mg^{\#}73$, respectively. With rapid re-equilibration, while olivine crystallizes on the wall, the residual melts progress from M1 and M2, towards B1 and B2, respectively. Fractionation paths B1 to C1, and B2 to C2 are reversible by heating, but with increasing temperature the melt progresses towards Fo_{84} and Fo_{90}, not M1 and M2, respectively. The similarity in FeO* content of heated melt inclusions in Fo_{84} (within 1 wt%), but relatively lower FeO* contents of a heated melt inclusion in Fo_{90} (~4 wt% lower) compared to the trapped melt and whole rock analyses, represent minor and large extents of re-equilibration at high temperatures, respectively, before quenching.

4.5 Recalculation procedure used in this study

The compositions of melt inclusions affected by "Fe-loss" and experimental underheating (or overheating) are not directly representative of the trapped melt. The recalculation procedure described below reconstructs the composition of heated melt inclusions by reversing the affect of "Fe-loss", underheating and overheating using a program written by L.V Danyushevsky. This program is based upon the re-equilibration model presented in section 4.3. A detailed description of this recalculation procedure is given in Appendix 4.1 and is summarized below using four case examples, A, B, C and D. These examples were selected to cover the range in FeO* and MgO of heated melt inclusion compositions after quenching. This range is shown as fields in Figure 4.7 for melt inclusion trapped in Fo_{91} that were naturally quenched (NQ) during eruption, or were underheated (UH), homogenized (H) or overheated (OH) during the experiment. Thus each case (A, B, C and D) represents the aliquants of a primitive melt M of Mg#75 trapped in Fo_{91} that re-equilibrated differently with the host olivine, or were heated above or below the homogenization temperature during the experiment. The recalculation paths of these melt inclusions are described below with reference to Figure 4.7.

CASE-A represents a completely re-equilibrated melt inclusion with lowest FeO* content after heating and quenching. In this case the melt inclusion is also underheated and therefore it has a lower MgO content compared to M but a higher Mg# due to extensive "Fe-loss".

CASE-B represents a melt inclusion that is slightly affected by Fe-Mg re-equilibration and therefore its FeO* content is only slightly lower than M. The composition of this melt inclusion also represents underheating and thus it has a lower MgO content and a lower Mg# compared to M.

CASE-C is a composition with MgO content higher than M due to experimental overheating. This melt inclusion is affected by moderate "Fe-loss" and consequently has a lower FeO* content and higher Mg# compared to M.

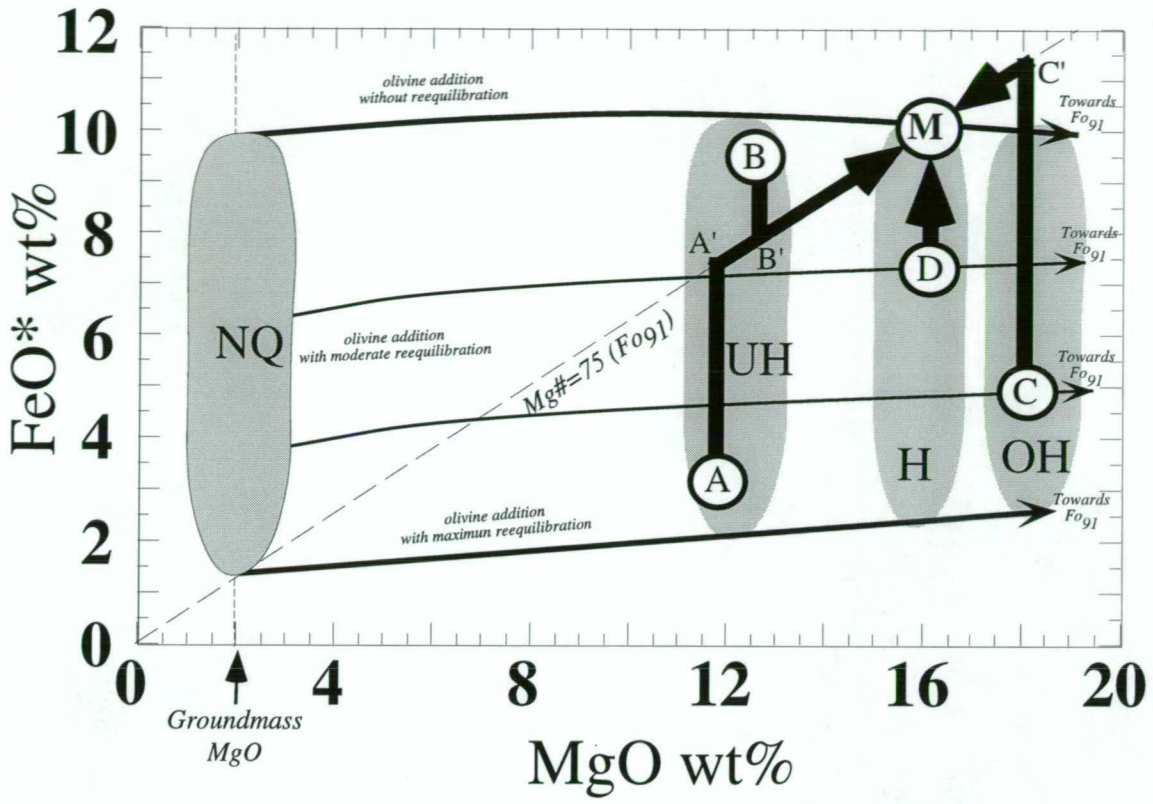

Figure 4.7 Recalculation paths (thick arrows) of four typical heated melt inclusion compositions A, B, C and D originaly trapped as melt M (Mg#=75) by an olivine phenocrysts Fo91. The recalculation procedure involves two main procedures. PROCEDURE-1 drives the composition of heated melt inclusions from A, B, C and D towards A', B', C', and M respectively. PROCEDURE-2 drives compositions A', B' and C' towards M. Shaded areas represent the maximun and minimun range in FeO* of melt inclusion glasses hosted in Fo91 after quenching. NQ indicates composition of naturally quenched melt inclusion glasses after eruption. UH and OH are the compositional range of experimentally underheated and overheated glasses respectively, after quenching. Field H represents the compositional range of homogenized melt inclusion glasses. Thin arrows represent the shift in composition of melt inclusions during the remelting of olivine component in the heating experiment. These trends enclose the minimun and maximum range in FeO* content inherited by heated melt inclusions in Fo91 due to least and complete reequilibration respectively. Groundmass MgO indicates the MgO content of the melt hosted in Fo91, at the moment of eruption.

CASE-D represents an ideal case where homogenization at correct temperature was achieved and therefore the melt inclusion has a major element composition similar to M with the exception of lower FeO* due to "Fe-loss".

The composition of all heated melt inclusion in this study belong to one of the four cases described above. Most of the heated melt inclusions however are represented by CASE-A, i.e., underheated melt inclusions affected by complete Fe-Mg re-equilibration. In all cases the recalculation process described here involves two main steps:

STEP 1 involves a stepwise Fe*-Mg cation exchange between the heated melt composition and the host olivine at constant temperature until chemical equilibrium is attained, i.e., a $K_D^{Ol-Melt}_{Fe-Mg}$ value of 0.30 (Roeder & Emslie 1970). In this step, compositions A, B, C and D are driven towards A', B' C' and M respectively (Figure 4.7). Compositions A', B', and C' have the same Mg# as M (Mg#=75) and are in chemical equilibrium with the host olivine (Fo_{91}) but differ from each other in composition and temperature due to experimental underheating or overheating.

STEP 2 involves the stepwise addition (if underheated) or substruction (if overheated) of equilibrium olivine component from the melt inclusion followed by stepwise re-equilibration. This is carried out at constant mg#, not temperature, until the FeO* content of the recalculated melt composition matches the FeO* content of the original melt M. In this step, compositions A', B' and C' are driven towards the original composition of the trapped melt M (Figure 4.7).

This recalculation procedure assumes that the original FeO* content of the trapped melt is similar to the wholerock FeO* content of the most primitive samples in each suite. This is based upon the assumption that the fractionation of olivine and clinopyroxene phenocrysts cause only minor variations to wholerock FeO* values (<1 wt% FeO*). This assumption is supported by a) calculated olivine fractionation paths, b) nearly constant wholerock FeO* *versus* mg# variation trends of each ankaramite suite (Figures 4.1) and c) small (<1 wt%) variations in the FeO* *versus* mg# content of other primitive olivine-clinopyroxene phyric suites. This assumption has proved useful in the reconstruction of primitive melt compositions from wholerock analyses that have only experienced olivine fractionation (Frey *et al.* 1991, Sato *et al.* 1991, Wilkinson 1991, Eggins 1993), as it happens in homogenized melt inclusions that are hosted by olivine.

The wholerock FeO* contents assumed for the recalculations of melt inclusions hosted in magnesian olivines ($Fo_{>88}$) are estimated from ankaramite FeO* *versus* MgO trends in Figure 4.6. In the Rinjani ankaramite suite, samples with >10 wt% MgO have 9-10 wt% FeO* and therefore a value of 9.5 wt% FeO* is selected for the recalculation. Similarly, in the Ulakan ankaramite suite the FeO* content of samples with ~8-18 wt% MgO vary between ~10-11 wt% FeO* and therefore a value of 10.5 wt% FeO* is selected. A similar approach to the ankaramite suite of Merelava yields an average FeO* content of 9.00 wt%. In Epi, 9.0 wt% FeO* is selected for melt inclusions trapped in olivines with $Fo_{>90}$ and 9.40 wt% for olivines trapped in Fo<90.

The Fe_2O_3/FeO_{melt} values used in the recalculation of melt inclusions from each suite were estimated from olivine-spinel inclusion pairs (Maurel & Maurel 1982) in Section 2.5.3 and

summarized in Table 4.1. To assess the effect of variation in Fe_2O_3/FeO_{melt} values, higher and lower Fe_2O_3/FeO_{melt} values were also used in the recalculation of melt inclusion from each suite. The complete set of recalculated analyses, within the range of Fe_2O_3/FeO values listed in Table 4.1, are given in Appendix 3. The largest range in Fe_2O_3/FeO_{melt} values (0.19-0.56) was tested in the melt inclusion hosted in olivines form the Rinjani suite. In those inclusions hosted in ~Fo_{90} these recalculations yield a range of mg# values that vary from ~66 to ~70. In other melt inclusion from the Ulakan, Merelava and Epi suites, the range in Fe_2O_3/FeO_{melt} values selected for the recalculations yield variations that are less than 2 Mg# units.

TABLE 4.1

	Fe_2O_3/FeO_{spl}	Fe_2O_3/FeO_{melt}	FeO^*_{melt}
		(0.56)	
Rinjani	~0.91	0.30	9.50
		(0.19)	
		(0.28)	
Ulakan	~0.68	0.20	10.50
		(0.13)	
		(0.22)	
Merelava	~0.52	0.15	9.00
		(0.11)	
		(0.19)	
Epi	~0.43	0.12	9.40
		(0.09)	

Range of Fe_2O_3/FeO_{melt} values obtained from olivine-spinel inclusion pairs (Maurel & Maurel 1982). Values in brackets are highest and lowest range in values used in the recalculation. Fe_2O_3/FeO_{spl} values are from section 2.5.2. FeO^*_{melt} indicates the original FeO* content used for the recalculation. Recalculated analyses listed in Appendix 3.

4.6 Conclusions

Due to the diffusion of Fe in olivine, the composition of residual melts of inclusions trapped in olivine are modified by re-equilibration of their Mg# with the host. This process causes "Fe-loss" from the melt to the host and is summarized below with reference to Figure 4.8. Three stages (1, 2 and 3) are considered where the re-equilibration paths of three melt inclusions (A, B and C) in separate olivine crystals are described.

Stage 1 represents a hypothetical slowly cooling magma (aggregate of melt+crystals) at the moment of eruption. The earliest formed olivine crystals in this magma are Fo_{91} and the last olivine crystals to form before eruption are Fo_{84}. Melt inclusions trapped just before eruption in Fo_{84} (A, Figure 4.8) preserve the composition of the melt (now rock groundmass) at the moment of eruption. As a result of magma-cooling however, melt inclusions trapped in Fo_{91} (case C, Figure 4.8) crystallize a rim of olivine on the walls. This rim depletes the residual melt within the inclusion in olivine component. Slow cooling of the host olivine crystal (Fo_{91}) allows this olivine rim to re-equilibrate simultaneously with the host as it crystallizes on the wall. The composition of

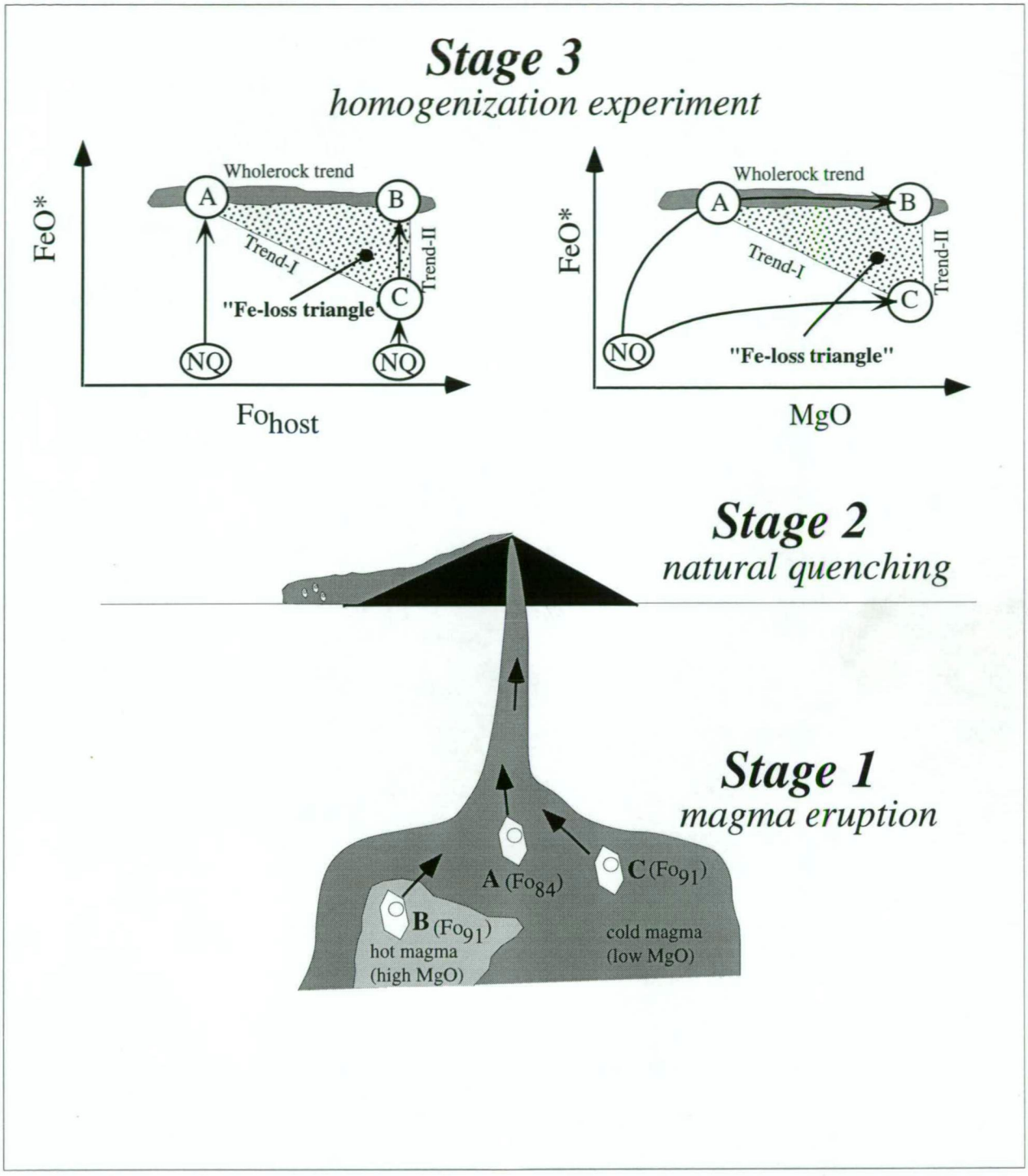

Figure 4.8 Schematic model illustrating possible paths and stages of re-equilibration for three melt inclusions (A, B and C) in three olivine crystals within a recharging magma chamber.

Stage 1: Mixing of hot and cold magma before eruption. A and C are slowly cooling melt inclusions in a slowly cooling magma. Mixing of the new hot batch of magma leads to the relatively rapid cooling of B. Melt inclusion B therefore has a short residence time compared to C. Melt inclusion C therefore is affected by a larger extent of "Fe-loss". Melt inclusion A is trapped just before eruption and therefore not affected by re-equilibration.

Stage 2: All melt inclusions are naturally quenched during and after magma eruption.

Stage 3: The composition of melt inclusions after natural quenching (NQ) is further depleted in MgO and FeO* by the growth of quench crystals. After homogenization, the original FeO* content of melt inclusions A and B is attained, but melt inclusion C inherits a relatively low FeO* content compared to B because of re-equilibration. The composition of melt inclusions A, B and C define an "Fe-loss triangle" within which the composition of homogenized melt inclusions trapped in olivine are to be found.

this olivine rim in these melt inclusions are therefore not zoned and maintain a composition similar to the host olivine (Fo_{91}). The residual melt within these inclusion also re-equilibrate by "Fe-loss" and thus become much more depleted in Fe.

Provided re-equilibration does not occur, the olivine rim formed on the walls of melt inclusions trapped in olivine with Fo_{91} will be zoned form Fo_{91} down to Fo_{84}. This case is represented by melt inclusion B. In this case cooling of the host crystal takes place relatively fast as a result of mixing between a new batch of recharging hot magma and the slowly cooling fractionated host magma. The residence time of melt inclusion B is therefore shorter, compared to C.

Stage 2 represents the rapid cooling during and after eruption, where more olivine crystallizes on the wall of the inclusion and the residual liquid is naturally quenched to a glass. The composition of this glass (NQ) is highly depleted in olivine component and other daughter phases that may have grown during quenching (e.g., clinopyroxene). No re-equilibration occurs at this stage. Stage 3 represents the homogenization experiment when daughter phases are remelted. If re-equilibration did not occur, the compositions of quenched glasses are ultimately driven along an olivine-addition trend that coincides with the wholerock trend (e.g., A to B). However, if "Fe-loss" occurred by re-equilibration, the composition of melt inclusions inherit abnormally low FeO* contents after homogenization (e.g., C). These compositions are therefore not representative of the original trapped melt.

These three cases represent compositional end members A, B and C, which define a "Fe-loss triangle" zone. According to the model presented here, the composition of heated melt inclusions in olivine must lie within this triangle. This "Fe-loss triangle" is bounded by Trend-I and Trend-II of Figure 4.1. Trend-II is governed by the rate of re-equilibration whereas Trend I is governed by the residence time of crystals in the magma, before eruption. Inclusions trapped immediately before eruption have virtually no residence time and their FeO* content after heating will always be representative of the trapped melt.

Most analyses of heated melt inclusions in this study are modified by "Fe-loss", and therefore their compositions require recalculation of their FeO* contents. However, FeO* contents of some inclusions in magnesian olivines ($Fo_{>88}$) range up to values that are similar to those of ankaramite bulk compositions (Figure 4.1). These melt inclusions have experienced least "Fe-loss" and their compositions are thus only modified by the crystallization of olivine on the wall.

Chapter 5: Dry, hydrous and CO_2-bearing phase relations of an ankaramite composition based on melt inclusion compositions

5.1 Introduction

Experimental studies on ankaramite rocks (e.g, Maaløe *et al.* 1986, Flower 1973) are yet to show that, ankaramitic wholerock compositions could be primary mantle peridotite partial melts (Chapter 1). However, a notable chemical characteristic of melt inclusions in ankaramite rocks, in addition to high CaO/Al_2O_3 values, is a strong silica-undersaturation with nepheline(*ne*)-, leucite(*lc*)-, and larnite(*cs*)-normative compositions (refer to Section 3.5.2). These compositions resemble those of naturally occurring highly silica-undersaturated rocks such as nephelinites and melilitites, but differ in terms of silica saturation, from the ankaramite host rocks which are *ne*- to *hy*-normative (Section 3.6). This observation led to the consideration of a model where highly silica-undersaturated melts played the role of parental melts, for the formation of primitive ankaramitic magmas (Section 3.7, and 3.8).

Extensive experimental results have shown that CO_2-rich fluids might be an essential ingredient for the generation of highly silica-undersaturated primary melts by partial melting of garnet lherzolite (cf. Eggler 1974, Wyllie & Huang 1976, Brey & Green 1976, Adam 1988, 1989, 1990). In particular, the experimental results of Mysen & Boettcher (1975b), Brey & Green (1977), and Mysen & Kushiro (1977) demonstrate that primary melts with chemical characteristics closely resembling those of melt inclusions in ankaramite rocks, namely silica-undersaturation and high CaO/Al_2O_3 values (Table 4.6), can be generated by melting at pressures <3 GPa in the presence of CO_2-H_2O bearing fluids. Primitive melt inclusions trapped by olivines in ankaramites could therefore have been produced by melting under these conditions (Section 3.7).

The work in this chapter complements the model presented in Chapter 3 by conducting a liquidus study at high pressures (<3 GPa) with variable CO_2-H_2O contents, using the average analyses of two melt inclusions as starting composition. If the trapped inclusions are aliquots of primary mantle partial melts, then the phase relations require that these melts must coexist at equilibrium with a peridotite mineralogy (*i.e,* at least ol+opx±cpx) provided P, T, $X_{H_2O\text{-}CO_2}$, fO_2 conditions of the source are experimentally duplicated.

5.2 *Experimental methods*

5.2.1 *Selection of starting material*

The starting material ANK2376 (Table 5.1) is a synthetic glass that was made from the average composition of two melt inclusions (Table 5.1, column 4 and 8). The inclusions are hosted in olivines (~Fo_{91}, Table 5.1) which were separated from the most magnesian sample of the Rinjani volcano ankaramite suite (sample UTas48001, $Mg^{\#}$~73, Table 1.3). The use of melt inclusion analyses as starting composition, instead of wholerock analyses, avoids the "circular argument trap" introduced by the possibility of crystal accumulation. Thus melt inclusions are highly suitable as a starting material because they represent the least modified melts trapped early in the evolution of the magma. These analyses are however, corrected for the effect of olivine crystallization on the walls of the inclusion, and for the effect of Fe-loss to the host. These two processes and the recalculation procedure employed, are fully documented in Chapter 4. The resultant composition ANK2376, is *ol-*, *ne-*, *lc-* and *cs*-normative (Table 5.1, analysis 11), which may therefore be described as an olivine melilite nephelinite (Green 1969).

The host rock sample UTas48001 contains abundant phenocrysts of diopsidic clinopyroxene (~$Wo_{45}En_{50}Fs_5$, 36%), lesser olivine ($Fo_{74\text{-}91.5}$, 12%) with rare inclusions of chromian spinel ($Cr^{\#}74$), and minor plagioclase ($An_{85\text{-}90}$, <4%). This sample belongs to a primitive *ne*-normative suite with typical geochemical affinities typical of convergent-margin magmatism. Wholerock chemical variations within this suite can be explained as a result of fractionation of observed phenocryst phases. This suite however, is compositionally distinct to other more evolved volcanics erupted on Lombok, and is thus considered to be a derivative from a compositionally distinct separate magma (Foden & Varne 1981a). Detailed petrology and geochemistry of this suite are given in Chapter 2.

5.2.2 *Preparation of the starting mix ANK2376*

The major element composition of the synthetic starting glass was prepared by adding the respective masses of oxides and carbonates, with the exception of iron (added as fayalite), to achieve the required proportion in a ~2 g batch of starting mix. Only analytical reagents with >99 % purity, or where unavailable, laboratory reagents with ~99 % purity, were used in the mix. CaO, Na_2O and K_2O were added as $CaCO_3$, $NaCO_3$ and KCO_3 respectively. P_2O_5 was added as $Ca_2P_2O_7$, and the remainder as oxides; SiO_2, TiO_2, Al_2O_3, Cr_2O_3, MnO and MgO. Allowance was made for the SiO_2 content of fayalite that was added later to prevent the oxidation of iron to its Fe^{3+} state. The mixture was placed in an agate mortar and ground to dryness under acetone several times, to achieve homogeneity. The mixture was then dried at 120°C, pressed into pellets, and ignited in a platinum (Pt) crucible at 1000°C overnight to release CO_2 and then cooled to room temperature. The pellets were then ground in an agate mortar, dried, placed in a Pt crucible and melted at 1410°C for 45 minutes in a 1 atm furnace. The melt was quenched by dropping the crucible into a reservoir of distilled water situated directly beneath the furnace. This glass was re-ground under acetone and

TABLE 5.1

	RUN 83/1				RUN 43/5				AVERAGE
	Host	*Heated glass*			*Host*	*Heated glass*			
	Olivine	*Probed*	*Sum*	*Rec.*	*Olivine*	*Probed*	*Sum*	*Rec.*	
Column	*1*	*2*	*3*	*4*	*5*	*6*	*7*	*8*	*9*
SiO_2	40.59	45.79	45.83	44.11	40.84	46.66	46.35	43.67	43.89
TiO_2		0.88	0.88	0.75		1.07	1.06	0.88	0.82
Al_2O_3		16.82	16.84	14.43		17.08	16.97	14.12	14.28
Cr_2O_3	0.04	0.05	0.05	0.05	0.02		0.00	0.07	0.06
FeO	8.74	7.26	7.27	9.80	8.59	5.35	5.31	9.80	9.80
MgO	49.35	8.63	8.64	13.26	49.63	8.95	8.89	13.59	13.43
CaO	0.26	16.77	16.79	14.42	0.33	17.60	17.48	14.58	14.50
MnO	0.17	0.10	0.10	0.10	0.16	0.00	0.00	0.02	0.06
Na_2O		2.35	2.35	2.01		2.87	2.85	2.37	2.19
K_2O		1.16	1.16	0.99		0.95	0.94	0.78	0.89
P_2O_5		0.10	0.10	0.08		0.14	0.14	0.12	0.10
NiO	0.24				0.19				
TOTAL	99.39	99.91	100.00	100.00	99.76	100.67	100.00	100.00	100.00
Mg#	91.0	68.0		70.7	91.2	74.9		71.2	71.0
K_D*		0.21		0.24		0.29		0.24	
FeO^{2+}		5.72		7.72		4.21		7.72	
mg#		72.9		75.4		79.1		75.9	
K_D		0.27		0.30		0.37		0.30	

STARTING MATERIAL ANK2376					
	Probed	*Mol CIPW*		*Traces (ppm)*	
Column	*10*		*11*		*12*
SiO_2	**43.98**	An	26.5	La	100.0
TiO_2	**0.84**	Ne	10.0	Ce	100.3
Al_2O_3	**14.15**	Lu	4.1	Sm	50.0
Cr_2O_3	**0.06**	Di	27.6	Eu	50.0
FeO	**9.16**	Ol	26.6	Yb	50.4
MgO	**13.21**	Cs	3.1		
CaO	**14.74**	Cm	0.1	Sr	450.0
MnO	**0.07**	Ill	1.6	Nb	496.8
Na_2O	**2.11**	Hap	0.5	Ta	503.0
K_2O	**0.80**			Zr	103.6
P_2O_5	**0.24**			Y	50.1
NiO				Sc	51.1
TOTAL	**99.36**				
Mg#	**72.0**				

Starting mix composition ANK2376. Columns 2 and 6 are the composition of heated melt inclusions hosted in olivines (columns 1 and 5) after homogenization experiment run 83/1 (1238°C) and run 43/5 (1250°C) respectively. Columns 3 and 7 are analyses summed to 100 wt%. Columns 4 and 8 are recalculated analyses following the method described in Chapter 4. This recalculation involves the mass-balanced addition of ~11.2 wt% and ~12.1 wt% host olivine material to columns 3 and 7 respectively, as well as the adjustment of FeO* content in the melt to ~9.80 wt%. Column 9 is the average of 4 and 8. Column 10 and 11 are the microprobe analyses and molecular CIPW norm of the prepared starting glass ANK2376. Column 12 are calculated trace element concentrations based on weighted mass of trace element oxide added into standard solution. Mg#= 100Mg/(Mg+Fe*), mg#= $100Mg/(Mg+Fe^{2+})$, $K_D^* = (Fe/Mg)_{Ol}/(Fe^*/Mg)_{Melt}$, $K_D = (Fe/Mg)_{Ol}/(Fe^*/Mg)_{Melt}$.

remelted again at 1410C° for 45 minutes to ensure homogeneity. The homogeneity of this glass was confirmed optically under the microscope and by mounting a sample of this glass on epoxy and analysing with an electron microprobe. The glass was then re-crushed in acetone and dried at 120 °C for 1.5 hours. The amount of synthetic fayalite powder required to make up the FeO* content was then added to the mix and ground under acetone until homogeneous in colour. Finally, the mix was dried and stored in a desiccator.

It is noted that the experimental composition used here are not suitable for investigations of the role of Cr-spinel as the starting mix contains only a trace amount of Cr_2O_3 (~800ppm). Thus in the discussion and application of these experiments the role of Cr-spinel is ignored.

5.2.3 Trace elements

Trace elements Ta, Nb, Zr, Sc, Y, Sr, and rare earth elements La, Ce, Sm, Eu, Yb were also added to the starting mix to study their partitioning under the range of experimental conditions investigated here. This partitioning study was not completed and will not be discussed in this thesis. The trace elements were added as solutions prepared from analytical reagent oxide powders (>99 % purity): Ta_2O_5, Nb_2O_5, ZrO_2, Sc_2O_3, Y_2O_3, La_2O_3, CeO_2, Sm_2O_3, Eu_2O_3, Yb_2O_3. All powders were ignited overnight in ceramic crucibles at 900°C, with the exception of $SrCO_3$ that was heated at 120°C. The required mass of trace element oxide was added into separate flasks with acid solutions of known concentration. Ta_2O_5, Nb_2O_5, and ZrO_2 powders required excess of both HNO_3 and HF acid solutions (1 Molar) to dissolve, whereas all other powders were dissolved in HNO_3 acid solutions (1 Molar). Once dissolved, each of the solutions was made up to a standard solution with the desired concentration. These standard trace element solutions were then added directly to the major element starting mixture during its preparation, and then left to dry. This procedure allows the unreacted acids in each trace element solution to neutralise (observed as effervescence) in a mixture of MgO, Al_2O_3, and $CaCO_3$. The remaining oxides (except Fa) were then continued to be added and the starting mixture prepared as described previously. Calculated concentrations of trace elements in ANK2376 are listed in Table 5.1.

5.2.4 Experimental techniques

All experiments were synthesis runs performed in a 1/2 inch (1.27 cm) piston-cylinder apparatus (Boyd & England 1960) at the University of Tasmania, Hobart, using standard techniques similar to those described in Green & Ringwood (1967). Run conditions ranged from 1030 to 1480°C, and from 1.0 to 3.5 GPa. The experimental assemblages used boron nitride internal components and NaCl-pyrex sleeves. These were kept dry at 120°C until each run. Pressures in the range 1.0 to 3.5 GPa range have been estimated to have an accuracy of approximately ±1% (Mirwald *et al.* 1975) and therefore no pressure correction was applied to any of the runs. Pressure was maintained during the run to within ±0.01 GPa. Temperatures were monitored with $Pt/Pt_{90}Rh_{10}$ thermocouples, and were controlled automatically to ±1°C. All capsules were loaded with approximately 10 to 15 grams of sample. Graphite capsules were used in dry experiments, $Ag_{75}Pd_{25}$ and $Ag_{50}Pd_{50}$ capsules in the hydrous experiments and Pt capsules in the CO_2-H_2O

bearing experiments. Water was added to the loaded capsules using a micro-syringe whereas CO_2 was generated by adding $Ag_2C_2O_4$ (silver oxalate) to the starting mix. All metal capsules were hermetically sealed with an electric-arc welder. Capsules were kept frozen during welding to prevent volatile loss, and their weight noted before and after welding, to detect any mass change. Once the capsule was welded, closure was confirmed by weighing the capsule after immersion in acetone and after heating to 120°C. Hydrous runs were carried out unbuffered (*i.e.*, buffered by the environment external to the capsule). An initial series of CO_2-bearing experiments was also run unbuffered, but led to the formation of water in the sample. This was interpreted as a result of rapid migration of H_2 from the outer assembly (boron nitride/pyrex), through the inner Pt capsule and into the sample (see text below). The experiments were therefore repeated using a double-capsule technique (Huebner 1971). The outer Pt capsule was packed with ~100 to ~170 mg of Specpure haematite to maintain a high H_2 fugacity outside the inner sample capsule by the reaction $Ht+H_2 \rightarrow Mt+H_2O$ and thus, prevent the migration of H_2.

Retention of volatiles after each experiment was confirmed by weighing before and after piercing the capsules (inner and outer) and identifying any weight change at room temperature, and after ~10 minutes at 120°C. In all cases up to ~1.4 mg weight loss was observed in outer capsules (buffer) demonstrating the formation of water during the run occurred by the reaction listed above. Examination of the buffer after each run demonstrated the presence of magnetite and haematite, and thus exhaustion of the buffer did not occur. The oxygen fugacities (fO_2) for the range of pressure and temperature conditions in magnetite-haematite (MH) buffered experiments can be estimated from the equations of Hemingway (1990). With reference to the fayalite-magnetite-quartz (FMQ) buffer, quoted as $\Delta \log fO_2$(FMQ) log units, fO_2 values in these experiments vary from -4.2 to -5.1. In hydrous and CO_2-unbuffered experiments, fO_2 are buffered by the furnace assemblage at approximately the NNO buffer (Green 1976). The experiments were run for durations ranging from 1 to 6 hours in the dry and hydrous experiments, and from 30 to 45 minutes in the CO_2-bearing runs. The shorter run times were used to minimize Fe-loss and to prevent premature exhaustion of the oxygen buffer components.

5.2.5 Analytical techniques

All glass and mineral phases were analysed using a SX-50 CAMECA electron microprobe at the University of Tasmania that was calibrated with natural mineral standards. Analytical conditions for experimental run products were 15 kV accelerating voltage, 10 nA beam current for glasses and 20 nA for minerals, and a beam size of 10 μm for glasses and 1μm for minerals. All elements were analysed at 20 seconds except Na that was analysed at 10 seconds. The number of analyses in each run was limited by the small size of crystals, a problem that often led to overlap with the surrounding glass or mineral phases. Full descriptions of microprobe analytical conditions are given in Appendix 2.1.

Some-crystal free glass fragments from sub-liquidus and above liquidus runs were carefully hand-picked using a binocular microscope and prepared for elemental analysis of Carbon and Hydrogen. If it is assumed that the concentrations of C and H in these analyses are representative of

CO_2 and H_2O contents respectively, in the quenched glass, then a direct measurement of their solubility in the melt can be obtained (Section 5.8). These analyses were performed on quenched glasses principally to confirm that migration of H_2 into the sample capsule was minimized by the MH buffer.

5.2.6 Iron absorption by Pt capsules

FeO* contents of quenched glasses are plotted against temperature in Figure 5.1. This figure is constructed using average (n=10) glass analyses of CO_2-bearing runs in Pt capsules that are above liquidus, near-liquidus (with less than ~10% crystals), and those runs in which clinopyroxene is the only phase. The later are underestimates because fractionation of clinopyroxene with less than ~3 wt% FeO* is likely to increase the iron concentration of the residual melt.

Most of glasses in MH-buffered runs have FeO* contents that range from 6.6 to 7.6 wt% (Figure 5.1, filled symbols) compared with an FeO* content of 9.16 wt% in the starting glass. Run T-4121 is an exception in which FeO* is as low as 4.5 wt%. These results suggest that at least ~25% iron loss occurred in MH-buffered runs. In the CO_2-bearing unbuffered experiments, the magnitude of iron loss is larger. At 2 GPa, the compositions of glasses above liquidus contain ~6 wt% FeO*, whereas at 1.5 GPa they contain ~4 wt% FeO* (Figure 5.1). At 1.0 GPa, the FeO* content of near-liquidus glasses decreases from ~4 wt% at 1280°C down to ~1.5 wt% at 1250°C (Figure 5.1, open circles). The composition of glasses in run T-4063, with low FeO* contents and high $Mg^{\#}$ ~98 compared with the starting glass ANK2376 ($Mg^{\#}$ 72) cannot be explained by crystal fractionation. Rather they indicate a strong iron loss to the capsule of ~7 wt% FeO* (~77% iron loss). Thus glass composition and phase relations in the experiments presented here must be interpreted with care. The large iron loss observed in the unbuffered experiments compared with the MH-buffered ones is the result of lower fO_2 and the presence of H_2O formed by migration of H_2 into the sample capsule (Stern & Wyllie 1975).

5.2.7 H-diffusion and formation of H_2O in the sample capsule

The migration of H_2 from the outer assemblage during the experiment forms unwanted H_2O in the sample capsule. This process has been widely documented (cf. Brey & Green 1975, 1976, Stern & Wyllie 1975, Wendant & Mysen 1980, Grove 1981, Taylor & Green 1987 and Canil & Scarfe 1988), and therefore precaution was taken in an initial series where a pure CO_2-fluid phase was desired. Formation of H_2O was minimized in these experiments by using short run times (<30 minutes), boron nitride/pyrex assemblages (dried at 110°C for >24 hours before assembling), and storing the final ANK2376 + $Ag_2C_4H_4$ starting mix in the dark, under vacuum, and over desiccant (Brey & Green 1975, 1976, Taylor & Green 1987, and Mattey *et al.* 1990). However, even under these conditions it was found that the elemental analysis of quenched glasses (Table 5.2) contained appreciable amounts of H_2O dissolved. These results are plotted in Figure 5.2, and indicate that the amount of H_2O formed is temperature and pressure dependent. At a constant temperature of ~1280°C the H_2O content in these glasses increased linearly with

TABLE 5.2

RUN	P (GPa)	T (°C)	C[1]	wt% CO_2[2]	H[1]	wt% H_2O[2]
Starting mix						
ANK2376+$Ag_2C_2O_4$			2.17	7.96	<DL	<0.18
Magnetite-haematite buffered runs						
T-4111	1.0	1290	0.52	1.91	0.03	0.27
T-4121	1.0	1320	0.38	1.39	<DL	<0.18
T-4092	1.5	1300	1.01	3.70	0.09	0.81
T-4088	1.5	1330	0.99	3.63	<DL	<0.18
T-4157	2.0	1350	0.68	2.49	0.04	0.36
T-4159	2.25	1320	1.49	5.46	0.04	0.36
Furnace buffered runs						
T-4062	1.0	1280	0.55	2.02	0.21	1.89
T-4043	1.5	1280	0.81	2.97	0.31	2.79
T-4052	2.0	1260	1.62	5.94	0.38	3.42
T-4051	2.0	1300	1.37	5.02	0.42	3.78

([1]) Bulk carbon (C) and hydrogen (H) elemental analyses of the starting mix and near liquidus glasses. ([2]) CO_2 and H_2O contents dissolved in the glass calculated from C and H analyses respectively. <DL indicates below detection limit ~0.02 =0.18 wt%

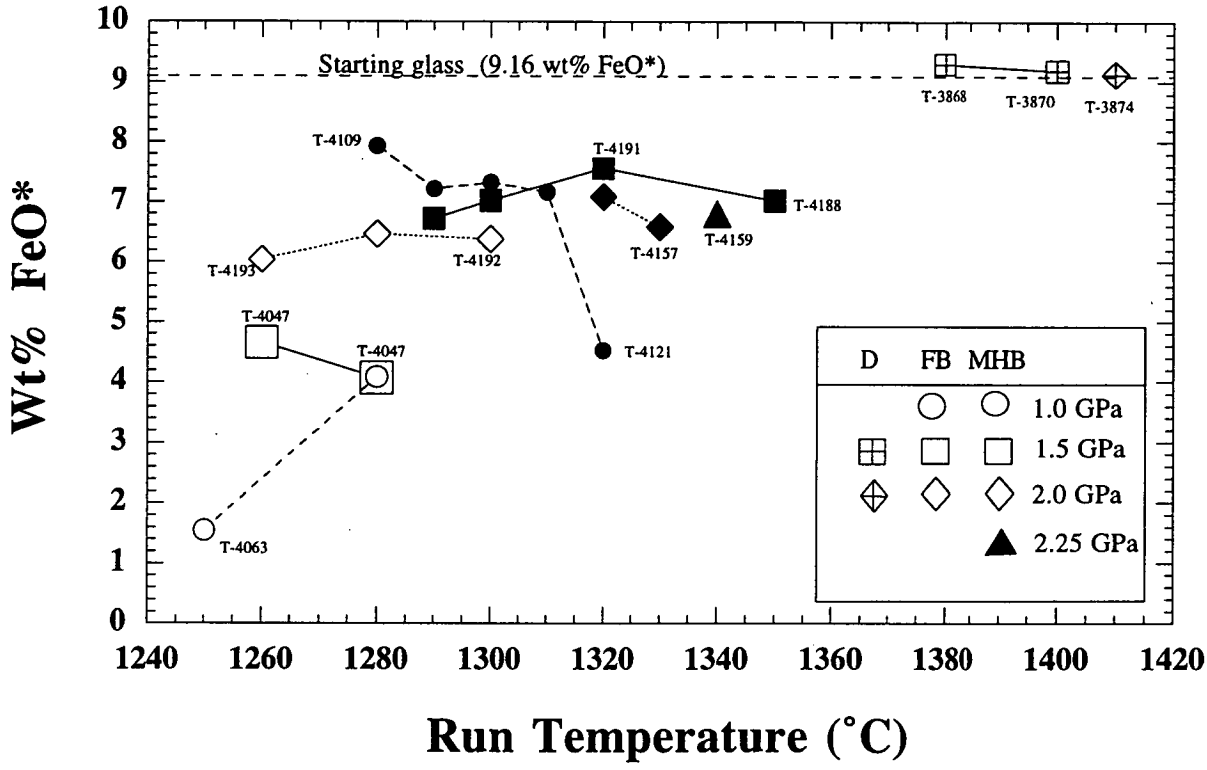

Figure 5.1 Variation in FeO* content of near liquidus and above liquidus glasses (total iron as FeO) *versus* temperature of quenching at various pressures (circles=1.0, squares=1.5, diamonds=2.0 and triangle=2.25 GPa), under dry (D), furnace buffered (FB) and magnetite-haematite buffered (MHB) conditions. Glass analyses are averages (n>10) normalized to 100 wt% volatile free (Appendix 5.9). Note FeO* content of glasses from runs T-3870 and T-3874 above liquidus in the graphite capsule. The average analysis of starting glass is shown for comparison (FeO*=9.16 wt%). Analytical errors are smaller than symbols.

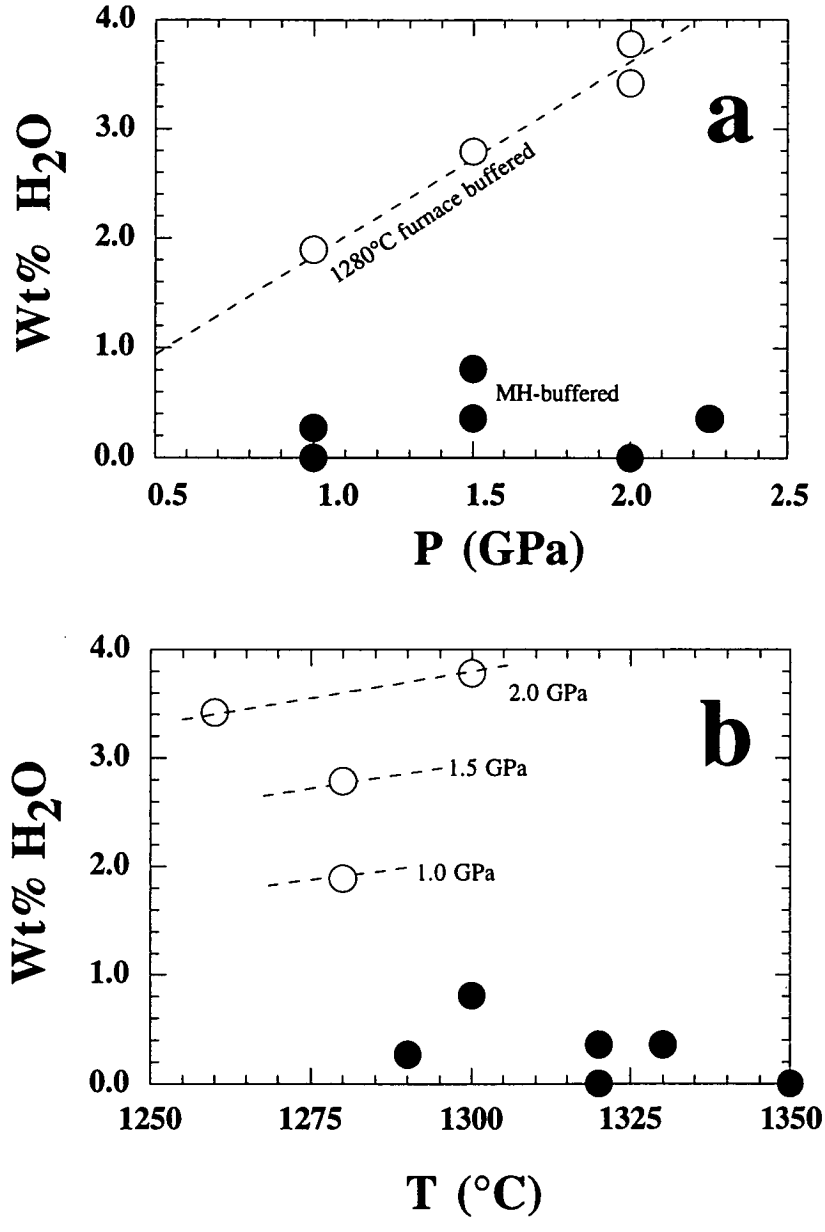

Figure 5.2 H_2O content dissolved in quenched glasses produced in furnace buffered (open circles) and MH buffered (filled circles) experiments as a result of H migration. a) Variation in H_2O content with pressure. Note the pressure dependence in furnace buffered experiments at a constant temperature of 1280°C. b) Variation in H_2O content with temperature relative to pressure. Note the small temperature dependence at 2.0 GPa. Data from Table 5.2.

pressure from ~1.8 wt% at 1.0 GPa up to ~3.6 wt% at 2.0 GPa (Figure 5.2a). An analysis of the starting mix (ANK2376+$Ag_2C_4H_4$) contained <0.18 wt% H_2O and 7.96 wt% CO_2 (Table 5.2) and can therefore be ruled out as a source of water. Hence the migration of H_2 from the outer assemblage was suspected. As these experiments were intended to investigate the liquidus phase relations of ANK2376 under more CO_2 rich conditions they were rerun using a double capsule technique. In this series of experiments the outer capsule was packed with haematite to "trap" the migrating H_2 (Section 5.2.4). Analysis of quenched glasses produced under these MH-buffered conditions (Table 5.2) show a successful decrease in the amounts of H_2O that range up to 0.8 wt% (Figure 5.2, filled symbols).

5.3 Recognition of primary and quench phases

Aliquots of run products were crushed in a mortar and mounted for optical examination in immersion oil of accurately known refractive index. Epoxy mounts of run material were also prepared for further optical examination and microprobe analysis. Back-scattered X-Ray scanned element images were also used to examine large portions of run products and confirm the identification of all crystal phases. Typically, subliquidus runs produced primary crystal phases together with a mixture of quench clinopyroxene and interstitial glass. Primary phases observed in the experiments consist of olivine, clinopyroxene, garnet and spinel. These are recognized by their euhedral habit, sharp optical extinction and by their composition.

The spinel phase is aluminous and tends to form interstitially amongst olivine and clinopyroxene crystals as a result of extensive crystallization of non-aluminous bearing phases such as plagioclase or garnet, in runs T-3875, T-3896 and T-3975 (Chapter 3). Garnet has a pale yellow colour and forms poikilitic textures. Olivine forms clear euhedral crystals. The chemical compositions of dendritic quench clinopyroxene crystals that formed during quenching of runs from above the liquidus, aid in identification of quench clinopyroxene crystals in sub-liquidus runs. The quenched pyroxenes form a fine grained groundmass, and have anomalous extinction. This population of "quench" pyroxenes defines a trend that ranges from the composition primary clinopyroxenes towards the composition of the residual glass. Compositionally, quenched pyroxenes are characterized by relatively higher Ti and Al contents and lower Ca contents and $Mg^{\#}$ values, compared with compositions of coexisting primary clinopyroxene crystals. In hydrous runs the liquid quenched to a feathery-textured clinopyroxene groundmass at all pressures and temperatures investigated. Under anhydrous and CO_2-bearing conditions the amount of quenched clinopyroxene produced was less than was formed in hydrous runs, particularly at low pressures. It is notable that the least aluminous clinopyroxenes found in dry and CO_2-bearing experiments have 8 to 10 wt% Al_2O_3, unlike those in hydrous experiments which have 2 to 3 wt% Al_2O_3. The former, although aluminous, are in Mg-Fe equilibrium with coexisting olivines and therefore are interpreted as primary (not quench) crystals. No evidence for metastable nucleation was found amongst primary clinopyroxenes. Hydrous and other oxide phases, other than aluminous spinels, were not identified within the range of pressure and temperature investigated, but may be confined to the groundmass.

5.4 Phase relations of ANK2376

Experimental results and conditions are listed in Table 5.3 and the phase relations illustrated in Figures 5.3 to 5.6. From these results, a diagram is constructed in Figure 5.7 where the variation in liquidus phases from dry to hydrous and CO_2-bearing conditions are summarized. These diagrams represent reconnaissance synthesis diagrams. Some of the phase boundaries are not tightly constrained, and no run reversals were carried out.

5.4.1 ANK2376-anhydrous

Under anhydrous conditions, olivine is the liquidus phase up to 2.0 GPa. Olivine was not found above 2.0 GPa and is replaced by clinopyroxene at higher pressures (Figure 5.3). At 2.0 GPa the crystallization interval is ~10°C. In run T-3878, olivine Fo_{87} coexists with clinopyroxene $Wo_{46}En_{47.4}Fs_{6.6}$ near the liquidus. This run contains ~80% crystals in contrast to run T-3874, at 10°C higher, which is above liquidus. Near the liquidus at higher pressures (2.5 GPa), the most magnesian clinopyroxenes analyzed in run T-3898 are less calcic ~$Wo_{41}En_{48}Fs_{11}$ (Appendix 5.2), whereas at lower temperatures in T-3896 (~90% crystals) they range up to $Wo_{46}En_{46}Fs_8$ and are accompanied by the crystallization of Al-spinel. Al-spinels also forms near the solidus at 2.0 GPa in T-3875 (~80% crystals) where clinopyroxene ($Wo_{47}En_{46}Fs_7$) is dominant and olivine (Fo_{85}) rare. At lower pressures (1.5 GPa) there is a pronounced increase in the crystallization interval and clinopyroxene ($Wo_{48}En_{45}Fs_7$) joins olivine (Fo_{87}) after ~40-50% crystallization. Orthopyroxene was not found in any of the anhydrous experiments.

5.4.2 ANK2376-H_2O

In hydrous experiments, the presence of water lowers the liquidus temperature by ~300°C, compared with anhydrous conditions, and expands the limit of liquidus olivine stability throughout the pressure range investigated (1.0 to 3.0 GPa), (Figure 5.4). Olivine is joined on the liquidus curve by high-Ca clinopyroxene (~$Wo_{48}En_{47}Fs_5$) at around 2.2 GPa (T-3898) and by garnet and high-Ca clinopyroxene (~$Wo_{48}En_{46}Fs_6$) at 2.5 GPa (T-4008). In one run at 2.5 GPa (T-3975), garnet is replaced by Al-spinel at lower temperatures, with larger degrees of crystallization (~80%). This run is comparable to the anhydrous run T-3896 (Figure 5.3), near the solidus at 2.5 GPa, where Al-spinel also formed. Orthopyroxene was not found under any of the hydrous conditions investigated and all pyroxenes analysed contained high Ca (~23 wt% CaO) and low Al (~4 wt% Al_2O_3) contents. Below ~1060°C, run products are highly crystalline (<10% liquid, dotted line in Figure 5.4) and therefore close to the hydrous solidus of ANK2376.

5.4.3 ANK2376-CO_2, furnace-buffered

Without the use of an external buffer, larger amounts of H_2O formed with increasing pressure in the sample capsule (Section 5.2.7). Consequently, these experiments are saturated by fluids of decreasing CO_2/H_2O ratio with increasing pressure and their liquidus temperatures are intermediate between those of anhydrous and hydrous experiments (Figure 5.5). With increasing pressure the

TABLE 5.3

RUN	T (°C)	P (GPa)	t (hr:min)	Assemblage[1]	%[2]	~Fo3	~Wo	En	Fs4
Anhydrous									
T-3868	1380	1.50	3:00	OL*+L*	<5	89.1			
T-3869	1350	1.50	4:00	OL*+CPX*+L*	~50	87.3	47.9	45.0	7.1
T-3870	1400	1.50	2:00	L*					
T-3871	1320	1.50	6:00	OL*+CPX*	~90	81.3	50.0	42.6	7.4
T-3874	1410	2.00	2:00	L*+CPXq					
T-3875	1390	2.00	2:00	CPX*+OL*+SPL	~80	85.3	47.4	45.8	6.8
T-3878	1400	2.00	3:00	CPX*+OLV*+L*	>90	87.3	46.0	47.4	6.6
T-3896	1420	2.50	3:00	CPX*+SPL	~95		46.2	46.3	7.5
T-3898	1460	2.50	2:00	CPX*+L*	<90		41.1	48.0	10.8
T-3899	1480	2.50	1:00	L*					
T-3900	1470	2.50	1:30	L	~50				
ANK2376 + 20 wt% H_2O									
T-3955	1100	1.50	4:00	OL*+L	~85	88.0			
T-3956	1060	1.50	5:00	OL*+CPX*+L+V	>90	84.2	48.9	45.5	5.6
T-3957	1040	1.50	5:00	OL*+CPX*+L+V	>90	84.1	48.9	45.6	5.4
T-3958	1120	1.50	1:30	OL*+L+V	<5	89.2			
T-3960	1140	1.50	1:00	L+V					
T-3961	1070	1.00	3:45	OL*+CPX*+L+V	~25	86.1	48.0	47.0	5.1
T-3962	1030	1.00	6:00	OL*+CPX*+L+V	>90	80.2	50.5	43.5	5.9
T-3964	1070	1.25	4:00	OL*+CPX*+L+V	~50	86.2	50.2	45.2	4.6
T-3965	1120	1.00	1:00	OL*+L+V	~10	89.8			
T-3966	1140	1.00	1:00	L+V					
T-3967	1120	2.00	2:00	L+CPXq*					
T-3968	1100	2.00	2:00	OL*+CPX*+L+V		85.9			
T-3969	1070	2.00	3:00	OL+CPX+L+V					
T-3970	1100	1.80	2:00	OL*+L+V	<20	86.6			
T-3971	1100	2.50	2:00	L+V					
T-3972	1100	3.00	2:00	L+V					
T-3974	1060	3.00	2:00	OL*+CPX*+GRT*+L+V	>90	83.1	46.4	45.8	7.8
T-3975	1060	2.50	4:00	OL*+CPX*+SPL+L+V	>90	81.8	46.8	46.6	6.6
T-3988	1120	1.90	3:00	L+V					
T-3989	1100	2.20	4:00	OL*+CPX*+L		87.4	48.0	47.5	4.5
T-3991	1080	2.20	5:00	OL*+CPX*+L+V		85.5	49.0	46.0	5.0
T-4007	1080	3.00	6:00	OL*+CPX*+GRT*+L		84.6	46.5	47.6	5.9
T-4008	1085	2.50	6:00	OL+CPX*+GRT*+L					

(*) Indicates phases analysed by electron microprobe. (1) Run phase assemblage, OL=Olivine, CPX=Clinopyroxene, CPXq=quenched clinopyroxene, GRT=Garnet, L=Liquid. (2) Visualy estimated percentage of primary crystals present in run. (†) Indicates runs where quenched glasses were analysed for CO_2 and H_2O (Table 5.2). (3) Average Fo composition from Appendix 5.1. (4) Most primitive composition of clinopyroxene in the run (Appendix 5.2).

TABLE 5.3 (continued)

RUN	T (°C)	P (GPa)	t (hr:min)	Assemblage[1]	%[2]	~Fo3	~Wo	En	Fs4
ANK2376 + 7.5 wt%CO_2, Furnace buffered (FB)									
T-4043†	1280	1.50	0:30	L*					
T-4045	1240	1.50	0:30	OL*+CPX*+L*		84.4	41.8	52.3	5.9
T-4047	1260	1.50	0:30	CPX*+OL+L			43.9	53.7	2.3
T-4050	1280	2.00	0:30	L*					
T-4051†	1300	2.00	0:30	L*					
T-4052†	1260	2.00	0:45	L*					
T-4054	1240	2.00	0:45	CPX*+L			42.0	50.7	7.3
T-4055	1240	2.50	0:45	CPX*+GRT*+L			43.5	50.0	6.5
T-4056	1260	2.50	0:45	CPX*+GRT*+L			44.4	48.3	7.3
T-4062†	1280	1.00	0:30	OL*+L*		90.9			
T-4063	1250	1.00	0:30	OL*+L*		91.7			
T-4068	1280	2.50	0:30	CPX+GRT+L					
T-4070	1260	2.25	0:30	CPX+GRT+L					
T-4071	1250	1.80	0:30	CPX+L					
ANK2376 + 7.5 wt%CO_2, Magnetite-haematite buffered (MHB)									
T-4087	1280	1.50	0:30	OL*+CPX		90.9			
T-4088†	1350	1.50	0:30	>L*					
T-4091	1320	1.50	0:30	>L*					
T-4092†	1300	1.50	0:30	>L*					
T-4093	1290	1.50	0:30	>L*					
T-4096	1280	2.00	0:30	CPX					
T-4098	1280	2.50	0:30	CPX+GRT*					
T-4109	1280	1.00	0:30	OL*+CPX*+L*		90.2	46.3	47.4	6.3
T-4111†	1290	1.00	0:30	OL*+CPX*+L*		90.4	45.8	47.0	7.2
T-4115	1300	1.00	0:30	OL+L*	<5				
T-4117	1310	1.00	0:30	OL+L*	<5				
T-4118	1280	1.75	0:30	CPX					
T-4119	1300	2.50	0:30	CPX+GRT*					
T-4120	1310	2.50	0:30	CPX+GRT*					
T-4121†	1320	1.00	0:30	OL*+L*	<1	92.6			
T-4131	1285	2.25	0:30	CPX+GRT					
T-4132	1280	1.25	0:30	OL*+CPX		88.6			
T-4134	1270	2.25	0:30	GRT+L					
T-4136	1270	2.00	0:30	CPX					
T-4137	1250	1.75	0:30	CPX					
T-4143	1250	1.60	0:30	OL*+CPX		84.5			
T-4145	1220	1.75	0:30	CPX					
T-4146	1200	1.75	0:45	OL*+CPX		82.3			
T-4149	1295	1.75	0:45	CPX*+L*			37.1	54.5	8.4
T-4150	1290	1.75	0:30	CPX					
T-4156	1330	2.25	0:30	CPX+GRT					
T-4157†	1330	2.00	0:30	CPX*+L*			37.3	56.0	6.6
T-4158†	1320	2.00	0:40	CPX*+L*	<90		40.6	52.4	7.0
T-4159	1340	2.25	0:30	CPX*+L*+CPXq			30.4	62.7	6.9
T-4160	1285	1.50	0:30	OL*+CPX*+L*		90.0	36.3	54.5	9.2
T-4161	1290	1.25	0:30	OL*+CPX*+L*		89.8	44.6	48.8	6.6

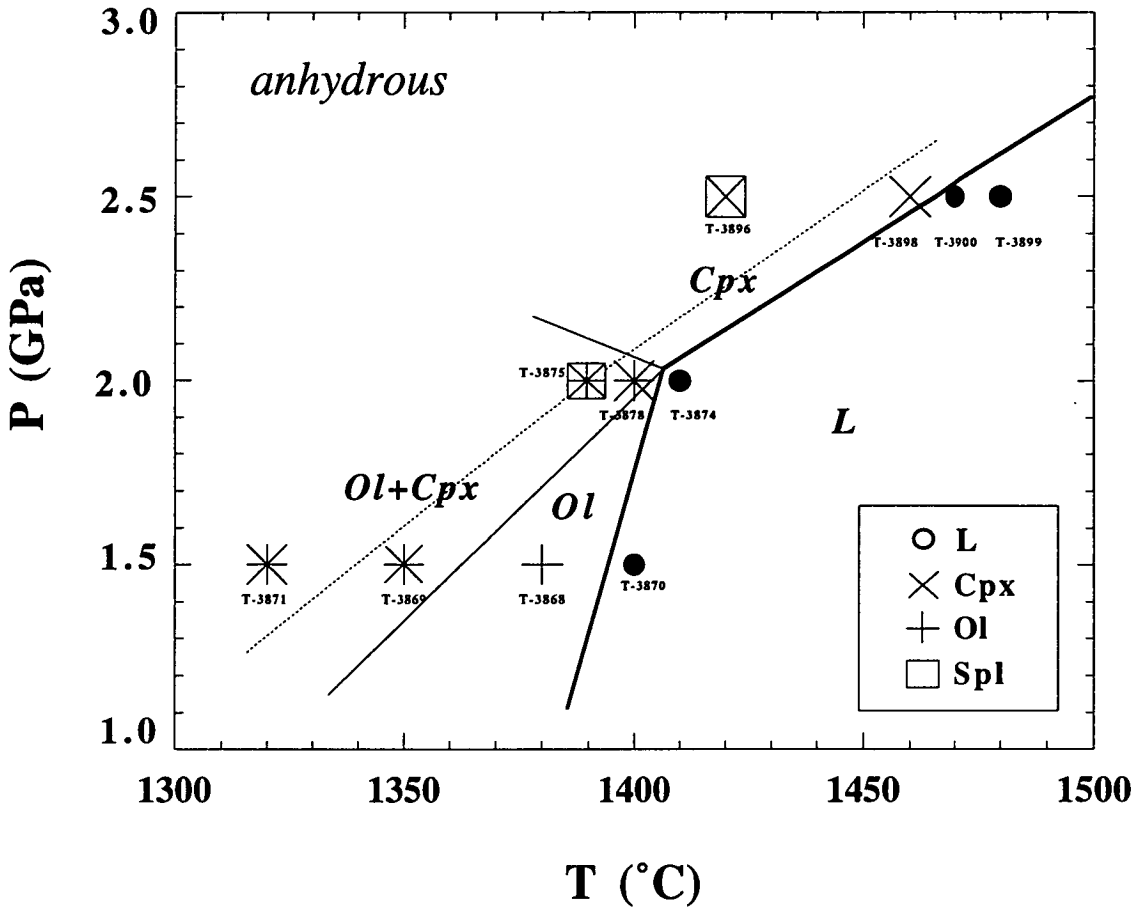

Figure 5.3 P, T diagram for the crystallization of ANK2376 under anhydrous conditions. Dotted line indicates approximately >50% crystals . Mineral symbols indicate phases coexisting with liquid. L=liquid, Cpx= clinopyroxene, Ol=olivine, Spl=spinel.

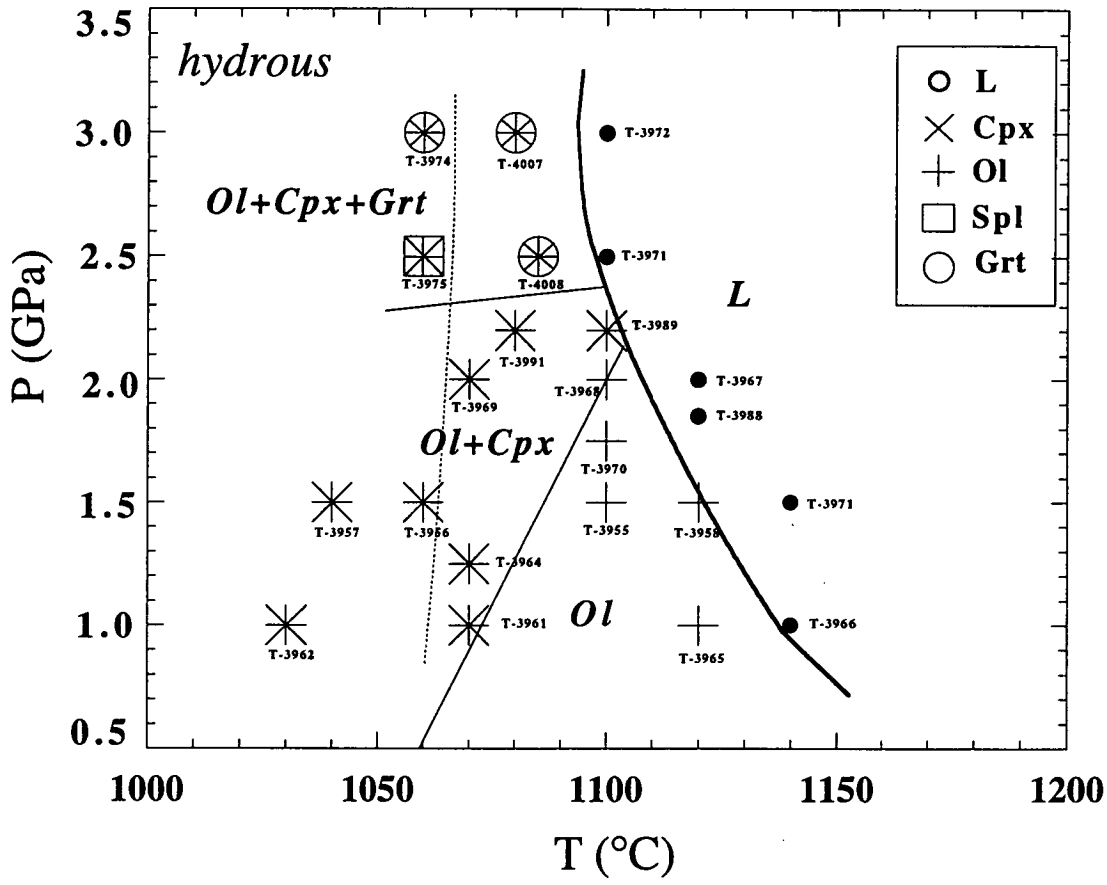

Figure 5.4 P, T diagram for the crystallization of ANK2376+20 wt% H_2O. Dotted line shows approximate boundary where run products are highly crystalline (~>90% crystals). L=liquid, Cpx= clinopyroxene, Ol=olivine, Spl=spinel, Grt=garnet.

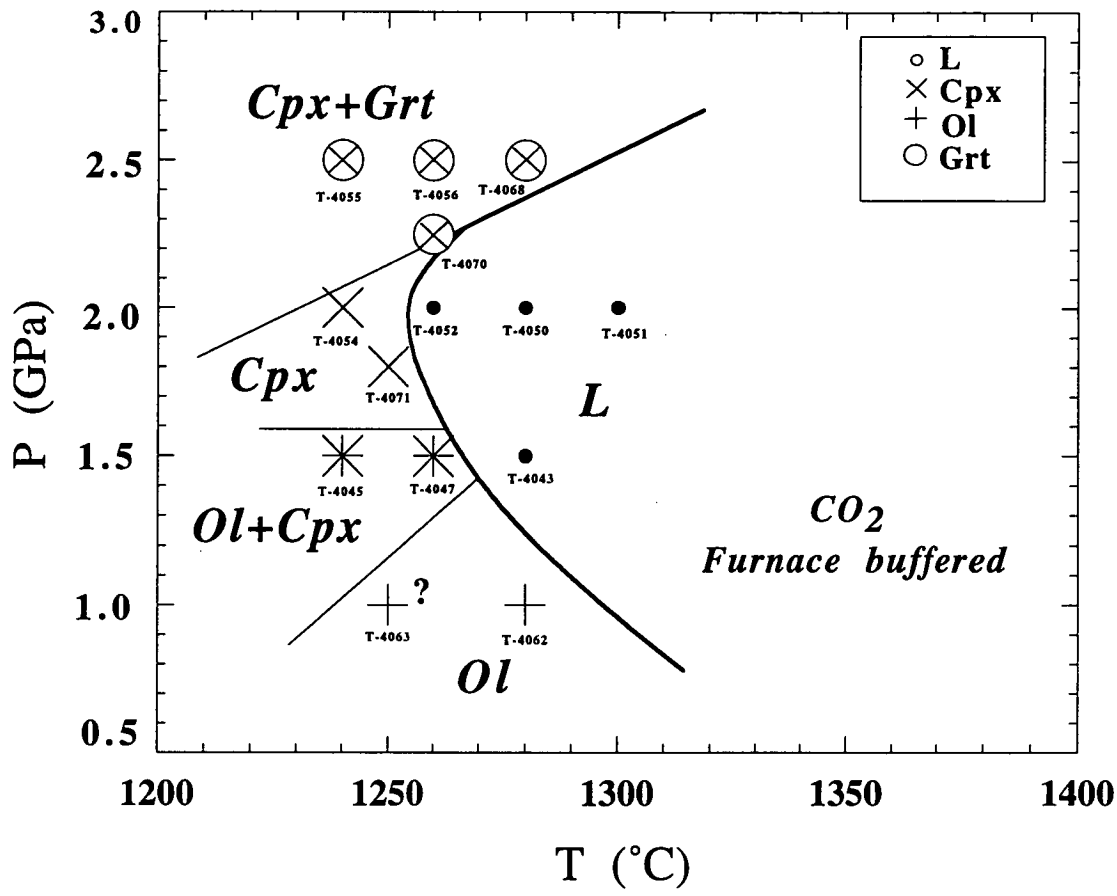

Figure 5.5 P, T diagram for crystallization of ANK2376+7.5 wt% CO_2 under furnace buffered conditions. "?" sign indicates experiment where mineral compositions are inconsistant with P, T trends (Section 5.7). L=liquid, Cpx= clinopyroxene, Ol=olivine, Grt=garnet.

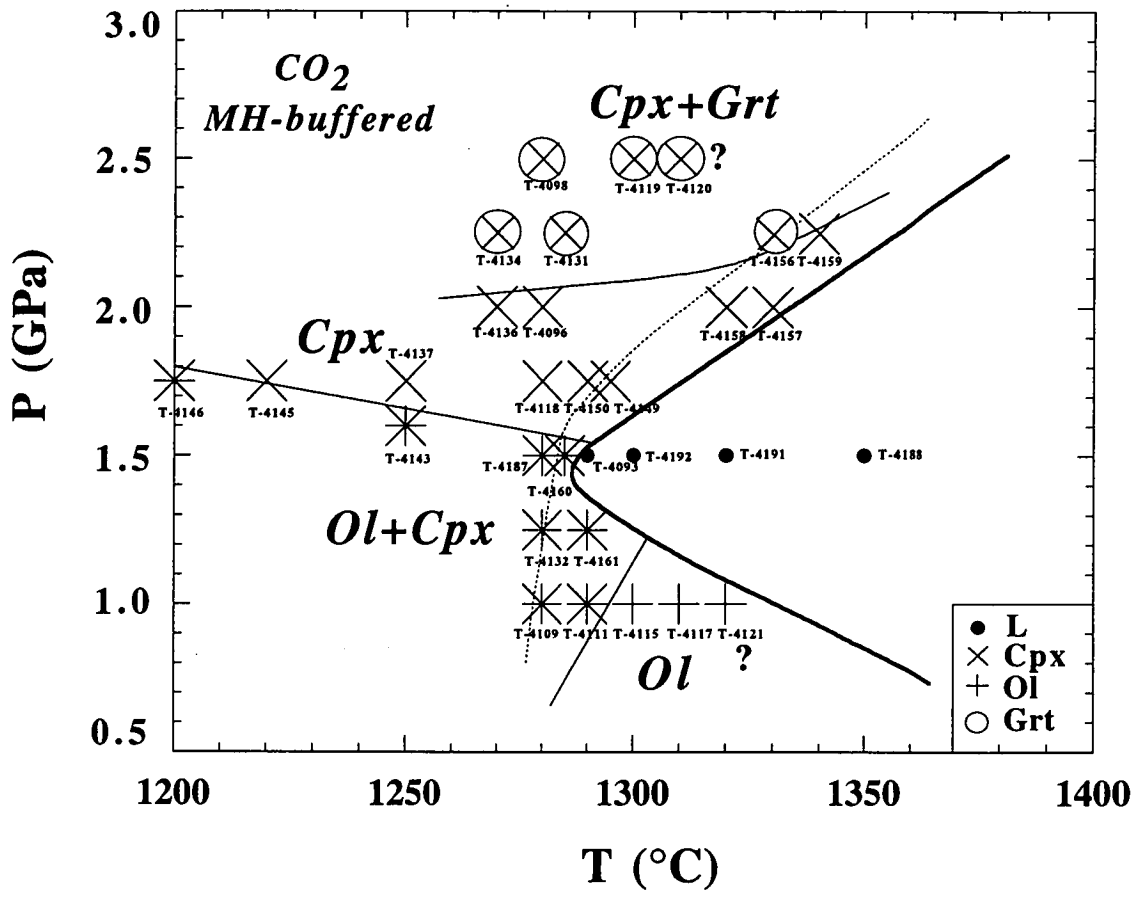

Figure 5.6 P, T diagram of crystallization for ANK2376+7.5wt%CO_2 under magnetite-haematite (MH) buffered conditions. Dotted line indicates ~50% crystallization. "?" signs indicate experiments where mineral compositions are inconsistent with P, T trends (Section 5.7). L=liquid, Cpx= clinopyroxene, Ol=olivine, Grt=garnet.

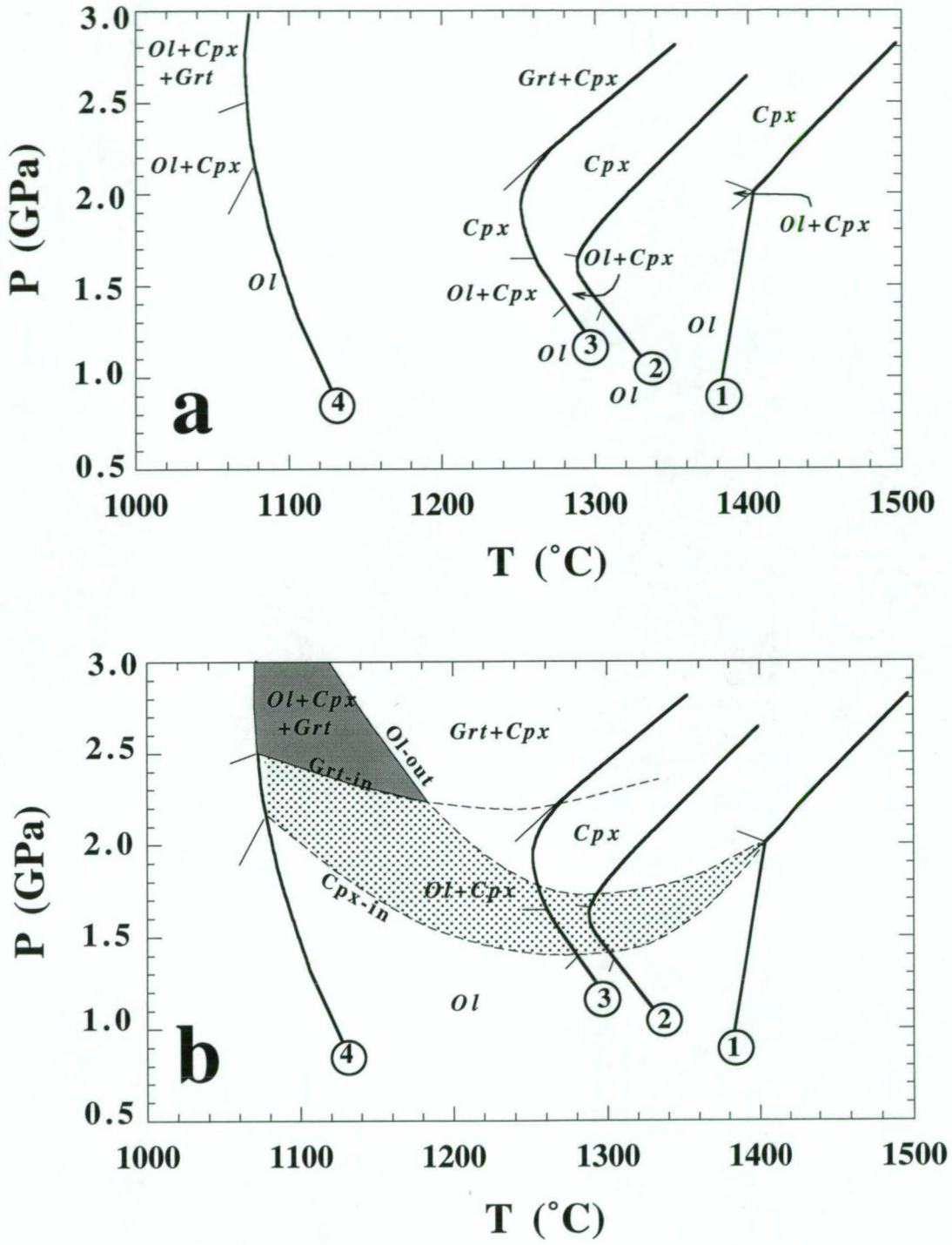

Figure 5.7 a: P, T summary diagram for the liquidus phases of ANK2376 under: (1) unhydrous, (2) +7.5wt% CO_2 furnace buffered, (3) +7.5wt% CO_2 magnetite-haematite (MH) buffered, and (4) +20wt% H_2O conditions.

b: Possible distribution of liquidus phases with pressure and temperature under dry, to hydrous, and CO_2 bearing conditions. Experimental conditions 1,2,3 and 4 as described above. Shaded area= Ol+Cpx+Grt. Dotted area= Ol+Cpx.

liquidus phases change from; olivine, to olivine+clinopyroxene, to clinopyroxene and to clinopyroxene+garnet. The upper limit of olivine stability is decreased and is not stable above 1.5 GPa. At this pressure olivine coexists in very small proportions (<2%) with low-Ca clinopyroxene ($Wo_{43}En_{54}Fs_3$, T-4047). Microprobe analysis of olivine in this run was not possible due to its small grain size. Clinopyroxene is the only liquidus phase from ~2.0 to 2.3 GPa, and it is joined by garnet at higher pressures (Figure 5.5). At 2.5 GPa the proportion of garnet compared to clinopyroxene decreases towards the liquidus. Liquidus temperatures in these experiments are not bracketed accurately because variable amounts of H_2O were introduced in the sample as a result of H_2 migration.

5.4.4 ANK2376-CO_2, MH-buffered

In this series of experiments a MH-buffer maintained a relatively CO_2-pure H_2O-free volatile phase during the runs (Section 5.2.7). Liquidus temperatures are slightly higher than those of furnace-buffered runs and show a pronounced temperature depression at the olivine-clinopyroxene stability field. Phase relations are much the same to those in furnace-buffered experiments, except garnet appears below the liquidus at high pressures (Figure 5.6). At pressures >1.5 GPa, the crystallization interval is relatively narrow (~10 to 20°C) but increases at lower pressures. As in furnace-buffered experiments, a field of clinopyroxene widely separates garnet from olivine, but olivine and clinopyroxene coexistence to lower pressures. The upper limit of olivine stability is well constrained by near solidus runs and has a negative slope. A thorough search at sub-liquidus and near-solidus pressure-temperature conditions found no orthopyroxene.

5.4.5 Summary of phase relations

It can be seen from Figure 5.7 that only under hydrous conditions does the olivine stability field extend into the garnet-clinopyroxene field at high pressures. Presence of CO_2 diminishes the lower pressure limit of garnet stability compared to hydrous conditions by about 0.5 GPa, but also lowers the upper limit of olivine stability much more rapidly down to 1.5 GPa. Thus, under CO_2-bearing conditions, the solidus fields of olivine and garnet are widely separated by clinopyroxene. Under the more CO_2-pure conditions of MH-buffered experiments, garnet does not appear as a liquidus phase. This suggests that both CO_2 and H_2O are needed to stabilize garnet on the liquidus of ANK2376 at high pressures. Olivine and clinopyroxene coexist on the liquidus; at ~2.25 GPa under hydrous conditions, at ~1.5 GPa under CO_2 furnace-buffered conditions, from ~1.25 to 1.5 GPa under CO_2 MH-buffered conditions, and at ~2.0 GPa under anhydrous conditions. Orthopyroxene was not found to crystallize from the liquid under any of the conditions investigated.

5.5 Absence of orthopyroxene

The lack of orthopyroxene on the liquidus of supposedly primary melts is commonly attributed to a reaction between orthopyroxene and liquid that can be confirmed by "orthopyroxene-addition" experiments (e.g., Brey & Green 1977, Maaløe *et al.* 1986 and Adam 1989). Multiple saturation in olivine, clinopyroxene and garnet was only achieved in ANK2376 under hydrous conditions at

pressures >2.5 GPa. Under all other CO_2-bearing and anhydrous conditions investigated, olivine and garnet were widely separated by a field of clinopyroxene (Figure 5.7b). Orthopyroxene may therefore be in a reaction relationship with the liquid in the region defined by the garnet-in and olivine-out curves under fluid saturated/undersaturated conditions of relatively high H_2O/CO_2 ratios (shaded area in Figure 5.7b). This possibility, of a "hidden" P, T stability range remains to be explored for ANK2376, but has been demonstrated to exist in other undersaturated compositions (e.g., Bultitude & Green 1971).

Nucleation and metastability of low Ca-pyroxenes at high temperatures may hinder the growth of orthopyroxene as a separate phase (Green & Hibberson 1970, Brey & Green 1977 and Gust & Perfit 1987). This possibility is discarded in these experiments based upon the compositions of pyroxenes crystals crystallized from ANK2376 that show no evidence of metastability (see Section 5.6.3 below). It is therefore concluded that under the conditions investigated here, orthopyroxene saturation did not occur.

5.6 Composition of experimental phases

Microprobe analyses of representative mineral phases from the experiments are listed in Appendix 5 and summarized in Table 5.3. These analyses were made to confirm optical identification of mineral phases and to establish their compositions. A detailed analytical study on compositional relationships is not intended Observations made from the limited amount of data are given below. Generally, only one microprobe analysis per crystal was possible without overlap of the electron beam on surrounding material. These were mostly limited to near-liquidus runs where the number of crystal phases were fewer and their sizes larger. Quenched overgrowth was common, but its amount varied between runs. Ferric iron contents in the analysis of spinel, garnet and clinopyroxene are calculated from microprobe analyses following the method described by Robinson (1980). This procedure calculates an equivalent number of oxygens assuming a perfect cation stochiometry, and attributes a deviation from the ideal total oxygen to the presence of Fe^{3+}.

5.6.1 Olivine

Average olivine analyses from selected runs are listed in Appendix 5.1. The compositions of near-liquidus olivines (~Fo_{90-92}) resemble the host olivine of melt inclusions that were analysed to prepare ANK2376 (~Fo_{91}, Table 5.1), and are similar to the most magnesian olivines found in the ankaramite rock UTas48001 (Figure 1.16a). At a constant pressure, the average fosterite content of olivine increases with run temperature at all conditions except in those of ANK2376+CO_2 furnace-buffered experiments (Figure 5.8). In these experiments, T-4063 has olivine with a higher Fo content than a run quenched at 30°C higher (T-4062). This reflects the high $Mg^{\#}$ (~94) of the coexisting liquid in this run (now glass, T-4063), after considerable iron loss to the Pt capsule (~77% FeO loss) under furnace-buffered condition (Section 5.2.6 and run T-4063 in Figure 5.1).

The $K_D{}^{Ol\text{-}Melt}_{Fe\text{-}Mg}$ values calculated directly from olivine and residual glass analyses in these

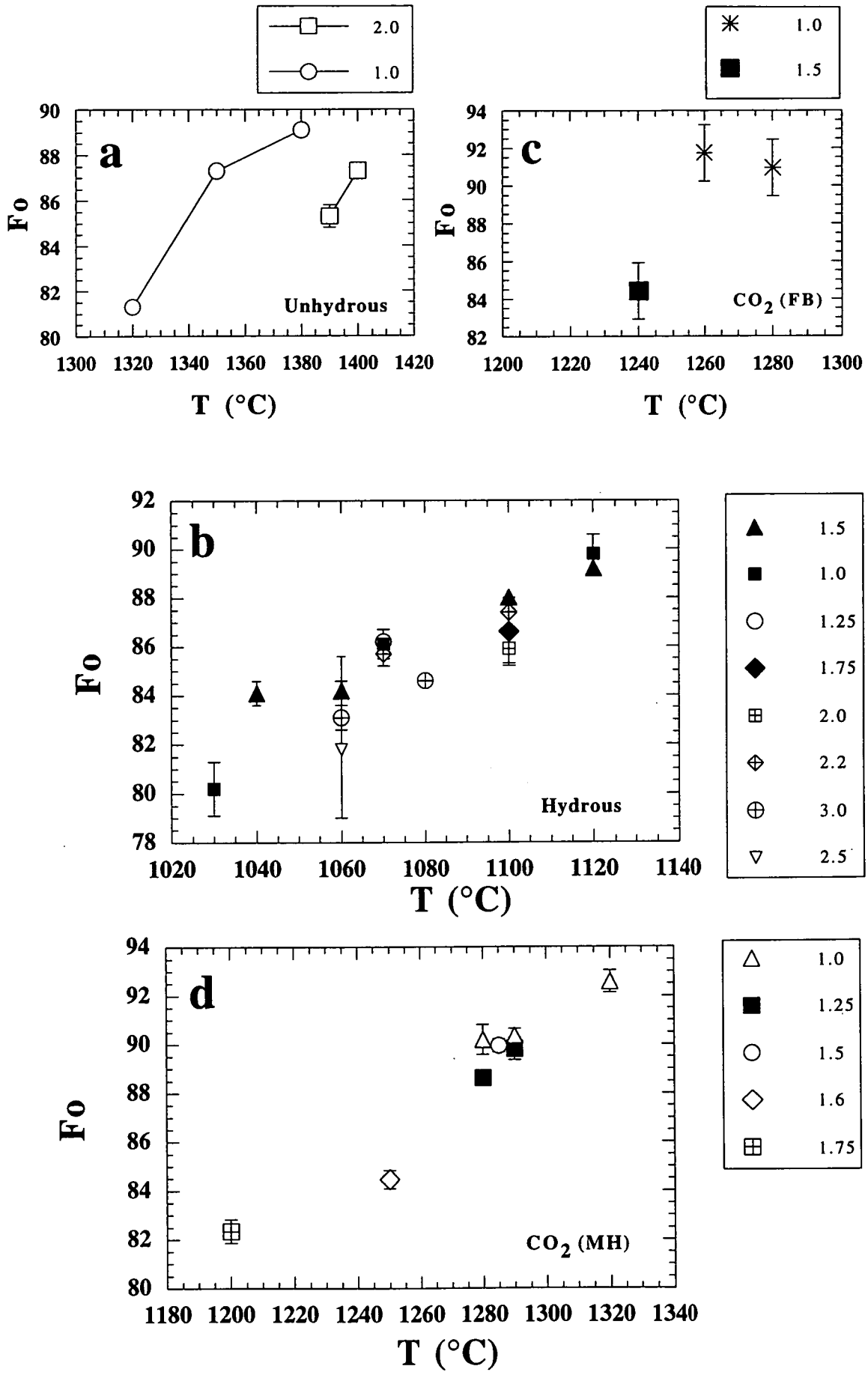

Figure 5.8 Variation in average fosterite (Fo) content of synthesized olivines *versus* temperature (T) of quenching in runs under a) dry, b) ANK2376+H20, c) ANK2376+CO_2 (furnace buffered), and d) ANK2376+CO_2 (MH buffered) conditions. Error bars represent standard deviation based on the number of analyses (Appendix 5.1). Symbols represent run pressure in GPa.

experiments are likely affected by iron loss to the capsule (Figure 5.1), as well as by quench overgrowth. Some of the $K_D^{Ol\text{-}Melt}_{Fe\text{-}Mg}$ values are alternatively calculated using the average composition of near-liquidus olivines (Appendix 5.1) and the composition of the starting glass ANK2376 (Table 5.1). These results are plotted against run temperature and pressure in Figure 5.9, where it can be seen that the calculated $K_D^{Ol\text{-}Melt}_{Fe\text{-}Mg}$ values show no correlation with temperature but a good pressure dependence (Figure 5.9b). The lack of temperature correlation rules out the possibility of a "hidden temperature effect" on the $K_D^{Ol\text{-}Melt}_{Fe\text{-}Mg}$ *versus* pressure trend as suggested by Sobolev and Danyushevsky (1994).

The average CaO content of olivine analyses from each run, are plotted in Figure 5.10 against Fo. The analyses have no detected Al_2O_3 to suggest electron beam overlap with the surrounding material. These olivine analyses are presented in Figure 5.10 as the composition of olivines coexisting with liquid, clinopyroxene+liquid, and garnet+clinopyroxene+liquid. Keeping in mind the potential risk of beam overlap, CaO contents in olivines vary within the analytical error and do not reveal the onset of clinopyroxene crystallization, although olivines coexisting with garnet in hydrous runs have consistently lower values (Figure 5.10). It is also notable that the ranges in CaO content (including uncertainties) of olivines from dry and CO_2 bearing experiments are much the same (~0.4 to ~0.8 wt%, Figure 5.10a, c, and d), yet they are systematically higher than CaO contents in olivines from hydrous runs (~0.1 to ~0.4 wt%, Figure 5.10b).

5.6.2 Clinopyroxene

Primary clinopyroxene crystals are surrounded by a distinctive rim of quench overgrowth despite careful search for rimless examples. As a result, microprobe analyses of primary clinopyroxene crystals within runs vary widely in composition due to beam overlap with these quench overgrowths. Typically, a range is present where compositions vary from the most primary compositions trending towards the residual glass. Consequently, the "average" clinopyroxene composition in each run is meaningless. Instead, the most "primitive" clinopyroxene analysis found in each run will be considered representative of the clinopyroxene composition formed at run conditions.

Primary clinopyroxene analyses are recognized by relatively low Al_2O_3, TiO_2 and high CaO contents, and by $Mg^{\#}$ values that are similar to those of coexisting olivines. The analyses of the most primary-seeming clinopyroxenes selected from each run are listed in Appendix 5.2 and plotted against run temperature in Figure 5.11. Within analytical error, the $Mg^{\#}$ values of clinopyroxenes increase with increasing run temperature. In Figure 5.11a, run T-3898 is an exception to this trend, as it has a lower $Mg^{\#}$ (81.6) than a run 40°C lower ($Mg^{\#}$ 86.0) at similar pressures, and the analysis is therefore considered to be slightly modified by quench overgrowths. In addition to this $Mg^{\#}$-temperature correlation, it also appears that at constant temperature, clinopyroxenes at higher pressures have lower $Mg^{\#}$. This is best shown by hydrous runs in Figure 5.11b.

Calculated $Fe^{3+}/Fe^{2+}+Fe^{3+}$ values of clinopyroxenes are highly variable and do not correlate

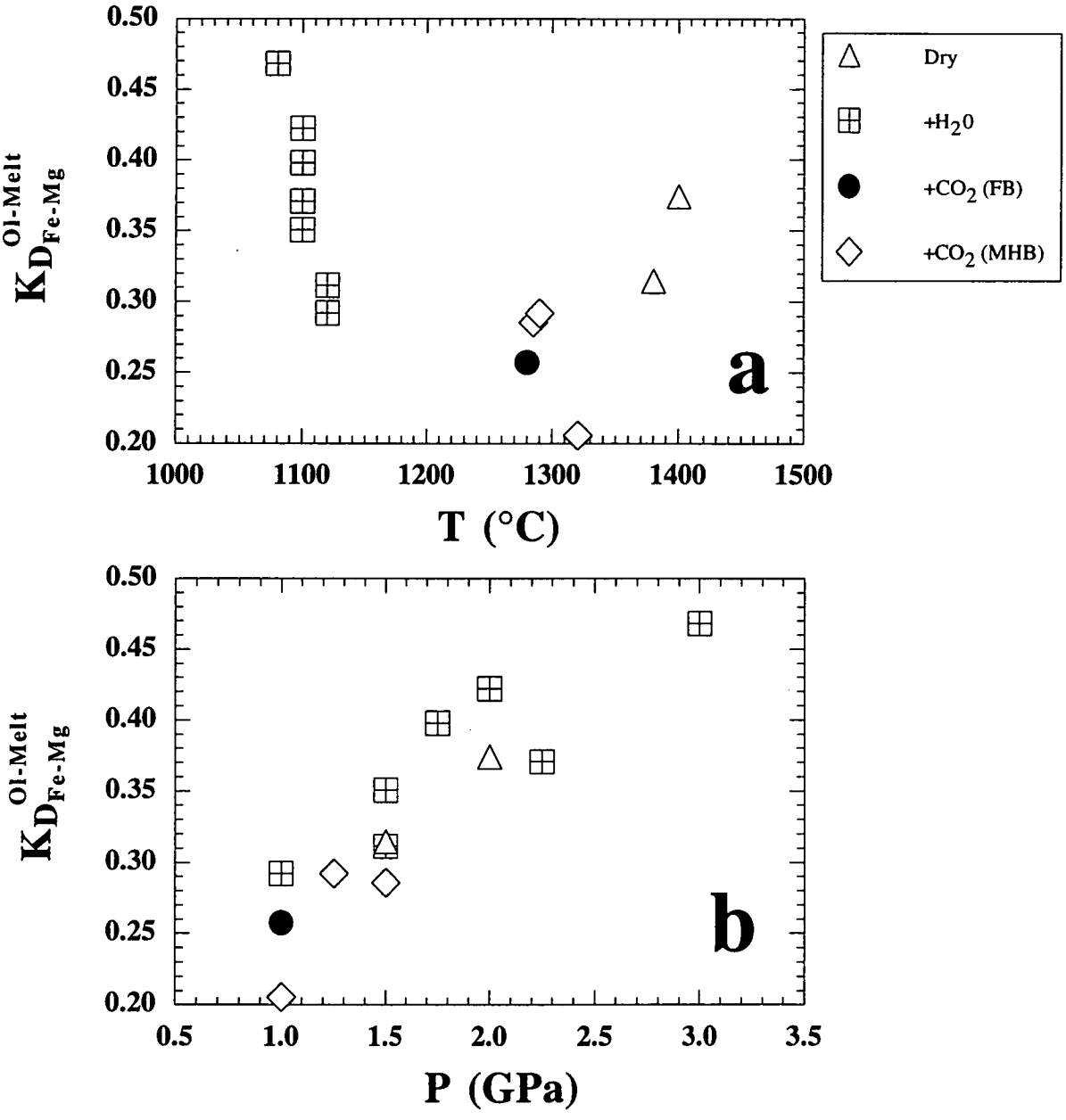

Figure 5.9 Variation in K_D values with a) temperature and b) pressure. K_D calculated as $(Fe/Mg)_{Olivine}/(Fe^*/Mg)_{Starting\ glass}$ using average composition of near liquidus olivines (Appendix 5.3) and bulk composition of starting glass ANK2376. Experimental conditions as follows: triangles=unhydrous, squares=hydrous, circle=CO_2 furnace buffered (FB), and diamonds=CO_2 magnetite-haematite buffered (MHB). Error bars in K_D values are smaller than symbols (<0.01).

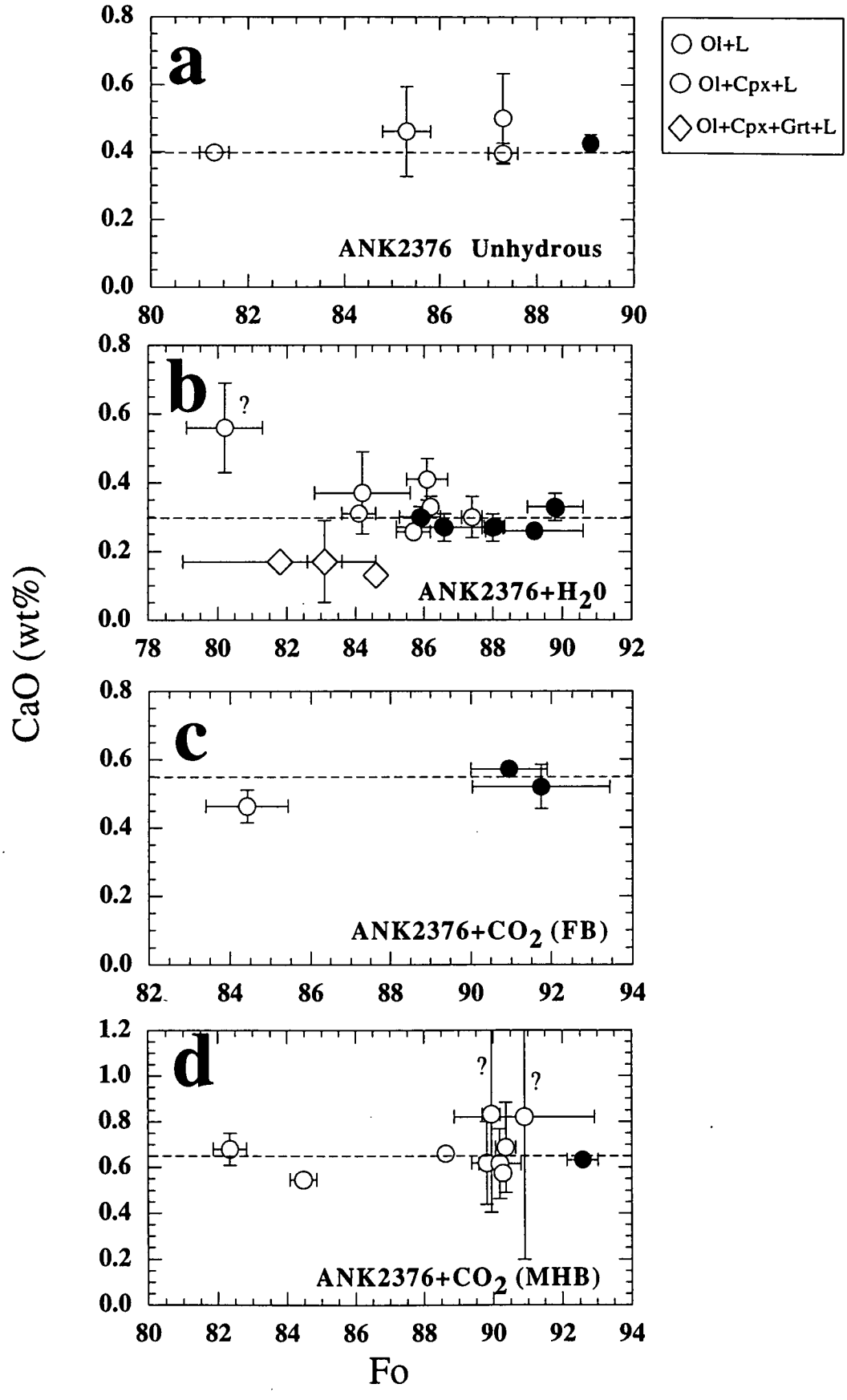

Figure 5.10 Average CaO content (wt%) in olivines *versus* fosterite (Fo) content, from runs under a) unhydrous, b) hydrous c) CO_2 unbuffered, and d) CO_2 magnetite-haematite buffered conditions. Filled symbols are near liquid olivines coexisting with liquid, open symols are olivines coexisting with clinopyroxene+liquid, and open diamonds are olivines coexisting with clinopyroxene+garnet+liquid. Question mark indicates olivine analyses with possible overlap on the surrounding matrix. Error bars are standard deviations based on number of analyses (Appendix 5.1). Ol=olivine, Cpx=clinopyroxene, Grt=garnet, L=liquid.

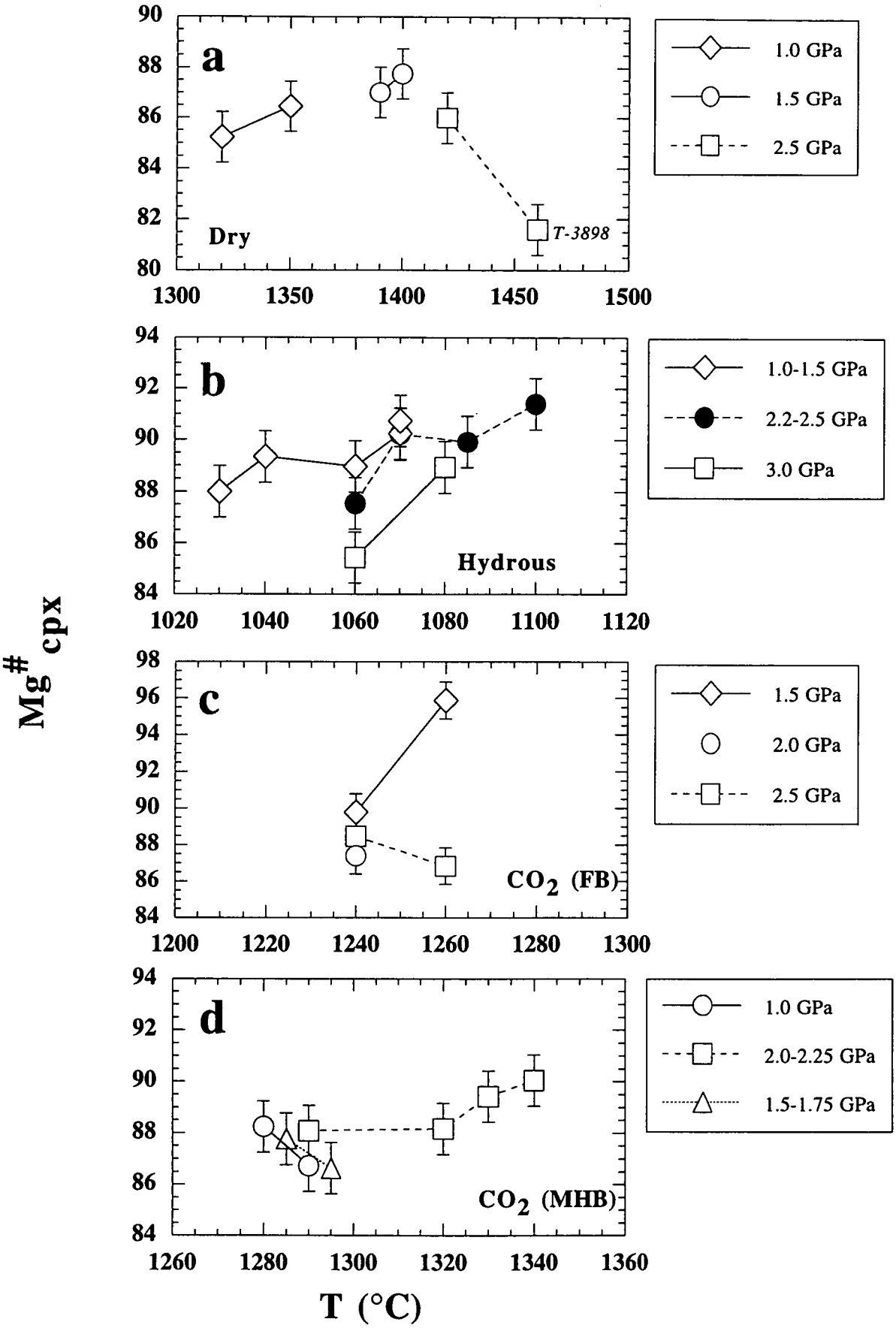

Figure 5.11 Variation in Mg# =100Mg/(Mg+Fe*) of the least aluminous clinopyroxene in each run versus temperature (T). a) unhydrous, b) hydrous, c) +CO_2 furnace buffered (FB) and d) +CO_2 magnetite-haematite buffered (MHB) conditions. Error bars are ±1 Mg# unit. Data from Appendix 5.2.

with the fO_2 conditions imposed by the buffer or furnace assemblage used. In MH-buffered runs for example, $Fe^{3+}/Fe^{2+}+Fe^{3+}$ values range from ~0.1 to ~0.9 and overlap with the compositions of clinopyroxenes formed under other fO_2 conditions, (Figure 5.12). Therefore, $Mg^{\#}$ values, calculated with all iron as Fe*, are used for these clinopyroxenes rather than their mg# values[1]. Within analytical error, $Mg^{\#}$-Fo values of coexisting clinopyroxene-olivine pairs (Appendix 5.3) are close to experimentally and naturally established relationships (Figure 5.13). It is notable that clinopyroxene $Mg^{\#}$ values under MH-buffered conditions are slightly lower than Fo, whereas all others are higher (Figure 5.13, dotted line)

The most primary-seeming clinopyroxenes in hydrous runs have <5 wt% Al_2O_3, ~23-24 wt% CaO, and $Mg^{\#}$ of ~90-91. As a group these clinopyroxenes plot within the augite field and resemble the calcic nature of the clinopyroxene phenocryst from sample UTas48001 (Figure 5.14).

Clinopyroxenes from anhydrous runs have similar Wo contents to UTas48001 phenocrysts, but are higher in Al (~8-10 wt% Al_2O_3), lower in Ca (~20-22 wt% CaO), and yet retain high $Mg^{\#}$ values, unlike their quenched counterparts with lower Mg# values.

Clinopyroxenes formed in experiments with CO_2 added and furnace-buffered conditions are also aluminous with ~6-9 wt% Al_2O_3, but less calcic (around 19 to 20 wt% CaO, Appendix 5.2), and plot within the augite field (Figure 5.14). However, although the compositions of primary clinopyroxenes formed in CO_2 experiments at MH-buffered conditions are similarly high in Al_2O_3 (~7-13 wt%) they have a much larger range in Wo contents varying from ~Wo_{45} to ~Wo_{30} at constant $Mg^{\#}$, with CaO values as low as 14 wt% (Figure 5.14). This variation seems to reflect a trend of decreasing Wo content with increasing pressure (Trend B, Figure 5.15). Clinopyroxenes from hydrous and dry experiments (with exception of run T-3898) also show similar trends, but the decrease in Wo with pressure is much more (Trend A, Figure 5.15). It is also notable that clinopyroxenes from CO_2 experiments at furnace-buffered conditions have Wo contents that range between these two trends, thus reflecting the increasing amount of H_2O formed in the run at higher pressures as a result of H_2 diffusion (Figure 5.2a).

5.6.3 Metastable clinopyroxene?

In Figure 5.16, the composition of primary clinopyroxenes under MH-buffered conditions that coexist with olivine at low pressures are shown to have highest Wo content (filled symbols). However those primary clinopyroxenes that coexist alone near the liquidus in higher pressure runs range towards lower Wo contents at nearly constant $Mg^{\#}$ (open symbols, Trend B, Figure 5.16). Also shown for comparison are analyses of clinopyroxenes modified by quenched overgrowths that define a trend towards the liquid composition (Trend A, Figure 5.16). Thus, Trend-B differs from Trend A, and must therefore represent a process other than compositional variation caused by quench overgrowth.

In particular, run T-4159 had clinopyroxene crystals sufficiently large to permit core-rim

---

[1] $Mg^{\#}$=100Mg/(Mg+Fe) whereas $mg^{\#}$=100Mg/(Mg+Fe^{2+}). Fo=100Mg/(Mg+Fe)

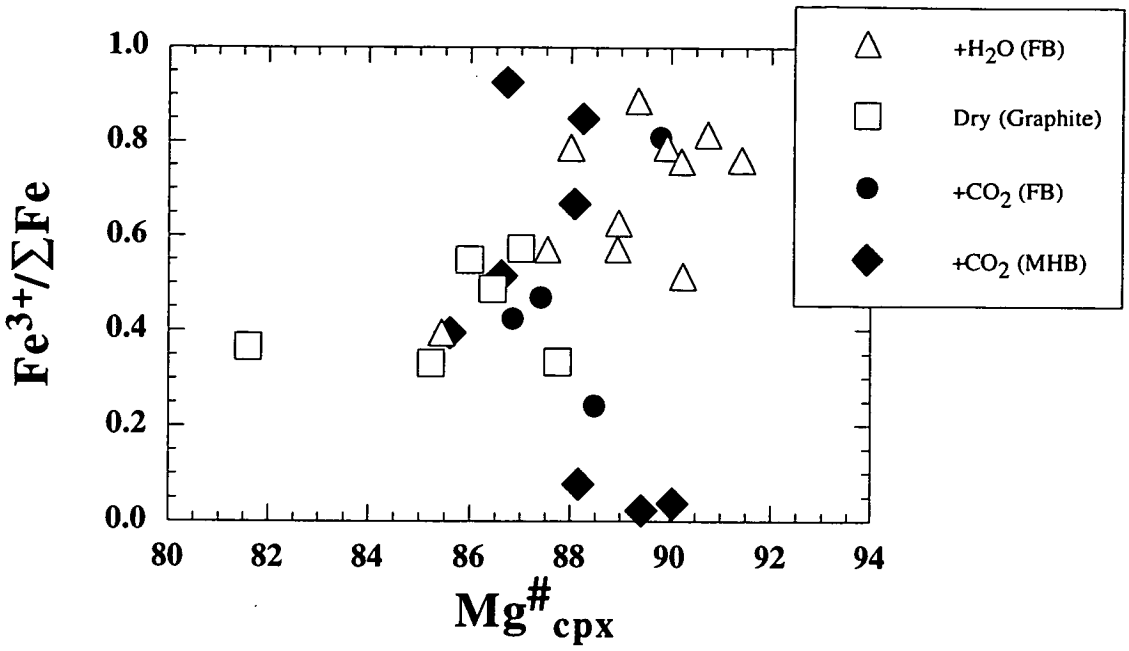

Figure 5.12 Variations in calculated $Fe^{3+}/(Fe^{3+}+Fe^{3+})$ values *versus* Mg#=100Mg/(Mg+Fe*) of the most primitive clinopyroxene analysis in each run. Square=unhydrous runs in graphire capsules, tringles=hydrous runs furnace buffered (FB), circles=CO_2 runs furnace buffered (FB), diamonds=CO_2 runs magnetite-haematite buffered (MHB). Fe^{3+} values in clinopyroxene are estimated assuming perfect stochiometry (see Section 5.6).

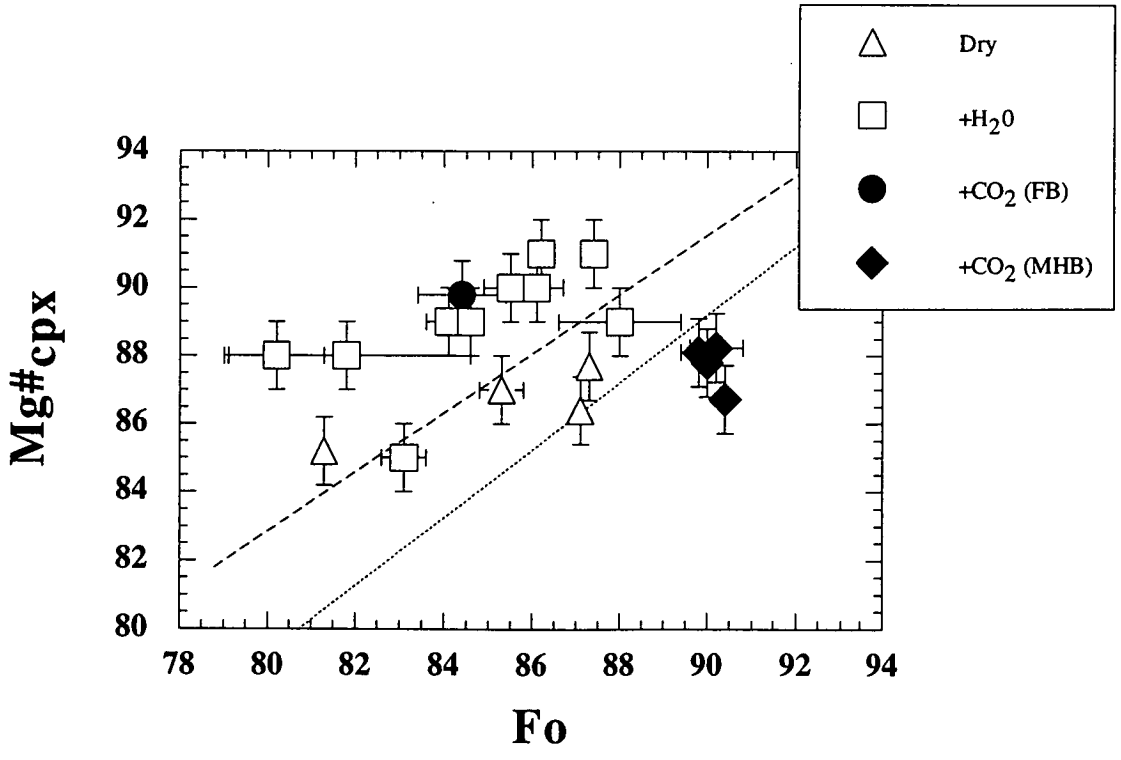

Figure 5.13 $Mg^{\#}$=100Mg/(Mg+Fe*) of clinopyroxene *versus* fosterite (Fo) content of coexisting olivine under unhydrous (triangles), hydrous (squares), CO_2 furnace buffered (FB) (circle), and CO_2 magnetite-haematite buffered (MHB) conditions. Filled symbols indicate runs in Pt capsules. Dashed line represents experimental and naturaly determined relationship after Barsdell (1988) on the basis of all iron as Fe2+. Dotted line indicates 1:1 ratio. Clinopyroxene compositions represent the most primitive analyses in each run, whereas olivine composition represent averages of several analyses within each run. Error bars in clinopyroxene are ±1 Mg# unit, and in olivines are ±standard deviations. Data from Appendix 5.1 and 5.2.

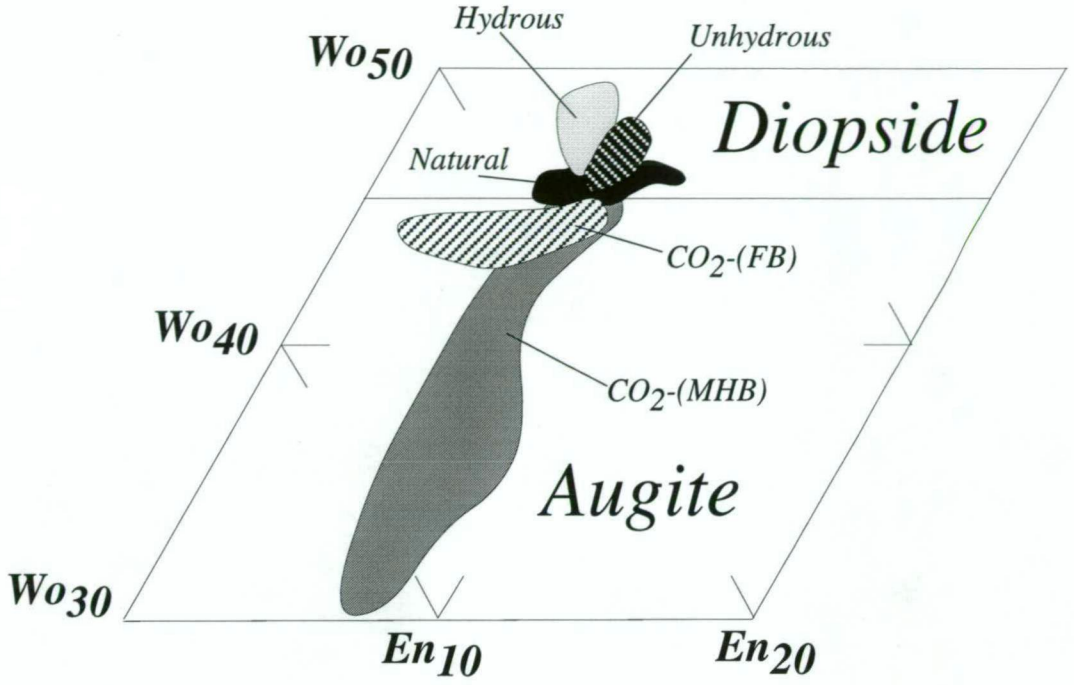

Figure 5.14 Composition of experimental and natural clinopyroxenes in the quadrilateral (Wo,En,Fs) after Marimoto (1989). Fields of experimental clinopyroxenes enclose the compositions of the most primitive analysis in each near liquidus run (~L, Appendix 5.2), under unhydrous, hydrous, CO_2 furnace buffered (FB), and CO_2 magnetite-haematite buffered (MHB) conditions. Natural clinopyroxenes are from sample UTas48001.

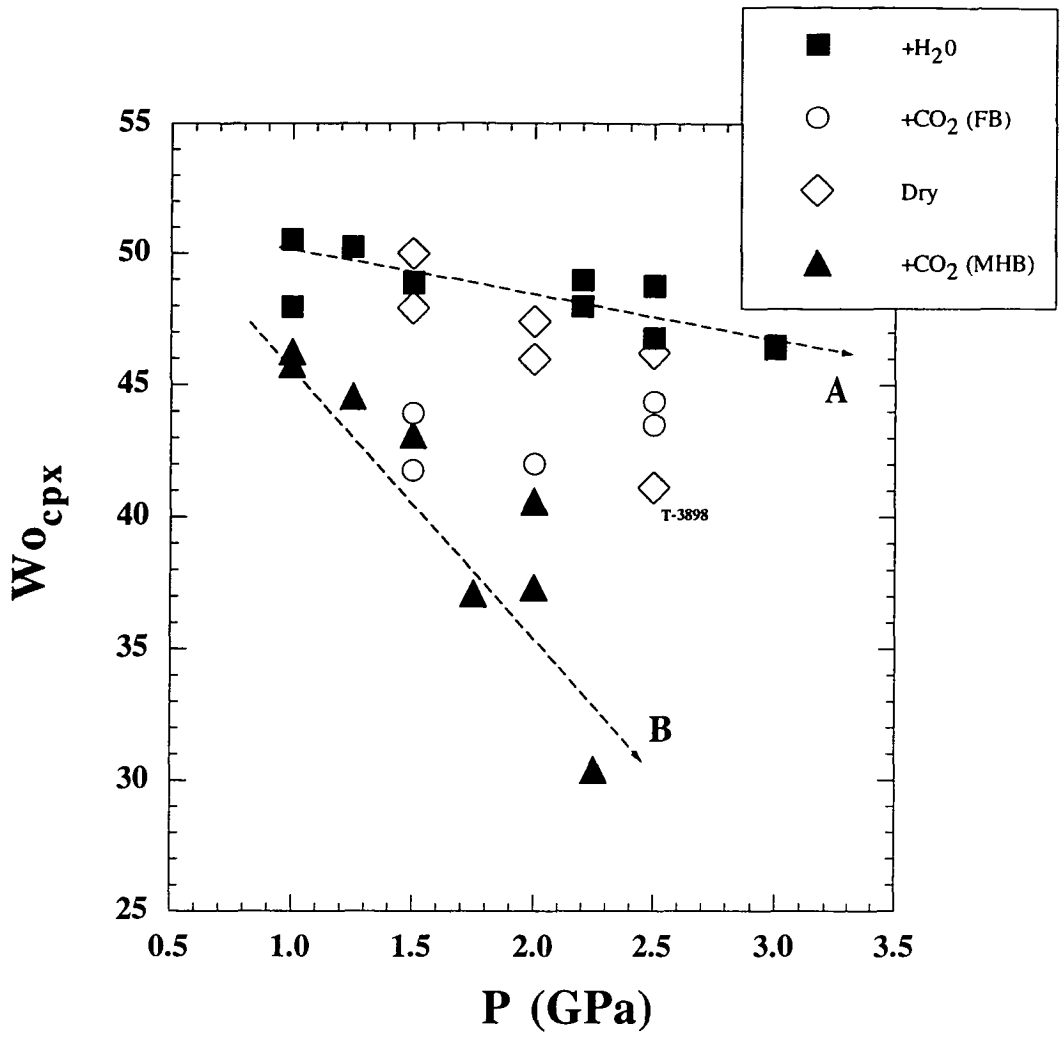

Figure 5.15 Variation in wollastonite (Wo=Ca/(Ca+Mg+ΣFe)) content of clinopyroxenes *versus* run pressure (P). Arrow labeled A indicates the slight trend of decreasing Wo content with increasing pressure in hydrous runs (filled squares), whereas arrow labeled B indicates a more pronounced trend in CO_2 magnetite-haematite buffered (MHB) runs. Dry (diamonds) and CO_2 furnace buffered (FB, circles) runs have an intermediate range. Data from Appendix 5.2.

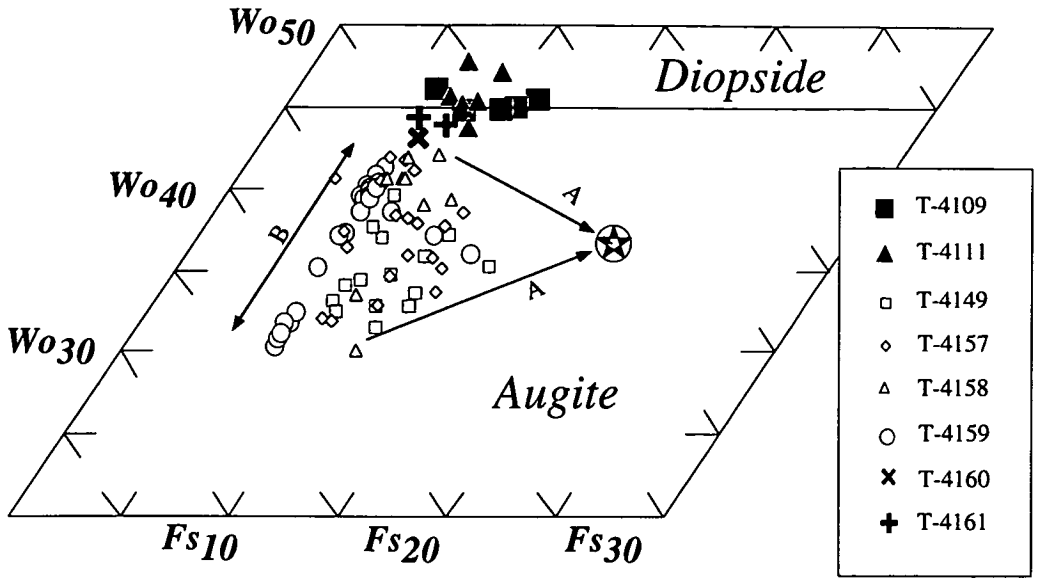

Figure 5.16 Variation in the composition of synthesized clinopyroxenes in experiments with CO_2 added under magnetite-haematite (MH) buffered conditions. Filled symbols are primitive compositions of clinopyroxenes coexisting with olivine in runs T-4109, T-4111, T-4160, and T-4161, (cf. Figure 5.8). Other symbols represent primary and quench compositions from near liquidus runs in which clinopyroxene is the only mineral phase (T-4149, T-4157, 4158, 4159). The star indicates the starting glass composition of ANK2376. Trend-A towards star indicates variation caused by quench overgrowth. Trend-B indicates variation in primary compositions at constant Mg# that is unrelated to quenching. Pyroxene quadrilateral Wo-En-Fs after Morimoto (1989).

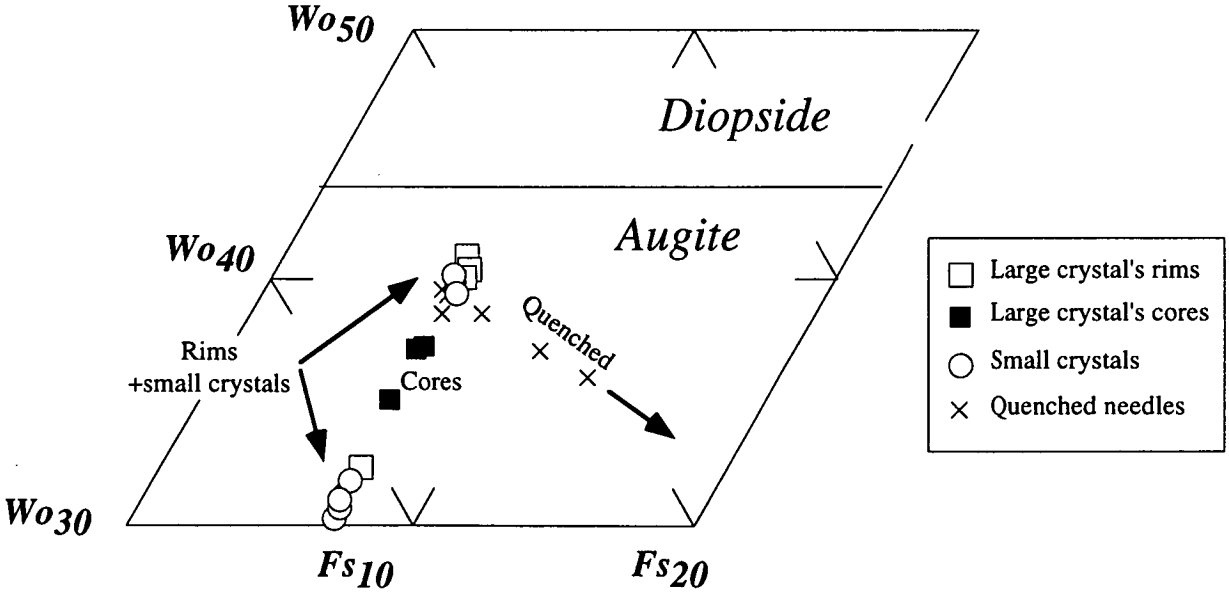

Figure 5.17 Compositional variations of clinopyroxenes in run T-4159 in the quadrilateral Wo-En-Fs after Marimoto (1989). Small clinopyroxene crystals have a bimodal composition (open circles) that is also displayed by the rims of larger crystals (open squares), as opposed to their cores (filled squares) that have intermediate compositions. Note that these variations are of constant Mg#, (~Fs_8) and differ from the quench trend defined by tiny brown clinopyroxene needles (crosses). Data from Appendix 5.4.

analyses. Their compositions together with those of single analyses from smaller clinopyroxene crystals and analyses from tiny brown needles of quenched clinopyroxene, are plotted in Figure 5.17 and listed in Appendix 5.4. It is notable that the smaller clinopyroxenes have bimodal distribution (open circles) with clusters at around ~Wo_{40} and ~Wo_{31}. A similar bimodal distribution is present in rim compositions of larger crystals (open squares), but not observed in their core (filled circles) which have intermediate compositions (~Wo_{36}). Thus the core and rim analyses of the larger clinopyroxene crystals reveal marked zoning, with similar core compositions but bimodal rims. The range in bimodal compositions has constant $Mg^{\#}$ (~Fs_8) similar to Trend-B in Figure 5.16, but differs from the oblique trend towards glass generated by quenching (crosses, Figure 5.17). This bimodal distribution is only present in CO_2 runs at MH-buffered conditions where clinopyroxene coexist alone near the liquidus. This range in composition is larger than observed in other runs and is the only indication of metastability in clinopyroxene compositions unrelated to quenching.

5.6.4 Garnet

Garnets have highly poikilitic textures with inclusions mainly of glass and possibly clinopyroxene. Reliable analyses were therefore difficult to obtain. Average compositions are listed in Appendix 5.5. At nearly constant pressures (2.5-3.0 GPa), garnets from hydrous runs have notably higher grossular (gross) and spessartine (spess) contents than those from CO_2-bearing runs (Figure 5.18a and b, open symbols). Within analytical error, $Mg^{\#}$ values increase with temperature, with the exception of run T-4120, which fall off the trend (Figure 5.18b).

5.6.5 Spinel

Aluminous spinels (Al-spinel) with ~65 wt% Al_2O_3 and very low chromium contents (Appendix 5.6), occur as an interstitial phase in some runs that are well below the liquidus and almost fully crystalline. In anhydrous runs, Al-spinel occurs at 2.0 and 2.5 GPa in association with olivine+clinopyroxene and clinopyroxene respectively (T-3875 and T-3896, Figure 5.3). Under hydrous conditions, Al-spinel coexists with olivine and clinopyroxene at 2.5 GPa (T-3975) but is replaced by garnet 25°C higher (Figure 5.4). These spinels nucleate and grow as a result of increased concentration of Al_2O_3 in the residual liquid, after continued crystallization of non-aluminous phases such as olivine and clinopyroxene. This process is similar to that leading to the formation of Al-spinels in melt inclusions trapped by olivine, as discussed in Chapter 6.

5.6.6 Liquid

Although the composition of residual liquids can be directly determined by microprobe analyses of interstitial glasses (Appendix 5.7), their compositions are of little petrological significance as a result of modifications by quench products. However, anhydrous glasses and, to a lesser extent, glasses from CO_2-bearing runs yielded portions of clear glass that permit measurements of CO_2 and H_2O solubility (discussed in Sections 5.2.7 and 5.8) as well as a quantitative assessment of iron loss to the platinum capsule (discussed in Section 5.2.6).

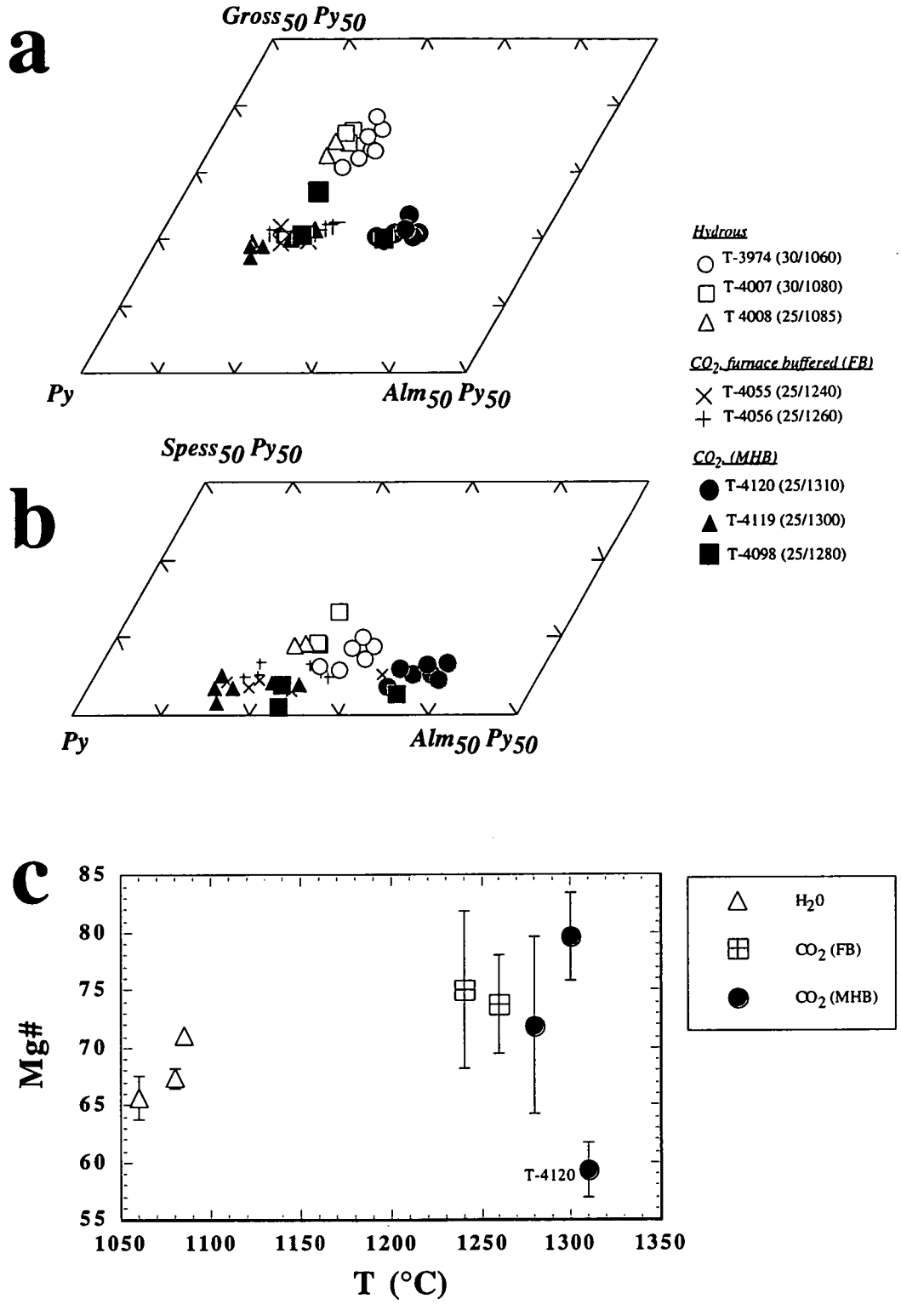

Figure 5.18 a) Compositional variations of garnets in the quadrilateral (Gross-Py-Alm) with molecular end members calculated as follows: Grossular (Gross)=Ca, Pyrope (Py)=Mg, and Almandine (Alm)=Fe^{2+}.

b) Compositional variations of garnets in the quadrilateral Spess-Py-Alm. Spessertine (Spess)=Mn. Symbols as in (a).

c) Average Mg# of synthesized garnets *versus* run temperature under hydrous (H_2O), CO_2 furnace buffered (FB) and magnetite-haematite buffered (MHB) conditions. Error bars are standard deviations based on number of analyses. T-4120 indicates run with anomalously low Mg#. Note run T-4120 with low Mg#. Data from Appendix 5.5.

5.7 Assessment of chemical equilibrium

All experiments in this work are synthesis runs. A more rigorous method of demonstrating phase equilibrium in these experiments would have been to successfully reproduce the experimental results using reground crystalline run products as starting material, instead of glass ANK2376, that is reversal experiments (Gust & Perfit 1987, Johnson & Rutherford 1989). Run reversals were not carried out. Therefore, not having strictly demonstrated run equilibrium, these experiments are regarded as "redundancy experiments", as opposed to "consistency experiments" (Pattinson 1994). The consistency of compositional trends however, is a sufficient indicator that chemical equilibrium was at least approached during the runs.

In the previous section, the experimental data were assessed against the following criteria: (1) does chemical homogeneity exists amongst phases within runs? (2) is there compositional zoning in large crystals? and, in particular (3) do variations in compositions between run products correlate with variations in pressure and temperature?. Some anomalous runs (see below) were rejected and these three criteria are generally satisfied by the analytical data, suggesting that equilibrium was approached. Some key factors are summarized below:

(1) Standard deviations values of olivine compositions within a single run are typically less than ~1 Fo unit (Appendix 5.1). In hydrous run T-3975, ~40°C below the liquidus, 8 olivine analyses have a standard deviation of ~2.8 Fo units, but the average Fo content is consistent with increasing Fo-temperature trends (Figure 5.8c).

When clinopyroxene it is the only liquidus phase under CO_2-MH-buffered conditions (Runs T-4149, T-4157, T-4158 and T-4159), its Wo content varies between ~30 to ~42 (Figure 5.14, Section 5.6.3). However, the Wo content of the most primary clinopyroxene compositions consistently decreases with pressure at constant $Mg^{\#}$ (Figure 5.15, Section 5.6.2). In all other runs , the compositions of primary clinopyroxenes show no marked variations (Figure 5.14).

Glass analyses within particular runs have uniform compositions, with standard deviations in $Mg^{\#}$ values typically <1%, (Appendix 5.7). The overlap of the electron microprobe beam with the inclusions in highly poikilitic garnets was unavoidable. Consequently, variations in the composition of garnet analyses within runs are relatively large (Appendix 5.4).

(2) Core and rim analyses of sufficiently large olivine crystals from runs T-3955, T-4007, T-4062 and T-4063 indicate no evidence of chemical zoning (Appendix 5.8). Analyses of clinopyroxene crystals from run T-4159 show pronounced Wo zoning with bimodal rim compositions and intermediate cores, but all have similar $Mg^{\#}$ values (Figure 5.17) possibly as the result of metastability (Section 5.6.3).

(3) Chemical variations of primary mineral phases were described in Section 5.6 and reflect, within analytical uncertainties, responses to variations in pressure and temperature. However, four of the runs likely to be removed from equilibrium are listed below.

T-3898: The highest Mg# value encountered among clinopyroxene analyses in this run is lower than that of lower temperature runs (Figure 5.11a), and the much lower Wo content than that defined by the Wo-Pressure trend of other anhydrous runs, is contrary to general trends (Figure 5.15). This is attributed to overlap of the electron beam with the surrounding matrix material, as primary euhedral

clinopyroxene crystals in this and other runs are small, and typically enveloped by a rim of quench overgrowth.

T-4020: Garnets in this run have a much lower Mg# values than those in run T-4119 at 10°C lower, as well as other runs at lower temperature (Figure 5.18c, Appendix 5.5). This run seems to have failed to attain equilibrium.

T-4021: Analyses of residual glasses in this run are anomalously low in FeO* content (~4.5 wt%) compared to those from other runs at similar conditions (~7 wt%, Figure 5.1). This run is therefore considered to be affected by iron loss to the platinum capsule and thus removed from equilibrium. T-4063: Olivine compositions (~$Fo_{91.5}$) in this run are anomalously higher than the Fo-temperature trend defined by the other runs (Figure 5.8c). Also, glass analyses in these runs have considerably low FeO* contents (~1.5 wt%, Figure 5.1). This run is therefore also considered to be affected by iron loss to the platinum capsule and thus removed from equilibrium.

In summary, although the phase relations in Figures 5.3 to 5.6 are internally consistent, complete chemical equilibrium can not be demonstrated. The phase diagrams can therefore be best regarded as an approach to equilibrium, and as records of the results of synthesis experiments in which changes in mineral chemistry are consistent with pressure and temperature variations. Equilibrium may not have been achieved in runs T-3898, T-4020, T-4021 and T-4063, and these results are indicated by "?" in the phase diagrams.

5.8 Reconnaissance solubility measurements of CO_2 in glasses

Reconnaissance solubility measurements were made to confirm the presence of a H_2O-free, CO_2-rich volatile phase in the MH-buffered runs. These results are described in Section 5.2.7 and were not planned as a detailed solubility study. Nevertheless, some broad interpretations can be made in this section regarding the amount of CO_2 dissolved in the liquid of ANK2376.

Typically, the CO_2 contents of near-liquidus glasses (Table 5.2) follow established solubility trends, with positive pressure but negative temperature dependence (Mattey *et al.* 1990, Thibault & Holloway 1994, Blank & Brooker 1994 and Holloway & Blank 1994). Despite 2 to 4 wt% H_2O being dissolved in the glasses of unbuffered experiments (Figure 5.19a), their CO_2 content does not differ markedly from the CO_2 content of near anhydrous (<0.8 wt% H_2O) glasses produced under MH-buffered conditions. CO_2 measurements from both furnace- and MH-buffered experiments are therefore combined and tested as a group.

Pressure dependence of CO_2 solubility at constant temperature is illustrated with isotherms at 1280°C and 1330°C in Figure 5.19b (lines I and II, respectively), and are sub-parallel to trends established for natural melts of olivine leucitite, and basanite compositions from Blank & Brooker (1994) (lines 2 and 3, Figure 5.2b). The temperature independence at constant pressure of CO_2 in ANK2376, is well constrained at 1.0 and 2.0 GPa, but less precisely at 1.5 GPa (Figure 5.19c).

In summary, the CO_2 content dissolved in ANK2376 near the liquidus is a function of pressure and temperature and is not coupled with the H_2O formed in the runs as a result of H_2 migration into the capsule. From Figure 5.19c, and using liquidus temperatures from Figures 5.5 and 5.6, the

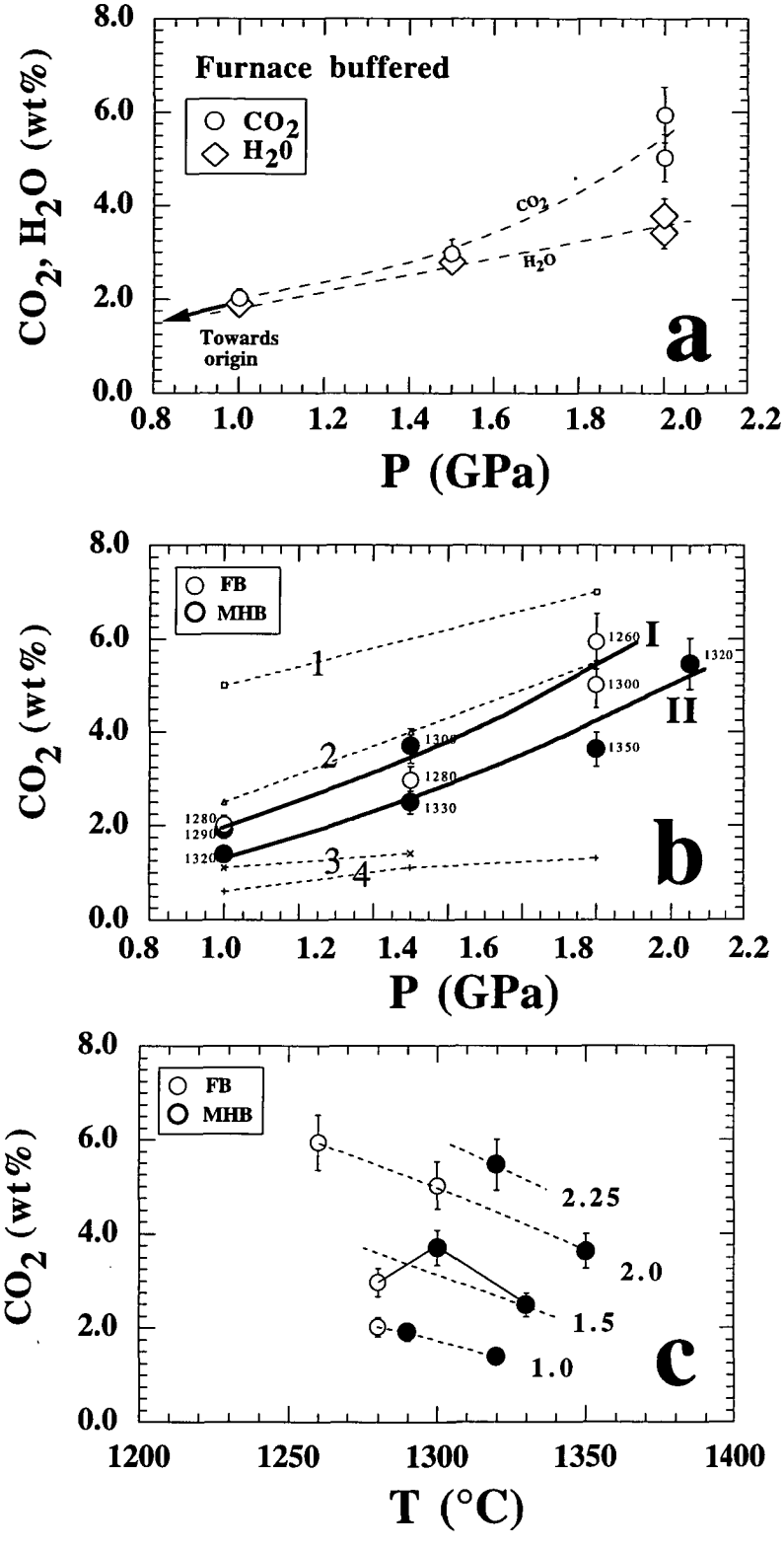

Figure 5.19 CO_2 and H_2O solubilities (measured as total C and H, Section 5.2.5) in near liquidus glasses of ANK2376, under furnace buffered (open symbols) and MH buffered (filled symbols) conditions. Error bars in all diagrams represent ±10% of measured value. Analyses are listed in Table 5.2.

a) Increase in CO_2 and H_2O solubility in unbuffered experiments as a function of pressure. Dashed lines indicate approximate contour at ~1280°C.

b) Increase in solubility of CO_2 in ANK2376 with pressure. Numbers next to symbols indicate run temperature in °C. Full lines I and II are approximate contours at 1280°C and 1330°C respectively. Dashed lines show the influence of pressure at ~1400°C on CO_2 solubility for a range of silicate melts, 1: Sodamelilite, 2: Ol-leucitite, 3: Basanite, 4: Basalt (Blank & Brooker 1994).

c) Decreasing solubility of CO_2 with temperature.

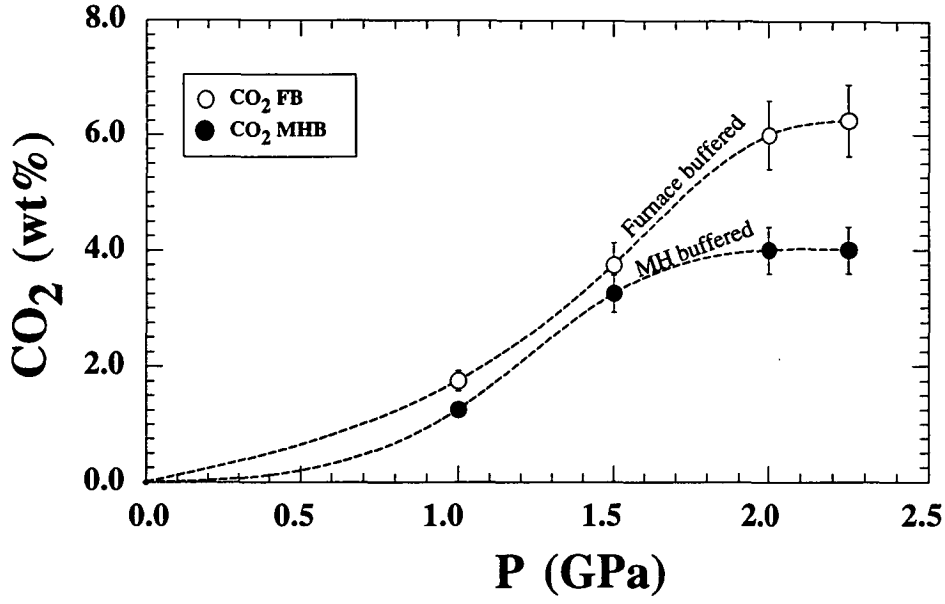

P (GPa)	Furnace buffered ~T_L (°C)	~CO_2 wt%	MH buffered ~T_L (°C)	~CO_2 wt%
1.00	1300	1.75	1295	3.25
1.50	1270	3.75	1340	4.00
2.00	1255	6.00	1400	4.00
2.25	1300	6.25	1340	1.25

Figure 5.20 Approximate CO_2 content dissolved in ANK2376 near the liquidus under furnace buffered (FB) and magnetite-haematite (MH) buffered conditions. Liquidus temperatures (T_L) are estimated from phase diagrams in Figures 5.5 and 5.6 (see table above), and the corresponding CO_2 contents at these temperatures are transferred from trends of Figure 5.19c. Estimated values are listed in the table above. Error bars are ±10%.

approximate CO_2 content at the liquidus under furnace and MH-buffered conditions can be estimated. These are plotted against pressure in Figure 5.20, where the solubility of CO_2 particularly at high pressures (>2.0 GPa), is higher under furnace-buffered conditions (~6 wt% CO_2) than under MH-buffered conditions (~4 wt% CO_2). This reflects the higher liquidus temperatures under MH-buffered conditions as a result of lower H_2O contents. The appearance of garnet on the liquidus of furnace-buffered experiments, compared to its absence under MH-buffered conditions, may reflect higher contents of CO_2 dissolved in the melt.

5.9 Deductions from experimental data

Work in this chapter was designed to complement and test one of the models proposed in Chapter 4 for the formation of ankaramitic magmas. In this model (described in Chapter 4), primitive melts, similar in composition to those trapped in melt inclusions, rise through, collect and continue to crystallize in the sub-arc mantle while re-equilibrating with the surrounding peridotite rock by melt-rock reactions. During this reaction, the magma becomes increasingly less silica-undersaturated and attains the silica richness observed in the natural rock samples of ankaramite. According to this model, the primitive chemical characteristics of the parent melts are lost, except for those preserved in melt inclusions of early formed phenocrysts. This experimental study was therefore aimed to test if the melt inclusions were indeed primary melts unmodified from their magma source, or instead whether they represent a derivative liquid. The experimental results are now assessed in view of this.

5.9.1 ANK2376 not a primary melt?

By definition, if primary arc melts such as ANK2376 are generated in the mantle wedge, their potential source rock is likely to be peridotite and the residual mineral assemblage with which ANK2376 are supposed to be in equilibrium contains olivine+orthopyroxene±clinopyroxene. It therefore follows that if a basaltic melt has this assemblage on the liquidus, then it becomes a possible candidate as a primary melt of mantle peridotite (Bultitude & Green 1971). When the experimental results are examined this way, the absence of orthopyroxene in the crystallization interval of ANK2376 (Section 5.5) precludes any model that involves the generation of this melt by direct partial melting of a peridotite source. More significant, the absence of olivine on the liquidus above ~1.5 GPa in CO_2-bearing experiments, discard the role of CO_2 in the generation of ANK2376 as a primary melt at high pressures, unless considerable olivine fractionation occurred.

5.9.2 ANK2376 as a fractionated but primitive (parent) melt

Although not primary, the composition of melt inclusions represented by ANK2376 may represent a primitive parental melt to the ankaramite rock suites. If a decline in the CaO content of olivine phenocrysts with decreasing Fo is interpreted to indicate the onset of clinopyroxene crystallization, then the mineral data obtained from UTas48001 indicates that clinopyroxene joined olivine at around Fo_{89-90} (Section 2.5). Thus ANK2376, trapped in Fo_{91}, could well represent a primitive melt derived from even more mafic liquids undergoing fractionation of

olivine+spinel±clinopyroxene on the way to the surface. This process would correspond to Stage 2 of the model illustrated by Figure 4.12 in Chapter 3.

5.9.3 Depth of magma aggregation

Recalling that CaO/Al_2O_3 values of melt inclusions in early formed phenocrysts vary between grains, but are consistently similar within them, it was suggested in Section 3.7 that the aggregation of magma must have occurred well after trapping of these primitive inclusions (Stage 3 of Figure 3.12). During aggregation of the magma, olivine (~Fo_{74-92}) and clinopyroxene ($Mg^{\#}$ ~80-93) were crystallizing phases until the moment of eruption (Section 3.8); thus a possible depth of aggregation can be estimated from the liquidus phase relationships of ANK2376.

The primitive phenocryst assemblage of UTas48001 (cpx>>ol) is duplicated on the liquidus of ANK2376 under dry, hydrous and CO_2-bearing conditions at pressures of around ~2.0, ~2.3, and ~1.5 GPa and temperatures of around 1400, 1070 and 1290 °C, respectively (Figure 5.7). Under CO_2 MH-buffered conditions, the synthesized clinopyroxenes show a decrease in Wo content with pressure (Figure 5.15), and at around the pressures corresponding to the olivine-clinopyroxene liquidus (~1.5 GPa), they attain compositions of ~$Wo_{40}En_{52}Fs_8$. These are unlike those observed in the natural sample that are much more calcic (~$Wo_{47}En_{47}Fs_8$) and similar to those formed in hydrous experiments (Figure 5.14). Compositional matching and trends with P, T and CO_2-H_2O contents are thus consistent with the aggregation of the magma aliquots (now represented by UTas48001) at hydrous conditions in the pressure range of around 2.2 GPa, equivalent to depths of about 60 Km, or lower pressures if CO_2 is present. The thickness of arc crust in the Lombok sector is estimated to 25 Km or less, and the Benioff subduction related seismic zone is approximately less than 200 Km below the surface (Foden 1979, p18). Magma aggregation and formation of the ankaramitic magma is likely to have occurred at sub-arc mantle depths. This agrees with the lack of crustal material in the melt.

5.10 Conclusion & further experiments

The experiments in this chapter aimed to find a link between the primitive composition of melt inclusions in olivine (ANK2376) and the composition of primary melts, by partial melting of mantle peridotite in the presence of CO_2 rich fluids. Instead the results indicate that the composition ANK2376 cannot represent a primary melt under either dry, hydrous or CO_2-bearing conditions up to pressures of about ~3 GPa. Nevertheless, experimental duplication of the natural phenocryst assemblage of ankaramite (UTas48001) suggests that its parent magma aggregated, and continued to crystallize at pressures of around ~2.2 GPa under hydrous conditions, or lower if some CO_2 were also present in the fluid phase. If olivine and clinopyroxenes are liquidus phases in the magma, then prolonged crystallization at these pressures would lead to the formation of olivine-clinopyroxene crystal-rich rocks, with phenocrysts of wide compositional range, as is typical of the ankaramites rocks described here. This process can be reconciled with the aggregation stage (Stage 3) of the model presented in Chapter 3 (Figure 3.12).

ANK2376 may therefore be representative of melts parental to the ankaramites but derived from more mafic precursors that rose, aggregated and continue to crystallize in the sub-arc mantle. This process is also open to the possibility that some olivine fractionation may have taken place in the primary melts during ascent, as a result of expansion of the olivine stability field (Section 3.7). Olivine addition experiments could then be useful, as olivine stability would be enhanced and extended to higher pressures under CO_2 bearing conditions. It would also be advantageous to explore the crystallization interval of ANK2376 at conditions of moderately high H_2O/CO_2 ratios, at around 2.5-3.0 GPa, to intersect a region defined in Figure 5.7 where olivine+clinopyroxene+garnet coexist. Under these conditions, olivine stability will not be significantly reduced and would coexist with garnet in the presence of small amounts of CO_2.

Chapter 6: The formation of aluminous spinels in melt inclusions

6.1 Introduction

Aluminous green spinel (Al-spl) belonging to the $Mg(Fe^{3+}Al)_2O_4$ - $Fe(AlFe^{3+})_2O_4$ pleonaste series with $Cr^{\#}<5$ and Al_2O_3 contents >50 wt% are common in peridotites and some metamorphic rocks, but are rare in primitive volcanic rocks, in which chromian spinels with $Cr^{\#}>70$ and Al_2O_3 <13 wt% are common (Roedder & Weiblen 1972). Nonetheless, Al-spl phenocrysts are reported in basaltic lavas from Guadalupe Island, Lesser Antilles arc (Bissainte *et al.* 1993) and in high alumina basalts from Akutan Island, Aleutian arc (Romick *et al.* 1990).

Al-spl may also occur as solid inclusions in phenocrysts (Arculus 1978, Romick *et al.* 1990, Green 1992, Bissainte *et al.* 1993, Nono *et al.* 1994) and as daughter crystals in melt inclusions (Frezzotti *et al.* 1991). Accordingly, Della-Pasqua *et al.* (1995) recognized two petrographic types of Al-spl: Type-1, in which Al-spl occurs as solid inclusions in phenocrysts ($Al\text{-}spl_s$), and Type-2, in which Al-spl occurs as daughter crystals in primary melt inclusions ($Al\text{-}spl_d$). Compositionally, both Al-spl types are similar and both may coexist with chromian spinel inclusions in the same phenocryst. Della-Pasqua *et al.* (1995), therefore, considered a possible origin for Al-spl involving the contamination of basaltic magma chambers by localized aluminous melt pockets from which the Al-spl crystallized. Two possible mechanisms were suggested for formation of the aluminous melt, (1) complete breakdown of assimilated lower crustal gabbroic rocks and (2) incongruent breakdown of amphibole in amphibole-rich cumulates to produce a melt with ~20-22% of Al_2O_3, aluminous clinopyroxene, Al-spl and olivine. Della-Pasqua *et al.* (1995) envisaged that Al-spl and aluminous melt produced by these mechanisms may be incorporated into the host basaltic magma and subsequently trapped, together with the coexisting chromian spinels, by the crystallizing olivine and clinopyroxene phenocrysts.

In this chapter, it is shown that Type-1 Al-spl may be "remnants" of $Al\text{-}spl_d$ crystals in melt inclusions (Type-2), accidentally exposed on the surface of the host grain during polishing. The review and conclusions presented in Della Pasqua *et al.* (1995) (Appendix 6.1) represent an earlier stage of this investigation and will not be reiterated. This chapter describes an additional mechanism for the formation of Al-spl in melt inclusions. The possible involvement of this mechanism arose from a written communication by Peter L. Roeder (15th August 1995) and is tested using results from melt inclusion heating experiments (Chapter 3) as

well as results from the high pressure phase relationships of melt inclusion compositions (Chapter 5).

6.2 Sample selection and preparation

While studying the primary melt inclusions in olivine and clinopyroxene phenocrysts from primitive ankaramites, Al-spl inclusions were also found. Full details of sample descriptions and preparation techniques were given in Chapter 2. Briefly, primitive samples from each ankaramite suite were crushed, sieved, and their phenocrysts (olivine and clinopyroxene) were hand-picked from size fractions 0.3-0.5 mm. The grains were mounted in epoxy, sectioned and polished to expose their magmatic inclusions. Both, the inclusions and host were then analysed by microprobe.

6.3 Melt inclusions with Al-spl$_d$ (Type-2)

Primary melt inclusions in olivine and clinopyroxene phenocrysts vary from glassy to crystalline, range in size up to a few hundred μm, and may contain accidentally trapped crystals of chromian spinel (Chapter 2). Rarely, melt inclusions hosted by olivine contain a distinct daughter crystal of green Al-spl (Al-spl$_d$), together with pale-green daughter clinopyroxene crystals (cpx$_d$), interstitial glass (L), a shrinkage bubble (V) and daughter olivine (Ol$_d$) on the walls (Figure 6.1a-f). Volumetrically, cpx$_d$ and L are the dominant phases in these melt inclusions, whereas Al-spl$_d$ is minor and ol$_d$ forms a rim on the walls (Figure 6.1a-b and d). Only one clinopyroxene phenocryst was found to contain a melt inclusion with an Al-spl$_d$ crystal, residual glass, and presumably cpx$_d$ that crystallized on the walls. In combined inclusions where chromian spinel, is accidentally trapped with melt (L+S), Al-spl$_d$ has nucleated and overgrown the chromian spinel to form a rim. This relationship demonstrates that this Al-spl$_d$ crystallized after trapping and that therefore some or all, may not be of xenocrystic origin (Della-Pasqua *et al.* 1995, their Figure 1).

A previous estimate of the (melt inclusion size)/(Al-spl$_d$ size) ratio ($R_{mi/spl}$), indicates that the volume proportion of Al-spl$_d$ varies approximately from 1 to 5 % (Della-Pasqua *et al.* 1995). However, additional measurements (Appendix 6.2) indicate that the value of $R_{mi/spl}$ averages ~5 (Figure 6.2) which consequently implies that Al-spl$_d$ occupies approximately ~0.8 vol% of the inclusion[1]. In this estimate, the sizes were measured from photographed melt inclusions assuming spherical forms for both the daughter crystals and inclusions, as described in Appendix 6.2. These measurements, however, exclude the volume of ol$_d$ crystallized on the inclusion walls and therefore represent an overestimation of the Al-spl$_d$ volume. The results imply that Al-spl$_d$, with up to 65 wt% Al_2O_3, contains less than ~0.5 wt% of the Al_2O_3 originally present in the trapped melt.

---

[1] $V_{sphere} = 4\pi r^3$ and therefore proportional to r^3. Thus $V_{mi}/V_{spl} = (R_{mi/spl})^3 = \sim 5^3 = 125$, i.e., V_{spl}= ~0.8 vol% of the melt incluSion.

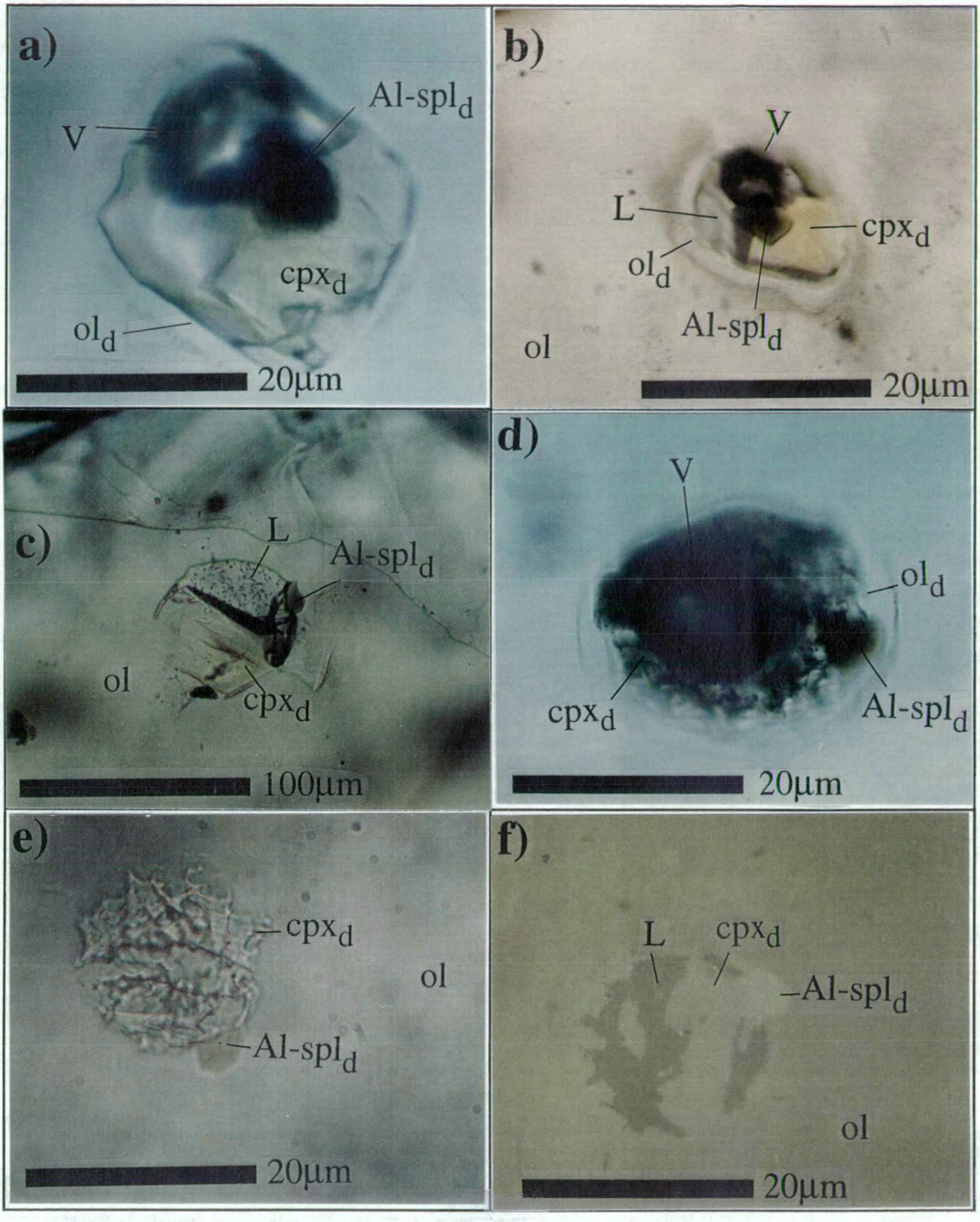

Figure 6.1 Melt inclusions in olivine phenocrysts (ol) having daughter-phase assemblages that contain Al-spl$_d$ + cpx$_d$ + ol$_d$ + L from a-d) Merelava sample 31551 and e-f) Ulakan sample UTas67424.

a) PPL, 100x. b-c) PPL, 20x. d) PPL, 100x. e) PPL, 100x. f) same inclusion as in e) but under reflected light (RL). Note cpx$_d$ forms a discrete single crystal in a-c, whereas in d-f cpx$_d$ form fine-grained aggregates.

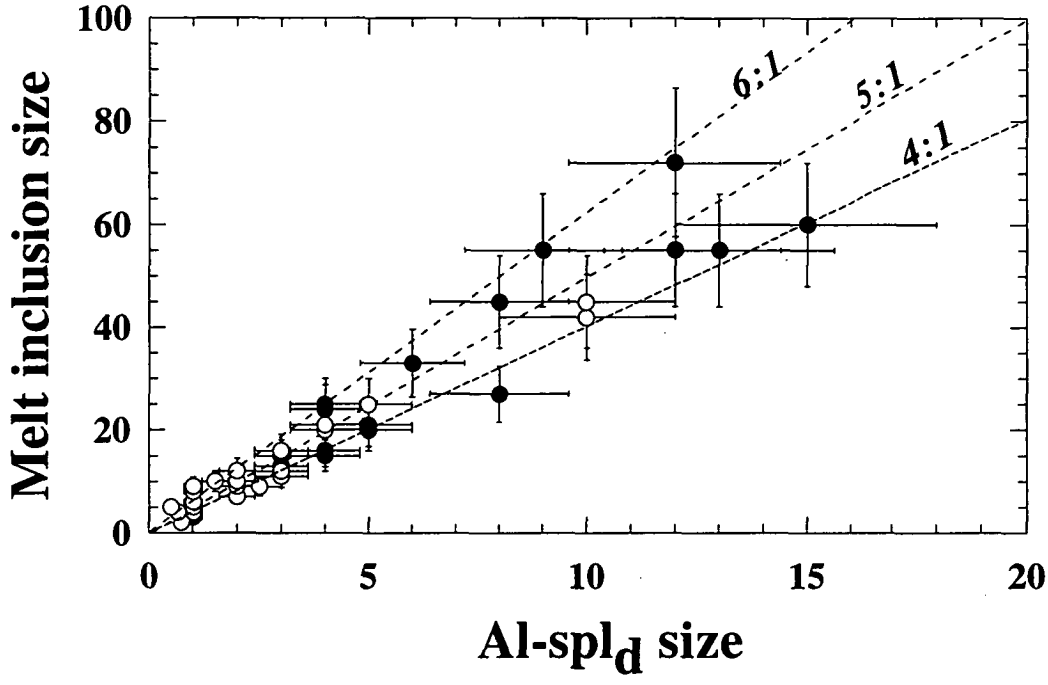

Figure 6.2 Relative sizes (arbitrary units) of melt inclusions *versus* size of their Al-spl$_d$ daughter crystals. Slope of ~5 indicates a inclusion/spinel volume ratio of ~125, thus suggesting that Al-spl$_d$ occupies aproximately <0.8% volume. Open symbols are data from Della-Pasqua *et al.* (1995), filled symbols are additional sizes measured from photographs (Appendix 6.2). Error bars are ±20%.

Textural relations of daughter phases in melt inclusions suggest that Al-spl_d began to grow shortly after olivine started to crystallize on the wall. This relationship is illustrated in Figure 6.1c-f where Al-spl_d crystals are embedded within ol_d rims on the walls of the melt inclusion. Olivine, therefore, continued to crystallize on the walls with Al-spl_d, and thus partially envelop it. Comparatively, cpx_d crystals are not embedded within olivine, but themselves enclose Al-spl_d (Figure 6.1a-b, d). Thus the crystallization sequence of daughter phases in olivine can be tentatively postulated as:

$ol_d \rightarrow ol_d \pm$Al-$spl_d \rightarrow cpx_d \pm$Al-spl $\rightarrow cpx_d$+L ...(Figure 6.3).

6.4 Composition of Al-spl_d and coexisting daughter phases

Daughter phases within melt inclusions range up to 10 μm in size and, due to their small sizes, reported compositions are modified by beam overlap with surrounding material during analysis. Interstitial glass (gl) was analysed with a small beam size (~1-3 μm), which generated high oxide totals and likely affected the concentration of Na and K (cf. Section 3.3.3). The compositions of daughter phases hosted by clinopyroxene and olivine phenocrysts are listed in Table 6.1 and Table 6.2, respectively, and are discussed below.

TABLE 6.1

	gl	cpx_h	Al-spl_d
SiO_2	61.38	52.47	0.10
TiO_2	0.68	0.25	0.18
Al_2O_3	16.45	2.36	48.70
Cr_2O_3	0.01	0.78	3.71
Fe_2O_3(1)		0.23	17.89
FeO	2.39	4.80	10.43
MgO	3.00	16.08	18.78
CaO	6.39	22.29	n/a
MnO	0.00	0.03	0.46
Na_2O	3.87	0.20	n/a
K_2O	3.80	n/a	n/a
P_2O_5	0.21	n/a	n/a
NiO	n/a	n/a	0.17
ZnO	n/a	n/a	0.19
TOTAL	98.18	99.49	100.61
mg#	69.1	85.7	76.3
Mg#		85.2	55.8
Cr#			4.9

Analysis of a Al-spl_d crystal and residual glass (gl) in a melt inclusion hosted in a clinopyroxene phenocryst (cpx_h) from ankaramite sample UTas67424. (1) indicate calculated Fe_2O_3 assuming perfect stochiometry. n/a= not analysed.

6.4.1 Daughter Al-spl crystals in melt inclusions (Al-spl_d)

Compositional variations of spinel solid inclusions in olivine phenocrysts from all four ankaramite suites are described in chapter 2. In the suites from Epi and Ulakan, the spinel solid inclusions were subdivided into aluminous Type-1 spinels (Al-spl_s) with Cr# <5, and chromian spinels with Cr# typically >50 (Cr-spl_s) (Della-Pasqua *et al.* 1995). These two spinel

TABLE 6.2

Location	Epi											Ulakan Fm.	Merelava				
Host rock	Utas71046											UTas67424	31551				
Grain/Inclusion	E122/1	E90/1	E90/2	E65/1	E35/1	E35/2	E33993	E108/1	E159/1	E159/2	E156/1	B77/1	M3/1	M3/2	M4/1	M4/2	M4/3
Set no.	1	2	3	4	5	6	7	8	9	10	11	12	13	14	15	16	17
												(heated)					
Host Olivine																	
Fo	82.7	83.7	83.7	84.4	76.6	85.7	85.7	85.1	84.2	84.7	84.2	89.1	86.9	86.9	84.0	83.5	82.2
Daughter aluminous spinel (Al-spl$_d$)																	
SiO_2	0.16	0.13	0.05	0.01	0.13	0.15	*small*	0.18	0.18	*small*	0.10	0.20	*small*	*small*	*small*	*small*	*small*
TiO_2	0.18	0.10	0.51	0.19	1.22	0.24		0.13	0.20		0.22	0.09					
Al_2O_3	57.75	60.86	49.01	60.59	51.22	58.86		62.78	61.05		56.51	67.44					
Cr_2O_3	1.94	0.06	1.31	0.42	0.52	0.07		0.16	0.36		0.35	0.12					
MgO	17.61	19.15	15.64	18.34	12.45	18.40		18.21	17.73		16.06	20.87					
MnO	0.14	0.14	0.13	0.12	0.12	0.08		0.11	0.12		0.12	0.08					
Fe_2O_3	8.43	7.31	17.84	7.42	11.87	6.85		2.37	6.52		9.83	-					
FeO	14.27	11.93	15.82	13.48	21.59	12.32		13.31	14.89		15.99	9.61					
NiO	0.15	0.20	0.21	0.21	0.09	0.17		0.12	0.22		0.16	0.16					
ZnO	0.19	0.35	0.22	0.14	0.24	0.04		0.08	0.10		0.19	0.26					
TOTAL	100.80	100.23	100.75	100.93	99.46	97.18		97.44	101.37		99.53	98.81					
mg#	68.7	74.1	63.8	70.8	50.7	72.7		70.9	68.0		64.2	79.5					
Cr#	2.2	0.1	1.8	0.5	0.7	0.1		0.2	0.4		0.4	0.1					
Fe^{2+}/Fe^{3+}	1.88	1.81	0.99	2.02	2.02	2.00		6.25	2.54		1.81	0.00					
$Fe^{2+}/(Fe^{2+}+Fe^{3+})$	0.65	0.64	0.50	0.67	0.67	0.67		0.86	0.72		0.64	1.00					
Daughter clinopyroxene (cpx$_d$)																	
SiO_2	41.21	41.67	41.74	46.40	42.71	45.28	44.78	42.70	45.86	44.11	*small*	53.21	51.57	39.22	52.96	*small*	*small*
TiO_2	1.66	1.04	0.79	0.68	2.92	0.58	0.61	0.76	0.91	0.53		0.45	0.37	1.78	0.18		
Al_2O_3	14.91	13.35	14.50	10.23	12.21	8.68	9.72	12.65	20.11	9.79		1.78	5.84	13.46	5.10		
Cr_2O_3	n.d.	0.03	0.02	n.d.	0.04	0.06	0.12	n.d.	0.01	n.d.		0.46	0.37	0.04	0.34		
FeO*	9.39	10.79	9.46	9.31	9.18	8.20	9.39	10.84	7.50	10.07		3.49	9.73	11.86	5.38		
MgO	10.14	10.35	10.11	13.09	10.93	13.29	12.24	10.83	6.67	12.28		17.95	15.78	11.68	14.74		
CaO	21.90	21.88	22.98	21.87	21.13	23.38	21.45	22.54	18.71	21.26		22.65	19.58	20.73	20.23		
MnO	0.13	0.05	0.03	0.14	0.19	0.15	0.20	0.08	0.11	0.09		0.15	0.10	0.07	0.13		
Na_2O	0.32	0.32	0.28	0.23	0.54	0.16	0.24	0.24	0.97	0.18		0.16	0.33	0.35	0.76		
TOTAL	99.68	100.37	100.78	102.58	100.35	100.68	99.40	101.59	100.85	99.08		100.45	103.95	99.95	99.81		
Mg#	65.9	63.1	65.6	71.5	68.0	74.3	70.0	64.1	61.4	68.5		90.2	74.3	63.7	83.0		
%Ca (Wo)	50.55	48.96	51.73	46.19	48.57	48.44	46.83	48.93	55.29	46.02		45.00	39.86	44.84	45.03		
%Mg (En)	32.55	32.20	31.65	38.46	34.95	38.30	37.17	32.70	27.41	36.96		49.60	44.68	35.14	45.63		
%Fe (Fs)	16.91	18.84	16.62	15.35	16.47	13.27	16.00	18.37	17.30	17.02		5.41	15.46	20.03	9.35		
FeO	3.01	2.76	1.81	3.55	4.47	0.15	3.51	2.37	7.50	3.16		2.12	7.16	0.00	5.38		
Fe_2O_3	7.09	8.92	8.50	6.41	5.24	8.95	6.53	9.42	0.00	7.68		1.52	2.85	13.18	0.00		
$Fe^{3+}/(Fe^{2+}+Fe^{3+})$	0.68	0.74	0.81	0.62	0.51	0.98	0.63	0.78	0.00	0.69		0.39	0.26	1.00	0.00		
mg#	85.8	87.0	90.9	86.8	81.4	99.4	86.2	89.1	61.4	87.4		93.8	79.7	63.7	83.0		
Residual glass (gl)																	
SiO_2	61.64	65.12	*small*	62.51	64.22	66.61	64.73	62.96	54.28	*small*	*small*	49.72	*small*	57.40	65.41	51.18	53.58
TiO_2	0.59	0.24		0.39	0.71	0.43	0.45	0.46	0.49			1.00		0.28	0.26	0.81	0.97
Al_2O_3	19.62	25.60		24.98	23.59	24.56	24.38	22.01	21.97			10.18		26.29	23.82	22.42	22.14
Cr_2O_3	0.06	0.04		n.d.	n.d.	0.03	n.d.	0.12	n.d.			0.07		0.06	n.d.	n.d.	n.d.
MgO	3.28	2.45		0.72	0.38	0.33	0.25	1.63	3.43			12.35		0.91	0.68	0.95	0.77
CaO	6.16	1.01		3.92	2.69	2.36	1.91	4.71	10.58			19.43		1.08	3.63	16.32	15.32
MnO	n.d.	n.d.		n.d.	n.d.	n.d.	0.02	n.d.	n.d.			n.d.		0.04	n.d.	n.d.	n.d.
FeO	2.86	3.14		1.67	1.55	1.15	1.19	1.62	4.67			4.08		1.17	1.32	2.91	2.68
Na_2O	3.99	3.33		6.05	3.21	3.06	3.23	5.42	4.07			1.59		12.96	5.64	3.38	3.47
K_2O	1.56	2.55		2.45	2.93	3.03	2.99	2.19	1.21			0.71		0.99	1.56	0.52	1.13
P_2O_5	0.38	0.34		0.44	0.48	0.49	0.58	0.40	0.33			0.51		0.87	0.26	0.49	0.43
TOTAL	100.14	103.82		103.12	99.76	102.05	99.73	101.52	101.07			99.63		102.04	102.58	98.97	100.49
Mg#	67.2	58.2		43.4	30.6	34.0	26.9	64.2	56.7			84.4		58.2	47.9	36.8	33.9
K_D	0.43	0.27		0.14	0.13	0.09	0.06	0.31	0.25			0.66		0.21	0.18		0.11
Na_2O/K_2O	2.56	1.30		2.47	1.10	1.01	1.08	2.47	3.37			2.23		13.13	3.61	6.47	3.07
TiO_2/P_2O_5	1.54	0.70		0.89	1.48	0.86	0.78	1.13	1.46			1.97		0.32	0.99	1.66	2.25

Composition of Al-spl$_d$ and associated daughter phases in melt inclusions within olivine phenocrysts from Epi, Ulakan and Merelava ankaramites. Observed phases which are not sufficiently large for microprobe analyses are indicated by "small". Sets number 2-3, 5-6, 9-10, 13-14 and 15-17 are analyses from coexisting melt inclusions in olivine grains E90, E35, E159, M3 and M4, respectively. Analysis in bold are from a partially homogenized melt inclusion (B77/1) quenched below the melting of the last cpx$_d$ crystal.

Mg#=100Mg/(Mg+Fe*), mg#=100Mg/(Mg+Fe^{2+}), Cr#=100Cr/(Cr+Al), K_D= $(Fe/Mg)_{host\ olivine}/(Fe^*/Mg)_{residual\ glass}$. n.d. = no detected.

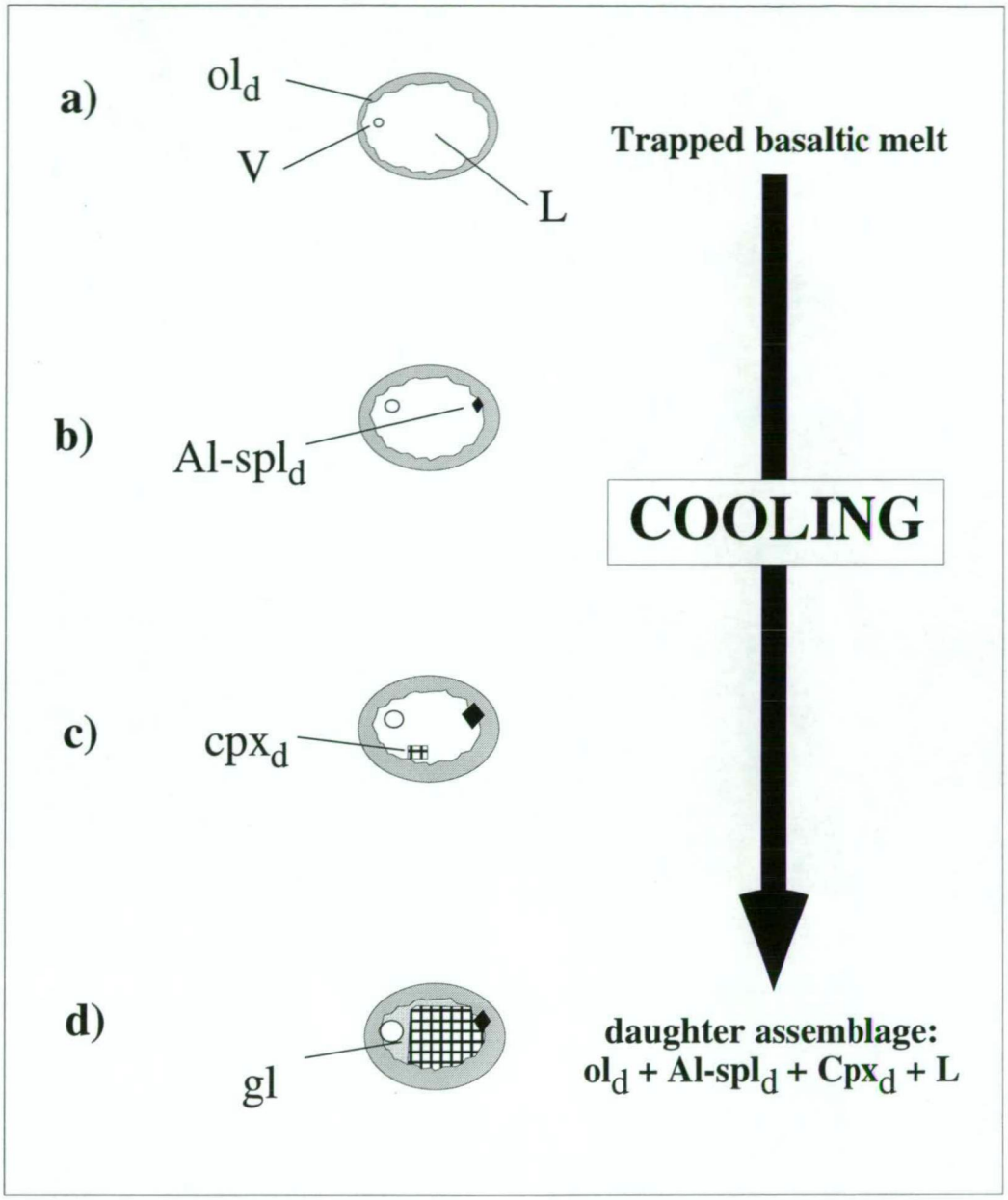

Figure 6.3 Proposed crystallization sequence of a melt inclusion trapped by an olivine phenocryst.

a) crystallization of olivine on the walls (ol_d) and nucleation of a shrinkage bubble (V),

b) continued growth of olivine on the wall and crystallization of Al-spl_d,

c) initiation of clinopyroxene crystallization (cpx_d),

d) continued growth of cpx_d followed by natural quenching of the residual liquid (L) to a glass (gl).

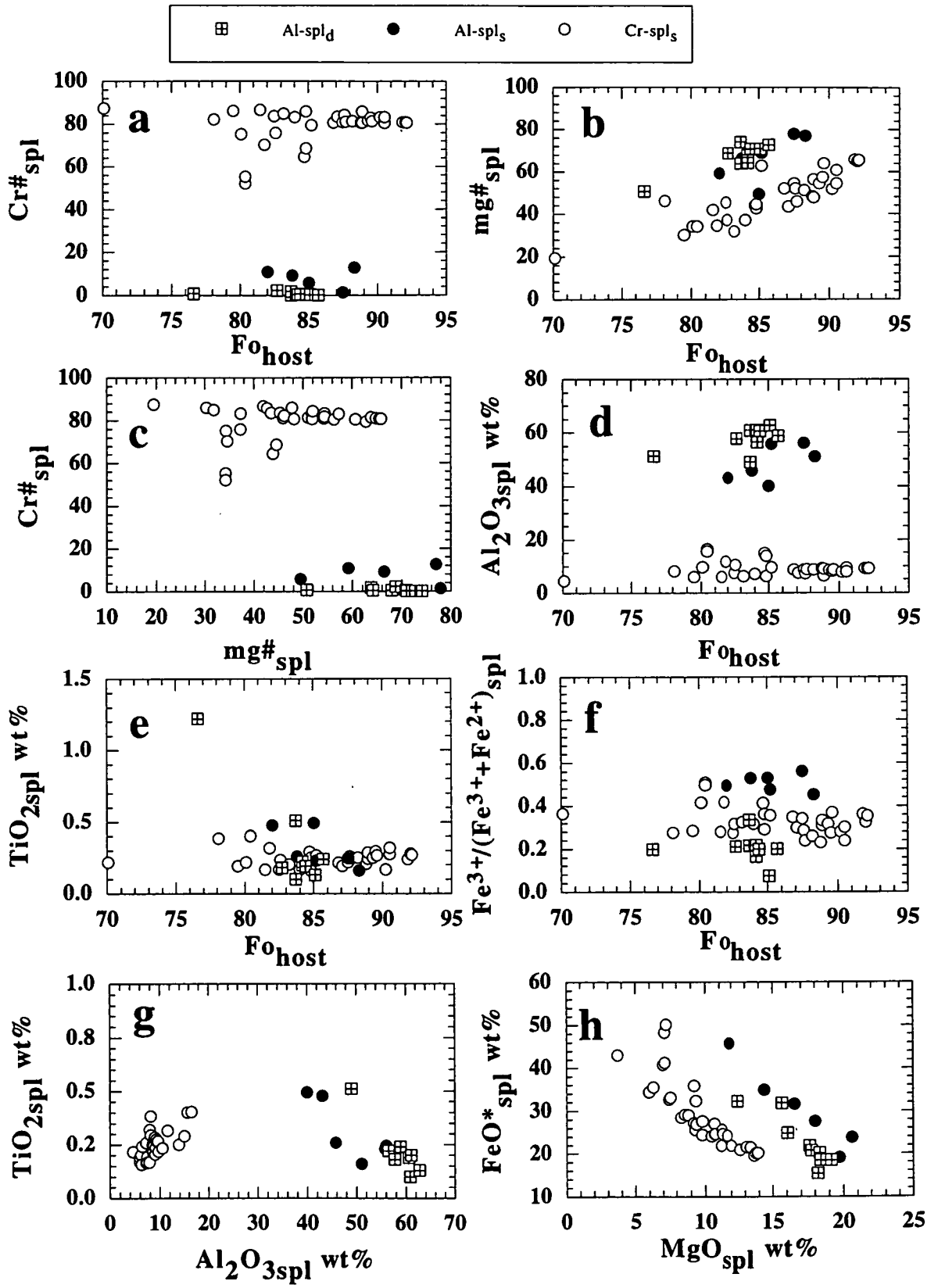

Figure 6.4 Composition of solid spinel inclusions in olivine phenocrysts from Epi ankaramites. Filled circles are spinels with Cr#<10 (Al-spl$_s$) and open circles are spinels with Cr#>50 (Cr-spl$_s$). The composition of Al-Spl$_d$ crystals in melt inclusion are shown as crossed squares for comparison.

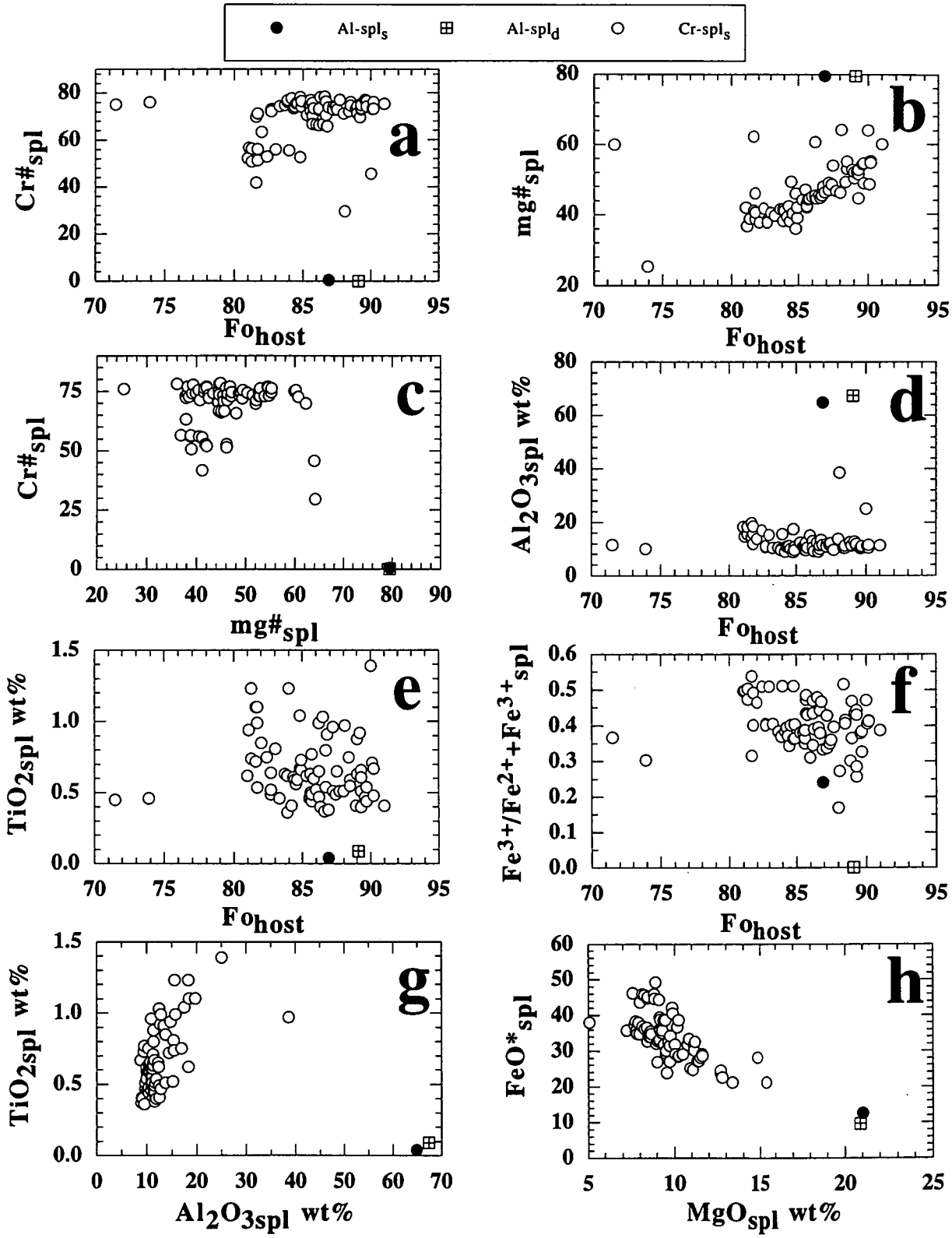

Figure 6.5 Composition of solid chromian spinels (Cr-spl$_s$) and solid Al-spl (Al-spl$_s$) inclusions in olivine phenocrysts from Ulakan ankaramite sample UTas67424. Crossed square indicates the composition of a daughter Al-spl crystal (Al-spl$_d$) in a melt inclusion hosted by olivine.

populations are plotted together with analyses of Al-spl_d crystals in Figures 6.4 and 6.5, and are represented within a spinel prism in Figure 6.6.

Figures 6.4 to 6.6 highlight the compositional similarity between Al-spl_s and Al-spl_d. Both spinel types have similar ranges in Cr# and $Fe^{3+}/(Fe^{2+}+Fe^{3+})$ values and similar MgO, FeO*, Al_2O_3 and TiO_2 contents. The olivine phenocrysts that host Al-spl_s and Al-spl_d inclusions have a similar range in fosterite and NiO contents, that are in turn, similar in composition to those that host chromian spinels. Therefore the textural distinction between Al-spl_s and Al-spl_d is not justified by their compositional variations which, suggest that the two spinel types may be genetically related

6.4.2 Daughter clinopyroxene crystals (cpx_d)

Crystals of cpx_d in melt inclusions have a wide range in composition with high Al_2O_3 (up to ~20 wt%), low SiO_2 (down to ~39 wt%) and lower $Mg^{\#}$ compared to the composition of clinopyroxene phenocrysts (Table 6.3, Figure 6.7a-c). These chemical features are typical of "quench" clinopyroxenes (Edgar *et al.* 1975) and suggest disequilibrium growth within the melt inclusion due to rapid closed system growth after trapping. Moreover, most cpx_d crystals have a much wider range in Ti and Al contents but similar Ti/Al values compared to the composition of clinopyroxene phenocrysts (Figure 6.7e). This feature reflects the incorporation of larger amounts of Al and Ti by cpx_d during rapid growth, enhanced by the absence of plagioclase and ilmenite nucleation within the inclusion (Walker *et al.* 1976). In particular, the lack of plagioclase nucleation within the melt inclusion has a significant role in the formation of Al-spl_d as discussed later. Recalculated cpx_d analyses have variable Fe_2O_3 contents with $Fe^{3+}/(Fe^{3+}+Fe^{2+})$ values ranging from 0 to 1 (Table 6.2) and the cpx_d $mg^{\#}$ values are closer to equilibrium with the host olivine than their corresponding Mg# values (Figure 6.7d).

6.4.3 Residual glasses (gl)

The interstitial glasses in melt inclusions are residual after the fractional crystallization of ol_d, Al-spl_d and cpx_d. These glasses typically have high SiO_2 (to ~65 wt%), Al_2O_3 (to ~26 wt%), Na_2O (to ~6 wt%) and K_2O (to ~3 wt%) contents, with low FeO (to ~4 wt%) and MgO (to ~3 wt%) contents (Table 6.2). One residual glass analysis from Merelava has ~13 wt% Na_2O, ~26 wt% Al_2O_3 and ~57 wt% SiO_2, and resembles the composition of albite (Table 6.2, Set 14).

6.5 Results from melt inclusion heating experiments

This section describes the composition of homogenized melt inclusion glasses that contain Al-spl_d crystals (Figure 6.8c). These melt inclusions will be referred to as Type-B throughout the text to distinguish them from homogenized melt inclusions that do not contain Al-spl_d (Type-A, Figure 6.8d). Type-A melt inclusions are considered parental to the

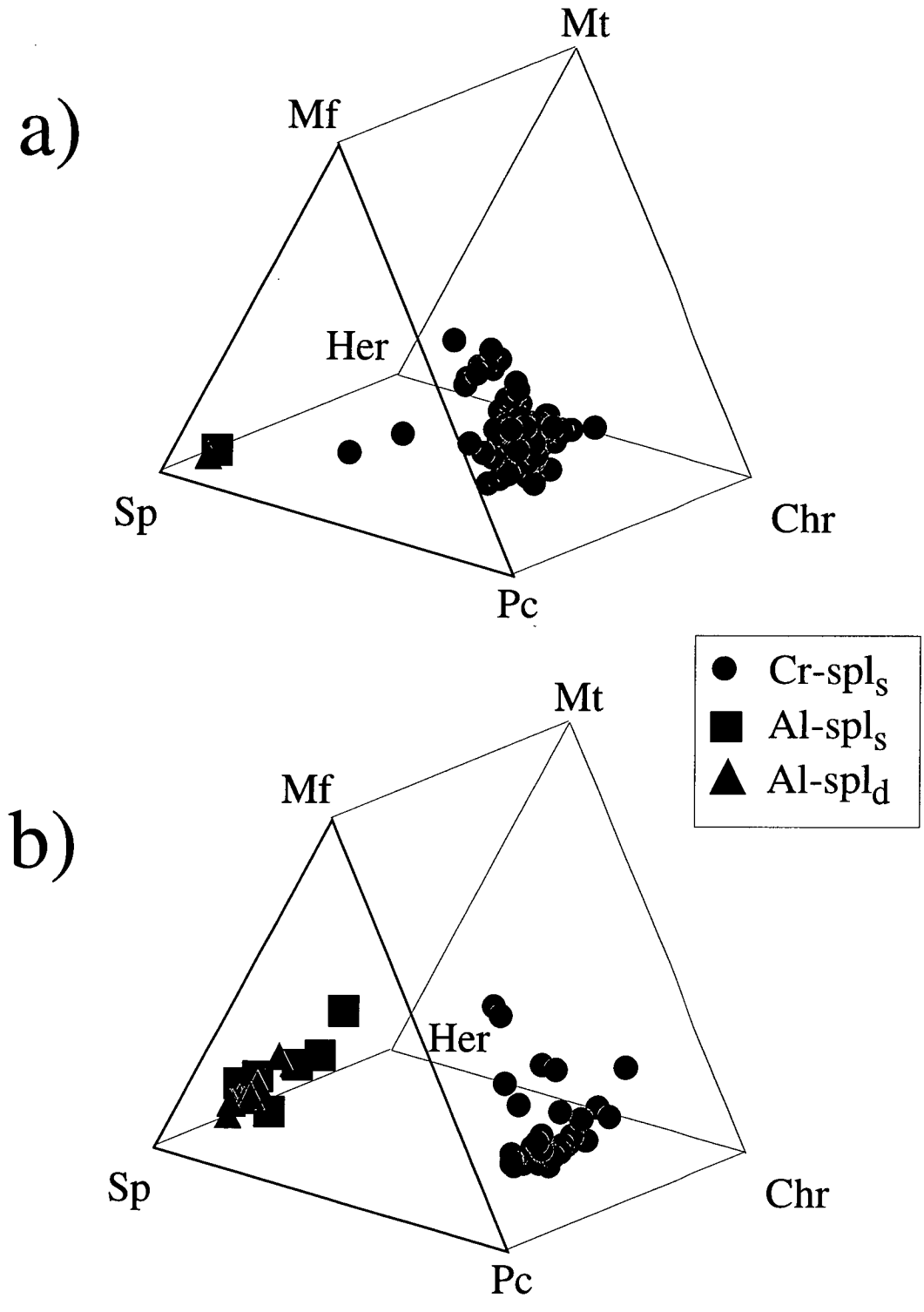

Figure 6.6 Composition of spinel inclusions hosted in olivine phenocrysts from the a) Ulakan and b) Epi ankaramite suites plotted in the oxidized (magnetite) spinel prism of Williams *et al.* (1990). Cr-spl$_S$= solid chromian spinel, Al-spl$_S$= solid Al-spl, Al-spl$_d$= daughter Al-spl. In this prism spinel analyses are subdivided into three series according to whether the trivalent ion is Al, Fe^{3+} or Cr as follows:

Spinel series [Sp-Her]= Spinel($MgAl_2O_4$) - Hercynite($Fe^{2+}Al_2O_4$),

Magnetite series [Mf-Mt]= Magnesioferrite($MgFe^{3+}_2O_4$) - Magnetite($Fe^{2+}Fe^{3+}_2O_4$),

Chromite series [Pc-Chr]= Magnesiochromite($MgCr_2O_4$) - Chromite($Fe^{2+}Cr_2O_4$).

Pleonaste series = $Mg(Fe^{3+},Al)_2O_3$ - $Fe(Al,Fe^{3+})_2O_4$

TABLE 6.3

Host rock	*Epi (UTas71046)*					*Rinjani (UTas48002)*				
Grain / Tq	Grain RW2 / 1280°C					Grain 43/1220°C				
Inclusion	1	2	3	4	*av (2-4)*	1	2	3	4	*av (2-4)*
Type	Type-B	Type-A	Type-A	Type-A	Type-A	Type-B	Type-B	Type-A	Type-A	Type-A
Melt inclusion (summed to 100 wt%)										
SiO_2	**44.37**	45.02	45.49	43.83	*44.78*	**46.17**	**45.76**	44.16	45.45	*44.81*
TiO_2	**0.76**	0.71	0.67	0.71	*0.70*	**1.06**	**1.22**	1.19	1.28	*1.24*
Al_2O_3	**15.18**	14.89	14.22	15.51	*14.87*	**16.90**	**18.15**	18.00	17.40	*17.70*
Cr_2O_3	**0.09**	0.15	0.03	0.07	*0.08*	**0.08**	**0.02**	0.02	0.00	*0.01*
FeO	**8.92**	9.45	9.59	9.86	*9.63*	**5.30**	**5.29**	5.80	5.69	*5.75*
MgO	**11.20**	10.40	11.08	10.44	*10.64*	**8.86**	**8.46**	8.86	8.87	*8.87*
CaO	**16.96**	16.69	16.45	17.36	*16.84*	**17.41**	**17.09**	17.73	17.24	*17.49*
MnO	**0.13**	0.09	0.01	0.11	*0.07*	**0.00**	**0.07**	0.11	0.03	*0.07*
Na_2O	**1.80**	1.93	1.79	1.55	*1.76*	**2.84**	**2.81**	2.81	2.75	*2.78*
K_2O	**0.54**	0.54	0.53	0.44	*0.50*	**0.94**	**0.92**	1.07	1.11	*1.09*
P_2O5	**0.08**	0.14	0.14	0.12	*0.13*	**0.45**	**0.21**	0.24	0.18	*0.21*
Mg#	**69.1**	66.2	67.3	65.3	*65.3*	**74.9**	**74.0**	73.1	73.5	*73.5*
Fo host	**83.6**	85.0	84.8	84.7	*84.7*	**91.1**	**90.7**	90.4	90.4	*90.4*
K_D	**0.44**	0.35	0.37	0.34	*0.34*	**0.29**	**0.29**	0.29	0.30	*0.30*
CaO/Al_2O_3	**1.12**	1.12	1.16	1.12	*1.13*	**1.03**	**0.94**	0.99	0.99	*0.97*
SiO_2/Al_2O_3	**2.92**	3.02	3.20	2.83	*3.01*	**2.73**	**2.52**	2.45	2.61	*2.53*
Na_2O/K_2O	**3.35**	3.56	3.35	3.54	*3.48*	**3.02**	**3.05**	2.63	2.48	*2.72*

Host rock	*Rinjani (UTas48002)*							
Grain / Tq	Grain 39 / 1220°C							
Inclusion	1	2	3	4	5	6	7	*av (2-7)*
Res. phase	Type-B	Type-A	Type-A	Type-A	Type-A	Type-A	Type-A	Type-A
Melt inclusion (summed to 100 wt%)								
SiO_2	**48.37**	48.05	47.49	47.68	47.26	46.43	46.60	*47.25*
TiO_2	**1.51**	1.24	1.25	1.19	1.18	1.55	0.99	*1.23*
Al_2O_3	**16.98**	18.36	17.82	18.68	19.00	17.76	18.18	*18.30*
Cr_2O_3	**0.00**	0.04	0.08	0.05	0.03	0.02	0.00	*0.04*
FeO	**5.11**	4.98	6.19	5.06	4.92	5.86	5.77	*5.46*
MgO	**7.91**	7.39	7.44	7.35	7.72	7.89	7.90	*7.62*
CaO	**14.87**	15.29	15.59	15.46	15.51	16.57	15.75	*15.70*
MnO	**0.03**	0.13	0.12	0.10	0.21	0.12	0.19	*0.15*
Na_2O	**3.38**	2.98	2.77	3.07	2.82	2.61	2.99	*2.87*
K_2O	**1.62**	1.21	1.11	1.17	1.21	1.05	1.35	*1.18*
P_2O5	**0.22**	0.32	0.16	0.19	0.12	0.15	0.27	*0.20*
Mg#	**73.4**	72.5	68.2	72.1	73.7	70.6	70.9	*70.9*
Fo host	**89.5**	89.8	89.5	89.2	89.5	89.5	89.4	*89.4*
K_D	**0.33**	0.30	0.25	0.31	0.33	0.28	0.29	*0.29*
CaO/Al_2O_3	**0.88**	0.83	0.87	0.83	0.82	0.93	0.87	*0.87*
SiO_2/Al_2O_3	**2.85**	2.62	2.66	2.55	2.49	2.61	2.56	*2.58*
Na_2O/K_2O	**2.09**	2.46	2.50	2.62	2.33	2.49	2.21	*2.34*

Analyses of heated melt inclusions Type-A and Type-B hosted by olivine T_q indicates temperature of quenching after melting of all cpx_d crystals. Numbers in italics indicate average compositions of melt inclusions without Al-spl_d (Type A). Mg#=100Mg/(Mg+Fe*), $K_D = (Fe/Mg)_{host\ olivine}/(Fe^*/Mg)_{residual\ glass}$

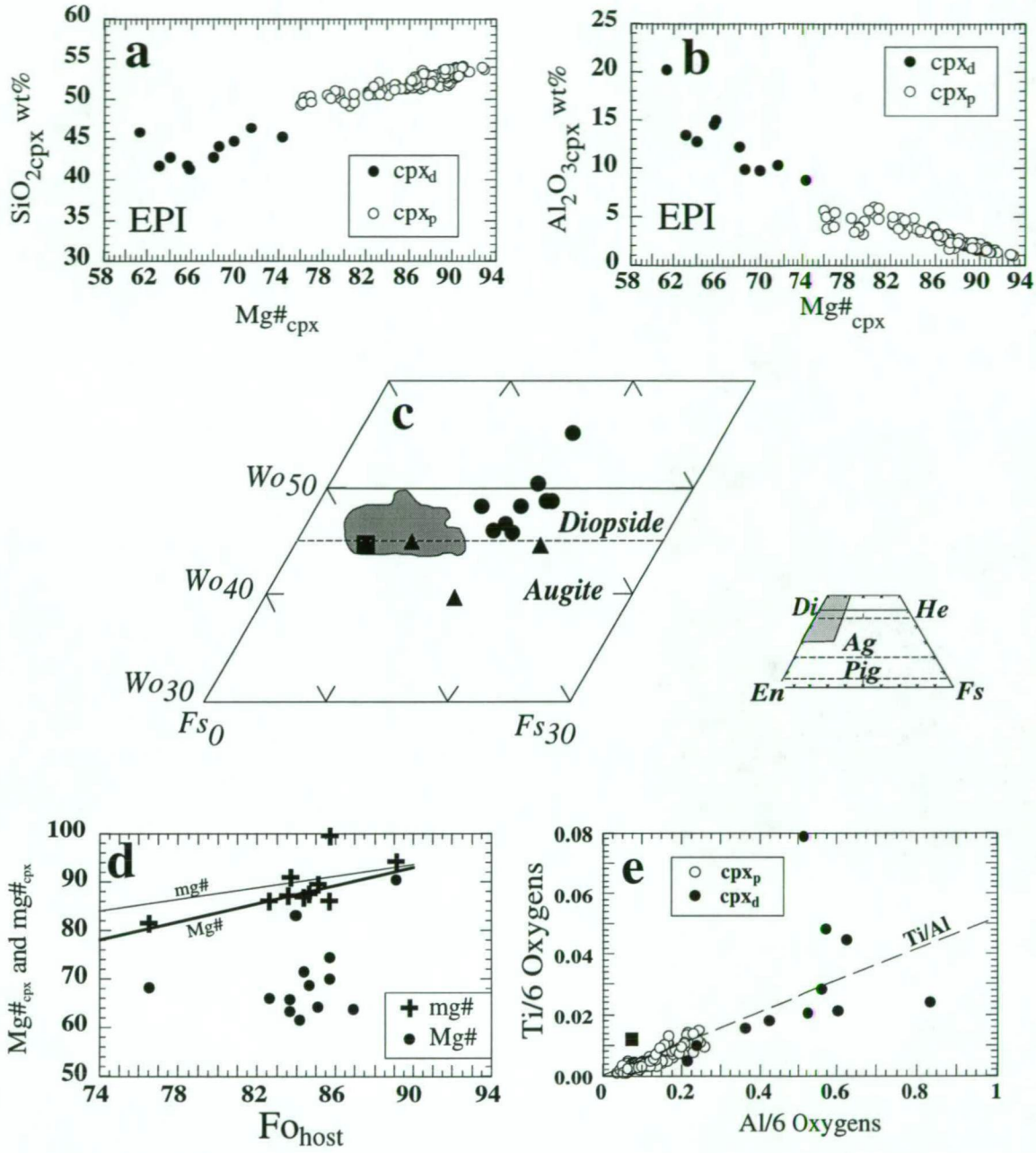

Figure 6.7 a-b) SiO_2 and Al_2O_3 content *versus* Mg# (=100Mg/(Mg+Fe*)) of Cpx_d (filled circles) coexisting with Al-spl_d in melt inclusions trapped in olivine from Epi. Open circles represent clinopyroxene phenocrysts (cxp_p).

c) Composition of cpx_d coexisting with Al-spl_d in olivine from Epi (filled circle) and Merelava (filled triangle). Filled square indicates composition of a "heated" cpx_d crystal. Shaded area indicates the field for clinopyroxene phenocrysts (cxp_p).

d) Mg# =100Mg/(Mg+Fe*) (filled circles) and mg# =100Mg/(Mg+Fe^{2+}) (crosses) values of cpx_d *versus* Fo of the host. Lines labeled Mg# and mg# are values calculated using coexisting clinopyroxene-olivine relations of Barsdell (1988) (Chapter 2).

e) Ti-Al content of clinopyroxene phenocrysts (open circles) and in cpx_d crystals (filled circles). Filled square indicates composition of cpx_d in heated melt inclusion.

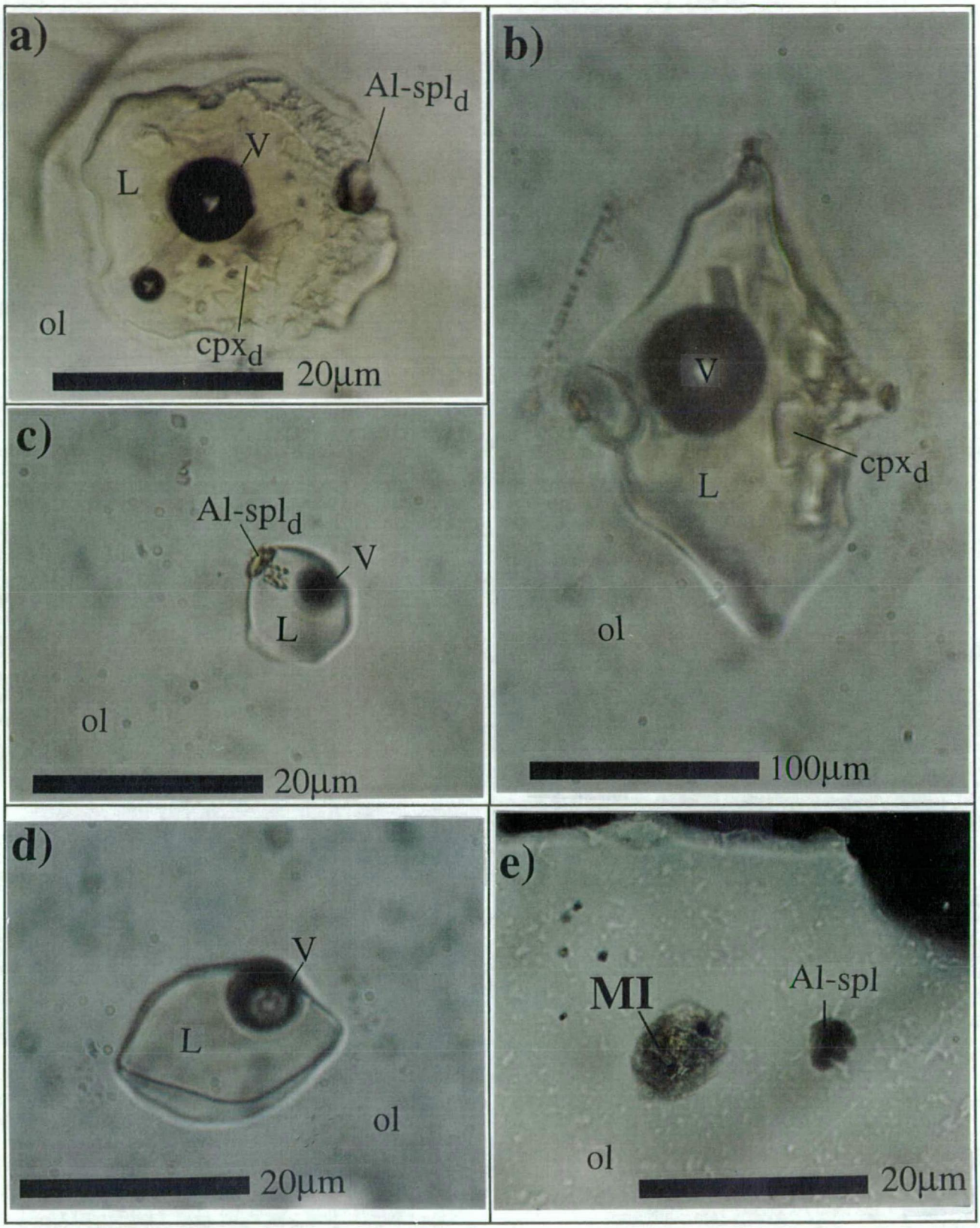

Figure 6.8 Al-spl$_d$ crystals in melt inclusions hosted by olivine.

a) Partially homogenized melt inclusion in olivine (ol) with residual "heated" Al-spl$_d$ and cpx$_d$ crystals. Note rim of unmelted Ol$_d$ on the walls of the inclusion. Temperature of quenching (Tq) = ~1230°C. Sample UTas67424, PPL, 100x.

b) Partially heated melt inclusion in olivine (ol) with residual "heated" Al-spl$_d$ and cpx$_d$ crystals. Note rim of unmelted Ol$_d$ on the walls of the inclusion. Tq=1242°C. Sample 31551, PPL, 100x.

c) Heated melt inclusion in olivine with partially dissolved residual Al-spl$_d$ crystal. Sample UTas71046, PPL, 100x.

d) Optically homogenized melt inclusion. Tq=1230°C. Sample 31551, PPL, 100x.

e) Al-spl$_d$ exposed on the surface of polished olivine grain. Also present within the olivine grain is a crystalline melt inclusion (MI). Sample UTas71046, PPL, 40x.

ankaramites (Chapter 3) and do not contain Al-spl_d. To test a model in which Al-spl_d is considered to crystallize from trapped contaminant aluminous melt (Della-Pasqua *et al.* 1995), both, Type-A and B melt inclusions are used. If Type-B melt inclusions are trapped contaminant melts, then their compositions should differ from Type-A melt inclusions. However, the original composition of trapped melts may be modified by (1) depletion in olivine component by unmelted ol_d from the walls (Chapter 3), (2) dilution caused by excess of ol_d melted from the walls (Chapter 3) and (3) Mg# re-equilibration of the melt by Fe-loss (Chapter 4). Although the extent of each process may differ between grains, the composition of melt inclusions that coexist within a single olivine grain will be equally modified. Thus, within a single olivine grain, the composition of coexisting Type-A and B melt inclusions may be compared directly.

This test is based on experiments applied to three olivine grains that have coexisting Type-A and B melt inclusions. One olivine grain is from the Epi ankaramite suite (grain RW2, Table 6.3) and the other two are from the Rinjani volcano suite (grain 39 and 43, Table 6.3). Each grain was individually prepared and heated to dissolve all daughter phases within the melt inclusions, following the experimental procedures described in Chapter 3. With increasing temperature, all daughter phases were progressively melted with the exception of Al-spl_d crystals that remained partially undissolved even at temperatures approaching 1300°C (Figure 6.8a-c). These "partially" homogenized melt inclusions were then quenched to a homogeneous glass and prepared for electron microprobe analysis using analytical techniques as described in Appendix 2.1. The results from these melt inclusion heating experiments are discussed below.

6.5.1 Composition of "heated" cpx_d and Al-spl_d crystals in partially homogenized melt inclusions

A melt inclusion with Al-spl_d was heated and quenched before the last cpx_d crystal melted (Figure 6.8a-b). The melt inclusion was then sectioned and carefully polished to expose the "heated" Al-spl_d and cpx_d phases for microprobe analysis.

The "heated" clinopyroxene crystal has distinctively higher SiO_2 and MgO contents with lower Al_2O_3 and FeO contents, than analyses of unheated cpx_d (bold analysis, Table 6.2). Whereas the compositions of unheated cpx_d crystals vary towards the compositional field of clinopyroxene phenocrysts (Figure 6.9), the composition of the "heated" cpx_d lies within this field (filled square, Figure 6.9). Results tentatively suggest that the composition of the "heated" cpx_d was re-adjusted by chemical diffusion that occurred in the duration of the heating experiment (~20 minutes at ~1240°C).

A similar phenomenon is observed in the composition of the "heated" Al-spl_d crystal, which acquired highest Al_2O_3 and MgO, and lowest FeO compared to the composition of unheated Al-spl_d (filled triangle, Figure 6.9). The recalculated analysis of this Al-spl_d crystal has no Fe^{3+}, unlike the unheated Al-spl_d crystals that have a Fe_2O_3 component (Table 6.2). The composition of this heated Al-spl_d therefore resembles a pleonaste spinel $(Mg\text{-}Fe^{2+})Al_2O_4$.

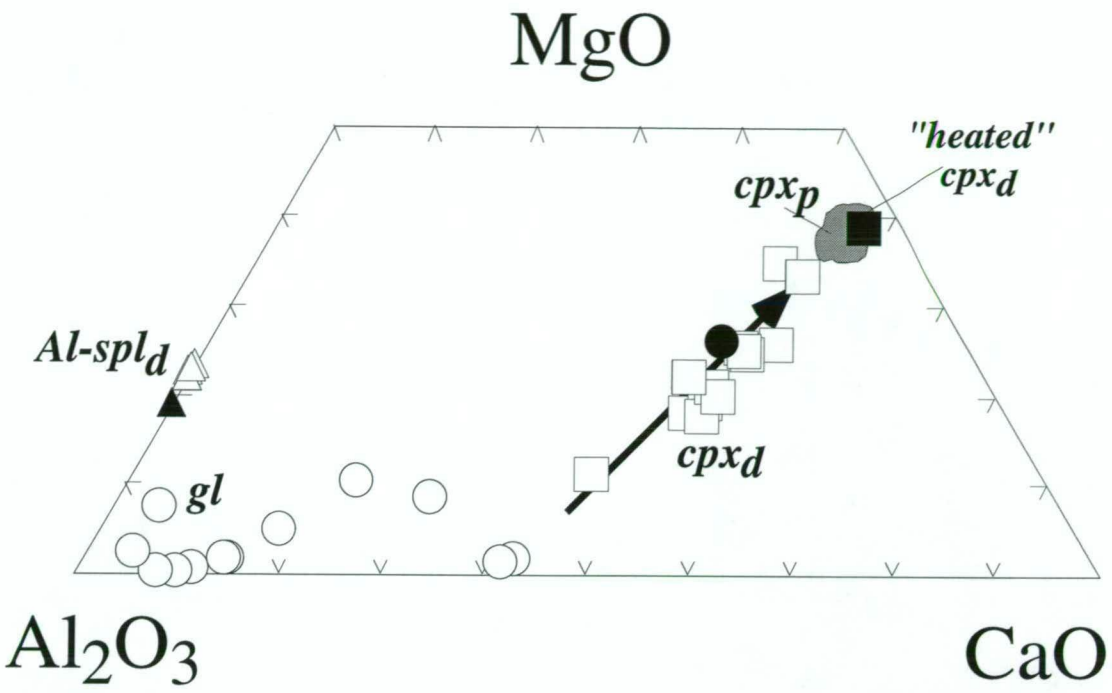

Figure 6.9 Chemical variation of daughter phases in melt inclusions trapped by olivine phenocrysts from Epi ankaramites. Analyses from Table 6.2. Open triangles=daughter Al-spl(Al-spl$_d$), open squares=daughter cpx(cpx$_d$), open circles=quenched glass(gl), cpx$_p$=compositional field of clinopyroxene phenocrysts from Epi (Table 6.2).

Filled symbols indicate compositions of "heated" daughter phases: Al-spl$_d$, cpx$_d$, and gl$_d$ from a partially homogenized melt inclusion hosted by olivine.

The observed change in Al-spl_d composition may have contributed to its failure to dissolve during the heating experiments.

6.5.2 Composition of melt inclusions that contain Al-spl_d

The heated glass compositions from coexisting Type-A and B inclusions in three olivine grains are listed in Table 6.3. The incompatible major element ratios (CaO/Al_2O_3, Na_2O/K_2O) and absolute major oxide abundances of these glasses are remarkably similar. These analyses, therefore, suggest that both melt inclusion types were trapped from the same parent melt. They contradict a model where the Al-spl_d are inferred to crystallize preferentially from contaminant aluminous melts. Further, if Type-A and B represent a common melt, then the effect of Al-spl_d crystallization can be assessed. Melt inclusions that crystallized Al-spl_d (Figure 6.8c) will be more depleted in Al-spl_d components (e.g., Al_2O_3) compared to coexisting melt inclusions in which Al-spl_d did not crystallize (Figure 6.8d). Comparison of CaO/Al_2O_3 values and Al_2O_3 contents between these two types of melt inclusions in each grain, however, vary non-systematically, and absolute Al_2O_3 variations are <1 wt%, as estimated in Section 6.3.

6.5.3 Results of least square mixing

An estimate of the volume of Al-spl_d in melt inclusions can also be obtained by solving mass balance equations of the form:

(1) $ol_{host} + cpx_d + gl_d + \text{Al-}spl_d = \text{melt}$

(2) $ol_{host} + cpx_d + gl_d = \text{melt}$

for each of the six complete sets of daughter phase analyses listed in Table 6.2 (analyses 1-2, 4-6 and 8). The second equation excludes Al-spl_d as a reactant, to asses its influence on the result. In each calculation, the composition of the host olivine from each set (Fo_{77-86}) is used as an approximation for Ol_d, whereas "melt" represents the average composition of three homogenized melt inclusions in ~Fo_{84-85} from the same suite (Table 6.3, grain RW2 analyses 2-4).

Mass balance calculations were made using the mixing program GENMIX (LeMaitre 1982). The results are given in Appendix 6.3 and summarized in Table 6.4. Solutions to equation (1) give unsatisfactory $\Sigma r2$ values (0.6-5.8) (Table 6.4a) which arise from discrepancies between calculated and target compositions of up to ~1.7 wt%, but typically <1 wt%. Modal proportions calculated by GENMIX indicate cpx_d > gl > Al-spl_d and agree with the observed natural abundances, but the actual proportions of Al-spl_d calculated by GENMIX (~1-8 vol%) are much higher than estimated in previous sections (<1 vol%). Solutions to equation (2) yield even more unsatisfactory results with differences in compositions of up to ~4.4 wt%, but mostly <1 wt%. (Table 6.4b).

GENMIX results can be explained with the aid of Figure 6.10a where the compositions of reactants (sets 1-9, Table 6.2) and target melt composition (M) are plotted. In Figure 6.10a, the mass balance calculations using equation (1) for sets-1 and set-9 are

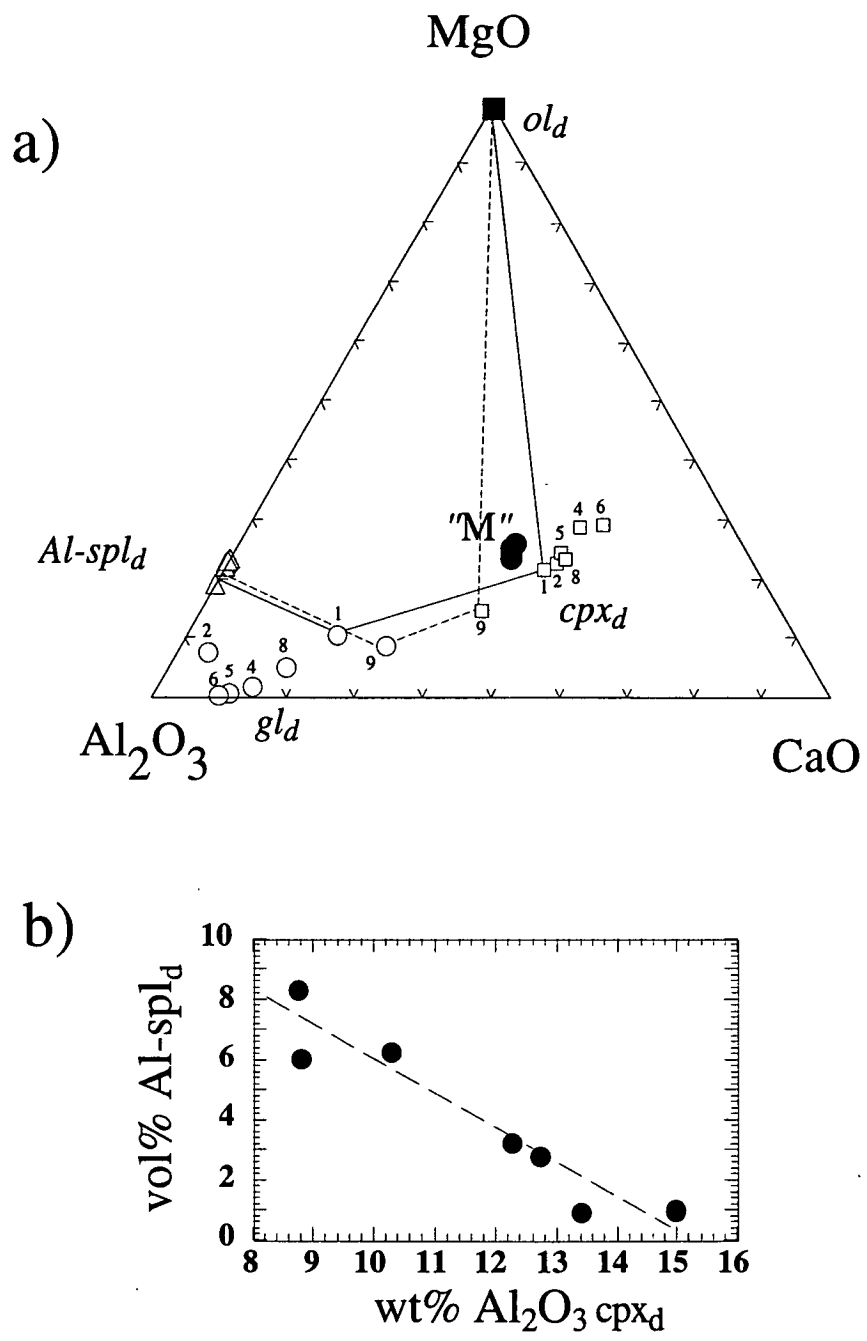

Figure 6.10 a) Al_2O_3-MgO-CaO (wt%) compositional variation of daughter phases in melt inclusions (Table 6.1).

open squares: daughter clinopyroxene (cpx_d),
open triangle: daughter Al-spl ($Al\text{-}spl_d$)
open circles: residual glasses (gl)
filled square: olivine (ol_d)
filled circles: melt composition M from analyses of Table 6.3.

Numbers adjacent to symbols indicate set number from Table 6.1. Tie lines join daughter phases used in the mass balance calculation of sets 1 and 9 (Table 6.2). Solution to mass balance calculations are summarized in Table 6.4 as listed in Appendix 6.3.

b) Variation in the proportion of $Al\text{-}spl_d$ calculated by mixing program GENMIX (LeMaitre 1982) *versus* Al_2O_3 content in Cpx_d.

illustrated with tie lines joining the composition of the reactants. It is clear from Figure 6.10a that Set-9 (broken lines) gives an inconclusive results as it excludes the target melt composition (M). Set-1 instead (thin lines), includes (M) and gives an Σr^2 value of ~2. Cpx_d compositions in Figure 6.10a are close to the target melt composition (M), and are interpreted to have the greatest influence on the calculated proportions of Al-spl_d. Thus if the cpx_d crystals are compositionally zoned, then the single-spot cpx_d analyses used for the mixing calculations could give inaccurate results. This is demonstrated in Figure 6.10b where the calculated proportions of Al-spl_d by GENMIX are negatively correlated to the Al_2O_3 content of cpx_d. Another contributing factor is the assumption that the composition M represents the original composition of melt from which Al-spl_d crystals formed. Further uncertainties are introduced by Fe-loss and the assumption that ol_d has a composition similar to the host. In conclusion, the volumes of Al-spl_d estimated by mass-balancing are, in this particular case, inaccurate. The results obtained in Section 6.3 are therefore preferred in comparison.

TABLE 6.4

Host rock	71046	71046	71046	71046	71046	71046
Set no.	1	2	4	5	6	8
Grain/Inclusion	122/1	90/1	65/1	35/1	35/2	108/1
a) ol_d + Al-spl_d + cpx_d + gl = heated melt						
% Ol_h	7.0	5.3	0.3	4.7	0.8	5.3
% Al-spl_d	1.1	1.0	6.4	3.3	8.4	2.9
% cpx_d	71.9	76.3	77.6	76.0	73.1	72.1
Σr^2	1.9	1.2	1.9	3.7	5.8	0.6
b) ol_d + cpx_d + gl = heated melt						
% ol_h	7.2	5.4	2.3	5.6	3.7	5.7
% cpx_d	73.5	77.2	79.7	79.0	76.6	74.8
% gl	19.4	17.4	18.0	15.4	19.6	19.5
Σr^2	2.3	1.7	22.2	8.4	42.9	4.8

Solution to mass balance calculation using least square mixing model GENMIX (LeMaitre 1982). Reactants= analyses of daughter phases (Al-spl_d, cpx_d, gl) and host olivine (ol_h) from Table 6.2. Product= average analysis of heated melt inclusion glasses from Grain RW2 (Table 6.3). (a) are solutions that include Al-spl_d. All calculations are made with analyses summed to 100%. Set no. refers to analyses in Table 6.2.

6.6 Results from high pressure experiments

The liquidus phase relations of a homogenized Type-A melt inclusion (ANK2376) were investigated at high pressures (1-3 GPa) in Chapter 5. In these experiments, despite the absence of Al-spl_d in the melt inclusion and the presence of ~14 wt% Al_2O_3 and ~800 ppm Cr in the starting mix, Al-spl crystallized. Compositionally, these synthesized Al-spl are similar to the naturally occurring Al-spl_d found in melt inclusions having $Cr^{\#}<1$, Al_2O_3 >60 wt% and $Mg^{\#}>60$ (Table 6.5). The Al-spl occurred in runs T-3975, T-3896 and T-3875, as described below.

Hydrous run T-3975 (0.25 GPa, 1060°C) is ~40°C below the liquidus and almost fully crystallized. In this run Al-spl coexists with olivine (Fo_{79-85}) and calcic augite (<4 wt%

Al_2O_3). At higher pressures and temperatures (T-3974, T-4008, T-4009) garnet replaces Al-spl and becomes the stable aluminous phase coexisting with clinopyroxene. Anhydrous run T-3875 (0.20 GPa, 1390°C) is also largely crystallized (~80% crystals) and the mineral assemblage is dominated by augite, olivine (Fo_{85}) and minor Al-spl. With increasing temperature, the Al-spl disappears and olivine+clinopyroxene become the only liquidus phases. At higher pressures and approximately 50°C below the liquidus, anhydrous run T-3896 (0.25 GPa, 1390°C) is almost fully crystalline (~90% crystals) with augite and interstitial Al-spl crystals. At higher temperatures, Al-spl disappears and augite becomes the only crystaline phase near the liquidus.

TABLE 6.5

Run	T-3975	T-3875
Pressure	2.5 GPa	2.0 GPa
Temperature	1060°C	1390°C
SiO_2	0.80	1.20
TiO_2	0.19	0.23
Al_2O_3	63.71	65.38
Cr_2O_3	0.04	0.77
Fe_2O_3	2.80	0.00
FeO	14.94	10.09
MgO	17.82	21.64
MnO	0.04	0.07
NiO	0.01	0.01
TOTAL	100.35	99.39
mg#	68.0	79.3
Mg#	64.6	79.3
Cr#	0.0	0.8
$Fe^{3+}/\Sigma Fe$	0.144	0.000

Analysis of Al-spl synthesized in high pressure experiments (Chapter 5). Mg#=100Mg/(Mg+Fe*), mg#=100Mg/(Mg+Fe^{2+}), Cr#=100Cr/(Cr+Al), *=all iron as FeO, $\Sigma Fe=(Fe^{2+}+Fe^{3+})$

Other authors[2] have also documented the crystallization of Al-spl (pleonaste) in basaltic melts in place of chromian spinel. These experimental results are often cited as evidence to support a high pressure origin for the formation of Al-spl in basaltic melts. However, any pressure dependence on the partitioning of Al between spinel and melt phases is yet to be shown. Rather, the conclusions of Dick & Bullen (1984) suggest that any pressure effects on the composition of spinel are largely the result of variations in the partition coefficient of chromium, producing spinels with lower $Cr^{\#}$ at high pressures. On this basis therefore, it has been commonly suggested that Cr-poor spinels may form by crystallization at high pressures (e.g., Irvine 1967, Sigurdsson & Schilling 1976, Dick & Bryan 1978, Fisk & Bence 1980) and

[2]Kushiro & Yoder (1966), Green *et al.* (1972), Råheim & Green (1974), Falloon & Green (1987), Delano (1980), Bartels *et al.* (1991), Thy (1991), Johnston & Draper (1992), Kinzler & Grove (1992a)

that the coexistence of both aluminous and chromian spinels within the same rock may represent crystallization at relatively high and low pressures respectively (Romick *et al.* 1990). However, the Al-spl compositions described in this work are virtually Cr-free. In addition, Al-spl can coexist in the same phenocrysts with chromian spinel inclusions as well as form rims around chromian spinel. These observations are difficult to explain by a high pressure crystallization model, particularly the occurrence of rims, which suggest that the Al-spl crystallized after, not before, chromian spinel (i.e., at lower pressures).

An alternative possibility for the formation of Al-spl in experimental charges was suggested by Peter L. Roeder (written. comm. August 15, 1995). Extensive crystallization of olivine and augite (<4 wt% Al_2O_3) rapidly depletes the residual melt in chromium and causes an Al_2O_3 enrichment in the residual melt. Unlike natural systems, the Al_2O_3 enrichment with continued crystallization is enhanced in the experimental charges by the lack of plagioclase nucleation. These conditions therefore generate fractionated aluminous melts that are optimal for the crystallization of Al-spl (Maurel & Maurel 1983) and thus explains their occurrence in the near-solidus of high-pressure experiments.

6.7 An alternative interpretation for the origin of Al-spl in melt inclusions

Della-Pasqua *et al.* (1995) considered the crystallization of Al-spl_d in melt inclusions as evidence for "localized aluminous melt pockets" in primitive basaltic melts. However, testing of this model using experimental techniques yield contradicting results. These are summarized below.

(1) the volume of Al-spl_d occupies <1% of the total melt inclusion volume (Section 6.3) and therefore the required addition of ~5% Al-spl using mass balance to reconstruct the original melt composition, is not justified.

(2) melt inclusions with and without Al-spl_d crystals are similar in composition (Section 6.5) and contradict the derivation of inclusions from contaminant aluminous melt in the basaltic magma.

(3) the compositions of cpx_d crystals coexisting with Al-spl_d suggest rapid disequilibrium growth with no plagioclase crystallization (Section 6.4).

(4) the continued crystallization of ol_d on the walls after trapping is sufficient to alone increase the Al_2O_3 concentration of the residual melt up to ~16-19 wt% as demonstrated by the composition of glassy melt inclusions in olivine (Table 3.3). Further crystallization of olivine without plagioclase, will result in an even higher Al_2O_3 content.

(5) phase relations of a basaltic melt inclusion composition (Chapter 5) demonstrate that Al-spl can nucleate after extensive crystallization of non-aluminous phases.

In summary, points (1) and (2) disprove the entrapment of a contaminant aluminous melt, whereas (3) and (4) discard the need for such contamination processes to generate aluminous, chromian free melt inclusion. It is therefore considered that the crystallization of Al-

spl_d in melt inclusions may be the result of alumina-enrichment and chromium-depletion, after crystallization of non-aluminous daughter phases.

6.8 What about the solid Al-spl inclusions?

Only seven solid inclusions of Al-spl (Al-spl_s) were found at the polished surface of sectioned olivine grains and these are compositionally similar to the Al-spl_d crystals found in melt inclusions (Figure 6.5 and 6.4). Despite an extensive search for additional Al-spl_s inclusions, none were found within the phenocrysts. All Al-spl crystals found within phenocrysts were daughter crystals in melt inclusions. It is therefore possible that the reported Al-spl_s inclusions are "remnants" of Al-spl_d crystals from melt inclusions that were partially removed by polishing as illustrated in Figure 6.8e. This possibility was proposed to me by Peter L. Roedder (15th August 1995, written. comm.) and is not considered by Della-Pasqua *et al.* (1995). This explanation could also account for the occurrence of aluminous cpx solid inclusions in olivine phenocrysts, with similar composition to cpx_d crystals, that were equivocally interpreted as evidence for high pressure crystallization (Della-Pasqua *et al.* 1995).

6.9 Conclusion

A model for the origin of Al-spl inclusions that requires "contamination by localised high-Al melts" (Della-Pasqua *et al.* 1995) is retracted. The preferred alternative model is proposed where Al-spl crystallizes as a daughter phase from aluminous melts that are residual after the fractional crystallization in basaltic melt inclusions of non-aluminous phases. Rare solid inclusions of Al-spl (and Al-cpx) exposed on the surface of polished grains may represent "remnants" of daughter phases exposed by polishing, and not solid inclusions *sensu stricto.* Finally, two points are noted:

1) The occurrence of Al-spl_d in melt inclusions has no petrogenetic implications, and
2) Al-spl_d may form in any basaltic melt inclusion provided crystallization of daughter phases led to an enrichment in alumina and depletion in chromium,

Therefore, the occurrence of Al-spl ought to be a widespread phenomenon within melt inclusions trapped by olivine.

Chapter 7: Synthesis

A compilation of ankaramite and picrite wholerock analyses indicates that ankaramite rocks have higher CaO/Al_2O_3 values (>1) and higher normative *di/ol* values (>0.7) than picrite (Table 1.3). These chemical characteristics of ankaramite rocks reflect their relative richness in clinopyroxene and differ from the composition of experimental partial melts of dry peridotite (up to ~4 GPa), which are picritic not ankaramitic. Ankaramite and picrite however share similar "primitive" characteristics. These include magnesian olivine (>Fo_{90}) and diopsidic clinopyroxene phenocrysts, high Mg# values (>~70), and high MgO, Ni and Cr contents. Moreover, if ankaramite rocks occur they are the most primitive rocks of the differentiation series. Ankaramite rocks are therefore often viewed as the result of clinopyroxene accumulation, rather than rocks that were derived from a magma of their own composition. However, many silica-undersaturated rocks are also characterised by high CaO/Al_2O_3 values (>1), yet these rock types are often olivine-phyric. Aphanitic alnöitic rocks and in particular, olivine-phyric komatiites rocks with CaO/Al_2O_3 values of up to ~2 (Table 1.4) are also additional examples. The experimental results of Herzberg (1992), in particular, demonstrate that the CaO/Al_2O_3 values of partial melts within the garnet lherzolite field increase with pressure and exceed 1 above 5 GPa. These results suggest that chemical characteristics of ankaramite rocks such as CaO/Al_2O_3 values >1(Table 1.3) could be primary and not the result of clinopyroxene accumulation. This thesis has focussed directly on this controversy, and concentrates on the results of melt inclusion homogenization experiments in primitive magnesian olivines of four well-studied arc-ankaramite suites (Chapter 2). Most of the conclusions of this thesis were already discussed in previous chapters and will only be briefly sumarized here.

A critical assessment of the data obtained from opticaly-homogenized inclusions (Chapter 3) indicates that the compositions of melt inclusions hosted in olivine phenocrysts from arc-rocks can be affected by: (1) Mg-Fe re-equilibration between the melt inclusion and the host phenocryst after trapping and before eruption, and (2) olivine fractionation by experimental underheating of the inclusion during the experiment. The effect of the first process is to lower the original FeO* content of the melt ("Fe-loss") whereas the effect of the second process is to lower the MgO content. Both processes may operate independently of one other and could considerably modify the original composition of the trapped melt. A model developed in Chapter 4 to explain how this re-equilibration may occur indicates that the extent of Fe-loss in melt inclusions is dependent on: (a) the time spent by the host olivine phenocryst in the magma before eruption (residence time) and (b) the rate at which the re-equilibration occurs. Melt inclusions trapped in early-formed magnesian olivines have the longest residence time in the magma and therefore they can undergo the largest extent of Fe-loss. In comparison, melt inclusions that are trapped in the least magnesian olivines that formed shortly before

the eruption, undergo least Fe-loss. Thus, those melt inclusions that re-equilibrated at a fast rate within magnesian olivine phenocrysts will have the lowest FeO* content (e.g., Ulakan, Merelava and Epi). Alternatively, if the re-equilibration rates between inclusions differ, the FeO* contents of homogenized melt inclusions in olivines of similar Fo content will vary (e.g. Rinjani). Melt inclusions hosted in the least magnesian olivines will have highest FeO* content regardless of the re-equilibration rate.

From the re-equilibration model described in Chapter 4, a recalculation procedure is developed to reconstruct the original composition of melt inclusions at the moment of trapping. The electron microprobe analyses of optically homogenized melt inclusions hosted in olivines from this study are therefore considered not directly representative of the originally trapped melt, but their CaO/Al_2O_3 values are unaffected. Three main observations from this data are:

(1) The CaO/Al_2O_3 values of all four ankaramite suites decrease with Fo_{host} and range up to values that are typical of ankaramite (up to ~1.7) in the most magnesian olivines.

(2) Within the same olivine grain, CaO/Al_2O_3 values of coexisting melt inclusions are remarkably similar.

(3) Although the CaO/Al_2O_3 values of melt inclusions within the same grain are similar, the CaO/Al_2O_3 values of melt inclusions between grains can vary over a wide range at constant Fo (e.g., ~1.0 to 1.7 in ~Fo_{91}, Figure 3.9b).

From (1) above, it is suggested that the early formed olivine phenocrysts crystallized from primitive basaltic melts that were ankaramitic, not picritic. Thus, the high CaO/Al_2O_3 values observed in ankaramite rock samples are not necessarily the result of clinopyroxene accumulation. Similarly, (2) and (3) above suggest that the primitive olivine phenocrysts crystallized from primitive ankaramitic basaltic melt pockets are regionally variable, but locally similar, CaO/Al_2O_3 values. These melts were later aggregated to form the ankaramite magma. If the high CaO/Al_2O_3 values of some melt inclusions are caused by the accidental trapping of clinopyroxene crystals (that were later dissolved and mixed during the homogenization experiment), it would be very unlikely for every inclusion within an olivine grain to have the same CaO/Al_2O_3 value, in every grain. Instead, this observation suggests that the high CaO/Al_2O_3 values in the melt inclusion do represent those of the parent melt.

If the compositions of recalculated melt inclusions are considered as representative of the original trapped melt, then the data indicate that the parent melts to ankaramite rocks were ankaramitic, not picritic, with normative *di/ol* values varying between 0.9 to ~4 (Appendix 3) that are typical of ankaramite (Table 1.3). The CIPW normative compositions of recalculated melt inclusions are, however, invariably more silica-undersaturated (*ne*-, *lc*- and *cs*-normative) compared with the host ankaramite rocks which vary from *ne*-normative (Sunda arc) to *hy*-normative (Vanuatu arc). The composition of melt inclusions therefore suggests that the aggregating primitive melts parental to ankaramite magmas were characterized both by high CaO/Al_2O_3 values and by silica-undersaturation. This association between high CaO/Al_2O_3 values and silica-undersaturated compositions is also documented in natural silica-undersaturated rock suites such as alnöites and therefore a genetic link may exist between such primitive melts and the generation of ankaramitic magmas.

This link was explored experimentally at high pressures, using the composition of a representative melt inclusion in Fo_{91} from Rinjani as starting mix composition (Chapter 5). Phase relations of this melt under dry, hydrous, CO_2-H_2O- and CO_2-bearing conditions, and 1 to 3 GPa pressures, lack orthopyroxene near the liquidus and are therefore inconsistent with the hypothesis that the melt of the inclusions represent a direct product of partial melting of mantle peridotite. Instead, the natural phenocryst assemblage and composition of the host ankaramite rock are duplicated under hydrous conditions in the pressure range of ~2.1 to 2.5 GPa and the temperature range of 1060 to 1080°C. With increasing CO_2:H_2O ratio of the fluid composition, the natural phenocryst assemblage is reproduced at relatively lower pressures and higher temperatures, but the composition of the clinopyroxene crystals becomes less calcic. Thus, if ankaramite magmas from Rinjani are formed by the aggregation of highly undersaturated melts (*ne*- to *cs*-normative), as suggested by the melt inclusion data, then the high pressure experimental results indicate that this process may occur at around ~2 to 2.5 GPa, where olivine and clinopyroxene are co-crystallizing phenocryst phases. This corresponds to depths of at least 60 Km and thus well below the base of the crust in the Lombok sector (~25 Km, Foden 1979). The aggregated magma may mix and continue to crystallize isobarically and in-situ, to produced the wide compositional range observed in olivine (~Fo_{75-91}) and clinopyroxene (~$Wo_{45-47}En_{5-10}Fs_{50-43}$) phenocrysts. These conclusions support the model of Thompson & Flower (1971) who suggested the formation of ankaramite rocks may be related to prolonged in-situ crystallization at high pressures. At relatively lower pressures, olivine is the only liquidus phase, and crystallization at these conditions would produce olivine-rich (picritic) magmas instead.

The possibility that ankaramite rocks may form as a mixture of crystals plus melts at low pressures is supported by the variable zoning and resorption textures displayed by olivine and clinopyroxene phenocrysts of ankaramite. Melt inclusions in magnesian olivines (>Fo_{90}) in the aggregated magma are therefore samples of primitive melts parental to the ankaramites before aggregation occurred. It is consequently suggested that these melts with variable CaO/Al_2O_3 values were in existence at higher temperatures and pressures than those prevailing when the ankaramitic magmas aggregated. Two mechanisms are considered for the formation of such melts, with high and variable CaO/Al_2O_3 values: (1) partial melting of lherzolite at high pressures (>5 GPa) and (2) melting of lherzolite in the presence of mantle CO_2-rich fluids. These melts ascend, collect, mix and continue to crystallize at lower pressures (~2 to 2.5 GPa) while continuing to react and re-equilibrate with the sub-arc mantle before eruption. Dissolution of pyroxene from the wall-rock during this reaction, leads to the silica-enrichment that distinguishes the ankaramite rock compositions from the compositions of melt inclusions trapped and preserved in early formed olivine phenocrysts.

Rare pleonastic spinels $(Mg, Fe^{2+})Al_2O_4$ with up to 65 wt% Al_2O_3 can crystallize within these melt inclusions, provided that the trapped melt becomes Al-enriched and Cr-depleted after fractional crystallization of daughter phases. The crystallization of olivine on the walls of an inclusion causes an Al_2O_3 enrichment in the residual melt above ~20 wt% (Table 3.3) and these melt inclusions may therefore provide ideal conditions for the formation of daughter aluminous spinel crystals. Aluminous spinels can therefore crystallize within any ordinary basaltic melt inclusions and their

presence are not evidence for the trapping of contaminant aluminous melts (Della-Pasqua *et al.* 1995). The occurrence of aluminous spinels in melt inclusions, should therefore become a widely documented phenomenon in olivine phenocrysts.

In short, this thesis has used melt inclusions to (1) demonstrate that ankaramitic melts may exist, with CaO/Al_2O_3 values >1 and normative *di/ol* values >0.7, and are parental to ankaramite rocks; 2) described a process of Fe-Mg re-equilibration ("Fe-loss") that affects melt inclusions in olivine phenocrysts before magma eruption; and 3) re-interpreted the formation of aluminous spinel crystals in melt inclusions, previously inferred as evidence for contaminant aluminous melts in basaltic magma chambers.

References

ADAM, J. (1988):
Dry, hydrous and CO_2-bearing liquidus phase relationships in the CMAS system at 28 Kb, and their bearing on the origin of alkali basalts.
J. Geol. **96**, 709-719.

ADAM, J. (1989):
Experimental studies of alkaline basalt genesis.
Ph.D. thesis, University of Tasmania, Hobart, Australia.

ADAM, J. (1990):
The geochemistry and experimental petrology of sodic alkaline basalts from Oatlands, Tasmania.
J. Petrol. **31**, 1201-1223.

ALLÈGRE, C. J., POIRIER, J., HUMLER, E. & HOFMANN, A. (1995):
The chemical composition of the earth.
Earth Planet. Sci. **134**, 515-526.

ANDERSON, A. T. (1974):
Evidence for a picritic, volatile-rich magma beneath Mt. Shasta, California.
J. Petrol. **15**, 243-267.

ANDERSON, A. T. & WRIGHT, T. (1972):
Phenocrysts and glass inclusions and their bearing on oxidation and mixing of basaltic magmas, Kilauea volcano, Hawaii.
Am. Mineral. **57**, 188-216.

ARCULUS, R. J. (1975):
Melting behaviour of two basanites in the range 10-35 Kbar and the effect of TiO_2 on the olivine-diopside reactions at high-pressures.
Carn. Inst. Wash. Year Book **74**, 512-515.

ARCULUS, R. J. (1976):
Geology and geochemistry of the alkali basalt-andesite association of Grenada, Lesser Antilles island arc.
Geol. Soc. Am. Bull. **87**, 612-624.

ARCULUS, R. J. (1978):
Mineralogy and petrology of Grenada, Lesser Antilles island arc.
Contrib. Mineral. Petrol. **65**, 413-424.

BACON, C. R., NEWMAN, S. & STOLPER, E. (1992):
Water, CO_2, CL and F in melt inclusions in phenocrysts from three Holocene explosive eruptions, Crater Lake, Oregon.
Am. Mineral. **77**, 1021-1030.

BAKER, M. B. & STOLPER, E. M. (1994):
Determining the composition of high-pressure mantle melts using diamond aggregates.
Geochim. Cosmochim. Acta **58**, 2811-2827.

BALLARD, H. R. (1987):
Tholeiitic arc-ankaramite in the Permian Brook Street terrane: Possible primary melts? (Abstr.). *In* Geological Society of New Zealand miscellaneous publication 37A, p12.

BALLHAUS, C., BERRY, R. F. & GREEN, D. H. (1991):
High pressure experimental calibration of the olivine-orthopyroxene-spinel oxygen geobarometer: implications for the oxidation state of the upper mantle.
Contrib. Mineral. Petrol. **107**, 27-40.

BARNES, S. J., LESHER, C. M. & KEAYS, R. R. (1995):
Geochemistry of mineralised and barren komatiites from the Perseverance nickel deposit, Western Australia.
Lithos **34**, 209-234.

BARSDELL, M. (1980):
Petrological variation in the Banks Islands, New Hebrides.
Ph.D. thesis, Auckland University, Auckland, New Zealand.

BARSDELL, M. (1988):
Petrology and petrogenesis of clinopyroxene-rich tholeiitic lavas, Merelava volcano, Vanuatu.
J. Petrol. **29**, 927-964.

BARSDELL, M. & BERRY, R. F. (1990):
Origin and evolution of primitive island arc ankaramites from western Epi, Vanuatu.
J. Petrol. **31**, 747-777.

BARSDELL, M. & SMITH, I. E. M. (1989):
Petrology of recrystallized ultramafic xenoliths from Merelava volcano, Vanuatu.
Contrib. Mineral. Petrol. **102**, 230-241.

BARTELS, K. S., KINZLER, R. J. & GROVE, T. L. (1991):
High pressure phase relations of primitive high-alumina basalts from Medicine Lake volcano, northern California.
Contrib. Mineral. Petrol. **108**, 253-270.

BEATTIE, P., FORD, C. & RUSSELL, D. (1991):
Partition coefficients for olivine-melt and orthopyroxene-melt systems.
Contrib. Mineral. Petrol. **109**, 212-224.

BISSAINTE, M., HERNANDEZ, J., SEMET, M. P. & BOUDON, G. (1993):
Al-bearing paragenesis in the lavas and cumulates from the Monts Caraïbes (South Guadeloupe-West Indies). *In* Ancient volcanics and modern analogues (Abstr.). IAVCEI 1993 General assembly. Canberra, Australia. (p3).

BLANK, J. G. & BROOKER, R. A. (1994):
Experimental studies of carbon dioxide in silicate melts: solubility, speciation, and stable carbon isotope behaviour. *In* Volatiles in magmas (M. R. Carroll & J. R. Holloway, eds.).
Rev. Mineral. **30**, 157-186.

BLACK, P. M. & BROTHERS, R. N. (1965):
Olivine nodules in olivine nephelinite from Tokatoka, Northland.
N. Z. J. Geol. Geophys. **8**, 62-80.

BOYD, F. R. & ENGLAND, J. L. (1960):
Apparatus for phase-equilibrium measurements at pressures up to 50 kilobars and temperatures up to 1750°C.
J. Geophys. Res. **65**, 741-748.

BREY, G. & GREEN, D. H. (1975):
The role of CO_2 in the genesis of olivine melilitite.
Contrib. Mineral. Petrol. **49**, 93-103.

BREY, G. & GREEN, D. H. (1976):
The role of CO_2 in the genesis of olivine melilitite: Reply to Eggler and Mysen.
Contrib. Mineral. Petrol. **55**, 237-239.

BREY, G. & GREEN, D. H. (1977):
Systematic study of liquidus phase relations in olivine melilitite+H_2O+CO_2 at high pressures and petrogenesis of an olivine melilitite magma.
Contrib. Mineral. Petrol. **61**, 141-162.

BULTTITUDE, R. J. & GREEN D. H. (1971):
Experimental study of crystal-liquid relationships at high pressure in olivine nephelinite and basanite compositions.
J. Petrol. **12**, 121-147.

CANIL, D. & SCARFE, C. M. (1990):
Phase relations in peridotite + CO_2 systems to 12 GPa: Implications for the origin of kimberlite and carbonate stability in the earth's upper mantle.
J. Geophys. Res. **95**, 15805-15816.

CHEN, C.-Y. (1993):
High-magnesium primary magmas from Haleakala Volcano, east Maui, Hawaii: petrography, nickel, and major-element constraints.
J. Volc. Geotherm. Res. **55**, 143-153.

CLARKE, D. B. (1970):
Tertiary basalts of Baffin Bay: possible primary magma from the mantle.
Contrib. Mineral. Petrol. **25**, 203-224.

CLOCCHIATTI, R. & MASSARE, D. (1985):
Experimental crystal growth in glass inclusions: the possibilities and limits of the method.
Contrib. Mineral. Petrol. **89**, 193-204.

CROSS, W. (1915):
Lavas of Hawaii and their relations.
U. S. Geol. Surv., Prof. Paper **88.**

DANYUSHEVSKY, L. V., SOBOLEV, A. V. & KONONKOVA, N. N. (1992):
Methods of studying melt inclusions in minerals during investigations on water-bearing primitive mantle melts (Tonga trench boninites).
Geochem. Int. **29**(7), 48-62.

DAWSON, J. B., POWELL, D. G. & REID, A. M. (1970):
Ultrabasic xenoliths and lava from the Lashaine volcano, Northern Tanzania.
J. Petrol. **11**, 519-548.

DEER, W. A., HOWIE, R. A. & ZUSSMAN, J. (1985):
An introduction to rock forming minerals.
Longman, Essex, U. K.

DE FINO, M., VOLPE, L. L. & LIRER, L. (1973):
Volcanology and petrology of the Assab Range (Ethiopia).
Bull. Volc. **37**, 95-110

DELANO, J. M. (1980):
Chemistry and liquidus phase relations of Apollo 15 red glass: implications for the deep lunar interior.
Proc. 11th Lunar Planet. Sci. Conf. **1**, 251-288.

DELLA-PASQUA, F. N., KAMENETSKY, V. S., GASPARON, M., CRAWFORD, A. J. & VARNE, R. (1995):
Al-spinels in primitive arc volcanics.
Mineral. Petrol. **53**, 1-26.

DELLA-PASQUA, F. N. & VARNE, R. (1997):
Primitive ankaramitic magmas in volcanic arcs: a melt inclusion approach.
Can. Mineral. **35**, 291-312.

DICK, H. J. B. & BRYAN, W. B. (1978):
Variation of basalt phenocryst mineralogy and rock compositions in DSDP Hole 396B.
DSDP Initial Reports **46**, 215-226.

DICK, H. & BULLEN, T. (1984):
Chromian spinel as a petrogenetic indicator in abyssal and alpine-type peridotites and spatially associated lavas.
Contrib. Mineral. Petrol. **86**, 54-76.

DONALDSON, C. H. & BROWN, R. W. (1977):
Refractory megacrysts and magnesium-rich melt inclusions within spinel in oceanic tholeiites: indicators of magma mixing and parental composition.
Earth Planet. Sci. Lett. **37**, 81-89.

DUNCAN, R. A. & GREEN, D. H. (1987):
The genesis of refractory melts in the formation of oceanic crust.
Contrib. Mineral. Petrol. **96**, 236-342.

DUNGAN, M. A. & RHODES, J. M. (1978):
Residual glasses and melt inclusions on basalts from DSDP Legs 45 and 46: evidence for magma mixing.
Contrib. Mineral. Petrol. **67**, 417-431.

EGGINS, S. (1989):
The origin of primitive ocean island and island arc basalts.
Ph.D. thesis, University of Tasmania, Hobart, Australia.

EGGINS, S. (1993):
Origin and differentiation of picritic arc magmas, Ambae (Aoba), Vanuatu.
Contrib. Mineral. Petrol. **114**, 79-100.

EGGLER, D. H. (1974):
Effect of CO_2 on the melting of peridotite.
Carnagie Inst. Wash. Year Book **73**, 215-224.

EGGLER, D. H. (1978):
The effect of CO_2 upon partial melting of peridotite in the system Na_2O-CaO-Al_2O_3-MgO-SiO_2-CO_2 to 35 kb, with an analysis of melting in a peridotite system.
Am. Mineral. **278**, 305-343.

EDGAR, A. D., GREEN, D. H. & HIBBERSON, W. O. (1975):
Experimental petrology of a highly potassic magma.
J. Petrol. **17**, 339-356.

FALLOON, T. J. & GREEN, D. H. (1986):
Glass inclusions in magnesian olivine phenocrysts from Tonga: evidence for highly refractory parental magmas in the Tonga arc.
Earth Planet. Sci. Lett. **81**, 95-103.

FALLOON, T. J. & GREEN, D. H. (1987):
Anhydrous partial melting of MORB pyrolite and other peridotite compositions at 10 Kbar: implications for the origin of primitive MORB glasses.
Mineral. Petrol. **37**, 181-219.

FALLOON, T. J. & GREEN, D. H. (1988):
Anhydrous partial melting of peridotite from 8 to 35 Kb and the petrogenesis of MORB.
J. Petrol., Spec. Lithosphere Issue 379-414.

FALLOON, T. J., GREEN, D. H., HATTON, C. J. & HARRIS, K. L. (1988):
Anhydrous partial melting of a fertile and depleted peridotite from 2-30 kb and application to basalt petrogenesis.
J. Petrol. **29**, 1257-1282.

FISK, M. R. & BENCE, A. E. (1980):
Experimental crystallization of chrome spinel in FAMOUS basalt 527-1-1.
Earth Planet. Sci. Lett. **48**, 111-123.

FLOWER, M. F. J. (1973):
Evolution of basaltic and differentiated lavas from Anjuan, Comores archipelago.
Contrib. Mineral. Petrol. **38**, 237-260.

FODEN, J. D. (1979):
The petrology of some young volcanic rocks from Lombok and Sumbawa, Lesser Sunda islands.
Ph.D. thesis, University of Tasmania, Hobart, Australia.

FODEN, J. D. (1983): The petrology of the calcalkaline lavas of Rinjani volcano, East Sunda arc: a model for island arc petrogenesis.
J. Petrol. **24**, 98-130.

FODEN, J. D. & VARNE, R. (1981a):
The geochemistry and petrology of the basalt-andesite-dacite suite from Rinjani volcano, Lombok: Implications for the petrogenesis of island arc, calc-alkaline magmas. *In* Geology and tectonics of eastern Indonesia (A. J. Barber & S. Wiryosujono, eds.).
Geological Research and Development Centre (Bandung), Spec. Publ. **2**, 115-134.

FODEN, J. D. & VARNE, R. (1981b):
Petrogenetic and tectonic implications of near coeval calc-alkaline to highly alkaline volcanism on Lombok and Sumbawa islands in the eastern Sunda arc. *In* Geology and tectonics of eastern Indonesia (A. J. Barber & S. Wiryosujono, eds.).
Geological Research and Development Centre (Bandung), Spec. Publ. **2**, 135-152.

FODEN, J. D. & VARNE, R. (1983):
Arc ankaramites, Sangean Api xenoliths and cordilleran ultramafic to dioritic intrusive complexes: an updated concept of arc growth and development. *In* Sixth Australia geological convention. Lithosphere dynamics and evolution of continental crust
Geol. Soc. Aust. Abst. Series **9**, 153-154.

FORD, C. E., RUSSEL, D. G., CRAVEN, J. A. & FISK, M. R. (1983):
Olivine-liquid equilibria: temperature, pressure and composition dependence of the crystal/liquid cation partition coefficients for Mg, Fe^{2+}, Ca and Mn.
J. Petrol. **24**, 256-265.

FREY, F. A., GARCIA, M. O., WISE, W. S., KENNEDY, A., GURRIET, P. & ALBAREDE, F. (1991):
The evolution of Manua Kea volcano, Hawaii: Petrogenesis of tholeiitic and alkali basalts.
J. Geophys. Res. **96**, 14347-14375.

FREY, F. A., GREEN, D. H. & ROY, S. D. (1978):
Integrated models of basalt petrogenesis: a study of quartz tholeiites to olivine melilitites from south eastern Australia utilizing geochemical and experimental petrological data.
J. Petrol. **19**, 463-513.

FREZZOTTI, M. L., DE VIVO, B. & CLOCCHIATTI, R. (1991):
Melt-mineral-fluid interaction in ultramafic nodules from alkaline lavas of Mount Etna (Sicily, Italy): melt and fluid inclusion evidence.
J. Volc. Geotherm. Res. **47**, 209-219.

GAETANI, G. A., GROVE, T. L. & BRYAN, W. B. (1994):
The influence of water on the petrogenesis of subduction-related rocks.
Nature **365**, 332-334.

GHIORSO, M. S. & CARMICHAEL, I. S. E. (1985):
Chemical mass-transfer in magmatic processes 2. Applications in equilibrium crystallization, fractionation and assimilation.
Contrib. Mineral. Petrol. **90**, 121-141.

GORTON, M. P. (1977):
The geochemistry and origin of quaternary volcanism in the New Hebrides.
Geochim. Cosmochim. Acta **41**, 1257-1270.

GOVOROV, I. N., KISELEV, V. V., GOVOROV, G. I., MARTYNOV, Y. A. & SIMANENKO, V. P. (1994):
Independent ankaramite association of the Marcus-Wake Mountains (Central Pacific).
Dokl. USSR Acad. Sci. **327**, 89-94.

GRAHAM, A. M. (1981):
Melting relations of island arc lavas from Grenada, Lesser Antilles.
Prog. Exp. Petrol. **5** 126-132.

GREEN, D. H. (1969):
The origin of basaltic and nephelinitic magmas in the earth's mantle.
Tectonophysics **7**, 409-422.

GREEN, D. H. (1976):
Experimental testing of "equilibrium" partial melting of peridotite under water-saturated, high-pressure conditions.
Can. Mineral. **14**, 255-268.

GREEN, D. H., FALLOON, T. J., BREY, G. P. & NICKEL, K. G. (1986):
Peridotite melting to 6 GPa and genesis of primary mantle-derived magmas. *In* Fourth international kimberlite conference.
Geol. Soc. Aust. Abstr. Series. **16**, 181-183.

GREEN, D. H., FALLOON, T. J. & TAYLOR, W. R. (1987):
Mantle-derived magmas--roles of variable source peridotite and variable C-H-O fluid compositions. *In* Magmatic processes: Physicochemical principles (B.O. Mysen, ed.).
Geochem. Soc., Spec. Publ. **1**, 139-154.

GREEN, D. H. & HIBBERSON, W. H. (1970):
Experimental duplication of conditions of precipitation of high-pressure phenocrysts in basaltic magmas.
Phys. Earth Planet. Int. **3**, 247-254.

GREEN, D. H. & RINGWOOD, A. E. (1967):
The stability fields of aluminous pyroxene peridotite and garnet peridotite and their relevance in upper mantle structure.
Earth Planet. Sci. Lett. **3**, 151-160.

GREEN, D. H., RINGWOOD, A. E., WARE, N. G. & HIBBERSSON, W. O. (1972):
Experimental petrology and petrogenesis of Apollo 14 basalts. *In* Proc. Third Lunar Sci. Conf. (Supplement 3, Geochim. Cosmochim. Acta). **1**, 179-206.

GREEN, T. H. (1992):
Petrology and geochemistry of basaltic rocks from the Belleny Is, Antarctica.
Aust. J. Earth Sci. **39**, 603-617.

GREENE, H. G., MACFARLANE, A., JOHNSON, D. P. & CRAWFORD, A. J. (1988):
Structure and tectonics of the central New Hebrides arc. *In* Geology and offshore resources of Pacific islands arcs - Vanuatu region, (H.G. Greene & F.L. Wong, eds.). Circum-Pacific council for energy and mineral resources. Earth science series **8**, 377-412.

GROVE, T. L. (1981):
Use of Fe-Pt alloys to eliminate the iron loss problem in 1 atmosphere gas mixing experiments: theoretical and practical considerations.
Contrib. Mineral. Petrol. **78**, 298-304.

GRUBB, P. L. C. (1965):
Undersaturated potassic lavas and hypabassal intrusives in North Johore.
Geol. Mag. **102**, 338-346.

GUNN, B. M., COY-YLL, R., WATKINS, N. D., ABRANSON, E. & NOUGIER, J. (1970):
Geochemistry of an oceanite-ankaramite-basalt suite from East Island, Crozet archipelago.
Contrib. Mineral. Petrol. **28**, 319-339.

GURENKO, A. A., SOBOLEV, A. V. & KONONKOVA, N. N. (1992):
New petrological data on Icelandic rift alkali basalts.
Geochem. Int. **29**(4), 41-53.

GURENKO, A. A., SOBOLEV, A. V., POLYAKOV, A. I. & KONONKOVA, N. N. (1988):
Primary melt of Iceland rift tholeiites: composition and conditions of crystallization.
Dokl. USSR Acad. Sci. **301**, 179-184.

GUST, D. A. & PERFIT, M. R. (1987):
Phase relations of a high-Mg basalt from the Aleutian Island Arc - Implications for primary island arc basalts and high Al-basalts.
Contrib. Mineral. Petrol. **97**, 7-18.

HANSTEEN, T. H. (1991):
Multi-stage evolution of the picritic Maelifell rocks, SW Iceland: constraints from mineralogy and inclusions of glass and fluid in olivine.
Contrib. Mineral. Petrol. **109**, 225-239.

HARANGI, S. (1994):
Geochemistry and petrogenesis of the Early Cretaceous continental rift-type volcanic rocks of the Mecsek Mountains, South Hungary.
Lithos **33**, 303-321.

HAWKINS, J. W. & NATLAND, J. H. (1975):
Nephelinites and basanites of the Samoan linear volcanic chain: their possible tectonic significance.
Earth Planet. Sci. Lett. **24**, 427-439.

HEMINGWAY, B. S. (1990):
Thermodynamic properties for bunsenite, NiO, magnetite, Fe_3O_4, and haematite, Fe_2O_3, with comments on selected oxygen buffer reactions.
Am. Min. **75**, 781-790.

HERZBERG, C. (1992):
Depth and degree of melting of komatiites.
J. Geophys. Res. **97**, 4521-4540.

HERZBERG, C., GASPARIK, T. & SAWAMOTO, H. (1990):
Origin of mantle peridotite: Constrains from melting experiments to 16.5 GPa.
J. Geophys. Res. **95**, 15779-15803.

HERZBERG, C. T. & OHTANI, E. (1988):
Origin of komatiite at high pressures.
Earth Planet. Sci. Lett. **88**, 321-329.

HIROSE, K. & KUSHIRO, I. (1993):
Partial melting of dry peridotites at high pressures: Determination of compositions of melts segregated from peridotite using aggregates of diamond.
Earth Planet. Sci. Lett. **114**, 477-489.

HOLLOWAY, J. R. & BLANK, J. R. (1994):
Application of experimental results to C-O-H species in natural melts. *In* Volatiles in magmas (M.H. Carroll & J.R. Holloway, eds.).
Rev. Mineral. **30**, 187-221.

HUEBNER, J. S. (1971):
Buffering techniques for hydrostatic systems at elevated pressures. *In*: Research techniques for high pressures and high temperatures (G. C. Ulmer, ed.).
Springer, Berlin Heidelberg New York. (123-177).

HUGHES, C. J. (1982):
Igneous Petrology.
Elsevier, Amsterdam, The Netherlands.

IRVINE, T.N. (1967):
Chromian spinel as a petrogenitic indicator. Part 2. Petrological implications.
Can. J. Earth Sci. **4**, 71-103.

JAMBON, A., LUSSIEZ, P., CLOCCHIATTI, R., WEISZ, J. & HERNANDEZ, J. (1992):
Olivine growth rates in a tholeiitic basalts: An experimental study of melt inclusions in plagioclase.
Chem. J. **96**, 277-287.

JAQUES, A. L. & GREEN, D. H. (1980):
Anhydrous melting of peridotite at 0-15 Kb pressure and the genesis of tholeiitic basalts.
Contrib. Mineral. Petrol. **73**, 287-310.

JAROSEWICH, E., NELEN, J. A. & NORBERG, J. A. (1980):
Reference samples for electron microprobe analysis.
Geostandards Newsletter **4**, 43-47.

JOHNSTON, A. D. & DRAPER, D. S. (1992):
Near-liquidus phase relations of an anhydrous high-magnesia basalts from the Aleutian Islands: implications for arc magma genesis and ascent.
J. Volc. Geotherm. Res. **52**, 27-41.

JOHNSON, M. C. & RUTHERFORD, M. J. (1989):
Experimentally determined compositions in the Fish Canyon Tuff, Colorado, magma chamber.
J. Petrol. **30**, 711-737.

JUREWICZ, A. J. G. & WATSON, E. B. (1988):
Cations in olivine, Part 1: calcium partitioning and calcium-magnesium distribution between olivines and coexisting melts, with petrologic applications.
Contrib. Mineral. Petrol. **99**, 176-185.

KATO, T., RINGWOOD, A. E. & IRIFUNE, T. (1988):
Experimental determination of element partitioning between silicate perovskites, garnets and liquids: constraints on the early differentiation of the mantle.
Earth Planet. Sci. Lett. **89**, 123-145.

KELEMEN, P. B. (1990):
Reaction between ultramafic rock and fractionating basaltic magma I. Phase relations, the origin of calc-alkaline magma series, and the formation of discordant dunite.
J. Petrol. **31**, 51-98.

KELEMEN, P. B., DICK, H. J. B. & QUICK, J. E. (1992):
Formation of harzburgite by pervasive melt/rock reaction in the upper mantle.
Nature **358**, 635-641.

KINZLER, R. J. & GROVE, T. L. (1992a):
Primary magmas of mid-ocean ridge basalts 1. Experiments and methods.
J. Geophys. Res. **97**, 6885-6906.

KINZLER, R. J. & GROVE, T. L. (1992b):
Primary magmas of mid-ocean ridge basalts 2. Applications.
J. Geophys. Res. **97**, 6907-6926.

KRISHNAMURTHY, P. & COX, K. G. (1977):
Picrite basalts and related lavas from the Deccan Traps of Western India.
Contrib. Mineral. Petrol. **62**, 53-75.

KUSHIRO, I. & KUNO, H. (1963):
Origin of primary basalt magmas and classification of basaltic rocks.
J. Petrol. **4**, 75-89.

KUSHIRO, I. & YODER, H. S. (1966):
Anorthite-forsterite and anorthite-enstatite relations and their bearing on the basalt-eclogite transformation.
J. Petrol. **7**, 337-362.

LACROIX, A. (1916):
Sur quelques roches volcaniques mélanocrates des possessions françaises de l'océan Indien et du Pacifique.
C. R. Acad. Sci. **158**, 177-183.

LANGMUIR, C. H. (1989):
Geochemical consequences of in-situ crystallization.
Nature 340, 199-205.

LANGMUIR, C. H., KLEIN, E. M. & PLANK, T. (1992):
Petrological systematics of Mid-Ocean Ridge Basalts: constraints on melt generation beneath ocean ridges. *In* Mantle flow and melt generation at mid-ocean ridges.
AGU Geophysical Monograph 71. (183-280).

LE MAITRE, R. W. (1989):
Numerical petrology - Statistical interpretation of geochemical data
Elsevier, Amsterdam, The Netherlands.

LE MAITRE, R. W., BATEMAN, P., DUDEK, A., KELLER, J., LAMEYRE, J., LE BAS, M. J., SABINE, P. A., SCHMID, R., SØRENSEN, H., STRECKEISEN, A., WOOLLEY, A. R. & ZANETTIN, B. (1989):
A classification of igneous rocks and glossary of terms.
Blackwell, Oxford, U.K.

LESHER, C. M. & ARDNT, A. N. (1995):
REE and Nd isotope geochemistry, petrogenesis and volcanic evolution of contaminated komatiites ant Kambalda, Western Australia.
Lithos **34**, 127-157.

LIANG, Y. & ELTHON, D. (1990):
Evidence from chromium abundances in mantle rocks for the extraction of picrite and komatiite melts.
Nature **343**, 551-553.

MACDONALD, G. A. & POWERS, H. A. (1968):
A further contribution to the petrology of Haleakala volcano, Hawaii.
Geol. Soc. Am. Bull. **79**, 877-888.

MAALØE, S., PEDERSEN, R. B. & JAMES, D. (1988):
Delayed fractionation of basaltic lavas.
Contrib. Mineral. Petrol. **98**, 401-407.

MAALØE, S., SORENSEN, I. & HARTOGEN, J. (1986):
The trachybasaltic suite of Jan Mayen.
J. Petrol. **27**, 439-466.

MALLICK, D. I. J. & ASH, R. (1975):
Geology of the southern Banks Islands.
New Hebrides Geol. Surv. Reg. Rept.

MATTEY, D. P., TYLOR, W. R., GREEN, D. H. & PILLINGER, C. T. (1990):
Carbon isotope fractionation between CO_2 vapour, silicate and carbonate melts: an experimental study to 30 Kbar.
Contrib. Mineral. Petrol. **104**, 492-505.

MAUREL, C. & MAUREL, P. (1982):
Étude expérimentale de la distribution de l'éauilibre Fe^{2+}-Fe^{3+} dans le spinelles chromifères et les liquides silicatés basiques coexistants, à 1 atm.
C. R. Acad. Sc. Paris, **295**, 209-212.

MAUREL, C. & MAUREL, P. (1983):
Influence du fer ferrique sur la distribution de l'aluminium entre bain silicaté basique et spinelle chromifère.
Bull. Minéral. **106**, 623-624.

MIRWALD, P. W., GETTING, I. C. & KENNEDY, G. C. (1975):
Low-friction cell for piston-cylinder high-pressure apparatus.
J. Geophys. Res. **80**, 1519-1525.

MITCHELL, R. S. (1985):
Dictionary of rocks.
Van Nostrand Reinhold, Melbourne, Australia.

MONZIER, M., DANYUSHEVSKY, L. V., CRAWFORD, A. J., BELLON, H. & COTTEN, J. (1993):
High-Mg andesites from the southern termination of the New Hebrides island arc (SW Pacific).
J. Volc. Geotherm. Res. **57**, 193-217.

MORIMOTO, N. (1989):
Nomenclature of pyroxenes.
Can. Mineral. **27**, 143-156.

MORIYAMA, J., KAWABE, I., FUJINO, K. & OHTANI, E. (1992):
Experimental study of element partitioning between majorite, olivine, merwinite, diopside and silicate melts at 16 GPa and 2000°C.
Geochem. J. **26**, 357-382.

MYSEN, B. & BOETTCHER, A. L. (1975a):
Melting of a hydrous mantle: I. Phase relations of natural peridotite at high pressures and temperatures with controlled activities of water, carbon dioxide and hydrogen.
J. Petrol. **16**, 520-548.

MYSEN, B. O. & BOETTCHER, A. (1975b):
Melting of a hydrous mantle: II. Geochemistry of crystals and liquids formed by anatexis of mantle peridotite at high pressures and high temperatures as a function of controlled activities of water, hydrogen and carbon dioxide.
J. Petrol. **16**, 549-593.

MYSEN, B. O. & KUSHIRO, I. (1977):
Compositional variations of coexisting phases with degree of melting of peridotite in the upper mantle.
Am. Mineral. **62**, 843-865.

NAKAMURA, Y. & TATSUMOTO, M. (1988):
Pb, Nd and Sr isotopic evidence for multicomponent source for rocks of Cook-Austral Islands and heterogeneities of mantle plumes.
Geochim. Cosmochim. Acta **52**, 2909-2924.

NICHOLLS, G. D. (1955):
The geology of North-East Jan Mayen.
Geol. Mag. **92**, 127-140.

NIXON, P. H., MITCHELL, R. H. & ROGERS, N. W. (1980):
Petrogenesis of alnöitic rocks from Malaita, Solomon islands, Melanesia.
Min. Mag. **43**, 587-596.

NONO, A., DÉRUELLE, B., DEMAIFFE, D. & KAMBOU, R. (1994):
Tchabal Nganha volcano in Adamawa (Cameroon): petrology of a continental alkaline lava series.
J. Volc. Geotherm. Res. **60**, 147-178.

OHTANI, E., NAGATA, Y., SUZUKI, A. & KATO, T. (1995):
Melting relations of peridotite and the density crossover in planetary mantles.
Chem. Geol. **120**, 207-221.

PATTINSON, D. R. M. (1994):
Are reversed Fe-Mg exchange and solid solution experiments really reversed?
Am. Min. **79**, 938-950.

PERFIT, M. R., GUST, D. A., BENCE, A. E., ARCULUS, R. J. & TAYLOR, S. R. (1980):
Chemical characteristics of island-arc basalts: implications for mantle sources.
Chem. Geol. **30**, 227-256.

RÅHEIM, A. & GREEN, D. H. (1974):
Experimental petrology of lunar highland basalt composition and applications to models for the lunar interior.
J. Petrol. **82**, 607-622.

RAMSAY, W. R. H, CRAWFORD, A. J. & FODEN, J. D. (1984):
Field setting, mineralogy, chemistry and genesis of arc picrites, New Georgia, Solomon Islands.
Contrib. Mineral. Petrol. **88** 386-402.

ROBINSON, P. (1980):
The composition space of terrestrial pyroxenes - internal and external limits. *In* Pyroxenes (C.T. Prewitt, ed.).
Rev. Mineral. **7**, (419-494).

ROEDDER, E. (1971):
Natural and laboratory crystallization of lunar glasses from Apollo 11.
Mineral. Soc. Japan, Spec. Paper **1**, 5-12.

ROEDDER, E. (1979):
Origin and significance of magmatic inclusion.
Bull. Minéral. **102**, 487-510.

ROEDDER, E. (1984):
Fluid inclusions.
Rev. Mineral. **12.**

ROEDDER, E. & WEIBLEN, P.W. (1972):
Silicate melt inclusions and glasses in lunar soil fragments from the Luna 16 core sample.
Earth Planet. Sci. Lett. **13**, 272-285.

ROEDER, P.L. & EMSLIE, R.F. (1970):
Olivine-liquid equilibrium.
Contrib. Mineral. Petrol. **29**, 275-289.

ROMICK, J. D., PERFIT, M. R., SWANSON, S. E. & SHUSTER, R. D. (1990):
Magamatism in the Eastern Alleutian arc: temporal characteristics of igneous activity on Akutan island.
Contrib. Mineral. Petrol. **104**, 700-721.

SATO, H., TCHOUA, F. & KUSAKABE, M. (1991):
Olivine phenocrysts in some Cameroonian basalts - Implications for primary magma composition.
Mineral. Petrol. **44**, 253-269.

SHIBATA, T. (1976):
Phenocryst-bulk rock composition relations of abyssal tholeiites and their petrogenetic significance.
Geochim. Cosmochim. Acta **40**, 1407-1417.

SHERATON, J. S., BLANCK, L. P., MCCULLOCH, M. T. & OLIVER, R. L. (1990):
Age and origin of a compositionally varied mafic dyke swarm in the Bunger Hills, East Antarctica.
Chem. Geol. **85**, 215-246.

SIGURDSSON, I. A. (1994):
Primitive magmas in convergent margins and at oceanic spreading ridges: evidence from early formed phenocryst phases and their melt inclusions.
Ph.D. thesis, University of Tasmania, Hobart.

SIGURDSSON, H. & SCHILLING, J. G. (1976):
Spinels in Mid-Atlantic ridge basalts: chemistry and occurrence.
Earth Planet. Sci. Lett. **29**, 7-20.

SISSON, T. W. & LAYNE, G. D. (1993):
H_2O in basalt and basaltic andesite glass inclusions from four subduction-related volcanoes.
Earth Planet. Sci. Lett. **117**, 619-635.

SIVELL, W. & RANKIN, P. (1983):
Arc-tholeiite and ultramafic cumulate, Brook Street volcanics, west D'Urville island, New Zealand.
N. Z. J. Geol. Geophys. **26**, 239-257.

SIVELL, W. J. & WATERHOUSE, J. B. (1988):
Petrogenesis of Gympie Group volcanics: evidence for remnants of an early Permian arc in eastern Australia.
Lithos **21**, 81-95.

SMITH, H. S. & ERLANK, A. J. (1982):
Geochemistry and petrogenesis of komatiites from the Barberton greenstone belt, South Africa. *In* Komatiites (N.T. Arndt & E.G. Nisbet, eds.).
Allen & Unwin, London, U.K. (347-397).

SOBOLEV, A. V. & DANYUSHEVSKY, L. V. (1994):
Petrology and geochemistry of the high-Ca boninite primary magmas: evidence from the north Tonga trench.
J. Petrol. **35**, 1183-1211.

SOBOLEV, A. V., DMITRIEV, L. V., BARUSKOV, V. L., NEVSOROV, V. N. & SLUTSKY, A. B. (1980):
The formation conditions of the high-magnesium olivines from the monomineralic fraction of Luna 24 regolith. *In* Proceedings of the 11th Lunar Science Conference (105-116).

SOBOLEV, A. V., DMITRIEV, L. V., TSAMERYAN, O. P., KONONKOVA, N. N. & ROBINSON, P. T. (1991):
A possible primary melt composition for the ultramafic lavas on the Margi Area, Troodos Ophiolite, Cyprus. *In* Cyprus crustal study project: Initial report, Holes CY-I and IA (I.L. Gibson, J. Malpas, P.T. Robinson & C. Xenophontos, eds.).
Geol. Surv. Can., Pap. **90-20**, 203-218.

SOBOLEV, A. V., KAMENETSKY, V. S. & KONONKOVA, N. N. (1989):
New data on the petrology and geochemistry of the ultramafic volcanites of Valayinskiy Range, eastern Kamchatka.
Geokhimiya **12**, 1694-1709 (in Russ).

SOBOLEV, A. V., KAMENETSKY, V. S., METRICH, N., CLOCCHIATTI, N. N., DEVIRTS, A. L. & USTINOW, V. I. (1990):
Volatile regime and crystallization conditions in Etna Hawaiite lavas.
Geochem. Int. **28**, 53-65.

SPRAY, J. G. & RAE, D. A. (1995):
Quantitative electron-microprobe analysis of alkali silicate glasses: A review and user guide.
Can. Mineral. **33**, 323-332.

STAUDIGEL, H. & BRYAN. W. B. (1981):
Contrasted glass-whole rock compositions and phenocryst re-distribution ODP Sites 417 and 418.
Contrib. Mineral. Petrol. **78**, 255-262.

STERN, C. R. & WYLLIE, P. J. (1975):
Effect of iron absorption by noble-metal capsules on phase boundaries in rock-melting experiments at 30 kilobars.
Am. Mineral. **60**, 681-689.

STORMER, J. C. Jr. (1973):
Calcium zoning in olivine and its relationship to silica activity and pressure.
Geochim. Cosmochim. Acta **37**, 1815-1821.

SULLIVAN, G. E. (1991):
Chemical evolution of basalts from 23°N along the mid-Atlantic ridge: evidence from melt inclusions.
Contrib. Mineral. Petrol. **106**, 296-308.

SUN S.-S. & MCDONOUGH W.F. (1989):
Chemical and isotopic systematics of oceanic basalts: implications for mantle composition and processes. *In* Magmatism in the ocean basins (A.D. Saunders & M. J. Norry, eds.).
Geol. Soc., Spec. Publ. **42**, 313-345.

TAIT, S. (1992):
Selective preservation of melt inclusions in igneous phenocrysts.
Am. Mineral. **77**, 146-155.

TAKAHASHI, E. (1986):
Melting of a dry peridotite KLB-1 up to 14 GPa: Implications on the origin of peridotite upper mantle.
J. Geophys. Res. **91**, 9367-9382.

TAYLOR, W. R. & GREEN, D. H. (1987):
The petrogenetic role of methane: Effect on liquidus phase relations and the solubility mechanism of reduced C-H volatiles. *In* Magmatic processes: Physicochemical principles (B.O. Mysen, ed.).
Geochem. Soc., Spec. Publ. **1**, 121-138.

TELFORD, W. M., GELDART, L. P., SHERIFF, R. E. & KEYS, D. A. (1976):
Applied geophysics.
Cambridge University press, New York, N. Y.

THIBAULT, Y. & HOLLOWAY, J. R. (1994):
Solubility of CO_2 in a Ca-rich leucitite: effects of pressure, temperature and oxygen fugacity.
Contrib. Mineral. Petrol. **116**, 216-224.

THIRWALL, M. F. & GRAHAM A. M. (1984):
Evolution of high-Ca, high-Sr C-series basalts from Grenada, Lesser Antilles: the effects of intra-crustal contamination.
J. Geol. Soc. London **141**, 427-445.

THOMPSON, R. N. & FLOWER, F. J. (1971):
Evidence for upper-crust ankaramitic liquids.
Am. Geophys. Union Trans. **52**, 377 (abstr.).

THØRNNES, R. G. (1990):
Basaltic melt evolution of the Hengill volcanic system, SW Iceland, and evidence for clinopyroxene assimilation in primitive tholeiitic magmas.
J. Geophys. Res. **95**, 15893-15910.

THY, P. (1991):
High and low pressure phase equilibria of a mildly alkalic lava from the 1965 Surtsey eruption: Experimental results.
Lithos **26**, 223-243.

TRØNNES, R. G., CANIL, D. & WEI, K. (1992):
Element partitioning between silicate minerals and coexisting melts at pressures of 1 - 27 GPa, and implications for mantle evolution.
Earth Planet. Sci. Lett. **111**, 241-255.

TOMKEIEFF, S. I. (1983):
Dictionary of petrology.
J. Wiley & Sons, Chichester, U.K.

VARNE, R. & FODEN, J. D. (1986):
Geochemical and isotopic systematics of eastern Sunda arc volcanics: implications for mantle sources and mantle mixing processes. *In* The origin of arcs (F. C. Wezel, ed.).
Elsevier, Amsterdam, The Netherlands (159-185).

WATSON, E.B. (1976):
Glass inclusions as samples of early magmatic liquid: determinative method and application to a South Atlantic basalt.
J. Volc. Geotherm. Res. **1**, 73-84.

WALKER, D., KIRKPATRICK, R. J., LONGHI, J. & HAYS, J. F. (1976):
Crystallization history of lunar picritic basalt sample 12002: Phase-equilibria and cooling rates.
Geol. Soc. Am. Bull. **87**, 646-656.

WALKER, D., SHIBATA, T. & DELONG, S. (1979):
Abyssal tholeiites from the Oceanographer fracture zone.
Contrib. Mineral. Petrol. **70**, 111-125.

WARDEN, A. J. (1970):
Evolution of Aoba caldera volcano, New Hebrides.
Bull. Volc. 34, 107-143

WEI, K., TRØNNES, R. G. & SCARFE, C. M. (1990):
Phase relations of aluminium-undepleted and aluminium-depleted komatiites at pressures of 4 - 12 GPa.
J. Geophys. Res. **95**, 15817-15827.

WEIBLEN, P. W. (1977):
Examination of the liquid line of descent of mare basalts in light of data from melt inclusions in olivine.
Proc. 8th Lunar Sci. Conf. (1751-1765).

WENDLANDT, R. F. & MYSEN, B. O. (1980):
Melting phase relations of natural peridotite + CO_2 as a function of degree of partial melting at 15 and 30 Kbar.
Am. Mineral. **65**, 37-44.

WHELLER, G. E. (1986):
Petrogenesis of Batur caldera, Bali and the geochemistry of Sunda-Banda arc basalts.
Ph.D. thesis, University of Tasmania, Hobart, Australia.

WHELLER, G. E. VARNE, R. FODEN, J. D. & ABBOT, M. J. (1987):
Geochemistry of quaternary volcanism in the Sunda-Banda arc, Indonesia, and three-component genesis of island-arc basaltic magmas.
J. Volc. Geotherm. Res. **32**, 137-160.

WHITFORD, D. J. (1975):
Geochemistry and petrology of volcanic rocks from the Sunda Arc, Indonesia.
Ph. D. thesis, Australian National University, Canberra, Australia.

WHITFORD, D. J., NICHOLS, I. A. & TAYLOR, S. R. (1979):
Spatial variations in the geochemistry of quaternary lavas across the Sunda arc in Java and Bali.
Contrib. Mineral. Petrol. **70**, 341-356.

WILKINSON, J. F. G. (1991):
Manua Loan and Kilauean tholeiites with low ferromagnesian fractionated (100Mg/Mg+Fe^{2+}) ratios: Primary liquids from the upper mantle?
J. Petrol. **32**, 863-907.

WILLIAMS, K. L., ROCK N. M. S. & CARROLL, G. W. (1990):
SPINEL and SPINELTAB: Macintosh programs to plot spinel analyses in the oxidized (magnetite) and reduced (ulvöspinel) prisms.
Am. Mineral. **75**, 1428-1430.

WOOD, D. A. (1978):
Major and trace element variations in the Tertiary lavas of eastern Iceland and their significance with respect to the Iceland geochemical anomaly.
J. Petrol. **19**, 393-436.

WYLLIE, P. J. & HUANG, W. L. (1976):
High CO_2 solubilities in mantle magmas.
Geology **4**, 21-24.

Appendix 1

Appendix 1.1

A1.1a Compiled analyses of reported ankaramite rocks.

	Sample no.	Location	SiO_2	TiO_2	Al_2O_3	FeO	MgO	CaO	MnO	Na_2O	K_2O	P_2O_5	TOTAL	Mg^a	CaO/Al_2O_3
1	5	North Johore	47.74	0.97	8.98	10.48	10.59	11.96	0.18	1.31	3.78	0.44	96.43	64.3	1.33
2	JM1	Jan Majen	47.57	1.83	8.98	8.41	15.19	14.00	0.12	1.51	1.00	0.23	98.84	76.3	1.56
3	JM2	Jan Majen	47.46	1.98	10.30	8.78	13.54	13.52	0.13	1.61	1.07	0.27	98.66	73.4	1.31
4	JM3	Jan Majen	47.65	2.02	10.35	8.53	13.29	13.76	0.13	1.61	1.01	0.25	98.60	73.6	1.33
5	BC13	Merelava, Vanuatu	50.20	0.46	10.30	8.06	13.71	13.69	0.17	1.60	0.38	0.05	98.62	75.2	1.33
6	UTas71041	Epi, Vanuatu	47.80	0.43	13.60	9.50	10.70	14.20	0.18	1.29	0.09	0.09	97.88	66.8	1.04
7	UTas71065	Epi, Vanuatu	48.00	0.45	13.90	9.50	11.20	13.50	0.18	1.55	0.05	0.05	98.38	67.8	0.97
8	UTas71046	Epi, Vanuatu	48.20	0.39	11.50	8.90	13.50	14.40	0.16	1.05	0.07	0.07	98.24	73.0	1.25
9	UTas71042	Epi, Vanuatu	48.20	0.45	13.80	9.71	10.50	14.20	0.17	1.26	0.07	0.07	98.43	65.9	1.03
10	5	Hawaii, Manua Kea	46.72	2.83	10.66	12.96	12.57	9.62	0.20	2.20	0.71	0.34	98.81	63.4	0.90
11	O231	D'Urville Is, NZ.	50.59	0.63	10.13	8.66	16.18	11.03	0.16	1.88	0.29	0.19	99.74	76.9	1.09
12	2	Ankaramy, Madagascar	43.27	1.25	7.54	8.27	17.65	13.72		1.26	1.14	0.49	94.59	79.2	1.82
13	4B	Nganha, Cameroon	39.69	4.14	12.92	12.72	10.38	11.92	0.18	2.61	0.83	1.23	96.62	59.3	0.92
14	220	Nganha, Cameroon	41.84	3.23	11.49	11.71	11.53	12.31	0.20	2.32	0.52	0.62	95.77	63.7	1.07
15	5823	Bunger Hills	43.90	1.82	7.33	12.09	16.58	12.47	0.18	1.50	0.55	0.18	96.60	71.0	1.70
16	5688	Bunger Hills	41.90	2.68	10.41	14.00	12.41	10.10	0.20	2.43	1.06	0.39	95.58	61.3	0.97
17	ms1	Mecsek Mt, Hungary	44.39	3.39	13.29	11.87	11.11	9.78	0.17	2.82	1.08	0.60	98.50	62.6	0.74
18	AJ35	Anjouan, Comores Arch.	47.33	2.26	10.52	11.85	11.97	12.30	0.18	1.99	0.75	0.39	99.54	64.3	1.17
19	CE0021	East Is., Crozet Arch.	45.26	2.58	11.23	11.46	13.47	12.00	0.16	2.21	0.95	0.37	99.69	67.7	1.07
20	D209d	Marcus-Wake Rise	45.81	2.33	7.26	9.58	13.78	15.95	0.16	0.88	0.35	0.54	96.64	72.0	2.20
21	D900/1	Marcus-Wake Rise	44.54	2.94	8.40	11.29	11.22	15.18	0.18	1.58	0.52	0.44	96.29	64.0	1.81
22	B43	Sangean Api, Sunda arc	47.77	0.81	13.05	9.41	8.65	13.90	0.17	3.79	1.85	0.44	99.84	62.1	1.07
23	UTas48001	Lombok, Sunda arc	48.39	0.69	10.55	9.20	14.04	14.40	0.17	1.50	0.90	0.15	99.99	73.2	1.36
24	UTas67424	Bali, Sunda arc	46.44	0.56	9.12	10.30	17.48	11.78	0.20	1.22	0.61	0.21	97.92	75.2	1.29

A1.1b Compiled analyses of reported picrite rocks.

	Sample #	location	SiO_2	TiO_2	Al_2O_3	FeO	MgO	CaO	MnO	Na_2O	K_2O	P_2O_5	TOTAL	Mg^a	CaO/Al_2O_3
25	498	Aoba	46.38	0.47	8.84	10.35	22.61	8.53	0.21	1.43	0.81	0.21	99.84	79.6	0.97
26	531	Aoba	47.26	0.59	10.70	10.24	16.19	11.94	0.21	1.67	0.85	0.17	99.82	73.8	1.12
27	576	Aoba	48.93	0.74	13.49	9.99	11.08	11.64	0.21	2.34	1.18	0.18	99.78	66.4	0.86
28	507	Aoba	49.67	0.81	15.42	10.04	8.31	10.87	0.20	2.73	1.52	0.26	99.83	59.6	0.71
29	1567	Ambrym	48.92	0.63	13.40	9.37	11.50	11.96	0.20	1.99	1.03	0.17	99.17	68.7	0.89
30	1569	Ambrym	52.43	1.07	16.74	11.67	4.13	9.13	0.23	3.24	0.97	0.17	99.78	38.7	0.55
31	thol	Ambrym	49.36	2.50	13.94	11.23	8.44	10.30	0.16	2.13	0.38	0.26	98.70	57.3	0.74
32	R-44692	Solomon	45.70	0.35	7.20	9.54	25.20	8.00	0.18	1.32	0.83	0.18	98.50	82.5	1.11
33	R-44691	Solomon	47.10	0.37	8.90	9.37	23.00	7.90	0.20	1.30	0.82	0.17	99.13	81.4	0.89
34	R-44679	Solomon	47.10	0.46	9.70	9.11	21.00	8.30	0.20	1.43	0.76	0.22	98.28	80.5	0.86
35	R-44688	Solomon	48.40	0.47	9.80	10.26	15.70	9.90	0.20	2.06	1.35	0.28	98.42	73.2	1.01
36	R-44682	Solomon	48.60	0.50	11.20	12.05	12.00	10.40	0.18	1.88	1.22	0.31	98.34	64.0	0.93
37	6	Hawaii, Manua Kea	44.43	2.52	10.47	12.90	15.90	8.82	0.19	1.74	0.32	0.31	97.60	68.8	0.84
38	3	Hawaii, Manua Kea	44.38	1.55	7.63	11.97	24.24	7.38	0.19	1.08	0.08	0.16	98.66	78.3	0.97
39	5954	Bunger Hills	42.60	2.40	8.79	12.58	15.59	8.78	0.18	2.09	1.47	0.41	94.89	68.9	1.00
40	2	Atiu, Cook Is	45.54	2.26	11.94	11.05	13.39	10.30	0.20	2.46	0.91	0.17	98.22	68.4	0.86
41	G20	Gaua	46.50	0.74	11.36	10.45	14.81	11.78	0.26	2.04	0.60	0.15	98.69	71.7	1.04
42	5954	Bunger Hill	42.60	2.40	8.79	12.09	15.59	8.78	0.18	2.09	1.47	0.41	94.40	69.7	1.00
43	EG670	Vanuatu	49.13	0.52	11.13	9.18	17.37	10.50	0.21	1.54	0.31		99.89	77.2	0.94
44	EG71065	Vanuatu	46.32	0.02	12.43	10.18	19.19	9.98	0.19	1.34	0.28		99.93	77.1	0.80
45	EG4DI-E	Vanuatu	47.44	0.38	11.78	9.38	17.76	11.45	0.17	1.31	0.29		99.96	77.2	0.97
46	EG698	Vanuatu	47.77	0.40	12.79	9.13	17.31	10.55	0.17	1.26	0.55		99.93	77.2	0.83
47	EGAYC55	Vanuatu	48.60	0.53	10.52	9.98	18.81	9.04	0.19	1.53	0.65		99.85	77.1	0.86
48	EGG20	Vanuatu	48.52	0.46	10.47	9.72	18.26	10.27	0.17	1.32	0.66		99.85	77.0	0.98
49	EG68638	Vanuatu	46.46	0.66	10.22	10.27	19.04	10.60	0.25	1.83	0.54		99.87	76.8	1.04
50	EG1567	Vanuatu	47.81	0.53	10.76	9.82	18.31	9.86	0.17	1.77	0.81		99.84	76.9	0.92
51	EG68567	Vanuatu	47.64	0.52	11.11	9.79	18.20	9.91	0.19	1.64	0.85		99.85	76.9	0.89
52	EGFMAC18	Vanuatu	47.13	0.54	10.21	9.91	18.54	10.43	0.19	1.29	1.42		99.66	77.0	1.02
53	EG68578	Vanuatu	49.97	0.95	14.17	10.69	10.17	10.57	0.15	2.45	0.67		99.79	62.9	0.75

Arch.=archipelago. Molecular CIPWnorm calculated with all oxides summed to 100, with all iron as FeO*.

Appendix 1.1 (continued)

	or	ab	an	ne	lc	di	hy	ol	cs	ilm	ap	di/ol	Mineralogy	Source
1	16.50		5.94	9.37	1.30	39.04		24.70		2.69	0.46	1.58	cpx_{80}, ol_7	Grubb (1965)
2	4.43	5.22	11.08	4.95		39.91		29.39		4.78	0.23	1.36	cpx_{57}, ol_{36}, plg_{54}	Maaløe *et al.* (1986)
3	4.86	7.29	13.62	3.82		36.59		28.25		5.30	0.27	1.30	cpx_{72}, ol_7	Maaløe *et al.* (1986)
4	4.62	7.81	13.95	3.37		37.61		26.95		5.44	0.25	1.40	cpx_{28}, ol_{11}	Maaløe *et al.* (1986)
5	1.68	10.78	14.85			35.85	13.31	22.27		1.20	0.05	1.61	cxp_{46}, ol_8	Barsdell (1988)
6	0.41	8.99	24.10			30.11	15.13	20.00		1.16	0.09	1.51	abundant cpx	Barsdell & Berry (1990)
7	0.23	10.80	23.93			27.81	11.83	24.13		1.22	0.05	1.15	abundant cpx	Barsdell & Berry (1990)
8	0.31	7.04	19.75			33.23	15.67	22.92		1.01	0.07	1.45	cpx_{78}, ol_{28}	Barsdell & Berry (1990)
9	0.31	8.61	24.19			29.07	19.08	17.47		1.19	0.07	1.66	abundant cpx	Barsdell & Berry (1990)
10	3.15	14.82	12.85			21.31	5.61	34.53		7.40	0.33	0.62	ol_{13}, cpx_{14}	Frey *et al.* (1991)
11	1.17	11.56	12.56			24.06	23.63	25.34		1.50	0.17	0.95	cpx>ol>plg	Sivell & Rankin (1983)
12			8.49	8.32	4.95	37.55		36.19	0.83	3.20	0.47	1.04	cpx>ol	Dawson et al. (1970)
13	3.66	1.81	15.73	15.67		22.39		28.79		10.75	1.20	0.78	cpx_{24}, ol_2, hnb_{31}	Nono *et al.* (1994)
14	2.34	4.27	14.76	11.58		28.63		29.24		8.56	0.62	0.98	cpx_{56}, ol_{12}	Nono *et al.* (1994)
15	2.37	1.96	8.48	7.85		35.73		38.82		4.62	0.17	0.92	$cpx_{20\text{-}50}$, $ol_{5\text{-}20}$	Sheraton *et al.* (1990)
16	4.65	3.43	10.68	12.79		24.67		36.47		6.94	0.38	0.68	$cpx_{20\text{-}50}$, $ol_{5\text{-}20}$	Sheraton *et al.* (1990)
17	4.81	10.64	15.40	8.46		18.25		32.94		8.91	0.59	0.55	$cpx_{20\text{-}25}$, $ol_{10\text{-}15}$	Harangi (1994)
18	3.43	11.92	13.57	1.89		31.63		31.09		6.08	0.39	1.02	cpx_{30}, ol_{44}, plg_{26}	Thompson & Flower (1971)
19	4.10	5.02	13.08	9.47		28.63		32.79		6.56	0.35	0.87	cpx>ol	Gunn *et al.* (1970)
20	1.64	5.87	11.73	0.38		48.09		25.31		6.42	0.56	1.90	$cxp_{15\text{-}50}$, ol<20	Govorov *et al.* (1994)
21	2.41	4.41	11.23	6.74		45.69		21.02		8.04	0.45	2.17	$cxp_{15\text{-}50}$, ol<20	Govorov *et al.* (1994)
22	8.10	0.63	9.73	24.59		39.24		15.21		2.09	0.43	2.58	cpx_{13}, ol_7	Foden (1979)
23	4.04	5.24	14.70	4.99		38.78		30.26		1.83	0.16	1.28	cpx_{37}, ol_{12}, plg_{46}	Foden (1983)
24	2.69	7.16	13.16	1.02		29.49		44.81		1.46	0.21	0.66	cpx_{38}, ol_{14}	Wheller (1986)

	or	ab	an	ne	lc	di	hy	ol	cs	ilm	ap	di/ol	Mineralogy	Source
25	3.29	7.16	10.53	1.67		17.64		58.38		1.13	0.19	0.30	olv_{35}	Gorton (1977)
26	3.69	6.21	14.11	4.81		28.62		40.89		1.51	0.16	0.70	olv-bearing	Gorton (1977)
27	5.48	12.45	17.94	4.07		26.54		31.32		2.03	0.19	0.85	olv-bearing	Gorton (1977)
28	7.33	16.50	20.67	3.51		21.95		27.47		2.30	0.28	0.80	olv-bearing	Gorton (1977)
29	4.87	13.47	19.69	0.84		26.93		32.27		1.76	0.18	0.83	olv-bearing	Gorton (1977)
30	4.31	21.89	21.27			11.98	33.81	3.77		2.80	0.17	3.18	olv-bearing	Gorton (1977)
31	1.54	13.15	18.80			15.16	41.03	4.10		5.98	0.23	3.69	olv-bearing	Gorton (1977)
32	3.31	5.55	7.60	2.44		18.37		61.75		0.82	0.16	0.30	ol_{36}, cpx_{10}	Ramsay *et al.* (1984)
33	3.26	7.86	10.79			14.85	8.26	53.95		0.87	0.15	0.28	ol_{30}, cpx_7	Ramsay *et al.* (1984)
34	3.08	8.82	12.23			15.07	10.83	48.67		1.10	0.20	0.31	ol_{32}, cpx_4	Ramsay *et al.* (1984)
35	6.02	11.47	10.19	2.49		25.50		42.82		1.24	0.28	0.60	ol_{22}, cpx_7	Ramsay *et al.* (1984)
36	5.57	13.04	14.31			23.99	7.62	33.82		1.35	0.31	0.71	ol_{16}, cpx_{22}, plg_{21}	Ramsay *et al.* (1984)
37	1.37	11.31	14.34			15.87	7.02	43.45		6.35	0.29	0.37	ol_{21}	Frey *et al.* (1991)
38	0.31	6.25	10.14			12.78	11.93	54.99		3.48	0.14	0.23	ol_{33}	Frey et al. (1991)
39	6.37	4.27	7.53	9.50		22.47		43.32		6.13	0.39	0.52	ol>cpx	Sheraton *et al.* (1990)
40	4.01	9.02	14.06	7.46		23.23		36.18		5.87	0.17	0.64	ol	Wood (1978)
41	2.65	7.30	14.98	6.37		27.91		38.72		1.92	0.15	0.72	cpx_4, ol_{23}	Barsdell (1980)
42	6.42	4.65	7.58	9.21		22.63		42.93		6.18	0.40	0.53	ol>cpx	Sheraton *et al.* (1990)
43	1.20	8.47	19.58	0.22		16.20		54.28		0.05		0.30	ol>cpx	Eggins (1989)
44	1.25	8.59	18.50			22.89	3.13	44.66		0.97		0.51	ol>cpx	Eggins (1989)
45	2.31	8.04	19.56			17.55	11.41	40.15		0.99		0.44	ol>cpx	Eggins (1989)
46	2.62	9.38	13.55			17.01	15.35	40.83		1.26		0.42	ol>cpx	Eggins (1989)
47	2.72	8.26	14.39			21.07	12.71	39.73		1.12		0.53	ol>cpx	Eggins (1989)
48	2.25	5.71	12.68	5.88		24.28		47.59		1.62		0.51	ol>cpx	Eggins (1989)
49	3.47	9.62	13.76	1.91		21.65		48.25		1.34		0.45	ol>cpx	Eggins (1989)
50	3.66	9.26	14.83	1.46		20.90		48.58		1.32		0.43	ol>cpx	Eggins (1989)
51	6.04	4.37	12.82	3.96		24.33		47.13		1.35		0.52	ol>cpx	Eggins (1989)
52	3.04	16.88	19.70			20.53	11.62	25.68		2.55		0.80	ol>cpx	Eggins (1989)
53	2.87	10.23	17.11	1.39		22.35		43.66		2.40		0.51	ol>cpx	Eggins (1989)

Numbers in *mineralogy* column indicate modal proportion of phenocrysts phases.

Appendix 2

Appendix 2.1
Analytical details

A2.1a Electron microprobe analyses

All analyses were performed from epoxy grain mounts using a CAMECA SX-50 electron microprobe (Central Science Laboratory, University of Tasmania) calibrated with natural glass and mineral standards listed in Table A2.1a (Jarosewich *et al.* 1980). Concentrations were calculated from relative peak intensities using the PAP matrix correction procedure that is incorporated into the Cameca software.

Table A2.1a Natural standards

Olivine, San Carlos		USNM 111312/444
Fayalite, Rockport		USNM 85276
Basaltic glass, Makaopuhi Lava Lake	VG-A99	USNM 113498/1
Basaltic glass, Juan de Fuca Ridge	VG-2	USNM 111249/52
Plagioclase, Lake Country		USNM 115900
Augite, Kakanui, NZ.		USNM 122142
Chromite, Tiebaghi Mine, NC.		USNM 117075

Routine analytical labels used for most microprobe analyses are given in Table A2.1b together with their corresponding analytical conditions and counting times. A multi-purpose analytical label "MISCELLAN" was also used in which all elements were analyzed at 20 seconds on the peak and 10 seconds on the background except for Si and Na that were analysed at 10 and 5 seconds.

Analytical conditions for the analyses of olivine and clinopyroxene phenocrysts as well as experimental crystal phases were 15 kV accelerating voltage, 20 nA beam current, and 1-2 μm beam size. Mineral inclusions in phenocrysts were analysed as pairs with the coexisting host, separated by a distance of approximately 20 to 30μm. Most crystal phases in high pressure experiments were analyzed using the MISCELLAN label.

Some olivine phenocrysts analysed with the MISCELLAN label were re-analyzed for trace elements Ca, Ni, Mn and Cr using the analytical label "KSPCOLTR" to confirm accuracy of analyses. The "KSPCOLTR" label was programmed with longer counting times (120 seconds), 200 nA beam current, 20 kV accelerating voltage and a 20-μm beam size (Table A2.1b). This label however has a matrix correction based on the San Carlos Olivine composition and therefore Fo contents cannot be determined. These analyses nonetheless confirm that CaO variations in olivine phenocrysts from Rinjani and Ulakan ankaramite suites are related to the onset of clinopyroxene crystallization(Figure 2.6a-b). The correlation between measured Ca, Ni and Mn contents in olivine with KSPCOLTR and MISCELLAN analytical labels indicate that the later yields reliable analyses under normal operating conditions (Figure A2.1a).

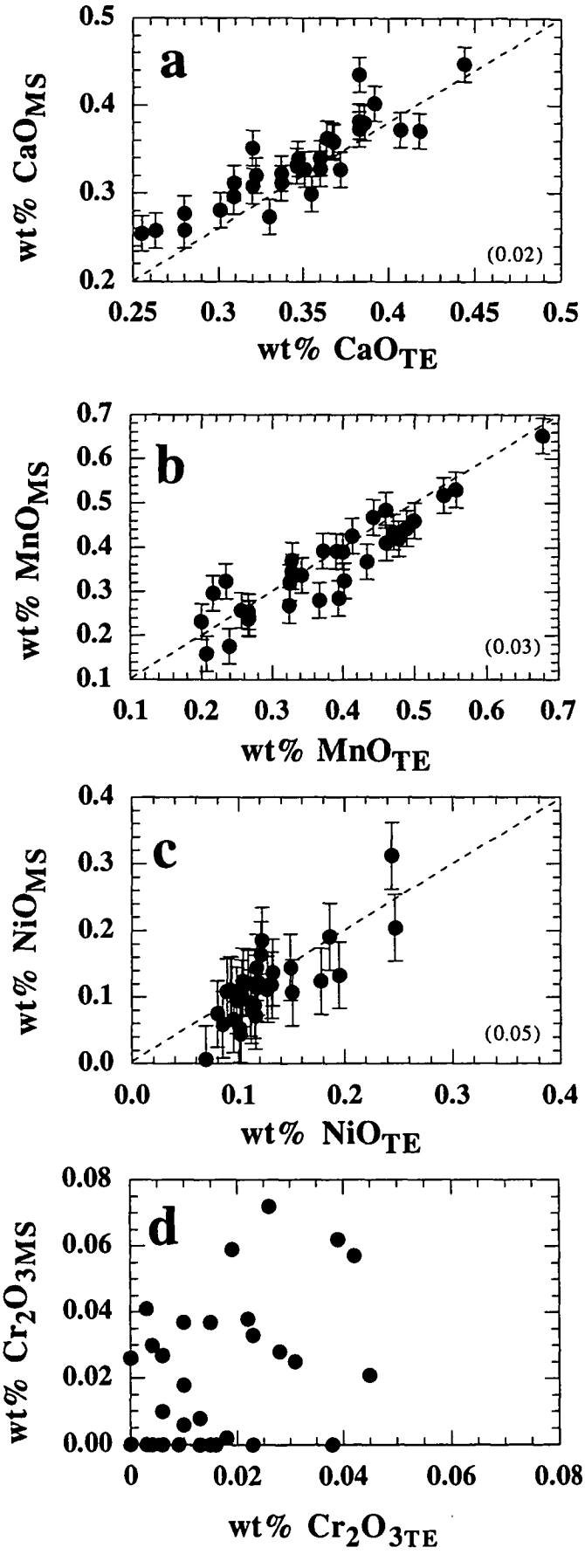

Figure A2.1a Comparison of measured CaO, MnO, NiO and Cr_2O_3 contents in olivine phenocrysts using the "MISCELLAN" (MS) and "KSPCOLTR" (TE) analytical labels. Dashed line indicates 1:1 relationship. Numbers in brackets indicate error bar amplitude. Data from Appendix 2.5.

Analytical conditions for glass analyses were 15 kV accelerating voltage and 10 nA beam current. Glasses from experimental runs were analyzed with a 10 μm beam size. For melt inclusion glasses, the beam size was varied between 2 to 10 μm depending on the size of the melt inclusion. A detailed assessment of volatilization in glasses under these operating conditions is discussed in Section 3.3.3.

TABLE A2.1b Analytical label conditions.

Phase	olivine	olivine	pyroxene	olivine	spinel	glass	multi-purpose
Label	DIMA	OLIVINE	LEOPYR	KSPCOLTR	UVSPLEO	GLASSLEO	MISCELLAN
Peak/background counting times							
SiO_2	10/5	10/5	10/5		10/5	10/5	10/5
TiO2			10/5		20/10	10/5	20/10
Al2O3			10/5		20/10	20/10	20/10
FeO	10/5	20/10	20/10		20/10	20/10	20/10
MnO		20/10	20/10	120/60	20/10	20/10	20/10
MgO	10/5	10/5	10/5		10/5	10/5	20/10
CaO	10/5	20/10	10/5	120/60		10/5	20/10
Na_2O			20/10			20/10	10/5
K_2O						20/10	20/10
P_2O_5						20/10	20/10
Cr_2O_3		20/10	20/10	120/60	10/10	20/10	20/10
NiO		20/10		120/60	10/10		20/10
ZnO					10/10		20/10
Analytical conditions							
V (kV)		15	15	20	15	15	15
I (nA)		20	20	200	20	10	10 or 20[1]
Ø (μm)		1-2	1-2	20	1	5-10	1-10

V=accelerating voltage, I=beam current, Ø=beam size, Peak and background times are in seconds, ([1]) 10nA for glasses and 20nA for minerals

A2.1b Wholerock trace and rare earth elements

Rock samples were crushed in a steel jaw-crusher and the fragments hand picked and recrushed in a tungsten carbide mill. This powder fraction was analysed for Ba, Th, Hf, Ta and REE by INAA at the Becquerel Laboratories, Lucas Heights research Laboratories, NSW (Dr Helen Waldron, analyst). Detection limits are listed in Table A2.1c and actual analyses in Table 2.1b.

A2.1c Elemental analyses for CO_2 and H_2O

Near liquidus experimental glasses (Chapter 5) were analysed for their CO_2 and H_2O content using a Carlo Erba Elemental Analyser EA1108 at the Central Science Laboratory, University of Tasmania (Dr. Graham Rowbottom, analyst).

A2.1d Laser Raman Specroscopy

Primary fluid inclusions in olivine phenocrysts were scanned for CO_2 and CH_4 using a DILOR MICRODIL-28® Raman microprobe at the Australian Geological Survey Organisation (AGSO), Canberra (Dr. Khin Zaw, analyst).

TABLE A2.1c Detection limits of INAA

Element	Detection limit (ppm)
Ba	50
La	0.1
Ce	1.0
Nd	2.0
Sm	0.05
Eu	0.1
Tb	0.5
Ho	0.5
Yb	0.1
Lu	0.05
Th	0.2
Hf	0.2
Ta	0.5

Appendix 2.2

Electron microprobe analyses of olivine phenocrysts

2.2a Rinjani ankaramite suite, sample UTas48001

Sample	48001	48001	48001	48001	48001	48001	48001	48001	48001	48001	48001	48001
Grain	1	2	3	4	5	6	7	8	9	10	11	12
SiO_2	40.23	40.59	40.31	40.43	40.18	38.86	40.24	40.67	40.67	38.11	39.51	40.57
MgO	47.00	47.92	47.34	47.08	45.47	41.21	47.08	48.90	48.25	37.92	42.32	48.51
CaO	0.42	0.45	0.36	0.44	0.49	0.34	0.35	0.24	0.35	0.36	0.37	0.33
MnO	n/a	n/a	n/a	n/a	n/a	n/a	n/a	n/a	n/a	n/a	n/a	0.16
FeO	11.77	10.36	10.99	11.90	13.11	19.56	11.79	9.06	10.00	22.81	17.27	10.76
TOTAL	99.42	99.32	99.00	99.85	99.25	99.97	99.46	98.87	99.27	99.20	99.47	100.34
Fo	87.7	89.2	88.5	87.6	86.1	79.0	87.7	90.6	89.6	74.8	81.4	88.9

Sample	48001	48001	48001	48001	48001	48001	48001	48001	48001	48001	48001	48001
Grain	13	14	15	16	17	18	19	20	21	22	23	24
SiO_2	40.46	38.75	37.93	37.90	37.85	38.30	37.95	38.14	40.24	38.07	39.17	39.95
MgO	48.45	43.19	38.81	38.68	38.88	39.92	38.31	41.17	48.51	38.84	44.56	47.79
CaO	0.35	0.25	0.32	0.29	0.33	0.28	0.32	0.38	0.29	0.32	0.26	0.33
MnO	0.23	0.37	0.43	0.47	0.46	0.39	0.39	0.47	0.25	0.48	0.34	0.22
FeO	10.90	16.99	22.40	22.54	22.05	20.97	22.52	19.12	10.30	22.68	15.39	11.75
TOTAL	100.39	99.54	99.88	99.88	99.57	99.86	99.50	99.28	99.58	100.38	99.73	100.04
Fo	88.8	81.9	75.5	75.4	75.9	77.2	75.2	79.3	89.4	75.3	83.8	87.9

Sample	48001	48001	48001	48001	48001	48001	48001	48001	48001	48001	48001	48001
Grain	25	26	27	28	29	30	31	32	33	34	35	36
SiO_2	38.24	40.83	37.63	40.44	38.56	38.52	40.27	39.84	40.43	37.96	38.91	37.58
MgO	40.28	49.55	38.24	49.23	40.71	41.21	48.49	45.90	48.79	39.54	43.54	38.83
CaO	0.33	0.27	0.34	0.28	0.32	0.34	0.35	0.34	0.38	0.34	0.31	0.32
MnO	0.38	0.27	0.46	0.28	0.47	0.40	0.23	0.30	0.14	0.46	0.33	0.48
FeO	20.52	9.91	23.11	9.60	20.42	19.32	11.15	13.97	9.89	21.28	16.68	21.91
TOTAL	99.75	100.83	99.77	99.82	100.47	99.78	100.48	100.34	99.64	99.58	99.76	99.12
Fo	77.8	89.9	74.7	90.1	78.0	79.2	88.6	85.4	89.8	76.8	82.3	76.0

Sample	48001	48001	48001	48001	48001	48001	48001	48001	48001	48001	48001	48001
Grain	37	38	39	40	41	42	43	44	45	46	47	48
SiO_2	37.54	40.29	38.62	39.56	39.71	37.65	39.87	39.39	37.95	37.57	37.74	40.29
MgO	38.39	48.88	42.40	46.07	46.95	37.66	48.54	47.13	38.81	37.94	38.27	48.83
CaO	0.35	0.26	0.32	0.39	0.33	0.32	0.26	0.30	0.33	0.32	0.32	0.31
MnO	0.52	0.20	0.37	0.31	0.33	0.43	0.23	0.24	0.50	0.58	0.46	0.21
FeO	22.80	10.41	17.51	14.18	12.32	23.03	10.26	11.49	22.17	23.07	22.74	10.69
TOTAL	99.59	100.03	99.21	100.52	99.65	99.09	99.14	98.55	99.76	99.48	99.52	100.34
Fo	75.0	89.3	81.2	85.3	87.2	74.4	89.4	88.0	75.7	74.6	75.0	89.1

Sample	48001	48001	48001	48001	48001	48001
Grain	49	50	51	52	53	54
SiO_2	40.07	39.93	39.94	39.68	38.81	38.59
MgO	46.28	46.65	45.82	43.85	41.85	39.47
CaO	0.37	0.39	0.40	0.42	0.27	0.31
MnO	n/a	n/a	n/a	n/a	n/a	n/a
FeO	12.13	12.23	12.88	15.03	18.22	20.58
TOTAL	98.85	99.20	99.04	98.98	99.15	98.95
Fo	87.2	87.2	86.4	83.9	80.4	77.4

n/a= not analysed

Appendix 2.2 (continued)

Electron microprobe analyses of olivine phenocrysts

2.2b Ulakan Formation ankaramite suite, sample UTas67424

Sample	67424	67424	67424	67424	67424	67424	67424	67424	67424	67424	67424	67424
Grain	1	2	3	4	5	6	7	8	9	10	11	12
SiO_2	39.72	39.99	39.91	38.82	40.78	40.74	39.68	40.61	39.85	40.71	40.67	40.83
MgO	44.42	45.99	45.21	41.84	48.65	48.76	45.59	48.91	45.10	49.77	48.13	49.15
CaO	0.33	0.27	0.33	0.35	0.41	0.40	0.40	0.26	0.37	0.35	0.42	0.27
MnO	0.22	0.22	0.37	0.40	0.23	0.12	0.33	0.17	0.31	0.16	0.18	0.24
FeO	14.34	12.73	13.08	17.58	9.03	9.08	12.99	8.89	13.36	8.21	9.53	8.33
TOTAL	99.21	99.44	99.10	99.15	99.29	99.31	99.13	99.20	99.19	99.53	99.16	99.10
Fo	84.7	86.6	86.1	81.0	90.6	90.6	86.2	90.8	85.8	91.5	90.0	91.3

Sample	67424	67424	67424	67424	67424	67424	67424	67424	67424	67424	67424	67424
Grain	13	14	15	16	17	18	19	20	21	22	23	24
SiO_2	39.25	40.88	39.56	40.15	39.22	40.67	39.24	40.14	40.33	40.29	40.20	39.58
MgO	42.99	49.31	43.56	45.86	43.53	48.65	42.33	47.18	46.49	47.18	47.17	44.97
CaO	0.34	0.31	0.30	0.44	0.33	0.49	0.42	0.47	0.39	0.44	0.45	0.41
MnO	0.35	0.26	0.27	0.27	0.33	0.28	0.36	0.19	0.28	0.32	0.25	n/a
FeO	16.08	8.63	15.52	12.49	15.56	9.50	16.66	11.09	12.62	10.93	10.86	14.17
TOTAL	99.18	99.66	99.36	99.35	99.10	99.78	99.21	99.28	100.24	99.35	99.10	99.13
Fo	82.7	91.1	83.4	86.8	83.3	90.1	81.9	88.4	86.8	88.5	88.6	85.0

Sample	67424	67424	67424	67424	67424	67424	67424	67424	67422	67422	67422	67422
Grain	25	26	27	28	29	30	31	32	33	34	35	36
SiO_2	40.51	39.43	39.55	39.00	40.32	40.59	39.97	40.67	40.67	40.39	40.52	40.57
MgO	48.58	42.35	43.59	43.58	47.26	48.95	45.13	48.18	46.61	47.98	48.28	47.63
CaO	0.45	0.41	0.28	0.36	0.37	0.48	0.44	0.36	0.52	0.41	0.38	0.47
MnO	n/a	n/a	n/a	n/a	n/a	n/a	n/a	n/a	n/a	n/a	n/a	n/a
FeO	9.72	17.03	15.59	16.41	11.12	9.47	13.57	10.12	11.26	10.41	9.90	10.43
TOTAL	99.26	99.22	99.00	99.34	99.07	99.49	99.11	99.33	99.06	99.19	99.08	99.10
Fo	89.9	81.6	83.3	82.6	88.4	90.2	85.6	89.5	88.1	89.2	89.7	89.1

Sample	67422	67422	67424	67424	67424	67424	67424	67424	67424	67424	67424	67424
Grain	37	38	39	40	41	42	43	44	45	46	47	48
SiO_2	41.00	40.70	40.05	39.45	39.25	40.37	38.99	40.20	39.24	40.84	40.32	40.04
MgO	48.88	49.32	46.16	43.51	43.69	47.12	41.93	47.83	42.85	49.44	48.21	47.28
CaO	0.53	0.47	0.27	0.35	0.35	0.27	0.34	0.27	0.36	0.28	0.40	0.44
MnO	n/a	n/a	0.32	0.29	0.27	0.17	0.36	0.20	0.31	0.24	0.10	n/a
FeO	8.67	8.58	14.36	14.95	14.91	10.51	17.19	10.07	16.00	7.93	9.56	10.94
TOTAL	99.08	99.07	101.50	98.70	98.65	98.82	98.98	98.89	98.95	98.88	98.75	98.70
Fo	91.0	91.1	85.2	83.9	84	88.9	81.3	89.5	82.7	91.8	90	88.5

Sample	67424	67424	67424	67424	67424	67424	67424	67424	67424
Grain	49	50	51	52	53	54	55	56	57
SiO_2	39.58	39.64	40.26	39.68	39.60	39.74	39.15	39.23	40.04
MgO	46.50	45.86	47.07	44.59	44.30	44.89	44.44	42.23	45.92
CaO	0.45	0.27	0.46	0.40	0.38	0.38	0.38	0.41	0.36
MnO	n/a	n/a	n/a	n/a	n/a	n/a	n/a	n/a	n/a
FeO	12.22	12.86	11.04	14.20	14.35	13.86	14.83	16.99	12.61
TOTAL	98.75	98.63	98.83	98.87	98.63	98.87	98.80	98.86	98.93
Fo	87.2	86.4	88.4	84.9	84.6	85.3	84.3	81.6	86.7

Appendix 2.2 (continued)

Electron microprobe analyses of olivine phenocrysts

2.2c Merelava ankaramite suite, sample 31551

Sample	31551	31551	31551	31551	31551	31551	31551	31551	31551	31551	31551	31551
Grain	1	2	3	4	5	6	7	8	9	10	11	12
SiO_2	41.04	38.21	38.99	39.00	38.56	40.30	39.42	40.41	39.55	38.59	40.21	38.39
MgO	49.03	39.37	39.49	43.08	40.76	44.49	45.31	49.49	45.14	40.60	48.69	38.82
CaO	0.09	0.18	0.19	0.15	0.18	0.24	0.22	0.26	0.22	0.22	0.23	0.17
MnO	n/a	n/a	n/a	n/a	n/a	n/a	n/a	n/a	n/a	n/a	n/a	n/a
FeO	9.48	21.24	21.29	17.88	20.10	14.69	14.07	9.30	14.12	19.97	9.75	22.18
TOTAL	99.64	99.00	99.96	100.10	99.61	99.72	99.03	99.46	99.03	99.38	98.88	99.57
Fo	90.2	76.8	76.8	81.1	78.4	84.4	85.2	90.5	85.1	78.4	89.9	75.8

Sample	31551	31551	31551	31551	31551	31551	31551	31551	31551	31551	31551	31551
Grain	13	14	15	16	17	18	19	20	21	22	23	24
SiO_2	40.51	40.14	40.60	39.27	40.84	40.54	40.51	40.86	39.04	39.77	40.12	41.05
MgO	49.03	48.48	48.00	42.33	49.45	47.77	48.64	48.84	42.71	48.49	47.69	48.24
CaO	0.22	0.22	0.23	0.17	0.25	0.20	0.25	0.27	0.16	0.19	0.25	0.25
MnO	n/a	n/a	n/a	n/a	n/a	n/a	n/a	n/a	n/a	n/a	n/a	n/a
FeO	9.83	10.11	10.68	17.68	9.32	12.19	10.44	10.19	17.52	9.98	11.12	10.65
TOTAL	99.59	98.95	99.51	99.43	99.87	100.70	99.85	100.17	99.43	98.43	99.18	100.18
Fo	89.9	89.5	88.9	81.0	90.5	87.5	89.3	89.5	81.3	89.7	88.5	89.0

Sample	31551	31551	31551	31551	31551	31551	31551	31551	31551	31551	31551	31551
Grain	25	26	27	28	29	30	31	32	33	34	35	36
SiO_2	40.56	40.94	38.44	40.49	40.04	40.62	38.62	38.64	40.30	40.77	38.15	40.28
MgO	48.82	48.90	39.06	48.80	45.90	49.01	40.10	41.43	49.52	49.84	40.01	49.00
CaO	0.26	0.24	0.17	0.23	0.18	0.22	0.21	0.24	0.22	0.25	0.24	0.23
MnO	0.00	0.00	0.00	0.00	0.00	0.00	0.00	0.00	0.00	0.00	0.00	0.00
FeO	10.14	9.72	21.35	9.55	13.37	9.83	20.73	19.03	8.90	8.29	19.59	9.69
TOTAL	99.79	99.80	99.02	99.08	99.50	99.68	99.66	99.34	98.94	99.16	97.99	99.19
Fo	89.6	90.0	76.6	90.1	86.0	89.9	77.6	79.5	90.9	91.5	78.5	90.0

Sample	31551	31551	31551	31551	31551	31551	31551	31551	31551	31551	31551	31551
Grain	37	38	39	40	41	42	43	44	45	46	47	48
SiO_2	38.41	38.54	38.28	39.04	40.44	40.96	38.35	40.74	41.02	39.16	40.46	40.03
MgO	39.46	39.43	38.84	42.96	46.51	49.60	37.90	48.75	48.38	41.92	47.01	47.19
CaO	0.18	0.17	0.21	0.24	0.23	0.28	0.20	0.22	0.25	0.21	0.24	0.21
MnO	n/a	n/a	n/a	n/a	n/a	n/a	n/a	n/a	n/a	n/a	n/a	n/a
FeO	21.84	21.05	21.73	17.13	12.69	9.19	23.06	10.09	9.75	18.27	12.42	12.01
TOTAL	99.89	99.19	99.06	99.35	99.87	100.03	99.51	99.81	99.38	99.56	100.12	99.43
Fo	76.3	77.0	76.1	81.7	86.7	90.6	74.6	89.6	89.9	80.4	87.1	87.5

Sample	31551	31551	31551	31551	31551	31551	31551	31551	31551	31551	31551	31551
Grain	49	50	51	52	53	54	55	56	57	58	59	60
SiO_2	40.76	38.29	38.86	39.62	37.83	40.19	38.61	38.50	39.21	39.80	39.48	40.36
MgO	49.27	39.75	41.57	43.87	39.47	47.73	40.51	40.14	43.04	44.41	43.47	46.52
CaO	0.24	0.21	0.18	0.24	0.20	0.24	0.21	0.18	0.24	0.18	0.18	0.24
MnO	n/a	n/a	n/a	n/a	n/a	n/a	n/a	n/a	n/a	n/a	n/a	n/a
FeO	9.90	20.88	18.08	16.19	21.53	11.27	20.03	20.33	16.54	15.33	17.03	12.73
TOTAL	100.17	99.12	98.70	99.93	99.04	99.43	99.36	99.15	99.03	99.73	100.16	99.85
Fo	89.9	77.3	80.4	82.9	76.6	88.3	78.3	77.9	82.3	83.8	82.0	86.7

Appendix 2.2 (continued)

Electron microprobe analyses of olivine phenocrysts

2.2d Epi ankaramite suite, sample UTas71041

Sample	71046	71046	71046	71046	71046	71046	71046	71046	71046	71046	71046	71046
Grain	1	2	3	4	5	6	7	8	9	10	11	12
SiO_2	40.78	39.95	39.89	39.09	39.40	39.78	40.32	38.97	39.02	38.68	38.58	39.95
MgO	49.43	45.05	45.40	41.43	43.67	45.22	47.47	40.86	42.24	40.80	40.78	45.29
CaO	0.09	0.24	0.31	0.22	0.23	0.24	0.24	0.20	0.27	0.21	0.26	0.27
MnO	n/a	n/a	n/a	n/a	n/a	n/a	n/a	n/a	n/a	n/a	n/a	n/a
FeO	9.65	14.95	14.48	18.69	15.83	14.21	11.56	19.49	17.53	19.84	19.70	14.27
TOTAL	99.95	100.19	100.08	99.43	99.13	99.45	99.59	99.52	99.06	99.53	99.32	99.77
Fo	90.1	84.3	84.8	79.8	83.1	85.0	88.0	78.9	81.1	78.6	78.7	85.0

Sample	71046	71046	71046	71046	71046	71046	71046	71046	71046	71046	71046	71046
Grain	13	14	15	16	17	18	19	20	21	22	23	24
SiO_2	38.81	38.69	39.39	39.52	39.49	38.55	39.79	39.43	38.28	42.23	40.15	38.64
MgO	42.98	40.99	44.60	44.24	43.57	41.08	41.54	42.91	39.67	39.39	47.58	41.09
CaO	0.24	0.27	0.25	0.23	0.22	0.25	0.22	0.25	0.22	0.21	0.26	0.28
MnO	n/a	n/a	n/a	n/a	n/a	n/a	n/a	n/a	n/a	n/a	n/a	n/a
FeO	16.99	18.25	15.73	15.46	16.74	19.19	18.84	16.92	20.85	17.42	11.76	18.99
TOTAL	99.02	98.20	99.97	99.45	100.02	99.06	100.39	99.51	99.02	99.25	99.74	99.00
Fo	81.9	80.0	83.5	83.6	82.3	79.3	79.7	81.9	77.3	80.2	87.8	79.4

Sample	71046	71046	71046	71046	71046	71046	71046	71046	71046	71046	71046	71046
Grain	25	26	27	28	29	30	31	32	33	34	35	36
SiO_2	39.75	40.88	40.80	41.16	40.74	39.74	38.53	38.82	39.15	40.87	38.27	39.93
MgO	45.36	50.07	48.85	50.40	49.82	45.66	41.12	40.37	42.58	50.29	40.94	46.15
CaO	0.28	0.25	0.26	0.30	0.28	0.25	0.22	0.22	0.26	0.25	0.23	0.24
MnO	n/a	n/a	n/a	n/a	n/a	n/a	n/a	n/a	n/a	n/a	n/a	n/a
FeO	14.09	8.66	9.12	8.13	8.44	13.76	19.17	20.32	17.53	8.32	19.77	12.90
TOTAL	99.48	99.86	99.03	99.99	99.28	99.41	99.04	99.73	99.52	99.73	99.20	99.21
Fo	85.2	91.2	90.5	91.7	91.3	85.6	79.3	78.0	81.3	91.5	78.7	86.5

Sample	71046	71046	71046	71046	71046	71046	71046	71046	71046	71046	71046	71046
Grain	37	38	39	40	41	42	43	44	45	46	47	48
SiO_2	40.91	40.51	40.41	38.96	40.68	40.06	39.68	39.21	40.17	38.94	39.17	38.68
MgO	50.52	49.19	48.11	42.08	49.11	46.59	43.60	44.56	47.96	42.15	43.03	40.75
CaO	0.24	0.27	0.20	0.27	0.27	0.25	0.22	0.25	0.18	0.25	0.23	0.20
MnO	n/a	n/a	n/a	n/a	n/a	n/a	n/a	n/a	n/a	n/a	n/a	n/a
FeO	7.62	9.94	10.66	17.58	8.82	12.35	15.64	15.22	10.87	18.31	17.64	20.17
TOTAL	99.29	99.91	99.37	98.89	98.88	99.24	99.14	99.24	99.18	99.65	100.07	99.80
Fo	92.2	89.8	89.0	81.0	90.9	87.1	83.3	83.9	88.7	80.4	81.3	78.3

Sample	71046	71046	71046	71046	71046	71046	71046	71046	71046	71046	71046	71046
Grain	49	50	51	52	53	54	55	56	57	58	59	60
SiO_2	40.15	40.43	40.37	40.61	40.54	39.08	39.07	40.49	38.72	39.43	39.48	39.64
MgO	47.51	47.96	48.45	48.92	48.77	42.95	43.36	49.31	40.45	43.49	45.03	44.76
CaO	0.33	0.30	0.12	0.25	0.27	0.28	0.23	0.26	0.22	0.22	0.24	0.27
MnO	n/a	n/a	n/a	n/a	n/a	n/a	n/a	n/a	n/a	n/a	n/a	n/a
FeO	11.94	10.52	10.72	9.81	9.74	16.83	16.62	9.58	19.65	16.60	14.50	14.74
TOTAL	99.93	99.21	99.65	99.59	99.32	99.14	99.28	99.63	99.04	99.74	99.25	99.41
Fo	87.7	89.1	89.0	89.9	89.9	82.0	82.3	90.2	78.6	82.4	84.7	84.4

Appendix 2.3

Electron microprobe analyses of clinopyroxene phenocrysts

2.3a Rinjani volcano ankaramite suite, sample UTas48001

Sample	48001	48001	48001	48001	48001	48001	48001	48001	48001	48001	48001	48001
Grain	1	2	3	4	5	6	7	8	9	10	11	12
SiO_2	53.16	52.66	52.94	52.63	52.93	52.90	53.39	53.21	52.77	52.76	52.42	52.94
TiO_2	0.23	0.35	0.29	0.29	0.32	0.21	0.31	0.26	0.26	0.28	0.33	0.22
Al_2O_3	1.93	2.59	2.32	2.29	2.38	1.74	2.08	2.14	2.48	2.05	2.63	1.96
Cr_2O_3	0.30	0.11	0.18	0.53	0.37	0.47	0.16	0.23	0.19	0.32	0.19	0.19
MgO	17.31	16.72	17.10	16.84	16.86	17.59	17.01	16.98	16.96	17.16	16.77	17.09
CaO	23.34	22.89	22.78	22.86	23.03	23.01	23.37	23.34	23.21	23.26	22.95	23.33
MnO	0.02	0.02	0.02	0.02	0.02	0.02	0.02	0.02	0.02	0.02	0.02	0.02
FeO*	4.08	4.86	4.51	4.29	4.50	3.69	4.39	4.46	4.62	4.05	4.46	4.27
Na_2O	0.15	0.18	0.16	0.18	0.14	0.17	0.17	0.16	0.17	0.15	0.15	0.15
TOTAL	100.53	100.38	100.31	99.93	100.55	99.80	100.90	100.81	100.68	100.05	99.92	100.17
Mg#	88.30	86.00	87.10	87.50	87.00	89.50	87.40	87.20	86.80	88.30	87.00	87.70
mg#	93.06	90.03	90.66	90.78	89.96	94.56	90.86	91.17	92.20	93.18	90.96	92.57
Fe_2O_3	1.98	1.73	1.52	1.38	1.27	2.10	1.49	1.70	2.29	2.01	1.66	2.03
FeO	2.30	3.30	3.14	3.05	3.35	1.80	3.05	2.93	2.56	2.24	2.97	2.45
$Fe^{3+}/Fe^{3+}+Fe^{2+}$	0.44	0.32	0.30	0.29	0.25	0.51	0.31	0.34	0.45	0.45	0.33	0.43
TOTAL'	100.72	100.56	100.46	100.07	100.68	100.01	101.05	100.98	100.91	100.25	100.09	100.37
Wo	46.11	45.82	45.47	46.04	46.05	45.68	46.30	46.26	46.03	46.23	46.11	46.24
En	47.56	46.55	47.47	47.18	46.89	48.57	46.87	46.81	46.78	47.45	46.86	47.12
Fs	6.33	7.63	7.06	6.78	7.06	5.75	6.82	6.94	7.19	6.32	7.03	6.64

Sample	48001	48001	48001	48001	48001	48001	48001	48001	48001	48001	48001	48001
Grain	13	14	15	16	17	18	19	20	21	22	23	24
SiO_2	52.98	51.97	52.67	53.65	52.92	53.15	53.21	53.43	51.20	52.52	52.78	50.52
TiO_2	0.31	0.30	0.34	0.21	0.30	0.31	0.27	0.29	0.54	0.33	0.34	0.67
Al_2O_3	2.54	2.97	2.67	1.75	2.13	2.12	2.09	2.08	4.03	2.67	2.57	4.54
Cr_2O_3	0.37	0.17	0.20	0.40	0.44	0.24	0.20	0.25	0.27	0.22	0.18	0.28
MgO	16.82	16.21	16.88	17.84	17.13	17.04	17.01	17.14	15.70	16.82	17.08	15.47
CaO	23.33	23.07	23.15	23.17	23.25	23.48	23.11	22.88	22.06	22.97	22.96	22.09
MnO	0.02	0.02	0.02	0.02	0.02	0.02	0.02	0.02	0.02	0.02	0.02	0.02
FeO*	4.69	5.14	4.73	3.69	4.09	4.33	4.24	4.07	6.70	4.60	4.39	6.19
Na_2O	0.19	0.15	0.17	0.14	0.14	0.14	0.10	0.13	0.24	0.15	0.13	0.27
TOTAL	101.25	100.00	100.82	100.87	100.42	100.83	100.26	100.29	100.77	100.30	100.44	100.04
Mg#	86.50	84.90	86.40	89.60	88.20	87.50	87.80	88.30	80.70	86.70	87.40	81.70
mg#	91.33	89.90	91.61	93.57	92.29	91.84	89.80	89.26	86.61	90.92	91.21	87.68
Fe_2O_3	2.05	2.10	2.20	1.67	1.71	1.81	0.88	0.43	2.64	1.78	1.62	2.58
FeO	2.84	3.25	2.75	2.18	2.55	2.70	3.44	3.68	4.32	2.99	2.93	3.87
$Fe^{3+}/Fe^{3+}+Fe^{2+}$	0.39	0.37	0.42	0.41	0.38	0.38	0.19	0.10	0.35	0.35	0.33	0.37
TOTAL'	101.46	100.21	101.04	101.04	100.59	101.01	100.35	100.33	101.03	100.48	100.60	100.30
Wo	46.29	46.47	45.99	45.53	46.23	46.43	46.14	45.84	44.89	45.97	45.77	45.59
En	46.41	45.42	46.64	48.77	47.38	46.85	47.22	47.76	44.43	46.82	47.36	44.40
Fs	7.30	8.12	7.37	5.70	6.39	6.72	6.64	6.39	10.68	7.22	6.87	10.01

Sample	48001	48001	48001	48001	48001	48001	48001	48001	48001	48001	48001	48001
Grain	25	26	27	28	29	30	31	32	33	34	35	36
SiO_2	52.97	53.27	52.81	52.03	51.40	52.58	53.72	52.72	52.97	52.76	53.00	52.55
TiO_2	0.24	0.35	0.23	0.35	0.49	0.29	0.29	0.27	0.27	0.29	0.32	0.26
Al_2O_3	2.34	2.37	1.90	2.85	3.49	2.42	2.02	2.47	2.32	2.61	2.30	2.39
Cr_2O_3	0.51	0.15	0.80	0.16	0.28	0.20	0.24	0.28	0.76	0.17	0.23	0.20
MgO	17.11	17.23	17.39	16.41	16.16	16.84	17.23	17.03	16.94	16.88	17.17	16.78
CaO	23.05	23.08	23.18	22.93	22.96	22.82	23.41	23.37	23.38	23.22	23.10	23.24
MnO	0.02	0.02	0.02	0.02	0.02	0.02	0.02	0.02	0.02	0.02	0.02	0.02
FeO*	3.98	4.30	3.54	5.01	5.19	4.68	4.01	4.44	4.18	4.60	4.25	4.33
Na_2O	0.17	0.16	0.17	0.13	0.16	0.18	0.11	0.15	0.17	0.14	0.13	0.14
TOTAL	100.38	100.93	100.04	99.88	100.14	100.03	101.05	100.75	101.01	100.68	100.52	99.91
Mg#	88.50	87.70	89.80	85.40	84.80	86.50	88.50	87.30	87.90	86.80	87.80	87.40
mg#	91.79	91.19	94.33	89.92	90.74	90.86	90.38	93.02	91.96	91.37	91.55	91.67
Fe_2O_3	1.39	1.48	1.86	1.92	2.50	1.85	0.82	2.40	1.71	1.96	1.58	1.79
FeO	2.73	2.97	1.86	3.28	2.94	3.02	3.27	2.28	2.64	2.84	2.82	2.72
$Fe^{3+}/Fe^{3+}+Fe^{2+}$	0.31	0.31	0.47	0.35	0.43	0.35	0.18	0.49	0.37	0.38	0.34	0.37
TOTAL'	100.52	101.07	100.23	100.07	100.39	100.22	101.13	100.99	101.18	100.88	100.68	100.09
Wo	46.14	45.78	46.22	46.16	46.38	45.71	46.34	46.24	46.56	46.16	45.91	46.50
En	47.62	47.53	48.23	45.93	45.40	46.93	47.44	46.86	46.92	46.67	47.46	46.70
Fs	6.25	6.69	5.54	7.91	8.22	7.36	6.22	6.89	6.53	7.17	6.63	6.80

Mg#=100Fe^{2+}/(Fe^{2+}+Fe^{3+}), mg#=100Fe^{2+}/(Fe^{*}+Fe^{2+}), TOTAL'= Oxide total including Fe_2O_3 and FeO.

Appendix 2.3 (continued)

Electron microprobe analyses of clinopyroxene phenocrysts

2.3b Ulakan Formation ankaramite suite, sample UTas67424

Sample	67424	67424	67424	67424	67424	67424	67424	67424	67424	67424	67424	67424
Grain	1	2	3	4	5	6	7	8	9	10	11	12
SiO_2	49.38	53.29	52.78	51.04	52.95	53.69	52.59	53.61	51.30	52.50	53.09	52.62
TiO_2	0.93	0.39	0.21	0.39	0.24	0.14	0.27	0.15	0.29	0.18	0.19	0.27
Al_2O_3	3.06	1.55	1.81	3.29	1.75	1.29	2.06	1.37	2.63	1.62	1.51	1.84
Cr_2O_3	0.01	0.31	0.76	0.04	0.80	0.60	0.42	0.56	0.48	0.55	0.41	0.08
MgO	12.69	17.62	17.51	15.69	17.16	17.73	16.52	17.91	16.01	17.37	17.51	17.10
CaO	21.96	23.61	23.11	23.26	23.61	23.68	23.50	23.48	23.60	23.63	23.59	23.59
MnO	0.16	0.05	0.07	0.00	0.06	0.07	0.05	0.08	0.05	0.06	0.05	0.09
FeO*	10.66	3.97	3.47	6.37	3.64	3.09	4.99	3.34	5.49	3.75	3.38	4.04
Na_2O	0.39	0.14	0.16	0.14	0.15	0.13	0.14	0.16	0.16	0.15	0.11	0.12
TOTAL	99.24	100.90	99.88	100.20	100.40	100.40	100.50	100.70	100.00	99.82	99.83	99.75
Mg#	68.00	88.80	90.00	81.50	89.40	91.10	85.50	90.50	83.90	89.20	90.20	88.30
mg#	75.98	94.80	94.92	90.39	94.04	94.82	91.10	95.68	93.26	97.01	94.94	94.40
Fe_2O_3	3.90	2.50	2.00	3.78	1.89	1.51	2.35	2.11	3.81	3.11	1.90	2.48
FeO	7.15	1.72	1.67	2.97	1.94	1.73	2.87	1.44	2.06	0.95	1.66	1.81
$Fe^{3+}/Fe^{2+}+Fe^{3+}$	0.33	0.57	0.52	0.53	0.47	0.44	0.42	0.57	0.62	0.75	0.51	0.55
TOTAL'	99.63	101.20	100.10	100.60	100.50	100.60	100.80	100.90	100.40	100.10	100.00	100.00
Wo	45.71	46.06	46.01	46.47	46.88	46.61	46.62	45.98	47.02	46.55	46.60	46.62
En	36.73	47.81	48.48	43.60	47.39	48.53	45.59	48.79	44.37	47.59	48.11	47.01
Fs	17.56	6.12	5.50	9.93	5.73	4.86	7.80	5.23	8.62	5.86	5.28	6.37

Sample	67424	67424	67424	67424	67424	67424	67424	67424	67424	67424	67424	67424
Grain	13	14	15	16	17	18	19	20	21	22	23	24
SiO_2	52.85	53.46	50.39	53.56	53.15	52.53	52.53	52.75	52.45	53.20	52.28	51.80
TiO_2	0.23	0.15	0.44	0.17	0.22	0.24	0.21	0.14	0.25	0.16	0.26	0.24
Al_2O_3	2.09	1.47	3.76	1.46	1.58	2.09	1.76	1.32	1.93	1.44	2.04	2.28
Cr_2O_3	0.11	0.46	0.18	0.61	0.38	0.30	0.51	0.39	0.17	0.48	0.30	0.31
MgO	16.78	17.28	15.39	17.75	17.61	16.71	17.06	17.90	17.06	17.68	16.75	16.22
CaO	23.49	23.79	23.34	23.50	23.69	23.88	23.52	23.86	23.58	22.91	23.51	23.56
MnO	0.09	0.02	0.00	0.09	0.07	0.11	0.11	0.03	0.06	0.08	0.05	0.07
FeO*	4.72	3.83	6.23	3.03	3.55	4.12	4.24	3.00	4.15	3.51	4.48	5.53
Na_2O	0.13	0.12	0.17	0.14	0.13	0.14	0.15	0.14	0.12	0.13	0.12	0.18
TOTAL	100.50	100.60	99.90	100.30	100.40	100.10	100.10	99.51	99.77	99.59	99.78	100.20
Mg#	86.40	89.00	81.50	91.30	89.90	87.90	87.80	91.40	88.00	90.00	87.00	84.00
mg#	91.71	93.34	91.60	94.85	95.87	93.95	94.81	99.76	94.70	93.45	93.19	92.94
Fe_2O_3	2.24	1.82	4.13	1.46	2.44	2.45	2.86	3.24	2.72	1.45	2.55	3.71
FeO	2.70	2.20	2.52	1.72	1.35	1.92	1.66	0.08	1.70	2.21	2.18	2.19
$Fe^{3+}/Fe^{2+}+Fe^{3+}$	0.43	0.43	0.60	0.43	0.62	0.53	0.61	0.97	0.59	0.37	0.51	0.60
TOTAL'	100.70	100.80	100.30	100.50	100.60	100.40	100.40	99.84	100.00	99.74	100.00	100.60
Wo	46.43	46.80	47.05	46.42	46.45	47.36	46.44	46.67	46.60	45.54	46.70	46.66
En	46.14	47.29	43.15	48.77	48.02	46.09	46.86	48.71	46.91	48.88	46.28	44.68
Fs	7.42	5.91	9.80	4.81	5.53	6.55	6.70	4.62	6.49	5.58	7.02	8.65

Sample	67424	67424	67424	67424	67424	67424	67424	67424	67424	67424	67424	67424
Grain	25	26	27	28	29	30	31	32	33	34	35	36
SiO_2	52.50	52.11	52.42	52.42	50.60	52.90	52.64	51.72	51.19	50.84	53.69	50.93
TiO_2	0.24	0.25	0.29	0.26	0.49	0.22	0.22	0.27	0.50	0.45	0.23	0.38
Al_2O_3	1.84	1.99	1.88	2.04	4.16	1.83	1.86	2.85	3.48	4.16	1.60	3.32
Cr_2O_3	0.24	0.31	0.28	0.02	0.44	0.40	0.57	0.52	0.47	0.48	0.21	0.21
MgO	17.14	17.01	17.19	16.82	15.55	17.28	17.13	15.90	16.09	15.56	17.59	15.79
CaO	23.93	23.86	23.21	23.85	22.13	22.82	22.72	22.52	22.23	22.48	22.95	22.61
MnO	0.08	0.08	0.10	0.12	0.06	0.08	0.09	0.08	0.14	0.14	0.08	0.10
FeO*	4.02	4.38	4.62	4.59	6.29	4.43	3.96	5.47	5.40	6.24	4.13	5.95
Na_2O	0.12	0.11	0.13	0.15	0.21	0.15	0.15	0.18	0.21	0.18	0.11	0.15
TOTAL	100.10	100.10	100.10	100.30	99.94	100.10	99.34	99.51	99.70	100.50	100.60	99.44
Mg#	88.40	87.40	86.90	86.70	81.50	87.40	88.50	83.80	84.20	81.70	88.40	82.60
mg#	96.37	96.58	94.24	95.06	87.81	92.10	91.85	87.64	89.42	88.29	91.11	89.43
Fe_2O_3	3.19	3.67	3.05	3.37	2.72	1.99	1.39	1.64	2.22	2.85	1.19	2.91
FeO	1.15	1.07	1.87	1.56	3.85	2.64	2.71	4.00	3.39	3.68	3.06	3.32
$Fe^{3+}/Fe^{2+}+Fe^{3+}$	0.71	0.75	0.59	0.66	0.39	0.40	0.32	0.27	0.37	0.41	0.26	0.44
TOTAL'	100.40	100.50	100.40	100.60	100.20	100.30	99.48	99.67	99.92	100.80	100.70	99.73
Wo	46.95	46.78	45.69	46.84	45.43	45.30	45.71	45.99	45.43	45.78	45.27	45.87
En	46.76	46.39	47.06	45.94	44.39	47.71	47.93	45.16	45.74	44.08	48.24	44.55
Fs	6.28	6.83	7.25	7.22	10.18	6.98	6.36	8.85	8.83	10.14	6.49	9.58

Appendix 2.3 (continued)

Electron microprobe analyses of clinopyroxene phenocrysts

2.3c Merelava Island ankaramite suite, sample 31551

Sample	31551	31551	31551	31551	31551	31551	31551	31551	31551	31551	31551	31551
Grain	1	2	3	4	5	6	7	8	9	10	11	12
SiO_2	52.05	54.36	51.85	54.11	54.14	54.41	49.38	54.96	53.74	53.36	52.78	54.61
TiO_2	0.52	0.06	0.32	0.08	0.10	0.14	0.32	0.04	0.17	0.06	0.23	0.05
Al_2O_3	5.65	1.19	2.92	1.17	1.28	1.26	5.25	1.06	2.01	1.80	2.48	1.07
Cr_2O_3	0.66	0.46	0.18	0.61	0.14	0.12	0.28	0.56	0.30	0.32	0.33	0.62
MgO	16.30	18.85	16.98	18.52	18.39	18.08	15.83	18.71	17.83	17.96	17.09	18.55
CaO	20.80	22.62	20.11	22.60	22.68	22.57	21.24	22.62	22.32	22.76	21.21	22.47
MnO	0.01	0.05	0.16	0.10	0.11	0.05	0.05	0.13	0.04	0.17	0.06	0.14
FeO*	4.32	3.07	7.66	3.16	3.18	3.58	8.09	2.69	4.42	4.14	5.56	3.06
Na_2O	0.79	0.13	0.18	0.15	0.14	0.12	0.28	0.13	0.13	0.12	0.23	0.15
TOTAL	101.11	100.77	100.36	100.49	100.14	100.32	100.74	100.89	100.96	100.69	99.96	100.72
Mg#	87.08	91.64	79.83	91.28	91.17	90.02	77.75	92.55	87.81	88.57	84.59	91.54
mg#	89.77	94.82	85.17	94.29	93.55	90.31	91.72	92.53	90.36	94.22	86.95	92.59
Fe_2O_3	1.12	1.37	2.66	1.29	1.02	0.14	6.16	0.00	1.15	2.42	1.10	0.46
FeO	3.31	1.84	5.27	2.00	2.26	3.46	2.55	2.69	3.39	1.96	4.57	2.65
$Fe^{3+}/Fe^{2+}+Fe^{3+}$	0.23	0.40	0.31	0.37	0.29	0.03	0.69	0.00	0.23	0.53	0.18	0.14
TOTAL'	101.22	100.91	100.62	100.62	100.25	100.34	101.35	100.89	101.08	100.93	100.07	100.77
Wo	44.40	44.12	40.35	44.39	44.63	44.66	42.81	44.49	44.11	44.54	42.96	44.26
En	48.38	51.13	47.39	50.61	50.32	49.74	44.38	51.18	49.01	48.87	48.15	50.82
Fs	7.22	4.75	12.26	5.00	5.05	5.61	12.81	4.33	6.88	6.59	8.88	4.92

Sample	31551	31551	31551	31551	31551	31551	31551	31551	31551	31551	31551	31551
Grain	13	14	15	16	17	18	19	20	21	22	23	24
SiO_2	52.36	53.88	51.75	52.47	54.19	54.14	52.68	52.72	53.16	53.51	52.98	54.37
TiO_2	0.26	0.06	0.20	0.21	0.11	0.07	0.30	0.12	0.14	0.17	0.18	0.09
Al_2O_3	3.07	1.10	2.96	2.58	1.42	1.23	2.73	2.11	1.61	1.94	2.17	1.42
Cr_2O_3	0.28	0.42	0.17	0.26	0.41	0.39	0.19	0.22	0.40	0.31	0.32	0.23
MgO	16.83	18.28	16.68	17.23	18.03	18.45	17.12	17.46	17.90	17.70	17.53	18.70
CaO	21.93	22.95	22.16	21.28	22.41	22.88	21.18	22.26	22.53	22.06	22.19	21.91
MnO	0.13	0.07	0.14	0.14	0.02	0.03	0.22	0.11	0.06	0.12	0.09	0.07
FeO*	5.97	2.97	5.56	6.08	4.29	3.33	6.84	4.94	4.26	4.64	4.97	4.12
Na_2O	0.18	0.12	0.16	0.20	0.15	0.13	0.21	0.16	0.13	0.16	0.16	0.10
TOTAL	101.01	99.85	99.77	100.44	101.02	100.65	101.46	100.10	100.19	100.61	100.59	101.01
Mg#	83.43	91.66	84.27	83.50	88.24	90.82	81.72	86.32	88.24	87.20	86.30	89.02
mg#	88.77	94.58	90.59	88.77	90.59	94.36	87.33	92.11	93.41	90.11	91.27	91.34
Fe_2O_3	2.42	1.22	2.75	2.44	1.06	1.52	2.69	2.53	2.24	1.31	2.20	1.07
FeO	3.79	1.87	3.09	3.88	3.34	1.97	4.42	2.67	2.25	3.46	2.99	3.16
$Fe^{3+}/Fe^{2+}+Fe^{3+}$	0.36	0.37	0.45	0.36	0.22	0.41	0.35	0.46	0.47	0.25	0.40	0.23
TOTAL'	101.25	99.97	100.05	100.69	101.13	100.80	101.73	100.35	100.41	100.74	100.81	101.11
Wo	43.77	45.22	44.49	42.47	44.07	44.72	41.94	44.09	44.35	43.77	43.92	42.80
En	46.72	50.10	46.57	47.83	49.32	50.16	47.14	48.10	49.01	48.85	48.26	50.81
Fs	9.51	4.68	8.94	9.69	6.61	5.12	10.92	7.81	6.64	7.38	7.82	6.39

Sample	31551	31551	31551	31551	31551	31551	31551	31551	31551	31551	31551	31551
Grain	25	26	27	28	29	30	31	32	33	34	35	36
SiO_2	53.71	51.49	52.82	51.55	51.71	53.52	52.83	51.84	53.20	53.24	54.06	54.12
TiO_2	0.05	0.33	0.25	0.36	0.25	0.08	0.18	0.23	0.17	0.19	0.10	0.11
Al_2O_3	1.19	2.98	2.45	3.87	3.44	1.20	2.09	3.06	1.83	1.97	1.09	1.31
Cr_2O_3	0.56	0.15	0.32	0.35	0.21	0.60	0.25	0.23	0.16	0.19	0.62	0.65
MgO	18.56	16.42	17.10	16.65	16.86	18.05	17.32	16.51	17.58	17.60	18.28	18.12
CaO	22.75	21.06	20.05	21.04	21.39	22.69	21.60	21.43	21.86	21.83	22.62	22.68
MnO	0.05	0.11	0.21	0.14	0.09	0.08	0.06	0.06	0.03	0.08	0.62	0.65
FeO*	3.12	7.09	6.32	6.53	6.25	3.20	5.05	6.16	4.72	5.23	2.52	2.83
Na_2O	0.11	0.21	0.27	0.21	0.21	0.14	0.14	0.15	0.13	0.17	0.14	0.13
TOTAL	100.10	99.84	99.77	100.70	100.40	99.55	99.52	99.67	99.67	100.49	100.03	100.59
Mg#	91.40	80.53	82.85	81.99	82.81	90.97	85.96	82.72	86.93	85.73	92.83	91.96
mg#	95.75	86.52	84.04	87.60	89.44	93.81	88.31	86.59	89.18	89.64	94.48	93.60
Fe_2O_3	1.84	2.81	0.59	2.59	3.00	1.20	1.07	1.78	1.02	1.78	0.69	0.69
FeO	1.47	4.56	5.79	4.20	3.55	2.12	4.08	4.56	3.80	3.63	1.90	2.21
$Fe^{3+}/Fe^{2+}+Fe^{3+}$	0.53	0.36	0.08	0.36	0.43	0.34	0.19	0.26	0.19	0.31	0.24	0.22
TOTAL'	100.29	100.12	99.83	100.96	100.70	99.67	99.63	99.85	99.77	100.67	100.10	100.66
Wo	44.57	42.53	40.97	42.59	42.96	45.06	43.48	43.51	43.71	43.27	44.80	44.82
En	50.57	46.12	48.61	46.87	47.10	49.86	48.49	46.63	48.89	48.52	50.34	49.80
Fs	4.85	11.35	10.42	10.54	9.94	5.08	8.03	9.86	7.41	8.21	4.86	5.37

Appendix 2.3 (continued)

Electron microprobe analyses of clinopyroxene phenocrysts

2.3d Epi Island ankaramite suite, sample UTas71046

Sample	71046	71046	71046	71046	71046	71046	71046	71046	71046	71046	71046	71046
Grain	1	2	3	4	5	6	7	8	9	10	11	12
SiO_2	52.35	51.34	52.99	52.19	52.72	53.19	53.40	53.32	52.00	50.39	51.92	53.88
TiO_2	0.16	0.23	0.12	0.16	0.14	0.13	0.06	0.10	0.19	0.33	0.18	0.07
Al_2O_3	2.56	3.67	2.22	2.96	2.22	1.70	1.52	1.65	2.90	4.88	3.33	1.09
Cr_2O_3	0.18	0.04	0.38	0.10	0.24	0.32	0.70	0.43	0.11	0.24	0.25	0.59
MgO	16.53	15.91	17.08	16.43	16.84	17.02	17.48	17.16	16.39	15.44	16.01	17.73
CaO	23.67	23.56	23.79	23.70	23.76	24.18	23.78	23.82	24.07	23.66	23.48	23.98
MnO	0.14	0.14	0.06	0.16	0.08	0.13	0.11	0.12	0.09	0.18	0.15	0.17
FeO*	4.21	5.28	3.71	4.70	3.93	3.66	2.93	3.45	4.47	5.22	4.61	2.48
Na_2O	0.12	0.16	0.12	0.16	0.14	0.12	0.13	0.13	0.17	0.18	0.16	0.14
TOTAL	99.94	100.38	100.47	100.67	100.13	100.47	100.13	100.20	100.40	100.54	100.10	100.15
Mg#	87.52	84.33	89.16	86.19	88.44	89.25	91.42	89.88	86.75	84.08	86.11	92.74
mg#	93.00	93.10	94.00	94.00	94.00	94.70	95.20	93.80	95.50	94.30	91.30	96.00
Fe_2O_3	2.21	3.53	1.97	3.14	2.23	2.18	1.53	1.61	3.42	3.95	2.12	1.28
FeO	2.22	2.10	1.93	1.87	1.93	1.70	1.55	2.00	1.39	1.66	2.71	1.33
$Fe^{3+}/Fe^{2+}+Fe^{3+}$	0.47	0.60	0.48	0.60	0.51	0.54	0.47	0.42	0.69	0.68	0.41	0.46
TOTAL'	100.04	100.57	100.55	100.82	100.21	100.57	100.15	100.23	100.57	100.76	100.15	100.14
Wo	47.30	47.20	47.10	47.10	47.20	47.60	47.10	47.20	47.70	47.90	47.50	47.30
En	45.90	44.30	47.10	45.40	46.60	46.60	48.20	47.30	45.20	43.50	45.00	48.60
Fs	6.80	8.50	5.80	7.50	6.20	5.80	4.70	5.50	7.10	8.50	7.50	4.10

Sample	71046	71046	71046	71046	71046	71046	71046	71046	71046	71046	71046	71046
Grain	13	14	15	16	17	18	19	20	21	22	23	24
SiO_2	52.14	51.28	51.15	51.45	53.44	52.09	52.78	52.50	51.77	53.52	53.69	53.28
TiO_2	0.21	0.25	0.21	0.18	0.08	0.11	0.16	0.11	0.15	0.04	0.04	0.18
Al_2O_3	3.03	3.93	3.70	3.86	1.26	2.58	1.92	2.50	3.53	1.44	0.90	1.52
Cr_2O_3	0.09	0.33	0.18	0.30	0.54	0.08	0.37	0.37	0.02	0.51	0.72	0.50
MgO	16.32	16.04	15.34	15.85	17.89	16.63	17.03	16.64	15.93	17.70	18.10	17.22
CaO	23.71	23.36	23.58	23.99	24.32	25.65	23.43	24.08	23.28	23.58	24.03	23.57
MnO	0.12	0.12	0.16	0.11	0.07	0.07	0.11	0.14	0.07	0.05	0.09	0.11
FeO*	4.67	4.75	5.40	4.67	2.92	4.50	3.90	4.14	5.12	3.06	2.44	3.53
Na_2O	0.15	0.22	0.20	0.18	0.14	0.13	0.17	0.14	0.14	0.13	0.13	0.14
TOTAL	100.45	100.38	99.95	100.62	100.69	101.85	99.88	100.62	100.01	100.08	100.18	100.07
Mg#	86.19	85.78	83.53	85.84	91.63	86.84	88.63	87.77	84.75	91.17	92.98	89.70
mg#	92.90	94.20	91.10	94.40	99.40	102.80	93.90	94.90	90.15	95.24	98.60	93.35
Fe_2O_3	2.72	3.34	3.04	3.32	3.04	5.89	2.16	2.85	2.24	1.65	2.20	1.50
FeO	2.23	1.75	2.66	1.68	0.18	-0.80	1.96	1.58	3.10	1.58	0.46	2.18
$Fe^{3+}/Fe^{2+}+Fe^{3+}$	0.52	0.63	0.51	0.64	0.94	1.18	0.50	0.62	0.39	0.49	0.81	0.38
TOTAL'	100.57	100.49	100.05	100.77	100.85	102.31	99.93	100.77	100.10	100.12	100.27	100.08
Wo	47.30	47.20	47.90	48.20	47.20	49.00	46.60	47.60	47.04	46.58	46.95	46.80
En	45.30	45.10	43.30	44.30	48.30	44.20	47.10	45.80	44.77	48.63	49.19	47.56
Fs	7.50	7.70	8.80	7.50	4.50	6.80	6.20	6.60	8.19	4.80	3.86	5.64

Sample	71046	71046	71046	71046	71046	71046	71046	71046	71046	71046
Grain	25	26	27	28	29	30	31	32	33	34
SiO_2	52.94	50.07	52.42	52.57	53.01	52.51	51.58	53.11	52.98	50.75
TiO_2	0.13	0.33	0.13	0.14	0.09	0.12	0.14	0.07	0.07	0.23
Al_2O_3	1.48	4.52	1.79	1.98	1.72	2.31	2.85	1.57	1.38	4.16
Cr_2O_3	0.18	0.18	0.53	0.39	0.16	0.23	0.31	0.24	0.39	0.16
MgO	17.25	14.90	17.06	16.76	16.94	16.68	16.33	17.07	17.59	15.63
CaO	24.18	22.24	23.53	23.92	23.59	24.02	23.80	23.74	24.18	23.25
MnO	0.03	0.17	0.08	0.14	0.19	0.11	0.08	0.11	0.10	0.19
FeO*	3.29	6.80	3.70	3.83	4.22	4.13	4.21	3.48	3.30	5.45
Na_2O	0.11	0.24	0.10	0.16	0.13	0.17	0.15	0.14	0.13	0.17
TOTAL	99.59	99.58	99.35	99.91	100.05	100.30	99.55	99.53	100.13	100.01
Mg#	90.35	79.65	89.17	88.65	87.76	87.82	87.38	89.75	90.49	83.66
mg#	96.37	87.74	94.78	95.01	93.04	95.33	95.61	93.91	98.89	92.53
Fe_2O_3	2.37	3.43	2.25	2.51	2.18	2.97	3.20	1.68	3.28	3.56
FeO	1.16	3.71	1.67	1.57	2.26	1.46	1.34	1.97	0.35	2.25
$Fe^{3+}/Fe^{2+}+Fe^{3+}$	0.65	0.45	0.55	0.59	0.47	0.65	0.68	0.43	0.89	0.59
TOTAL'	99.72	99.68	99.48	100.00	100.14	100.43	99.72	99.56	100.33	100.20
Wo	47.63	45.95	46.86	47.53	46.63	47.54	47.73	47.21	47.13	47.07
En	47.26	42.81	47.26	46.32	46.57	45.91	45.55	47.22	47.69	44.01
Fs	5.11	11.24	5.88	6.16	6.81	6.55	6.72	5.57	5.18	8.92

Appendix 2.4

Microprobe analyses of olivine-spinel inclusion pairs

2.4a Ulakan Formation ankaramite suite

Sample	67424	67424	67424	67424	67424	67424	67424	67424	67424	67424	67424	67424	67424	67424	67424
Grain	1	2	3	4	5	6	7	8	9	10	11	12	13	14	15
TiO_2	0.51	0.51	0.54	1.10	0.51	0.55	0.67	0.41	0.49	0.56	0.65	0.97	0.71	0.63	0.61
Al_2O_3	11.21	9.70	10.01	18.42	11.70	11.15	8.84	12.57	11.54	10.95	12.29	38.59	11.25	11.27	11.15
Cr_2O_3	50.95	48.25	48.10	29.04	49.71	48.57	47.20	50.60	49.38	50.09	49.18	24.11	45.44	48.31	45.71
Fe_2O_3	7.71	14.31	13.43	22.10	10.77	12.73	14.43	8.44	11.35	10.83	10.88	6.39	14.36	11.80	15.23
FeO	19.96	19.57	19.70	20.62	18.96	16.74	22.81	17.49	18.97	18.61	17.40	15.36	18.85	18.43	18.12
MgO	8.99	9.66	9.40	9.88	10.24	11.54	7.22	10.91	10.05	10.19	11.42	15.44	10.03	10.46	10.75
MnO	0.30	0.17	0.24	0.23	0.24	0.24	0.42	0.23	0.41	0.33	0.17	0.15	0.24	0.20	0.23
NiO	0.09	0.03	0.08	0.19	0.08	0.09	0.15	0.13	0.16	0.17	0.13	0.29	0.15	0.04	0.02
ZnO	0.19	0.09	0.20	0.12	0.11	0.07	0.18	0.13	0.15	0.09	0.00	0.09	0.20	0.06	0.09
TOTAL	99.97	102.32	101.77	101.75	102.37	101.76	102.00	100.96	102.56	101.86	102.15	101.46	101.29	101.26	101.99
mg#	44.5	46.8	46.0	46.1	49.0	55.1	36.1	52.6	48.6	49.4	53.9	64.2	48.7	50.3	51.4
Cr#	75.3	76.9	76.3	51.4	74.0	74.5	78.2	73.0	74.2	75.4	72.9	29.5	73.0	74.2	73.3
Fe^{3+}/Fe^{3+}_{spl}	2.88	1.52	1.63	1.04	1.96	1.46	1.76	2.30	1.86	1.91	1.78	2.67	1.46	1.74	1.32
Fe^{3+}/Fe^{3+}_{melt}	11.22	4.87	5.33	2.95	6.77	4.62	5.88	8.38	6.32	6.55	5.97	10.17	4.61	5.79	4.05
Fo_{host}	89.3	87.7	86.7	81.7	87.2	88.5	84.8	88.9	87.4	84.5	87.5	88.1	90.1	89.0	89.3

Sample	67424	67424	67424	67424	67424	67424	67424	67424	67424	67424	67424	67424	67424	67424	67424
Grain	16	17	18	19	20	21	22	23	24	25	26	27	28	29	30
TiO_2	0.37	0.50	0.60	0.44	0.62	0.48	0.66	0.99	0.72	0.67	0.40	0.41	0.88	0.51	0.04
Al_2O_3	9.00	11.20	10.59	10.40	9.95	10.47	10.77	12.85	14.48	11.54	11.86	11.30	11.35	13.72	64.88
Cr_2O_3	48.65	47.92	43.69	50.48	47.25	49.75	45.92	37.38	49.93	46.94	52.35	51.59	41.99	50.41	0.44
Fe_2O_3	14.52	12.49	17.09	11.73	13.97	13.18	14.09	20.13	7.41	13.36	7.85	10.57	17.37	4.50	3.40
FeO	19.97	20.85	20.34	16.85	21.38	16.80	22.07	20.46	14.44	17.13	17.71	15.00	17.72	19.79	9.64
MgO	9.12	8.95	9.18	11.38	8.53	11.63	7.96	9.36	13.37	11.60	11.07	12.69	10.82	9.54	21.01
MnO	0.41	0.35	0.28	0.24	0.35	0.28	0.46	0.33	0.20	0.27	0.27	0.22	0.28	0.16	0.14
NiO	0.08	0.01	0.06	0.08	0.12	0.12	0.11	0.26	0.08	0.07	0.09	0.08	0.05	0.06	0.27
ZnO	0.02	0.10	0.09	0.08	0.04	0.00	0.10	0.04	0.04	0.05	0.15	0.05	0.17	0.27	0.25
TOTAL	102.21	102.45	102.02	101.80	102.35	102.81	102.18	101.88	100.73	101.90	101.99	101.96	100.73	99.30	100.14
mg#	44.9	43.3	44.6	54.6	41.6	55.2	39.1	44.9	62.3	54.7	52.7	60.1	52.1	46.2	79.5
Cr#	78.4	74.2	73.5	76.5	76.1	76.1	74.1	66.1	69.8	73.2	74.7	75.4	71.3	71.1	0.5
Fe^{3+}/Fe^{3+}_{spl}	1.53	1.86	1.32	1.60	1.70	1.42	1.74	1.13	2.16	1.42	2.51	1.58	1.13	4.89	3.15
Fe^{3+}/Fe^{3+}_{melt}	4.90	6.31	4.06	5.19	5.63	4.44	5.81	3.30	7.73	4.47	9.37	5.11	3.31	22.45	12.65
Fo_{host}	86.6	85.6	85.8	89.7	83.9	90.2	84.9	86.2	81.6	90.2	89.3	91.0	89.0	88.0	86.9

Sample	67424	67424	67424	67424	67424	67424	67424	67424	67424	67424	67424	67424	67424	67424	67424
Grain	31	32	33	34	35	36	37	38	39	40	41	42	43	44	45
TiO_2	0.47	0.41	0.62	0.47	0.52	1.03	0.63	0.65	0.47	0.63	0.77	0.73	0.80	0.61	0.94
Al_2O_3	9.67	9.06	12.31	12.84	11.06	12.44	11.36	10.57	10.22	10.45	9.57	9.42	11.39	10.90	14.71
Cr_2O_3	48.07	46.88	43.81	50.62	42.61	37.12	44.06	42.89	50.95	46.04	44.40	45.69	40.86	44.67	28.58
Fe_2O_3	13.27	14.84	13.84	8.64	16.72	20.53	14.62	16.95	11.49	14.78	17.38	15.96	17.60	15.25	25.60
FeO	20.75	21.51	20.27	14.73	22.43	20.16	20.77	19.84	16.90	21.36	20.34	21.15	19.87	21.00	23.13
MgO	8.42	7.82	9.03	12.77	7.68	9.46	8.60	9.27	11.32	8.49	9.14	8.61	9.30	8.67	7.57
MnO	0.42	0.33	0.15	0.06	0.29	0.31	0.32	0.27	0.30	0.32	0.25	0.32	0.21	0.27	0.35
NiO	0.15	0.14	0.21	0.17	0.02	0.18	0.10	0.05	0.07	0.11	0.13	0.07	0.19	0.11	0.21
ZnO	0.20	0.13	0.09	0.19	0.04	0.08	0.22	0.00	0.02	0.12	0.16	0.04	0.00	0.00	0.14
TOTAL	101.48	101.16	100.37	100.56	101.39	101.38	100.76	100.56	101.81	102.35	102.23	102.07	100.28	101.51	101.31
mg#	42.0	39.3	44.2	60.7	37.9	45.5	42.5	45.4	54.4	41.5	44.5	42.0	45.5	42.4	36.8
Cr#	76.9	77.6	70.5	72.6	72.1	66.7	72.2	73.1	77.0	74.7	75.7	76.5	70.6	73.3	56.6
Fe^{3+}/Fe^{3+}_{spl}	1.74	1.61	1.63	1.89	1.49	1.09	1.58	1.30	1.64	1.61	1.30	1.47	1.25	1.53	1.00
Fe^{3+}/Fe^{3+}_{melt}	5.79	5.25	5.32	6.49	4.74	3.15	5.11	3.97	5.35	5.23	3.97	4.67	3.78	4.91	2.83
Fo_{host}	85.6	84.2	85.3	86.2	82.7	86.5	85.6	86.2	89.6	83.7	85.7	84.9	86.7	84.3	81.1

Appendix 2.4 (continued)

Microprobe analyses of olivine-spinel inclusion pairs

2.4b Epi Island ankaramite suite

Sample	71046	71046	71046	71046	71046	71046	71046	71046	71046	71046	71046	71046	71046	71046	71046
Grain	1	2	3	4	5	6	7	8	9	10	11	12	13	14	15
TiO_2	0.30	0.17	0.17	0.16	0.28	0.26	0.50	0.32	0.22	0.24	0.19	0.40	0.20	0.40	0.17
Al_2O_3	8.17	5.95	7.52	6.31	9.35	7.27	39.99	11.66	9.68	6.43	7.44	16.43	6.29	15.64	7.21
Cr_2O_3	59.36	57.30	56.95	57.29	57.47	58.47	3.61	41.24	43.91	58.49	56.17	26.74	52.67	28.75	53.52
Fe_2O_3	6.65	8.88	8.30	9.43	6.99	7.87	26.98	19.16	18.93	9.48	9.63	28.29	12.84	26.69	11.45
FeO	15.87	20.51	19.77	20.56	14.61	17.51	21.55	24.00	23.85	19.04	20.35	24.65	23.96	24.32	22.34
MgO	11.96	8.33	9.22	8.59	12.65	10.66	11.81	7.13	6.98	9.79	8.81	7.21	6.29	7.10	7.45
MnO	0.28	0.36	0.24	0.26	0.26	0.21	0.35	0.31	0.28	0.35	0.42	0.26	0.39	0.38	0.25
NiO	0.00	0.06	0.00	0.04	0.12	0.13	0.18	0.02	0.02	0.13	0.12	0.05	0.06	0.13	0.06
ZnO	0.00	0.00	0.00	0.00	0.00	0.00	0.00	0.00	0.00	0.00	0.00	0.00	0.00	0.00	0.00
TOTAL	102.63	101.63	102.25	102.69	101.77	102.41	105.03	103.90	103.91	103.99	103.18	104.09	102.76	103.47	102.48
mg#	57.32	41.97	45.38	42.67	60.67	52.03	49.41	34.63	34.28	47.82	43.55	34.26	31.87	34.22	37.27
Cr#	82.97	86.59	83.55	85.89	80.48	84.36	5.71	70.34	75.26	85.92	83.51	52.18	84.88	55.21	83.27
Fe^{3+}/Fe^{2+}_{spl}	2.65	2.57	2.65	2.42	2.32	2.47	0.89	1.39	1.40	2.23	2.35	0.97	2.07	1.01	2.17
Fe^{3+}/Fe^{2+}_{melt}	10.09	9.66	10.06	8.96	8.47	9.20	2.41	4.33	4.37	8.05	8.59	2.70	7.30	2.86	7.74
Fo_{host}	89.5	81.5	82.5	84.8	90.5	87.6	85.0	81.8	80.1	88.9	87.1	80.4	83.2	80.4	84.0

Sample	71046	71046	71046	71046	71046	71046	71046	71046	71046	71046	71046	71046	71046	71046	71046
Grain	16	17	18	19	20	21	22	23	24	25	26	27	28	29	30
TiO_2	0.48	0.17	0.22	0.39	0.25	0.25	0.32	0.23	0.19	0.25	0.21	0.26	0.27	0.27	0.29
Al_2O_3	43.05	7.91	4.65	8.16	8.78	13.90	7.97	10.57	5.98	8.76	9.11	45.80	8.73	9.61	8.95
Cr_2O_3	7.82	58.60	48.16	55.88	56.07	45.36	59.10	49.37	55.18	57.16	56.55	6.85	56.85	55.49	55.45
Fe_2O_3	19.15	7.71	17.44	8.27	6.79	13.04	5.79	11.67	10.90	6.97	6.24	18.62	8.84	8.53	8.96
FeO	17.66	17.75	27.36	19.47	19.53	20.62	16.67	22.61	24.60	17.86	18.82	14.92	13.54	13.88	16.15
MgO	14.40	10.70	3.72	9.38	9.32	9.33	11.16	7.54	5.99	10.46	9.80	16.55	13.41	13.12	11.65
MnO	0.23	0.31	0.37	0.38	0.22	0.31	0.21	0.39	0.46	0.29	0.18	0.05	0.08	0.16	0.20
NiO	0.13	0.06	0.07	0.07	0.00	0.03	0.07	0.07	0.00	0.12	0.06	0.13	0.01	0.01	0.14
ZnO	0.00	0.00	0.00	0.00	0.00	0.00	0.00	0.00	0.00	0.00	0.00	0.00	0.00	0.00	0.00
TOTAL	102.97	103.26	102.06	102.00	101.02	102.85	101.33	102.46	103.38	101.93	101.06	103.27	101.76	101.12	101.86
mg#	59.24	51.80	19.50	46.18	45.96	44.64	54.39	37.26	30.26	51.06	48.14	66.40	63.83	62.74	56.24
Cr#	10.86	83.24	87.41	82.13	81.07	68.63	83.26	75.80	86.09	81.40	80.62	9.12	81.37	79.47	80.60
Fe^{3+}/Fe^{2+}_{spl}	1.02	2.56	1.74	2.62	3.20	1.76	3.20	2.15	2.51	2.85	3.35	0.89	1.70	1.81	2.00
Fe^{3+}/Fe^{2+}_{melt}	2.90	9.62	5.82	9.90	12.87	5.88	12.90	7.68	9.37	11.07	13.69	2.42	5.64	6.10	6.98
Fo_{host}	82.0	90.2	70.1	78.1	87.7	84.8	90.5	82.6	79.5	88.2	88.8	83.8	89.6	85.2	88.9

Sample	71046	71046	71046	71046	71046	71046	71046	71046	71046	71046
Grain	31	32	33	34	35	36	37	38	39	40
TiO_2	0.25	0.25	0.16	0.28	0.24	0.27	0.22	0.22	0.23	0.29
Al_2O_3	8.52	56.04	51.06	9.24	9.16	9.25	8.65	8.71	55.74	14.98
Cr_2O_3	56.92	1.18	11.01	58.22	57.54	57.46	54.22	55.26	0.50	40.58
Fe_2O_3	8.66	14.81	9.61	7.09	8.17	7.91	10.42	9.75	14.64	16.52
FeO	16.83	10.43	10.50	13.20	12.88	12.94	17.58	16.83	14.48	20.99
MgO	11.26	20.61	19.74	13.68	13.93	13.80	10.64	11.22	18.00	9.21
MnO	0.34	0.05	0.14	0.23	0.21	0.19	0.22	0.24	0.13	0.26
NiO	0.12	0.17	0.16	0.10	0.10	0.11	0.14	0.06	0.10	0.11
ZnO	0.00	0.00	0.00	0.00	0.00	0.00	0.00	0.00	0.00	0.00
TOTAL	102.94	103.63	102.44	102.10	102.33	101.97	102.11	102.31	103.93	102.97
mg#	54.39	77.89	77.01	64.87	65.85	65.52	51.89	54.28	68.90	43.88
Cr#	81.75	1.39	12.64	80.87	80.81	80.64	80.78	80.97	0.60	64.50
Fe^{3+}/Fe^{2+}_{spl}	2.16	0.78	1.21	2.07	1.75	1.82	1.88	1.92	1.10	1.41
Fe^{3+}/Fe^{2+}_{melt}	7.70	2.04	3.63	7.29	5.85	6.15	6.40	6.60	3.18	4.42
Fo_{host}	89.3	87.5	88.3	92.0	91.8	92.1	86.8	87.5	85.2	84.7

Appendix 2.4 (continued)

Microprobe analyses of olivine-spinel inclusion pairs

2.4c Rinjani volcano ankaramite suite

Sample	48001	48001	48001	48001	48001	48001	48001	48001	48001	48001	48001	48001	48001	48001	48001
Grain	1	2	3	4	5	6	7	8	9	10	11	12	13	14	15
TiO_2	0.61	0.62	0.93	0.62	0.80	0.63	0.59	0.74	1.00	0.93	0.71	0.98	0.78	0.94	0.66
Al_2O_3	12.65	13.70	11.08	18.36	9.71	11.94	11.83	14.51	10.73	15.11	16.17	14.34	14.66	11.81	15.19
Cr_2O_3	41.51	41.88	25.32	31.26	21.57	45.66	28.34	40.13	26.46	38.60	40.14	36.87	39.16	45.59	43.30
Fe_2O_3	17.10	16.10	32.89	21.65	38.96	15.06	31.49	16.68	32.99	16.72	14.96	19.44	16.91	14.34	13.29
FeO	20.08	18.68	25.58	21.07	24.37	16.31	23.64	19.00	25.24	16.90	14.99	18.70	19.49	17.16	13.61
MgO	9.51	10.54	5.91	9.67	6.48	12.00	7.30	10.48	6.31	11.88	13.23	10.74	10.11	11.60	13.83
MnO	0.33	0.33	0.27	0.34	0.33	0.22	0.34	0.33	0.31	0.25	0.29	0.24	0.24	0.10	0.19
NiO	0.12	0.09	0.04	0.08	0.16	0.22	0.08	0.17	0.00	0.11	0.19	0.08	0.16	0.19	0.12
ZnO	0.00	0.00	0.00	0.00	0.00	0.00	0.00	0.00	0.00	0.00	0.00	0.00	0.00	0.00	0.00
TOTAL	102.00	102.00	102.10	103.10	102.60	102.10	103.70	102.10	103.10	100.60	101.00	101.40	101.50	101.80	100.30
mg#	45.77	50.13	29.15	44.99	32.15	56.74	35.49	49.56	30.82	55.59	61.13	50.58	48.04	54.63	64.42
Cr#	68.75	67.21	60.51	53.31	59.83	71.94	61.63	64.96	62.32	63.14	62.47	63.29	64.17	72.13	65.66
Fe^{3+}/Fe^{3+}_{spl}	1.31	1.29	0.86	1.08	0.70	1.20	0.83	1.27	0.85	1.12	1.11	1.07	1.28	1.33	1.14
Fe^{3+}/Fe^{3+}_{melt}	3.98	3.92	2.32	3.12	1.75	3.58	2.22	3.83	2.27	3.28	3.24	3.07	3.89	4.09	3.33
Fo_{max}	83.9	84.0	75.0	83.6	78.5	89.4	81.1	85.5	75.3	87.1	89.3	86.1	83.0	88.6	88.4

Sample	48001	48001	48001	48001	48001
Grain	16	17	18	19	20
TiO_2	0.68	0.68	0.69	0.70	0.75
Al_2O_3	14.83	15.43	15.12	12.12	14.69
Cr_2O_3	44.52	42.99	43.73	45.04	40.03
Fe_2O_3	13.47	13.61	13.81	14.29	16.28
FeO	13.79	15.13	14.23	15.21	15.94
MgO	13.84	13.01	13.63	12.51	12.19
MnO	0.28	0.27	0.16	0.15	0.28
NiO	0.20	0.14	0.18	0.08	0.08
ZnO	0.00	0.00	0.00	0.00	0.00
TOTAL	101.70	101.30	101.60	100.20	100.30
mg#	64.14	60.51	63.06	59.44	57.66
Cr#	66.81	65.13	65.98	71.36	64.63
Fe^{3+}/Fe^{3+}_{spl}	1.14	1.24	1.15	1.18	1.09
Fe^{3+}/Fe^{3+}_{melt}	3.33	3.71	3.36	3.50	3.14
Fo_{max}	90.3	87.6	90.1	90.6	88.0

2.4d Merelava Island ankaramite suite

Sample	31551	31551	31551	31551	31551	31551	31551
Grain	1	2	3	4	5	6	7
TiO_2	0.25	0.57	0.92	0.32	0.33	0.20	0.32
Al_2O_3	9.75	11.74	14.95	10.25	12.19	7.13	9.88
Cr_2O_3	48.96	37.35	39.27	50.24	52.87	52.49	47.58
Fe_2O_3	13.41	19.33	17.01	12.05	8.00	12.51	14.12
FeO	18.96	21.12	17.56	17.42	14.74	21.36	20.94
MgO	9.56	7.94	11.30	10.76	12.62	7.91	8.60
MnO	0.52	0.28	0.48	0.33	0.37	0.25	0.37
NiO	0.03	0.06	0.17	0.02	0.09	0.07	0.00
ZnO	0.02	0.06	0.12	0.15	0.17	0.06	0.04
TOTAL	101.50	98.45	101.80	101.60	101.40	102.00	102.00
mg#	47.33	40.10	53.43	52.39	60.40	39.76	42.26
Cr#	77.10	68.09	63.79	76.68	74.42	83.16	76.36
Fe^{3+}/Fe^{3+}_{spl}	1.57	1.21	1.15	1.61	2.05	1.90	1.65
Fe^{3+}/Fe^{3+}_{melt}	5.08	3.63	3.37	5.23	7.19	6.50	5.41
Fo_{max}	83.90	84.00	75.00	83.60	78.50	89.40	81.10

Appendix 2.5

Duplicated electron microprobe analyses of olivine phenocrysts using trace element label "KSPCOLTR"

2.5a Rinjani volcano ankaramite suite, UTas48001

Sample	48001	48001	48001	48001	48001	48001	48001	48001	48001	48001	48001	48001	48001
no.	1	2	3	4	5	6	7	8	9	10	11	12	13
SiO_2	38.83	38.03	38.07	39.46	39.29	38.17	38.19	37.52	37.72	38.42	38.12	39.79	37.11
MgO	43.01	38.54	40.33	46.67	44.85	40.23	43.01	38.30	39.08	41.56	39.64	46.91	36.55
FeO	16.01	21.32	19.10	10.96	13.72	18.85	16.16	21.25	20.21	17.96	20.13	11.05	23.83
CaO	0.33	0.32	0.28	0.37	0.33	0.34	0.26	0.30	0.32	0.36	0.36	0.38	0.31
CaO_{TE}	**0.36**	**0.32**	**0.28**	**0.41**	**0.37**	**0.35**	**0.28**	**0.36**	**0.34**	**0.57**	**0.37**	**0.39**	**0.32**
Cr_2O_3	0.00	0.00	0.00	0.04	0.04	0.03	0.03	0.00	0.00	0.00	0.00	0.06	0.03
Cr_2O_{3TE}	**0.02**	**0.01**	**0.02**	**0.02**	**0.01**	**0.01**	**0.03**	**0.00**	**0.00**	**0.01**	**0.02**	**0.02**	**0.00**
MnO	0.29	0.44	0.43	0.25	0.27	0.39	0.37	0.46	0.48	0.37	0.41	0.26	0.65
MnO_{TE}	**0.39**	**0.47**	**0.41**	**0.27**	**0.32**	**0.40**	**0.33**	**0.50**	**0.46**	**0.43**	**0.46**	**0.26**	**0.68**
NiO	0.10	0.08	0.12	0.11	0.11	0.09	0.12	0.11	0.07	0.12	0.05	0.12	0.01
NiO_{TE}	**0.10**	**0.11**	**0.13**	**0.13**	**0.12**	**0.12**	**0.18**	**0.09**	**0.10**	**0.10**	**0.10**	**0.12**	**0.07**
TOTAL	98.71	98.81	98.35	97.91	98.69	98.11	98.17	98.01	97.90	99.05	98.84	98.53	98.56
Fo	82.8	76.4	79.0	88.4	85.4	79.2	82.6	76.3	77.5	80.5	77.9	88.4	73.3

Sample	48001	48001	48001	48001	48001	48001	48001	48001	48001	48001	48001	48001	48001
no.	14	15	16	17	18	19	20	21	22	23	24	25	26
SiO_2	37.20	40.27	38.45	38.65	38.40	37.63	39.97	39.12	39.38	39.65	37.29	38.72	40.23
MgO	37.26	46.88	42.85	42.12	40.07	37.89	48.17	43.41	44.99	47.89	37.19	42.24	48.91
FeO	22.38	11.26	15.48	16.98	19.42	21.90	9.95	15.42	13.59	9.81	22.84	17.20	8.82
CaO	0.31	0.30	0.37	0.28	0.27	0.31	0.33	0.38	0.37	0.44	0.36	0.35	0.26
CaO_{TE}	**0.34**	**0.31**	**0.42**	**0.30**	**0.33**	**0.31**	**0.35**	**0.38**	**0.38**	**0.38**	**0.36**	**0.32**	**0.26**
Cr_2O_3	0.03	0.00	0.01	0.07	0.04	0.02	0.00	0.00	0.01	0.03	0.00	0.00	0.06
Cr_2O_{3TE}	**0.00**	**0.02**	**0.01**	**0.03**	**0.02**	**0.01**	**0.04**	**0.00**	**0.01**	**0.03**	**0.01**	**0.00**	**0.04**
MnO	0.53	0.24	0.35	0.39	0.47	0.42	0.32	0.34	0.32	0.30	0.52	0.39	0.16
MnO_{TE}	**0.56**	**0.27**	**0.33**	**0.37**	**0.44**	**0.48**	**0.23**	**0.34**	**0.33**	**0.22**	**0.54**	**0.39**	**0.21**
NiO	0.11	0.15	0.07	0.14	0.11	0.05	0.19	0.15	0.09	0.11	0.08	0.12	0.20
NiO_{TE}	**0.09**	**0.15**	**0.12**	**0.13**	**0.10**	**0.10**	**0.19**	**0.12**	**0.11**	**0.15**	**0.08**	**0.11**	**0.25**
TOTAL	97.82	99.16	97.65	98.58	98.77	98.31	98.90	98.79	98.78	98.13	98.31	98.98	98.72
Fo	74.8	88.1	83.2	81.6	78.7	75.5	89.6	83.4	85.5	89.7	74.4	81.4	90.8

Sample	48001	48001	48001	48001	48001
no.	27	28	29	30	31
SiO_2	38.56	38.87	40.08	39.75	37.89
MgO	42.43	42.82	48.82	46.69	38.82
FeO	16.57	15.77	8.85	11.31	21.04
CaO	0.36	0.34	0.25	0.40	0.33
CaO_{TE}	**0.37**	**0.36**	**0.26**	**0.39**	**0.35**
Cr_2O_3	0.04	0.03	0.06	0.01	0.00
Cr_2O_{3TE}	**0.00**	**0.02**	**0.04**	**0.01**	**0.01**
MnO	0.32	0.28	0.23	0.24	0.44
MnO_{TE}	**0.40**	**0.37**	**0.20**	**0.27**	**0.49**
NiO	0.11	0.16	0.31	0.19	0.06
NiO_{TE}	**0.09**	**0.12**	**0.24**	**0.12**	**0.09**
TOTAL	98.43	98.33	98.49	98.54	98.68
Fo	82.1	82.9	90.8	88.1	76.7

Analyses are form "MISCELLAN" and "KSPCOLTR" (bold numbers) microprobe lables.

Appendix 2.5 (continued)

Duplicated electron microprobe analyses of olivine phenocrysts using trace element label "KSPCOLTR"

2.5a Ulakan Formation ankaramite suite, sample UTas67424

Sample	67424	67424	67424	67424	67424	67424	67424	67424	67424	67424	67424	67424	67424	67424
no.	1	2	3	4	5	6	7	8	9	10	11	12	13	14
SiO_2	41.05	40.78	38.97	39.45	40.45	39.73	39.56	40.05	40.03	39.56	39.58	39.71	39.41	40.41
MgO	50.26	49.92	42.48	44.17	47.66	45.21	45.12	47.01	45.32	45.28	44.22	44.85	44.08	49.44
FeO	7.87	8.15	17.10	15.03	11.07	13.97	14.16	11.68	14.10	13.80	14.94	14.95	15.28	8.74
CaO	0.32	0.31	0.26	0.45	0.33	0.38	0.36	0.33	0.28	0.36	0.30	0.31	0.30	0.38
CaO_{TE}	**0.32**	**0.34**	**0.32**	**0.44**	**0.35**	**0.39**	**0.39**	**0.33**	**0.33**	**0.38**	**0.33**	**0.32**	**0.33**	**0.34**
Cr_2O_3	0.08	0.10	0.05	0.02	0.06	0.08	0.08	0.00	0.02	0.02	0.06	0.03	0.01	0.08
$Cr2O3_{TE}$	**0.06**	**0.06**	**0.03**	**0.02**	**0.05**	**0.03**	**0.02**	**0.04**	**0.03**	**0.02**	**0.03**	**0.03**	**0.03**	**0.05**
MnO	0.16	0.12	0.39	0.32	0.29	0.33	0.30	0.25	0.33	0.33	0.35	0.34	0.36	0.16
MnO_{TE}	**0.22**	**0.19**	**0.39**	**0.33**	**0.26**	**0.31**	**0.32**	**0.24**	**0.31**	**0.32**	**0.34**	**0.33**	**0.34**	**0.21**
NiO	0.31	0.22	0.18	0.11	0.16	0.03	0.15	0.19	0.16	0.11	0.14	0.22	0.18	0.22
NiO_{TE}	**0.23**	**0.23**	**0.17**	**0.14**	**0.22**	**0.16**	**0.17**	**0.22**	**0.20**	**0.18**	**0.19**	**0.19**	**0.20**	**0.19**
TOTAL	100.00	99.67	99.45	99.57	100.05	99.80	99.74	99.57	100.31	99.53	99.63	100.37	99.66	99.38
Fo	91.9	91.6	81.6	84.0	88.5	85.2	85.1	87.8	85.2	85.4	84.1	84.3	83.7	91.0

Sample	67424	67424	67424	67424	67424	67424	67424	67424	67424	67424	67424	67424	67424	67424
no.	15	16	17	18	19	20	21	22	23	24	25	26	27	28
SiO_2	39.39	40.20	39.94	38.95	39.34	39.65	39.01	39.35	40.15	38.87	39.53	39.88	39.57	39.09
MgO	43.95	47.49	46.13	42.75	44.13	44.91	43.60	44.86	47.16	41.99	42.89	48.32	44.32	43.12
FeO	15.69	11.07	12.70	17.05	15.19	14.30	15.98	13.97	11.24	17.46	16.35	9.60	14.87	16.85
CaO	0.34	0.34	0.40	0.38	0.43	0.36	0.26	0.39	0.36	0.40	0.32	0.37	0.34	0.40
CaO_{TE}	**0.36**	**0.39**	**0.42**	**0.39**	**0.42**	**0.41**	**0.32**	**0.43**	**0.40**	**0.37**	**0.34**	**0.36**	**0.38**	**0.40**
Cr_2O_3	0.03	0.05	0.03	0.04	0.09	0.04	0.00	0.12	0.04	0.01	0.06	0.06	0.07	0.00
Cr_2O_{3TE}	**0.02**	**0.03**	**0.03**	**0.02**	**0.03**	**0.02**	**0.02**	**0.03**	**0.06**	**0.01**	**0.03**	**0.05**	**0.03**	**0.01**
MnO	0.28	0.23	0.33	0.36	0.34	0.31	0.38	0.32	0.27	0.39	0.35	0.24	0.39	0.37
MnO_{TE}	**0.35**	**0.26**	**0.28**	**0.36**	**0.35**	**0.33**	**0.36**	**0.31**	**0.26**	**0.40**	**0.39**	**0.23**	**0.34**	**0.39**
NiO	0.16	0.18	0.13	0.17	0.15	0.15	0.09	0.17	0.20	0.16	0.19	0.12	0.16	0.17
NiO_{TE}	**0.17**	**0.18**	**0.17**	**0.16**	**0.16**	**0.18**	**0.18**	**0.17**	**0.18**	**0.15**	**0.16**	**0.17**	**0.17**	**0.16**
TOTAL	99.91	99.62	99.67	99.68	99.63	99.80	99.47	99.12	99.45	99.26	99.69	98.61	99.68	100.02
Fo	83.3	88.5	86.6	81.7	83.8	84.9	83.0	85.2	88.2	81.1	82.4	90.0	84.2	82.1

Sample	67424	67424	67424	67424	67424	67424	67424	67424	67424	67424	67424	67424	67424	67424
no.	29	30	31	32	33	34	35	36	37	38	39	40	41	42
SiO_2	39.78	40.14	38.78	39.55	39.76	39.24	41.26	39.62	38.48	40.52	39.58	40.36	40.90	40.30
MgO	45.32	48.21	40.50	43.64	46.64	43.80	50.28	43.66	41.02	48.01	45.77	48.35	50.64	48.13
FeO	13.52	9.71	19.34	15.63	12.27	15.57	8.01	16.20	18.62	10.96	13.44	10.13	7.22	10.21
CaO	0.39	0.45	0.31	0.47	0.25	0.37	0.30	0.32	0.30	0.45	0.40	0.37	0.25	0.40
CaO_{TE}	**0.39**	**0.44**	**0.32**	**0.41**	**0.32**	**0.36**	**0.29**	**0.35**	**0.60**	**0.44**	**0.43**	**0.39**	**0.29**	**0.43**
Cr_2O_3	0.02	0.02	0.04	0.06	0.06	0.07	0.02	0.04	0.00	0.05	0.02	0.04	0.07	0.05
Cr_2O_{3TE}	**0.03**	**0.05**	**0.01**	**0.02**	**0.04**	**0.01**	**0.04**	**0.02**	**0.02**	**0.04**	**0.02**	**0.04**	**0.07**	**0.04**
MnO	0.33	0.18	0.45	0.40	0.28	0.36	0.13	0.41	0.40	0.26	0.32	0.21	0.18	0.25
MnO_{TE}	**0.32**	**0.24**	**0.46**	**0.34**	**0.32**	**0.34**	**0.20**	**0.37**	**0.42**	**0.25**	**0.29**	**0.23**	**0.17**	**0.23**
NiO	0.17	0.13	0.13	0.15	0.17	0.14	0.23	0.14	0.15	0.09	0.12	0.17	0.25	0.19
NiO_{TE}	**0.17**	**0.20**	**0.14**	**0.15**	**0.20**	**0.15**	**0.27**	**0.16**	**0.15**	**0.15**	**0.18**	**0.23**	**0.34**	**0.17**
TOTAL	99.53	98.98	99.55	99.73	99.56	99.47	100.35	100.38	99.31	100.37	99.72	99.71	99.62	99.51
Fo	85.7	89.9	78.9	83.3	87.2	83.4	91.8	82.8	79.7	88.7	85.9	89.5	92.6	89.4

Appendix 3

NOTES

Appendix 3.1 Recalculated analyses of optically homogenized melt inclusions

Recalculation procedure is described in Chapter 4. Compositions are presented for each melt inclusion as 1) the composition of optically homogenized melt inclusions as determined by electron microprobe, b) the recalculated composition after STEP-1 (italics) and c) the composition of melt inclusions after complete recalculation (bold). Full lines separate groups of coexisting melt inclusions within the same olivine grain.

T_q=temperature of quenching, Fo_h=host fosterite content, Mg#=100Mg/(Mg+Fe*), T_c=calculated melt composition using olivine-melt thermometer of Ford *et al.* (1983), Fo_c=calculated equilibrium Fo composition (Ford *et al.* 1983), ol%= percentage of olivine added (+) or substracted (-) from the melt during the recalculation.

Appendix 3.2 Molecular CIPWnorm compositions

Normative compositions of recalculated melt inclusion analyses in Appendix 3.1. Normative components are calculated using the program MINPET (LeMaitre 1981).

Appendix 3.3 Electron microprobe analyses of host olivine phenocrysts

Each analyses represents the composition of the host olivine adjacent to the melt inclusion.

Appendix 3.4 Della-Pasqua & Varne 1997.

Appendix 3.1

Composition of optically homogenized melt inclusions

Rinjani ankaramite suite, sample UTas48001

Grain	Melt	T_1	Fo_h	SiO_2	TiO_2	Al_2O_3	Fe_2O_3	FeO	MnO	MgO	CaO	Na_2O	K_2O	P_2O_5	FeO*	Mg#	CaO/Al_2O_3	Tc	Fo_c	ol%
39	1	1220	89.8	48.00	1.24	18.34	1.18	3.91	0.13	7.38	15.27	2.98	1.20	0.31	4.97	72.6		1171	92.3	0.00
				47.48	*1.21*	*17.79*	*1.57*	*5.23*	*0.13*	*7.37*	*14.82*	*2.89*	*1.17*	*0.30*	*6.64*	*66.5*		*1171*	*89.8*	*2.27*
				46.15	1.06	15.55	2.25	7.49	0.11	10.60	12.95	2.53	1.02	0.27	9.51	66.6	0.83	1268	89.8	14.42
39	2	1220	89.5	47.41	1.24	17.79	1.46	4.87	0.12	7.43	15.56	2.76	1.10	0.16	6.19	68.2		1168	90.6	0.00
				47.19	*1.23*	*17.57*	*1.63*	*5.43*	*0.12*	*7.41*	*15.37*	*2.73*	*1.09*	*0.16*	*6.90*	*65.7*		*1167*	*89.5*	*0.94*
				46.02	1.09	15.58	2.25	7.49	0.11	10.23	13.63	2.42	0.97	0.14	9.52	65.7	0.87	1255	89.5	11.74
39	3	1220	89.2	47.62	1.19	18.66	1.20	3.98	0.10	7.34	15.44	3.07	1.17	0.19	5.06	72.1		1171	92.2	0.00
				47.00	*1.15*	*17.97*	*1.68*	*5.59*	*0.10*	*7.35*	*14.87*	*2.95*	*1.13*	*0.18*	*7.10*	*64.9*		*1171*	*89.2*	*2.83*
				45.94	1.03	16.12	2.25	7.49	0.09	9.88	13.34	2.65	1.01	0.16	9.51	65.0	0.83	1249	89.2	12.57
39	4	1220	89.5	47.22	1.18	18.98	1.16	3.87	0.21	7.71	15.49	2.82	1.21	0.12	4.91	73.7		1180	92.8	0.00
				46.53	*1.13*	*18.19*	*1.71*	*5.69*	*0.20*	*7.71*	*14.84*	*2.70*	*1.16*	*0.12*	*7.22*	*65.6*		*1180*	*89.5*	*3.21*
				45.56	1.02	16.38	2.25	7.48	0.18	10.17	13.36	2.43	1.04	0.10	9.50	65.7	0.82	1254	89.5	12.65
39	6	1220	89.5	46.36	1.55	17.74	1.38	4.60	0.12	7.88	16.55	2.60	1.05	0.15	5.85	70.6		1180	91.8	0.00
				45.89	*1.50*	*17.20*	*1.77*	*5.90*	*0.11*	*7.86*	*16.05*	*2.52*	*1.02*	*0.14*	*7.49*	*65.2*		*1180*	*89.5*	*2.30*
				45.08	1.37	15.68	2.25	7.49	0.10	10.01	14.63	2.30	0.93	0.13	9.52	65.2	0.93	1247	89.5	10.63
39	7	1220	89.4	46.54	0.99	18.15	1.36	4.54	0.19	7.89	15.73	2.99	1.35	0.27	5.76	71.0		1190	91.9	0.00
				46.00	*0.96*	*17.52*	*1.80*	*5.99*	*0.18*	*7.90*	*15.19*	*2.89*	*1.30*	*0.26*	*7.61*	*65.0*		*1190*	*89.4*	*2.66*
				45.23	0.88	16.07	2.25	7.48	0.17	9.90	13.93	2.65	1.19	0.24	9.51	65.0	0.87	1251	89.4	10.43
39	5	1220	89.5	48.31	1.51	16.96	1.21	4.02	0.03	7.90	14.86	3.37	1.62	0.22	5.11	73.4		1204	92.8	0.00
				47.52	*1.44*	*16.18*	*1.79*	*5.95*	*0.03*	*7.94*	*14.18*	*3.22*	*1.54*	*0.21*	*7.56*	*65.2*		*1204*	*89.5*	*3.54*
				46.59	1.31	14.79	2.25	7.48	0.03	10.06	12.95	2.94	1.41	0.19	9.50	65.4	0.88	1266	89.5	11.69
42	1	1184	88.0	45.63	1.04	18.66	1.22	4.06	0.00	7.79	16.51	2.91	1.49	0.65	5.16	72.9		1184	92.7	0.00
				44.69	*0.98*	*17.48*	*2.04*	*6.79*	*0.00*	*7.79*	*15.47*	*2.73*	*1.40*	*0.61*	*8.62*	*61.7*		*1184*	*88.0*	*4.92*
				44.39	0.94	16.85	2.25	7.48	0.00	8.58	14.91	2.63	1.35	0.59	9.50	61.7	0.88	1211	88.0	8.18
42	2	1184	88.3	50.20	0.77	17.74	1.44	4.80	0.17	6.71	13.41	2.14	2.34	0.27	6.09	66.3		1155	89.3	0.00
				50.00	*0.76*	*17.56*	*1.57*	*5.24*	*0.17*	*6.71*	*13.28*	*2.12*	*2.32*	*0.27*	*6.65*	*64.3*		*1155*	*88.3*	*0.77*
				48.43	0.67	15.51	2.25	7.48	0.15	9.63	11.73	1.87	2.05	0.24	9.50	64.4	0.76	1244	88.3	11.97
42	3	1184	88.3	46.98	1.04	17.47	1.33	4.43	0.03	8.25	16.44	2.15	1.31	0.56	5.62	72.4		1187	92.2	0.00
				46.13	*0.98*	*16.55*	*2.01*	*6.69*	*0.03*	*8.22*	*15.57*	*2.04*	*1.24*	*0.53*	*8.50*	*63.3*		*1186*	*88.3*	*4.08*
				45.71	0.94	15.84	2.25	7.48	0.03	9.20	14.90	1.95	1.19	0.51	9.51	63.3	0.94	1218	88.3	8.04
43	1	1220	90.4	44.10	1.19	17.98	1.37	4.56	0.11	8.85	17.71	2.81	1.06	0.23	5.79	73.2		1217	93.1	0.00
				43.53	*1.13*	*17.17*	*1.92*	*6.40*	*0.11*	*8.88*	*16.92*	*2.68*	*1.02*	*0.22*	*8.13*	*66.1*		*1217*	*90.4*	*3.49*
				43.10	1.06	16.06	2.25	7.48	0.10	10.43	15.83	2.51	0.95	0.21	9.51	66.2	0.99	1264	90.4	9.48
43	3	1220	90.4	45.39	1.28	17.38	1.34	4.47	0.03	8.86	17.23	2.74	1.11	0.18	5.68	73.6		1217	93.1	0.00
				44.77	*1.22*	*16.61*	*1.88*	*6.27*	*0.03*	*8.89*	*16.47*	*2.62*	*1.06*	*0.17*	*7.96*	*66.6*		*1217*	*90.4*	*3.43*
				44.19	1.13	15.39	2.25	7.49	0.03	10.68	15.26	2.43	0.98	0.16	9.52	66.7	0.99	1270	90.4	10.30
43	5	1220	91.1	46.23	1.06	16.92	1.25	4.17	0.00	8.87	17.44	2.84	0.94	0.20	5.29	75.0		1216	93.5	0.00
				45.66	*1.02*	*16.28*	*1.72*	*5.73*	*0.00*	*8.90*	*16.78*	*2.74*	*0.91*	*0.19*	*7.28*	*68.6*		*1216*	*91.1*	*2.93*
				44.75	0.91	14.51	2.25	7.48	0.00	11.68	14.95	2.44	0.81	0.17	9.51	68.7	1.03	1294	91.1	13.39
43	4	1220	90.7	45.69	1.21	18.13	1.25	4.17	0.07	8.45	17.07	2.81	0.92	0.21	5.29	74.0		1200	93.2	0.00
				45.17	*1.17*	*17.48*	*1.71*	*5.68*	*0.07*	*8.44*	*16.46*	*2.71*	*0.89*	*0.20*	*7.22*	*67.6*		*1200*	*90.7*	*2.73*
				44.30	1.04	15.61	2.25	7.48	0.06	11.15	14.70	2.42	0.79	0.18	9.50	67.7	0.94	1280	90.7	12.98
82	1	1255	90.0	47.14	0.88	14.16	1.75	5.83	0.06	9.32	17.55	1.91	1.21	0.13	7.40	69.2		1220	91.1	0.00
				46.85	*0.87*	*13.91*	*1.97*	*6.54*	*0.06*	*9.31*	*17.24*	*1.87*	*1.19*	*0.13*	*8.31*	*66.7*		*1220*	*90.0*	*1.37*
				46.29	0.82	13.12	2.25	7.48	0.06	10.66	16.26	1.77	1.12	0.12	9.50	66.7	1.24	1259	90.0	6.65
82	2	1255	90.1	51.34	0.74	11.97	1.61	5.34	0.10	10.24	15.36	1.69	1.30	0.20	6.79	72.9		1246	91.9	0.00
				50.71	*0.72*	*11.58*	*1.98*	*6.58*	*0.10*	*10.27*	*14.87*	*1.64*	*1.26*	*0.19*	*8.36*	*68.7*		*1246*	*90.1*	*2.51*
				49.92	0.68	10.90	2.25	7.48	0.09	11.69	13.99	1.54	1.19	0.18	9.51	68.7	1.28	1282	90.1	8.04
83	1	1238	91.0	45.75	0.88	16.81	1.72	5.72	0.10	8.62	16.76	2.35	1.16	0.09	7.26	68.0		1203	90.8	0.00
				45.82	*0.88*	*16.89*	*1.66*	*5.54*	*0.10*	*8.60*	*16.84*	*2.36*	*1.16*	*0.09*	*7.04*	*68.6*		*1202*	*91.0*	*-0.38*
				44.80	0.78	14.88	2.25	7.48	0.09	11.66	14.84	2.08	1.03	0.08	9.50	68.7	1.00	1291	91.0	11.08
83	3	1238	90.5	45.82	0.93	17.02	1.57	5.23	0.18	7.67	17.29	2.69	1.33	0.20	6.64	67.3		1174	90.6	0.00
				45.82	*0.93*	*17.02*	*1.58*	*5.25*	*0.18*	*7.65*	*17.28*	*2.69*	*1.33*	*0.20*	*6.67*	*67.2*		*1174*	*90.5*	*0.00*
				44.69	0.81	14.85	2.25	7.49	0.16	10.92	15.08	2.35	1.16	0.18	9.51	67.2	1.02	1275	90.5	12.29
84	1	1260	90.2	45.08	0.96	12.75	2.26	7.52	0.17	10.17	18.34	1.62	1.01	0.07	9.55	65.5		1244	89.9	0.00
				45.18	*0.97*	*12.84*	*2.18*	*7.26*	*0.17*	*10.16*	*18.46*	*1.64*	*1.02*	*0.07*	*9.23*	*66.3*		*1244*	*90.2*	*-0.54*
				45.06	0.96	12.66	2.25	7.48	0.16	10.47	18.21	1.61	1.01	0.07	9.51	66.3	1.44	1253	90.2	0.71
86	1	1230	89.6	46.91	0.92	12.91	2.22	7.39	0.16	9.75	16.63	1.74	1.18	0.13	9.39	65.0		1232	89.1	0.00
				47.04	*0.93*	*13.02*	*2.12*	*7.07*	*0.16*	*9.75*	*16.77*	*1.76*	*1.19*	*0.13*	*8.98*	*66.0*		*1232*	*89.6*	*-0.65*
				46.79	0.91	12.69	2.25	7.48	0.16	10.33	16.35	1.71	1.16	0.13	9.50	66.0	1.29	1248	89.6	1.65
87	1	1240	89.7	45.82	0.97	15.32	1.98	6.59	0.10	9.04	16.62	2.11	1.29	0.14	8.38	65.8		1216	89.8	0.00
				45.80	*0.97*	*15.30*	*2.00*	*6.65*	*0.10*	*9.04*	*16.60*	*2.11*	*1.28*	*0.14*	*8.45*	*65.6*		*1216*	*89.7*	*0.10*
				45.35	0.92	14.55	2.25	7.49	0.09	10.18	15.79	2.01	1.22	0.13	9.51	65.7	1.09	1250	89.7	4.61

Appendix 3.1 (continued)

Composition of optically homogenized melt inclusions

Rinjani ankaramite suite, sample UTas48001 (cont.)

Grain	Melt	T_a	Fo_a	SiO_2	TiO_2	Al_2O_3	Fe_2O_3	FeO	MnO	MgO	CaO	Na_2O	K_2O	P_2O_5	FeO*	Mg#	CaO/Al_2O_3	Tc	Fo_x	ol%
87	2	1240	89.6	46.67	0.99	15.26	1.95	6.50	0.12	8.32	17.03	1.86	1.07	0.18	8.26	64.3		1185	88.8	0.00
				46.86	*1.00*	*15.44*	*1.81*	*6.02*	*0.12*	*8.32*	*17.23*	*1.88*	*1.09*	*0.19*	*7.65*	*66.0*		*1185*	*89.6*	*-0.89*
				46.03	0.92	14.16	2.25	7.48	0.11	10.32	15.80	1.73	1.00	0.17	9.50	66.0	1.12	1246	89.6	6.89
87	3	1240	89.3	45.15	1.02	15.11	2.00	6.66	0.14	9.31	17.16	2.04	1.20	0.20	8.47	66.2		1223	90.1	0.00
				44.95	*1.01*	*14.89*	*2.17*	*7.22*	*0.14*	*9.32*	*16.91*	*2.01*	*1.18*	*0.20*	*9.17*	*64.5*		*1223*	*89.3*	*1.13*
				44.82	0.99	14.66	2.25	7.48	0.14	9.67	16.65	1.98	1.16	0.19	9.51	64.5	1.14	1233	89.3	2.53
88	1	1250	89.7	45.31	0.93	14.17	2.05	6.83	0.14	9.50	17.69	1.84	1.32	0.16	8.67	66.2		1228	90.1	0.00
				45.21	*0.92*	*14.07*	*2.13*	*7.11*	*0.14*	*9.51*	*17.56*	*1.83*	*1.31*	*0.16*	*9.03*	*65.3*		*1228*	*89.7*	*0.58*
				45.01	0.90	13.75	2.25	7.49	0.14	10.03	17.16	1.79	1.28	0.15	9.52	65.3	1.25	1244	89.7	2.67
88	3	1250	88.8	45.23	0.95	13.59	2.07	6.91	0.18	11.27	17.85	0.94	0.67	0.32	8.77	69.6		1259	91.3	0.00
				44.54	*0.90*	*12.91*	*2.64*	*8.80*	*0.17*	*11.23*	*16.95*	*0.89*	*0.63*	*0.31*	*11.18*	*64.2*		*1258*	*88.8*	*3.99*
				45.22	0.98	14.01	2.24	7.46	0.19	9.49	18.40	0.97	0.69	0.33	9.48	64.1	1.31	1207	88.8	-3.38
89	1	1240	90.4	46.61	0.79	14.50	2.15	7.17	0.10	10.77	14.85	1.84	1.02	0.17	9.10	67.9		1260	90.3	0.00
				46.66	*0.79*	*14.55*	*2.12*	*7.07*	*0.10*	*10.75*	*14.90*	*1.85*	*1.03*	*0.17*	*8.98*	*68.1*		*1259*	*90.4*	*-0.26*
				46.39	0.77	14.15	2.25	7.49	0.10	11.38	14.49	1.80	1.00	0.16	9.51	68.1	1.02	1276	90.4	2.26

Ulakan ankaramite suite, sample UTas67424

Grain	Melt	T_a	Fo_a	SiO_2	TiO_2	Al_2O_3	Fe_2O_3	FeO	MnO	MgO	CaO	Na_2O	K_2O	P_2O_5	FeO*	Mg#	CaO/Al_2O_3	Tc	Fo_x	ol%
R92	1	1280	89.8	48.30	1.05	12.65	0.90	4.50	0.08	11.74	16.06	2.36	1.58	0.65	5.31	82.3	1.27	1302	94.5	0.00
				46.72	*0.95*	*11.41*	*1.71*	*8.53*	*0.07*	*11.88*	*14.48*	*2.13*	*1.42*	*0.59*	*10.06*	*71.3*		*1301*	*89.8*	*8.08*
				46.49	0.93	11.14	1.78	8.91	0.07	12.40	14.13	2.08	1.39	0.58	10.51	71.3		1314	89.8	10.29
R93	1	1280	91.5	48.20	0.98	13.65	0.75	3.74	0.14	11.73	15.92	2.71	1.69	0.33	4.41	84.9	1.17	1311	95.6	0.00
				46.84	*0.89*	*12.47*	*1.45*	*7.26*	*0.13*	*11.95*	*14.54*	*2.47*	*1.54*	*0.30*	*8.57*	*74.6*		*1311*	*91.5*	*7.10*
				45.79	0.79	11.02	1.78	8.91	0.11	14.79	12.86	2.18	1.36	0.27	10.51	74.8		1374	91.5	18.41
R94	1	1280	91.0	48.52	0.84	14.72	0.63	3.13	0.11	10.76	16.70	2.56	1.65	0.36	3.69	86.0	1.13	1280	95.9	0.00
				47.05	*0.76*	*13.40*	*1.40*	*6.98*	*0.10*	*10.91*	*15.21*	*2.33*	*1.50*	*0.33*	*8.24*	*73.6*		*1280*	*91.0*	*7.26*
				45.85	0.67	11.71	1.78	8.92	0.09	14.03	13.29	2.04	1.31	0.28	10.52	73.7		1354	91.0	19.60
R96	1	1280	87.4	46.61	1.18	13.16	0.94	4.71	0.13	12.74	15.52	2.21	2.07	0.65	5.55	82.9	1.18	1334	94.9	0.00
				44.04	*0.96*	*10.74*	*2.38*	*11.90*	*0.11*	*13.12*	*12.67*	*1.80*	*1.69*	*0.53*	*14.04*	*66.3*		*1334*	*87.4*	*16.16*
				45.53	1.15	12.84	1.78	8.90	0.13	9.64	15.15	2.16	2.02	0.63	10.50	65.9		1247	87.4	0.05
R 101	1	1280	88.8	47.43	1.16	14.24	0.85	4.26	0.07	10.98	16.33	1.60	2.35	0.67	5.02	82.2	1.15	1278	94.5	0.00
				45.77	*1.03*	*12.71*	*1.76*	*8.81*	*0.06*	*11.10*	*14.58*	*1.43*	*2.10*	*0.60*	*10.39*	*69.2*		*1278*	*88.8*	*8.83*
				45.72	1.03	12.63	1.78	8.91	0.06	11.22	14.50	1.42	2.09	0.59	10.51	69.2		1281	88.8	9.35
R102	1	1300	88.3	46.11	1.01	12.64	0.96	4.82	0.13	12.05	17.82	1.91	1.98	0.51	5.68	81.7	1.41	1313	94.6	0.00
				44.15	*0.87*	*10.84*	*2.12*	*10.58*	*0.12*	*12.24*	*15.28*	*1.64*	*1.70*	*0.43*	*12.49*	*67.4*		*1313*	*88.3*	*12.08*
				44.94	0.96	11.99	1.78	8.89	0.13	10.20	16.90	1.81	1.88	0.48	10.49	67.2		1259	88.3	2.99
R103	1	1280	90.5	50.93	0.87	15.12	0.59	2.93	0.10	10.88	13.91	3.03	1.37	0.17	3.46	86.9	0.92	1293	96.0	0.00
				49.02	*0.78*	*13.56*	*1.45*	*7.24*	*0.09*	*11.20*	*12.47*	*2.71*	*1.23*	*0.16*	*8.54*	*73.4*		*1293*	*90.5*	*8.52*
				47.77	0.70	12.08	1.78	8.90	0.08	13.86	11.11	2.42	1.09	0.14	10.50	73.6		1351	90.5	19.15
R104	1	1280	90.1	48.51	0.84	12.89	0.76	3.83	0.14	11.96	17.31	2.06	1.33	0.23	4.51	84.8	1.34	1303	95.5	0.00
				46.69	*0.74*	*11.44*	*1.69*	*8.48*	*0.13*	*12.12*	*15.36*	*1.83*	*1.18*	*0.21*	*10.00*	*71.9*		*1303*	*90.1*	*9.32*
				46.43	0.72	11.12	1.78	8.90	0.12	12.74	14.93	1.78	1.15	0.20	10.50	71.9		1318	90.1	11.88
R105	1	1290	90.1	48.94	0.80	12.35	0.77	3.87	0.03	12.22	17.14	2.25	1.22	0.24	4.57	84.9	1.39	1312	95.5	0.00
				47.01	*0.71*	*10.90*	*1.73*	*8.65*	*0.03*	*12.41*	*15.14*	*1.99*	*1.08*	*0.22*	*10.21*	*71.9*		*1312*	*90.1*	*9.75*
				46.84	0.70	10.72	1.78	8.90	0.03	12.77	14.89	1.95	1.06	0.21	10.51	71.9		1320	90.1	11.26
R107	1	1300	87.7	46.63	1.04	13.47	1.10	5.50	0.16	12.76	15.47	1.62	1.83	0.30	6.48	80.6	1.15	1322	93.9	0.00
				44.52	*0.89*	*11.47*	*2.26*	*11.31*	*0.13*	*12.95*	*13.17*	*1.38*	*1.56*	*0.26*	*13.34*	*67.2*		*1322*	*87.7*	*12.74*
				45.76	1.02	13.26	1.78	8.90	0.16	10.09	15.22	1.59	1.80	0.30	10.50	66.9		1250	87.7	-0.34
R107	2	1300	87.6	46.93	1.02	12.67	1.03	5.18	0.18	13.47	16.09	1.35	1.67	0.30	6.11	82.3	1.27	1334	94.6	0.00
				44.43	*0.85*	*10.46*	*2.39*	*11.94*	*0.15*	*13.66*	*13.29*	*1.11*	*1.38*	*0.25*	*14.09*	*67.1*		*1334*	*87.6*	*15.20*
				46.05	1.02	12.61	1.78	8.89	0.18	10.05	16.01	1.34	1.66	0.30	10.49	66.9		1244	87.6	-1.64
R108	1	1280	90.9	48.05	0.88	15.56	0.64	3.18	0.04	11.58	16.38	2.32	1.13	0.10	3.76	86.7	1.05	1294	96.1	0.00
				46.43	*0.79*	*13.96*	*1.51*	*7.54*	*0.04*	*11.73*	*14.70*	*2.08*	*1.02*	*0.09*	*8.90*	*73.5*		*1294*	*90.9*	*8.40*
				45.61	0.72	12.68	1.78	8.90	0.03	13.92	13.35	1.89	0.92	0.08	10.50	73.6		1345	90.9	17.22
R109	1	1300	90.9	47.78	1.29	10.87	0.74	3.71	0.07	12.39	18.64	1.56	2.41	0.41	4.37	85.6	1.71	1323	95.9	0.00
				46.02	*1.14*	*9.61*	*1.68*	*8.39*	*0.06*	*12.63*	*16.49*	*1.38*	*2.13*	*0.36*	*9.90*	*72.9*		*1323*	*90.9*	*9.65*
				45.71	1.10	9.27	1.78	8.90	0.06	13.43	15.90	1.33	2.06	0.35	10.51	72.9		1342	90.9	12.96
R109	2	1300	91.2	46.52	1.29	12.32	0.82	4.12	0.07	11.52	18.96	1.41	2.28	0.48	4.86	83.3	1.54	1294	95.2	0.00
				45.35	*1.19*	*11.32*	*1.51*	*7.54*	*0.06*	*11.60*	*17.41*	*1.30*	*2.10*	*0.45*	*8.90*	*73.3*		*1294*	*91.2*	*6.58*
				44.63	1.08	10.29	1.78	8.90	0.06	13.79	15.82	1.18	1.91	0.40	10.50	73.5		1348	91.2	15.32
R109	3	1300	90.9	47.04	1.18	11.88	0.83	4.16	0.07	11.80	19.31	1.45	1.82	0.28	4.91	83.5	1.63	1299	95.2	0.00
				45.68	*1.07*	*10.80*	*1.59*	*7.96*	*0.07*	*11.90*	*17.54*	*1.32*	*1.65*	*0.25*	*9.39*	*72.8*		*1299*	*90.9*	*7.45*
				45.16	1.00	10.12	1.78	8.90	0.06	13.37	16.44	1.24	1.55	0.24	10.50	72.9		1335	90.9	13.40

Appendix 3.1 (continued)

Composition of optically homogenized melt inclusions

Ulakan ankaramite suite, sample UTas67424 (cont.)

Grain	Melt	T_i	Fo_i	SiO_2	TiO_2	Al_2O_3	Fe_2O_3	FeO	MnO	MgO	CaO	Na_2O	K_2O	P_2O_5	FeO*	Mg#	CaO/Al_2O_3	Tc	Fo_c	ol%
1	1	1240	89.8	47.91	0.77	14.00	0.83	4.13	0.00	13.94	14.37	1.91	1.40	0.59	4.87	85.8	1.03	1348	95.7	0.00
				45.63	*0.65*	*11.87*	*1.99*	*9.96*	*0.00*	*14.28*	*12.18*	*1.62*	*1.19*	*0.50*	*11.75*	*71.9*		*1348*	*89.8*	*13.18*
				46.29	0.70	12.80	1.78	8.89	0.00	12.70	13.14	1.74	1.28	0.54	10.49	71.8		1313	89.8	6.29
2	1	1240	91.8	48.20	0.94	13.47	0.65	3.26	0.05	12.66	16.30	2.34	1.59	0.42	3.85	87.4	1.21	1329	96.4	0.00
				46.57	*0.84*	*12.05*	*1.50*	*7.50*	*0.05*	*12.91*	*14.59*	*2.10*	*1.42*	*0.37*	*8.85*	*75.5*		*1329*	*91.8*	*8.74*
				45.67	0.76	10.80	1.78	8.90	0.04	15.41	13.07	1.88	1.28	0.33	10.50	75.6		1383	91.8	18.82
2	2	1240	91.8	48.04	0.83	13.38	0.86	4.28	0.00	13.38	15.68	1.77	1.26	0.48	5.05	84.8	1.17	1332	95.4	0.00
				46.72	*0.76*	*12.22*	*1.53*	*7.66*	*0.00*	*13.54*	*14.33*	*1.61*	*1.15*	*0.44*	*9.04*	*75.9*		*1332*	*91.8*	*7.15*
				45.88	0.68	11.06	1.78	8.90	0.00	15.79	12.96	1.46	1.04	0.40	10.51	76.0		1379	91.8	16.35
3	1	1220	89.6	50.32	1.17	12.65	0.70	3.48	0.06	11.23	15.39	1.90	2.14	0.80	4.11	85.2	1.22	1286	95.4	0.00
				48.37	*1.04*	*11.29*	*1.60*	*8.03*	*0.05*	*11.40*	*13.73*	*1.70*	*1.91*	*0.71*	*9.47*	*71.7*		*1286*	*89.6*	*8.84*
				47.75	0.99	10.66	1.78	8.90	0.05	12.67	12.97	1.60	1.80	0.67	10.51	71.8		1315	89.6	14.06
4	1	1240	88.7	47.00	0.78	12.14	1.07	5.37	0.07	14.34	14.94	2.16	1.92	0.10	6.34	82.7	1.23	1374	94.8	0.00
				44.47	*0.64*	*9.91*	*2.39*	*11.98*	*0.06*	*14.84*	*12.20*	*1.77*	*1.57*	*0.08*	*14.13*	*68.9*		*1374*	*88.7*	*16.31*
				46.21	0.79	12.17	1.78	8.89	0.07	10.80	14.99	2.17	1.93	0.10	10.49	68.5		1282	88.7	-2.32
5	1	1240	89.3	48.56	0.87	17.65	1.00	5.02	0.06	6.98	14.16	2.56	2.62	0.49	5.93	71.3	0.80	1171	89.7	0.00
				48.49	*0.87*	*17.58*	*1.05*	*5.23*	*0.06*	*6.97*	*14.10*	*2.55*	*2.61*	*0.49*	*6.17*	*70.4*		*1171*	*89.3*	*0.30*
				46.32	0.71	14.25	1.78	8.91	0.05	11.96	11.43	2.07	2.12	0.40	10.51	70.6		1312	89.3	19.36
6	1	1240	85.3	51.07	0.71	13.43	0.82	4.09	0.00	12.60	12.82	2.15	1.94	0.28	4.83	84.6	0.95	1329	95.1	0.00
				46.92	*0.55*	*10.39*	*2.59*	*12.96*	*0.00*	*13.22*	*9.91*	*1.66*	*1.50*	*0.22*	*15.29*	*64.6*		*1329*	*85.3*	*20.61*
				49.74	0.69	13.11	1.78	8.90	0.00	8.92	12.51	2.10	1.89	0.27	10.50	64.2		1228	85.3	-0.36
22	1	1250	89.6	43.19	1.38	14.36	1.27	6.35	0.10	11.26	18.18	1.49	1.51	0.86	7.49	76.0	1.27	1280	92.6	0.00
				42.49	*1.29*	*13.48*	*1.77*	*8.87*	*0.10*	*11.25*	*17.07*	*1.40*	*1.42*	*0.81*	*10.47*	*69.4*		*1280*	*89.6*	*4.89*
				42.48	1.29	13.45	1.78	8.91	0.10	11.30	17.03	1.40	1.42	0.81	10.51	69.4		1281	89.6	5.08
25	1	1205	89.9	49.79	0.91	16.71	0.78	3.91	0.06	6.74	15.24	2.65	2.95	0.23	4.61	75.5	0.91	1164	91.7	0.00
				49.44	*0.89*	*16.41*	*0.96*	*4.78*	*0.06*	*6.74*	*14.96*	*2.61*	*2.90*	*0.23*	*5.64*	*71.6*		*1164*	*89.9*	*1.36*
				46.81	0.70	12.88	1.78	8.90	0.05	12.62	11.74	2.05	2.27	0.18	10.50	71.7		1331	89.9	23.42
27	1	1220	89.4	49.12	0.90	15.68	0.74	3.70	0.00	10.40	15.90	1.76	1.52	0.12	4.37	83.4	1.01	1255	94.8	0.00
				47.58	*0.82*	*14.30*	*1.52*	*7.59*	*0.00*	*10.44*	*14.51*	*1.60*	*1.39*	*0.11*	*8.95*	*71.1*		*1254*	*89.4*	*7.08*
				46.76	0.76	13.17	1.78	8.91	0.00	12.27	13.36	1.48	1.28	0.10	10.51	71.1		1301	89.4	14.56
27	2	1220	89.7	49.05	0.82	14.39	0.92	4.59	0.03	10.78	17.26	1.04	0.94	0.09	5.41	80.8	1.20	1248	93.6	0.00
				47.90	*0.77*	*13.46*	*1.49*	*7.46*	*0.03*	*10.73*	*16.14*	*0.97*	*0.88*	*0.08*	*8.80*	*72.0*		*1247*	*89.7*	*5.17*
				46.96	0.70	12.27	1.78	8.90	0.03	12.79	14.72	0.89	0.80	0.08	10.50	72.0		1300	89.7	13.57
27	3	1220	89.9	48.36	0.84	15.95	0.81	4.03	0.08	10.75	16.43	1.30	1.33	0.11	4.76	82.7	1.03	1255	94.5	0.00
				47.08	*0.78*	*14.73*	*1.48*	*7.42*	*0.07*	*10.74*	*15.17*	*1.20*	*1.22*	*0.10*	*8.75*	*72.1*		*1254*	*89.9*	*6.14*
				46.18	0.70	13.39	1.78	8.90	0.07	12.89	13.78	1.09	1.11	0.09	10.50	72.1		1308	89.9	14.86
28	1	1290	87.3	49.93	1.09	14.17	1.02	5.09	0.00	10.64	13.91	1.99	1.54	0.48	6.00	78.9	0.98	1267	92.8	0.00
				48.17	*0.99*	*12.78*	*1.83*	*9.18*	*0.00*	*10.74*	*12.56*	*1.80*	*1.39*	*0.43*	*10.83*	*67.6*		*1266*	*87.3*	*8.01*
				48.36	1.00	12.99	1.78	8.89	0.00	10.40	12.76	1.83	1.41	0.44	10.49	67.6		1258	87.3	6.54
29	1	1300	88.5	48.34	0.66	13.29	1.08	5.38	0.17	11.63	15.63	1.99	1.54	0.14	6.35	79.4	1.18	1294	93.3	0.00
				46.73	*0.59*	*11.96*	*1.88*	*9.43*	*0.16*	*11.74*	*14.07*	*1.79*	*1.39*	*0.13*	*11.12*	*69.0*		*1294*	*88.5*	*8.24*
				47.06	0.61	12.36	1.78	8.89	0.16	11.04	14.54	1.85	1.43	0.13	10.49	68.9		1277	88.5	5.26
30	1	1300	86.0	48.44	0.83	14.07	0.97	4.86	0.08	11.69	15.16	2.03	1.47	0.32	5.74	81.1	1.08	1295	94.0	0.00
				45.79	*0.69*	*11.79*	*2.31*	*11.54*	*0.07*	*11.85*	*12.70*	*1.70*	*1.23*	*0.27*	*13.62*	*64.7*		*1294*	*86.0*	*13.96*
				47.30	0.80	13.64	1.78	8.88	0.08	9.04	14.69	1.96	1.42	0.31	10.48	64.5		1220	86.0	0.81
95	1	1280	86.9	47.13	0.97	12.46	1.03	5.16	0.11	11.32	18.27	1.71	1.49	0.25	6.09	79.7	1.47	1284	93.7	0.00
				45.06	*0.84*	*10.77*	*2.17*	*10.84*	*0.10*	*11.38*	*15.79*	*1.47*	*1.29*	*0.21*	*12.80*	*65.2*		*1284*	*86.9*	*11.40*
				46.06	0.93	11.99	1.78	8.89	0.11	9.26	17.58	1.64	1.44	0.24	10.49	65.0		1224	86.9	1.74
97	1	1290	89.6	48.39	0.88	12.44	0.90	4.52	0.22	12.02	16.77	2.04	1.44	0.14	5.33	82.6	1.35	1305	94.7	0.00
				46.65	*0.78*	*11.09*	*1.79*	*8.93*	*0.20*	*12.17*	*14.96*	*1.82*	*1.28*	*0.13*	*10.54*	*70.9*		*1305*	*89.6*	*8.98*
				46.67	0.78	11.12	1.78	8.89	0.20	12.10	15.00	1.82	1.28	0.13	10.49	70.9		1303	89.6	8.72
98	1	1280	88.6	49.42	0.93	14.67	0.81	4.05	0.16	11.29	13.94	2.27	1.77	0.60	4.78	83.3	0.95	1291	94.7	0.00
				47.40	*0.82*	*12.95*	*1.78*	*8.92*	*0.14*	*11.51*	*12.30*	*2.00*	*1.56*	*0.53*	*10.53*	*69.7*		*1291*	*88.6*	*9.80*
				47.42	0.82	12.97	1.78	8.89	0.14	11.47	12.32	2.01	1.57	0.53	10.49	69.7		1290	88.6	9.64
100	1	1280	91.4	48.27	0.80	15.39	0.69	3.45	0.06	10.76	15.39	2.79	2.00	0.31	4.07	84.8	1.00	1289	95.5	0.00
				47.03	*0.74*	*14.20*	*1.34*	*6.71*	*0.06*	*10.92*	*14.20*	*2.58*	*1.84*	*0.29*	*7.92*	*74.4*		*1289*	*91.4*	*6.22*
				45.66	0.63	12.11	1.78	8.90	0.05	14.66	12.11	2.20	1.57	0.25	10.50	74.6		1374	91.4	20.84

Appendix 3.1 (continued)

Composition of optically homogenized melt inclusions

Merelava ankaramite suite, sample 31551

Grain	Melt	T_x	Fo_x	SiO_2	TiO_2	Al_2O_3	Fe_2O_3	FeO	MnO	MgO	CaO	Na_2O	K_2O	P_2O_5	FeO*	Mg#	CaO/Al_2O_3	Tc	Fo_x	ol%
60		1230	87.9	49.23	0.47	16.91	0.87	5.83	0.14	8.23	14.69	2.85	0.46	0.31	6.62	71.6		1195	89.6	0.00
				48.86	*0.46*	*16.56*	*1.02*	*6.80*	*0.14*	*8.21*	*14.40*	*2.79*	*0.45*	*0.30*	*7.72*	*68.3*		*1195*	*87.9*	*1.55*
				48.19	0.44	15.64	1.19	7.94	0.13	9.55	13.59	2.63	0.43	0.28	9.01	68.2	0.87	1235	87.9	6.78
61		1237	89.4	49.67	0.63	16.12	0.82	5.45	0.02	9.15	14.85	2.43	0.53	0.31	6.19	75.0		1219	91.1	0.00
				49.24	*0.61*	*15.74*	*0.98*	*6.54*	*0.02*	*9.15*	*14.51*	*2.37*	*0.52*	*0.31*	*7.42*	*71.4*		*1219*	*89.4*	*1.82*
				48.33	0.56	14.53	1.19	7.93	0.02	11.08	13.39	2.19	0.48	0.28	9.01	71.4	0.92	1272	89.4	9.12
62	1	1240	82.6	47.99	0.75	16.77	1.18	7.90	0.07	7.92	13.91	2.27	0.74	0.48	8.96	64.2		1183	85.5	0.00
				47.36	*0.72*	*16.16*	*1.44*	*9.60*	*0.07*	*7.86*	*13.40*	*2.18*	*0.71*	*0.46*	*10.89*	*59.4*		*1183*	*82.6*	*2.86*
				48.22	0.77	17.33	1.19	7.91	0.07	6.50	14.37	2.34	0.76	0.49	8.98	59.5	0.83	1134	82.6	-3.39
62	2	1240	83.8	49.45	0.77	15.19	1.15	7.65	0.12	8.28	14.43	2.08	0.34	0.47	8.68	65.9		1186	86.2	0.00
				48.91	*0.75*	*14.76*	*1.35*	*9.02*	*0.12*	*8.21*	*14.01*	*2.02*	*0.33*	*0.45*	*10.24*	*61.9*		*1186*	*83.8*	*2.23*
				49.55	0.78	15.48	1.19	7.92	0.12	7.23	14.70	2.12	0.35	0.48	8.99	62.0	0.95	1153	83.8	-2.09
63	1	1209	87.1	47.82	0.60	17.56	0.90	5.98	0.10	8.29	16.09	1.94	0.41	0.28	6.78	71.2		1180	89.4	0.00
				47.35	*0.58*	*17.09*	*1.10*	*7.30*	*0.10*	*8.23*	*15.65*	*1.89*	*0.40*	*0.27*	*8.29*	*66.8*		*1180*	*87.1*	*2.07*
				47.03	0.56	16.58	1.19	7.93	0.09	8.91	15.19	1.83	0.39	0.26	9.00	66.7	0.92	1202	87.1	4.82
63	2	1209	87.6	47.84	0.61	16.87	0.94	6.26	0.21	8.37	16.29	1.94	0.32	0.34	7.10	70.5		1181	89.0	0.00
				47.55	*0.60*	*16.59*	*1.06*	*7.08*	*0.21*	*8.33*	*16.02*	*1.91*	*0.31*	*0.33*	*8.03*	*67.8*		*1181*	*87.6*	*1.26*
				47.10	0.57	15.90	1.19	7.93	0.20	9.29	15.35	1.83	0.30	0.32	9.01	67.7	0.97	1212	87.6	5.09
63	3	1209	85.7	48.05	0.62	17.03	0.92	6.15	0.08	8.32	16.20	1.89	0.36	0.35	6.98	70.7		1180	89.1	0.00
				47.35	*0.59*	*16.34*	*1.22*	*8.13*	*0.08*	*8.23*	*15.55*	*1.81*	*0.34*	*0.33*	*9.22*	*64.4*		*1180*	*85.7*	*3.12*
				47.45	0.60	16.49	1.19	7.93	0.08	8.04	15.69	1.83	0.35	0.34	9.00	64.4	0.95	1173	85.7	2.33
63	4	1209	87.0	47.88	0.55	17.30	0.88	5.84	0.09	8.26	16.50	2.02	0.35	0.28	6.63	71.6		1179	89.6	0.00
				47.34	*0.54*	*16.75*	*1.11*	*7.38*	*0.09*	*8.20*	*15.99*	*1.96*	*0.34*	*0.27*	*8.37*	*66.5*		*1179*	*87.0*	*2.42*
				47.06	0.52	16.31	1.19	7.93	0.09	8.79	15.56	1.91	0.33	0.27	9.01	66.4	0.95	1199	87.0	4.82
64A	1	1242	90.4	48.57	0.56	15.66	0.71	4.76	0.07	8.99	17.75	1.77	0.64	0.47	5.40	77.1		1199	92.2	0.00
				48.18	*0.55*	*15.32*	*0.88*	*5.85*	*0.07*	*8.93*	*17.37*	*1.73*	*0.62*	*0.46*	*6.64*	*73.2*		*1199*	*90.4*	*1.64*
				46.94	0.48	13.53	1.19	7.94	0.06	12.00	15.34	1.53	0.55	0.40	9.01	73.0	1.13	1287	90.4	13.01
64A	2	1242	90.2	47.97	0.52	15.91	0.76	5.08	0.00	8.98	17.94	1.80	0.59	0.42	5.77	75.9		1200	91.8	0.00
				47.63	*0.51*	*15.59*	*0.91*	*6.06*	*0.00*	*8.94*	*17.58*	*1.77*	*0.58*	*0.41*	*6.87*	*72.5*		*1200*	*90.2*	*1.52*
				46.57	0.46	13.98	1.19	7.94	0.00	11.62	15.76	1.58	0.52	0.37	9.01	72.3	1.13	1278	90.2	11.52
64B	3	1248	87.9	48.66	0.52	17.41	0.82	5.49	0.00	8.41	16.00	2.01	0.32	0.36	6.24	73.2		1184	90.2	0.00
				48.16	*0.51*	*16.92*	*1.03*	*6.86*	*0.00*	*8.37*	*15.55*	*1.95*	*0.31*	*0.35*	*7.78*	*68.5*		*1184*	*87.9*	*2.15*
				47.56	0.48	16.02	1.19	7.93	0.00	9.63	14.72	1.85	0.29	0.33	9.01	68.4	0.92	1223	87.9	7.10
64B	4	1248	87.6	48.21	0.52	17.78	0.87	5.81	0.11	8.61	15.52	1.87	0.31	0.36	6.60	72.6		1188	89.9	0.00
				47.72	*0.51*	*17.28*	*1.08*	*7.17*	*0.11*	*8.56*	*15.08*	*1.81*	*0.30*	*0.35*	*8.14*	*68.1*		*1188*	*87.6*	*2.17*
				47.30	0.49	16.62	1.19	7.94	0.10	9.44	14.51	1.74	0.29	0.33	9.01	68.0	0.87	1215	87.6	5.67
65	1	1257	89.1	47.68	0.57	15.97	0.96	6.40	0.14	9.92	15.66	1.85	0.41	0.38	7.26	73.5		1230	90.5	0.00
				47.33	*0.56*	*15.63*	*1.11*	*7.37*	*0.14*	*9.90*	*15.32*	*1.81*	*0.41*	*0.38*	*8.37*	*70.6*		*1230*	*89.1*	*1.65*
				47.02	0.54	15.15	1.19	7.93	0.13	10.63	14.85	1.76	0.39	0.36	9.00	70.5	0.98	1251	89.1	4.51
65	2	1257	89.4	49.05	0.59	16.06	0.85	5.66	0.04	9.45	15.65	1.98	0.34	0.33	6.43	74.9		1218	91.0	0.00
				48.64	*0.57*	*15.69*	*1.01*	*6.73*	*0.04*	*9.44*	*15.29*	*1.93*	*0.33*	*0.32*	*7.63*	*71.5*		*1218*	*89.4*	*1.79*
				47.88	0.54	14.65	1.19	7.93	0.04	11.09	14.27	1.80	0.31	0.30	9.00	71.4	0.97	1264	89.4	8.08
66	1	1220	88.8	48.46	0.60	14.27	1.16	7.73	0.04	9.39	15.71	1.85	0.45	0.35	8.77	68.5		1218	87.9	0.00
				48.68	*0.61*	*14.45*	*1.07*	*7.15*	*0.04*	*9.41*	*15.90*	*1.88*	*0.46*	*0.35*	*8.12*	*70.2*		*1218*	*88.8*	*-0.95*
				48.19	0.58	13.85	1.19	7.94	0.04	10.40	15.24	1.80	0.44	0.34	9.01	70.1	1.10	1247	88.8	2.94
66	2	1220	88.2	47.35	0.55	14.98	1.13	7.56	0.17	9.60	15.88	1.92	0.50	0.36	8.58	69.4		1225	88.7	0.00
				47.24	*0.54*	*14.88*	*1.18*	*7.87*	*0.17*	*9.60*	*15.76*	*1.91*	*0.49*	*0.35*	*8.93*	*68.5*		*1225*	*88.2*	*0.56*
				47.20	0.54	14.83	1.19	7.93	0.17	9.68	15.71	1.90	0.49	0.35	9.00	68.6	1.06	1227	88.2	0.85
70	2	1200	87.9	49.27	0.84	15.21	0.89	5.94	0.07	8.82	15.79	2.20	0.57	0.40	6.74	72.6		1204	90.0	0.00
				48.77	*0.82*	*14.80*	*1.09*	*7.25*	*0.07*	*8.77*	*15.36*	*2.14*	*0.56*	*0.38*	*8.23*	*68.4*		*1204*	*87.9*	*2.09*
				48.35	0.79	14.29	1.19	7.93	0.07	9.58	14.83	2.06	0.54	0.37	9.00	68.3	1.04	1228	87.9	5.28
71	1	1247	85.4	44.89	0.65	12.29	1.53	10.21	0.21	9.84	17.96	1.65	0.38	0.36	11.59	63.3		1235	86.1	0.00
				44.74	*0.64*	*12.16*	*1.60*	*10.68*	*0.21*	*9.81*	*17.77*	*1.63*	*0.37*	*0.35*	*12.13*	*62.1*		*1235*	*85.4*	*0.83*
				45.95	0.73	13.81	1.19	7.91	0.23	7.28	20.19	1.86	0.43	0.40	8.98	62.2	1.46	1148	85.4	-10.59
71	2	1247	85.1	44.93	0.60	11.13	1.67	11.15	0.10	9.37	18.57	1.64	0.44	0.40	12.65	60.0		1225	84.3	0.00
				45.13	*0.61*	*11.29*	*1.58*	*10.55*	*0.10*	*9.38*	*18.83*	*1.67*	*0.45*	*0.41*	*11.98*	*61.4*		*1225*	*85.1*	*-1.12*
				46.29	0.69	12.70	1.19	7.93	0.11	7.07	21.19	1.87	0.50	0.46	9.00	61.4	1.67	1142	85.1	-11.63
74		1300	87.7	46.58	0.42	14.16	1.15	7.64	0.13	12.13	15.44	1.57	0.46	0.32	8.67	73.9		1290	90.9	0.00
				45.60	*0.39*	*13.21*	*1.56*	*10.41*	*0.12*	*12.11*	*14.40*	*1.47*	*0.43*	*0.30*	*11.81*	*67.5*		*1290*	*87.7*	*5.45*
				46.90	0.45	15.14	1.19	7.92	0.14	9.23	16.51	1.68	0.49	0.35	8.99	67.5	1.09	1210	87.7	-6.92
75	1	1300	87.9	48.43	0.55	12.53	1.02	6.78	0.02	11.64	16.34	1.86	0.45	0.36	7.69	75.4		1281	91.5	0.00
				47.29	*0.51*	*11.67*	*1.46*	*9.74*	*0.02*	*11.59*	*15.21*	*1.73*	*0.42*	*0.33*	*11.05*	*68.0*		*1280*	*87.9*	*5.53*
				48.39	0.56	12.89	1.19	7.93	0.02	9.44	16.80	1.91	0.46	0.37	9.00	68.0	1.30	1221	87.9	-3.48

Appendix 3.1 (continued)

Composition of optically homogenized melt inclusions

Merelava ankaramite suite, sample 31551 (cont.)

Grain	Melt	T_s	Fo_s	SiO_2	TiO_2	Al_2O_3	Fe_2O_3	FeO	MnO	MgO	CaO	Na_2O	K_2O	P_2O_5	FeO*	Mg#	CaO/Al_2O_3	Tc	Fo_c	ol%
75	2	1300	87.3	52.24	0.73	14.90	0.85	5.64	0.04	10.18	11.62	2.77	0.72	0.27	6.40	76.3		1266	91.4	0.00
				50.86	*0.68*	*13.88*	*1.29*	*8.58*	*0.04*	*10.31*	*10.82*	*2.58*	*0.67*	*0.25*	*9.74*	*68.2*		*1266*	*87.3*	*5.58*
				51.36	0.71	14.38	1.19	7.93	0.04	9.50	11.22	2.67	0.70	0.26	9.00	68.2	0.78	1246	87.3	2.33
78	1	1390	83.2	48.15	0.48	12.24	1.27	8.48	0.25	15.51	11.15	1.72	0.38	0.29	9.63	76.6		1364	91.6	0.00
				44.40	*0.36*	*9.23*	*2.61*	*17.41*	*0.19*	*15.52*	*8.41*	*1.30*	*0.29*	*0.22*	*19.76*	*61.4*		*1364*	*83.2*	*22.95*
				50.22	0.61	15.50	1.19	7.92	0.32	7.02	14.12	2.18	0.48	0.37	8.99	61.3	0.91	1149	83.2	-23.74
79	1	1250	84.2	52.09	0.56	16.03	1.03	6.88	0.07	8.74	10.82	3.06	0.46	0.23	7.81	69.4		1230	88.0	0.00
				51.00	*0.53*	*15.17*	*1.38*	*9.23*	*0.07*	*8.79*	*10.24*	*2.89*	*0.43*	*0.22*	*10.48*	*63.0*		*1230*	*84.2*	*4.28*
				51.94	0.56	16.13	1.19	7.91	0.07	7.51	10.89	3.08	0.46	0.23	8.98	62.9	0.68	1193	84.2	-1.25

Epi ankaramite suite, sample UTas71046

Grain	Melt	T_s	Fo_s	SiO_2	TiO_2	Al_2O_3	Fe_2O_3	FeO	MnO	MgO	CaO	Na_2O	K_2O	P_2O_5	FeO*	Mg#	CaO/Al_2O_3	Tc	Fo_c	ol%
RW1	1	1260	86.6	45.18	0.68	14.01	0.92	7.64	0.12	10.86	17.82	1.96	0.66	0.03	8.47	71.7		1270	90.6	0.00
				44.18	*0.63*	*12.98*	*1.31*	*10.93*	*0.11*	*10.77*	*16.52*	*1.81*	*0.61*	*0.03*	*12.11*	*63.8*		*1270*	*86.6*	*5.90*
				45.19	0.71	14.63	1.02	8.48	0.13	8.34	18.62	2.05	0.69	0.03	9.39	63.7	1.27	1193	86.6	-4.88
RW1	1	1260	87.3	46.11	0.61	13.94	0.83	6.93	0.11	10.78	17.76	2.02	0.66	0.18	7.68	73.5		1266	91.2	0.00
				45.09	*0.57*	*12.97*	*1.21*	*10.10*	*0.10*	*10.71*	*16.53*	*1.88*	*0.61*	*0.17*	*11.19*	*65.4*		*1266*	*87.3*	*5.60*
				45.83	0.62	14.07	1.02	8.48	0.11	8.99	17.93	2.04	0.67	0.18	9.39	65.4	1.27	1214	87.3	-1.79
RW2	1	1280	83.6	44.31	0.76	15.16	0.97	8.04	0.13	11.19	16.94	1.80	0.54	0.08	8.91	71.3		1275	90.4	0.00
				42.67	*0.66*	*13.21*	*1.65*	*13.75*	*0.11*	*11.00*	*14.76*	*1.57*	*0.47*	*0.07*	*15.24*	*58.8*		*1275*	*83.6*	*10.78*
				44.57	0.84	16.74	1.02	8.46	0.14	6.76	18.70	1.98	0.60	0.09	9.38	58.8	1.12	1134	83.6	-10.40
RW2	7	1280	84.8	45.44	0.67	14.20	1.04	8.65	0.01	11.07	16.44	1.79	0.53	0.14	9.58	69.6		1271	89.3	0.00
				44.25	*0.61*	*12.98*	*1.49*	*12.38*	*0.01*	*10.98*	*15.03*	*1.63*	*0.48*	*0.13*	*13.72*	*61.3*		*1272*	*84.8*	*7.03*
				45.92	0.73	15.58	1.02	8.47	0.01	7.51	18.03	1.96	0.58	0.15	9.38	61.3	1.16	1162	84.8	-9.33
RW2	8	1280	85.0	44.97	0.71	14.87	1.02	8.52	0.09	10.39	16.67	1.93	0.54	0.14	9.44	68.5		1253	88.9	0.00
				44.06	*0.66*	*13.88*	*1.38*	*11.53*	*0.08*	*10.26*	*15.56*	*1.80*	*0.50*	*0.13*	*12.77*	*61.4*		*1253*	*85.0*	*5.33*
				45.28	0.76	15.97	1.02	8.47	0.10	7.55	17.90	2.07	0.58	0.15	9.38	61.4	1.12	1164	85.0	-7.22
RW2	10	1280	84.7	43.78	0.71	15.49	1.07	8.89	0.11	10.43	17.34	1.55	0.44	0.12	9.85	67.7		1250	88.6	0.00
				42.92	*0.66*	*14.43*	*1.44*	*11.98*	*0.10*	*10.30*	*16.15*	*1.44*	*0.41*	*0.11*	*13.27*	*60.6*		*1250*	*84.7*	*5.53*
				44.14	0.77	16.89	1.02	8.48	0.12	7.31	18.90	1.69	0.48	0.13	9.40	60.6	1.12	1149	84.7	-8.58
R15		1305	91.6	44.94	0.60	14.73	0.62	5.14	0.05	11.81	19.46	2.00	0.45	0.16	5.70	80.4		1296	94.3	0.00
				44.25	*0.57*	*13.96*	*0.91*	*7.55*	*0.05*	*11.78*	*18.43*	*1.89*	*0.43*	*0.15*	*8.36*	*73.6*		*1296*	*91.6*	*4.18*
				44.01	0.55	13.44	0.98	8.13	0.05	12.68	17.76	1.82	0.41	0.15	9.00	73.6	1.32	1320	91.6	7.61
R54	1	1275	84.0	46.89	0.58	15.54	0.93	7.77	0.08	12.25	14.41	1.03	0.41	0.11	8.61	73.8		1284	90.6	0.00
				44.93	*0.50*	*13.53*	*1.61*	*13.40*	*0.07*	*12.05*	*12.55*	*0.90*	*0.36*	*0.10*	*14.85*	*61.6*		*1284*	*84.0*	*10.90*
				47.35	0.64	17.16	1.02	8.47	0.09	7.67	15.91	1.14	0.45	0.12	9.38	61.8	0.93	1155	84.0	-10.49
R55	3	1230	81.0	48.00	0.85	15.30	1.06	8.84	0.18	9.19	13.60	2.21	0.64	0.14	9.80	65.0		1223	86.2	0.00
				46.72	*0.79*	*14.15*	*1.48*	*12.32*	*0.17*	*9.05*	*12.58*	*2.04*	*0.59*	*0.13*	*13.65*	*56.7*		*1223*	*81.0*	*6.09*
				48.66	0.92	16.54	1.02	8.48	0.19	6.25	14.71	2.39	0.69	0.15	9.39	56.8	0.89	1127	81.0	-7.94

Appendix 3.2

Molecular CIPWnorm compositions

Rinjani ankaramite suite, sample UTas48001

Grain	Melt	T_n	Fo_n	*or*	*ab*	*an*	*ne*	*lc*	*di*	*hy*	*ol*	*cs*	*cm*	*mt*	*ilm*	*ap*	*di/ol*
39	1	1220	89.8	5.71	6.85	26.67	14.70		32.70		7.87		0.06	1.66	3.48	0.33	4.16
				5.56	*7.02*	*25.81*	*13.84*		*31.71*		*10.11*		*0.06*	*2.20*	*3.39*	*0.32*	*3.14*
				4.65	6.82	21.67	10.71		26.58		23.37		0.04	3.03	2.85	0.27	1.14
39	2	1220	89.5	5.21	5.12	26.36	14.74		34.64		8.16		0.12	2.04	3.46	0.17	4.25
				5.15	*5.18*	*25.98*	*14.43*		*34.20*		*9.06*		*0.12*	*2.27*	*3.43*	*0.17*	*3.78*
				4.43	5.26	22.26	11.53		29.32		20.99		0.10	3.03	2.93	0.14	1.40
39	3	1220	89.2	5.50	4.88	26.81	17.06		33.17		7.35		0.07	1.66	3.30	0.20	4.51
				5.31	*5.21*	*25.79*	*15.84*		*31.90*		*10.18*		*0.07*	*2.33*	*3.18*	*0.19*	*3.13*
				4.60	5.31	22.45	13.03		27.79		20.80		0.06	3.02	2.77	0.16	1.34
39	4	1220	89.5	5.67	3.41	28.21	16.68		32.14		8.86		0.04	1.60	3.26	0.12	3.63
				5.43	*3.89*	*27.01*	*15.32*		*30.70*		*12.01*		*0.04*	*2.36*	*3.12*	*0.12*	*2.56*
				4.73	4.13	23.63	12.65		26.86		22.10		0.04	3.02	2.73	0.10	1.22
39	6	1220	89.5	4.87	0.70	26.40	17.62		37.28		6.81		0.03	1.89	4.24	0.15	5.48
				4.73	*1.11*	*25.59*	*16.65*		*36.18*		*9.06*		*0.03*	*2.42*	*4.10*	*0.14*	*3.99*
				4.21	1.63	22.74	14.17		32.16		18.27		0.03	3.00	3.65	0.13	1.76
39	7	1220	89.4	6.20	0.30	24.96	20.56		34.32		8.87			1.84	2.68	0.27	3.87
				5.97	*0.79*	*24.07*	*19.36*		*33.14*		*11.37*			*2.44*	*2.60*	*0.26*	*2.91*
				5.34	1.34	21.61	16.74		29.71		19.71			2.98	2.33	0.24	1.51
39	5	1220	89.5	7.46	4.56	20.56	19.04		35.81		6.60			1.64	4.10	0.22	5.42
				7.09	*5.01*	*19.59*	*17.50*		*34.14*		*10.13*			*2.43*	*3.91*	*0.21*	*3.37*
				6.34	5.06	17.49	15.01		30.43		19.03			2.98	3.47	0.19	1.60
42	1	1184	88.0	1.93		25.94	20.25	4.90	34.27		7.55		0.04	1.65	2.81	0.66	4.54
				3.53		*24.24*	*18.98*	*2.87*	*32.10*		*12.23*		*0.04*	*2.75*	*2.64*	*0.62*	*2.62*
				4.03		23.18	18.13	2.10	30.66		15.75		0.04	3.01	2.51	0.59	1.95
42	2	1184	88.3	11.81	12.16	27.23	4.25		28.08		11.74			2.14	2.29	0.30	2.39
				11.69	*12.14*	*26.90*	*4.09*		*27.78*		*12.50*			*2.33*	*2.26*	*0.30*	*2.22*
				9.88	11.16	22.73	2.53		23.45		24.89			3.20	1.90	0.26	0.94
42	3	1184	88.3	6.25	2.80	27.57	12.78		35.32		9.90			1.87	2.92	0.59	3.57
				5.90	*3.44*	*26.03*	*11.31*		*33.36*		*13.85*			*2.82*	*2.75*	*0.56*	*2.41*
				5.59	3.57	24.59	10.33		31.49		18.18			3.11	2.60	0.53	1.73
43	1	1220	90.4			24.77	18.76	4.66	27.50		13.24	5.97	0.03	1.77	3.08	0.22	2.08
						23.66	*17.90*	*4.48*	*27.44*		*15.73*	*5.14*	*0.03*	*2.49*	*2.93*	*0.21*	*1.74*
						21.81	16.52	4.12	26.22		21.25	4.28	0.03	2.87	2.71	0.20	1.23
43	3	1220	90.4			24.10	18.61	4.96	35.29		9.52	2.20		1.77	3.37	0.18	3.71
						23.02	*17.80*	*4.74*	*34.95*		*12.13*	*1.51*		*2.48*	*3.21*	*0.17*	*2.88*
						20.95	16.21	4.30	32.77		18.90	0.88		2.91	2.92	0.16	1.73
43	5	1220	91.1			23.40	19.47	4.24	40.63		6.93	0.52	0.11	1.66	2.82	0.20	5.86
						22.45	*18.76*	*4.10*	*40.01*		*9.34*	*0.05*	*0.11*	*2.29*	*2.71*	*0.19*	*4.29*
				1.36		19.45	16.23	2.19	34.68		20.58		0.09	2.90	2.35	0.16	1.68
43	4	1220	90.7			26.21	19.37	4.17	37.19		7.63	0.28	0.03	1.67	3.23	0.21	4.87
				0.47		*25.25*	*18.67*	*3.57*	*36.42*		*9.97*		*0.03*	*2.29*	*3.13*	*0.20*	*3.65*
				1.82		21.93	16.20	1.66	31.59		20.97		0.03	2.92	2.70	0.18	1.51
82	1	1255	90.0	2.98		20.78	13.45	2.63	46.84		8.31		0.09	2.39	2.40	0.13	5.64
				3.46		*20.42*	*13.16*	*2.05*	*45.97*		*9.65*		*0.09*	*2.69*	*2.38*	*0.13*	*4.76*
				3.98		18.92	12.25	1.12	42.66		15.64		0.08	3.02	2.20	0.12	2.73
82	2	1255	90.1	6.25	12.34	17.27			43.64	5.06	10.70		0.15	2.28	2.10	0.21	4.08
				5.99	*11.84*	*16.50*			*41.84*	*6.34*	*12.36*		*0.15*	*2.77*	*2.02*	*0.20*	*3.39*
				5.50	10.81	15.10			38.25	7.50	17.61		0.13	3.07	1.85	0.18	2.17
83	1	1238	91.0			24.65	16.31	5.30	38.62		10.02	0.27	0.07	2.32	2.37	0.09	3.86
						24.80	*16.39*	*5.30*	*38.76*		*9.69*	*0.30*	*0.07*	*2.24*	*2.37*	*0.09*	*4.00*
				0.96		21.10	13.96	3.59	33.55		21.76		0.05	2.93	2.03	0.08	1.54
83	3	1238	90.5			23.46	18.62	6.06	38.93		6.67	1.36	0.10	2.11	2.50	0.20	5.84
						23.47	*18.62*	*6.06*	*39.00*		*6.61*	*1.32*	*0.10*	*2.12*	*2.50*	*0.20*	*5.90*
						19.78	15.72	5.11	34.58		19.28	0.25	0.08	2.92	2.10	0.18	1.79
84	1	1260	90.2			18.61	11.03	4.53	40.88		14.69	4.59	0.07	2.99	2.54	0.07	2.78
						18.71	*11.17*	*4.57*	*41.00*		*14.26*	*4.71*	*0.07*	*2.88*	*2.56*	*0.07*	*2.88*
						18.40	10.93	4.51	40.50		15.49	4.53	0.07	2.96	2.53	0.07	2.62
86	1	1230	89.6	5.47	0.60	18.78	11.66		45.31		12.42		0.07	3.04	2.51	0.13	3.65
				5.52	*0.47*	*18.93*	*11.93*		*45.71*		*11.79*		*0.07*	*2.90*	*2.54*	*0.13*	*3.88*
				5.34	0.67	18.33	11.29		44.22		14.41		0.07	3.06	2.47	0.13	3.07
87	1	1240	89.7	0.53		22.05	14.64	5.36	40.98		10.99		0.03	2.67	2.61	0.14	3.73
				0.60		*22.02*	*14.64*	*5.25*	*40.92*		*11.09*		*0.03*	*2.69*	*2.61*	*0.14*	*3.69*
				1.16		20.65	13.76	4.33	38.45		16.04		0.03	2.99	2.44	0.13	2.40

Appendix 3.2 (continued)

Molecular CIPWnorm compositions

Rinjani ankaramite suite, sample UTas48001 (cont.)

Grain	Melt	T_s	Fo_s	*or*	*ab*	*an*	*ne*	*lc*	*di*	*hy*	*ol*	*cs*	*cm*	*mt*	*ilm*	*ap*	*di/ol*
87	2	1240	89.6	5.06	0.93	24.11	12.43		42.56		9.19		0.06	2.72	2.76	0.19	4.63
				5.16	*0.78*	*24.40*	*12.74*		*43.05*		*8.30*		*0.06*	*2.53*	*2.79*	*0.20*	*5.19*
				4.61	**1.28**	**21.78**	**10.83**		**38.51**		**17.20**		**0.06**	**3.06**	**2.50**	**0.17**	**2.24**
87	3	1240	89.3			21.83	14.02	5.43	38.33		12.82	2.00		2.67	2.72	0.20	2.99
						21.52	*13.81*	*5.33*	*38.18*		*13.64*	*1.75*		*2.89*	*2.69*	*0.20*	*2.80*
						21.10	**13.55**	**5.22**	**37.64**		**15.05**	**1.63**		**2.99**	**2.63**	**0.19**	**2.50**
88	1	1250	89.7			20.25	12.62	5.96	39.53		12.97	3.24	0.07	2.73	2.47	0.16	3.05
						20.09	*12.55*	*5.91*	*39.39*		*13.42*	*3.13*	*0.07*	*2.83*	*2.45*	*0.16*	*2.93*
						19.51	**12.20**	**5.74**	**38.54**		**15.52**	**2.92**	**0.07**	**2.98**	**2.38**	**0.15**	**2.48**
88	3	1250	88.8			24.20	6.61	3.10	42.61		17.22	0.48	0.03	2.83	2.59	0.33	2.47
				0.60		*22.97*	*6.25*	*2.31*	*41.22*		*20.26*		*0.03*	*3.60*	*2.45*	*0.32*	*2.03*
				25.48		**6.97**	**3.26**	**45.07**			**12.60**	**0.39**	**0.03**	**3.12**	**2.73**	**0.35**	**3.58**
89	1	1240	90.4	4.72	4.01	22.15	8.92		34.66		20.24		0.03	2.93	2.15	0.17	1.71
				4.76	*3.93*	*22.20*	*9.07*		*34.80*		*19.98*		*0.03*	*2.89*	*2.15*	*0.17*	*1.74*
				4.59	**3.97**	**21.41**	**8.58**		**33.60**		**22.54**		**0.03**	**3.04**	**2.08**	**0.16**	**1.49**

Ulakan ankaramite suite, sample UTas67424

Grain	Melt	T_s	Fo_s	*or*	*ab*	*an*	*ne*	*lc*	*di*	*hy*	*ol*	*cs*	*cm*	*mt*	*ilm*	*ap*	*di/ol*
R92	1	1280	89.8	7.14	1.92	14.72	14.28		42.94		14.20		0.17	1.20	2.79	0.65	3.02
				6.36	*2.64*	*13.18*	*11.86*		*38.38*		*22.08*		*0.15*	*2.26*	*2.51*	*0.58*	*1.74*
				6.19	**2.67**	**12.77**	**11.40**		**37.19**		**24.29**		**0.15**	**2.34**	**2.44**	**0.57**	**1.53**
R93	1	1280	91.5	6.07		15.02	18.19	1.40	42.43		12.80		0.23	0.98	2.55	0.32	3.31
				6.77	*0.13*	*13.68*	*16.36*		*38.51*		*19.86*		*0.22*	*1.88*	*2.30*	*0.29*	*1.94*
				5.79	**0.61**	**11.73**	**13.50**		**33.00**		**30.70**		**0.18**	**2.24**	**1.98**	**0.25**	**1.08**
R94	1	1280	91.0	6.25		18.19	17.57	1.20	43.34		9.95		0.06	0.84	2.24	0.36	4.36
				6.73	*0.30*	*16.46*	*15.59*		*39.22*		*17.45*		*0.06*	*1.85*	*2.01*	*0.33*	*2.25*
				5.67	**0.74**	**13.86**	**12.67**		**33.09**		**29.69**		**0.04**	**2.27**	**1.71**	**0.27**	**1.11**
R96	1	1280	87.4	1.52		14.66	14.64	7.50	39.02		17.68		0.11	1.21	3.03	0.63	2.21
				4.27		*11.85*	*11.80*	*3.02*	*31.50*		*31.50*		*0.09*	*3.03*	*2.44*	*0.51*	*1.00*
				3.17		**14.70**	**14.72**	**5.89**	**39.22**		**16.17**		**0.11**	**2.35**	**3.04**	**0.62**	**2.43**
R101	1	1280	88.8	5.20		19.19	11.14	5.58	40.27		13.59		0.09	1.15	3.13	0.68	2.96
				6.55		*16.95*	*9.87*	*2.99*	*35.62*		*22.24*		*0.07*	*2.36*	*2.76*	*0.60*	*1.60*
				6.50		**16.81**	**9.78**	**2.97**	**35.42**		**22.72**		**0.07**	**2.38**	**2.75**	**0.59**	**1.56**
R102	1	1300	88.3			14.77	12.62	8.61	38.10		16.67	4.87	0.05	1.23	2.59	0.49	2.29
						12.57	*10.76*	*7.34*	*34.92*		*26.09*	*2.94*	*0.05*	*2.70*	*2.21*	*0.41*	*1.34*
						14.23	**12.15**	**8.30**	**38.35**		**17.76**	**3.87**	**0.05**	**2.32**	**2.50**	**0.47**	**2.16**
R103	1	1280	90.5	6.38	11.58	18.62	9.87		34.93		15.11		0.13	0.81	2.39	0.18	2.31
				5.66	*11.24*	*16.52*	*7.71*		*30.86*		*23.64*		*0.11*	*1.97*	*2.12*	*0.16*	*1.31*
				4.84	**10.16**	**14.20**	**6.18**		**26.57**		**33.64**		**0.10**	**2.33**	**1.83**	**0.14**	**0.79**
R104	1	1280	90.1	4.69		16.78	14.11	1.31	47.59		11.84		0.21	1.01	2.23	0.23	4.02
				5.27	*0.46*	*14.76*	*11.96*		*41.83*		*21.15*		*0.18*	*2.23*	*1.95*	*0.21*	*1.98*
				5.10	**0.56**	**14.22**	**11.43**		**40.38**		**23.72**		**0.18**	**2.33**	**1.88**	**0.20**	**1.70**
R105	1	1290	90.1	5.49	0.79	15.22	14.58		48.31		12.01		0.22	1.02	2.12	0.24	4.02
				4.81	*1.73*	*13.28*	*11.74*		*42.24*		*21.66*		*0.19*	*2.27*	*1.86*	*0.22*	*1.95*
				4.70	**1.76**	**13.03**	**11.38**		**41.38**		**23.19**		**0.19**	**2.33**	**1.83**	**0.21**	**1.78**
R107	1	1300	87.7	2.56		18.09	10.93	5.56	38.11		20.11		0.18	1.44	2.72	0.29	1.90
				4.75		*15.24*	*9.21*	*2.11*	*32.08*		*30.98*		*0.15*	*2.93*	*2.30*	*0.25*	*1.04*
				4.02		**18.29**	**11.00**	**4.17**	**38.40**		**18.52**		**0.17**	**2.39**	**2.74**	**0.30**	**2.07**
R107	2	1300	87.6	2.08		17.76	9.13	5.36	40.90		20.32		0.14	1.35	2.68	0.30	2.01
				4.72		*14.48*	*7.41*	*1.34*	*33.31*		*33.08*		*0.12*	*3.09*	*2.20*	*0.24*	*1.01*
				3.74		**18.30**	**9.37**	**3.90**	**42.05**		**17.02**		**0.14**	**2.42**	**2.77**	**0.31**	**2.47**
R108	1	1280	90.9	5.11	0.91	21.96	15.03		39.71		13.80		0.18	0.85	2.34	0.10	2.88
				4.57	*1.70*	*19.53*	*12.46*		*35.35*		*22.05*		*0.17*	*2.00*	*2.09*	*0.09*	*1.60*
				4.02	**1.93**	**17.29**	**10.61**		**31.27**		**30.51**		**0.15**	**2.29**	**1.85**	**0.08**	**1.03**
R109	1	1300	90.9			11.55	10.41	10.58	47.18		11.40	4.01	0.18	0.96	3.34	0.40	4.14
						10.13	*9.14*	*9.28*	*43.38*		*19.91*	*2.55*	*0.16*	*2.16*	*2.93*	*0.35*	*2.18*
						9.68	**8.73**	**8.90**	**41.74**		**23.10**	**2.29**	**0.15**	**2.27**	**2.80**	**0.33**	**1.81**
R109	2	1300	91.2			15.39	9.48	10.09	41.03		13.00	5.84	0.26	1.07	3.36	0.47	3.16
						14.05	*8.70*	*9.25*	*39.01*		*18.68*	*4.58*	*0.25*	*1.96*	*3.09*	*0.44*	*2.09*
						12.47	**7.71**	**8.21**	**35.28**		**27.02**	**3.73**	**0.21**	**2.26**	**2.74**	**0.38**	**1.31**
R109	3	1300	90.9			15.41	9.77	8.07	44.68		12.17	5.22	0.25	1.09	3.08	0.27	3.67
						13.93	*8.85*	*7.28*	*41.99*		*18.73*	*3.90*	*0.23*	*2.07*	*2.78*	*0.24*	*2.24*
						12.82	**8.17**	**6.72**	**39.19**		**24.48**	**3.35**	**0.21**	**2.28**	**2.56**	**0.23**	**1.60**

Appendix 3.2 (continued)

Molecular CIPWnorm compositions

Ulakan ankaramite suite, sample UTas67424 (cont.)

Grain	Melt	T_s	Fo_s	*or*	*ab*	*an*	*ne*	*lc*	*di*	*hy*	*ol*	*cs*	*cm*	*mt*	*ilm*	*ap*	*di/ol*
1	1	1240	89.8	6.32	4.61	19.46	8.48		32.03		25.14		0.22	1.10	2.05	0.59	1.27
				5.28	*5.08*	*16.22*	*5.84*		*26.70*		*35.89*		*0.19*	*2.60*	*1.70*	*0.49*	*0.74*
				5.80	**5.27**	**17.90**	**6.72**		**29.40**		**29.90**		**0.21**	**2.38**	**1.87**	**0.54**	**0.98**
2	1	1240	91.8	5.73		16.18	15.77	1.33	42.47		14.65		0.15	0.85	2.46	0.41	2.90
				6.24	*0.27*	*14.33*	*13.76*		*37.73*		*23.04*		*0.14*	*1.94*	*2.18*	*0.36*	*1.64*
				5.47	**0.62**	**12.47**	**11.59**		**32.86**		**32.41**		**0.12**	**2.24**	**1.91**	**0.31**	**1.01**
2	2	1240	91.8	5.71	2.91	19.05	9.27		38.19		20.94		0.08	1.15	2.22	0.48	1.82
				5.16	*3.40*	*17.27*	*7.58*		*34.58*		*27.44*		*0.08*	*2.03*	*2.01*	*0.44*	*1.26*
				4.54	**3.38**	**15.18**	**6.30**		**30.38**		**35.73**		**0.07**	**2.29**	**1.75**	**0.39**	**0.85**
3	1	1220	89.6	10.15	7.50	15.79	6.19		41.31		13.71		0.26	0.98	3.27	0.84	3.01
				8.93	*7.61*	*13.88*	*4.47*		*36.37*		*22.70*		*0.23*	*2.21*	*2.87*	*0.73*	*1.60*
				8.27	**7.36**	**12.90**	**3.81**		**33.73**		**27.96**		**0.21**	**2.41**	**2.68**	**0.68**	**1.21**
4	1	1240	88.7			12.79	13.96	8.17	39.26		21.87	0.42	0.13	1.34	1.96	0.09	1.80
				2.12		*10.30*	*11.33*	*4.49*	*32.46*		*34.56*		*0.10*	*2.97*	*1.59*	*0.07*	*0.94*
				0.46		**13.22**	**14.50**	**8.02**	**41.63**		**17.58**		**0.14**	**2.31**	**2.05**	**0.10**	**2.37**
5	1	1240	89.3	12.54	3.59	23.44	15.03		30.89		10.11		0.01	1.41	2.45	0.52	3.06
				12.49	*3.64*	*23.33*	*14.90*		*30.73*		*10.44*		*0.01*	*1.48*	*2.45*	*0.52*	*2.94*
				9.51	**3.67**	**17.70**	**10.43**		**23.35**		**30.70**		**0.01**	**2.35**	**1.88**	**0.40**	**0.76**
6	1	1240	85.3	9.09	11.95	16.86	3.36		32.12		23.09		0.15	1.13	1.96	0.29	1.39
				6.81	*10.95*	*12.65*	*0.50*		*24.02*		*39.80*		*0.11*	*3.47*	*1.47*	*0.22*	*0.60*
				9.17	**13.12**	**17.05**	**2.36**		**32.47**		**20.87**		**0.15**	**2.55**	**1.97**	**0.29**	**1.56**
22	1	1250	89.6			20.82	9.94	6.63	27.21		21.90	7.39	0.07	1.64	3.57	0.83	1.24
						19.50	*9.32*	*6.22*	*26.60*		*25.52*	*6.38*	*0.07*	*2.29*	*3.33*	*0.78*	*1.04*
						19.42	**9.31**	**6.21**	**26.53**		**25.70**	**6.35**	**0.07**	**2.30**	**3.33**	**0.78**	**1.03**
25	1	1205	89.9	14.02	0.87	20.10	18.27		39.51		3.30		0.04	1.09	2.55	0.24	11.98
				13.76	*1.02*	*19.67*	*17.79*		*38.73*		*4.91*		*0.04*	*1.34*	*2.49*	*0.24*	*7.89*
				10.02	**1.79**	**14.37**	**11.96**		**28.26**		**29.27**		**0.03**	**2.32**	**1.82**	**0.18**	**0.97**
27	1	1220	89.4	7.21	4.67	24.40	8.01		38.29		13.53		0.22	1.03	2.52	0.13	2.83
				6.53	*5.05*	*22.04*	*6.37*		*34.60*		*20.73*		*0.20*	*2.10*	*2.27*	*0.11*	*1.67*
				5.86	**4.93**	**19.75**	**5.36**		**31.06**		**28.30**		**0.18**	**2.40**	**2.05**	**0.10**	**1.10**
27	2	1220	89.7	4.56	5.66	26.10	1.99		43.66		14.13		0.14	1.31	2.34	0.10	3.09
				4.23	*5.88*	*24.22*	*1.21*		*40.49*		*19.47*		*0.12*	*2.11*	*2.18*	*0.09*	*2.08*
				3.72	**5.66**	**21.37**	**0.64**		**35.76**		**28.29**		**0.12**	**2.44**	**1.92**	**0.08**	**1.26**
27	3	1220	89.9	6.33	3.11	27.18	6.29		37.87		15.60		0.01	1.14	2.36	0.12	2.43
				5.76	*3.66*	*24.91*	*4.94*		*34.66*		*21.73*		*0.01*	*2.06*	*2.17*	*0.10*	*1.59*
				5.08	**3.66**	**21.96**	**3.92**		**30.51**		**30.48**		**0.01**	**2.40**	**1.89**	**0.09**	**1.00**
28	1	1290	87.3	7.42	12.63	20.54	1.94		33.18		19.01		0.22	1.45	3.10	0.51	1.75
				6.61	*12.17*	*18.25*	*0.83*		*29.61*		*26.54*		*0.21*	*2.56*	*2.77*	*0.45*	*1.12*
				6.74	**12.39**	**18.66**	**0.90**		**30.23**		**25.08**		**0.21**	**2.51**	**2.82**	**0.47**	**1.21**
29	1	1300	88.5	7.00	1.41	17.53	12.34		41.43		16.74		0.20	1.45	1.77	0.14	2.48
				6.27	*2.17*	*15.64*	*10.09*		*36.98*		*24.48*		*0.18*	*2.50*	*1.57*	*0.13*	*1.51*
				6.51	**2.13**	**16.33**	**10.66**		**38.58**		**21.45**		**0.18**	**2.39**	**1.64**	**0.13**	**1.80**
30	1	1300	86.0	6.75	4.01	19.39	10.16		37.46		18.24		0.11	1.31	2.25	0.33	2.05
				5.56	*4.80*	*16.01*	*6.88*		*30.88*		*30.57*		*0.10*	*3.08*	*1.84*	*0.27*	*1.01*
				6.69	**4.91**	**19.30**	**9.11**		**37.15**		**17.71**		**0.12**	**2.47**	**2.22**	**0.32**	**2.10**
95	1	1280	86.9			16.62	11.64	6.67	46.46		12.11	2.20	0.12	1.36	2.56	0.25	3.84
						14.27	*9.93*	*5.73*	*42.29*		*21.76*	*0.66*	*0.11*	*2.84*	*2.20*	*0.21*	*1.94*
						16.29	**11.36**	**6.57**	**47.02**		**12.10**	**1.40**	**0.13**	**2.39**	**2.50**	**0.24**	**3.89**
97	1	1290	89.6	5.25		15.60	13.91	1.21	46.92		13.11		0.33	1.19	2.33	0.14	3.58
				5.70	*0.45*	*13.80*	*11.86*		*41.49*		*21.88*		*0.30*	*2.35*	*2.05*	*0.13*	*1.90*
				5.71	**0.48**	**13.88**	**11.85**		**41.63**		**21.63**		**0.30**	**2.34**	**2.05**	**0.13**	**1.92**
98	1	1280	88.6	8.30	8.80	19.52	7.36		32.23		19.36		0.12	1.12	2.57	0.62	1.66
				7.21	*8.77*	*17.01*	*5.27*		*28.01*		*28.42*		*0.10*	*2.43*	*2.23*	*0.54*	*0.99*
				7.26	**8.73**	**17.00**	**5.39**		**28.11**		**28.22**		**0.10**	**2.43**	**2.23**	**0.54**	**1.00**
100	1	1280	91.4	7.34		17.82	18.94	1.59	38.39		12.45		0.14	0.91	2.11	0.31	3.08
				8.18	*0.01*	*16.35*	*17.42*		*35.23*		*18.70*		*0.12*	*1.76*	*1.94*	*0.29*	*1.88*
				6.70	**0.62**	**13.38**	**13.65**		**28.82**		**32.67**		**0.11**	**2.24**	**1.58**	**0.24**	**0.88**

Appendix 3.2 (continued)

Molecular CIPWnorm compositions

Merelava ankaramite suite, sample 31551

Grain	Melt	T_s	Fo_s	*or*	*ab*	*an*	*ne*	*lc*	*di*	*hy*	*ol*	*cs*	*cm*	*mt*	*ilm*	*ap*	*di/ol*
60		1230	87.9	2.23	13.79	26.29	7.24		31.94		15.58			1.25	1.35	0.33	2.05
				2.18	*13.63*	*25.69*	*6.91*		*31.28*		*17.23*			*1.46*	*1.31*	*0.32*	*1.82*
				2.04	**12.82**	**23.77**	**6.14**		**28.91**		**23.12**			**1.67**	**1.23**	**0.29**	**1.25**
61		1237	89.4	2.59	14.56	26.06	3.48		33.19		16.77		0.03	1.18	1.81	0.33	1.98
				2.53	*14.35*	*25.36*	*3.18*		*32.30*		*18.75*		*0.03*	*1.41*	*1.75*	*0.33*	*1.72*
				2.27	**13.16**	**22.71**	**2.56**		**28.95**		**26.80**		**0.03**	**1.66**	**1.56**	**0.29**	**1.08**
62	1	1240	82.6	3.64	13.65	27.79	3.31		27.04		20.11		0.05	1.71	2.17	0.52	1.34
				3.48	*13.48*	*26.71*	*2.75*		*25.92*		*22.96*		*0.05*	*2.08*	*2.08*	*0.50*	*1.13*
				3.81	**14.40**	**29.33**	**3.44**		**28.50**		**15.89**		**0.05**	**1.76**	**2.28**	**0.54**	**1.79**
62	2	1240	83.8	1.61	14.99	24.98			30.04	11.86	12.14		0.12	1.61	2.15	0.49	2.47
				1.55	*14.46*	*24.10*			*28.97*	*12.39*	*13.98*		*0.12*	*1.88*	*2.08*	*0.47*	*2.07*
				1.68	**15.47**	**25.76**			**30.98**	**12.27**	**9.32**		**0.12**	**1.69**	**2.21**	**0.51**	**3.33**
63	1	1209	87.1	2.01	9.23	31.54	5.23		33.21		15.38		0.06	1.30	1.73	0.30	2.16
				1.96	*9.17*	*30.59*	*4.87*		*32.20*		*17.61*		*0.06*	*1.59*	*1.67*	*0.29*	*1.83*
				1.89	**8.91**	**29.36**	**4.54**		**30.93**		**20.74**		**0.06**	**1.70**	**1.60**	**0.28**	**1.49**
63	2	1209	87.6	1.57	9.47	30.17	4.98		35.02		15.27		0.03	1.36	1.76	0.37	2.29
				1.52	*9.43*	*29.61*	*4.77*		*34.38*		*16.65*		*0.03*	*1.53*	*1.73*	*0.36*	*2.07*
				1.45	**9.11**	**27.95**	**4.29**		**32.43**		**21.10**		**0.03**	**1.69**	**1.62**	**0.34**	**1.54**
63	3	1209	85.7	1.78	10.31	30.83	3.86		34.37		15.27		0.06	1.34	1.80	0.38	2.25
				1.67	*10.21*	*29.46*	*3.29*		*32.85*		*18.62*		*0.06*	*1.77*	*1.71*	*0.36*	*1.76*
				1.72	**10.26**	**29.79**	**3.43**		**33.23**		**17.67**		**0.06**	**1.73**	**1.74**	**0.37**	**1.88**
63	4	1209	87.0	1.71	8.49	30.69	6.51		35.51		13.87		0.06	1.27	1.58	0.30	2.56
				1.65	*8.43*	*29.57*	*6.07*		*34.32*		*16.47*		*0.06*	*1.59*	*1.55*	*0.29*	*2.08*
				1.59	**8.33**	**28.54**	**5.67**		**33.04**		**19.31**		**0.06**	**1.69**	**1.48**	**0.29**	**1.71**
64A	1	1242	90.4	3.12	6.18	27.13	6.92		42.96		10.47		0.08	1.02	1.61	0.51	4.10
				3.01	*6.25*	*26.50*	*6.53*		*41.93*		*12.37*		*0.08*	*1.26*	*1.58*	*0.49*	*3.39*
				2.55	**5.66**	**22.33**	**5.13**		**35.40**		**25.51**		**0.06**	**1.63**	**1.31**	**0.41**	**1.39**
64A	2	1242	90.2	2.84	4.11	27.41	9.08		42.98		10.54		0.03	1.08	1.48	0.45	4.08
				2.79	*4.17*	*26.76*	*8.77*		*42.05*		*12.26*		*0.03*	*1.29*	*1.45*	*0.44*	*3.43*
				2.41	**3.99**	**23.11**	**7.11**		**36.21**		**23.88**		**0.03**	**1.62**	**1.25**	**0.38**	**1.52**
64B	3	1248	87.9	1.59	12.30	31.55	2.87		33.19		15.38			1.20	1.52	0.40	2.16
				1.53	*12.17*	*30.56*	*2.49*		*32.12*		*17.76*			*1.50*	*1.49*	*0.38*	*1.81*
				1.41	**11.55**	**28.34**	**2.07**		**29.79**		**23.42**			**1.70**	**1.37**	**0.35**	**1.27**
64B	4	1248	87.6	1.54	12.58	32.97	1.54		29.80		18.29		0.08	1.27	1.52	0.40	1.63
				1.49	*12.47*	*31.96*	*1.14*		*28.82*		*20.59*		*0.08*	*1.58*	*1.49*	*0.38*	*1.40*
				1.41	**11.95**	**30.29**	**0.94**		**27.37**		**24.48**		**0.08**	**1.71**	**1.41**	**0.36**	**1.12**
65	1	1257	89.1	1.97	8.96	27.71	4.55		33.47		19.89		0.07	1.36	1.61	0.40	1.68
				1.96	*8.91*	*27.02*	*4.27*		*32.61*		*21.59*		*0.07*	*1.57*	*1.58*	*0.40*	*1.51*
				1.85	**8.66**	**25.89**	**4.01**		**31.30**		**24.67**		**0.07**	**1.66**	**1.51**	**0.38**	**1.27**
65	2	1257	89.4	1.67	12.98	28.19	1.79		34.53		17.54			1.23	1.71	0.36	1.97
				1.61	*12.84*	*27.48*	*1.52*		*33.62*		*19.48*			*1.46*	*1.64*	*0.35*	*1.73*
				1.48	**11.93**	**24.99**	**1.11**		**30.54**		**26.46**			**1.67**	**1.52**	**0.32**	**1.15**
66	1	1220	88.8	2.18	10.79	24.08	2.85		38.08		18.26			1.66	1.72	0.38	2.09
				2.24	*10.80*	*24.38*	*3.08*		*38.63*		*17.21*			*1.53*	*1.75*	*0.38*	*2.24*
				2.11	**10.36**	**23.01**	**2.72**		**36.42**		**21.71**			**1.68**	**1.64**	**0.36**	**1.68**
66	2	1220	88.2	2.38	6.82	24.76	7.05		36.72		18.77			1.58	1.54	0.38	1.96
				2.33	*6.84*	*24.58*	*6.94*		*36.43*		*19.35*			*1.65*	*1.51*	*0.37*	*1.88*
				2.32	**6.81**	**24.48**	**6.88**		**36.26**		**19.70**			**1.66**	**1.51**	**0.37**	**1.84**
70	2	1200	87.9	2.79	12.37	24.79	3.98		37.90		14.03			1.28	2.42	0.43	2.70
				2.73	*12.15*	*24.02*	*3.69*		*36.78*		*16.30*			*1.57*	*2.35*	*0.41*	*2.26*
				2.60	**11.75**	**22.93**	**3.31**		**35.02**		**20.07**			**1.69**	**2.24**	**0.39**	**1.75**
71	1	1247	85.4			19.23	11.39	1.73	43.08		18.19	2.20	0.03	2.05	1.74	0.36	2.37
						19.04	*11.25*	*1.68*	*42.78*		*18.91*	*2.10*	*0.03*	*2.14*	*1.71*	*0.35*	*2.26*
						22.31	**13.28**	**2.02**	**48.93**		**6.19**	**3.16**	**0.03**	**1.65**	**2.02**	**0.42**	**7.90**
71	2	1247	85.1			16.69	11.32	2.00	45.49		16.94	3.32		2.24	1.61	0.40	2.69
						16.91	*11.53*	*2.05*	*45.98*		*15.91*	*3.46*		*2.12*	*1.63*	*0.41*	*2.89*
						19.67	**13.32**	**2.34**	**52.12**		**3.88**	**4.63**		**1.65**	**1.91**	**0.48**	**13.42**
74		1300	87.7	2.12	4.44	23.57	6.56		34.53		25.76			1.56	1.14	0.33	1.34
				1.97	*4.59*	*21.81*	*5.62*		*31.97*		*30.58*			*2.10*	*1.05*	*0.30*	*1.05*
				2.34	**4.91**	**26.13**	**7.28**		**38.24**		**17.78**			**1.68**	**1.27**	**0.37**	**2.15**
75	1	1300	87.9	2.10	7.02	19.35	6.16		42.79		19.23		0.06	1.40	1.51	0.37	2.23
				1.94	*7.02*	*17.90*	*5.15*		*39.55*		*24.66*		*0.06*	*1.99*	*1.39*	*0.34*	*1.60*
				2.20	**7.62**	**20.44**	**6.27**		**45.11**		**14.65**		**0.06**	**1.68**	**1.58**	**0.39**	**3.08**

Appendix 3.2 (continued)

Molecular CIPWnorm compositions

Merelava ankaramite suite, sample 31551 (cont.)

Grain	Melt	T_a	Fo_a	*or*	*ab*	*an*	*ne*	*lc*	*di*	*hy*	*ol*	*cs*	*cm*	*mt*	*ilm*	*ap*	*di/ol*
75	2	1300	87.3	3.22	18.81	19.74			22.53	20.52	11.82		0.06	1.12	1.92	0.27	1.91
				2.95	*17.26*	*18.11*			*20.66*	*20.83*	*16.45*		*0.05*	*1.67*	*1.76*	*0.24*	*1.26*
				3.12	**18.08**	**18.99**			**21.70**	**21.19**	**13.18**		**0.06**	**1.56**	**1.86**	**0.26**	**1.65**
78	1	1390	83.2	1.62	11.15	17.73			20.84	13.05	32.46		0.08	1.60	1.21	0.27	0.64
				1.18	*8.06*	*12.78*			*15.06*	*15.28*	*43.36*		*0.06*	*3.14*	*0.87*	*0.20*	*0.35*
				2.27	**15.67**	**24.89**			**29.25**	**16.49**	**7.56**		**0.12**	**1.66**	**1.70**	**0.39**	**3.87**
79	1	1250	84.2	2.05	20.69	21.58			17.72	24.59	10.26		0.06	1.35	1.47	0.23	1.73
				1.89	*19.30*	*20.20*			*16.53*	*25.12*	*13.53*		*0.05*	*1.79*	*1.37*	*0.21*	*1.22*
				2.06	**21.01**	**21.90**			**18.00**	**25.63**	**8.06**		**0.06**	**1.57**	**1.48**	**0.23**	**2.23**

Epi ankaramite suite, sample UTas71046

Grain	Melt	T_a	Fo_a	*or*	*ab*	*an*	*ne*	*lc*	*di*	*hy*	*ol*	*cs*	*cm*	*mt*	*ilm*	*ap*	*di/ol*
RW1	1	1260	86.6			20.51	13.13	2.91	35.87		19.69	4.73	0.16	1.20	1.77	0.03	1.82
						18.97	*12.09*	*2.68*	*34.06*		*24.79*	*3.90*	*0.15*	*1.70*	*1.63*	*0.03*	*1.37*
						21.95	**14.09**	**3.12**	**38.55**		**13.80**	**5.03**	**0.18**	**1.36**	**1.89**	**0.03**	**2.79**
RW1	1	1260	87.3			20.48	13.75	2.96	41.37		16.45	2.02	0.10	1.10	1.61	0.18	2.52
						18.97	*12.73*	*2.72*	*39.17*		*21.61*	*1.44*	*0.10*	*1.59*	*1.50*	*0.17*	*1.81*
						21.01	**14.12**	**3.05**	**42.84**		**13.75**	**1.91**	**0.10**	**1.37**	**1.66**	**0.18**	**3.11**
RW2	1	1280	83.6			23.69	12.08	2.39	30.76		23.64	3.99	0.12	1.26	1.98	0.08	1.30
						20.51	*10.47*	*2.06*	*28.22*		*32.05*	*2.66*	*0.11*	*2.14*	*1.71*	*0.07*	*0.88*
						27.47	**13.95**	**2.78**	**35.58**		**11.67**	**4.64**	**0.14**	**1.39**	**2.29**	**0.09**	**3.05**
RW2	7	1280	84.8			22.19	12.23	2.38	38.94		20.78	0.13	0.04	1.38	1.78	0.14	1.87
				0.89		*20.20*	*11.08*	*1.26*	*35.60*		*27.24*		*0.04*	*1.96*	*1.61*	*0.13*	*1.31*
						25.40	**13.97**	**2.72**	**44.28**		**9.73**	**0.27**	**0.04**	**1.41**	**2.02**	**0.16**	**4.55**
RW2	8	1280	85.0			23.05	13.17	2.43	36.40		20.02	1.36	0.21	1.35	1.88	0.14	1.82
						21.45	*12.24*	*2.24*	*34.77*		*24.60*	*0.81*	*0.19*	*1.82*	*1.74*	*0.13*	*1.41*
						25.56	**14.59**	**2.69**	**40.15**		**11.55**	**1.61**	**0.23**	**1.39**	**2.08**	**0.15**	**3.48**
RW2	10	1280	84.7			25.77	10.55	1.97	29.38		24.10	4.72	0.10	1.41	1.87	0.12	1.22
						23.93	*9.76*	*1.83*	*28.11*		*28.58*	*3.95*	*0.10*	*1.89*	*1.74*	*0.11*	*0.98*
						29.12	**11.91**	**2.23**	**32.88**		**14.64**	**5.48**	**0.11**	**1.40**	**2.11**	**0.13**	**2.25**
R15		1305	91.6			21.98	13.21	1.96	31.67		20.35	8.30	0.05	0.79	1.54	0.15	1.56
						20.79	*12.45*	*1.86*	*30.49*		*24.05*	*7.54*	*0.05*	*1.16*	*1.46*	*0.14*	*1.27*
						19.83	**11.87**	**1.76**	**29.31**		**27.31**	**7.08**	**0.05**	**1.24**	**1.39**	**0.14**	**1.07**
R54	1	1275	84.0	1.91	7.29	28.84			26.98	3.17	28.83			1.28	1.59	0.11	0.94
				1.63	*6.18*	*24.34*			*22.80*	*5.67*	*35.81*			*2.15*	*1.33*	*0.10*	*0.64*
				2.23	**8.57**	**33.79**			**31.61**	**3.54**	**16.78**			**1.49**	**1.87**	**0.13**	**1.88**
R55	3	1230	81.0	3.06	11.92	24.21	4.12		29.62		23.03			1.49	2.39	0.15	1.29
				2.80	*11.47*	*22.22*	*3.22*		*27.15*		*28.74*			*2.07*	*2.21*	*0.14*	*0.94*
				3.43	**13.29**	**27.25**	**4.77**		**33.37**		**13.52**			**1.50**	**2.70**	**0.17**	**2.47**

Appendix 3.3

Host olivine analyses

Rinjani ankaramite suite, sample UTas48001

Grain	Melt	T_q	SiO_2	Cr_2O_3	FeO	MgO	CaO	MnO	NiO	Total	Fo
39	1	1220	40.32	0.04	9.78	48.17	0.30	0.14	0.26	99.00	89.8
39	2	1220	39.87	0.04	9.96	47.67	0.38	0.16	0.18	98.26	89.5
39	3	1220	39.88	0.01	10.27	47.68	0.31	0.13	0.22	98.51	89.2
39	4	1220	40.74	0.05	9.97	47.52	0.34	0.19	0.24	99.04	89.5
39	5	1220	40.51	0.05	10.15	48.40	0.33	0.18	0.24	99.85	89.5
39	6	1220	41.35	0.03	10.39	49.51	0.36	0.12	0.19	101.95	89.5
39	7	1220	39.97	0.03	10.22	48.17	0.31	0.27	0.19	99.16	89.4
42	1	1184	39.84	0.05	11.50	47.45	0.42	0.22	0.16	99.63	88.0
42	2	1184	39.97	0.05	11.22	47.41	0.32	0.19	0.13	99.29	88.3
42	3	1184	39.80	0.07	10.92	46.02	0.38	0.28	0.09	97.55	88.3
43	1	1220	40.53	0.05	9.29	49.18	0.34	0.20	0.27	99.86	90.4
43	3	1220	40.65	0.04	9.28	48.82	0.33	0.29	0.30	99.70	90.4
43	4	1220	40.28	0.02	9.01	49.20	0.33	0.18	0.30	99.31	90.7
43	5	1220	40.84	0.02	8.59	49.63	0.33	0.16	0.19	99.76	91.2
82	1	1255	39.06	0.03	9.31	47.14	0.34	0.25	0.07	96.20	90.0
82	2	1255	39.38	0.08	9.43	47.89	0.38	0.19	0.17	97.51	90.1
83	1	1238	40.59	0.04	8.74	49.35	0.26	0.17	0.24	99.39	91.0
83	3	1238	40.48	0.08	9.23	49.40	0.29	0.25	0.23	99.96	90.5
84	1	1260	39.60	0.05	9.18	47.58	0.38	0.30	0.15	97.23	90.2
86	1	1230	40.21	0.04	9.92	47.81	0.40	0.24	0.08	98.70	89.6
87	1	1240	40.31	0.03	9.90	48.23	0.30	0.24	0.12	99.12	89.7
87	2	1240	39.76	0.05	9.76	47.26	0.32	0.23	0.09	97.47	89.6
87	3	1240	40.44	0.07	10.43	48.82	0.31	0.24	0.13	100.44	89.3
88	1	1250	40.57	0.01	9.90	48.56	0.39	0.15	0.07	99.65	89.8
88	3	1250	40.31	0.00	10.84	48.22	0.39	0.22	0.05	100.03	88.8
89	1	1240	40.02	0.06	9.14	48.42	0.32	0.21	0.25	98.42	90.4

Ulakan ankaramite suite, sample UTas67424

Grain	Melt	T_q	SiO_2	Cr_2O_3	FeO	MgO	CaO	MnO	NiO	Total	Fo
R92	1	1280	40.28	0.03	9.90	49.08	0.37	0.25	0.12	100.00	89.9
R93	1	1280	40.65	0.06	8.41	50.58	0.37	0.16	0.15	100.40	91.5
R94	1	1280	40.31	0.07	8.76	49.91	0.31	0.20	0.15	99.69	91.1
R96	1	1280	39.93	0.00	12.16	47.29	0.45	0.22	0.12	100.20	87.4
R101	1	1280	40.40	0.04	10.99	49.06	0.47	0.23	0.14	101.30	88.9
R102	1	1300	39.13	0.01	11.23	47.44	0.52	0.26	0.15	98.74	88.3
R103	1	1280	39.94	0.06	9.22	49.24	0.33	0.16	0.28	99.24	90.5
R104	1	1280	40.42	0.04	9.72	49.73	0.43	0.21	0.24	100.80	90.1
R105	1	1290	40.03	0.05	9.57	49.12	0.42	0.25	0.19	99.64	90.2
R107	1	1300	39.57	0.00	11.78	47.14	0.40	0.28	0.20	99.37	87.7
R108	1	1280	40.05	0.03	8.87	49.78	0.46	0.10	0.24	99.53	90.9
R109	1	1300	39.62	0.05	8.82	49.66	0.43	0.18	0.21	98.97	91.0
R109	2	1300	40.31	0.03	8.61	50.03	0.42	0.13	0.13	99.66	91.2
R109	3	1300	39.91	0.04	8.83	49.37	0.41	0.16	0.19	98.92	90.9
1	1	1240	40.58	0.08	10.11	49.68	0.42	0.22	0.10	101.20	89.8
2	1	1240	41.21	0.06	8.09	50.95	0.34	0.24	0.14	101.00	91.8
2	2	1240	41.21	0.06	8.09	50.95	0.34	0.24	0.14	101.00	91.8
3	1	1220	40.51	0.44	10.20	49.32	0.44	0.19	0.16	101.30	89.6
4	1	1240	40.58	0.05	11.05	48.85	0.46	0.27	0.10	101.40	88.8
5	1	1240	41.03	0.06	10.76	50.10	0.34	0.20	0.21	102.70	89.3
6	1	1240	39.86	0.00	14.35	46.84	0.42	0.31	0.15	101.90	85.4
22	1	1250	40.48	0.00	10.30	49.82	0.35	0.22	0.13	101.30	89.6
25	1	1205	40.95	0.02	9.96	49.92	0.34	0.26	0.13	101.60	89.9
27	1	1220	40.88	0.05	10.50	49.45	0.36	0.33	0.11	101.70	89.4
27	2	1220	40.96	0.04	10.23	49.84	0.37	0.17	0.15	101.80	89.7

Appendix 3.3 (continued)

Host olivine analyses

Ulakan ankaramite suite, sample UTas67424 (cont.)

Grain	Melt	T_q	SiO_2	Cr_2O_3	FeO	MgO	CaO	MnO	NiO	Total	Fo
27	3	1220	41.15	0.04	10.10	50.29	0.33	0.20	0.12	102.20	89.9
28	1	1290	40.36	0.06	12.42	47.73	0.30	0.25	0.11	101.20	87.3
29	1	1300	40.84	0.02	11.41	49.02	0.37	0.19	0.10	102.00	88.5
30	1	1300	39.37	0.06	13.28	45.67	0.48	0.32	0.13	99.30	86.0
95	1	1280	39.62	0.06	12.50	46.45	0.47	0.30	0.16	99.55	86.9
97	1	1290	39.99	0.00	10.00	48.47	0.44	0.18	0.14	99.22	89.6
98	1	1280	39.56	0.10	11.02	47.94	0.31	0.11	0.17	99.20	88.6
100	1	1280	40.80	0.06	8.47	50.49	0.35	0.16	0.30	100.60	91.4
107	2	1300	38.93	0.06	11.82	46.67	0.43	0.25	0.20	98.36	87.6

Merelava ankaramite suite, sample 31551

Grain	Melt	T_q	SiO_2	Cr_2O_3	FeO	MgO	CaO	MnO	NiO	Total	Fo
60	1	1230	39.69	0.01	11.70	47.55	0.27	0.24	0.06	99.52	87.9
61	1	1237	40.28	0.05	10.46	49.52	0.23	0.16	0.00	100.70	89.4
62	1	1240	38.24	0.02	16.18	43.18	0.26	0.32	0.08	98.28	82.7
62	2	1240	38.82	0.00	15.51	44.85	0.23	0.23	0.05	99.69	83.8
63	1	1209	39.66	0.00	12.37	46.88	0.32	0.25	0.14	99.62	87.1
63	2	1209	39.58	0.08	11.99	47.61	0.30	0.18	0.22	99.96	87.6
63	3	1209	39.03	0.03	13.50	45.30	0.52	0.25	0.16	98.79	85.7
63	4	1209	39.18	0.02	12.33	46.25	0.49	0.29	0.14	98.69	87.0
64	1	1242	39.84	0.00	9.29	48.80	0.21	0.25	0.16	98.55	90.4
64	2	1242	39.80	0.04	9.48	48.69	0.28	0.18	0.19	98.65	90.2
64	3	1248	40.90	0.00	11.89	48.57	0.29	0.32	0.08	102.00	87.9
64	4	1248	40.27	0.01	12.13	48.04	0.33	0.20	0.12	101.10	87.6
65	1	1257	40.62	0.00	10.64	48.74	0.25	0.05	0.03	100.30	89.1
65	2	1257	40.35	0.02	10.43	49.10	0.23	0.33	0.14	100.60	89.4
66	1	1220	40.54	0.02	10.94	48.77	0.26	0.16	0.09	100.80	88.8
66	2	1220	39.07	0.04	11.17	46.96	0.28	0.24	0.17	97.93	88.2
70	2	1200	40.22	0.00	11.83	48.07	0.29	0.18	0.24	100.80	87.9
71	1	1247	40.20	0.03	14.04	46.17	0.33	0.43	0.15	101.40	85.4
71	2	1247	39.94	0.08	14.43	46.15	0.37	0.33	0.19	101.50	85.1
74	1	1300	40.49	0.02	12.04	47.96	0.28	0.20	0.18	101.20	87.7
75	1	1300	39.88	0.00	11.59	47.44	0.33	0.33	0.18	99.74	88.0
75	2	1300	39.51	0.05	12.09	46.76	0.21	0.26	0.09	98.96	87.4
78	1	1390	39.21	0.02	15.83	43.84	0.26	0.36	0.11	99.64	83.2
79	1	1250	38.75	0.00	14.68	43.86	0.27	0.31	0.06	97.93	84.2

Epi ankaramite suite, sample UTas71046

Grain	Melt	T_q	SiO_2	Cr_2O_3	FeO	MgO	CaO	MnO	NiO	Total	Fo
RW1	1	1260	40.56	0.00	12.75	46.16	0.23	0.14	0.17	100.00	86.6
RW1	1	1260	40.43	0.03	12.13	46.85	0.24	0.20	0.13	100.00	87.3
RW2	1	1280	40.04	0.00	15.35	44.05	0.24	0.26	0.07	100.00	83.7
RW2	7	1280	40.01	0.00	14.42	44.97	0.30	0.23	0.08	100.00	84.8
RW2	8	1280	40.15	0.05	14.15	44.91	0.35	0.27	0.12	100.00	85.0
RW2	10	1280	39.85	0.00	14.50	44.93	0.27	0.32	0.13	100.00	84.7
R15	1	1305	40.95	0.05	8.18	50.10	0.38	0.08	0.26	100.00	91.6
R54	1	1275	39.47	0.04	15.12	44.63	0.26	0.31	0.18	100.00	84.0
R55	3	1230	39.29	0.01	17.62	42.26	0.32	0.40	0.11	100.00	81.1

Appendix 3.4

Gamble, John A., Christie, Rob H.K., Wright, I.C., Wysoczanski , R.J. (1997) Primitive K-rich magmas from Clark Volcano, southern Kermadec Arc; a paradox in the K-depth relationship
Can Mineral, 35(2), 275-290

Appendix 4

Appendix 4.1

Melt inclusion recalculation procedure

This appendix presents additional details on the recalculation procedure described in Section 4.5. This recalculation involved mainly two procedures (PROCEDURE-1 and PROCEDURE-2) and were illustrated with the recalculations paths of four representative heated melt inclusions A, B, C and D in Figure 4.5. Each procedure consists of infinitesimal increments that are reiterated by the program until the procedure is fully completed. These increments are nearly similar in both procedures, but in PROCEDURE-1 they are carried keeping temperature constant whereas in PROCEDURE-2 they are carried out keeping Mg# constant. The scope of this appendix is simply to describe these increments in detail, first in PROCEDURE-1 and then in PROCEDURE-2.

Recalculation increments in PROCEDURE-1

Basically, each increment involves two stages of recalculation. These two stages are illustrated in the enlarged portions of the recalculation paths shown in Figure A4.1. The first stage of each increment in PROCEDURE-1 involves a one-to-one Fe^{2+}-Mg cation exchange between the melt and the host olivine. The molecular amount of Mg and Fe^{2+} exchanged in each stage is 0.00015 moles and causes at infinitesimal shift in the composition of the melt. This stage can involve either the exchange of Mg by Fe^{2+} or *vice versa,* depending on the Mg# of the melt. If the Mg# of the melt is higher than M, this stage involves replacing Mg with Fe^{2+}. This is illustrated by the increments of paths A to A', C to C' and D to M. Conversely, if the Mg# of the melt is lower than M then Fe^{2+} is replaced by Mg. This is illustrated by path B to B'. Temperatures are calculated after each increment using the equations of Ford *et al.* (1983).

Subsequent to this Fe^{2+}-Mg exchange stage, the composition of the melt will be either oversaturated in olivine (if Fe^{2+} is exchanged by Mg) or undersaturated in olivine (if Mg is exchanged by Fe^{2+}). This over- or undersaturation imparts a higher or lower calculated temperature to the melt. Thus, recalling that calculated temperature in PROCEDURE-1 is kept constant, the second stage of this increment consits of forcing melt back in equilibrium with olivine at this temperature. This is achieved by adding (or subtracting) enough equilibrium olivine (in units of 7.5×10^{-5} wt%) to (or from) the melt until saturation is achieved. This second stage causes a small change in MgO at nearly constant FeO*, i.e., a small horizontal shift in Figure A4.1. These two stages form a complete increment that is reiterated by the program until PROCEDURE-1 is completed.

Two types of increments are therefore possible and are summarized in the table below. One (Increment-I) involves the exchange of Mg by Fe^{2+} and the addition of olivine. This increment is applied to melt heated melt inclusion that has an Mg# higher than M. The other increment type (Increment-II) involves the exchange of Fe^{2+} by Mg and the substruction of olivine and is applied to melt inclusion with an Mg# lower than M.

These increments are reiterated in PROCEDURE-1 until the Mg# of the recalculated melt matches the Mg# of the trapped melt M. After PROCEDURE-1 all melt inclusions trapped in olivine (Fo_{91}) lie along the dashed line Mg#75 of Figure A4.1.

Procedure	Increment	Stages	Condition	Result	Path
1	I	exchange of Mg by Fe^{2+} and olivine addition	constant T	decrease in Mg# increase in FeO* ~constant MgO	A-A' D-M C-C'
1	II	exchange of Fe^{2+} by Mg and olivine substruction	constant T	increase in Mg# decrease in FeO* ~constant MgO	B-B'

Recalculation increments along PROCEDURE-2

The recalculation path in PROCEDURE-2 was described in Section 4.5. This procedure shifts the compositions of the melts towards M, at a constant Mg#. As for PROCEDURE-1, PROCEDURE-2 also consists of infinitesimal increments that involve two stages of calculation. These stages are reiterated by the program until PROCEDURE-2 is completed. In the first stage of each increment, 0.00045 wt% of equilibrium olivine is added (or subtracted) to (or from) the melt. Olivine is added to the melt by the program as long as the FeO of the recalculated melt is less than in M (e.g., A' and B'). If the FeO of the melt is higher than in M, then the program subtracts olivine (e.g., C').

The addition (or substruction) of olivine in the first stage of each PROCEDURE-2 increment, causes an oversaturation (or undersaturation) in olivine component in the melt. Thus after each stage the recalculated melt composition has a higher (or lower) Mg# compared to M. Recalling that PROCEDURE-2 is carried out at constant Mg#, then the second stage of each increment in PROCEDURE-2 is aimed to restore the Mg# of the recalculated melt by applying the increments described in PROCEDURE-1. If the first increment-stage of PROCEDURE-2 involves olivine addition then Increment-I of PROCEDURE-1 is applied to decrease the Mg# of the recalculated melt (e.g., path A' or B to M). Conversely, if the first increment-stage of PROCEDURE-2 involves substruction of olivine, then Increment-II of PROCEDURE-1 is applied to increase the Mg# of the recalculated melt (e.g., path C' to M). These increments are reiterated by the program until the FeO* of the recalculated melt matches the target FeO*. These procedures are summarized in the table below and illustrated in Figure A4.1 as enlarged portions of the recalculation paths.

Procedure	Increment	Stages	Conditions	Result	Path
2	I	olivine addition and Increment-I of PROCEDURE-1	constant Mg#	increase in MgO increase in FeO* constant Mg#	A'-M B'-M
2	II	olivine substruction and Increment-II of PROCEDURE-1	constant Mg#	decrease in MgO decrease in FeO* constant Mg#	C'-M

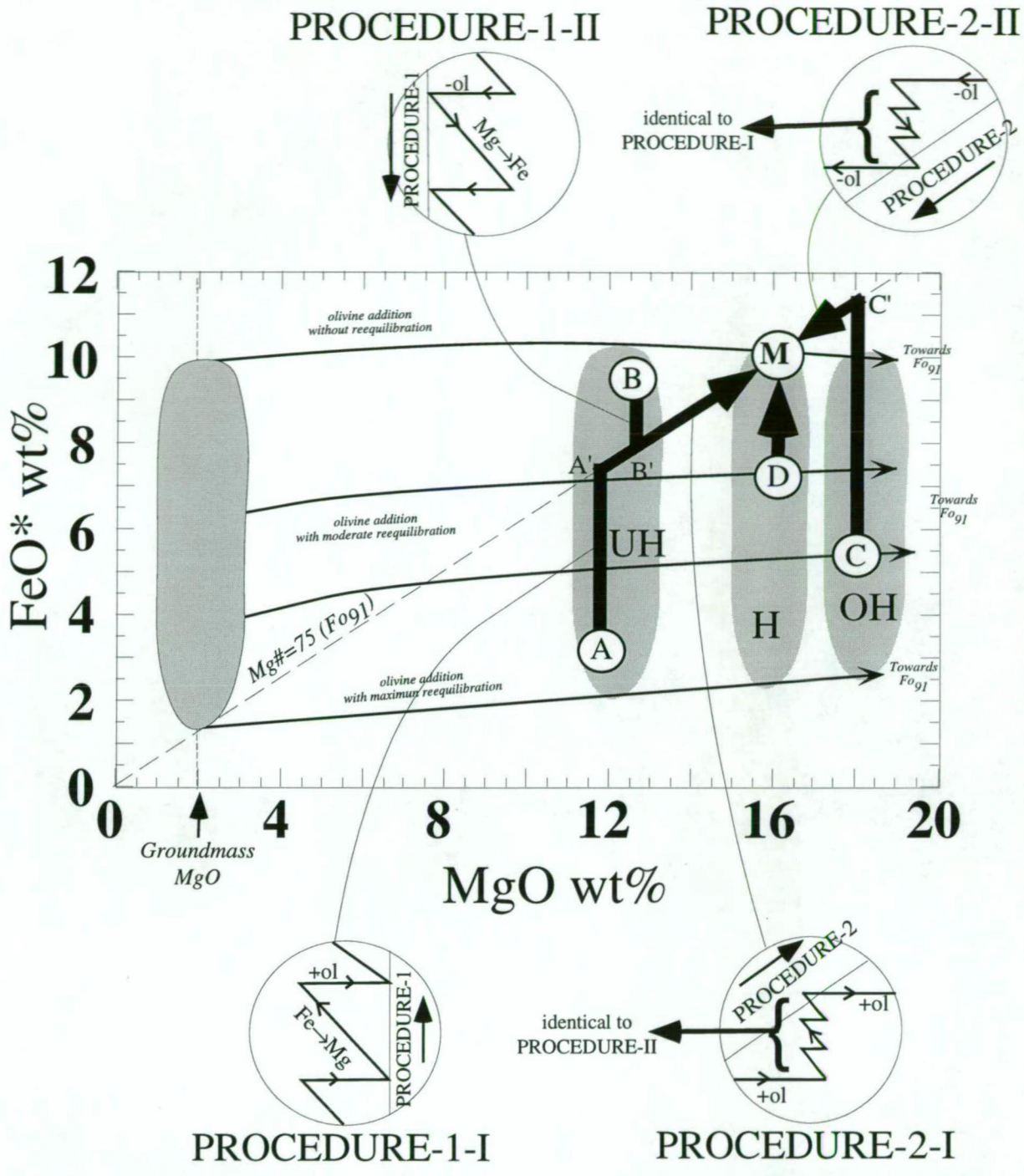

Figure A4.1 Modified after Figure 4.5 in Chapter 4. Recalculation paths (thick arrows) of four representative heated melt inclusion compositions A, B, C and D originaly trapped as melt M (Mg#=75) by an olivine phenocrysts with Fo91. Increments (I and II) in each procedure (1 and 2) are illustrated by enlargements. Each Fe^{2+}-Mg exchange in PROCEDURE-1 represents 0.00015 moles of Fe^{2+} and Mg. Each +ol or -ol increment in PROCEDURE-2 represents 0.000075 wt% of olivine.

Shaded areas represent compositional range of melt inclusion glasses hosted in Fo91 after quenching. NQ represents composition of glasses that were naturally quenched during eruption. UH and OH represent the compositional range of melt inclusion glasses that were underheated and overheated during the experiment, and therefore are relastively depleted or enriched in olivine component relative to M respectively. H represents compositional range of homogenized glasses. Thin arrows indicate shift in composition after the addition of olivine component during the heating experiment and enclose the maximum and minimun range possible in FeO* of heated melt inclusions in Fo91. Groundmass MgO indicates the MgO content of the residual melt trapped in Fo91 at the moment of eruption. See text of for further explanation.

The recalculated compositions of heated melt inclusions in olivine are given in Appendix 3. These are listed as 1) the composition of heated melt inclusion after quenching (before recalculation), 2) the composition of recalculated melt inclusions after PROCEDURE-1 and 3) the composition of melt inclusion after PROCEDURE-2.

Appendix 5

Appendix 5.1

Average electron microprobe analyses of olivine from experimental runs

Run	T-3875	T-3871	T-3869	T-3868	T-4045	T-4062	T-4063	T-4087
P (GPa)	2.00	1.50	1.50	1.50	1.50	1.00	1.00	1.50
T (°C)	1390	1320	1350	1380	1240	1280	1250	1280
	D	D	D	D	CO2 (FB)	CO2 (FB)	CO2 (FB)	CO2 (MHB)
n	4	4	4	4	4	6	6	5
SiO_2	39.59 *0.14*	38.80 *0.15*	39.82 *0.52*	40.27 *0.17*	39.51 *0.21*	40.64 *0.23*	40.98 *0.42*	38.16 *2.60*
$Cr2O_3$	0.02 *0.01*	0.04 *0.02*	0.06 *0.03*	0.04 *0.04*	0.03 *0.03*	0.03 *0.03*	0.05 *0.02*	0.00 *0.00*
MgO	45.41 *0.52*	42.59 *0.51*	46.77 *0.12*	48.48 *0.21*	44.60 *0.65*	49.99 *0.80*	50.81 *1.34*	45.56 *2.35*
CaO	0.46 *0.13*	0.40 *0.02*	0.50 *0.13*	0.42 *0.03*	0.46 *0.05*	0.57 *0.02*	0.52 *0.07*	0.82 *0.62*
MnO	0.08 *0.03*	0.13 *0.02*	0.05 *0.04*	0.04 *0.03*	0.02 *0.01*	0.09 *0.03*	0.07 *0.05*	0.00 *0.00*
FeO	13.93 *0.39*	17.44 *0.21*	12.16 *0.11*	10.59 *0.15*	14.67 *1.01*	8.86 *0.88*	8.14 *1.62*	8.15 *1.85*
NiO	0.01 *0.01*	0.01 *0.01*	0.00 *0.01*	0.02 *0.03*	0.01 *0.01*	0.01 *0.01*	0.01 *0.02*	0.00 *0.00*
TOTAL	99.48	99.39	99.36	99.86	99.30	100.19	100.56	92.69
Si	0.995 *0.006*	0.993 *0.005*	0.997 *0.008*	0.992 *0.004*	0.998 *0.004*	0.992 *0.001*	0.992 *0.003*	1.004 *0.021*
Cr	0.000 *0.000*	0.000 *0.000*	0.000 *0.000*	0.000 *0.000*	0.001 *0.001*	0.001 *0.001*	0.001 *0.000*	0.000 *0.000*
Mg	1.703 *0.013*	1.628 *0.010*	1.740 *0.015*	1.778 *0.004*	1.679 *0.016*	1.818 *0.020*	1.834 *0.033*	1.789 *0.079*
Ca	0.013 *0.005*	0.010 *0.000*	0.012 *0.004*	0.010 *0.000*	0.013 *0.001*	0.015 *0.001*	0.013 *0.002*	0.023 *0.017*
Mn	0.000 *0.000*	0.000 *0.000*	0.000 *0.000*	0.000 *0.000*	0.001 *0.000*	0.002 *0.001*	0.001 *0.001*	0.000 *0.000*
Fe	0.293 *0.010*	0.375 *0.006*	0.255 *0.005*	0.220 *0.000*	0.310 *0.021*	0.181 *0.019*	0.165 *0.034*	0.179 *0.037*
Ni	0.000 *0.000*	0.000 *0.000*	0.000 *0.000*	0.000 *0.000*	0.000 *0.000*	0.000 *0.000*	0.000 *0.000*	0.000 *0.000*
TOTAL	3.003 *0.005*	3.008 *0.005*	3.003 *0.008*	3.008 *0.004*	3.001 *0.005*	3.008 *0.001*	3.007 *0.003*	2.996 *0.021*
Fo	85.3 *0.5*	81.3 *0.3*	87.3 *0.1*	89.1 *0.1*	84.4 *1.0*	90.9 *0.9*	91.7 *1.7*	90.9 *2.0*

Run	T-4109	T-4111	T-4121	T-4132	T-4143	T-4146	T-4160	T-4161
P (GPa)	1.00	1.00	1.00	1.25	1.60	1.75	1.50	1.25
T (°C)	1280	1290	1320	1280	1250	1200	1285	1290
	CO2 (MHB)	CO2 (MHB)	CO2 (MHB)	CO2 (MHB)	CO2 (MHB)	CO2 (MHB)	CO2 (MHB)	CO2 (MHB)
n	7	5	4	1	3	2	8	7
SiO_2	40.46 *0.36*	40.56 *0.49*	41.27 *0.21*	40.27	39.18 *0.60*	38.86 *0.40*	39.90 *0.74*	40.65 *0.43*
$Cr2O_3$	0.03 *0.01*	0.03 *0.02*	0.05 *0.03*	0.02	0.02 *0.02*	0.00 *0.00*	0.05 *0.03*	0.02 *0.02*
MgO	48.54 *0.43*	49.52 *0.36*	51.10 *0.18*	47.28	44.59 *0.26*	41.68 *0.71*	47.28 *0.70*	48.25 *0.88*
CaO	0.62 *0.15*	0.69 *0.20*	0.63 *0.01*	0.66	0.55 *0.03*	0.68 *0.07*	0.83 *0.43*	0.62 *0.18*
MnO	0.06 *0.04*	0.06 *0.03*	0.09 *0.02*	0.12	0.08 *0.06*	0.08 *0.09*	0.06 *0.03*	0.06 *0.03*
FeO	9.40 *0.58*	9.41 *0.30*	7.30 *0.47*	10.81	14.61 *0.36*	15.93 *0.25*	9.41 *0.30*	9.74 *0.40*
NiO	0.01 *0.01*	0.03 *0.03*	0.00 *0.00*	0.05	0.01 *0.02*	0.02 *0.03*	0.01 *0.01*	0.02 *0.02*
TOTAL	99.11	100.31	100.43	99.21	99.04	97.25	97.54	99.35
Si	1.000 *0.004*	0.991 *0.007*	0.997 *0.003*	1.001	0.994 *0.007*	1.010 *0.000*	1.003 *0.011*	1.003 *0.006*
Cr	0.001 *0.000*	0.001 *0.000*	0.001 *0.001*	0.000	0.000 *0.001*	0.000 *0.000*	0.001 *0.001*	0.000 *0.000*
Mg	1.788 *0.015*	1.804 *0.014*	1.839 *0.005*	1.752	1.685 *0.018*	1.614 *0.012*	1.771 *0.028*	1.774 *0.018*
Ca	0.016 *0.004*	0.018 *0.005*	0.016 *0.000*	0.018	0.015 *0.001*	0.019 *0.002*	0.022 *0.011*	0.016 *0.005*
Mn	0.001 *0.001*	0.001 *0.001*	0.002 *0.000*	0.003	0.002 *0.001*	0.002 *0.002*	0.001 *0.001*	0.001 *0.001*
Fe	0.194 *0.012*	0.192 *0.007*	0.147 *0.009*	0.225	0.310 *0.006*	0.346 *0.009*	0.198 *0.007*	0.201 *0.009*
Ni	0.000 *0.000*	0.001 *0.001*	0.000 *0.000*	0.001	0.000 *0.000*	0.000 *0.001*	0.000 *0.000*	0.000 *0.000*
TOTAL	3.000 *0.004*	3.008 *0.007*	3.003 *0.003*	2.999	3.006 *0.006*	2.990 *0.000*	2.997 *0.011*	2.997 *0.006*
Fo	90.2 *0.6*	90.4 *0.3*	92.6 *0.4*	88.6	84.5 *0.4*	82.3 *0.5*	90.0 *0.3*	89.8 *0.4*

Average olivine analyses. *n* = numer of analyses obtained from each run. Numbers in italics are standard deviations.
Experimental conditions: D=dry, H=hydrous, FB= furnace buffered, MHB= magnetite-haematite-buffered.
Microprobe analytical conditions given in Appendix 2.1.

Appendix 5.1 (continued)

Average electron microprobe analyses of olivine from experimental runs

Run	T-3955	T 3956	T 3957	T-3958	T-3961	T-3962	T-3964	T-3965
P (GPa)	1.50	1.50	1.50	1.50	1.00	1.00	1.25	1.00
T (°C)	1100	1060	1040	1120	1070	1030	1070	1120
	H	H	H	H	H	H	H	H
n	5	4	4	1	6	5	3	4
SiO_2	40.34 *0.08*	39.70 *0.43*	39.51 *0.23*	40.64	39.87 *0.35*	38.57 *0.38*	39.54 *0.16*	40.00 *0.40*
$Cr2O_3$	0.05 *0.04*	0.03 *0.03*	0.02 *0.01*	0.01	0.03 *0.04*	0.03 *0.01*	0.02 *0.02*	0.05 *0.02*
MgO	47.94 *0.40*	45.36 *1.18*	45.07 *0.43*	48.81	46.25 *0.71*	41.60 *0.91*	45.98 *0.24*	48.56 *0.92*
CaO	0.27 *0.04*	0.37 *0.12*	0.31 *0.02*	0.26	0.41 *0.06*	0.56 *0.13*	0.33 *0.03*	0.33 *0.04*
MnO	0.07 *0.03*	0.10 *0.05*	0.09 *0.04*	0.01	0.08 *0.04*	0.11 *0.04*	0.08 *0.05*	0.08 *0.04*
FeO	11.60 *0.25*	15.11 *1.26*	15.21 *0.46*	10.53	13.32 *0.49*	18.31 *0.97*	13.14 *0.05*	9.80 *0.64*
NiO	0.03 *0.03*	0.02 *0.02*	0.01 *0.01*	0.03	0.02 *0.02*	0.01 *0.01*	0.00 *0.01*	0.01 *0.01*
TOTAL	100.30	100.67	100.22	100.29	99.98	99.18	99.09	98.82
Si	0.994 *0.003*	0.991 *0.004*	0.992 *0.003*	0.996	0.994 *0.001*	0.994 *0.002*	0.994 *0.003*	0.994 *0.004*
Cr	0.001 *0.001*	0.001 *0.001*	0.000 *0.000*	0.000	0.001 *0.001*	0.001 *0.000*	0.000 *0.000*	0.001 *0.000*
Mg	1.761 *0.011*	1.688 *0.029*	1.686 *0.010*	1.783	1.719 *0.014*	1.598 *0.025*	1.724 *0.007*	1.797 *0.018*
Ca	0.007 *0.001*	0.010 *0.003*	0.008 *0.001*	0.007	0.011 *0.002*	0.015 *0.004*	0.009 *0.001*	0.009 *0.001*
Mn	0.001 *0.001*	0.002 *0.001*	0.002 *0.001*	0.000	0.002 *0.001*	0.002 *0.001*	0.002 *0.001*	0.002 *0.001*
Fe	0.239 *0.005*	0.316 *0.029*	0.319 *0.011*	0.216	0.278 *0.012*	0.395 *0.022*	0.276 *0.002*	0.204 *0.015*
Ni	0.001 *0.001*	0.000 *0.000*	0.000 *0.000*	0.001	0.000 *0.000*	0.000 *0.000*	0.000 *0.000*	0.000 *0.000*
TOTAL	3.005 *0.003*	3.008 *0.004*	3.008 *0.003*	3.004	3.005 *0.002*	3.006 *0.002*	3.005 *0.003*	3.006 *0.004*
Fo	88.0 *0.3*	84.2 *1.4*	84.1 *0.5*	89.2	86.1 *0.6*	80.2 *1.1*	86.2 *0.1*	89.8 *0.8*

Run	T-3968	T-3970	T-3974	T-3975	T-3989	T-3991	T 4007	T-3878
P (GPa)	2.00	1.75	3.00	2.50	2.20	2.20	3.00	2.00
T (°C)	1100	1100	1060	1060	1100	1070	1280	1400
	H	H	H	H	H	H	H	D
n	3	4	7	8	3	4	5	4
SiO_2	39.97 *0.14*	39.67 *0.34*	39.40 *0.06*	39.30 *0.60*	40.03 *0.22*	39.52 *0.12*	39.54 *0.24*	40.01 *0.19*
$Cr2O_3$	0.03 *0.03*	0.03 *0.02*	0.01 *0.01*	0.02 *0.02*	0.02 *0.02*	0.04 *0.04*	0.03 *0.03*	0.03 *0.01*
MgO	46.50 *0.36*	46.36 *1.14*	44.38 *0.46*	43.67 *2.15*	47.25 *0.29*	45.88 *0.33*	45.28 *0.06*	47.09 *0.29*
CaO	0.30 *0.03*	0.27 *0.04*	0.17 *0.12*	0.17 *0.02*	0.30 *0.06*	0.26 *0.02*	0.13 *0.02*	0.40 *0.03*
MnO	0.09 *0.05*	0.07 *0.03*	0.09 *0.03*	0.10 *0.06*	0.05 *0.04*	0.10 *0.04*	0.09 *0.04*	0.07 *0.03*
FeO	13.56 *0.59*	12.82 *1.20*	16.13 *0.46*	17.30 *2.36*	12.16 *0.25*	13.82 *0.51*	14.69 *0.11*	12.19 *0.21*
NiO	0.02 *0.02*	0.03 *0.02*	0.03 *0.03*	0.04 *0.02*	0.01 *0.02*	0.01 *0.02*	0.03 *0.02*	0.00 *0.01*
TOTAL	100.47	99.24	100.20	100.60	99.82	99.63	99.78	99.79
Si	0.993 *0.002*	0.994 *0.002*	0.993 *0.003*	0.992 *0.002*	0.994 *0.004*	0.992 *0.001*	0.994 *0.003*	0.995 *0.006*
Cr	0.001 *0.000*	0.001 *0.000*	0.000 *0.000*	0.000 *0.000*	0.000 *0.000*	0.001 *0.001*	0.001 *0.001*	0.000 *0.000*
Mg	1.721 *0.010*	1.732 *0.029*	1.667 *0.015*	1.642 *0.056*	1.749 *0.007*	1.716 *0.008*	1.696 *0.004*	1.745 *0.006*
Ca	0.008 *0.001*	0.007 *0.001*	0.005 *0.003*	0.005 *0.001*	0.008 *0.001*	0.007 *0.000*	0.003 *0.001*	0.010 *0.000*
Mn	0.002 *0.001*	0.002 *0.001*	0.002 *0.001*	0.002 *0.001*	0.001 *0.001*	0.002 *0.001*	0.002 *0.001*	0.000 *0.000*
Fe	0.282 *0.013*	0.269 *0.027*	0.340 *0.010*	0.366 *0.055*	0.253 *0.006*	0.290 *0.011*	0.309 *0.003*	0.255 *0.006*
Ni	0.000 *0.000*	0.001 *0.000*	0.001 *0.001*	0.001 *0.000*	0.000 *0.000*	0.000 *0.000*	0.001 *0.000*	0.000 *0.000*
TOTAL	3.007 *0.002*	3.005 *0.002*	3.007 *0.003*	3.008 *0.001*	3.005 *0.004*	3.008 *0.002*	3.006 *0.003*	3.005 *0.006*
Fo	85.9 *0.6*	86.6 *1.4*	83.1 *0.5*	81.8 *2.8*	87.4 *0.3*	85.5 *0.6*	84.6 *0.1*	87.3 *0.3*

Appendix 5.2

Electron microprobe analyses of primitive clinopyroxenes from experimental runs

Run	T-3869	T-3871	T-3875	T-3878	T-3896	T-3898	T-3956	T-3957	T-3961	T-3962
P (GPa)	1.50	1.50	2.00	2.00	2.50	2.50	1.50	1.50	1.00	1.00
T (°C)	1350	1320	1390	1400	1420	1460	1060	1040	1070	1030
Analysis no	104-23	105	104-47	104-58			115-30	115-14	120-7	121-3
	-L		-L	-L					-L	
	D	D	D	D	D	D	H	H	H	H
SiO_2	46.05	48.39	48.46	49.12	47.51	45.28	50.70	51.31	52.52	49.57
TiO_2	0.93	0.65	0.56	0.50	0.66	0.97	0.35	0.41	0.31	0.66
Al_2O_3	13.30	10.30	10.71	10.50	11.92	14.89	4.85	4.56	2.45	4.71
Cr_2O_3	0.19	0.13	0.07	0.12	0.05	0.13	0.48	0.40	0.58	0.18
Fe_2O_3	2.11	1.54	2.46	1.41	2.53	2.37	2.44	3.43	1.85	3.22
FeO	2.01	2.80	1.66	2.53	1.89	3.69	1.31	0.39	1.58	0.78
CaO	20.72	22.13	20.95	20.60	19.95	17.24	23.66	24.39	23.97	24.44
MgO	13.99	13.57	14.54	15.27	14.36	14.48	15.83	16.36	16.88	15.14
MnO	0.00	0.09	0.05	0.03	0.05	0.00	0.03	0.02	0.01	0.00
Na_2O	0.52	0.65	0.86	0.65	0.93	0.74	0.23	0.20	0.15	0.17
TOTAL	99.82	100.25	100.32	100.73	99.85	99.79	99.89	101.46	100.31	98.87
4 cations sum										
Si	1.676	1.761	1.752	1.766	1.724	1.646	1.853	1.847	1.911	1.837
Ti	0.025	0.018	0.015	0.014	0.018	0.027	0.010	0.011	0.008	0.018
Al	0.571	0.442	0.457	0.445	0.510	0.638	0.209	0.193	0.105	0.206
Cr	0.005	0.004	0.002	0.003	0.001	0.004	0.014	0.011	0.017	0.005
Fe^{3+}	0.058	0.042	0.067	0.038	0.069	0.065	0.067	0.093	0.051	0.090
Fe^{2+}	0.061	0.085	0.050	0.076	0.057	0.112	0.040	0.012	0.048	0.024
Ca	0.808	0.863	0.812	0.794	0.776	0.672	0.927	0.941	0.934	0.971
Mg	0.759	0.736	0.784	0.818	0.777	0.785	0.863	0.878	0.915	0.836
Mn	0.000	0.003	0.002	0.001	0.002	0.000	0.001	0.001	0.000	0.000
Na	0.037	0.046	0.060	0.045	0.065	0.052	0.016	0.014	0.011	0.012
Mg#	86.4	85.2	87.0	87.7	86.0	81.6	89	89	90	88
mg#	92.5	89.6	94.0	91.5	93.1	87.5	95.6	98.7	95.0	97.2
Fe*	0.12	0.13	0.12	0.11	0.13	0.18	0.11	0.10	0.10	0.11
FeO*	3.91	4.19	3.87	3.80	4.17	5.82	3.50	3.48	3.25	3.68
$Fe^{3+}/\sum Fe$	0.49	0.33	0.57	0.33	0.55	0.37	0.63	0.89	0.51	0.79
%Ca	47.9	50.0	47.4	46.0	46.2	41.1	48.9	48.9	48.0	50.5
%Mg	45.0	42.6	45.8	47.4	46.3	48.0	45.5	45.6	47.0	43.5
$\%\sum Fe$	7.1	7.4	6.8	6.6	7.5	10.8	5.6	5.4	5.1	5.9
Coex. Fo	87.1	81.3	85.3	87.3			88.0	84.1	86.1	80.2

Run	T-3964	T-3974	T-3975	T-3989	T-3991	T-4007	T-4008	T-4045	T-4047	T-4054
P (GPa)	1.25	3.00	2.50	2.20	2.20	3.00	2.50	1.50	1.50	2.00
T (°C)	1070	1060	1060	1100	1070	1080	1085	1240	1260	1240
Analysis no	121-10	125-5	125-15			146-53	146-66	146-20	145-1	145-6
	-L			-L	-L	-L	-L	-L	-L	
	H	H	H	H	H	H	H	CO2 (FB)	CO2 (FB)	CO2 (FB)
SiO_2	51.25	52.40	52.10	52.75	50.84	52.77	52.00	49.96	51.71	50.01
TiO_2	0.30	0.25	0.26	0.13	0.29	0.15	0.18	0.29	0.29	0.39
Al_2O_3	3.47	2.64	3.11	2.15	4.05	2.36	3.53	7.38	5.45	8.95
Cr_2O_3	0.56	0.00	0.20	0.35	0.54	0.20	0.21	0.36	0.36	0.34
Fe_2O_3	2.64	2.17	2.68	2.44	2.61	2.41	2.85	3.17	1.18	2.21
FeO	0.54	3.00	1.83	0.69	0.75	1.63	0.69	0.67	0.35	2.25
CaO	24.76	23.02	23.34	24.20	23.76	23.30	23.98	19.32	20.92	19.02
MgO	16.00	16.33	16.71	17.24	16.05	17.14	16.28	17.39	18.40	16.50
MnO	0.04	0.03	0.05	0.03	0.05	0.07	0.00	0.12	0.06	0.09
Na_2O	0.16	0.27	0.21	0.16	0.26	0.25	0.41	0.75	0.45	0.87
TOTAL	99.71	100.12	100.49	100.14	99.20	100.27	100.11	99.41	99.17	100.62
4 cations sum										
Si	1.878	1.916	1.894	1.918	1.870	1.918	1.892	1.812	1.870	1.796
Ti	0.008	0.007	0.007	0.004	0.008	0.004	0.005	0.008	0.008	0.010
Al	0.150	0.114	0.133	0.092	0.176	0.101	0.151	0.316	0.232	0.379
Cr	0.016	0.000	0.006	0.010	0.016	0.006	0.006	0.010	0.010	0.010
Fe^{3+}	0.073	0.060	0.073	0.067	0.072	0.066	0.078	0.086	0.032	0.060
Fe^{2+}	0.016	0.092	0.055	0.021	0.023	0.050	0.021	0.020	0.011	0.068
Ca	0.972	0.902	0.909	0.943	0.936	0.908	0.935	0.751	0.811	0.732
Mg	0.874	0.890	0.905	0.934	0.880	0.929	0.883	0.940	0.992	0.883
Mn	0.001	0.001	0.002	0.001	0.002	0.002	0.000	0.004	0.002	0.003
Na	0.011	0.019	0.015	0.011	0.019	0.017	0.029	0.053	0.031	0.061
Mg#	91	85	88	91	90	89	90	89.8	95.9	87.4
mg#	98.1	90.6	94.2	97.8	97.4	94.9	97.7	97.9	98.9	92.9
Fe*	0.09	0.15	0.13	0.09	0.10	0.12	0.10	0.11	0.04	0.13
FeO*	2.91	4.96	4.24	2.89	3.10	3.80	3.25	3.52	1.41	4.24
$Fe^{3+}/\sum Fe$	0.82	0.39	0.57	0.76	0.76	0.57	0.79	0.81	0.75	0.47
%Ca	50.2	46.4	46.8	48.0	49.0	46.5	48.8	41.8	43.9	42.0
%Mg	45.2	45.8	46.6	47.5	46.0	47.6	46.1	52.3	53.7	50.7
$\%\sum Fe$	4.6	7.8	6.6	4.5	5.0	5.9	5.2	5.9	2.3	7.3
Coex. Fo	86.2	83.1	81.8	87.4	85.5	84.6		84.4		

Appendix 5.2 (continued)

Electron microprobe analyses of primitive clinopyroxenes from experimental runs

Run	T-4055	T-4056	T-4109	T-4111	T-4149	T-4157	T-4158	T-4159	T-4160	T-4161
P (GPa)	2.50	2.50	1.00	1.00	1.75	2.00	2.00	2.25	1.50	1.25
T (°C)	1240	1260	1280	1290	1295	1330	1320	1340	1285	1290
Analysis no	157-3	149-13	176-6	176-18	170-1	172-46	170-26	171-6	174-19	175-12
		~L		~L	~L	~L	~L	~L	~L	~L
	CO2 (FB)	CO2 (FB)	CO2 (MHB)	CO2 (MHB)	CO2 (MHB)	CO2 (MHB)	CO2 (MHB)	CO2 (MHB)	CO2 (MHB)	CO2 (MHB)
SiO_2	51.39	50.71	48.31	45.74	48.48	50.27	48.513	52.00	47.65	48.37
TiO_2	0.35	0.40	0.46	0.89	0.39	0.24	0.39	0.19	0.56	0.38
Al_2O_3	8.79	8.88	9.41	12.68	10.39	8.79	12.16	7.55	11.44	9.08
Cr_2O_3	0.16	0.09	0.43	0.25	0.23	0.40	0.19	0.34	0.26	0.77
Fe_2O_3	1.00	1.95	3.52	4.20	2.78	0.10	0.33	0.17	2.54	2.87
FeO	2.81	2.38	0.57	0.31	2.36	3.75	3.56	3.95	1.66	1.29
CaO	19.34	19.56	21.31	20.26	16.73	16.86	17.39	14.06	19.05	20.42
MgO	15.98	15.31	15.71	14.97	17.67	18.20	16.14	20.84	15.86	16.08
MnO	0.06	0.03	0.03	0.06	0.11	0.07	0.09	0.00	0.02	0.00
Na_2O	1.22	1.35	0.49	0.54	0.63	0.53	0.79	0.70	0.67	0.44
TOTAL	101.09	100.66	100.24	99.88	99.76	99.20	99.56	99.79	100.11	99.73
4 cations sum										
Si	1.832	1.820	1.750	1.662	1.750	1.818	1.751	1.854	1.726	1.760
Ti	0.009	0.011	0.013	0.024	0.011	0.007	0.010	0.005	0.015	0.011
Al	0.369	0.376	0.402	0.543	0.442	0.375	0.518	0.317	0.489	0.390
Cr	0.005	0.003	0.012	0.007	0.006	0.012	0.006	0.009	0.007	0.022
Fe^{3+}	0.027	0.053	0.096	0.115	0.076	0.003	0.009	0.005	0.069	0.079
Fe^{2+}	0.084	0.072	0.017	0.009	0.071	0.113	0.108	0.118	0.050	0.039
Ca	0.739	0.752	0.827	0.789	0.647	0.653	0.673	0.537	0.740	0.796
Mg	0.849	0.819	0.848	0.811	0.950	0.981	0.868	1.107	0.856	0.872
Mn	0.002	0.001	0.001	0.002	0.004	0.002	0.003	0.000	0.001	0.000
Na	0.084	0.094	0.035	0.038	0.044	0.037	0.055	0.048	0.047	0.031
Mg#	88.5	86.8	88.2	86.7	86.6	89.4	88.2	90.1	87.76	88.1
mg#	91.0	92.0	98.0	98.9	93.0	89.6	89.0	90.4	94.46	95.7
Fe*	0.11	0.12	0.11	0.12	0.15	0.12	0.12	0.12	0.12	0.12
FeO*	3.71	4.14	3.73	4.08	4.86	3.83	3.86	4.10	3.94	3.88
$Fe^{3+}/\sum Fe$	0.24	0.42	0.85	0.9	0.51	0.02	0.08	0.04	0.58	0.67
%Ca	43.5	44.4	46.3	45.8	37.1	37.3	40.6	30.4	43.1	44.6
%Mg	50.0	48.3	47.4	47.0	54.5	56.0	52.4	62.7	49.9	48.8
$\%\sum Fe$	6.5	7.3	6.3	7.2	8.4	6.6	7.0	6.9	7.0	6.6
Coex. Fo			90.2	90.4					90.0	89.8

Selected analyses of the most primitive clinopyroxene composition within each run. ~L indicates close to clinopyroxene-in boundary. D=dry, H=hydrous, FB=furnace buffered, MHB=magnetite-haematite buffered condition. Fe^{3+} calculated assuming perfect stochiometry after Robinson (1980). Mg#= 100Mg/(Mg+Fe*), mg#= 100Mg/(Mg+Fe^{2+}), (*) all iron as FeO. Coex. Fo indicates average composition of the coexisting olivine in run from Appendix 5.1. Microprobe analytical conditions given in Appendix 2.1.

Appendix 5.3

Olivine-Melt $K_D^{Fe\text{-}Mg}$ values from experimental runs

Run	P (GPa)	T (°C)	Fo	K_D
ANK2376 (Anhydrous)				
T-3868	1.50	1380	89.1 *0.1*	0.31
T-3878	2.00	1400	87.3 *0.3*	0.37
ANK2376 + 20 wt%H_2O (Hydrous)				
T-3955	1.50	1100	88.0 *0.3*	0.35
T-3958	1.50	1120	89.2	0.31
T-3965	1.00	1120	89.8 *0.8*	0.29
T-3968	2.00	1100	85.9 *0.6*	0.42
T-3970	1.75	1100	86.6 *1.4*	0.40
T-3989	2.25	1100	87.4 *0.3*	0.37
T-4007	3.00	1080	84.6 *0.1*	0.47
ANK2376 + 7.5 wt%CO_2 Furnace buffered (FB)				
T-4062	1.00	1280	90.9 *0.9*	0.26
ANK2376 + 7.5 wt%CO_2 Magnetite-Haematite buffered (MHB)				
T-4121	1.00	1320	92.6 *0.4*	0.21
T-4160	1.50	1285	90.0 *0.3*	0.29
T-4161	1.25	1290	89.8 *0.4*	0.29

K_D values $=(Fe/Mg)_{Ol}/(Fe^*/Mg)_{Melt}$ for near liquidus olivines calculated using starting glass ANK2376 as melt composition (Table 5.1, Column 10). Numbers in italics are standard deviation of average olivine analyses (Appendix 5.1). Standard deviation in K_D values are less than 0.01.

Appendix 5.4

Electron microprobe analyses of clinopyroxenes from run T-4159

Core-rim analyses from large crystals.

Grain	A		B		C		D		E	
Position	C	R	C	R	C	R	C	R	C	R
Anal. No.	171-3	171-2	171-4	171-5	173-2	173-3	173-4	173-5	173-14	173-15
SiO_2	50.78	52.02	48.63	48.71	48.44	48.68	48.78	48.40	49.33	48.46
TiO_2	0.17	0.14	0.37	0.32	0.20	0.27	0.29	0.35	0.27	0.28
Al_2O_3	9.42	7.63	12.57	12.48	12.00	11.56	12.12	12.39	12.02	12.11
Cr_2O_3	0.22	0.29	0.43	0.40	0.40	0.50	0.39	0.45	0.46	0.31
Fe_2O_3	0.01	0.37	0.77	0.38	0.84	1.13	0.43	1.06	0.00	1.12
FeO	3.69	3.69	2.80	3.08	2.73	2.52	3.22	2.70	3.49	2.63
CaO	15.71	14.96	17.64	17.42	17.08	17.12	15.89	17.36	15.75	17.19
MgO	18.69	20.07	15.99	16.10	16.44	16.54	17.09	16.31	17.15	16.39
MnO	0.04	0.06	0.05	0.05	0.09	0.07	0.10	0.08	0.02	0.04
Na_2O	0.80	0.79	0.98	0.95	0.89	0.96	0.96	0.89	0.91	0.93
TOTAL	99.52	100.02	100.23	99.90	99.12	99.34	99.28	99.98	99.40	99.45
Si	1.821	1.854	1.742	1.749	1.752	1.758	1.757	1.738	1.774	1.748
Ti	0.005	0.004	0.010	0.009	0.006	0.007	0.008	0.009	0.007	0.008
Al	0.398	0.321	0.531	0.528	0.512	0.492	0.515	0.525	0.510	0.515
Cr	0.006	0.008	0.012	0.011	0.012	0.014	0.011	0.013	0.013	0.009
Fe^{3+}	0.000	0.010	0.021	0.010	0.023	0.031	0.012	0.029	0.000	0.031
Fe^{2+}	0.111	0.110	0.084	0.093	0.083	0.076	0.097	0.081	0.105	0.079
Ca	0.603	0.571	0.677	0.670	0.662	0.662	0.613	0.668	0.607	0.664
Mg	0.999	1.066	0.854	0.862	0.886	0.890	0.917	0.873	0.919	0.881
Mn	0.001	0.002	0.002	0.002	0.003	0.002	0.003	0.002	0.001	0.001
Na	0.056	0.054	0.068	0.066	0.062	0.067	0.067	0.062	0.064	0.065
Mg#	90.0	89.9	89.1	89.3	89.4	89.3	89.4	88.8	89.8	88.9
mg#	90.0	90.7	91.1	90.3	91.5	92.1	90.4	91.5	89.8	91.7
Fe*	0.11	0.12	0.10	0.10	0.11	0.11	0.11	0.11	0.10	0.11
FeO*	3.70	4.02	3.49	3.43	3.49	3.54	3.61	3.65	3.49	3.64
$Fe^{3+}/\Sigma Fe$	0.00	0.08	0.20	0.10	0.22	0.29	0.11	0.26	0.00	0.28
%Ca (Wo)	35.2	32.5	41.4	41.0	40.0	39.9	37.4	40.5	37.2	40.1
%Mg (En)	58.3	60.7	52.2	52.7	53.6	53.6	56.0	52.9	56.3	53.2
%Fe* (Fs)	6.5	6.8	6.4	6.3	6.4	6.4	6.6	6.6	6.4	6.6

Single analyses on small grains.

Grain	F	G	H	I	J	K
Position						
Anal. No.	171-1	171-6	171-7	171-8	173-11	173-13
SiO_2	51.32	52.00	51.85	49.03	48.39	51.23
TiO_2	0.20	0.19	0.14	0.28	0.28	0.12
Al_2O_3	8.21	7.55	7.84	12.07	11.88	7.57
Cr_2O_3	0.35	0.34	0.35	0.37	0.37	0.37
Fe_2O_3	0.00	0.17	0.65	1.01	1.04	0.90
FeO	3.91	3.95	3.47	2.52	2.69	3.15
CaO	14.38	14.06	14.24	17.32	16.91	14.26
MgO	19.86	20.84	20.68	16.54	16.54	20.41
MnO	0.02	0.00	0.06	0.09	0.04	0.05
Na_2O	0.75	0.70	0.75	1.00	0.92	0.76
TOTAL	98.99	99.79	100.02	100.21	99.05	98.81
Si	1.846	1.854	1.844	1.754	1.752	1.845
Ti	0.006	0.005	0.004	0.008	0.008	0.003
Al	0.348	0.317	0.329	0.509	0.507	0.321
Cr	0.010	0.009	0.010	0.010	0.010	0.010
Fe^{3+}	0.000	0.005	0.017	0.027	0.028	0.024
Fe^{2+}	0.118	0.118	0.103	0.075	0.081	0.095
Ca	0.554	0.537	0.543	0.664	0.656	0.550
Mg	1.065	1.107	1.096	0.882	0.892	1.096
Mn	0.001	0.000	0.002	0.003	0.001	0.001
Na	0.052	0.048	0.052	0.069	0.064	0.053
Mg#	90.1	90.1	90.1	89.6	89.0	90.2
mg#	90.1	90.4	91.4	92.1	91.6	92.0
Fe*	0.12	0.12	0.12	0.10	0.11	0.12
FeO*	3.91	4.10	4.05	3.43	3.63	3.95
$Fe^{3+}/\Sigma Fe$	0.00	0.04	0.14	0.26	0.26	0.20
%Ca (Wo)	31.9	30.4	30.8	40.3	39.6	31.2
%Mg (En)	61.3	62.7	62.3	53.5	53.8	62.1
%Fe* (Fs)	6.8	6.9	6.9	6.2	6.6	6.7

Appendix 5.4 (continued)

Electron microprobe analyses of clinopyroxenes from run T-4159

Single analyses on quench needles

Grain	L	M	N	O	P	Q	R	S	T	U
Position										
Anal. No	171-9	171-10	170-11	170-12	173-6	173-7	173-8	173-9	173-10	173-12
SiO_2	49.21	48.68	48.68	48.73	45.01	46.59	45.07	48.69	48.66	51.39
TiO_2	0.29	0.20	0.30	0.31	1.01	0.65	0.86	0.29	0.25	0.14
Al_2O_3	11.81	11.96	12.07	12.19	15.47	14.43	15.44	12.50	11.97	7.55
Cr_2O_3	0.47	0.42	0.51	0.41	0.01	0.33	0.05	0.46	0.55	0.37
Fe_2O_3	0.98	0.73	0.31	0.41	1.92	1.15	1.24	0.91	0.97	0.69
FeO	2.64	2.73	3.23	3.14	3.90	3.30	5.43	2.83	2.80	3.19
CaO	17.40	16.93	16.82	16.99	15.06	16.15	14.06	16.89	16.58	14.62
MgO	16.65	16.62	16.58	16.32	15.16	16.03	14.29	16.50	16.87	20.30
MnO	0.04	0.03	0.03	0.01	0.00	0.00	0.10	0.02	0.03	0.03
Na_2O	0.96	0.93	0.89	0.98	0.98	0.80	1.22	0.99	0.92	0.74
TOTAL	100.44	99.23	99.41	99.48	98.52	99.43	97.75	100.08	99.60	99.01
Si	1.757	1.757	1.755	1.756	1.647	1.683	1.666	1.744	1.751	1.848
Ti	0.008	0.006	0.008	0.008	0.028	0.018	0.024	0.008	0.007	0.004
Al	0.497	0.509	0.513	0.518	0.667	0.614	0.673	0.528	0.508	0.320
Cr	0.013	0.012	0.014	0.012	0.000	0.009	0.001	0.013	0.016	0.010
Fe^{3+}	0.026	0.020	0.008	0.011	0.053	0.031	0.034	0.025	0.026	0.019
Fe^{2+}	0.079	0.082	0.097	0.095	0.119	0.100	0.168	0.085	0.084	0.096
Ca	0.666	0.655	0.650	0.656	0.590	0.625	0.557	0.648	0.639	0.563
Mg	0.886	0.894	0.891	0.876	0.826	0.863	0.787	0.881	0.904	1.088
Mn	0.001	0.001	0.001	0.000	0.000	0.000	0.003	0.000	0.001	0.001
Na	0.067	0.065	0.062	0.068	0.069	0.056	0.087	0.069	0.064	0.052
Mg#	89.4	89.8	89.4	89.2	82.7	86.8	79.6	88.9	89.1	90.5
mg#	91.8	91.6	90.2	90.2	87.4	89.7	82.4	91.2	91.5	91.9
Fe*	0.11	0.10	0.11	0.11	0.17	0.13	0.20	0.11	0.11	0.11
FeO*	3.52	3.38	3.51	3.51	5.63	4.33	6.54	3.65	3.67	3.82
$Fe^{3+}/(Fe^{3+}$	0.25	0.19	0.08	0.10	0.31	0.24	0.17	0.22	0.24	0.16
%Ca (W	40.2	39.7	39.5	40.0	37.1	38.6	36.0	39.6	38.6	31.9
%Mg (E	53.5	54.2	54.1	53.5	52.0	53.3	50.9	53.7	54.7	61.6
%Fe* (F	6.3	6.2	6.4	6.5	10.8	8.1	13.1	6.7	6.7	6.5

Selected pyroxene analyses from Run T-4159. Analyses from A to E are core (C) and rim (R) analyses from large crystals. F to K are single analyses on small pyroxene crystals, and from L to U are analyses of tiny quench clinopyrxene needles. Data plotted in Figure 5.14. Mg#=100Mg/(Mg+Fe*). mg#=100Mg/(Mg+Fe^{2+}). (*) indicates all iron as Fe^{2+}.

Appendix 5.5

Average electron microprobe analyses of garnets from experimental runs

Run	T-3974	T-4007	T-4008	T-4055	T-4056	T-4098	T-4119	T-4120
P (GPa)	3.0	3.0	2.5	2.5	2.5	2.5	2.5	2.5
T (°C)	1060	1080	1085	1240	1260	1280	1300	1310
Condition	H	H	H	CO2 (FB)	CO2 (FB)	CO2 (MHB)	CO2 (MHB)	CO2 (MHB)
n	7	3	3	5	6	4	6	7
SiO_2	40.02 *0.33*	39.31 *0.70*	40.16 *0.15*	41.43 *0.79*	41.07 *0.21*	42.59 *2.26*	41.34 *0.64*	40.05 *0.40*
TiO_2	0.70 *0.26*	0.61 *0.24*	0.63 *0.16*	0.34 *0.14*	0.47 *0.10*	0.54 *0.12*	0.31 *0.08*	0.71 *0.10*
Al_2O_3	21.86 *0.58*	21.88 *0.87*	21.82 *0.13*	22.70 *0.67*	22.54 *0.55*	21.22 *1.72*	23.27 *0.59*	21.19 *0.70*
$Cr2O_3$	0.09 *0.08*	0.26 *0.11*	0.13 *0.00*	0.15 *0.06*	0.10 *0.02*	0.06 *0.07*	0.23 *0.07*	0.09 *0.03*
Fe_2O_3	2.44 *0.33*	3.49 *0.74*	3.00 *0.10*	1.66 *0.32*	2.10 *0.39*	0.77 *0.79*	1.46 *0.50*	1.87 *0.44*
FeO	9.38 *0.54*	7.77 *0.18*	7.35 *0.11*	8.76 *2.59*	8.77 *1.69*	10.33 *3.13*	7.05 *1.42*	14.43 *0.80*
CaO	13.14 *0.96*	13.34 *0.43*	12.89 *0.52*	7.98 *0.57*	8.32 *0.23*	9.16 *1.68*	7.71 *0.46*	8.24 *0.47*
MgO	12.40 *0.82*	12.64 *0.33*	13.79 *0.43*	17.27 *1.85*	16.82 *1.05*	15.75 *1.64*	18.32 *1.28*	13.14 *0.70*
MnO	0.17 *0.04*	0.16 *0.05*	0.16 *0.04*	0.09 *0.06*	0.14 *0.04*	0.13 *0.01*	0.14 *0.04*	0.13 *0.03*
TOTAL	100.20	99.46	99.93	100.38	100.33	100.56	99.83	99.85
Cations, (Σ=8)								
Si	2.943 *0.007*	2.907 *0.051*	2.938 *0.003*	2.973 *0.029*	2.958 *0.021*	3.078 *0.149*	2.957 *0.024*	2.977 *0.024*
Ti	0.039 *0.015*	0.034 *0.013*	0.035 *0.009*	0.018 *0.008*	0.026 *0.006*	0.029 *0.007*	0.017 *0.005*	0.040 *0.006*
Al	1.895 *0.037*	1.908 *0.077*	1.882 *0.006*	1.920 *0.051*	1.913 *0.036*	1.809 *0.151*	1.962 *0.042*	1.856 *0.048*
Cr	0.005 *0.005*	0.015 *0.007*	0.007 *0.000*	0.008 *0.004*	0.006 *0.001*	0.003 *0.004*	0.013 *0.004*	0.005 *0.002*
Fe^{3+}	0.135 *0.019*	0.194 *0.041*	0.165 *0.005*	0.090 *0.018*	0.114 *0.021*	0.042 *0.042*	0.079 *0.027*	0.105 *0.025*
Fe^{2+}	0.577 *0.032*	0.481 *0.011*	0.450 *0.008*	0.527 *0.164*	0.528 *0.105*	0.626 *0.199*	0.422 *0.090*	0.898 *0.057*
Ca	1.036 *0.083*	1.057 *0.034*	1.010 *0.044*	0.614 *0.044*	0.642 *0.020*	0.709 *0.127*	0.591 *0.040*	0.656 *0.041*
Mg	1.359 *0.082*	1.394 *0.037*	1.503 *0.043*	1.844 *0.175*	1.805 *0.103*	1.695 *0.152*	1.951 *0.115*	1.455 *0.065*
Mn	0.011 *0.003*	0.010 *0.003*	0.010 *0.003*	0.005 *0.004*	0.009 *0.002*	0.008 *0.000*	0.008 *0.002*	0.008 *0.002*
Mg#	65.7 *1.9*	67.4 *0.9*	71.0 *0.8*	75.0 *6.8*	73.8 *4.3*	71.9 *7.7*	79.6 *3.9*	59.3 *2.4*
mg#	70.2 *2.0*	74.3 *1.0*	77.0 *0.8*	77.7 *7.0*	77.4 *4.5*	73.1 *7.8*	82.2 *4.0*	61.8 *2.5*
Fe^*	0.71 *0.04*	0.68 *0.05*	0.61 *0.00*	0.62 *0.17*	0.64 *0.10*	0.67 *0.20*	0.50 *0.09*	1.00 *0.07*
FeO*	11.57 *0.59*	10.91 *0.85*	10.05 *0.02*	10.26 *2.62*	10.66 *1.60*	11.02 *3.23*	8.36 *1.49*	16.12 *0.97*
$Fe^{3+}/\Sigma Fe$	0.19 *0.02*	0.29 *0.04*	0.27 *0.01*	0.15 *0.04*	0.18 *0.04*	0.06 *0.07*	0.16 *0.06*	0.10 *0.02*
%Ca (gross)	32.9 *2.4*	33.5 *0.6*	31.9 *1.4*	19.8 *1.3*	20.6 *0.6*	22.9 *4.1*	19.3 *1.1*	20.8 *1.1*
%Mg (py)	43.2 *3.0*	44.1 *1.5*	47.5 *1.4*	59.7 *5.9*	58.0 *3.5*	54.6 *4.7*	63.8 *3.8*	46.2 *2.5*
$\%Fe^{2+}$ (alm)	18.3 *1.0*	15.2 *1.5*	14.2 *0.1*	17.0 *5.4*	17.0 *3.1*	20.2 *6.5*	13.8 *2.7*	28.5 *1.8*
$\%Ti+Fe^{3+}$ (spess)	5.5 *1.3*	7.2 *1.5*	6.3 *0.2*	3.5 *0.7*	4.5 *0.8*	2.3 *1.2*	3.1 *0.6*	4.6 *1.1*

Average analyses of synthesized garnets. *n* =number of analyses. Numbers in itallics are standard deviations. Experimental conditions: H=hydrous, FB= Furnace buffered, MHB= Magnetite-haematite-buffered.

Mg#=100Mg/(Mg+Fe), mg#=100Mg/(Mg+Fe^{2+}). Fe^{3+} values calculated assuming perfect stochiometry following the method of Robinson (1980). py=pyrope, spess=spessartine, gross=grossular, alm=almandine.

Appendix 5.6

Electron microprobe analyses of spinel from experimental runs

Run	T-3975				T-3875	
P (GPa)	2.50				2.00	
T (°C)	1060				1320	
	H				D	
Analysis No.	125-26	125-27	125-28	125-29	104-49	104-53
SiO_2	0.06	0.09	0.08	0.09	4.65	1.20
TiO_2	0.21	0.29	0.36	0.19	0.28	0.23
Al_2O_3	63.22	61.96	60.82	63.71	62.06	65.38
Cr_2O_3	0.06	0.12	0.05	0.04	0.64	0.77
Fe_2O_3	2.93	3.41	4.40	2.80	0.00	0.00
FeO	15.00	15.83	17.72	14.94	10.53	10.09
MgO	17.62	16.91	15.61	17.82	20.60	21.64
MnO	0.00	0.03	0.12	0.04	0.07	0.07
NiO	0.02	0.00	0.06	0.01	0.00	0.01
ZnO	0.00	0.00	0.00	0.00	0.00	0.00
TOTAL	99.12	98.64	99.22	99.64	98.83	99.39
Cations						
Si	0.012	0.019	0.017	0.019	0.945	0.240
Ti	0.033	0.046	0.057	0.029	0.043	0.035
Al	15.444	15.313	15.143	15.464	14.869	15.439
Cr	0.010	0.020	0.008	0.007	0.103	0.122
Mg	5.441	5.283	4.913	5.468	6.239	6.460
Mn	0.000	0.006	0.021	0.006	0.012	0.012
Fe^{3+}	0.457	0.538	0.700	0.434	0.000	0.000
Fe^{2+}	2.600	2.775	3.129	2.572	1.790	1.690
Ni	0.003	0.000	0.010	0.002	0.000	0.002
Zn	0.000	0.000	0.000	0.000	0.000	0.000
TOTAL	24.00	24.00	24.00	24.00	24.00	24.00
mg#	67.67	65.56	61.09	68.01	77.71	79.26
Mg#	64.08	61.50	56.25	64.57	77.75	79.30
Cr#	0.06	0.13	0.06	0.04	0.69	0.78
$Fe^{3+}/\Sigma Fe$	0.15	0.16	0.18	0.14	0.00	0.00
Fe*	3.06	3.31	3.83	3.01	1.79	1.69
FeO*	17.64	18.90	21.68	17.46	10.53	10.09
Fe_2O_3/FeOmelt	0.04	0.05	0.06	0.04		

Selected analyses of aluminous spinels from runs under hydrous (H) and unhydrous (D) conditions. Note beam overlap indicated by preence of silica in analyses of unhydrous runs. Mg#= 100Mg/(Mg+Fe*), mg= 100Mg/(Mg+Fe^{2+} Cr#= 100Cr/(Cr+Al). (*) indicates all iron as FeO. Fe_2O_3/FeO value for the melt estimalted using Maurel & Maurel (1982) equations.

Appendix 5.7

Average microprobe analyses of glasses from experimental runs

Run	T-3869	T-3868	T-3870	T-3874	T-3878	T-3899	T-3898	T-4063
P (GPa)	1.50	1.50	1.50	2.00	2.00	2.50	2.50	1.00
T (°C)	1350	1380	1400	1410	1400	1480	1460	1250
	U	U	U	U	U	U	U	CO2-FB
n	*8*	*6*	*10*	*9*	*7*		*2*	*10*
SiO_2	43.93 *0.28*	44.29 *0.10*	44.02 *0.17*	43.95 *0.16*	43.55 *0.16*	44.74 *0.04*	43.02 *0.33*	44.90 *0.13*
TiO_2	0.88 *0.04*	0.87 *0.02*	0.81 *0.03*	0.86 *0.03*	0.91 *0.03*	0.81 *0.04*	0.91 *0.04*	0.86 *0.02*
Al_2O_3	14.90 *0.27*	14.36 *0.11*	14.01 *0.07*	14.32 *0.08*	14.15 *0.09*	14.37 *0.22*	14.26 *0.16*	14.22 *0.11*
Cr_2O_3	0.06 *0.02*	0.08 *0.03*	0.05 *0.03*	0.06 *0.03*	0.07 *0.03*	0.08 *0.06*	0.05 *0.04*	0.07 *0.04*
FeO	9.80 *0.22*	9.30 *0.11*	9.19 *0.10*	9.13 *0.11*	10.26 *0.09*	8.69 *0.23*	10.51 *0.21*	1.45 *0.19*
MgO	11.61 *0.45*	12.81 *0.11*	13.32 *0.13*	13.09 *0.09*	12.48 *0.06*	13.73 *0.05*	12.85 *0.13*	13.83 *0.07*
CaO	14.98 *0.27*	15.03 *0.18*	14.74 *0.06*	14.74 *0.19*	14.31 *0.20*	14.87 *0.06*	13.83 *0.06*	15.25 *0.10*
MnO	0.06 *0.04*	0.09 *0.05*	0.06 *0.04*	0.08 *0.04*	0.08 *0.04*	0.10 *0.08*	0.01 *0.01*	0.09 *0.03*
Na_2O	2.27 *0.08*	2.12 *0.05*	2.03 *0.05*	2.19 *0.12*	2.30 *0.07*	2.18 *0.00*	2.54 *0.07*	2.08 *0.06*
K_2O	0.84 *0.03*	0.81 *0.03*	0.78 *0.02*	0.83 *0.02*	0.92 *0.03*	0.80 *0.01*	0.99 *0.02*	0.75 *0.03*
P_2O_5	0.25 *0.04*	0.23 *0.09*	0.27 *0.08*	0.21 *0.09*	0.27 *0.08*	0.23 *0.00*	0.25 *0.01*	0.26 *0.03*
TOTAL	99.59 *0.67*	99.97 *0.31*	99.28 *0.34*	99.47 *0.34*	99.30 *0.23*	100.60 *0.12*	99.19 *0.77*	93.74 *0.29*
Mg#	67.9 *1.2*	71.1 *0.4*	72.1 *0.2*	71.9 *0.2*	68.5 *0.3*	73.8 *0.6*	68.6 *0.2*	94.5 *0.7*
CaO/Al_2O	1.0 *0.0*	1.0 *0.0*	1.1 *0.0*	1.0 *0.0*	1.0 *0.0*	1.0 *0.0*	1.0 *0.0*	98.3 *0.2*

Run	T-4062	T-4043	T-4052	T-4051	T-4050	T-4047	T-4045	T-4088
P (GPa)	1.00	1.50	2.00	2.00	2.00	1.50	1.50	1.00
T (°C)	1280	1280	1260	1300	1280	1260	1240	1350
	CO2-FB	CO2-FB	CO2-FB	CO2-FB	CO2-FB	CO2-FB	CO2-FB	CO2-MHB
n	*10*	*10*	*10*	*10*	*10*	*10*	*10*	*6*
SiO_2	44.19 *0.18*	42.78 *0.14*	40.88 *0.16*	40.89 *0.19*	40.74 *0.11*	42.66 *0.18*	41.07 *0.25*	43.14 *0.27*
TiO_2	0.87 *0.04*	0.84 *0.03*	0.77 *0.04*	0.79 *0.04*	0.80 *0.02*	0.85 *0.02*	0.84 *0.04*	0.79 *0.03*
Al_2O_3	14.10 *0.06*	13.52 *0.07*	12.89 *0.06*	12.80 *0.11*	12.78 *0.09*	13.84 *0.13*	13.63 *0.10*	13.99 *0.10*
Cr_2O_3	0.06 *0.03*	0.07 *0.02*	0.07 *0.03*	0.06 *0.02*	0.05 *0.03*	0.05 *0.03*	0.04 *0.02*	0.05 *0.03*
FeO	3.87 *0.20*	3.71 *0.27*	5.35 *0.10*	5.68 *0.09*	5.72 *0.15*	4.40 *0.23*	7.50 *0.22*	6.64 *0.14*
MgO	13.48 *0.06*	12.87 *0.06*	12.40 *0.09*	12.29 *0.12*	12.26 *0.06*	12.82 *0.15*	11.89 *0.08*	12.72 *0.12*
CaO	15.09 *0.05*	14.46 *0.18*	13.53 *0.14*	13.74 *0.12*	13.53 *0.12*	14.25 *0.12*	13.52 *0.17*	14.42 *0.05*
MnO	0.06 *0.04*	0.04 *0.03*	0.07 *0.03*	0.08 *0.03*	0.08 *0.05*	0.07 *0.03*	0.07 *0.05*	0.07 *0.03*
Na_2O	2.06 *0.04*	1.97 *0.06*	1.77 *0.05*	1.88 *0.07*	1.83 *0.10*	2.12 *0.07*	2.03 *0.05*	1.95 *0.04*
K_2O	0.74 *0.02*	0.67 *0.02*	0.62 *0.01*	0.64 *0.01*	0.63 *0.02*	0.74 *0.02*	0.73 *0.02*	0.69 *0.03*
P_2O_5	0.26 *0.02*	0.22 *0.02*	0.22 *0.02*	0.20 *0.02*	0.21 *0.01*	0.24 *0.03*	0.24 *0.03*	0.16 *0.02*
TOTAL	94.79 *0.15*	91.17 *0.20*	88.57 *0.22*	89.04 *0.24*	88.63 *0.25*	92.04 *0.38*	91.56 *0.38*	94.61 *0.63*
Mg#	86.2 *0.6*	86.1 *0.9*	80.5 *0.3*	79.4 *0.3*	79.3 *0.5*	83.9 *0.8*	73.9 *0.5*	77.4 *0.4*
CaO/Al_2O	95.4 *0.2*	95.4 *0.3*	93.2 *0.1*	92.8 *0.1*	92.7 *0.2*	94.5 *0.3*	90.4 *0.2*	91.9 *0.2*

Average glass analyses of residual glasses from runs under unhydrous (U), CO_2 furnace buffered (FB), and CO_2 magnetite haematite buffered (MHB) conditions. Number in italics are standard deviations. *n* = number of analyses. Mg#=100Mg/(Mg+Fe*). (*) all iron as FeO.

Appendix 5.7 (continued)

Average microprobe analyses of glasses from experimental runs

Run	T-4092		T-4092		T-4091		T-4109		T-4111		T-4115		T-4117	
P (GPa)	1.00		1.00		1.00		1.00		1.00		1.00		1.00	
T (°C)	1300		1300		1320		1280		1290		1300		1310	
	CO2-MHB		CO2-MHB		CO2-MHB		CO2-MHB		CO2-MHB		CO2-MHB		CO2-MHB	
n		*6*		*5*		*5*		*14*		*14*		*6*		*5*
SiO_2	43.03	*0.34*	42.94	*0.51*	43.22	*0.26*	43.80	*0.16*	44.35	*0.14*	44.31	*0.21*	44.29	*0.13*
TiO_2	0.79	*0.04*	0.80	*0.07*	0.81	*0.03*	0.88	*0.03*	0.87	*0.02*	0.85	*0.04*	0.84	*0.00*
Al_2O_3	14.01	*0.09*	13.94	*0.23*	14.02	*0.08*	15.09	*0.09*	15.25	*0.02*	14.84	*0.06*	14.65	*0.09*
Cr_2O_3	0.07	*0.02*	0.04	*0.01*	0.07	*0.05*	0.06	*0.03*	0.05	*0.03*	0.09	*0.03*	0.06	*0.03*
FeO	6.33	*0.26*	6.62	*0.05*	7.22	*0.05*	7.69	*0.15*	7.02	*0.13*	7.16	*0.11*	6.99	*0.11*
MgO	12.63	*0.06*	12.58	*0.16*	12.71	*0.08*	11.17	*0.06*	11.11	*0.03*	12.27	*0.05*	12.79	*0.07*
CaO	14.44	*0.10*	14.64	*0.16*	14.58	*0.20*	15.17	*0.05*	15.46	*0.17*	15.15	*0.13*	14.97	*0.16*
MnO	0.05	*0.03*	0.06	*0.04*	0.04	*0.03*	0.08	*0.03*	0.09	*0.02*	0.04	*0.03*	0.09	*0.05*
Na_2O	1.93	*0.02*	1.91	*0.04*	1.93	*0.01*	2.15	*0.04*	2.13	*0.02*	2.09	*0.03*	2.07	*0.05*
K_2O	0.69	*0.02*	0.69	*0.03*	0.69	*0.03*	0.74	*0.03*	0.76	*0.03*	0.74	*0.02*	0.73	*0.03*
P_2O_5	0.17	*0.03*	0.15	*0.03*	0.19	*0.04*	0.19	*0.02*	0.21	*0.03*	0.24	*0.03*	0.22	*0.01*
TOTAL	94.14	*0.25*	94.37	*1.11*	95.49	*0.51*	97.01	*0.18*	97.29	*0.22*	97.77	*0.25*	97.70	*0.37*
Mg#	78.1	*0.7*	77.2	*0.2*	75.9	*0.2*	72.2	*0.5*	73.9	*0.4*	75.4	*0.3*	76.6	*0.3*
CaO/Al_2O	92.2	*0.3*	91.9	*0.1*	91.3	*0.1*	89.6	*0.2*	90.4	*0.2*	91.1	*0.1*	91.6	*0.1*

Run	T-4121		T-4149		T-4157		T-4158		T-4159		T-4160		T-4161	
P (GPa)	1.00		1.75		2.00		2.00		2.25		1.50		2.25	
T (°C)	1320		1295		1330		1320		1340		1285		1290	
	CO2-MHB		CO2-MHB		CO2-MHB		CO2-MHB		CO2-MHB		CO2-MHB		CO2-MHB	
n		*6*		*8*		*10*		*10*		*10*		*2*		*10*
SiO_2	45.61	*0.14*	41.77	*0.41*	43.35	*0.79*	42.48	*0.19*	42.44	*0.17*	42.78	*0.86*	43.40	*0.25*
TiO_2	0.89	*0.04*	0.80	*0.04*	0.79	*0.02*	0.85	*0.03*	0.81	*0.03*	0.80	*0.02*	0.85	*0.03*
Al_2O_3	15.27	*0.11*	14.52	*0.06*	14.09	*0.22*	14.38	*0.08*	13.97	*0.06*	14.07	*0.31*	14.65	*0.12*
Cr_2O_3	0.04	*0.03*	0.03	*0.02*	0.06	*0.03*	0.04	*0.02*	0.05	*0.02*	0.05	*0.03*	0.05	*0.03*
FeO	4.45	*0.31*	6.76	*0.24*	6.17	*0.17*	6.60	*0.15*	6.31	*0.11*	7.37	*0.03*	7.60	*0.09*
MgO	13.01	*0.10*	12.65	*0.38*	12.61	*0.08*	12.30	*0.07*	12.44	*0.04*	11.35	*0.08*	11.77	*0.08*
CaO	15.98	*0.11*	13.79	*0.20*	14.25	*0.08*	13.65	*0.12*	13.95	*0.11*	13.26	*0.03*	14.74	*0.15*
MnO	0.09	*0.03*	0.06	*0.04*	0.08	*0.03*	0.07	*0.04*	0.08	*0.02*	0.05	*0.02*	0.08	*0.04*
Na_2O	2.18	*0.03*	2.11	*0.18*	1.92	*0.05*	2.09	*0.05*	1.98	*0.05*	2.31	*0.14*	2.13	*0.05*
K_2O	0.77	*0.03*	0.76	*0.12*	0.70	*0.03*	0.75	*0.02*	0.69	*0.02*	0.84	*0.07*	0.74	*0.02*
P_2O_5	0.20	*0.02*	0.19	*0.03*	0.02	*0.02*	0.02	*0.03*	0.01	*0.02*	0.18	*0.00*	0.21	*0.03*
TOTAL	98.49	*0.14*	93.43	*0.57*	94.05	*0.95*	93.22	*0.37*	92.75	*0.23*	93.05	*0.36*	96.24	*0.45*
Mg#	83.9	*1.0*	77.0	*1.0*	78.5	*0.5*	76.9	*0.4*	77.9	*0.3*	73.3	*0.2*	73.4	*0.3*
CaO/Al_2O	94.6	*0.4*	91.8	*0.4*	92.4	*0.2*	91.7	*0.2*	92.2	*0.1*	90.2	*0.1*	90.2	*0.1*

Appendix 5.8

Core-rim electron microprobe analyses of large olivines from experimental runs

Run	T-4007		T-4062		T-4063		T-3955	
P (GPa)	3.0		1.0		1.0		1.5	
T (°C)	1280		1280		1250		1100	
	C	R	C	R	C	R	C	R
Analysis No	146-46	146-47	157-10	157-12	157-16	157-17	118-5	118-6
SiO_2	39.88	39.38	40.86	40.69	41.46	41.56	40.41	40.23
Cr_2O_3	0.04	0.05	0.04	0.05	0.06	0.03	0.05	0.05
MgO	45.36	45.24	50.23	49.46	52.60	52.17	47.89	48.36
CaO	0.11	0.11	0.55	0.58	0.45	0.44	0.27	0.24
MnO	0.09	0.06	0.13	0.00	0.07	0.08	0.08	0.11
FeO	14.65	14.72	9.15	9.49	6.36	6.29	11.53	11.33
NiO	0.02	0.04	0.03	0.03	0.00	0.00	0.00	0.00
TOTAL	100.15	99.59	100.99	100.30	100.99	100.56	100.23	100.32
Cations								
Si	0.998	0.992	0.990	0.994	0.992	0.997	0.996	0.991
Cr	0.001	0.001	0.001	0.001	0.001	0.000	0.001	0.001
Mg	1.691	1.699	1.815	1.801	1.875	1.866	1.760	1.775
Ca	0.003	0.003	0.014	0.015	0.011	0.011	0.007	0.006
Mn	0.002	0.001	0.003	0.000	0.001	0.002	0.002	0.002
Fe^{2+}	0.306	0.310	0.186	0.194	0.127	0.126	0.238	0.233
Ni	0.000	0.001	0.001	0.001	0.000	0.000	0.000	0.000
TOTAL	3.002	3.007	3.009	3.005	3.008	3.003	3.003	3.009
Fo	84.7	84.6	90.7	90.3	93.6	93.7	88.1	88.4

Core (C) and rim (R) analyses pairs from synthesized olivine crystals.

Appendix 5.9

FeO* content of near liquidus glasses from experimental runs

RUN	Press. (GPa)	Temp. (°C)	Run time (min.)	wt% FeO[1] (analyzed)	wt% FeO*[2] (summed)	Assemblage	Total[3] crystals
Graphite capsules							
T-3868	1.5	1380	180	9.3 (0.11)	9.30	Ol+L	<10%
T-3870	1.5	1400	180	9.19 (0.10)	9.26	>L	
T-3874	2.0	1410	180	9.13 (0.13)	9.18	>L	
Pt capsules, furnace buffered							
T-4043	1.5	1280	30	3.71 (0.27)	4.07	>L	
T-4047	1.5	1260	30	4.40 (0.23)	4.66	<L	
T-4050	2.0	1280	30	5.72 (0.15)	6.46	>L	
T-4051	2.0	1300	30	5.68 (0.09)	6.38	>L	
T-4052	2.0	1260	45	5.35 (0.10)	6.04	>L	
T-4062	1.0	1280	30	3.87 (0.20)	4.08	Ol+L	<10%
T-4063	1.0	1250	30	1.45 (0.19)	1.55	Ol+L	<10%
Pt capsules, MH-buffered							
T-4088	1.5	1350	30	6.64 (0.14)	7.02	>L	
T-4091	1.5	1320	30	7.22 (0.05)	7.56	>L	
T-4092	1.5	1300	30	6.62 (0.06)	7.02	>L	
T-4093	1.5	1290	30	6.33 (0.26)	6.72	>L	
T-4121	1.0	1320	30	4.45 (0.31)	4.52	Ol+L	<5%
T-4115	1.0	1300	30	7.16 (0.11)	7.32	Ol+L	<5%
T-4117	1.0	1310	30	6.99 (0.11)	7.16	Ol+L	<5%
T-4157	2.0	1330	30	6.18 (0.17)	6.58	Cpx+L	<50%
T-4158	2.0	1320	30	6.60 (0.15)	7.08	Cpx+L	<50%
T-4159	2.25	1340	30	6.31 (0.11)	6.80	Cpx+L	<10%

([1]) Average (n=10) FeO* content of quenched glasses obtained by microprobe analysis.

Numbers in brackets are standard deviations. ([2]) FeO* content after summing to 100% total. ([3]) Percentage values indicate aproximate crystal content in run. Starting glass FeO*=9.16 wt%. Ol=olivine, Cpx=clinopyroxene, L=liquid.

Appendix 6

Appendix 6.1

Della-Pasqua, N., Kamenetsky, V.S., Gasparon, M., Crawford, A. J.Varne, R., (1995), Al-spinels in primitive arc volcanics, 53(1) 1-26

Appendix 6.2

Relative size of Al-spl$_d$ and melt inclusion

D_{mi}	D_{spl}	$R_{mi/spl}$
5	1	5.0
10	1.5	6.7
10	2	5.0
25	5	5.0
21	4	5.3
9	2	4.5
9	2	4.5
4	1	4.0
9	2	4.5
8	1	8.0
16	3	5.3
12	2	6.0
4	1	4.0
9	2	4.5
5	0.5	10.0
6	1	6.0
12	3	4.0
20	4	5.0
10	1.5	6.7
9	1	9.0
6	1	6.0
11	3	3.7
5	1	5.0
7	2	3.5
2	0.75	2.7
4	0.66	6.1
5	1	5.0
11	3	3.7
9	2.5	3.6
42	10	4.2
45	10	4.5
6	1	6.0
5	1	5.0
5.5	1	5.5
13	3	4.3
60	15	4.0

D_{mi}	D_{spl}	$R_{mi/spl}$
3	1	3.0
33	6	5.5
27	8	3.4
15	3	5.0
25	4	6.3
5	1	5.0
72	12	6.0
16	4	4.0
20	5	4.0
55	13	4.2
15	4	3.8
25	5	5.0
55	9	6.1
21	5	4.2
45	8	5.6
6	1	6.0
24	4	6.0
5	1	5.0
20	4	5.0
25	5	5.0
20	5	4.0
55	12	4.6
32	12	2.7

Average $R_{mi/spl}$ =	**~5.0**
$(R_{mi/spl})^3$ =	**~125**
Vol% $_{spl}$=100*$(1/R_{mi/spl})^3$ =	**~0.8%**

Values represent microscopic units and measurements obtained from photographs of melt inclusions. $R_{mi/spl}$= (inclusion size/spinel size). Sizes were measured assuming spherical forms to melt inclusions and crystals.

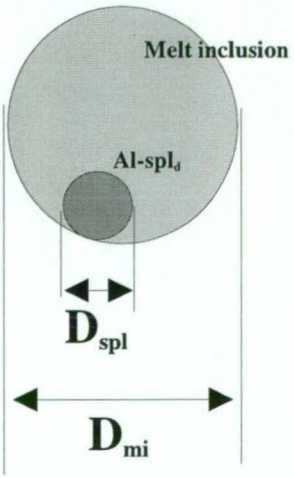

Appendix 6.3

Mass balance calculations $cpx_d + L + ol_d + Al\text{-}spl_d = Melt$

Set 122/1

% amounts		SiO_2	TiO_2	Al_2O_3	FeO	MgO	CaO	MnO	Na_2O	K_2O	P_2O_5	TOTAL
Reactants Used												
ol_d	7.0	40.21	0.00	0.00	16.25	43.54	0.00	0.00	0.00	0.00	0.00	100.00
Al-spl_d	1.1	0.16	0.18	57.96	21.94	17.67	0.00	0.14	0.00	0.00	0.00	98.05
cpx_d	71.9	41.35	1.67	14.96	9.42	10.17	21.97	0.13	0.32	0.00	0.00	100.00
L	20.0	61.55	0.59	19.59	2.86	3.28	6.15	0.00	3.98	1.56	0.38	99.94
Products Used												
Melt	1.0	44.71	0.71	14.96	9.46	10.79	16.88	0.08	1.77	0.51	0.12	100.00
Estimated Compositions												
Reactants		44.84	1.32	15.31	8.73	11.22	17.03	0.10	1.03	0.31	0.08	
Products		44.71	0.71	14.96	9.46	10.79	16.88	0.08	1.77	0.51	0.12	
Differences		0.13	0.61	0.35	-0.73	0.43	0.15	0.01	-0.74	-0.20	-0.04	
Residual Sum Squares=			**1.8**									

Set 90/1

% amounts		SiO_2	TiO_2	Al_2O_3	FeO	MgO	CaO	MnO	Na_2O	K_2O	P_2O_5	TOTAL
Reactants Used												
ol_d	5.3	40.40	0.00	0.00	15.30	44.30	0.00	0.00	0.00	0.00	0.00	100.00
Al-spl_d	1.0	0.13	0.10	61.51	18.70	19.35	0.00	0.14	0.00	0.00	0.00	99.94
cpx_d	76.3	41.89	1.05	13.42	10.85	10.40	21.99	0.05	0.32	0.00	0.00	99.97
L	17.4	62.72	0.23	24.66	3.02	2.36	0.97	0.00	3.21	2.46	0.33	99.96
Products Used												
Melt	1.0	44.71	0.71	14.96	9.46	10.79	16.88	0.08	1.77	0.51	0.12	100.00
Estimated Compositions												
Reactants		45.00	0.84	15.16	9.80	10.88	16.96	0.04	0.80	0.43	0.06	
Products		44.71	0.71	14.96	9.46	10.79	16.88	0.08	1.77	0.51	0.12	
Differences		0.28	0.13	0.20	0.34	0.09	0.08	-0.04	-0.96	-0.09	-0.06	
Residual Sum Squares=			**1.3**									

Set 65/1

% amounts		SiO_2	TiO_2	Al_2O_3	FeO	MgO	CaO	MnO	Na_2O	K_2O	P_2O_5	TOTAL
Reactants Used												
ol_d	0.3	40.52	0.00	0.00	14.68	44.80	0.00	0.00	0.00	0.00	0.00	100.00
Al-spl_d	6.4	0.01	0.19	60.70	20.19	18.37	0.00	0.12	0.00	0.00	0.00	99.58
cpx_d	77.6	45.51	0.67	10.03	9.13	12.84	21.45	0.14	0.23	0.00	0.00	100.00
L	15.8	60.61	0.38	24.22	1.62	0.70	3.80	0.00	5.87	2.38	0.43	100.00
Products Used												
Melt	1.0	44.71	0.71	14.96	9.46	10.79	16.88	0.08	1.77	0.51	0.12	100.00
Estimated Compositions												
Reactants		44.99	0.59	15.47	8.66	11.36	17.24	0.11	1.10	0.38	0.07	
Products		44.71	0.71	14.96	9.46	10.79	16.88	0.08	1.77	0.51	0.12	
Differences		0.28	-0.12	0.51	-0.80	0.57	0.36	0.03	-0.67	-0.14	-0.05	
Residual Sum Squares=			**1.9**									

Set 35/1

% amounts		SiO_2	TiO_2	Al_2O_3	FeO	MgO	CaO	MnO	Na_2O	K_2O	P_2O_5	TOTAL
Reactants Used												
ol_d	4.7	39.16	0.00	0.00	21.71	39.14	0.00	0.00	0.00	0.00	0.00	100.00
Al-spl_d	3.3	0.13	1.25	52.30	32.95	12.71	0.00	0.12	0.00	0.00	0.00	99.47
cpx_d	76.0	42.77	2.92	12.23	9.19	10.95	21.16	0.19	0.54	0.00	0.00	99.96
L	16.0	64.37	0.71	23.65	1.55	0.38	2.70	0.00	3.22	2.94	0.48	100.00
Products Used												
Melt	1.0	44.71	0.71	14.96	9.46	10.79	16.88	0.08	1.77	0.51	0.12	100.00
Estimated Compositions												
Reactants		44.64	2.38	14.81	9.35	10.64	16.50	0.15	0.93	0.47	0.08	
Products		44.71	0.71	14.96	9.46	10.79	16.88	0.08	1.77	0.51	0.12	
Differences		-0.07	1.67	-0.15	-0.11	-0.15	-0.38	0.06	-0.84	-0.04	-0.04	
Residual Sum Squares=			**3.7**									

Set 35/2

% amounts		SiO_2	TiO_2	Al_2O_3	FeO	MgO	CaO	MnO	Na_2O	K_2O	P_2O_5	TOTAL
Reactants Used												
ol_d	0.8	40.74	0.00	0.00	13.53	45.73	0.00	0.00	0.00	0.00	0.00	100.00
Al-spl_d	8.4	0.16	0.25	61.13	19.20	19.11	0.00	0.08	0.00	0.00	0.00	99.93
cpx_d	73.1	45.38	0.58	8.70	8.22	13.32	23.43	0.15	0.16	0.00	0.00	99.94
L	17.7	65.27	0.42	24.07	1.13	0.32	2.31	0.00	3.00	2.97	0.48	99.97
	100.0											
Products Used												
Melt	1.0	44.71	0.71	14.96	9.46	10.79	16.88	0.08	1.77	0.51	0.12	100.00
Estimated Compositions												
Reactants		45.05	0.52	15.75	7.93	11.77	17.54	0.12	0.65	0.52	0.08	
Products		44.71	0.71	14.96	9.46	10.79	16.88	0.08	1.77	0.51	0.12	
Differences		0.34	-0.19	0.80	-1.53	0.98	0.66	0.03	-1.12	0.01	-0.03	
Residual Sum Squares=			**5.8**									

Set 108/1

% amounts		SiO_2	TiO_2	Al_2O_3	FeO	MgO	CaO	MnO	Na_2O	K_2O	P_2O_5	TOTAL
Reactants Used												
ol_d	5.3	40.64	0.00	0.00	14.08	45.29	0.00	0.00	0.00	0.00	0.00	100.00
Al-spl_d	2.9	0.19	0.13	64.71	15.92	18.77	0.00	0.11	0.00	0.00	0.00	99.84
cpx_d	72.1	42.43	0.76	12.57	10.77	10.76	22.40	0.08	0.24	0.00	0.00	100.00
L	19.7	62.02	0.45	21.68	1.60	1.61	4.64	0.00	5.34	2.16	0.39	99.88
Products Used												
Melt	1.0	44.71	0.71	14.96	9.46	10.79	16.88	0.08	1.77	0.51	0.12	100.00
Estimated Compositions												
Reactants		44.95	0.64	15.21	9.29	11.03	17.07	0.06	1.22	0.42	0.08	
Products		44.71	0.71	14.96	9.46	10.79	16.88	0.08	1.77	0.51	0.12	
Differences		0.24	-0.07	0.25	-0.17	0.24	0.19	-0.02	-0.55	-0.09	-0.04	
Residual Sum Squares=			**0.6**									

Mass balanced solutions using mixing program GENMIX (LeMaitre 1982). Reactants are daughter phases of melt inclusion trapped in olivine from Table 6.2. $Alspl_d$, clinopyroxene=cpx_d, host olivine=ol_d and residual glass=L. Target composition (Melt) used as product is the average analysis of melts inclusion trapped in $Fo_{84\text{-}85}$ from Epi.

Appendix 6.3 (continued)

Mass balance calculations $cpx_d + L + ol_d = Melt$

Set 122/1

% amounts		SiO_2	TiO_2	Al_2O_3	FeO	MgO	CaO	MnO	Na_2O	K_2O	P_2O_5	TOTAL
Reactants Used												
ol_d	7.2	40.21	0.00	0.00	16.25	43.54	0.00	0.00	0.00	0.00	0.00	100.00
cpx_d	73.5	41.35	1.67	14.96	9.42	10.17	21.97	0.13	0.32	0.00	0.00	100.00
L	19.4	61.55	0.59	19.59	2.86	3.28	6.15	0.00	3.98	1.56	0.38	99.94
Products Used												
Melt	1.0	44.71	0.71	14.96	9.46	10.79	16.88	0.08	1.77	0.51	0.12	100.00
Estimated Compositions												
Reactants		45.18	1.34	14.79	8.64	11.22	17.34	0.10	1.01	0.30	0.07	
Products		44.71	0.71	14.96	9.46	10.79	16.88	0.08	1.77	0.51	0.12	
Differences		0.47	0.63	-0.17	-0.82	0.43	0.46	0.01	-0.76	-0.21	-0.05	
Residual Sum Squares=			**2.3**									

Set 90/2

% amounts		SiO_2	TiO_2	Al_2O_3	FeO	MgO	CaO	MnO	Na_2O	K_2O	P_2O_5	TOTAL
Reactants Used												
ol_d	5.4	40.40	0.00	0.00	15.30	44.30	0.00	0.00	0.00	0.00	0.00	100.00
cpx_d	77.2	41.89	1.05	13.42	10.85	10.40	21.99	0.05	0.32	0.00	0.00	99.97
L	17.4	62.72	0.23	24.66	3.02	2.36	0.97	0.00	3.21	2.46	0.33	99.96
Products Used												
Melt	1.0	44.71	0.71	14.96	9.46	10.79	16.88	0.08	1.77	0.51	0.12	100.00
Estimated Compositions												
Reactants		45.43	0.85	14.65	9.73	10.84	17.15	0.04	0.81	0.43	0.06	
Products		44.71	0.71	14.96	9.46	10.79	16.88	0.08	1.77	0.51	0.12	
Differences		0.71	0.14	-0.31	0.27	0.05	0.27	-0.05	-0.96	-0.09	-0.06	
Residual Sum Squares=			**1.7**									

Set 65/1

% amounts		SiO_2	TiO_2	Al_2O_3	FeO	MgO	CaO	MnO	Na_2O	K_2O	P_2O_5	TOTAL
Reactants Used												
ol_d	2.3	40.52	0.00	0.00	14.68	44.80	0.00	0.00	0.00	0.00	0.00	100.00
cpx_d	79.7	45.51	0.67	10.03	9.13	12.84	21.45	0.14	0.23	0.00	0.00	100.00
L	18.0	60.61	0.38	24.22	1.62	0.70	3.80	0.00	5.87	2.38	0.43	100.00
	100.0											
Products Used												
Melt	1.0	44.71	0.71	14.96	9.46	10.79	16.88	0.08	1.77	0.51	0.12	100.00
Estimated Compositions												
Reactants		48.12	0.60	12.36	7.90	11.38	17.78	0.11	1.24	0.43	0.08	
Products		44.71	0.71	14.96	9.46	10.79	16.88	0.08	1.77	0.51	0.12	
Differences		3.41	-0.11	-2.60	-1.56	0.59	0.90	0.03	-0.53	-0.08	-0.04	
Residual Sum Squares=			**22.2**									

Set 35/1

% amounts		SiO_2	TiO_2	Al_2O_3	FeO	MgO	CaO	MnO	Na_2O	K_2O	P_2O_5	TOTAL
Reactants Used												
ol_d	5.6	39.16	0.00	0.00	21.71	39.14	0.00	0.00	0.00	0.00	0.00	100.00
cpx_d	79.0	42.77	2.92	12.23	9.19	10.95	21.16	0.19	0.54	0.00	0.00	99.96
L	15.4	64.37	0.71	23.65	1.55	0.38	2.70	0.00	3.22	2.94	0.48	100.00
Products Used												
Melt	1.0	44.71	0.71	14.96	9.46	10.79	16.88	0.08	1.77	0.51	0.12	100.00
Estimated Compositions												
Reactants		45.89	2.42	13.30	8.72	10.90	17.13	0.15	0.92	0.45	0.07	
Products		44.71	0.71	14.96	9.46	10.79	16.88	0.08	1.77	0.51	0.12	
Differences		1.18	1.71	-1.66	-0.74	0.11	0.25	0.07	-0.84	-0.06	-0.05	
Residual Sum Squares=			**8.4**									

Set 35/2

% amounts		SiO_2	TiO_2	Al_2O_3	FeO	MgO	CaO	MnO	Na_2O	K_2O	P_2O_5	TOTAL
Reactants Used												
ol_d	3.7	40.74	0.00	0.00	13.53	45.73	0.00	0.00	0.00	0.00	0.00	100.00
cpx_d	76.6	45.38	0.58	8.70	8.22	13.32	23.43	0.15	0.16	0.00	0.00	99.94
L	19.6	65.27	0.42	24.07	1.13	0.32	2.31	0.00	3.00	2.97	0.48	99.97
	100.0											
Products Used												
Melt	1.0	44.71	0.71	14.96	9.46	10.79	16.88	0.08	1.77	0.51	0.12	100.00
Estimated Compositions												
Reactants		49.12	0.53	11.40	7.02	11.96	18.41	0.12	0.71	0.58	0.09	
Products		44.71	0.71	14.96	9.46	10.79	16.88	0.08	1.77	0.51	0.12	
Differences		4.41	-0.18	-3.56	-2.44	1.17	1.53	0.03	-1.05	0.07	-0.02	
Residual Sum Squares=			**42.9**									

Set 108/1

% amounts		SiO_2	TiO_2	Al_2O_3	FeO	MgO	CaO	MnO	Na_2O	K_2O	P_2O_5	TOTAL
Reactants Used												
ol_d	5.7	40.48	0.00	0.00	14.89	44.63	0.00	0.00	0.00	0.00	0.00	100.00
cpx_d	74.8	42.43	0.76	12.57	10.77	10.76	22.40	0.08	0.24	0.00	0.00	100.00
L	19.5	62.02	0.45	21.68	1.60	1.61	4.64	0.00	5.34	2.16	0.39	99.88
	100.0											
Products Used												
Melt	1.0	44.71	0.71	14.96	9.46	10.79	16.88	0.08	1.77	0.51	0.12	100.00
Estimated Compositions												
Reactants		46.13	0.65	13.63	9.22	10.91	17.66	0.06	1.22	0.42	0.08	
Products		44.71	0.71	14.96	9.46	10.79	16.88	0.08	1.77	0.51	0.12	
Differences		1.42	-0.06	-1.33	-0.24	0.12	0.78	-0.02	-0.55	-0.09	-0.04	
Residual Sum Squares=			**4.8**									

Mass balanced solutions using mixing program GENMIX (LeMeitre 1982). Reactants are daughter phases (excluding Al-spl_d) of melt inclusion trapped in olivine from Table 6.2. Clinopyroxene=cpx_d, host olivine=ol_d and residual glass=L. Target composition (Melt) used as product is the average analysis of melts inclusion trapped in Fo_{84-85} from Epi.